

World Scientific Series on Carbon Nanoscience

HANDBOOK OF CARBON NANO MATERIALS

Volume 1

Synthesis and Supramolecular Systems

Editors

Francis D'Souza

Karl M. Kadish

HANDBOOK OF CARBON NANO MATERIALS

Volume 1
Synthesis and Supramolecular Systems

This page intentionally left blank

World Scientific Series on Carbon Nanoscience

HANDBOOK OF CARBON NANO MATERIALS

Volume 1
Synthesis and Supramolecular Systems

Editors

Francis D'Souza

Wichita State University, USA

Karl M. Kadish

University of Houston, USA



NEW JERSEY • LONDON • SINGAPORE • BEIJING • SHANGHAI • HONG KONG • TAIPEI • CHENNAI

Published by

World Scientific Publishing Co. Pte. Ltd.

5 Toh Tuck Link, Singapore 596224

USA office: 27 Warren Street, Suite 401-402, Hackensack, NJ 07601

UK office: 57 Shelton Street, Covent Garden, London WC2H 9HE

British Library Cataloguing-in-Publication Data

A catalogue record for this book is available from the British Library.

HANDBOOK OF CARBON NANO MATERIALS

Volume 1: Synthesis and Supramolecular Systems

Copyright © 2011 by World Scientific Publishing Co. Pte. Ltd.

All rights reserved. This book, or parts thereof, may not be reproduced in any form or by any means, electronic or mechanical, including photocopying, recording or any information storage and retrieval system now known or to be invented, without written permission from the Publisher.

For photocopying of material in this volume, please pay a copying fee through the Copyright Clearance Center, Inc., 222 Rosewood Drive, Danvers, MA 01923, USA. In this case permission to photocopy is not required from the publisher.

ISBN-13 978-981-4327-81-7 (Set)

ISBN-10 981-4327-81-6 (Set)

ISBN-13 978-981-4350-20-4 (Vol. 1)

ISBN-10 981-4350-20-6 (Vol. 1)

Typeset by Stallion Press

Email: enquiries@stallionpress.com

Printed in Singapore.

Contents

<i>Preface</i>	xiii
<i>List of Contributors</i>	xv
<i>Contents of Volumes 1 and 2</i>	xxi
 1 / Chemistry with Fullerene Building Blocks	1
<i>Julien Iehl, Maxence Urbani and Jean-François Nierengarten</i>	
1. Introduction	1
2. Fullerene Building Blocks for Porphyrin Synthesis	2
3. Fullerene Building Blocks for Dendrimer Synthesis	6
3.1. Divergent synthesis	8
3.2. Convergent synthesis	10
4. Click Chemistry with Fullerene Building Blocks	16
4.1. Click chemistry with fullerene mono- and bis-adducts	16
4.2. Click chemistry with fullerene hexa-adducts	22
5. Conclusions and Perspectives	28
References	28
 2 / New Reactivity in Fullerene Chemistry	33
<i>Marta Izquierdo, Salvatore Filippone, Ángel Martín-Domenech and Nazario Martín</i>	
1. Introduction	33
2. Regioselective Intramolecular <i>cis-1</i> Cycloadditions to Fullerenes	34
2.1. Intramolecular nucleophilic addition of phenols	35
2.2. Intramolecular nucleophilic addition of alcohols and thiols	37
3. Fuller-1,6-enynes: New and Versatile Building Blocks in Fullerene Chemistry	38
3.1. The Pauson–Khand reaction on [60]fullerene	39
3.2. Thermally induced [2+2] cyclizations from fuller-1,6-enynes	45
3.3. Thermally induced intramolecular ene reaction of fuller-1,6-enynes: synthesis of fulleroallenes	46

3.4. Theoretical study of the thermal intramolecular reactions of fuller-1,6-enynes	47
4. Catalytic Enantioselective Cycloadditions: Chiral Fullerenes	49
References.	55

3 / Phthalocyanine Functionalized Carbon Nanostructures

59

Uwe Hahn, David González-Rodríguez and Tomás Torres

1. Introduction	59
2. Phthalocyanine-Fullerene Assemblies.	60
2.1. Covalent phthalocyanine-fullerene systems.	61
2.2. Non-covalent phthalocyanine-fullerene systems	75
3. Phthalocyanine-CNT Assemblies.	83
3.1. Covalent phthalocyanine-carbon nanotube systems	84
3.2. Non-covalent phthalocyanine-carbon nanotube systems	89
4. Conclusions and Perspectives	93
Acknowledgments	94
References.	94

4 / Perfluoroalkylation of Fullerenes

101

Olga V. Boltalina, Igor V. Kuvychko, Natalia B. Shustova and Steven H. Strauss

1. Methods of Synthesis	102
1.1. General remarks	102
1.2. <i>In situ</i> formation of PFAFs in an arc generator or mass spectrometer	103
1.3. Synthesis of PFAFs: reactions with metal trifluoroacetates.	105
1.4. Synthesis of PFAFs: reactions with perfluoroalkyl iodides	107
1.4.1. Reactions with CF_3I	108
1.4.2. Reactions with $\text{R}_\text{F}\text{I}$ ($\text{R}_\text{F} = \text{C}_2\text{F}_5, \text{C}_3\text{F}_7, \text{C}_4\text{F}_9, \text{C}_6\text{F}_{13},$ and $\text{C}_{12}\text{F}_{25}$)	112
2. Methods of Isolation and Characterization.	115
2.1. Selective syntheses of PFAFs.	115
2.2. Purification methods	119
2.3. Characterization	123
2.3.1. Mass spectrometry	123
2.3.2. Vibrational and UV-vis spectroscopy	125
2.3.3. NMR spectroscopy	127
2.3.4. X-ray crystallography	128

3. Physical Properties	134
4. Electrochemical Properties	135
5. Chemical Properties	137
6. Conclusions and Perspectives	139
References.	139

5 / New Vistas in Endohedral Metallofullerenes 145

Michio Yamada, Takeshi Akasaka and Shigeru Nagase

1. Introduction	146
2. Cage Frameworks, Positions, and Movements of Encaged Species	147
2.1. Monometallofullerenes.	147
2.2. Dimetallofullerenes	149
2.3. Clusterfullerenes	153
3. Electronic Properties of Pristine Endohedral Metallofullerenes	154
4. Chemistry of Endohedral Metallofullerenes	156
4.1. Bis-silylation	156
4.2. Electrophilic carbene addition.	160
4.3. 1,3-Dipolar cycloaddition.	165
4.4. Nucleophilic addition.	168
4.5. Diels–Alder reaction.	170
4.6. Radical reaction.	173
5. Electronic Tuning by Chemical Functionalization.	175
6. Conclusions and Perspectives	180
Acknowledgments	180
References.	180

6 / Metallic Oxide Clusters in Fullerene Cages 185

Steven Stevenson

1. Introduction	186
2. Synthesis	188
2.1. Historical perspective on oxometallic fullerene (OMF) and metallic nitride fullerene (MNF) synthesis.	188
2.2. Electric-arc synthesis of OMFs	189
3. Isolation	191
3.1. Stir and Filter Approach (SAFA) for $\text{Sc}_4\text{O}_2@\text{C}_{80}$ and $\text{Sc}_4\text{O}_3@\text{C}_{80}$	192
3.2. Selective precipitation method using Lewis acids	196
3.2.1. Isolation of a Stage 1 metallofullerene (<i>e.g.</i> , $\text{Sc}_4\text{O}_3@\text{C}_{80}$)	198

3.2.2. Isolation of a Stage 2 metallofullerene (<i>e.g.</i> , $\text{Sc}_2\text{O}@\text{C}_{82}$)	199
4. Reactivity	200
4.1. Reactivity comparison with other fullerenes	200
4.2. Reactivity comparison to electrochemical band gap	201
5. UV Characterization	203
6. Conclusions and Perspectives	203
Acknowledgments	203
References.	203
 7 / Synthesis of Electron Donor-[60]Fullerene Multi-Ring Interlocked Systems	 207
<i>Jackson D. Megiatto, Jr. and David I. Schuster</i>	
1. Introduction	207
2. Electron Transfer Reactions in Artificial Photosynthetic Systems	209
3. Supramolecular Artificial Photosynthesis — Catenanes and Rotaxanes	210
4. Synthesis of Ferrocene- C_{60} -Rotaxane	216
5. Synthesis of Zn(II)-Porphyrin-“Stoppered”- C_{60} -Rotaxane	221
6. Synthesis of Zn(II)-Porphyrin- C_{60} -[2]Catenates	224
7. Structural Characterization	226
8. Synthesis of [3]Catenates	228
9. Conclusion and Perspectives	238
References.	240
 8 / Solubilized Carbon Nanotubes and Their Redox Chemistry	 245
<i>Naotoshi Nakashima, Yasuhiko Tanaka and Tsuyohiko Fujigaya</i>	
1. Introduction	245
2. Characterizations of Individually Solubilized Carbon Nanotubes.	247
3. Individual Solubilization of SWNTs Using Surfactant Micelles	247
4. DNA/Carbon Nanotube Hybrids	249
5. Individual Solubilization of SWNTs Using Functional Aromatic Molecules	251
6. Nanotube/Polymer Composites	254
7. Redox Reaction and Determination of Electronic States of Carbon Nanotubes.	254

8. Electrocatalyst for Fuel Cell using Soluble CNTs	258
9. Concluding Remarks	262
References.	263

9 / Recent Advances in Covalent Functionalization and Characterization of Carbon Nanotubes 271

Maria Antonia Herrero, Ester Vazquez and Maurizio Prato

1. Introduction	272
2. Carbon Nanotubes: Type, Structure and Properties	273
3. Synthesis of Carbon Nanotubes.	274
4. Characterization of CNTs.	276
4.1. Thermogravimetric analysis.	276
4.2. Spectroscopic characterization	278
4.2.1. Electron energy loss spectroscopy (EELS)	278
4.2.2. Resonance Raman spectroscopy.	278
4.2.3. UV-vis–NIR absorption spectroscopy.	280
4.2.4. Infrared spectroscopy	282
4.2.5. Emission spectroscopy	283
4.2.6. Nuclear magnetic resonance spectrometry	284
4.2.7. X-ray photoelectron spectroscopy	285
4.3. Scanning probe microscopy	285
4.3.1. Atomic force microscopy.	286
4.3.2. Scanning tunneling microscopy	287
4.4. Electron microscopy	289
4.4.1. Transmission electron microscopy	289
4.4.2. Scanning electron microscopy	289
5. Organic Functionalization of CNTs.	291
5.1. Covalent surface chemistry of CNTs	291
5.1.1. Amidation and esterification of oxidized CNTs.	292
5.1.1.1. Esterification reactions	292
5.1.1.2. Amidation reactions.	293
5.1.2. Covalent sidewall (and tip) functionalization	295
5.1.2.1. Halogenation	296
5.1.2.2. Addition of carbenes and nitrenes.	297
5.1.2.3. 1,3-dipolar cycloaddition	298
5.1.2.4. Diels–Alder cycloadditions	301
5.1.2.5. Nucleophilic and electrophilic additions	303
5.1.2.6. Free-radical additions.	304
5.1.2.7. Reduction and reductive alkylations	305
5.1.2.8. Direct arylations	306

5.1.2.8.1. Diazonium coupling	306
5.1.2.8.2. C-C coupling chemistry catalyzed by palladium.	308
5.1.2.9. Ozonolysis	308
5.1.2.10. Grafting of polymers	309
5.1.2.11. Mechanochemical functionalizations	310
5.2. Non-covalent adsorption or wrapping of functional molecules	310
5.3. The endohedral filling of the CNTs inner empty cavity.	311
6. Double functionalization reactions	312
7. Applications: Supramolecular Chemistry	312
Conclusions and Perspectives	315
References.	316

10 / Reactions and Retro-Reactions of Fullerenes 325

*Angy L. Ortiz, Luis Echegoyen, Juan Luis Delgado
and Nazario Martín*

1. Introduction	326
2. Retro-Diels Alder Reaction.	327
2.1. Thermal <i>vs.</i> electrochemical stability of Diels-Alder adducts	327
2.2. Tether-directed remote functionalization	333
2.3. Orthogonal transposition approach	335
2.4. Diels-Alder adducts of substituted isobenzofurans and C ₆₀	337
3. Retro-cyclopropanation Reaction	339
3.1. Electrochemically induced retro-cyclopropanation reactions	340
3.1.1. C ₆₀ Fullerene derivatives	340
3.1.1.1. Walk-on-the-sphere rearrangements	350
3.1.2. C ₇₀ Fullerene derivatives and higher fullerenes.	352
3.2. Chemical retro-cyclopropanation reaction	355
3.2.1. Tandem reductive ring opening-retro-Bingel reaction	357
4. Retro-1,3-dipolar Cycloaddition Reactions	357
4.1. Chemical retro-cycloaddition of pyrrolo[3,4:1,2] [60]fullerenes	359
4.1.1. Electrochemical retro-cycloaddition of pyrrolo[3,4:1,2] [60]fullerenes	362
4.1.2. Endohedral derivatives and their stability	363

4.2. Retro-cycloaddition reaction of isoxazolo[3,4:1,2]	
[60]fullerenes	364
4.2.1. Chemical retro-cycloaddition.	365
4.2.2. Electrochemical retro-cycloaddition	365
4.3. Retro-cycloaddition reaction of pyrazolino[3,4:1,2]	
[60]fullerenes	366
4.3.1. Chemical retro-cycloaddition.	366
4.3.2. Competitive retro-cycloaddition of fullerene dimers . .	367
5. Conclusions and Outlook	368
Acknowledgments	369
References.	369

11 / Porphyrin-Fullerene Supramolecular Chemistry 375

*Peter D.W. Boyd, Ali Hosseini, John D. van Paauwe
and Christopher A. Reed*

1. Introduction	375
2. Molecular Porphyrin Hosts for Fullerenes	376
3. The Porphyrin-Fullerene Interaction	378
4. Cobalt(II) Porphyrins and Fullerenes.	380
4.1. Synthesis of bis-porphyrins	381
4.2. Binding constants and charge transfer bands	381
4.3. X-ray structures of T _{3,4,5-OMe} PP cocrystallates	383
5. Conclusions.	387
Acknowledgments	387
References.	387

12 / Supramolecular Hosts for Pristine Fullerenes. 391

Paris E. Georghiou

1. Introduction	391
2. Complexation in Organic Solutions.	392
2.1. General considerations	392
2.2. Calixarene-type hosts	393
2.3. Porphyrin-containing hosts.	395
2.4. Tetrathiafulvalene-containing hosts	397
2.5. Some other hosts.	399
3. Conclusions.	402
References.	402

Cumulative Index of Volumes 1 and 2

This page intentionally left blank

Preface

This *Handbook of Carbon Nanomaterials* celebrates the 25th anniversary of the discovery of Fullerenes, then known as Buckyballs. Since their discovery in 1985, fullerenes as well as carbon nanotubes and graphenes, two closely related carbon allotropes, have taken up a solid place in modern science and technology as evidenced by the awarding of two Nobel Prizes — the first, in Chemistry, was given in 1996 to Robert F. Curl Jr., Sir Harold Kroto and Richard E. Smalley for the discovery of fullerenes and the second, in Physics, was awarded in 2010 to Andre Geim and Konstantin Novoselov for the isolation of graphene using Scotch tape as a tool. Since 1985, more than 100,000 scientific papers have been published on topics devoted to fullerenes, carbon nanotubes and related materials and there is no doubt that these types of carbon nanomaterials, with their unique structures and properties, will continue to find many new applications in all areas of science and technology.

The present *Handbook of Carbon Nanomaterials* consists of 23 chapters in two volumes which, as a whole, summarize current work and the latest developments in the field of carbon nanomaterials as seen through the eyes of more than three dozen leading researchers from around the world. The topics covered in this two volume set of books can be divided into four general areas. The first deals with the chemistry of fullerenes and carbon nanotubes, including organic functionalization, reactivity, perfluoroalkylation and fullerenes linked to photosensitizers. The second covers the chemistry and physics of endohedral fullerenes. The third major area of coverage involves molecular and supramolecular chemistry of fullerenes and carbon nanotubes while the fourth includes topics related to photoinduced energy and electron transfer. Finally, applications of fullerenes, carbon nanotubes and graphenes as applied to organic molecular electronics, polymers composites, thermal conductive materials, photovoltaics and sensing are presented.

This Handbook was written as a hands on reference guide for scientists working in the fields of chemistry, physics, materials science, polymer science, solid-state physics, nanotechnology or supramolecular science. The coverage of topics presented is both in-depth and comprehensive, and when combined with the perspectives for future research given by the contributing authors makes this book an invaluable reference source which should be considered essential reading for both students and advanced researchers in the field.

The editors would like to acknowledge all of the contributors for their timely submission of the state-of-the-art review topics; We also acknowledge NSF, Kansas-EPSCoR, ACS-PRF (to FD) and the Robert A Welch Foundation (to KMK) for financial support; last but not least, the staff of World Scientific Publishing Co are acknowledged for their immense help in bringing out this publication in a timely manner.

Francis D'Souza
Wichita, KS, USA

Karl M. Kadish
Houston, TX, USA

December 18, 2010

This page intentionally left blank

List of Contributors*

Takeshi Akasaka

University of Tsukuba
Tsukuba, Ibaraki, Japan
E-mail: akasaka@tara.tsukuba.ac.jp
Chapter 5

Olga V. Boltalina

Colorado State University
Fort Collins, CO 80523, USA
Email: olga.boltalina@colostate.edu
Chapter 4

Peter D.W. Boyd

The University of Auckland
Auckland 1142, New Zealand
Email: pdw.boyd@auckland.ac.nz
Chapter 11

John W. Connel

NASA Langley Research Center
Hampton, VA 23681, USA
E-mail: john.w.connell@nasa.gov
Chapter 22

Juan Luis Delgado

Universidad Complutense
Madrid, Spain
Chapter 10

Francis D'Souza

Wichita State University
Wichita, KS 67260, USA
Email: Francis.DSouza@wichita.edu
Chapter 21

Luis Echegoyen

University of Texas at El Paso
El Paso, TX 79968, USA
E-mail: echegoyen@utep.edu
Chapter 10

Fernando Fernández-Lázaro

Universidad Miguel Hernández
Alicante, Spain
Chapter 19

Salvatore Filippone

Universidad Complutense
Madrid, Spain
Chapter 2

Tsuyohiko Fujigaya

Kyushu University
Fukuoka 819-0395, Japan
Chapter 8

*Full Contact Information for authors can be found on the title page of each chapter.

Shunichi Fukuzumi

Osaka University
Osaka 565-0871, Japan
Email: fukuzumi@chem.eng.
osaka-u.ac.jp

Chapter 16

Paris E. Georghiou

Memorial University of
Newfoundland
St. Johns, Canada
Email: parisg@mun.ca

Chapter 12

Sayata Ghose

National Institute of Aerospace
Hampton, VA 23666, USA

Chapter 22

David González-Rodríguez

Universidad Autónoma
Madrid, Spain

Chapter 3

Dirk M. Guldi

Friedrich-Alexander-Universität
Erlangen-Nürnberg
Erlangen, Germany
Email: guldi@chemie.uni-erlangen.de

Chapter 20

Uwe Hahn

Universidad Autónoma de Madrid
Madrid, Spain

Chapter 3

Maria Antonia Herrero

Universidad de Castilla-La Mancha
Ciudad Real, Spain

Chapter 9

Ali Hosseini

The University of Auckland
Auckland 1142
New Zealand

Chapter 11

Piétrick Hudhomme

Université d'Angers
Angers, France
Email: pietrick.hudhomme@univ-
angers.fr

Chapter 17

Julien Iehl

Université de Strasbourg et CNRS
Strasbourg Cedex 2, France

Chapter 1

Hiroshi Imahori

Kyoto University
Kyoto, Japan
Email: imahori@scl.kyoto-u.ac.jp

Chapter 18

Osamu Ito

CarbonPhotoScience
Sendai, Japan
Email: ito@tagen.tohoku.ac.jp

Chapters 14, 15

Marta Izquierdo

Universidad Complutense
Madrid, Spain

Chapter 2

Chang Yi Kong

Clemson University
Clemson, SC 29634, USA

Chapter 22

Włodzimierz Kutner

Polish Academy of Sciences
Warsaw, Poland

E-mail: wkutner@ichf.edu.pl

Chapter 21

Igor V. Kuvychko

Colorado State University
Fort Collins, CO 80523, USA

Chapter 4

Helge Lemmetyinen

Tampere University of
Technology

Tampere, Finland

Chapter 13

Yi Lin

National Institute of Aerospace
Hampton, VA 23666, USA

E-mail: yi.lin@nianet.org

Chapter 22

Nazario Martín

Universidad Complutense de
Madrid

Madrid, Spain

E-mail: nazmar@quim.ucm.es

Chapters 2, 10

Ángel Martín-Domenech

Universidad Complutense
Madrid, Spain

Chapter 2

Luis Martín-Gomis

Universidad Miguel Hernández
Alicante, Spain

Chapter 19

Aurelio Mateo-Alonso

Albert-Ludwigs-Universität
Freiburg

Freiburg i. Brsg, Germany

Chapter 20

Jackson D. Megiatto, Jr.

New York University

New York 10003, USA

Email: jackson.megiatto@nyu.edu

Chapter 7

Mohammed J. Meziani

Clemson University

Clemson, SC 29634, USA

Chapter 22

Shigeru Nagase

Institute for Molecular Science

Okazaki, Aichi, Japan

E-mail: nagase@ims.ac.jp

Chapter 5

Naotoshi Nakashima

Kyushu University

Fukuoka 819-0395, Japan

Email: nakashima-tcm@mail.

cstm.kyushu-u.ac.jp

Chapter 8

Jean-François Nierengarten

Université de Strasbourg et CNRS

Strasbourg Cedex 2, France

Email: nierengarten@chimie.u-

strasbg.fr

Chapter 1

Angy L. Ortiz

Clemson University

Clemson, SC 29634, USA

Chapter 10

Piotr Pieta

Polish Academy of Sciences
Warsaw, Poland
Chapter 21

Maurizio Prato

Università di Trieste
34127 Trieste, Italy
Email: prato@units.it
Chapter 9

Christopher A. Reed

University of California
Riverside CA 92521, USA
Chapter 11

Slava V. Rotkin

Lehigh University
Bethlehem, PA 18015, USA
E-mail: rotkin@lehigh.edu
Chapter 23

Ángela Sastre-Santos

Universidad Miguel Hernández
Alicante, Spain
E-mail: asastre@umh.es
Chapter 19

David I. Schuster

New York University
New York, 10003, USA
E-mail: david.schuster@nyu.edu
Chapter 7

Natalia B. Shustova

Colorado State University
Fort Collins, CO 80523, USA
Chapter 4

Steven Stevenson

University of Southern Mississippi
Hattiesburg, MS, 39406, USA
Email: Steven.Stevenson@usm.edu
Chapter 6

Steven H. Strauss

Colorado State University
Fort Collins, CO 80523, USA
Email: steven.strauss@colostate.edu
Chapter 4

Ya-Ping Sun

Clemson University
Clemson, SC 29634, USA
E-mail: syaping@clemson.edu
Chapter 22

Toshikazu Takata

Tokyo Institute of Technology,
Tokyo, 152-8552, Japan
Chapter 15

Yasuhiko Tanaka

Kyushu University
Fukuoka 819-0395, Japan
Email: ttakata@polymer.titech.ac.jp
Chapter 8

Leilei Tian

Clemson University
Clemson, SC 29634, USA
Chapter 22

Nikolai V. Tkachenko

Tampere University of Technology
Tampere, Finland
Email: nikolai.tkachenko@tut.fi
Chapter 13

Tomás Torres

Universidad Autónoma de Madrid
Madrid, Spain

Email: tomas.torres@uam.es

Chapter 3

Tomokazu Umeyama

Kyoto University
Kyoto 615-8510, Japan

Chapter 18

Maxence Urbani

Université de Strasbourg et CNRS
Strasbourg Cedex 2, France

Chapter 1

John D. van Paauwe

The University of Auckland
Auckland 1142, New Zealand

Chapter 11

Ester Vazquez

Universidad de Castilla-La Mancha
Ciudad Real, Spain

Chapter 9

L. Monica Veca

Clemson University
Clemson, SC 29634, USA

Email: lveca@clemson.edu

Chapter 22

Wei Wang

Clemson University
Clemson, SC 29634, USA

Chapter 22

Mateusz Wielopolski

Friedrich-Alexander-Universität
Erlangen-Nürnberg

Erlangen, Germany

Chapter 20

René M. Williams

Universiteit van Amsterdam
Amsterdam, The Netherlands

E-mail: r.m.williams@uva.nl

Chapter 17

Michio Yamada

Tokyo Gakugei University
Tokyo, Japan

Chapter 5

This page intentionally left blank

Contents of Volumes 1 and 2

Volume 1 Synthesis and Supramolecular Systems

1. Chemistry with Fullerene Building Blocks
Julien Iehl, Maxence Urbani and Jean-François Nierengarten
2. New Reactivity in Fullerene Chemistry
Marta Izquierdo, Salvatore Filippone, Ángel Martín-Domenech and Nazario Martín
3. Phthalocyanine Functionalized Carbon Nanostructures
Uwe Hahn, David González-Rodríguez and Tomás Torres
4. Perfluoroalkylation of Fullerenes
Olga V. Boltalina, Igor V. Kuvychko, Natalia B. Shustova and Steven H. Strauss
5. New Vistas in Endohedral Metallofullerenes
Michio Yamada, Takeshi Akasaka and Shigeru Nagase
6. Metallic Oxide Clusters in Fullerene Cages
Steven Stevenson
7. Synthesis of Electron Donor-[60]Fullerene Multi-Ring Interlocked Systems
Jackson D. Megiatto, Jr. and David I. Schuster
8. Solubilized Carbon Nanotubes and Their Redox Chemistry
Naotoshi Nakashima, Yasuhiko Tanaka and Tsuyohiko Fujigaya
9. Recent Advances in Covalent Functionalization and Characterization of Carbon Nanotubes
Maria Antonia Herrero, Ester Vazquez and Maurizio Prato

10. Reactions and Retro-reactions of Fullerenes
Angy L. Ortiz, Luis Echegoyen, Juan Luis Delgado and Nazario Martín
11. Porphyrin-Fullerene Supramolecular Chemistry
*Peter D.W. Boyd, Ali Hosseini, John D. van Paauwe
and Christopher A. Reed*
12. Supramolecular Hosts for Pristine Fullerenes
Paris E. Georghiou

Volume 2 Electron Transfer and Applications

13. Dynamics of Photoinduced Charge Transfer of Fullerene Based Donor–Acceptor Systems: From Solution to Organized Molecular Films
Nikolai V. Tkachenko and Helge Lemmetyinen
14. Photoinduced Electron Transfer Between Fullerenes and Electron-Donors Through Molecular Bridges
Osamu Ito
15. Photoinduced Electron Transfer Processes of Fullerene Rotaxanes
Toshikazu Takata and Osamu Ito
16. Electron Donor–Acceptor Nanohybrids and Their Application to Light–Energy Conversion
Shunichi Fukuzumi
17. Energy and Electron Transfer in Photo- and Electro-Active Fullerene Dyads
Piétrick Hudhomme and René M. Williams
18. Fullerenes for Photoelectrochemical and Photovoltaic Devices
Hiroshi Imahori and Tomokazu Umeyama
19. Fullerenes as Photosensitizers in Photorefractive Materials
*Ángela Sastre-Santos, Luis Martín-Gomis
and Fernando Fernández-Lázaro*

20. Functionalized Fullerene Derivatives in Organic Molecular Electronics
Mateusz Wielopolski, Aurelio Mateo-Alonso and Dirk M. Guldi
21. Preparation, Properties, and Application of Polymer Composites of Carbon Nanotubes
Piotr Pieta, Francis D'Souza and Wlodzimierz Kutner
22. Thermal Conductive Materials Based on Carbon Nanotubes and Graphene Nanosheets
L. Monica Veca, Wei Wang, Yi Lin, Mohammed J. Meziani, Leilei Tian, John W. Connel, Sayata Ghose, Chang Yi Kong and Ya-Ping Sun
23. Electronic Properties of DNA-SWNT Hybrids: From Charge Separation to Optical Sensing
Slava V. Rotkin

This page intentionally left blank

Chapter 1

Chemistry with Fullerene Building Blocks

*Julien Iehl, Maxence Urbani and Jean-François Nierengarten**

*Laboratoire de Chimie des Matériaux Moléculaires,
Université de Strasbourg et CNRS, Ecole Européenne de Chimie,
Polymères et Matériaux, 25 rue Becquerel, 67087 Strasbourg Cedex 2, France*

1. Introduction	1
2. Fullerene Building Blocks for Porphyrin Synthesis	2
3. Fullerene Building Blocks for Dendrimer Synthesis	6
3.1. Divergent synthesis	8
3.2. Convergent synthesis	10
4. Click Chemistry with Fullerene Building Blocks	16
4.1. Click chemistry with fullerene mono- and bis-adducts	16
4.2. Click chemistry with fullerene hexa-adducts	22
5. Conclusions and Perspectives	28
References	28

1. Introduction

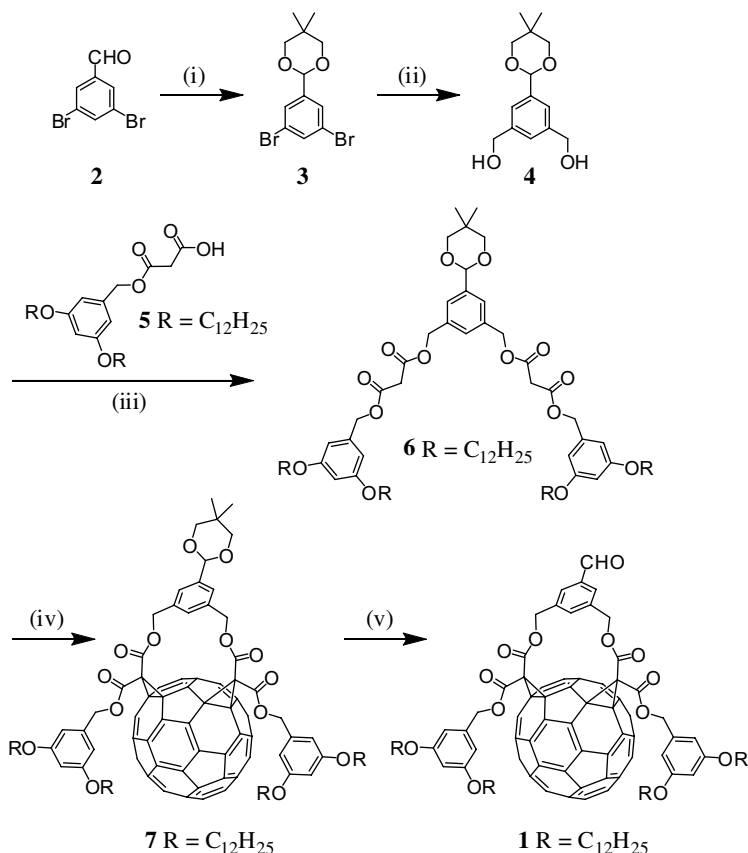
Following the discovery of the macroscopic-scale [60]fullerene synthesis,¹ the chemistry of this fascinating spherical molecule has been intensely investigated.² The chemical reactivity of C₆₀ is now well established and a large number of fullerene derivatives have been prepared.² Owing to their facile multiple reducibility, optical non-linearity and/or efficient singlet oxygen photosensitization, fullerene-containing compounds have found applications in materials science³ and biology.⁴ Whereas most of the fullerene derivatives

*Corresponding author. Email: nierengarten@chimie.u-strasbg.fr

reported to date have been prepared by the direct functionalization of C_{60} in the final step, the use of fullerene building blocks in multi-step synthesis has been scarcely considered. This is mainly associated with the chemical reactivity of the fullerene moiety. Effectively, C_{60} derivatives react readily with radicals, various nucleophiles, carbenes, and participate as reactive 2π components in a variety of cycloaddition reactions.² Thus, the range of reactions that can be used for the further transformations of fullerene derivatives appears to be quite limited. Nonetheless, an increasing number of reactions involving fullerene building blocks have been reported in recent years. Examples are activation of fullerene-carboxylic acid derivatives for subsequent esterification or preparation of amides, construction of porphyrins from fullerene-benzaldehydes, and copper catalyzed alkyne-azide click reactions involving either fullerene-azide or fullerene-alkyne derivatives. In this chapter, the most recent developments in the use of fullerene building blocks as synthetic intermediates will be presented. The aim of this chapter is not to give an exhaustive review on reactions using fullerene derivatives as starting material but to present significant examples to illustrate the current state-of-the-art of fullerene chemistry for the development of new nanomaterials and bioactive molecules.

2. Fullerene Building Blocks for Porphyrin Synthesis

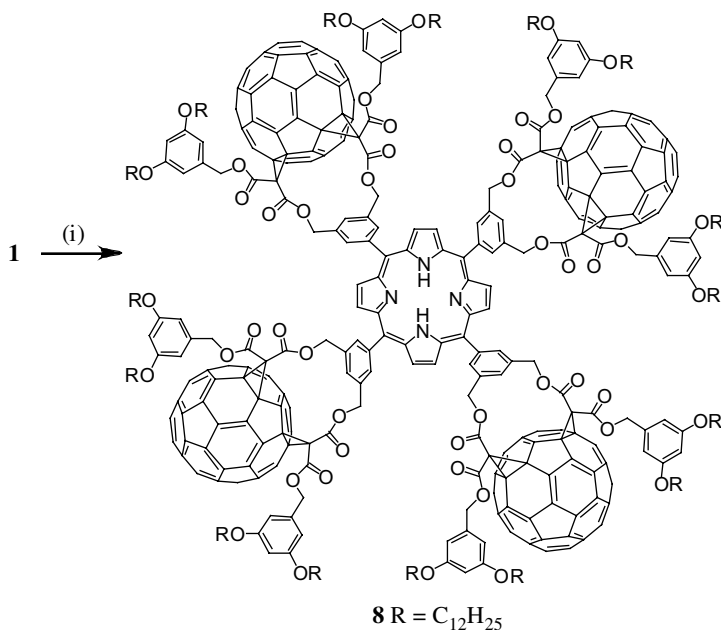
Owing to their electronic properties, porphyrins and fullerenes are interesting complementary building blocks for the preparation of artificial photosynthetic systems⁵ and molecular photonic devices.⁶ Indeed, many examples of covalently linked porphyrin-fullerene derivatives have been described in recent years.⁵ Their photophysical properties have been investigated in detail and intramolecular processes such as electron and energy transfer evidenced in such multicomponent hybrid systems.⁵ As far as their synthesis is concerned, most of the porphyrin- C_{60} dyads reported so far have been prepared by reaction of a preconstructed porphyrin derivative with C_{60} itself.⁷ In contrast, the use of fullerene building blocks in porphyrin synthesis has been scarcely considered. Actually, the compatibility of C_{60} derivatives with reaction conditions classically used for porphyrin synthesis is not obvious. The potential of fullerene-benzaldehyde derivatives as starting materials for the construction of functionalized porphyrins has been reported by Nierengarten and coworkers.⁸⁻¹² The synthesis of fullerene building block **1** is depicted in Scheme 1. Reaction of **2** with 2,2-dimethyl-1,3-propanediol in refluxing benzene in the presence of a catalytic amount of *p*-toluenesulfonic acid (*p*-TsOH) afforded **3** in 97% yield. Treatment of **3** with an excess of *t*-BuLi in THF followed by quenching with *N,N*-dimethylformamide (DMF), and subsequent reduction of the resulting dialdehyde with diisobutylaluminum hydride (DIBAL-H) gave



Scheme 1. Reagents and conditions: (i) 2,2-dimethyl-1,3-propanediol, C_6H_6 , *p*-TsOH cat., Δ , Dean-Stark trap (97%); (ii) *t*-BuLi (4 eq.), THF, -78 to 0°C , then DMF, -78 to 0°C , then aq. 2 M HCl, then DIBAL-H, CH_2Cl_2 , 0°C (56%); (iii) DCC, DMAP, CH_2Cl_2 , 0°C to r.t. (72%); (iv) C_{60} , DBU, I_2 , toluene, r.t. (48%); (v) $\text{CF}_3\text{CO}_2\text{H}$, H_2O , CH_2Cl_2 , r.t. (93%).

diol **4** in an overall 56% yield. *N,N'*-Dicyclohexylcarbodiimide (DCC)-mediated esterification of **4** with the malonic mono-ester **5** yielded bis-malonate **6**.

The functionalization of C_{60} was based on the highly regioselective reaction developed by Diederich and coworkers¹³ which yielded macrocyclic bis-adducts of C_{60} resulting from a macrocyclization reaction of the carbon sphere with bis-malonate derivatives in a double Bingel addition. Treatment of C_{60} with **6**, iodine and 1,8-diazabicyclo[5.4.0]undec-7-ene (DBU) in toluene at room temperature afforded the *cis*-2 bis-adduct **7** in 48% yield. The relative position of the two cyclopropane rings in **7** on the C_{60} core was determined based on the molecular symmetry (C_s) deduced from the ^1H - and ^{13}C NMR spectra. It is also well-established that the 1,3-phenylenebis(methylene)-tethered bis-malonates produce regioselectively the C_s symmetrical *cis*-2 addition

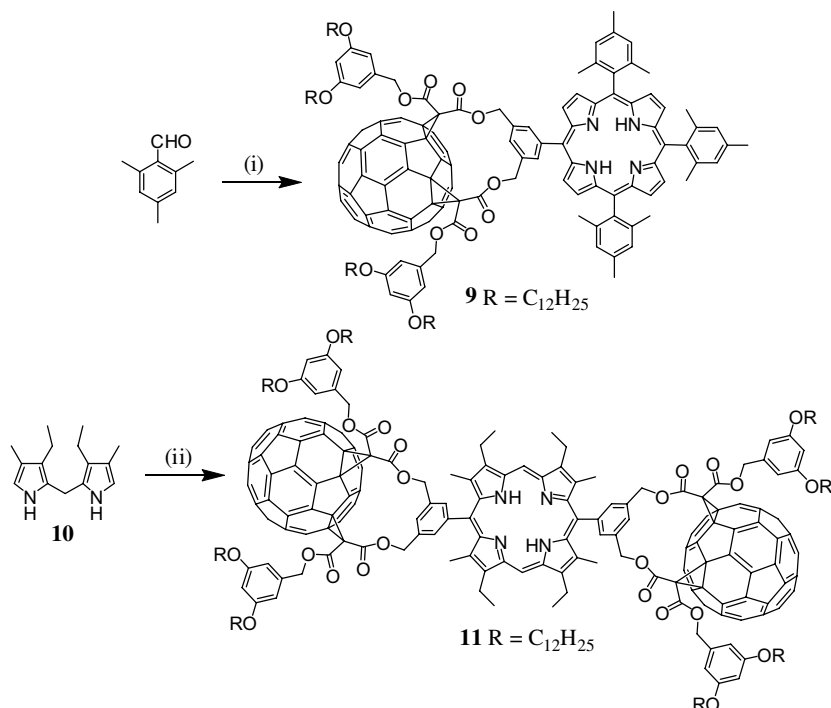


Scheme 2. Regents and conditions: (i) pyrrole, BF₃·Et₂O, CHCl₃ (containing 0.75% EtOH), r.t. then *p*-chloranil, Δ (12%).

pattern at C₆₀.¹³ Finally, treatment of **7** with CF₃CO₂H in CH₂Cl₂/H₂O 1:1 afforded benzaldehyde **1**. It was obtained in 93% yield as an orange-red glassy product and its preparation was easily carried out on a gram scale. Preparation of porphyrin **8** (Scheme 2) was first attempted from C₆₀-benzaldehyde **1** and pyrrole under the classical conditions reported by Lindsey *et al.*¹⁴

However, reaction of **1** with pyrrole in CH₂Cl₂ with CF₃CO₂H as catalyst followed by *p*-chloranil oxidation yielded unreacted **1** and polymers, and no trace of porphyrin **8** could be detected. However, **8** could be obtained by using the reaction conditions developed by Lindsey for the synthesis of sterically hindered porphyrins such as tetramesitylporphyrin.¹⁵ A key feature of these conditions involves BF₃-ethanol cocatalysis. The condensation of **1** and pyrrole was performed in CHCl₃ (commercial CHCl₃ containing 0.75% ethanol as stabilizer) at room temperature in the presence of BF₃·Et₂O. After 5 hours, *p*-chloranil (tetrachlorobenzoquinone) was added to irreversibly convert the porphyrinogen to the porphyrin. The desired tetraphenylporphyrin **8** was subsequently isolated in 12% yield by tedious chromatographic separations.⁹

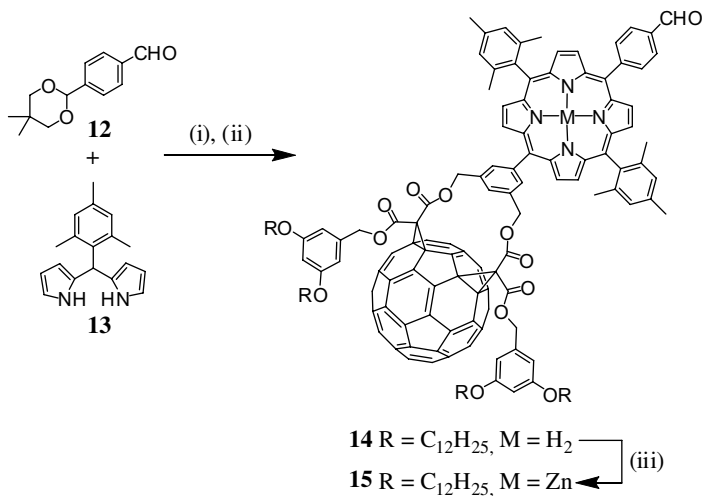
Reaction of **1** (1 equiv.) with mesitaldehyde (3 equiv.) and pyrrole (4 equiv.) in CHCl₃ in the presence of BF₃·Et₂O followed by treatment with *p*-chloranil gave fullerene-porphyrin conjugate **9** in 11% yield (Scheme 3). Finally, bis(*meta*-substituted-phenyl) porphyrin **11** was prepared in 38% yield from **1** and **10**.^{10,11}



Scheme 3. Reagents and conditions: (i) **1**, pyrrole, $BF_3 \cdot Et_2O$, $CHCl_3$ (containing 0.75% EtOH), r.t. then *p*-chloranil, Δ (11%); (ii) **1**, pyrrole, $BF_3 \cdot Et_2O$, $CHCl_3$ (containing 0.75% EtOH), r.t. then *p*-chloranil, Δ (38%).

Investigations of the photophysical properties of compounds **8**, **9** and **11** have revealed the occurrence of photoinduced electron transfer upon photo-excitation of the porphyrin moiety leading to a short-lived charge separated state.¹¹ With the aim of increasing the lifetime of the charge separated state, we became interested in the synthesis of fullerene derivatives bearing multi-porphyrinic donors. In such systems, the initial photoinduced electron transfer between the C_{60} unit and its neighboring porphyrin moiety can be followed by a charge shift from the first porphyrin moiety to the next one. Therefore, the distance between the fullerene radical anion and the terminal porphyrin radical cation is quite long and thus the lifetime of the charge separated state is increased.⁵ For this purpose, Nierengarten and coworkers have developed a fullerene-porphyrin conjugate bearing a benzaldehyde moiety allowing further porphyrin synthesis. The synthesis of this building block is depicted in Scheme 4.

Condensation of **1** (1 equiv.), **12** (1 equiv.) and **13** (2 equiv.) in $CHCl_3$ at room temperature in the presence of $BF_3 \cdot Et_2O$ followed by *p*-chloranil oxidation and subsequent treatment with CF_3CO_2H in CH_2Cl_2 gave porphyrin **14** in an overall 4.5% yield. This low yield is explained by partial cleavage of

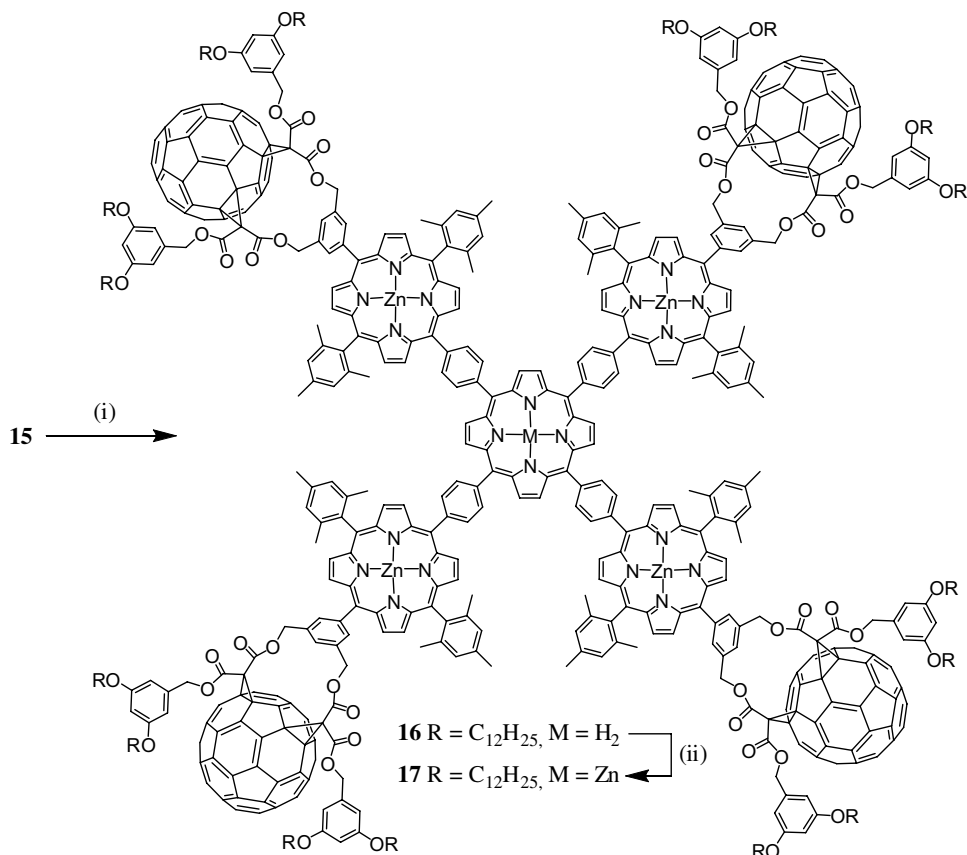


Scheme 4. Reagents and conditions: (i) **1**, $\text{BF}_3 \cdot \text{Et}_2\text{O}$, CHCl_3 (containing 0.75% EtOH), r.t. then *p*-chloranil, Δ (5%); (ii) $\text{CF}_3\text{CO}_2\text{H}$, CH_2Cl_2 , r.t. (90%); (iii) $\text{Zn}(\text{OAc})_2 \cdot 2\text{H}_2\text{O}$, $\text{CHCl}_3/\text{MeOH}$ (9:1), Δ (87%).

the acetal protecting group under the acidic conditions used for the condensation reaction. Metalation of porphyrin **14** with $\text{Zn}(\text{OAc})_2$ gave **15** in 87% yield. Condensation of aldehyde **15** with pyrrole in CHCl_3 with $\text{BF}_3 \cdot \text{Et}_2\text{O}$ as catalyst followed by *p*-chloranil oxidation yielded porphyrin **16** which was metalated with $\text{Zn}(\text{OAc})_2$ to give **17** (Scheme 5). The structure of both **16** and **17** was confirmed by MALDI-TOF mass spectrometry. The expected molecular ion peak were observed at m/z 10816.1 for **16** ($[M]^+$, calcd for $\text{C}_{740}\text{H}_{614}\text{N}_{20}\text{O}_{48}\text{Zn}_4$: 10815.35 (100%), 10816.36 (93.5%), 10814.36 (87.3%)) and m/z 10878.1 for **17** ($[M]^+$, calcd for $\text{C}_{740}\text{H}_{612}\text{N}_{20}\text{O}_{48}\text{Zn}_5$: 10879.27 (100%), 10879.26 (97.9%), 10877.27 (97.9%)).

3. Fullerene Building Blocks for Dendrimer Synthesis

In recent years, the rapid advances in dendrimer synthetic chemistry have moved towards the creation of functional systems with increased attention to potential applications.¹⁶ Among the large number of molecular subunits used for dendrimer chemistry, C_{60} has proven to be a versatile building block.¹⁷ C_{60} itself is a convenient core for dendrimer chemistry^{18,19} and the functionalization of C_{60} with a controlled number of dendrons dramatically improves the solubility of the fullerenes.²⁰ Furthermore, variable degrees of addition about the fullerene core are possible and its almost spherical shape leads to globular systems even with low-generation dendrons.²¹ On the other hand, specific advantages are brought about by the encapsulation of a fullerene moiety in



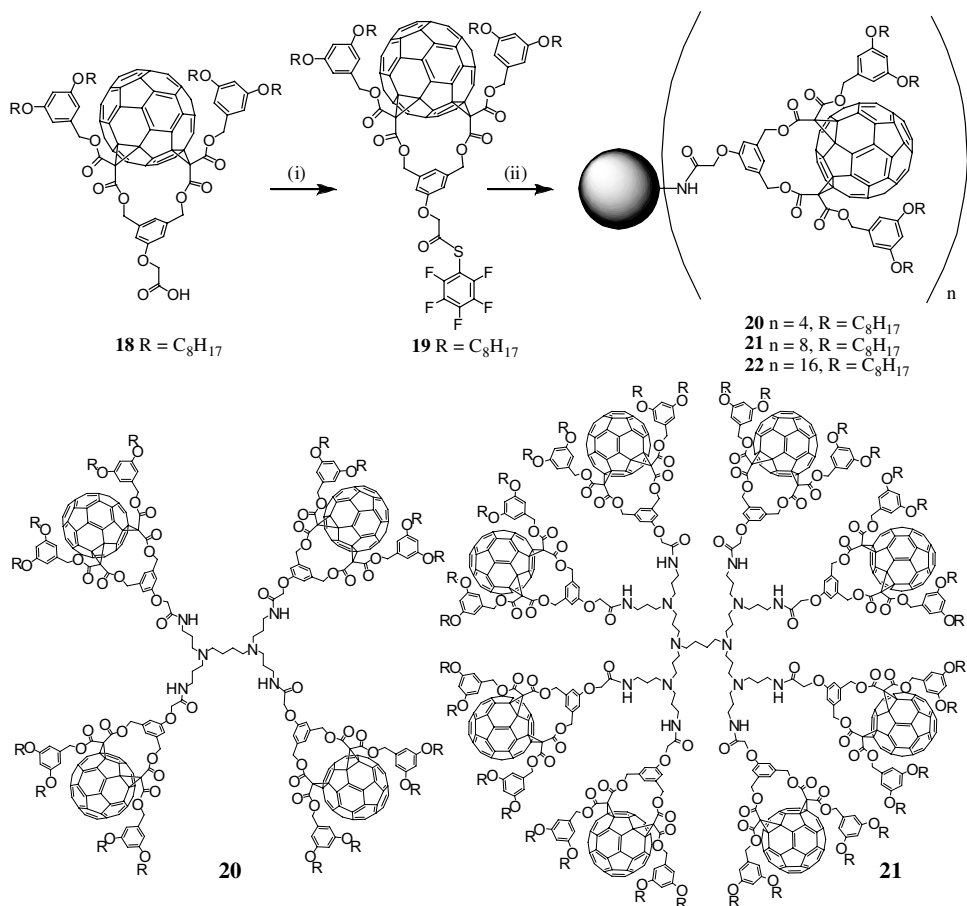
Scheme 5. Reagents and conditions: (i) pyrrole, $\text{BF}_3 \cdot \text{Et}_2\text{O}$, CHCl_3 (containing 0.75% EtOH), r.t. then *p*-chloranil, Δ (57%); (ii) $\text{Zn}(\text{OAc})_2 \cdot 2\text{H}_2\text{O}$, $\text{CHCl}_3/\text{MeOH}$ (9:1), Δ (82%).

the middle of a dendritic structure.²² The shielding effect resulting from the presence of the surrounding shell has been found to be useful in optimizing the optical limiting properties of C_{60} derivatives,²³ to obtain amphiphilic derivatives with good spreading characteristics,²⁴ or to prepare fullerene-containing liquid crystalline materials.²⁵ The use of the fullerene sphere as a photoactive core unit has also been reported.²⁶ In particular, the special photophysical properties of C_{60} have been used to evidence dendritic shielding effects²⁷ and to prepare dendrimer-based light-harvesting systems.²⁸ Whereas the majority of the fullerene-containing dendrimers reported so far have been prepared with a C_{60} core, dendritic structures with fullerene units at their surface or with C_{60} spheres in the dendritic branches have been essentially ignored. This is mainly associated with the difficulties related to the synthesis of fullerene-rich molecules.²⁹ Indeed, the two major problems for the preparation of such dendrimers are the low solubility of C_{60} and its

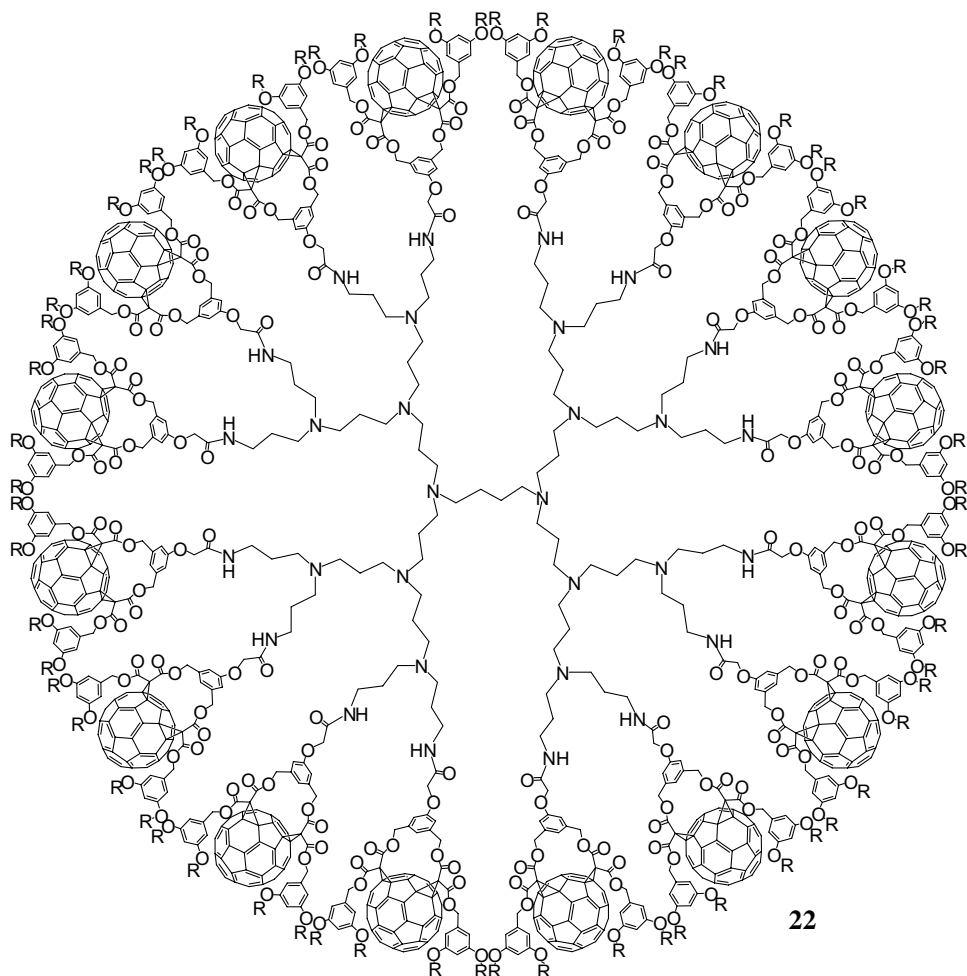
chemical reactivity limiting the range of reactions that can be used for the synthesis of branched structures bearing multiple C_{60} units. Over the past years, several examples of fullerene-rich dendrimers have been reported. These results will be summarized in the following sections.

3.1. Divergent synthesis

The divergent preparation of fullerodendrimers by grafting C_{60} units on the peripheral reactive groups of commercially available dendrimers is the easiest way to produce large dendritic structures.³⁰ This synthetic approach was applied to prepare compounds **20–22** (Scheme 6) from fullerene derivative



Scheme 6. Reagents and conditions: (i) pentafluorothiophenol, DCC, DMAP, CH_2Cl_2 , $0^\circ C$ to r.t. (99%); (ii) PPI, Et_3N , $CHCl_3$, r.t. (**20**: 61%, **21**: 82%, **22**: 51%).



Scheme 6. (Continued)

18 and polypropyleneimine (PPI) dendrimers.³¹ The choice of the appropriate activating group for the carboxylic acid function of the C₆₀ building block **18** was the key to this synthesis. Effectively, the reaction conditions for the activation step may not be strongly acidic or basic to preserve the ester functions. Furthermore, the grafting onto the dendritic polyamines requires an extremely efficient reaction to obtain the corresponding functionalized derivatives with good yields and to avoid the formation of defective dendrimers. The preparation of the pentafluorothiophenolester derived from compound **18** and pentafluorothiophenol under DCC-mediated esterification conditions appeared as a good choice. Indeed, the reaction conditions for the preparation

of this activated acid are mild and the efficient grafting of pentafluorothiophenolesters onto PPI dendrimers has already been reported.³² The activated acid (**19**) was obtained in nearly quantitative yields by reaction of carboxylic acid **18** with pentathiofluorothiophenol in the presence of DCC and a catalytic amount of 4-dimethylaminopyridine (DMAP). Subsequent reaction of the resulting pentafluorothiophenolester with the PPI dendrimers of 1st, 2nd and 3rd generation in the presence of triethylamine (Et_3N) provided the corresponding dendritic derivatives **20–22** in good yields.

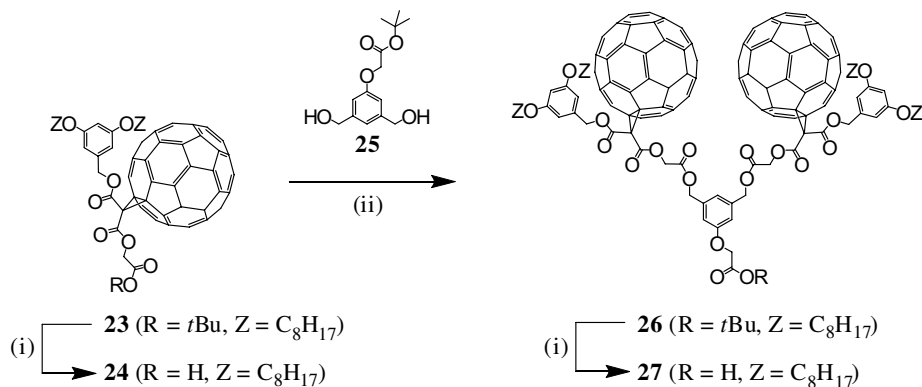
Owing to the presence of four pendant alkyl chains per fullerene moiety, compounds **20–22** are all well soluble in common organic solvents such as CH_2Cl_2 , CHCl_3 , THF or toluene, and spectroscopic characterization was easily achieved. The ^1H -NMR spectra of dendrimers **20–22** show the typical pattern of the fullerene cis-2 bis-adduct with the expected additional signals arising from the PPI skeleton. The integration ratios are also consistent with the proposed molecular structures. The structure of **20** and **21** was further confirmed by MALDI-TOF mass spectrometry. The expected molecular ion peaks were clearly observed for both compounds. It should be pointed out that no peaks corresponding to defected dendrimers were observed in the mass spectra of **20–21**, thus providing clear evidence for their monodispersity. For **22**, a high level of fragmentation prevented the observation of the expected molecular ion peak and its monodispersity could not be unambiguously demonstrated.

3.2. Convergent synthesis

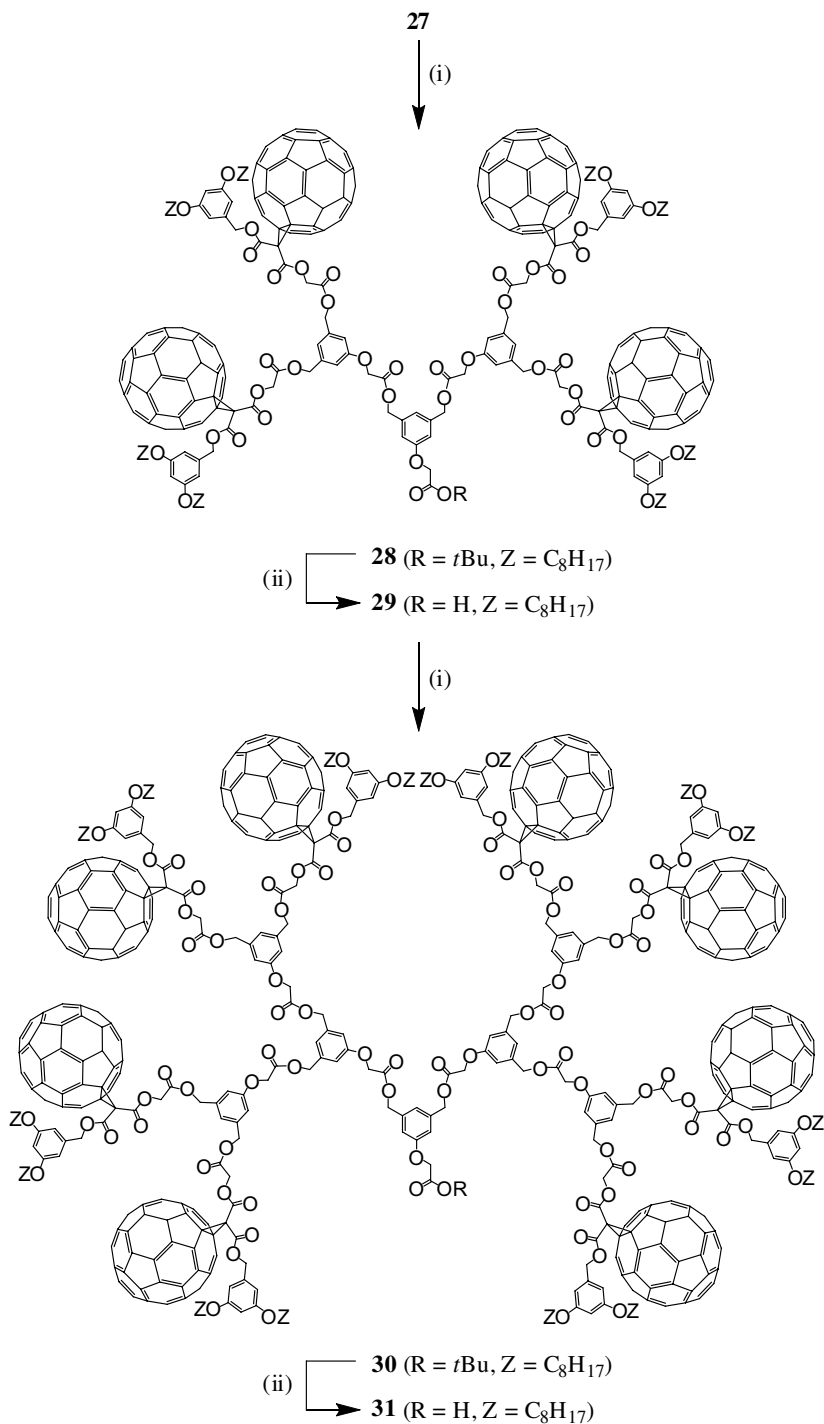
In the divergent strategy, dendrimers are constructed from the central core to the periphery.¹⁶ In each repeat cycle, the n reactive groups on the dendrimer periphery react with n monomer units to add a new generation to the dendrimer. However, due to the increasing number of reactive terminal units, defects in the structures appear rapidly. In the convergent strategy which has been introduced by Hawker and Fréchet,³³ dendritic branches are first built up, then attached to the central core in the final step. In this case, the number of coupling reactions needed to add each new generation — usually 2 or 3 — is the same throughout the synthesis making defective products easier to separate. Whereas exactly the same number of steps is required in using a divergent or convergent approach for the preparation of a given dendrimer, the convergent one appears to be more efficient for the construction of monodisperse dendrimers. In recent years, Nierengarten and coworkers have developed synthetic methodologies allowing for the preparation of dendrons substituted with several fullerene moieties.²⁹ As a typical example, the

convergent preparation of dendritic branches with fullerene subunits at the periphery is depicted in Schemes 7–9.

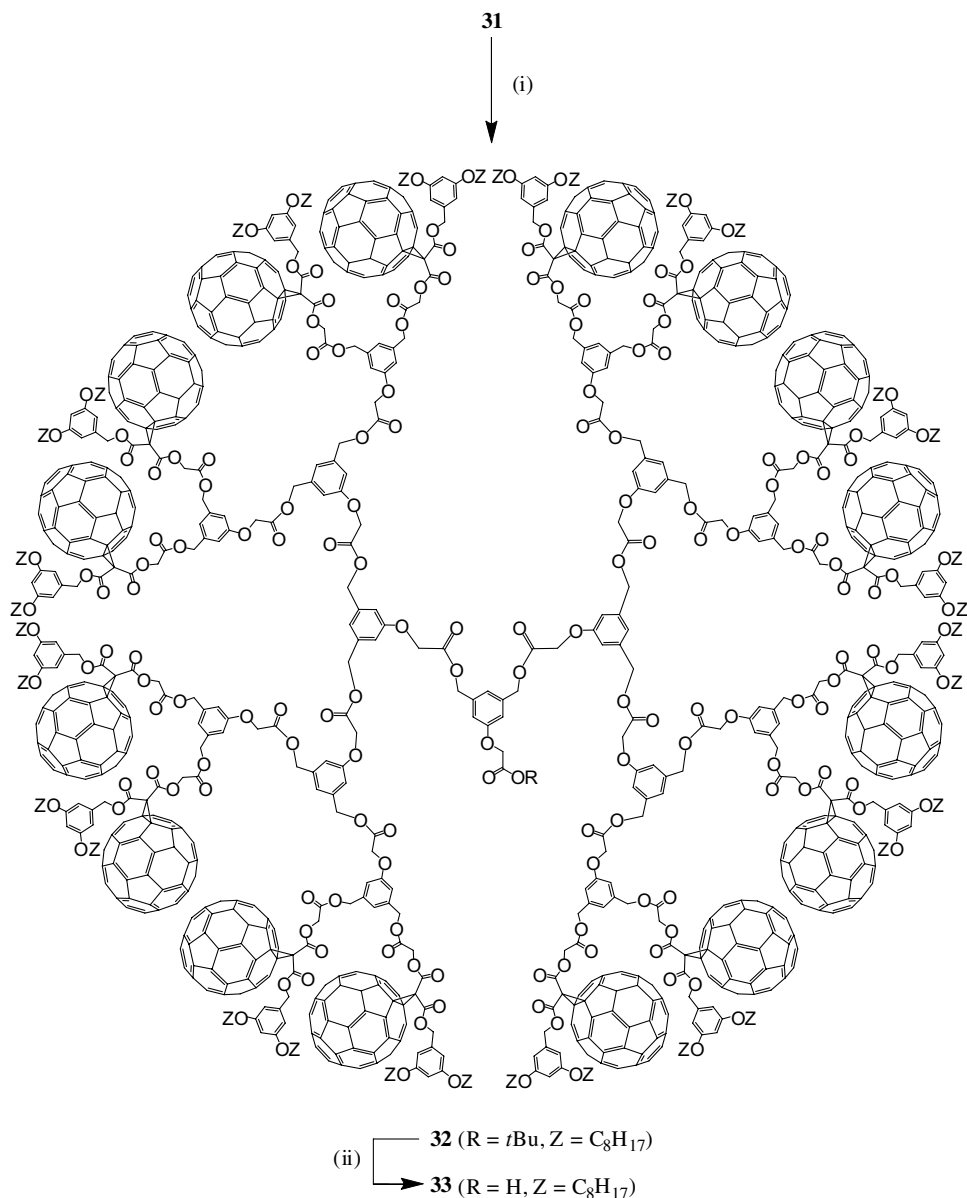
The starting fullerene derivative **23** is easily obtained on a multi-gram scale and is highly soluble in common organic solvents thanks to the presence of the two long alkyl chains.³⁴ The iterative reaction sequence used for the preparation of the subsequent dendrimer generations relies upon successive cleavage of a *t*-butyl ester moiety under acidic conditions followed by a *N,N'*-dicyclohexylcarbodiimide (DCC)-mediated esterification reaction with the A₂B building block **25** possessing two benzylic alcohol functions and a protected carboxylic acid function.³⁴ Selective cleavage of the *t*-butyl ester group in **23** was achieved by treatment with an excess of CF₃COOH (TFA) in CH₂Cl₂ to afford **24** in a quantitative yield. Reaction of diol **25** with carboxylic acid **24** under esterification conditions using DCC, DMAP, and 1-hydroxybenzotriazole (HOBT) in CH₂Cl₂ gave the protected dendron of second generation **26** in 90% yield. Hydrolysis of the *t*-butyl ester moiety under acidic conditions then afforded the corresponding carboxylic acid **27** in a quantitative yield. Esterification of **27** with diol **25** (DCC, HOBT, DMAP) afforded the *t*-butyl-protected fullerodendrion **28** in 87% yield (Scheme 8). Selective hydrolysis of the *t*-butyl ester under acidic conditions afforded acid **29** in 99% yield. Subsequent reaction of **29** with the branching unit **25** in the presence of DCC, HOBT and DMAP afforded fullerodendrion **30** (95%), which after treatment with CF₃CO₂H gave **31** (97%). By repeating the same reaction sequence from **31**, the fifth generation derivatives **32** and **33** were also prepared (Scheme 9). Compounds **26**–**33** are well soluble in common organic solvents such as CH₂Cl₂, CHCl₃, or THF and complete spectroscopic characterization was easily achieved.



Scheme 7. Reagents and conditions: (i) TFA, CH₂Cl₂; (ii) DCC, DMAP, HOBT, CH₂Cl₂.

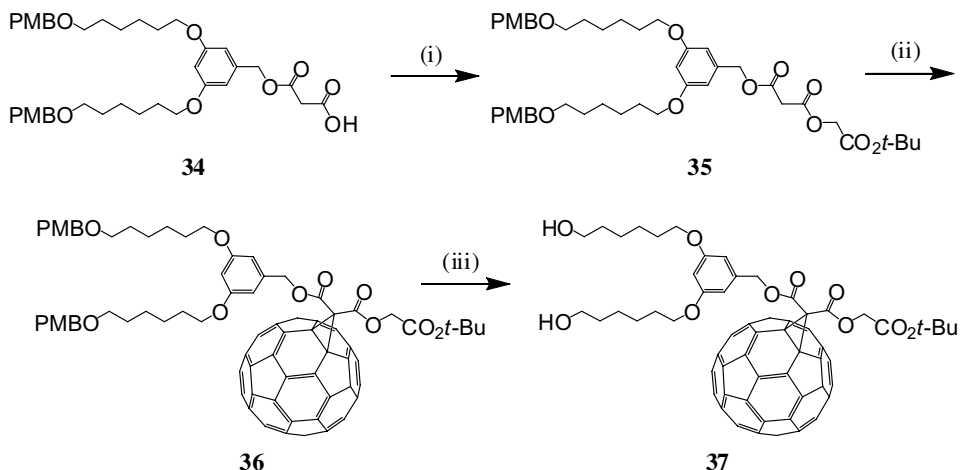


Scheme 8. Reagents and conditions: (i) **25**, DCC, DMAP, HOBT, CH_2Cl_2 ; (ii) TFA, CH_2Cl_2 .



Scheme 9. Reagents and conditions: (i) **25**, DCC, DMAP, HOBT, CH_2Cl_2 ; (ii) TFA, CH_2Cl_2 .

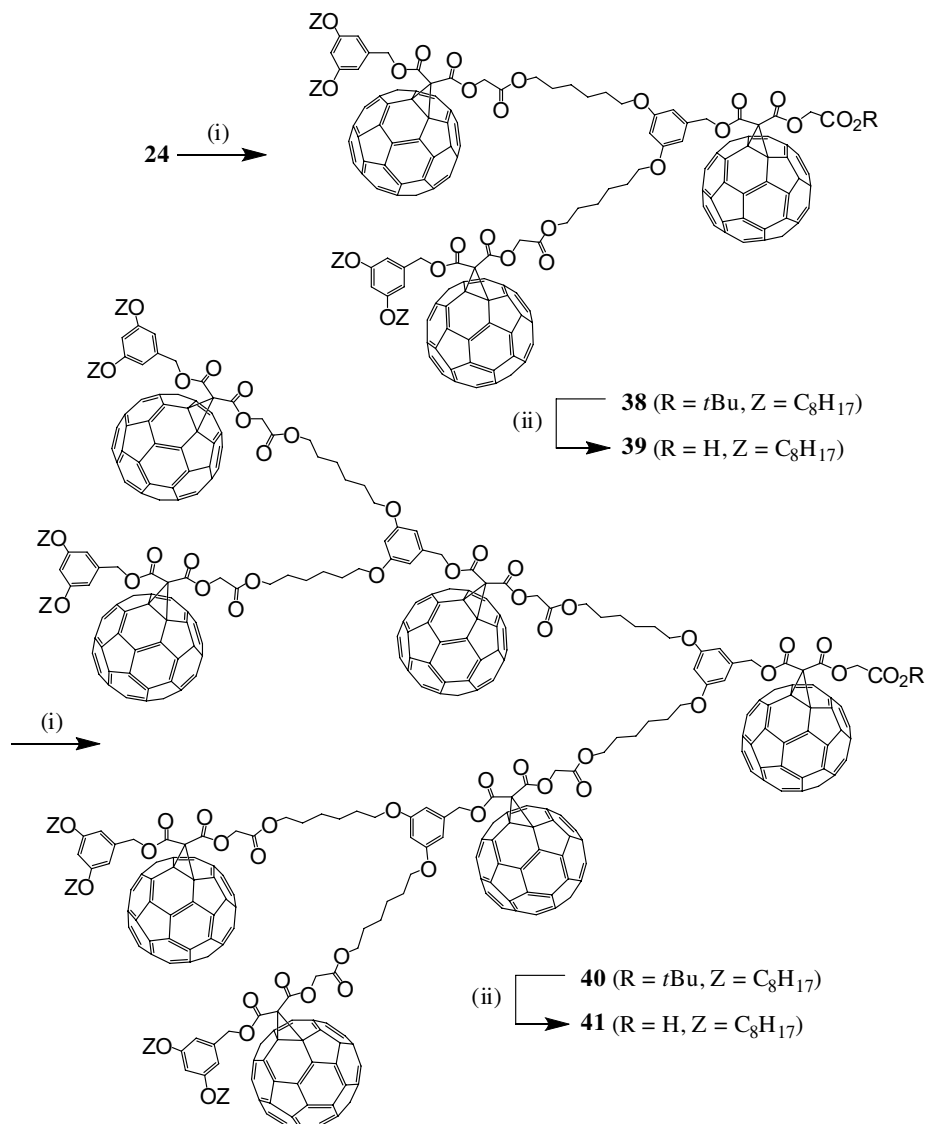
The preparation of fullerodendrons with a C_{60} group at each branching unit was also carried out by a convergent approach using successive esterification and deprotection steps.³⁵ The preparation of the key building block **37** is depicted in Scheme 10. This diol containing one *t*-butyl ester function appears to be the



Scheme 10. Reagents and conditions: (i) *t*-Butyl 2-hydroxyacetate, DCC, DMAP, BtOH, CH₂Cl₂, 0°C to r.t. (91%); (ii) C₆₀, DBU, I₂, toluene, r.t. (30%); (iii) DDQ, H₂O, CH₂Cl₂, r.t. (84%).

branching unit for the construction of the fullerodendrons. DCC-mediated esterification of **34** with *t*-butyl 2-hydroxyacetate in CH₂Cl₂ yielded malonate **35**, which after treatment with C₆₀, I₂ and DBU in toluene at room temperature gave methanofullerene **36** in 30% yield. The choice of the appropriate protecting group for the two alcohol groups in **36** was the key to this synthesis. Effectively, the deprotection conditions must not be acidic to preserve the *t*-butyl ester moiety nor basic to preserve the other ester functions. The PMB protecting groups in **36** could be removed with 2,3-dichloro-5,6-dicyanobenzoquinone (DDQ) in CH₂Cl₂ containing a small amount of water at room temperature. Under these neutral conditions, all the ester functions remained unchanged and compound **37** was thus obtained in a good yield (84%).

Fullerene derivative **24** substituted with two long alkyl chains (solubilizing groups) and a carboxylic function was used as a peripheral subunit for the constructions of the dendrons (Scheme 11). Esterification of acid **24** with diol **37** under conditions using DCC, BtOH and DMAP afforded the *t*-butyl-protected fullerodendron **38** in 70% yield. Selective hydrolysis of the *t*-butyl ester under acidic conditions afforded acid **39** in 98% yield. Subsequent reaction of **39** with the branching unit **37** in the presence of DCC, BtOH and DMAP afforded fullerodendron **40**, which after treatment with CF₃CO₂H gave **41**. The ¹H and ¹³C NMR, IR, UV/vis and elemental analysis data were consistent with the proposed molecular structures assigned to the fullerodendrons of each generation.



Scheme 11. Reagents and conditions: (i) **37**, DCC, DMAP, BtOH, CH_2Cl_2 , 0°C to r.t.; (ii) $\text{CF}_3\text{CO}_2\text{H}$, CH_2Cl_2 , r.t.

Several other syntheses of fullerodendrons having either peripheral C_{60} subunits or containing C_{60} groups at each branching units have been reported.³⁶ In all the cases, the synthesis of the dendrons relies upon the same iterative reaction sequence (esterification/cleavage of a *t*-butyl ester). These fullerodendrons are interesting building blocks for the preparation of monodisperse fullerene-rich macromolecules.³⁷ For example, Nierengarten

and coworkers³⁸ have also shown that C₆₀ derivatives bearing a carboxylic acid function undergo self-assembly with *n*-butylstannonic acid (*n*BuSn(O)OH) to produce fullerene-rich nanostructures with a stannoxane core.³⁸ The reaction conditions were first adjusted with compound **24** (Scheme 12). Under optimized conditions, a mixture of **24** (1 equiv.) and *n*BuSn(O)OH (1 equiv.) in benzene was refluxed for 12 h using a Dean-Stark trap. After cooling, the solution was filtered and evaporated to dryness to afford the hexameric organostannoxane derivative **42** in 99% yield.

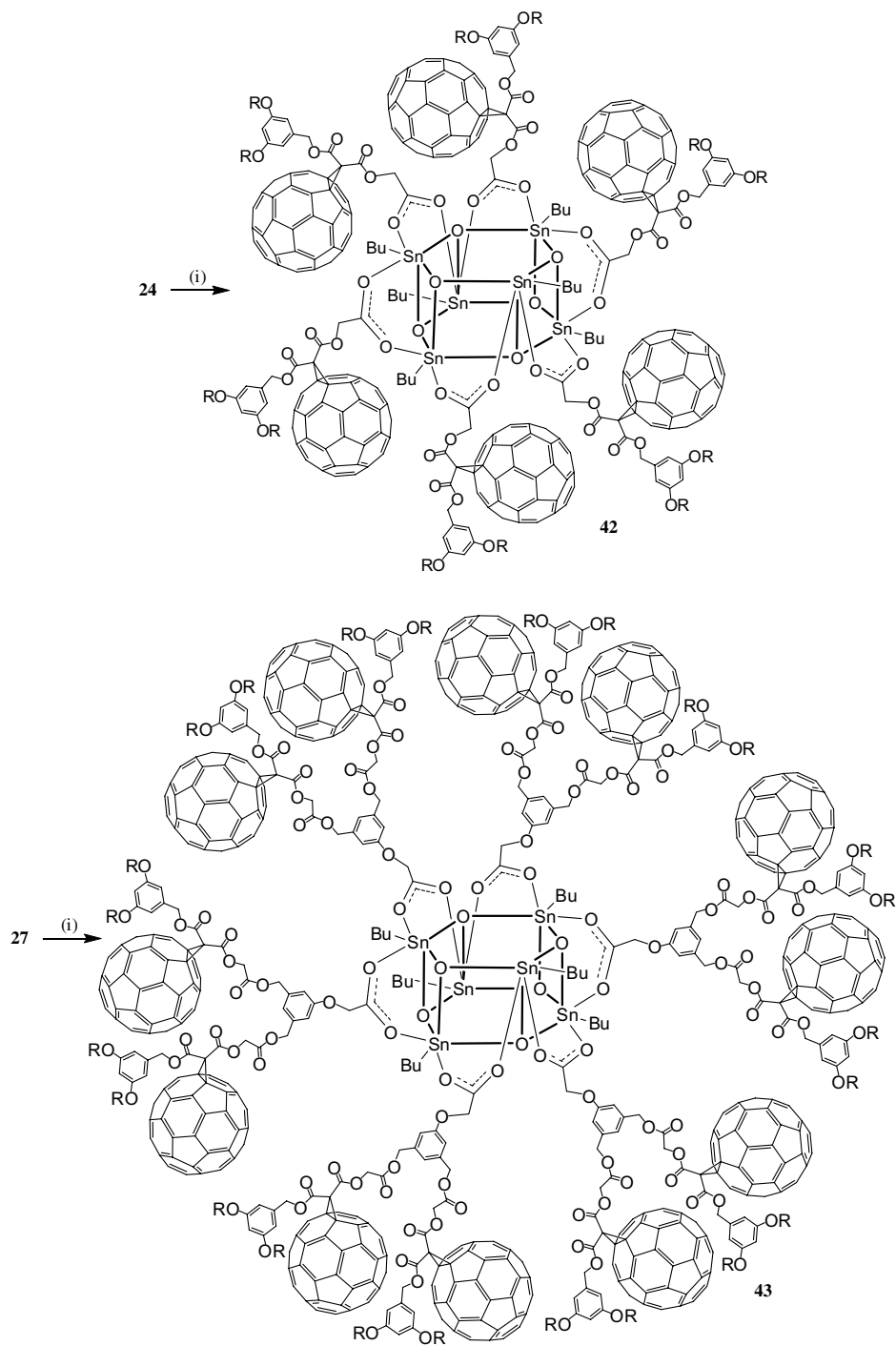
The reaction conditions used for the preparation of **42** from carboxylic acid **24** were then applied to fullerodendrons **27** and **29**. The corresponding organostannoxane derivatives **43–44** were thus obtained in almost quantitative yields (Schemes 12 and 13).

Interestingly, the self-assembly process is not affected by the increased size of the starting carboxylic acids when going from the first to the third generation derivative. Whatever the generation number is, the reaction was finished after 12 h and the hexameric assembly was obtained in a very high yield (96–99%).

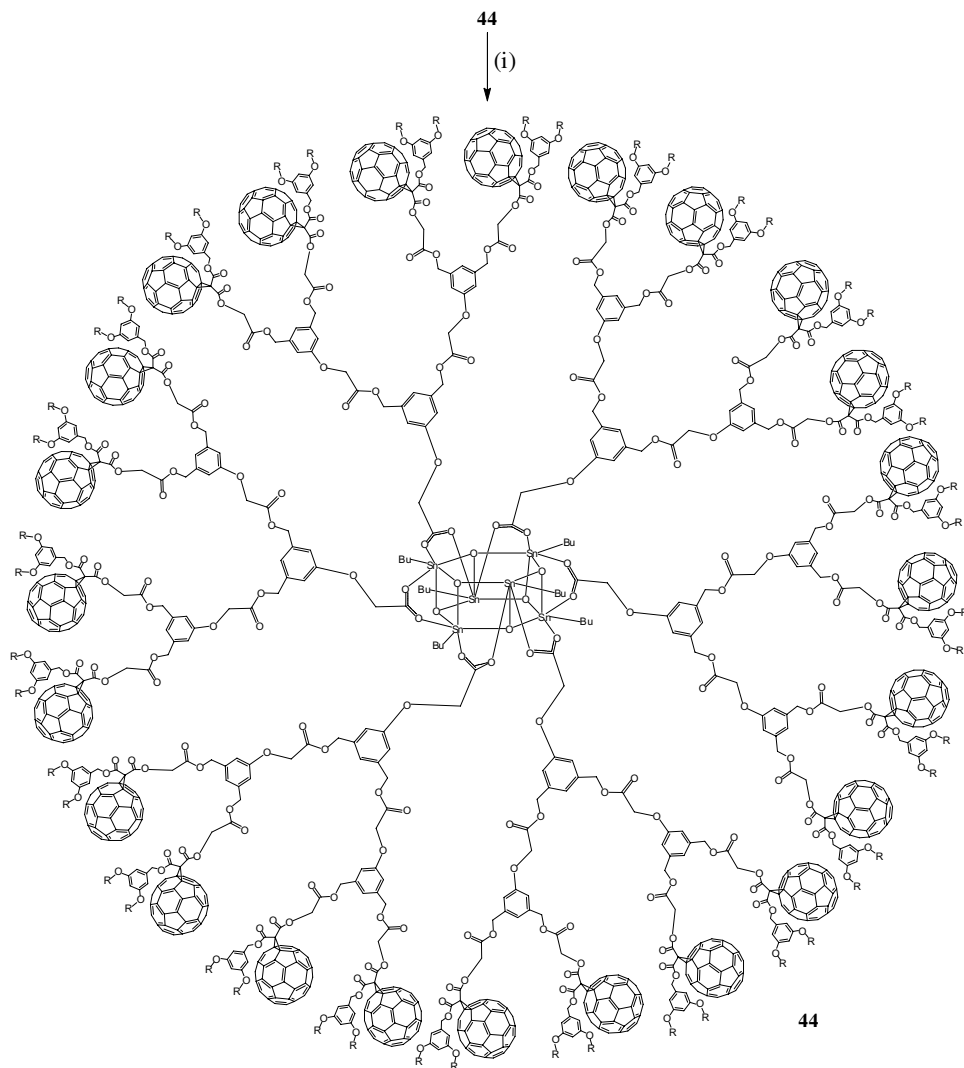
4. Click Chemistry with Fullerene Building Blocks

4.1. Click chemistry with fullerene mono- and bis-adducts

Click chemistry is an attractive tool for fullerene chemistry as click reactions are modular, tolerant to a wide range of functional groups, and high yielding.³⁹ The copper mediated Huisgen 1,3-dipolar cycloaddition of organic azides and alkynes⁴⁰ to give 1,2,3-triazoles is without any doubt the most useful member of this family of reactions. However, whereas this click reaction has proven to be powerful for a large variety of building blocks,³⁹ its compatibility with fullerene derivatives was not obvious, as organic azides may also undergo [3+2]cycloadditions to the [6,6]double bonds of fullerenes.⁴¹ Recently, the potential of click chemistry to functionalize fullerene derivatives has been systematically evaluated.⁴² The first series of click reactions was performed from fullerene derivatives functionalized with terminal alkyne groups (Scheme 14).⁴² Treatment of **45** (1 equiv.) with benzyl azide (3 equiv.), CuSO₄·5H₂O (0.1 equiv.) and sodium ascorbate (0.3 equiv.) in CH₂Cl₂/H₂O under vigorous stirring at room temperature for 96 h gave the cycloaddition product **46** in a moderate yield (48%). The solubility of compound **45** is quite low and all the starting material was not dissolved under the copper mediated Huisgen reaction conditions. Thus, the reaction was slow and side reactions, most probably cycloaddition of benzyl

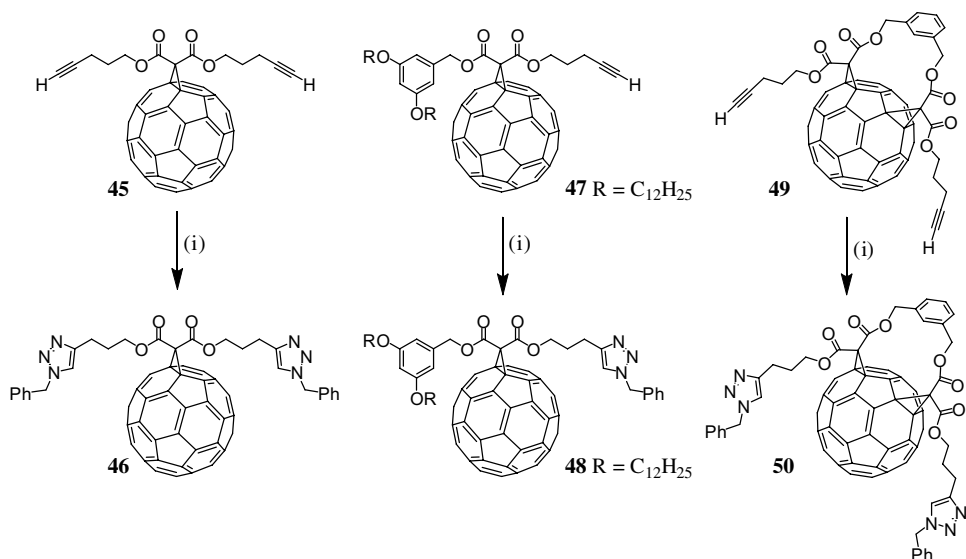


Scheme 12. Reagents and conditions: (i) BuSn(O)OH, C₆H₆, Dean Stark, Δ.



Scheme 13. Reagents and conditions: (i) $\text{BuSn}(\text{O})\text{OH}$, C_6H_6 , Dean Stark, Δ .

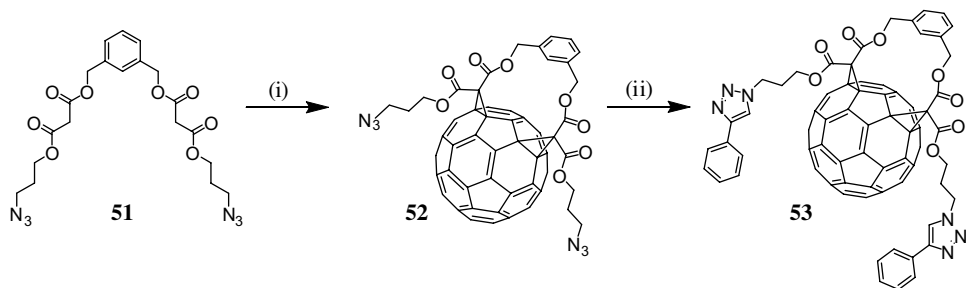
azides to the fullerene core, were observed. To solve this problem, it was decided to prepare a more soluble methanofullerene-alkyne derivative bearing a 3,5-didodecyloxybenzyl group (**47**). The reaction of this compound with benzyl azide in the presence of $\text{CuSO}_4 \cdot 5\text{H}_2\text{O}$ and sodium ascorbate in $\text{CH}_2\text{Cl}_2/\text{H}_2\text{O}$ could be achieved under optimized concentration conditions. Compound **48** was thus obtained in a good yield (80%), thus showing that the reactivity of the fullerene moiety with organic azides plays only a minor role under copper mediated Huisgen 1,3-dipolar cycloaddition conditions.



Scheme 14. Reagents and conditions: (i) benzyl azide, $\text{CuSO}_4 \cdot 5\text{H}_2\text{O}$, sodium ascorbate, $\text{CH}_2\text{Cl}_2/\text{H}_2\text{O}$, r.t.

To further decrease the reactivity of the C_{60} moiety towards the azide reagents in the click reactions, a fullerene bis-adduct bearing two terminal alkyne groups was prepared. It is well known that the reactivity of the fullerene unit is decreased by increasing the number of substituents on the carbon cage.⁴³ Reaction of **49** with benzyl azide under the conditions optimized for the preparation of compound **48** gave bis-1,2,3-triazole **50** in 70% yield. When compared to the preparation of compound **46** from methanofullerene **45**, the increased yield can be explained by both the higher solubility of the starting terminal alkyne and the decreased reactivity of the bis-substituted fullerene group.

In a second series of click reactions, the use of fullerene building blocks functionalized with azide groups was evaluated.^{42–44} To this end, the synthesis of methanofullerene derivatives substituted with one or two azide groups was attempted. Unfortunately, these compounds were found to be very unstable in the solid state although reasonably stable in solution. Most probably, intermolecular cycloaddition reactions between the C_{60} and the azide groups led to complex mixtures of polymeric compounds. Actually, only fullerene bis-adducts were sufficiently stable to be used as synthetic intermediates in click reactions. This observation confirms the decreased reactivity of the fullerene moiety by increasing the number of substituents on the carbon cage. Bis-adduct **52** was obtained in 16% yield

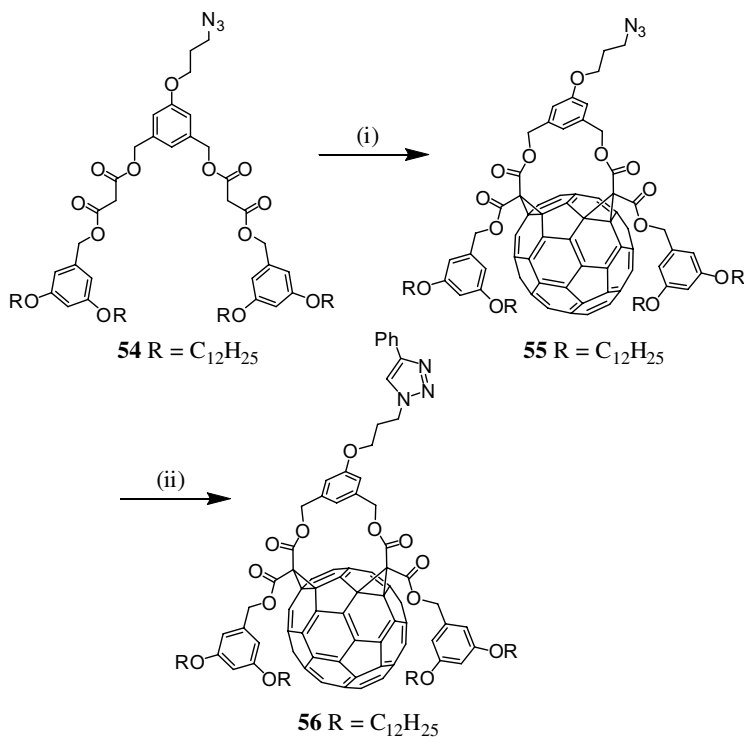


Scheme 15. Reagents and conditions: (i) C_{60} , DBU, I_2 , PhMe, r.t. (16%); (ii) phenylacetylene, $CuSO_4 \cdot 5H_2O$, sodium ascorbate, CH_2Cl_2/H_2O , r.t. (78%).

by reaction of **51** with C_{60} , I_2 , and DBU in toluene at room temperature (Scheme 15).

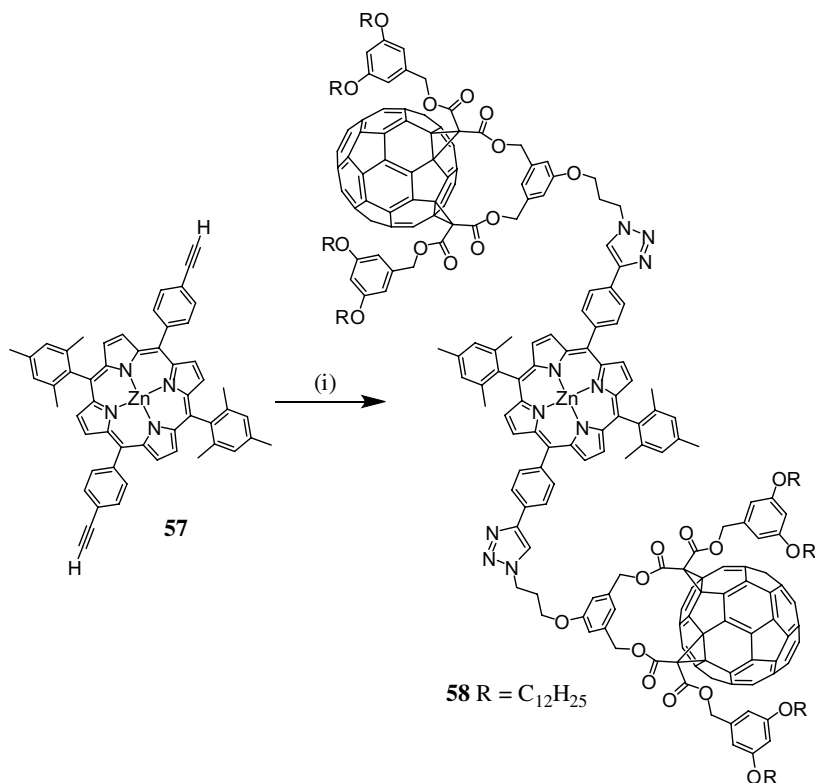
Reaction of **52** with phenylacetylene under optimized conditions afforded bis-1,2,3-triazole **53** in 78% yield. Indeed, upon preparation and purification, compound **52** must be used for the click reactions within the following couple of hours to obtain good yields. Therefore, the availability of this synthetic intermediate is quite limited. In order to obtain a stable fullerene azide derivative, it was decided to take advantage of the encapsulation of the fullerene sphere in a cyclic addend surrounded by two 3,5-didodecylbenzyl ester moieties;⁴⁵ the azide function being attached onto the bridging subunit. In this way, steric hindrance should prevent the reaction of the azide group with the C_{60} core and, thus, provide a stable compound. The synthesis of building block **55** is depicted in Scheme 16. Reaction of **54** with C_{60} , I_2 , and DBU in toluene at room temperature afforded the cyclization product **55** in 56% yield. Importantly, fullerene azide derivative **55** was found to be a stable compound under normal laboratory conditions. A sample was stored in the fridge for several months without any detectable decomposition. The reaction conditions for the 1,3-dipolar cycloaddition of compound **55** with terminal alkynes were adjusted with phenylacetylene. Under optimized conditions, a mixture of **55** (1 equiv.), phenylacetylene (2 equiv.), $CuSO_4 \cdot 5H_2O$ (0.1 equiv.) and sodium ascorbate (0.3 equiv.) in CH_2Cl_2/H_2O was vigorously stirred at room temperature for 12 h. After work-up and purification, compound **56** was thus obtained in 73% yield.

It appears clearly that click chemistry is an interesting tool for the functionalization of fullerene building blocks. The chemical transformation of fullerene derivatives bearing azides and alkynes under the copper mediated Huisgen 1,3-dipolar cycloaddition conditions has been demonstrated. Whereas the preparation of fullerene azide derivatives can be difficult due to



Scheme 16. Reagents and conditions: (i) C₆₀, DBU, I₂, PhMe, r.t. (56%); (ii) phenylacetylene, CuSO₄·5H₂O, sodium ascorbate, CH₂Cl₂/H₂O, r.t. (73%).

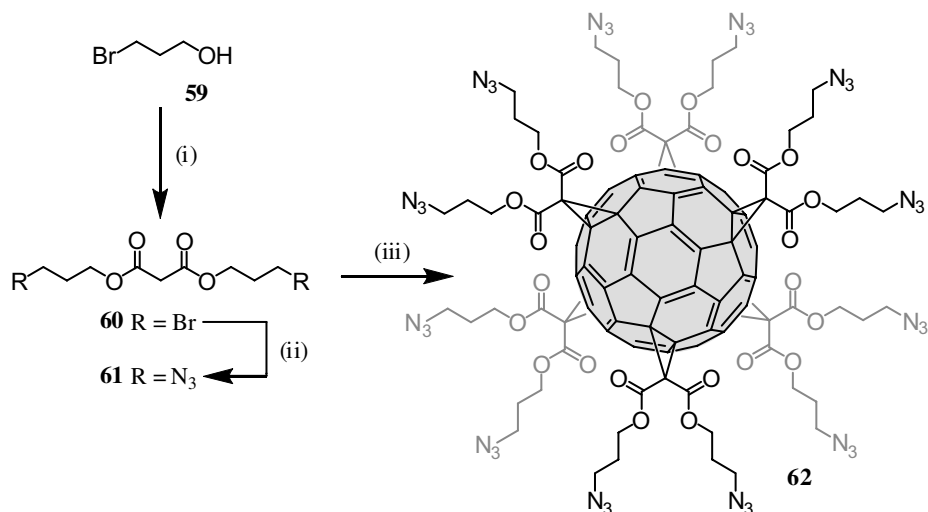
their fast decomposition, fullerene alkyne building blocks are easy to produce. In general, the reactivity of C₆₀ towards azides is not significantly competing with the cycloaddition leading to the desired 1,2,3-triazole derivatives and good yields can be obtained when fullerene derivatives with reasonable solubility are used as starting materials. In particular, bis-adduct derivatives bearing alkyne or azide groups appear to be the most promising building blocks for the synthesis of more complex fullerene derivatives. For example, compound **55** has been recently used for the synthesis of a fullerene-porphyrin conjugate.⁴⁴ As shown in Scheme 17, treatment of **57** with fullerene azide **55** in the presence of CuSO₄·5H₂O and sodium ascorbate gave compound **58** in 64% yield. The ¹H and ¹³C NMR spectra of **58** are in perfect agreement with proposed formulation. IR data also revealed that no terminal alkyne (3294 cm⁻¹) or azide (2092 cm⁻¹) residues remained in the final product. The MALDI-TOF mass spectrum confirmed the structure of **58** with a very intense signal at 4898.5 corresponding to the expected molecular ion peak ([MH]⁺, calcd. for C₃₃₂H₂₈₇N₁₀O₂₆Zn: 4898.36).



Scheme 17. Reagents and conditions: (i) **55**, CuSO₄·5H₂O, sodium ascorbate, CH₂Cl₂/H₂O, r.t. (73%).

4.2. Click chemistry with fullerene hexa-adducts

Fullerene hexakis-adducts with a T_h -symmetrical octahedral addition pattern have received increasing attention in the past few years.⁴⁶ As far as the synthesis of fullerene hexakis-adducts is concerned, most of them have been prepared by the one-pot reaction of C₆₀ with malonates under the conditions initially developed by Hirsch *et al.*⁴⁷ and further improved by Sun and collaborators.⁴⁸ Whereas these reaction conditions are efficient for the synthesis of hexa-substituted fullerenes when starting from relatively simple malonates, structurally more complicated hexakis-adducts are generally obtained in rather low yields and/or HPLC is often required for their purification. In order to overcome this problem, Nierengarten and coworkers synthesized simple C₆₀ hexakis-adduct derivatives bearing 12 terminal groups allowing their further functionalization. The grafting of 12 building blocks onto this core requires however an extremely efficient reaction to obtain functionalized derivatives

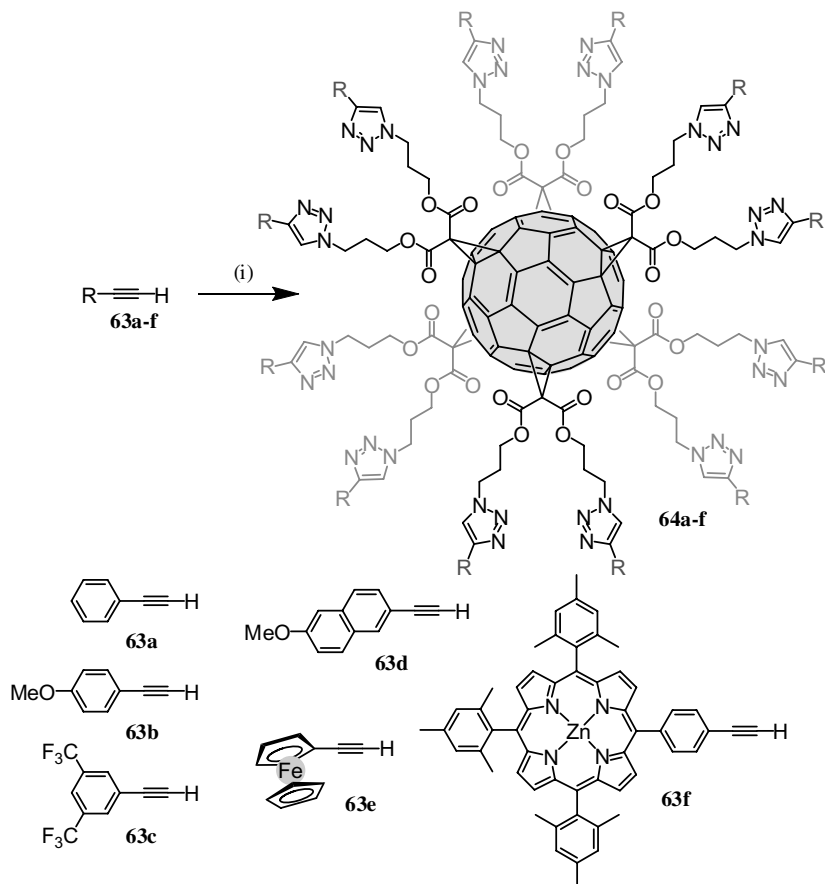


Scheme 18. Reagents and conditions: (i) CH₂Cl₂, pyridine, 0°C to rt, 18 h (83%); (ii) NaN₃, DMF, rt, 16 h (95%); (iii) C₆₀, ODCB, DBU, CBr₄, rt, 72 h (62%).

with good yields. Indeed, click chemistry³⁹ appears to be perfectly suited for this purpose. To this end, a C₆₀ hexakis-adduct bearing 12 azide groups has been prepared (Scheme 18).⁴⁹

Reaction of malonyl dichloride with 3-bromopropan-1-ol (**59**) in the presence of pyridine afforded malonate **60** in 83% yield. Subsequent treatment with sodium azide in DMF at room temperature gave **61** in 95% yield. Hexakis-adduct **62** was then readily synthesized by the reaction of C₆₀ (1 equiv.) with **61** (10 equiv.), CBr₄ (100 equiv.) and DBU (20 equiv.) in *o*-dichlorobenzene (ODCB) at room temperature. The mixture was stirred for 72 h and evaporated. The resulting sample was separated on a silica-gel column in a relatively straightforward fashion to obtain **62** in 62% yield. The reaction conditions for the 1,3-dipolar cycloaddition of compound **62** with terminal alkynes were first adjusted with phenylacetylene (**63a**) (Scheme 19). Under optimized conditions, a mixture of **62** (1 equiv.), **63a** (13 equiv.), CuSO₄·5H₂O (0.1 equiv.) and sodium ascorbate (0.3 equiv.) in CH₂Cl₂/H₂O was vigorously stirred at room temperature for 12 h. After work-up and purification, compound **64a** was thus obtained in 78% yield.

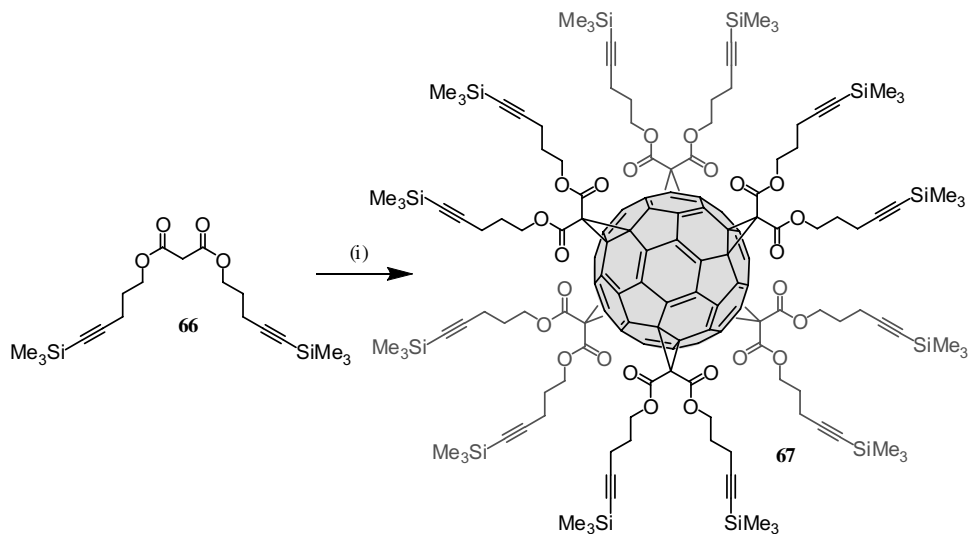
The reaction conditions used for the preparation of **64a** from phenylacetylene were then applied to the terminal alkynes **63b–f**. The clicked derivatives **65b–f** were thus obtained in 56 to 81% yields. The structures of compounds **65a–f** were confirmed by their ¹H and ¹³C NMR spectra as well as by mass spectrometry. Inspection of the ¹H NMR spectra clearly indicates



Scheme 19. Reagents and conditions: (i) **62**, CuSO₄·5H₂O, sodium ascorbate, CH₂Cl₂, H₂O, rt, 12 h (**63a**: 78%, **63b**: 61%, **63c**: 56%, **63d**: 63%, **63e**: 81%, **63f**: 74%).

the disappearance of the CH₂-azide signal at δ 3.33 ppm. IR data also confirmed that no azide (2092 cm⁻¹) residues remain in the final products. Importantly, the ¹H NMR spectra of **65a-f** show the typical singlet of the 1,2,3-triazole unit at ca. δ 7.5–7.8 ppm as well as the signal corresponding to the CH₂-triazole protons at ca. δ 4.3–4.4 ppm. Finally, the two expected resonances of the C atoms of the 1,2,3-triazole unit are clearly observed in the ¹³C NMR spectra of **65a-f**.

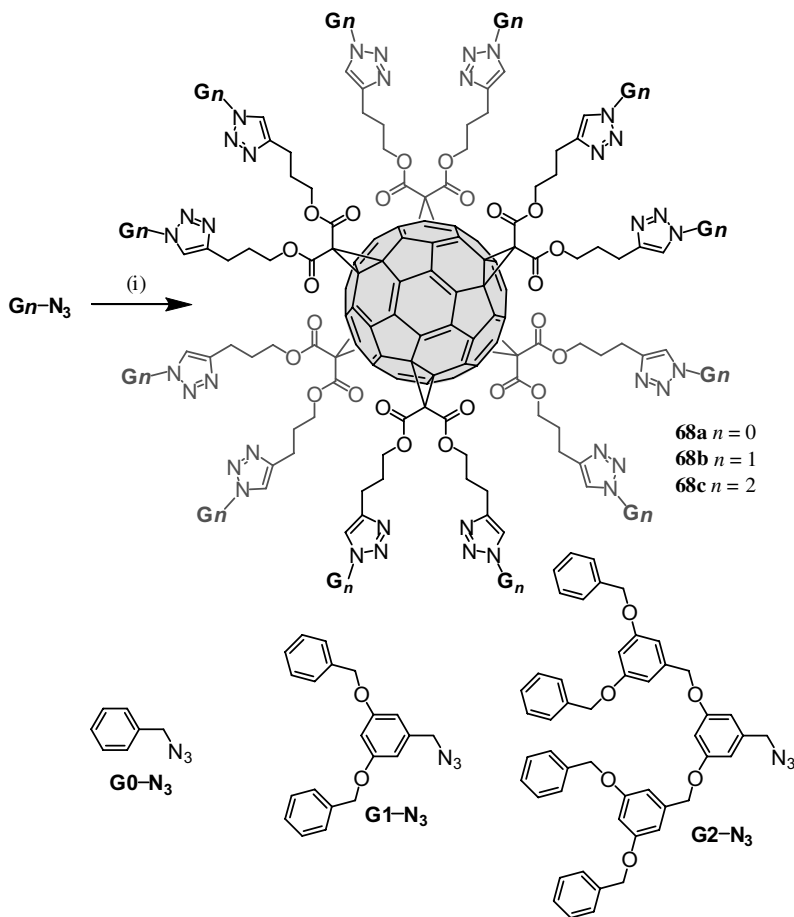
The preparation of a C₆₀ hexakis-adduct bearing 12 trimethylsilyl (TMS)-protected alkyne groups allowing the attachment of 12 azide units under the copper mediated Huisgen 1,3-dipolar cycloaddition conditions has also been reported.⁵⁰ Hexakis-adduct **67** was then obtained in 49% yield by the reaction of C₆₀ with **66**, CBr₄ and DBU in ODCB (Scheme 20).



Scheme 20. Reagents and conditions: (i) C_{60} , ODCB, DBU, CBr_4 , rt, 72 h (62%).

Compound **67** was desilylated *in situ* with tetrabutylammonium fluoride (TBAF) to form the corresponding hexa-adduct bearing 12 terminal alkyne units, to which a suitable azide precursor was subsequently clicked (Scheme 21). Under typical conditions, a mixture of **67** (1 equiv.), TBAF (14 equiv.), **Gn-N₃** (13 equiv.), $CuSO_4 \cdot 5H_2O$ (0.1 equiv.) and sodium ascorbate (0.3 equiv.) in CH_2Cl_2/H_2O was vigorously stirred at room temperature for 12 h. The resulting 1,2,3-triazole-linked fullerodendrimers **68a–c** were thus obtained in 58 to 84% yield. It is worth noting that a first generation dendritic C_{60} hexa-adduct similar to **68b** was already reported by Hirsch and co-workers.²¹ The latter was obtained in a low yield (5%) from C_{60} and the corresponding dendritic malonate, furthermore preparative HPLC was required for its purification. In contrast, compound **68b** was prepared in a good yield from **67** and its purification was easily achieved on a silica-gel column. Furthermore, the second generation derivative (**68c**) was also obtained in a good yield from **67**. Actually, the preparation of such a second generation fullerodendrimer is nearly impossible from the corresponding malonate and C_{60} . The latter observations clearly show the advantages of the synthetic method based on the post-functionalization of a readily available fullerene hexa-adduct under the copper-mediated Huisgen reaction conditions.

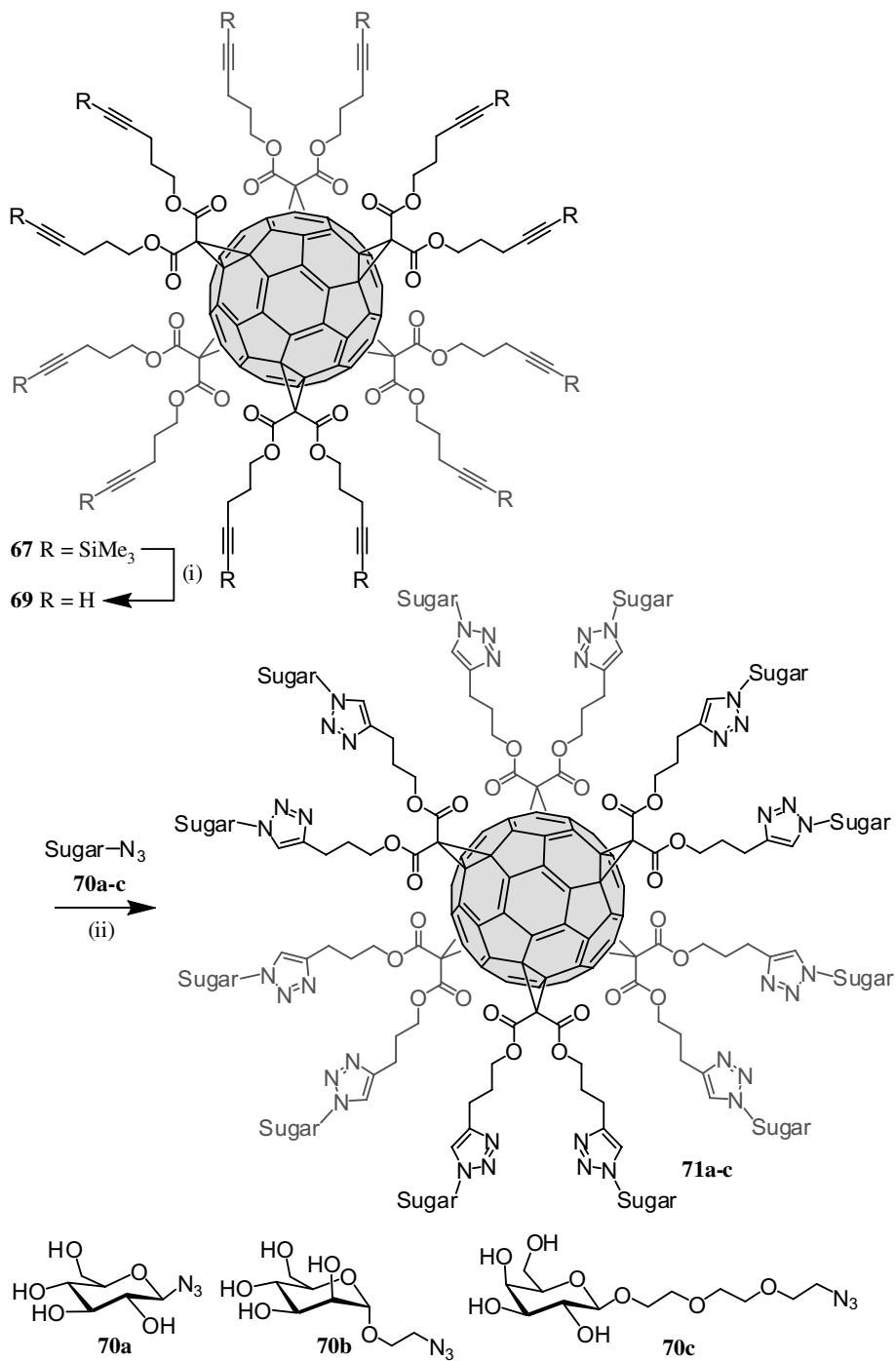
Compound **67** was also treated with an excess of tetrabutylammonium fluoride (TBAF) to give the corresponding hexa-adduct **69** bearing 12 terminal alkyne units (Scheme 22). This compound was the key precursor for



Scheme 21. Reagents and conditions: (i) **67**, TBAF, $\text{CuSO}_4 \cdot 5\text{H}_2\text{O}$, sodium ascorbate, CH_2Cl_2 , H_2O , rt, 12 h (**68a**: 58%, **68b**: 84%, **68c**: 67%).

the efficient preparation of fullerene hexakis-adducts functionalized with peripheral sugar residues (Scheme 22).⁵¹

A mixture of **69** (1 equiv.), **70a** (13 equiv.), $\text{CuSO}_4 \cdot 5\text{H}_2\text{O}$ (0.1 equiv.) and sodium ascorbate (0.3 equiv.) in DMSO was stirred at room temperature for 60 h. At the end of the reaction, the product was precipitated by addition of MeOH, filtered and extensively washed with MeOH and CH_2Cl_2 . Sugar ball **71a** was thus obtained in 74% yield. The reaction conditions used for the preparation of **71a** from azide **70a** were then applied to the more elaborated sugar azide derivatives **70b–c**. The clicked derivatives **71b–c** were thus obtained in excellent yields (72–90%) and their structure confirmed by their ^1H and ^{13}C NMR spectra as well as by IR spectroscopy. The methodology



Scheme 22. Reagents and conditions: (i) CuSO₄·5H₂O, sodium ascorbate, CH₂Cl₂, H₂O, rt (**71a**: 74%, **71b**: 90%, **71c**: 72%).

based on the Huisgen-type click chemistry is particularly efficient for the synthesis of fullerene glycoconjugates in which the C₆₀ core is completely surrounded by sugar residues. No protecting groups are requested and this approach allows for the easy preparation of a large variety of sugar balls.⁵¹ The peculiar spherical distribution of the sugar residues in **71a–c** also gives rise to unprecedented globular polytopic ligands for biological applications.

5. Conclusions and Perspectives

Despite the chemical reactivity of C₆₀, a large variety of reaction conditions can be applied to fullerene-containing building blocks for further chemical transformations. As shown in the first section, classical porphyrin chemistry can be performed from fullerene-benzaldehyde derivatives thus allowing the preparation of spectacular photoactive molecular devices. In the second section, the activation of fullerene-carboxylic acid derivatives for subsequent esterification or preparation of amides has been illustrated with the synthesis of fullerene-rich dendritic nanomaterials. Finally, the last part of this chapter shows that click chemistry is an attractive tool for the functionalization of fullerene building blocks. As click reactions are modular, tolerant to a wide range of functional groups, and high yielding; a large number of functionalized fullerene derivatives should become easily accessible by using this synthetic approach.

References

1. Krätschmer, W.; Lamb, L. D.; Fostiropoulos, K.; Huffman, D. R. *Nature* **1990**, *347*, 354.
2. Hirsch, A. *The Chemistry of the Fullerenes*; Thieme: Stuttgart, **1994**.
3. Nierengarten, J.-F. *New J. Chem.* **2004**, *28*, 1177.
4. Jensen, A. W.; Wilson, S. R.; Schuster, D. I. *Bioorg. Med. Chem.* **1996**, *4*, 767.
5. (a) Guldi, D. M. *Chem. Soc. Rev.* **2002**, *31*, 22; (b) Gust, D.; Moore, T. A.; Moore, L. *Acc. Chem. Res.* **2001**, *34*, 40; (c) Imahori, H.; Sakata, Y. *Eur. J. Org. Chem.* **1999**, 2445.
6. (a) Imahori, H. *J. Phys. Chem. B* **2004**, *108*, 6130; (b) Imahori, H. *Org. Biomol. Chem.* **2004**, *2*, 1425.
7. (a) Imahori, H.; Hagiwara, K.; Akiyama, T.; Taniguchi, S.; Okada T.; Sakata, Y. *Chem. Lett.* **1995**, 265; (b) Drovetskaya, T.; Reed, C. A.; Boyd, P. *Tetrahedron Lett.* **1995**, *36*, 7971; (c) Ranasinghe, M. G.; Olivier, A. M.; Rothenfluh, D. F.; Salek, A.; Paddon-Row, M. N. *Tetrahedron Lett.* **1996**, *37*, 4797.
8. Nierengarten, J.-F. *J. Porphyrins and Phthalocyanines* **2008**, *12*, 1022.
9. Nierengarten, J.-F.; Schall, C.; Nicoud, J.-F. *Angew. Chem. Int. Ed. Engl.* **1998**, *37*, 1934.
10. Nierengarten, J.-F.; Oswald, L.; Nicoud, J.-F. *Chem. Commun.* **1998**, 1545.
11. Urbani, M.; Iehl, J.; Osinska, I.; Louis, R.; Holler, M.; Nierengarten, J.-F. *Eur. J. Org. Chem.* **2009**, 3715.
12. Urbani M.; Nierengarten, J.-F.; *Tetrahedron Lett.* **2007**, *48*, 8111.

13. Nierengarten, J.-F.; Gramlich, V.; Cardullo, F.; Diederich, F. *Angew. Chem. Int. Ed. Engl.* **1996**, *35*, 2101.
14. (a) Lindsey, J. S.; Hsu, H. C.; Schreiman, I. C. *Tetrahedron Lett.* **1986**, *27*, 4969; (b) Lindsey, J. S.; Schreiman, I. C.; Hsu, H. C.; Kearney P. C.; Marguerettaz, A. M. *J. Org. Chem.* **1987**, *52*, 827.
15. (a) Wagner, R. W.; Lawrence, D. S.; Lindsey, J. S. *Tetrahedron Lett.* **1987**, *28*, 3069; (b) Lindsey, J. S.; Wagner, R. W. *J. Org. Chem.* **1989**, *54*, 828.
16. (a) Newkome, G. R.; Moorefield, C. N.; Vögtle, F. *Dendrimers and Dendrons: Concepts, Syntheses, Applications*; VCH: Weinheim, **2001**. (b) *Dendrimers and other Dendritic Polymers*; Fréchet, J. M. J.; Tomalia, D. A., Eds.; Wiley: Chichester, **2001**.
17. Nierengarten, J.-F. *Chem.-Eur. J.* **2000**, *6*, 3667.
18. Hirsch, A.; Vostrowsky, O. *Top. Curr. Chem.* **2001**, *217*, 51.
19. Nierengarten, J.-F. *Top. Curr. Chem.* **2003**, *228*, 87.
20. (a) Wooley, K. L.; Hawker, C. J.; Fréchet, J. M. J.; Wudl, F.; Srdanov, G.; Shi, S.; Li, C.; Kao, M. *J. Am. Chem. Soc.* **1993**, *115*, 9836; (b) Hawker, C. J.; Wooley K. L.; Fréchet, J. M. J. *J. Chem. Soc., Chem. Commun.* **1994**, 925; (c) Nierengarten, J.-F.; Habicher, T.; Kessinger, R.; Cardullo, F.; Diederich, F.; Gramlich, V.; Gisselbrecht, J.-P.; Boudon, C.; Gross, M. *Helv. Chim. Acta* **1997**, *80*, 2238; (d) Brettreich, M.; Hirsch, A. *Tetrahedron Lett.* **1998**, *39*, 2731; (e) Rio, Y.; Nicoud, J.-F.; Rehspringer, J.-L.; Nierengarten, J.-F. *Tetrahedron Lett.* **2000**, *41*, 10207.
21. (a) Camps, X.; Hirsch, A. *J. Chem. Soc., Perkin Trans. 1* **1997**, 1595; (b) Camps, X.; Schönberger, H.; Hirsch, A. *Chem.-Eur. J.* **1997**, *3*, 561; (c) Herzog, A.; Hirsch A.; Vostrowsky, O. *Eur. J. Org. Chem.* **2000**, 171.
22. Nierengarten, J.-F. *Comptes Rendus Chimie* **2003**, *6*, 725.
23. Rio, Y.; Accorsi, G.; Nierengarten, H.; Rehspringer, J.-L.; Hönerlage, B.; Kopitkovas, G.; Chugreev, A.; Van Dorsselaer, A.; Armaroli, N.; Nierengarten, J.-F. *New J. Chem.* **2002**, *26*, 1146.
24. (a) Cardullo, F.; Diederich, F.; Echegoyen, L.; Habicher, T.; Jayaraman, N.; Leblanc, R. M.; Stoddart J. F.; Wang, S. *Langmuir* **1998**, *14*, 1955; (b) Zhang, S.; Rio, Y.; Cardinali, F.; Bourgogne, C.; Gallani J.-L.; Nierengarten, J.-F. *J. Org. Chem.* **2003**, *68*, 9787.
25. Chuard, T.; Deschenaux, R. *J. Mater. Chem.* **2002**, *12*, 1944 and references therein.
26. Nierengarten, J.-F.; Armaroli, N.; Accorsi, G.; Rio Y.; Eckert, J.-F. *Chem. Eur. J.* **2003**, *9*, 36.
27. (a) Kunieda, R.; Fujitsuka, M.; Ito, O.; Ito, M.; Murata, Y.; Komatsu, K. *J. Phys. Chem. B.* **2002**, *106*, 7193; (b) Murata, Y.; Ito, M.; Komatsu, K. *J. Mater. Chem.* **2002**, *12*, 2009; (c) Rio, Y.; Accorsi, G.; Nierengarten, H.; Bourgogne, C.; Strub, J.-M.; Van Dorsselaer, A.; Armaroli, N.; Nierengarten, J.-F. *Tetrahedron* **2003**, *59*, 3833.
28. (a) Armaroli, N.; Barigelletti, F.; Ceroni, P.; Eckert, J.-F.; Nicoud, J.-F.; Nierengarten, J.-F. *Chem. Commun.* **2000**, 599; (b) Segura, J. L.; Gomez, R.; Martin, N.; Luo, C. P.; Swartz, A.; Guldi, D. M. *Chem. Commun.* **2001**, 707; (c) Accorsi, G.; Armaroli, N.; Eckert, J.-F.; Nierengarten, J.-F. *Tetrahedron Lett.* **2002**, *43*, 65; (d) Langa, F.; Gómez-Escalonilla, M. J.; Díez-Barra, E.; García-Martínez, J. C.; de la Hoz, A.; Rodríguez-López, J.; González-Cortés, A.; López-Arza, V. *Tetrahedron Lett.* **2001**, *42*, 3435; (e) Guldi, D. M.; Swartz, A.; Luo, C.; Gomez, R.; Segura, J. L.; Martin, N. *J. Am. Chem. Soc.* **2002**, *124*, 10875; (f) Pérez, L.; Garcia-Martinez, J. C.; Diez-Barra, E.; Atienzar, P.; Garcia, H.; Rodríguez-Lopez, J.; Langa, F. *Chem.-Eur. J.* **2006**, *12*, 5149; (g) Armaroli, N.; Accorsi, G.; Clifford, J. N.; Eckert, J.-F.; Nierengarten, J.-F. *Chem. Asian J.* **2006**, *1*, 564.

29. (a) Figueira-Duarte, T. M.; Gégout, A.; Nierengarten, J.-F. *Chem. Commun.* **2007**, 109; (b) Hahn, U.; Cardinali, F.; Nierengarten, J.-F. *New J. Chem.* **2007**, 31, 1128.
30. Hahn, U.; Nierengarten, J.-F.; Vögtle, F.; Listorti, A.; Monti, F.; Nicola Armaroli, *New J. Chem.* **2009**, 33, 337.
31. Schenning, A. P. H. J.; Elissen-Román, C.; Weener, J.-W.; Baars, M. W. P. L.; van der Gaast, S. J.; Meijer, E. W. *J. Am. Chem. Soc.*, **1998**, 120, 8199.
32. Baars, M. W. P. L.; Söntjens, S. H. M.; Fischer, H. M.; Peerlings, H. W. I.; Meijer, E. W. *Chem.-Eur. J.* **1998**, 4, 2456.
33. Hawker, C.; J. Fréchet, J. M. *J. Chem. Soc., Chem. Commun.* **1990**, 1010.
34. (a) Hahn, U.; Hosomizu, K.; Imahori, H.; Nierengarten, J.-F. *Eur. J. Org. Chem.* **2006**, 85; (b) Herschbach, H.; Hosomizu, K.; Hahn, U.; Leize, E.; Van Dorsselaer, A.; Imahori, H.; Nierengarten, J.-F. *Anal. and Bioanal. Chem.* **2006**, 386, 46.
35. (a) Nierengarten, J.-F.; Felder, D.; Nicoud, J.-F. *Tetrahedron Lett.* **2000**, 41, 41; (b) Felder, D.; Nierengarten, H.; Gisselbrecht, J.-P.; Boudon, C.; Leize, E.; Nicoud, J.-F.; Gross, M.; Van Dorsselaer, A.; Nierengarten, J.-F. *New J. Chem.* **2000**, 24, 687.
36. (a) Nierengarten, J.-F.; Felder, D.; Nicoud, J.-F. *Tetrahedron Lett.* **1999**, 40, 269; (b) Nierengarten, J.-F.; Eckert, J.-F.; Rio, Y.; Carreon, M. P.; Gallani, J.-L.; Guillon, D. *J. Am. Chem. Soc.* **2001**, 123, 9743.
37. (a) Nierengarten, J.-F.; Felder, D.; Nicoud, J.-F. *Tetrahedron Lett.* **1999**, 40, 273; (b) Armaroli, N.; Boudon, C.; Felder, D.; Gisselbrecht, J.-P.; Gross, M.; Marconi, G.; Nicoud, J.-F.; Nierengarten, J.-F.; Vicinelli, V. *Angew. Chem. Int. Ed. Engl.* **1999**, 38, 3730; (c) Hahn, U.; González, J. J.; Huerta, E.; Segura, M.; Eckert, J.-F.; Cardinali, F.; de Mendoza, J.; Nierengarten, J.-F. *Chem.-Eur. J.* **2005**, 11, 6666; (d) Elhabiri, M.; Trabolsi, A.; Cardinali, F.; Hahn, U.; Albrecht-Gary, A.-M.; Nierengarten, J.-F. *Chem.-Eur. J.* **2005**, 11, 4793; (e) Nierengarten, J.-F.; Hahn, U.; Trabolsi, A.; Herschbach, H.; Cardinali, F.; Elhabiri, M.; Leize, E.; Van Dorsselaer, A.; Albrecht-Gary, A.-M. *Chem.-Eur. J.* **2006**, 12, 3365; (f) Hahn, U.; Maisonhaute, E.; Amatore, C.; Nierengarten, J.-F.; *Angew. Chem. Int. Ed.* **2007**, 46, 951.
38. (a) Hahn, U.; Gégout, A.; Duhayon, C.; Coppel, Y.; Saquet, A.; Nierengarten, J.-F.; *Chem. Commun.* **2007**, 516; (b) Delavaux-Nicot, B.; Kaeser, A.; Hahn, U.; Gégout, A.; Brandli, P.-E.; Duhayon, C.; Coppel, Y.; Saquet, A.; Nierengarten, J.-F.; *J. Mater. Chem.* **2008**, 18, 1547.
39. Kolb, H. C.; Finn, M. G.; Sharpless, K. B. *Angew. Chem. Int. Ed.* **2001**, 40, 2004.
40. Huisgen, R. *Angew. Chem. Int. Ed. Engl.* **1968**, 7, 321.
41. Prato, M.; Li, Q. C.; Wudl, F.; Lucchini, V. *J. Am. Chem. Soc.* **1993**, 115, 1148.
42. (a) Iehl, J.; Pereira de Freitas, R.; Nierengarten, J.-F. *Tetrahedron Lett.* **2008**, 49, 4063; (b) Pereira de Freitas, R.; Iehl, J.; Delavaux-Nicot, B.; Nierengarten, J.-F. *Tetrahedron* **2008**, 64, 11409.
43. Cardullo, F.; Seiler, P.; Isaacs, L.; Nierengarten, J.-F.; Haldimann, R. F.; Diederich, F.; Mordasini-Denti, T.; Thiel, W.; Boudon, C.; Gisselbrecht, J.-P.; Gross, M. *Helv. Chim. Acta* **1997**, 80, 343.
44. Iehl, J.; Osinska, I.; Louis, R.; Holler, M.; Nierengarten, J.-F. *Tetrahedron Lett.* **2009**, 50, 2245.
45. Felder, D.; Gutiérrez Nava, M.; del Pilar Carreon, M.; Eckert, J.-F.; Luccisano, M.; Schall, C.; Masson, P.; Gallani, J.-L.; Heinrich, B.; Guillon, D.; Nierengarten, J.-F. *Helv. Chim. Acta* **2002**, 85, 288.

46. Hirsch, A.; Vostrowski, O. *Eur. J. Org. Chem.* **2001**, 829.
47. Hirsch, A.; Lamparth, I.; Grösser, T.; Karfunkel, H. R. *J. Am. Chem. Soc.* **1994**, *116*, 9385.
48. (a) Li, H.; Kitaygorodskiy, A.; Carino, R. A.; Sun, Y.-P. *Org. Lett.* **2005**, *7*, 859; (b) Li, H.; Haque, S. A.; Kitaygorodskiy, A.; Meziani, M. J.; Torres-Castillo, M.; Sun, Y.-P. *Org. Lett.* **2006**, *8*, 5641.
49. Iehl, J.; Pereira de Freitas, R.; Delavaux-Nicot, B.; Nierengarten, J.-F. *Chem. Commun.* **2008**, 2450.
50. Iehl, J.; Nierengarten, J.-F. *Chem.-Eur. J.* **2009**, *15*, 7306.
51. Nierengarten, J.-F.; Iehl, J.; Oerthel, V.; Holler, M.; Illescas, B. M.; Muñoz, A.; Martín, N.; Rojo, J.; Sánchez-Navarro, M.; Cecioni, S.; Vidal, S.; Buffet, K.; Durka, M.; Vincent, S. P. *Chem. Commun.* **2010**, *46*, 3860.

This page intentionally left blank

Chapter 2

New Reactivity in Fullerene Chemistry

*Marta Izquierdo, Salvatore Filippone, Ángel Martín-Domenech
and Nazario Martín**

*Departamento de Química Orgánica, Facultad de Ciencias Químicas,
Universidad Complutense, E-28040 Madrid, Spain*

1. Introduction	33
2. Regioselective Intramolecular <i>cis-1</i> Cycloadditions to Fullerenes	34
2.1. Intramolecular nucleophilic addition of phenols	35
2.2. Intramolecular nucleophilic addition of alcohols and thiols	37
3. Fuller-1,6-enynes: New and Versatile Building Blocks in Fullerene Chemistry	38
3.1. The Pauson–Khand reaction on [60]fullerene	39
3.2. Thermally induced [2+2] cyclizations from fuller-1,6-enynes	45
3.3. Thermally induced intramolecular ene reaction of fuller-1,6-enynes: synthesis of fulleroallenes	46
3.4. Theoretical study of the thermal intramolecular reactions of fuller-1,6-enynes	47
4. Catalytic Enantioselective Cycloadditions: Chiral Fullerenes	49
References	55

1. Introduction

Twenty five years after their discovery,¹ there is still unabated interest in fullerenes. The impressive number of review papers on the chemical reactivity, biological, electrochemical and photophysical properties of fullerenes give an idea of the attention dedicated to fullerenes as well as the

*Corresponding author. Email: nazmar@quim.ucm.es

most recent new forms of carbon allotropes such as nanohorns, nanoonions, graphenes and, particularly, endohedral fullerenes and carbon nanotubes.² Although the chemistry of fullerenes is nowadays considered a well known and established matter, a wide variety of reactions in the arsenal of the alkenes have not been explored. Among them, some important reactions, namely involving transition metals, that allow us to transform fullerenes into more sophisticated structures, have not been reported in the literature so far.

On the other hand, important issues, such as the complete control of the reactivity and selectivity, have not been satisfactorily addressed and often, the chemistry of fullerenes is characterized by the formation of isomeric mixtures to be further purified. Particularly, chirality in fullerenes,³ despite its importance, still remains an unsolved theme to this day. Indeed, chiral fullerenes have been obtained by employing only chiral starting materials or after chromatographic purification.

This singular three-dimensional alkene family constituted by closed cages containing thirty or more highly reactive, no coordinating, electron poor double bonds on a curved surface, represents a singular and unique scenario where a variety of different chemical reactions can be tested. The convex surface of fullerenes offers new possibilities for the study of new reactions and mechanisms under severe geometrical constraints involving carbon atoms with an unusual $sp^{2.3}$ hybridization.⁴

In this chapter we will give an overview of new concept in fullerene chemistry that goes beyond mere functionalization of the fullerenes. Therefore, new and unexpected reactions, developed in our own laboratory, and leading to useful and intriguing structures will be presented, with special attention to the control of the different levels of selectivity that the presence of different double bonds implies.

This new reactivity of fullerenes is an excellent starting point for the knowledge of the chemical behavior of the less accessible and still scarcely known endohedral fullerenes — only produced in low quantities — as well as the so-called higher fullerenes — still only produced in overwhelmingly minor amounts — or the most frequent single-wall carbon nanotubes (SWNTs), multi-wall carbon nanotubes (MWNTs) and the most recent nanoonions and nanohorns. Furthermore, the thorough exploitation of the outstanding optical and electronic properties of these new carbon allotropes relies on the ability of chemists to solubilize and functionalize such carbon nanostructures in order to produce easily processable materials for practical applications.

2. Regioselective Intramolecular *cis-1* Cycloadditions to Fullerenes

The regioselective preparation of multiadducts of fullerenes is of prime importance for obtaining functional fullerene derivatives and fullerene-based

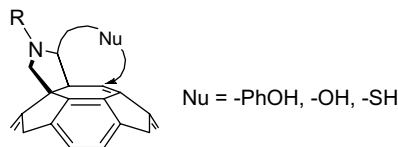


Figure 1. Intramolecular nucleophilic addition to fullerenes.

advanced materials. This is related to the fact that the properties of fullerene derivatives critically depend on the number of addends and that their structures play a crucial role in the relative arrangement of components in the materials.

Nevertheless, a very scarce level of control on the regioselectivity has been obtained so far, and fullerene polyadducts are generally obtained as byproducts of the fullerene derivatization formed generally as regioisomeric mixtures.

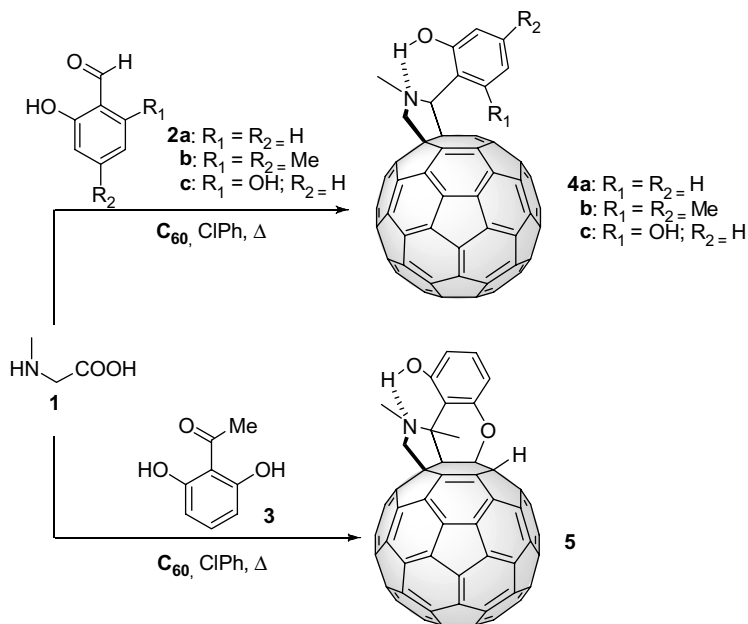
For this purpose, pyrrolidino[60]fullerenes endowed with suitable nucleophilic groups have been chosen as starting materials for the regioselective preparation of *cis-1* isomer (Figure 1). The formation of this kind of regioisomeric bisadduct is not common due mainly to steric reasons and its formation requires activation, for example with the presence of an imino group.⁵ On the other hand, this kind of addition opens an avenue to achieving new and sophisticated structures on the fullerene sphere.

2.1. Intramolecular nucleophilic addition of phenols

The nucleophilic addition of carbon nucleophiles as well as other species involving nitrogen (cyanide, amines), oxygen (alkoxides, hydroxides), phosphorus, and others such as silicon and germanium to fullerenes have been extensively studied and a wide variety of derivatives bearing heteroatoms have been prepared.⁶

Among them, the nucleophilic attack of a hydroxyl group on the fullerene generally requires basic conditions to generate *in situ* the alkoxide species,⁷ or photosensitized electron transfer.⁸ Defined alkoxy fullerenes have also been obtained by nucleophilic substitution reactions of alkoxides with previously prepared halogenofullerenes.⁹

With the aim to test the reactivity of the fullerene double bond adjacent to the saturation (*cis-1*) towards the nucleophilic addition of an hydroxyl group, a series of fuller-1,6-enols were obtained by 1,3 dipolar cycloaddition of sarcosine with the suitable *o*-hydroxybenzaldehyde or *o*-hydroxyketone (Scheme 1).¹⁰



Scheme 1. Intramolecular nucleophilic attack of phenols to [60]fullerene.

When the reaction is carried out with hydroxy aldehydes **2a,b** exclusively the formation of the atropoisomer with the hydroxyl group placed on the nitrogen side is observed. The lack of rotation due to steric reasons (an energy barrier of *ca.* 30 Kcal mol⁻¹ prevents the free rotation of the aryl group),¹¹ and/or the presence of hydrogen bond, hampered the cycloaddition on the adjacent double bond, and no cyclic compounds **4a,b** were formed.

Neither is the presence of a second OH group in ortho position sufficient to ensure the ring closure on the *cis-1* double bond as it was evident in the reaction involving the dihydroxy benzaldehyde **2c** that gives rise to pyrrolidinofullerene **4c**. The ring closing reaction does not take place even by heating fullereneol **4c**.

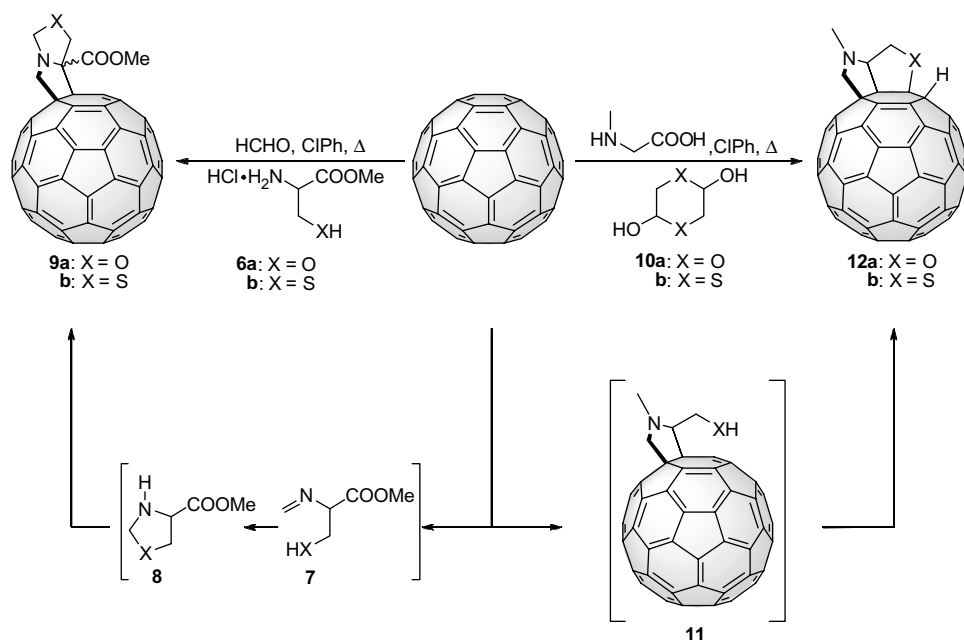
To overcome this lack of reactivity of such rigid 1,6 systems to undergo a ring closing reaction, we used the dihydroxyacetophenone **3** with sarcosine in order to fulfill simultaneously two conditions: the presence of a second OH group in ortho position and the presence of a double substitution at the C2 carbon of pyrrolidine ring, thus favoring a positive Thorpe-Ingold effect (Scheme 1). In such a way, the reaction occurs easily and together with the pyrrolidines analogous to **4a-c**, compound **5** resulting from the intramolecular nucleophilic addition of the OH to the

fullerene *cis-1* double bond is obtained. It is interesting to note that because of the chain length between the reactive OH and C=C groups, the favored cyclization process according to Baldwin's rules (*6-exo-trig*) affords a hexagonal heterocyclic ring (dihydropyran) fused simultaneously to the pyrrolidine and benzene rings.

2.2. Intramolecular nucleophilic addition of alcohols and thiols

The scope of the nucleophilic addition has also been extended to the more flexible aliphatic alcohols or thiols. To this aim, a variety of new pyrrolidino[3,4:1,2][60]fullerenes suitably endowed with a hydroxymethyl group or with a thiohydroxymethyl group able to further react with the fullerene double bond, were prepared.

The first chemical strategy consisted in the reaction of commercially available methylserinate or methyl cistinate chlorhydrate with formaldehyde in the presence of C₆₀. However, the only compound obtained was the unexpected fulleropyrrolidine derivative **9** (Scheme 2) whose formation can be accounted for by condensation reaction of the amino of the glycine moiety and the carbonyl group of formaldehyde to yield intermediate **7**, which can cyclise



Scheme 2. Intramolecular nucleophilic attack of alcohols and thiols to [60]fullerene.

spontaneously to **8**. Further reaction of **8** (bearing the glycine moiety) with formaldehyde generates *in situ* the required azomethine ylide, which reacts as a 1,3-dipole with [60]fullerene to afford fulleropyrrolidine derivative **9** in moderate yield.

Thus, we skipped our reaction design to the use of the commercially available N-methylglycine (sarcosine) with hydroxyacetaldehyde **10a** or thiohydroxiacetaldehyde **10b** and C₆₀ in refluxing chlorobenzene by following Prato's procedure. Under these conditions, the desired cyclized compounds **12a** and **12b** were obtained in 25% and 7% yield respectively (Scheme 2).¹²

Interestingly, the intermediate fulleropyrrolidine **11** bearing the hydroxymethyl group was not observed. This experimental finding is a clear indication of the favorable geometrical approach between the reactive O-H and fullerene double bond. A favored *5-exo-trig* cyclization¹³ by intramolecular nucleophilic addition of the O-H group to the adjacent double bond of the fullerene leads to the formation of the unprecedented compound **12a** in which a tetrahydrofuran ring is simultaneously fused to the pyrrolidine and fullerene moieties.

3. Fuller-1,6-enynes: New and Versatile Building Blocks in Fullerene Chemistry

1,6-Enynes are an important class of compounds in organic synthesis which have been used for the construction of a wide variety of carbo- and heterocyclic systems mostly through metal transition catalyzed processes (see below). With this in mind, the design of new and singular 1,6-enynes involving a highly reactive fullerene double bond as the ene moiety of the 1,6-enyne system was undertaken in our research group. These new building blocks were coined with the term "fuller-1,6-enynes" just to emphasise the singularity of this highly strained double bond component, belonging to a curved surface molecule. In order to favor the chemical reactivity of these fuller-1,6-enynes, a double substitution should be present on C-2 to take advantage of the Thorpe–Ingold effect (Figure 2). In this regard, fulleropyrrolidines bearing a propargyl group on the C-2 of the pyrrolidine ring fulfill all the above requirements and, in addition, were straightforward and readily available molecules, thus enhancing the utility and versatility of these new building blocks.

In the following sections the preparation of fuller-1,6-enynes, as well as the versatility of these building blocks to obtain different chemical structures will be discussed.

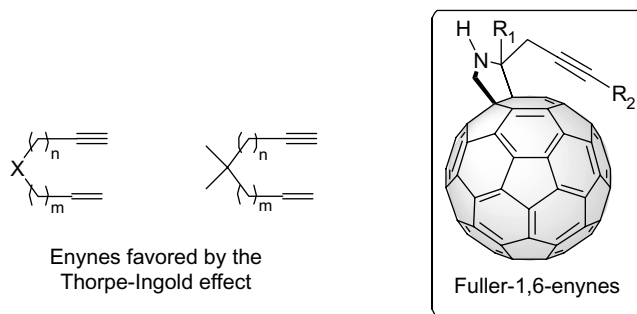


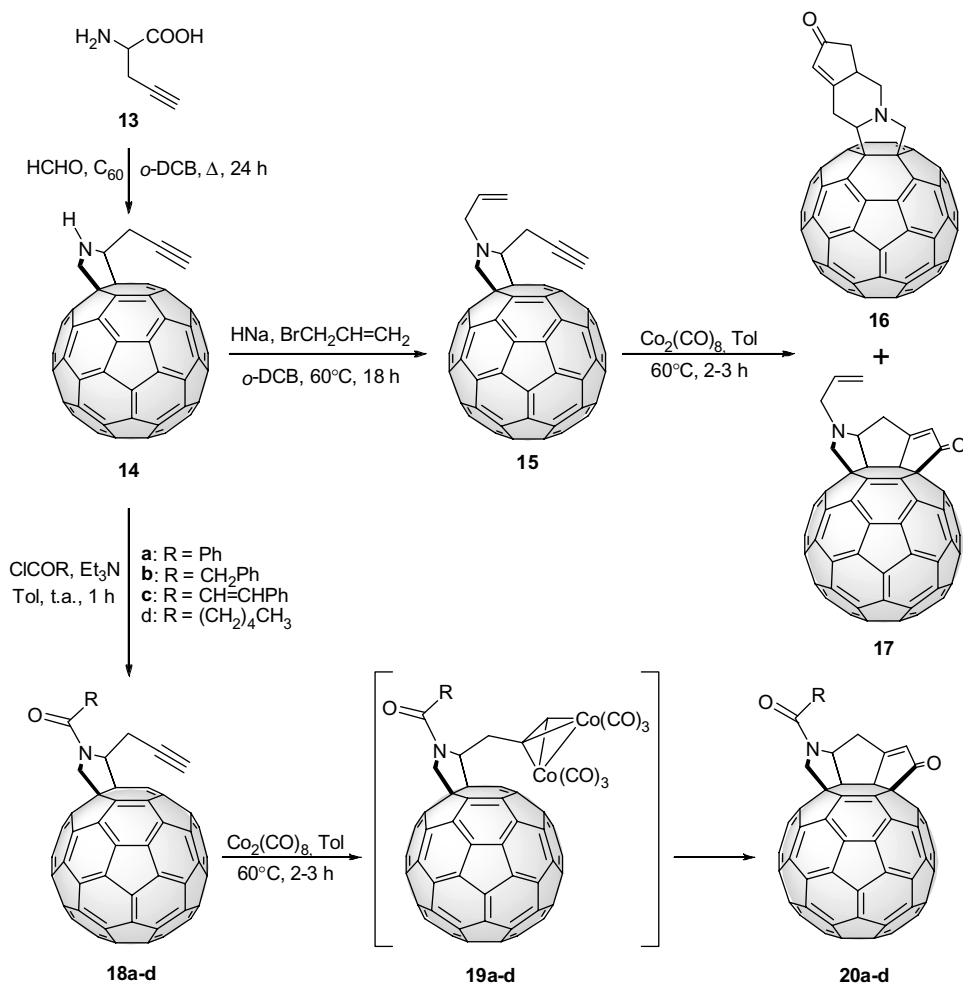
Figure 2. Chemical structure of the new building block Fuller-1,6-enynes.

3.1. The Pauson–Khand reaction on [60]fullerene

The well-known [2+2+1] cycloaddition of alkyne, alkene, and carbon monoxide mediated or catalyzed by a transition metal (mostly cobalt) — also known as the Pauson–Khand (PK) reaction — has been one of the most widely used organic reactions for the construction of biologically active five-membered carbocycles in a convergent approach.

Although electron-poor alkenes are not suitable substrates in PK reactions due to their low reactivity and the competitive elimination reaction affording 1,3-dienes, a wide variety of inter- and intramolecular PK reactions involving electron-withdrawing substituted alkenes have been reported in recent years.¹⁴ Therefore, despite the electron-poor character of the constituent fullerene double bonds, these carbon molecules emerge as suitable new substrates to explore the PK reaction since, in addition, the competitive β -hydride elimination reaction is prevented due to the absence of hydrogen atoms in their structure.

The Pauson–Khand reaction has a broad scope in terms of compatibility with many functional groups (ethers, alcohols, tertiary amines, acetals, esters, amides and heterocycles) as well as different experimental conditions, promoters and metal catalysts.¹⁵ An important drawback of the PK reaction is, however, that the intermolecular version is mainly limited to strained olefins. Fullerenes are known to show a strained spherical geometry and, therefore, they appear as suitable candidates to undergo the PK reaction. However, all attempts to carry out the intermolecular PK reaction with C₆₀ and alkynes using Co₂(CO)₈ were unsuccessful. Intramolecular PK reaction involving fullerenes requires the previous design of new fullerene derivatives suitably functionalized with an alkyne group. In this regard, fulleropyrrolidines endowed with an alkyne group at C-2 of the pyrrolidine ring fulfill the



Scheme 3. Intramolecular Pauson–Khand reaction of fuller-1,6-enynes.

requirements of appropriate geometry and variable length between the fullerene double bond and the alkyne.

We have recently explored this reaction on fullerene C_{60} , acting as the alkene component, and a highly efficient and regioselective intramolecular PK products showing three (or five) fused pentagonal rings on the same hexagon of the fullerene surface was formed (Scheme 3).¹⁶

Most of the reported intramolecular PK reactions have been carried out from systems derived from hept-1-en-6-yne or propargyl allyl ethers or amines, affording cyclopentenones fused to a carbo- or heterocyclic pentagonal ring. Enynes connected through aromatic rings have also been

successfully used in the PK reaction, thus allowing the synthesis of medium size rings (6–8 member rings).¹⁷

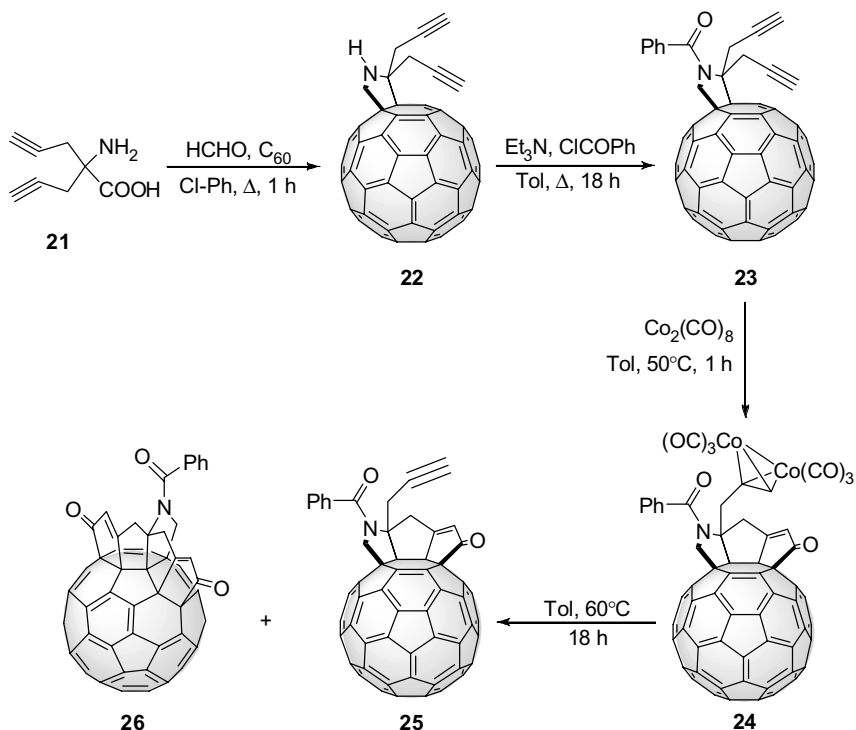
Since hept-1-en-6-yne are the most widely used substrates in the PK reaction, the synthesis of a new fuller-1,6-enyne **14** by following Prato's procedure was carried out.¹⁸

It is worth mentioning that despite fulleropyrrolidine **14** being suitably functionalized to undergo the PK reaction since it contains the required 1,6-enyne moiety, it did not afford the PK product due, probably, to the presence of the nitrogen lone pair of the pyrrolidine ring, which is able to coordinate to the catalyst cobalt complex. It has been previously reported that secondary amines are not compatible with the PK reaction. However, fulleropyrrolidines are known to exhibit a remarkably low basic and nucleophilic character due to the through-space interactions of the nitrogen lone pair with the fullerene π -system, resulting in them being six orders of magnitude less basic than their pyrrolidine model compound.¹⁹ Therefore, **14** was acylated in order to prevent the negative effect of the nitrogen lone pair. The resulting derivatives **18a–d** showed non-resolved broad signals at room temperature in the ¹H NMR spectra due to the rotational barrier of the acyl group linked to the nitrogen atom. This dynamic behavior has been previously found in related systems¹⁹ and, recently, it has been observed that the presence of the fullerene fragment close to the amide nitrogen accelerates amide rotation by a factor of 10³ at room temperature, due to the strong electron-withdrawing effect of the C₆₀ unit, thus lowering the N-CO rotational barrier ($\Delta H_{\text{N-CO}} = 16.0 \pm 0.1$ Kcal/mol).²⁰ In our case, the temperature variable high resolution (500 MHz) ¹H NMR experiments afforded an energy barrier of $\Delta H_{\text{N-CO}} = 14.2 \pm 0.1$ Kcal/mol for compound **18a**.

Stoichiometric reaction of N-acylfulleropyrrolidines **18a–d** with Co₂(CO)₈ in toluene at 60°C, in the presence of molecular sieves (4Å) previously activated,²¹ yielded the respective PK products **20a–d** almost quantitatively. Intermediate dicobalt carbonyl complexes **19** can be isolated by carrying out the reaction at room temperature.²²

Fulleropyrrolidine **14** was also reacted with allyl bromide under basic conditions to form compound **15** bearing a highly reactive allyl group. Further reaction of **15** with Co₂(CO)₈ under the same experimental conditions (molecular sieves, toluene, 60°C) afforded the PK product **17** (41% yield), together with compound **16** (41%) resulting from the PK reaction on the allyl moiety. This finding shows that the fullerene double bonds in the PK reaction are as reactive as those of the allyl moiety.

It was further decided to investigate the PK reaction on fulleropyrrolidines endowed with two propargyl groups on the same C2 of the pyrrolidine



Scheme 4. Double intramolecular Pauson–Khand reaction from dipropargyl fulleropyrrolidines.

ring. According to the above results, the PK reaction on fullerenes is strongly dependent of geometrical factors, and a two-fold cyclization should drastically increase the strain of the resulting triscycloadduct. Fulleropyrrolidine **22** was synthesized from dipropargyl glycine **21**, formaldehyde and C_{60} in refluxing chlorobenzene (Scheme 4).

In order to favor the subsequent PK reaction, acylation of the amino pyrrolidine ring was carried out with benzoyl chloride in refluxing toluene and the presence of triethylamine to form compound **23** in 95% yield. This compound (**23**) is suitably functionalized with two propargyl groups able to undergo further PK reaction by treatment with $\text{Co}_2(\text{CO})_8$ in the presence of activated molecular sieves in toluene at 50°C . Interestingly, *cis-1* biscycloadduct **25** resulting from only one $[2+2+1]$ cycloaddition reaction was obtained in 30% yield as the main reaction product. 1,2,3,4,11,12-triscycloadduct **26** formed from a two-fold PK reaction was also obtained, although in a very poor yield (5%) due, probably, to the high strain of the resulting geometry, presenting the unprecedented structure with five fused pentagonal rings on the fullerene surface.²³

Intermediate dicobalt complex **24** could be isolated after 2 hours reacting at 50°C in 95% yield. When **24** was heated at 60°C in toluene for 18 hours, mono-PK compound **25** was obtained in 30% yield together with the double PK product **26** in 5% yield. Attempts to obtain compound **26** from **25** under the same PK experimental conditions afforded **26** in trace amounts (TLC) and other unidentified decomposition compounds.

Therefore, the Pauson–Khand reaction on C₆₀ emerges as a highly efficient regioselective procedure to obtain *cis*-1 biscycloadducts (**17**, **20a–d**, **25**), as well as the rather unusual 1,2,3,4,11,12-triscycloadduct (**26**), endowed with cyclopentenone moieties able to undergo further chemical transformations. The PK reaction on fullerenes also reveals the potential interest of this reaction in materials science where it had never been previously explored. Furthermore, the electrochemical study by cyclic voltammetry [*o*-DCB/MeCN (4:1) as solvent at room temperature and using tetrabutylammonium perchlorate as supporting electrolyte] of the novel PK biscycloadducts reveals that they exhibit the same electron accepting ability than the precursor fulleropyrrolidines²⁴ due to the electron-withdrawing effect of the carbonyl group of the cyclopentenone moiety directly linked to the fullerene sphere. Remarkably, triscycloadduct **26** bearing two cyclopentenone rings shows an even better electron accepting ability with a first reduction potential value close to that of pristine C₆₀.

It is interesting to note the remarkable different reactivity observed for the fulleropyrrolidines endowed with a 1,6-enyne moiety leading to the PK products almost quantitatively, in comparison with those bearing larger enynes which, in any case yielded the [2+2+1] PK cyclization. Thus, fulleropyrrolidines **27** and **28** bearing 1,7-enyne moieties were suitably functionalized to undergo the PK reaction (Figure 3). However, in all cases the reaction formed the intermediate cobalt complexes (**29** and **30** respectively) as the only reaction product, despite the many changes in the reaction experimental conditions.¹⁶ In these compounds, the additional methylene group in the chain linking the olefin and the alkynyl groups should introduce important geometrical differences which prevent further cyclization.

In order to rationalize the different cyclization behavior observed for the fuller-1,6-enynes and fuller-1,7-enynes, we carried out BP86 theoretical calculations.

Theoretical studies had predicted that the rate-determining step in PK reactions is the loss of CO from intermediate dicobalt carbonyl complexes, such as complex **31**.²⁵ This finding is supported by the fact that these are the only intermediates that can be experimentally observed. The molecular structures of complexes **31** and **32** are depicted in Figure 4. Here a clear difference

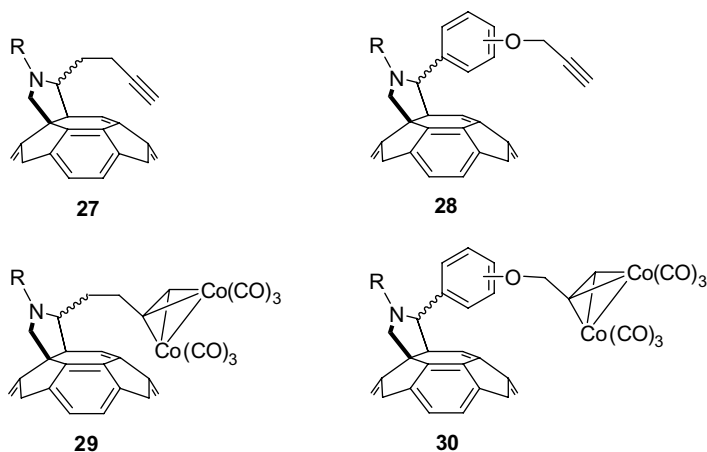


Figure 3. Different fuller-1,n-enynes ($n = 7, 8, 9$) and their dicobalt complexes.

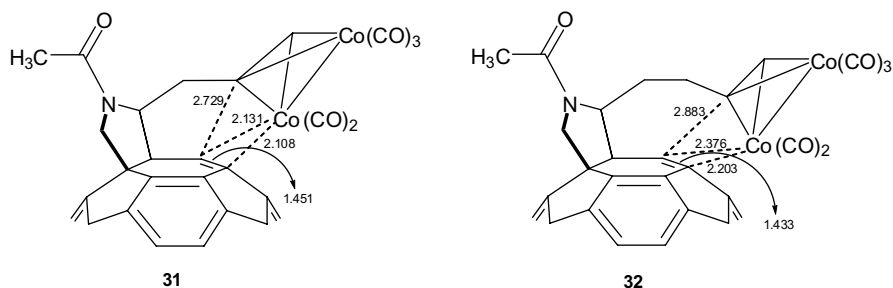


Figure 4. Geometry of complexes **31** and **32** with the most relevant distances (given in Å) calculated using BP86.

is observed between them. The distances from the coordinatively unsaturated Co to the C–C bond being attacked are 2.131 and 2.108 Å for complex **31**, about 0.1–0.2 Å shorter than those found for complex **32**. This is likely due to the fact that the donation and backdonation interactions between the coordinatively unsaturated Co and the π system of the fullerene are stronger in complex **31** than in **32**. The better π interaction in **31** is also seen in the bond length of the C–C double bond attacked which increases by 0.064 Å in **31** and no more than 0.050 Å in **32**. So, the fullerene C–C double bond that interacts with the Co is especially well activated in **31** to continue with the PK process.

In summary, the reason for the differences observed has been attributed to the different length of the organic chain bearing the alkyne functional

group for the two complexes, the organic chain being particularly well fitted in **31** to favor the metal- π interaction.

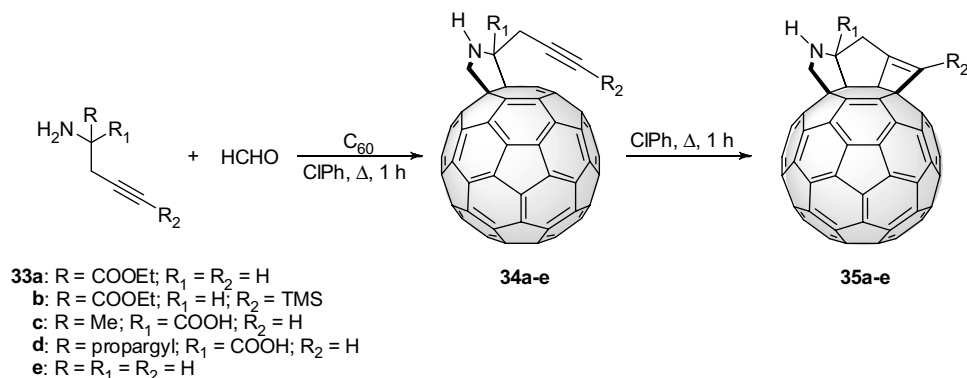
3.2. Thermally induced [2+2] cyclizations from fuller-1,6-enynes

Although cycloadditions are among the most useful and versatile reactions in fullerene chemistry, [2+2] cycloadditions of fullerenes are not common. However, several examples are known in which mostly photochemical methods are employed.²⁶

We have recently reported that the thermal treatment of fuller-1,6-enynes leads in an efficient and totally regioselective manner, to the formation of stable cyclobutene-fused adducts without involving the presence of any catalyst.²⁷ To the best of our knowledge, this is the first example of a thermal [2+2] cyclization involving a fullerene double bond as the alkene unit of the reactive 1,6-enyne, to form novel organofullerenes endowed with a rather unusual moiety constituted by a cyclopentane ring fused to a cyclobutene.

The synthesis of the starting fuller-1,6-enynes (**34a–e**) has been carried out by 1,3-dipolar cycloaddition reaction of the azomethine ylides, generated *in situ* from propargyl containing glycine derivatives²⁸ (**33a–e**) and formaldehyde, to [60]fullerene in refluxing chlorobenzene for 1 h by following Prato's procedure.¹⁸ The novel fulleropyrrolidines **34a–c** and previously reported compounds **34d–e**¹⁶ were obtained as stable brown solids in moderate yields (30–49%, 55–65% based on recovered C₆₀) (Scheme 5).

Compounds **34** undergo a thermal intramolecular cyclization by heating in refluxing chlorobenzene, leading to fullerocyclobutenes **35** in excellent yields (75–95%). Interestingly, gem-disubstituted fuller-1,6-enynes **34a–d**



Scheme 5. Formation of cyclobutenes (**35a–e**) through [2+2] cycloaddition reaction.

afforded the respective cyclobutenes **35a–d** as stable solids in very high yields. In contrast, cyclobutene **35e** ($R_1 = R_2 = H$) was obtained in a significantly lower yield (15%) and turned out to be unstable.

These findings support, like the previously studied PK reaction, that the reactivity of fuller-1,6-enynes is strongly influenced by the rigid geometry between the reactive ene and yne groups, which in turn depends on the substituents on the C2 of the pyrrolidine ring. Although fuller-1,6-enyne **34d** bearing two propargyl groups are able to undergo a two-fold thermal cyclization reaction, only compound **35d** resulting from a single thermal cyclization was obtained. The high strain resulting from the second cyclization prevents the formation of the bis-cyclobutene.

The intramolecular thermal reaction of compounds **34** leads regioselectively to the formation of the respective *cis-1* regioisomers, which are obtained as a mixture of enantiomers provided that the thermal cyclization yields, in addition to the chiral center on the pyrrolidine ring, two new chiral carbons on the fullerene surface with a well-defined stereochemistry. Furthermore, these results prove that cyclobutene structures **35** are stable and their thermal formation is possible from strained 1,6-enynes.

3.3. Thermally induced intramolecular ene reaction of fuller-1,6-enynes: synthesis of fulleroallenes

In order to determine the scope of the new thermal cycloaddition reaction of fuller-1,6-enynes for preparing novel modified fullerenes, the effect of alkyl substituents on the alkyne moiety was studied. Unexpectedly, we realized the strong impact that the presence of a methyl or alkyl group on the alkyne moiety in the 1,6-fullerenyne has on the reaction outcome. The thermal treatment of the novel alkyne-substituted fulleropyrrolidines (**37**, **39**) does not form the expected alkyl-substituted cyclobutene derivatives through a [2+2] cyclization and, instead, new allene derivatives (**38**, **40**) were obtained in a highly efficient way through a different mechanism involving an intramolecular ene reaction.²⁹

Allenes constitute a family of compounds not very well known which are currently receiving a lot of interest because of the important role that these compounds play in the mechanisms of enzyme inhibitors, cytotoxic, or antiviral agents. In fact, allenes are emerging as useful building blocks for a wide variety of synthetic applications, thus discarding the belief of unstable compounds.³⁰

They have also been isolated and characterized from many natural products and, up to now, over 150 compounds comprising this functionality in their structure are known.³¹

The very few examples reporting the preparation of allenes from enynes involve the use of Lewis catalyst³² or allenyl radicals.³³ To the best of our knowledge, only two allene compounds have previously been reported by thermal intramolecular ene reaction of enynes, and they involve the use of high temperature (210°C) with a moderate yield in one case,³⁴ and the formation of a non-isolated allene intermediate in the other.³⁵ The first intermolecular ene reaction of arynes with alkynes to form a wide variety of symmetric and asymmetric allenes has recently been reported.³⁶

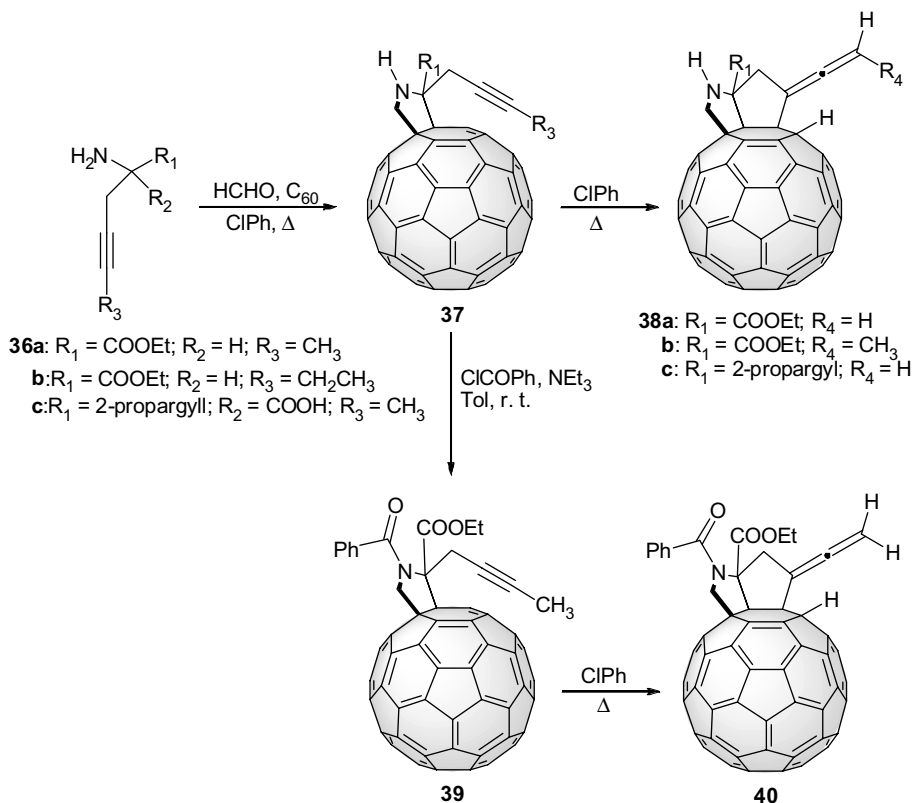
Our approach is the first example of synthesis of allenes involving a fullerene double bond as the ene moiety by simple and efficient thermal non-catalyzed intramolecular ene cyclization. Furthermore, the reaction proceeds with a methyl or ethyl groups on the alkyne moiety, thus enhancing the scope of this reaction to prepare new fullerene architectures.

The new 1,6-fullerenynes **37a–c** and **39** were obtained by following the standard protocol previously discussed, as stable brown solids in moderate (16–32%) yields (55–64% based on recovered fullerene). 1,6-fullerenyne **39** was readily prepared in 90% yield by benzylation reaction of compound **37a**. Further thermal treatment of the so-formed 1,6-fullerenynes by heating in refluxing chlorobenzene for 3 h afforded new fulleroallenes **38a–c** and **40** in quantitative yields (Scheme 6).³⁷ It is worth mentioning that allenes **38** were formed as by-products (6–10 %) in the synthesis of the precursor fuller-1,6-enynes **37**. This finding indicates that allenes can be prepared in a one-pot synthesis from the starting materials. However, the one-pot reaction affords lower yields due, probably, to the formation of bis-adducts (HPLC) and the recovery of unreacted C₆₀.

As diagnostic signatures of the allene functional group, the two hydrogen terminal atoms of the allene unit appear as two ddd at around 5.4 and 5.6 ppm. The characteristic allene central carbon atom appears at 204.0 ppm when two hydrogens atoms are on the allene moiety, whereas this signal is upfield shifted (200.6 ppm) when a methyl group is the substituent. Compound **38b** bearing simultaneously a hydrogen atom and a methyl group on the terminal carbon of the allene unit was obtained as a diastereomeric mixture (3.5:1 ratio determined by ¹H NMR) due to the atropisomerism of the allene group.

3.4. Theoretical study of the thermal intramolecular reactions of fuller-1,6-enynes

The substitution of a H atom by an alkyl group on the terminal carbon of the alkyne moiety in the thermal treatment of 1,6-fullerenynes has a strong impact on the reaction outcome.



Scheme 6. Formation of allene-containing fullerenes from propargylfulleropyrrolidines.

While the reaction of 1,6-fullerenynes bearing a terminal alkyne moiety results in the cycloaddition of the alkyne group to the fullerene double bond leading to cyclobutene-fused derivatives, the presence of an alkyl substituent leads to the formation of fulleroallenes (Figure 5). In order to gain a better understanding of the different reaction mechanisms involved in the cyclization processes, we have carried out theoretical calculations using the basis set (B3LYP/6-31G**//ONIOM2(B3LYP/6-31G*:BVWN/STO-3G)).³⁸

We have located all intermediates and transition states involved in the so-called carbene and diradical pathways. The carbene reaction mechanism proposed first by Gilbert and coworkers involves a [2+1] cycloaddition to give a cyclopropylcarbene intermediate that in a subsequent step evolves through 1,2-C shift to the final product.^{39,40} In our systems that have non-strained triple bonds (in contrast to cyclopentyne or benzyne) the carbene pathway can be totally ruled out according to the data obtained. The diradical mechanism, first suggested by Olivella and coworkers,⁴¹ involves a

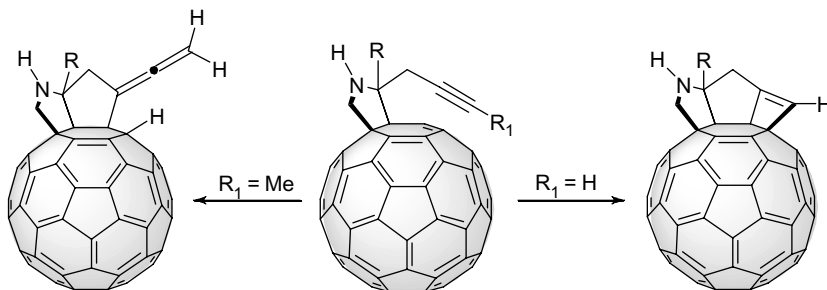


Figure 5. Influence of the nature of R (H or Me) on the reactivity of propargylfulleropyrrolidines.

diradical intermediate that already comprises one of the two C–C bonds to be formed. This diradical mechanism has been also considered by several authors for the reaction between cyclopentyne and ethene.^{42,43}

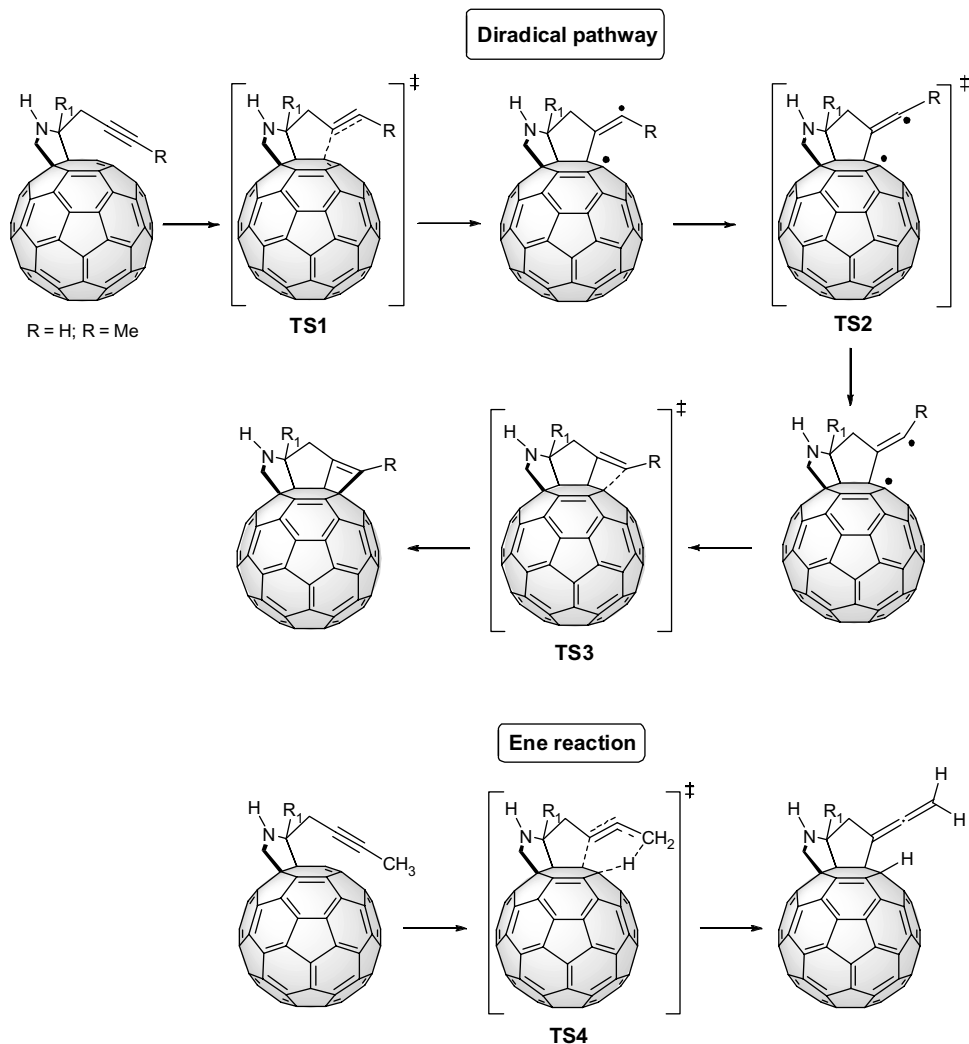
Theoretical calculations show that cyclobutene formation occurs through a diradical pathway with two intermediates and three transition states, the highest in energy having an energy barrier of about 34 kcal/mol (Scheme 7).

The change of a H atom by a methyl group reduces the energy barrier by about 1 kcal/mol, thus favoring the reaction. Therefore, the substituent effect is not responsible for the lack of cyclobutene formation which prefers to react through an unusual concerted ene reaction mechanism involving the triple and a C–H bonds of the alkyne moiety and the closer double bond of the fullerene cage. The Gibbs energy barrier for the allene formation is lower than that corresponding to the cyclobutene formation by about 4.8 kcal/mol, despite the latter product being thermodynamically preferred by about 5 kcal/mol.

4. Catalytic Enantioselective Cycloadditions: Chiral Fullerenes

The preparation of chiral fullerenes in a controlled way has been recognized as an important topic.⁴⁴ The lack of a general method of preparation of chiral derivatives has conditioned the possible application of fullerene compounds and often, racemic compounds have been used, even in fields such as medicinal chemistry (HIV protease inhibition) where the stereochemical configuration is not secondary.⁴⁵

Only a few examples of enantiomerically pure derivatives, employed as helicity inducer in polymers⁴⁶ or as homochiral prolinofullerenes in peptides synthesis,⁴⁷ have been reported where the enantiopure fullerene derivatives have been used after HPLC isolation on chiral column or prepared with chiral starting materials.⁴⁸



Scheme 7. Proposed mechanisms for the cyclization of propargylfulleropyrrolidines.

The main obstacle for a general method of synthesis of chiral fullerene derivatives lies, possibly, in the unavailability of most part of the known catalytic systems for the selective addition to a non-coordinating double bond of the fullerene sphere.

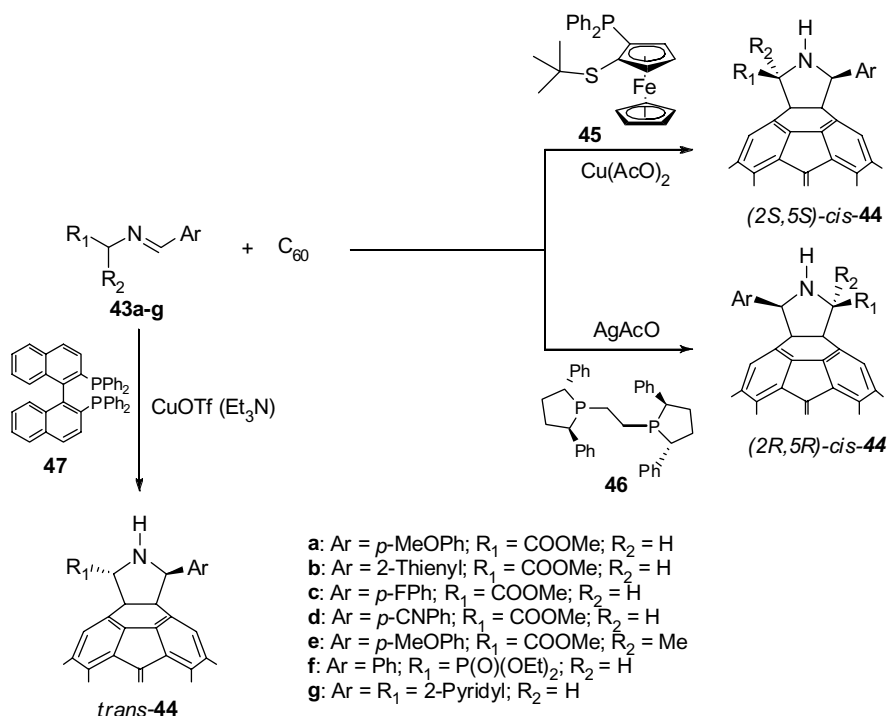
Recently, the enantioselective cycloaddition reactions of azomethine ylides⁴⁹ to fullerenes, appeared as a powerful methodology to address this issue for two reasons: firstly, this reaction gives rise to pyrrolidino[3,4:1,2][60]fullerenes. These heterocyclic-fused compounds are, probably, the most widely used fullerene derivatives because of their stability, versatility, as well as

the availability of the required starting materials.⁵⁰ Moreover, prolino-fullerene, the biggest non-natural amino acid belonging to this class, represents a valuable building block for the synthesis of fulleropeptides.⁵¹ Secondly, this 1,3 dipolar cycloaddition is not based on the activation of the LUMO orbital of the dipolarophile and, therefore, the lack of coordinating ability of fullerenes does not hamper the asymmetric induction.

In a first step, we focused our attention on the ability of a metal complex to carry out this transformation at room temperature by controlling the diastereoselectivity. To this purpose, we chose as a model reaction the addition of the iminoester **43a** onto C₆₀.⁵²

Thermal treatment of iminoester **43a** with C₆₀ displayed the formation of mixtures of two diastereomeric pyrrolidinofullerenes *cis*-**44a** and *trans*-**44a** in a 60/40 ratio (Scheme 8; Table 1, Entry 1) in line with other similar results described in literature.

A preliminary screening of different metal-ligand pairs demonstrated the feasibility of the metal mediated azomethine ylide cycloaddition onto the fullerene sphere that occurs easily (1–2 hours) at room temperature, giving



Scheme 8. Synthesis of nantiomerically pure fulleropyrrolidines by asymmetric catalysis.

Table 1. Asymmetric Cu(II) and Ag(I)-catalyzed 1,3-dipolar cycloadditions of azomethine ylides to C₆₀ by using different chiral ligands.^a

Entry	Dipole	Metal salt	Ligand	T (°C)	Yield (%)	<i>de</i> (%)	<i>ee</i> (%)
1	43a	—	—	110	30	20	—
2	43a	Cu(OTf) ₂ ^b	dppp ^d	r.t.	68	80	—
3	43a	Cu(AcN) ₄ ClO ₄ ^b	45	0	45	94	64 (2 <i>S</i> ,5 <i>S</i>)- 44a
4	43a	Cu(AcN) ₄ PF ₆ ^b	45	0	60	98	73 (2 <i>S</i> ,5 <i>S</i>)- 44a
5	43a	Cu(AcO) ₂	45	−15	88	>99	90 (2 <i>S</i> ,5 <i>S</i>)- 44a
6	43a	Cu(AcN) ₄ PF ₆ ^c	45	−15	60	>99	92 (2 <i>S</i> ,5 <i>S</i>)- 44a
7	43b	Cu(AcO) ₂	45	−15	49	>99	93 (2 <i>S</i> ,5 <i>S</i>)- 44b
8	43c	Cu(AcO) ₂	45	−15	40	>99	90 (2 <i>S</i> ,5 <i>S</i>)- 44c
9	43d	Cu(AcO) ₂	45	−15	60	>99	88 (2 <i>S</i> ,5 <i>S</i>)- 44d
10	43e	Cu(AcO) ₂	45	−15	40	95	80 (2 <i>S</i> ,5 <i>S</i>)- 44e
11	43f	Cu(AcO) ₂	45	r.t.	25	95	65 (2 <i>R</i> ,5 <i>S</i>)- 44f ^c
12	43g	Cu(AcO) ₂	45	r.t.	68	>99	—
13	43a	AgAcO	46	−15	60	>99	90 (2 <i>R</i> ,5 <i>R</i>)- 44a
14	43b	AgAcO	46	−15	45	>99	81 (2 <i>R</i> ,5 <i>R</i>)- 44b
15	43c	AgAcO	46	−15	35	>99	85 (2 <i>R</i> ,5 <i>R</i>)- 44c
16	43d	AgAcO	46	−15	60	>99	86 (2 <i>R</i> ,5 <i>R</i>)- 44d
17	43e	AgAcO	46	−15	33	80	70 (2 <i>R</i> ,5 <i>R</i>)- 44e

^aReaction conditions: Ligand: 10% (entry 11: 100%). ^bEt₃N (20%). ^cBuN₄AcO (20%). ^d1,3-Bis(diphenylphosphino)propane. ^eThe different priority of the phosphonate group is responsible for the change of configuration in the series.

rise to the pyrrolidinofullerenes in a high yield. More important, catalytic amounts (10%) of copper(II) triflate and the achiral ligand 1,3-bis(diphenylphosphino)propane (dppp), in the presence of triethylamine, were able to address the lack of diastereoselectivity to the formation of *cis*-**44a** with 80% of *de* (Scheme 8; Table 1, Entry 2).

The Fesulphos catalytic systems reported by Carretero,⁵³ gave rise to the formation of a unique diastereomer, *cis*-**44a**. Nevertheless, the obtained enantiomeric excesses were well below those reported for other non-fullerene dipolarophiles (Table 1, Entries 3 and 4).

We have attributed this result to the non-ligand properties of the [60]fullerene which, in sharp contrast to the other so far employed dipolarophiles, does not coordinate with the metal cation.

For this reason, we moved from non-ligand anions, such as PF₆[−] or ClO₄[−] to acetate that acts, also, as a base: we speculated that such ligand anion, occupying the vacant site — normally filled by a ligand dipolarophile — in the metal coordination sphere, could allow a better stereodifferentiation of the two faces of azomethine ylides. Indeed, even when the copper(I) acetate was

ineffective, copper(II) acetate along with Fesulphos **45**, was able to catalyze the cycloaddition of imine **43a** at -15°C without the use of any base, giving rise to (2*S*,5*S*)-*cis*-**44a** in 90% of enantiomeric excess (Table 1, Entry 5). Moreover, the fact that similar results were obtained using $\text{Cu}(\text{ACN})_4\text{PF}_6$ and tetrabutylammonium acetate, confirms the important role of the coordinating acetate anion in the catalytic system (Table 1, Entry 6). Copper (II) acetate together with (R)-Fesulphos **45** demonstrated an excellent catalytic activity in the cycloaddition of different iminecarboxylate esters (**43b–e**) to C_{60} (Table 1, entries 7–10). The pyrrolidine formation occurs in 2 hours at -15°C with a remarkable yield improvement, up to 60%, compared with the classical thermal process. This catalytic complex leads to the exclusive formation of the *cis* adducts, with a diastereoselectivity of >99%.⁵²

Excellent asymmetric induction results were also obtained since (2*S*,5*S*)-*cis*-**44b–d** enantiomers were formed with *ee* values ranging from 88% to 93%. Cycloaddition of iminoester **43e** derived from alanine occurs with a slightly lower asymmetric induction, similar to previously reported studies (Table 1, Entry 10).

A good control on the stereochemical outcome in the synthesis of chiral fulleropyrrolidines requires the efficient formation of the opposite enantiomers. In order to face this synthetic challenge we looked for a different metal catalyst. In particular, we focused our attention on the pair Ag(I)-**46** since preliminary tests showed the preferential formation of the (2*R*,5*R*)-**44a** enantiomer. The replacement of the non-ligand anion by acetate proved to be needed to obtain higher enantiomeric excesses. Thus, 10% of the chiral silver acetate-**46** complex promoted the cycloaddition of imines **43a–e** again with outstanding *cis* diastereoselectivities but with a reverse stereodifferentiation. The favored approach of C_{60} to the *Si* face of the dipole gave rise to the cycloadducts (2*R*,5*R*)-**44a–e** with slightly lower enantioselectivities, but still achieving very good *ee*, up to 90% (Table 1, Entries 13–17).

The presence of pairs of chiral fullerene systems is clearly evident in the circular dichroism (CD) spectra that appear with exact mirror symmetries (Figure 6). Remarkably, enantiomers obtained from the same catalytic complex give rise to CD spectra with the same sign and behavior in the 430 nm region of the electronic spectra. This relevant UV-vis band is considered the fingerprint for all fullerene monoadducts at 6,6 junctions (between two fused hexagons) regardless of the nature of the organic addend saturating the double bond. On this basis, a sector rule has been proposed^{54,55} that links the Cotton effect (CE) associated to this diagnostic UV-vis band and the stereochemical environment around the 6,6 junction. Since we have not been able to achieve suitable crystals for X-ray diffraction, we have used this rule to

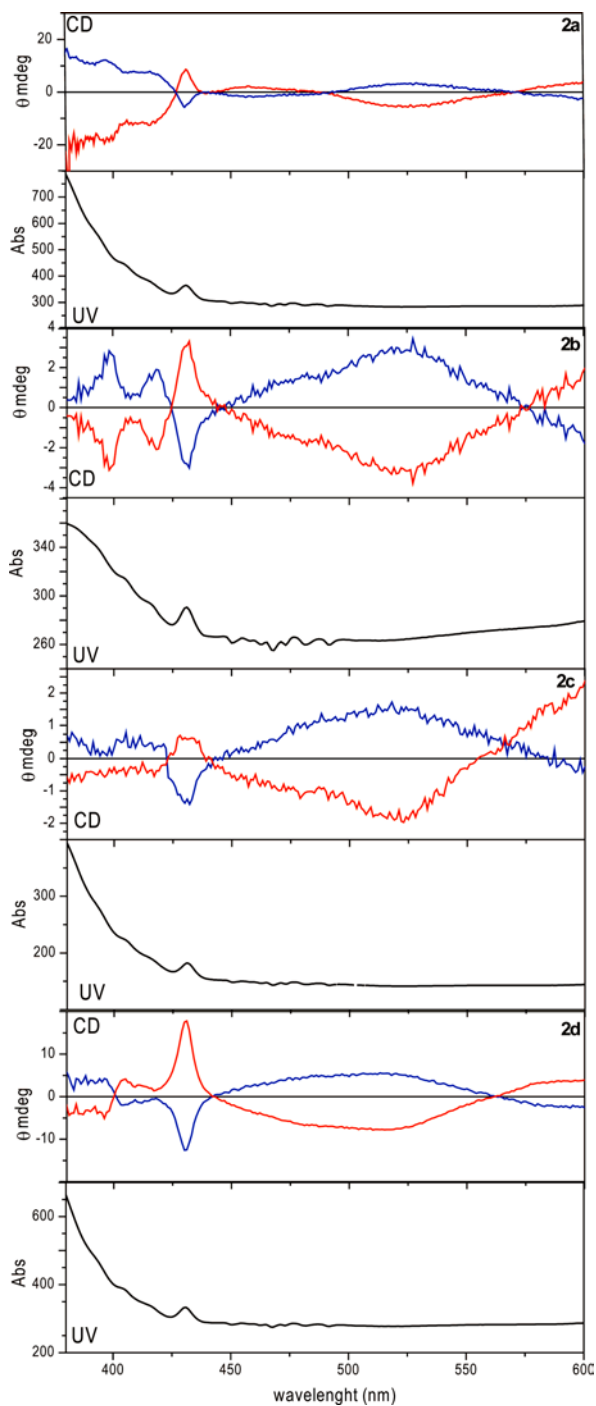


Figure 6. CD and UV spectra of fulleropyrrolidines **44a-d** (conc. 4×10^{-4} M in toluene). Red line: enantiomers from Ag(I)-**46**; Blue line: enantiomers from Cu(II)-**45**.

assign the absolute stereochemistry of the obtained compounds. All the pyrrolidinofullerenes formed from Ag(I)-**46** catalytic complex showed in their CD spectra a positive CE, that is consistent with a (2*R*,5*R*) stereochemistry. Likewise, the negative CE corresponding to the Cu(II)-**45** system is in agreement within the (2*S*,5*S*) configuration.

This assignement has been confirmed by comparison of the stereochemistry of the fullerene free pyrrolidines obtained from Cu(ACN)₄ClO₄-**45** catalyst by other authors,⁵³ and the pyrrolidino fullerene **44a** obtained by using the same catalytic system (Table 1, Entry 3). If we assume the same facial selectivity in the approach of [60]fullerene to the azomethine ylide, the (2*S*,5*S*) configuration could be easily demonstrated.

The scope of our methodology has been expanded to enable a complete switch in the diastereoselectivity. We screened a catalytic complex formed from copper(II)triflate (10%) and Binap **47**, with triethylamine as the base. This pair was able to efficiently catalyze the reaction at room temperature with high yields both with glycinate **43a** and **43b**. This catalytic complex proved to be very useful in inverting the diastereochemical outcome obtained with Cu(II)-Fesulphos or Ag(I)-**46**, forming *trans* pyrrolidinofullerenes **44a,b** with 90% and 80% diastereomeric excess, respectively (Scheme 8).⁵²

In summary, the above results have paved the way for the preparation of fullerenes “a la carte” in which a control on the stereochemical outcome of the reaction is possible by choosing the appropriate catalytic cocktail of metal, chiral ligand and anion. These new findings should facilitate its application to areas such as materials science and, in particular, in biomedical applications where chirality is of critical importance.

References

1. Kroto, H. W.; Heath, J. R.; O'Brien, S. C.; Curl, R. F.; Smalley, R. E. C₆₀: Buckminsterfullerene. *Nature* **1985**, *318*, 162–163.
2. (a) Taylor, R. Lecture notes on fullerene chemistry: a handbook for chemists. Imperial College Press: London, **1999**. (b) *Fullerenes: from synthesis to optoelectronic properties*. Guldi, D. M.; Martín, N.; Eds.; Kluwer Academic Publishers; Dordrecht, **2002** (c) Martín, N. *Chem. Commun.* **2006**, 2093. (d) Delgado, J. L.; Herranz, M. A.; Martín, N. *J. Mater. Chem.* **2008**, *18*, 1417–1426.
3. Thilgen, C.; Diederich, F. *Chem. Rev.* **2006**, *106*, 5049.
4. Haddon, R. C. *Acc. Chem. Rev.* **1992**, *25*, 127–133.
5. Hirsch, A.; Brettreich, M. *Fullerenes: chemistry and reactions*. Wiley-VCH, Weinheim, **2005**.
6. (a) Hirsch, A. *The chemistry of fullerenes*. Wiley-VCH, Weinheim, **2005**. (b) *Fullerenes*; Langa, F.; Nierengarten, J.-F.; Eds.; RSC Publishing, Cambridge, **2007**.

7. Fukuzumi, S.; Nakanishi, I.; Maruta, I.; Yorisue, T.; Suenobu, T.; Itoh, S.; Arakawa, R.; Kadish, K. M. *J. Am. Chem. Soc.* **1998**, *120*, 6673–6680.
8. Lem, G.; Schuster, D. I.; Courtney, S. H.; Lu, Q.; Wilson, S. R. *J. Am. Chem. Soc.* **1995**, *117*, 554–555.
9. Avent, A. G.; Birkett, P. R.; Darwish, A. D.; Houlton, S.; Taylor, R.; Thomson, K. S. T.; Wei, X.-W. *J. Chem. Soc. Perkin Trans.* **2001**, *2*, 782–786.
10. Izquierdo, M.; Osuna, S.; Filippone, S.; Martín-Domenech, A.; Solà, M.; Martín, N. *J. Org. Chem.* **2009**, *74*, 1480–1487.
11. Ajamaa, F.; Duarte, T. M. F.; Bourgogne, C.; Holler, M.; Fowler, P. W.; Nierengarten, J.-F. *Eur J. Org. Chem.* **2005**, 3766–3774.
12. (a) Izquierdo, M.; Osuna, S.; Filippone, S.; Martín-Domenech, A.; Solà, M.; Martín, N. *J. Org. Chem.* **2009**, *74*, 6253–6259. (b) Izquierdo, M.; Osuna, S.; Filippone, S.; Martín-Domenech, A.; Solà, M.; Martín, N. *Eur. J. Org. Chem.* **2009**, 6231–6238.
13. Baldwin, J. E. *J. Chem. Soc., Chem. Commun.* **1976**, 734–735.
14. For a review, see: Rivero, M. R.; Adrio, J.; Carretero, J. C. *Eur. J. Org. Chem.* **2002**, 2881–2889.
15. For recent reviews on the PK reaction see: (a) Sugihara, T.; Tamaguchi, M.; Nishizawa, M. *Chem. Eur. J.* **2001**, *7*, 1589–1595. (b) Gibson, S. E.; Stevenazzi, A. *Angew. Chem. Int. Ed.* **2003**, *42*, 1800–1810. (c) Blanco-Urgoiti, J.; Añorbe, L.; Pérez-Serrano, L.; Domínguez, G.; Pérez-Castells, J. *Chem. Soc. Rev.* **2004**, *33*, 32–42.
16. (a) Martín, N.; Altable, M.; Filippone, S.; Martín-Domenech, A. *Chem. Commun.* **2004**, 1338–1339. (b) Martín, N.; Altable, M.; Filippone, S.; Martín-Domenech, A.; Poater, A.; Solà, M. *Chem. Eur. J.* **2005**, *11*, 2716–2729.
17. (a) Pérez-Serrano, L.; Blanco-Urgoiti, J.; Casarrubios, L.; Domínguez, G.; Pérez-Castells, J. *J. Org. Chem.* **2000**, *65*, 3513–3519. (b) Lovely, C. J.; Seshadri, H.; Wayland, B. R.; Cordes, A. W. *Org. Lett.* **2001**, *3*, 2607–2610.
18. Prato, M.; Maggini, M. *Acc. Chem. Res.* **1998**, *31*, 519–526.
19. Bagno, A.; Claeson, S.; Maggini, M.; Martini, M. L.; Prato, M.; Scorrano, G. *Chem. -Eur. J.* **2002**, *8*, 1015–1023.
20. Borsato, A.; Della Negra, F.; Gasparrini, F.; Misiti, D.; Lucchini, V.; Possamai, G.; Villani, C.; Zambon, A. *J. Org. Chem.* **2004**, *69*, 5785–5788.
21. (a) Pérez-Serrano, L.; Casarrubios, L.; Domínguez, G.; Pérez-Castells, J. *Org. Lett.* **1999**, *1*, 1187–1188. (b) Blanco-Urgoiti, J.; Casarrubios, L.; Domínguez, G.; Pérez-Castells, J. *Tetrahedron Lett.* **2002**, *43*, 5763–5765.
22. Acetylene-linked di- and tetracobalt-carbonyl clusters covalently connected to C₆₀ have also been reported, see: Draper, S. M.; Delamesiere, M.; Champeil, E.; Twamley, B.; Byrne, J. J.; Long, C. *J. Organomet. Chem.* **1999**, *589*, 157–167.
23. AM1 calculations with the AMPAC 6.55 program have been carried out for carbon monoxide and complexes **23**, **25** and **26** in which the phenyl group has been substituted by a methyl group. The results give a reaction enthalpy of -73.3 and -116.2 Kcal/mol for the reactions **23** + CO for **25** and **23** + 2CO for **26**, respectively. The difference of 30.4 Kcal/mol [(-116.2)–(-73.3)] can be taken as an indication of excess strain energy in **26** compared with **25**.
24. (a) Echegoyen, L.; Echegoyen, L. E. *Acc. Chem. Res.* **1998**, *31*, 593–601. (b) Martín, N.; Sánchez, L.; Illescas, B.; Pérez, I. *Chem. Rev.* **1998**, *98*, 2527–2548. (c) Carano, M.; Da Ros, T.; Fanti, M.; Kordatos, K.; Marcaccio, M.; Paolucci, F.; Prato, M.; Roffia, S.;

- Zerbetto, F. *J. Am. Chem. Soc.* **2003**, *125*, 7139–7144. (d) Suzuki, T.; Maruyama, Y.; Akasaka, T.; Ando, W.; Kobayashi, K.; Nagase, S. *J. Am. Chem. Soc.* **1994**, *116*, 1359–1363.
25. (a) Pericàs, M. A.; Balsells, J.; Castro, J.; Marchueta, I.; Moyano, A.; Riera, A.; Vázquez, J.; Verdaguer, X. *Pure Appl. Chem.* **2002**, *74*, 167–174. (b) Yamanaka, M.; Nakamura, E. *J. Am. Chem. Soc.* **2001**, *123*, 1703–1708.
26. (a) Hoke II, S. H.; Molstad, J.; Dilettato, D.; Jay, M. J.; Carlson, D.; Kahr, B.; Cooks, R. G. *J. Org. Chem.* **1992**, *57*, 5069–5071. (b) Wilson, S. R.; Kaprinidis, N.; Wu, Y.; Schuster, D. I. *J. Am. Chem. Soc.* **1993**, *115*, 8495–8496. (c) Vassilikogiannakis, G.; Orfanopoulos, M. *J. Am. Chem. Soc.* **1997**, *119*, 7394–7395. (d) Bildstein, B.; Schweiger, M.; Angleitner, H.; Kopacka, H.; Wurst, K.; Ongania, K.-H.; Fontani, M.; Zanello, P. *Organometallics* **1999**, *18*, 4286–4295. (e) Hisao, T.-Y.; Chidambareswaran, S. K.; Cheng, Ch.-H. *J. Org. Chem.* **1998**, *63*, 6119–6122.
27. Martín, N.; Altable, M.; Filippone, S.; Martín-Domenech, A.; Güell, M.; Sola, M. *Angew. Chem. Int. Ed.* **2006**, *45*, 1439–1442.
28. López, A.; Pleixats, R. *Tetrahedron: Asymmetry* **1998**, *9*, 1967–1977.
29. Some examples of intermolecular ene reactions involving fullerenes have been previously reported, see: (a) Cronakis, N.; Orfanopoulos, M. *Org. Lett.* **1999**, *1*, 1909–1912. (b) Miles, W. H.; Siley, P. M. *J. Org. Chem.* **1996**, *61*, 2559–2560. (c) Komatsuk, K.; Murata, Y.; Sugita, N.; Wan, T. S. M. *Chem. Lett.* **1994**, 635–636. (d) Wu, S.; Shu, L.; Fan, K. *Tetrahedron Lett.* **1994**, *35*, 919–922.
30. For a recent review on the synthetic applications of allenes, see: Ma, S. *Chem. Rev.* **2005**, *105*, 2829–2872.
31. (a) *Modern allene chemistry*. Krause, N.; Hashmi, A. S. K., Eds., Wiley-VCH, Weinheim. **2004**. (b) Hoffmann-Röder, A.; Krause, N. *Angew. Chem. Int. Ed.* **2004**, *43*, 1196–1216.
32. Yamazaki, S.; Yamada, K.; Yamamoto, K. *Org. Biomol. Chem.* **2004**, *2*, 257–264.
33. Alameda-Angulo, C.; Quiclet-Sire, B.; Zard, S. *Tetrahedron Lett.* **2006**, *47*, 913–916.
34. Oppolzer, W.; Pfenninger, E.; Keller, K. *Helv. Chim. Acta* **1973**, *56*, 1807–1812.
35. Shea, K. J.; Burke, L. D.; England, W. P. *Tetrahedron Lett.* **1988**, *29*, 407–410.
36. Jayanth, T. T.; Jeganmohan, M.; Cheng, M.-J.; Chu, S.-Y.; Cheng, Ch.-H. *J. Am. Chem. Soc.* **2006**, *128*, 2232–2233.
37. Altable, M.; Filippone, S.; Martín-Domenech, A.; Güell, M.; Sloà, M.; Martín, N. *Org. Lett.* **2006**, *8*, 5959–5962.
38. Güell, M.; Martín, N.; Altable, M.; Filippone, S.; Martín-Domenech, A.; Sloà, M. *J. Phys. Chem. A* **2007**, *111*, 5253–5258.
39. Laird, D. W.; Gilbert, J. C. *J. Am. Chem. Soc.* **2001**, *123*, 6704–6705.
40. Su, M.-D. *J. Chin. Chem. Soc. (Taipei)* **2005**, *52*, 599–624.
41. Olivella, S.; Pericàs, M. A.; Riera, A.; Solé, A. *J. Chem. Soc., Perkin Trans* **1986**, *2*, 613–617.
42. Hariharan, P. C.; Pople, J. A. *Helv. Chim. Acta* **1973**, *28*, 213–222.
43. (a) Wiest, O.; Houk, K. N.; Black, K. A.; Thomas, B. I. V. *J. Am. Chem. Soc.* **1995**, *117*, 8594–8599. (b) Goldstein, E.; Beno, B.; Houk, K. N. *J. Am. Chem. Soc.* **1996**, *118*, 6036–6043. (c) Wiest, O.; Houk, K. N. *Top. Curr. Chem.* **1996**, *183*, 1–24. (d) Dinadayalane, T. C.; Vijaya, R.; Smith, A.; Narahari-Sastry, G. *J. Phys. Chem. A* **2002**, *106*, 1627–1633. (e) Isobe, H.; Yamanaka, S.; Yamaguchi, K. *Int. J. Quantum Chem.* **2003**, *95*, 532–545.

44. Thilgen, C.; Gosse, I.; Diederich, F. *Top. Stereochem.* **2003**, 1–124.
45. Friedman, S. H.; Ganapathi, P. S.; Rubin, Y.; Kenyon, G. L. *J. Med. Chem.* **1998**, *41*, 2424–2429.
46. Nishimura, T.; Tsuchiya, K.; Ohsawa, S. Maeda, K.; Yashima, E.; Nakamura, Y.; Nishimura, J. *J. Am. Chem. Soc.* **2004**, *126*, 11711–11717.
47. Bianco, A.; Maggini, M.; Scorrano, G.; Tonido, C.; Marconi, G.; Villani, C.; Prato, M. *J. Am. Chem. Soc.* **1996**, *118*, 4072–4080.
48. (a) Illescas, B. M.; Martín, N.; Poater, J.; Solà, M.; Aguado, G. P.; Ortuño, R. M. *J. Org. Chem.* **2005**, *70*, 6929–6932. (b) Djojo, F.; Hirsch, A. *Chem. -Eur. J.* **1998**, *4*, 344–356.
49. Nájera, C.; Sansano, J. M. *Angew. Chem. Int. Ed.* **2005**, *44*, 6272–6276.
50. (a) Maggini, M.; Scorrano, G.; Prato, M. *J. Am. Chem. Soc.* **1993**, *115*, 9798–9799. (b) Martín, N.; Altable, M.; Filippone, S.; Martín-Domenech, A.; Echegoyen, L.; Cardona, C. M. *Angew. Chem. Int. Ed.* **2006**, *45*, 110–114.
51. Pantarotto, D.; Bianco, A.; Pellarini, F.; Tossi, A.; Giangaspero, A.; Zelezetsky, I.; Briand, J.-P.; Prato, M. *J. Am. Chem. Soc.* **2002**, *124*, 12543–12549.
52. Filippone, S.; Maroto, E. E.; Martín-Domenech, A.; Suarez, M.; Martín, N. *Nature Chem.* **2009**, *1*, 578–582.
53. Cabrera, S.; Gómez-Arrayás, R.; Carretero, J. C. *J. Am. Chem. Soc.* **2005**, *127*, 16394–16395.
54. Wilson, S. R.; Lu, Q.; Cao, J.; Wu, Y.; Welch, C. J.; Schuster, D. I. *Tetrahedron* **1996**, *52*, 5131–5142.
55. Tan, X.; Schuster, D. I.; Wilson, S. R. *Tetrahedron Lett.* **1998**, *39*, 4187–4190.

Chapter 3

Phthalocyanine Functionalized Carbon Nanostructures

Uwe Hahn, David González-Rodríguez* and Tomás Torres*,†,‡*

**Departamento de Química Orgánica, Campus Cantoblanco,
Universidad Autónoma de Madrid, 28049 Madrid, Spain*

*†IMDEA-Nanociencia, Facultad de Ciencias, Ciudad Universitaria de
Cantoblanco, 28049 Madrid, Spain*

1. Introduction	59
2. Phthalocyanine-Fullerene Assemblies	60
2.1. Covalent phthalocyanine-fullerene systems	61
2.2. Non-covalent phthalocyanine-fullerene systems	75
3. Phthalocyanine-CNT Assemblies	83
3.1. Covalent phthalocyanine-carbon nanotube systems	84
3.2. Non-covalent phthalocyanine-carbon nanotube systems	89
4. Conclusions and Perspectives	93
Acknowledgments	94
References	94

1. Introduction

The intriguing properties of phthalocyanines (Pcs) are related to their two-dimensional 18 π -electron aromatic system.¹ As a consequence, this class of porphyrin synthetic analogues has demonstrated its value in the form of dyes and pigments. This is due to their intense *Q* band absorption in the red and near infrared region at wavelengths which typically lie between 630 to 670 nm,

‡Corresponding author. Email: tomas.torres@uam.es

along with remarkably high extinction coefficients of $\sim 10^5 \text{ L mol}^{-1} \text{ cm}^{-1}$.² However, in recent years they have also been at the center of attention as building blocks for the construction of new molecular materials for electronics and optoelectronics. As for porphyrins, in terms of electron-donating materials, Pc-based compounds represent an interesting kind of molecules with an extraordinary ability to harvest light and subsequently promote energy or electron transfer processes.³

On the other hand, carbonaceous materials⁴ such as fullerenes⁵ and carbon nanotubes (CNTs)^{6,7} have clearly demonstrated their huge potential over more than the last decade as versatile building blocks in material sciences.⁸ In fact, both the sphere-shaped fullerenes as well as the tubular one-dimensional CNTs exhibit excellent electron acceptor abilities, which are the origin for such nanostructures to be subjected in the construction of photo- and electroactive donor-acceptors systems.^{3,7b}

The design and development of Pc-fullerene or Pc-CNT ensembles can be accomplished by approaches either relying on the covalent or the non-covalent association.³ Both fundamental concepts and the corresponding research efforts devoted to the construction of materials consisting of Pcs and carbonaceous materials such as fullerenes and CNTs will be introduced in this Chapter. However, it shall be pointed out that we do not intend to present an exhausting overview of all such multi-component assemblies presented to date rather than to highlight the advances made during recent years.

2. Phthalocyanine-Fullerene Assemblies

The importance and complexity of energy and electron transfer reactions have prompted the design and preparation of a variety of donor-acceptor (D-A) molecular models. The basic structure of these systems is a dyad comprised of an electron-donating and an electron-accepting molecule that are separated by a covalent or a non-covalent spacer. Successful mimicry of nature's photosynthetic performance — to be applied in organic solar cells — requires careful optimization of a number of parameters in these synthetic ensembles: (i) the absorption of the system must cover a wide region of the solar spectrum and any energy transfer process should be directional and quantitative, (ii) the redox properties of the donor and the acceptor must be adjusted so that an exergonic electron transfer process can take place without significant energy loss, and (iii) the system should undergo a fast charge separation and a slow charge recombination process, in order to form a long-lived radical pair efficiently.

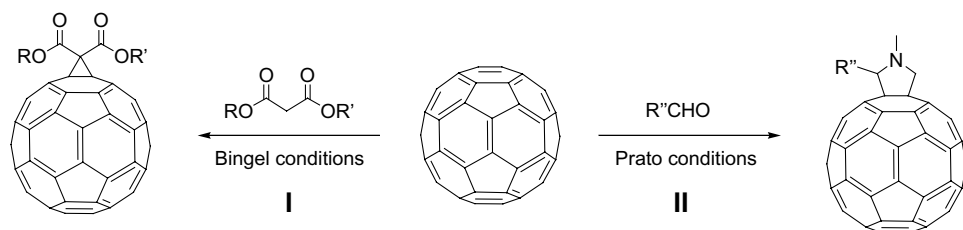
Regarding the electron-acceptor components, fullerenes and CNTs have been recognized as ideal candidates for being incorporated in D-A systems.

Pcs, on the other hand, have arisen as excellent light-harvesting and electron donor partners to these carbon materials due to their outstanding photo-physical and electrochemical properties as well as their high optical, thermal and chemical stability.³

2.1. Covalent phthalocyanine-fullerene systems

Since their discovery in the mid 1980s, fullerenes have been the focus of attention.⁵ However, pristine C₆₀ tends to be scarcely soluble in organic media. That is why modification of this all-carbon structure is the key for possible applications thereby not only imparting solubility but also offering the possibility to incorporate additional functions for tailoring the C₆₀ properties. Among the reactions that can be employed for the covalent functionalization of the spherical fullerene structure, the Bingel–Hirsch and the Prato reaction respectively, have demonstrated their potential in this regard. The former relies on the preparation of a malonate precursor which is reacted in the presence of a base and iodine or tetrachloromethane, thus giving rise to a cyclopropanation reaction with formation of the corresponding methanofullerene adducts (Scheme 1).⁹ On the other hand, the Prato reaction can be accomplished with azomethine ylides in a 1,3-cycloaddition thus leading to the formation of five-membered *N*-methylpyrrolidine ring structures (Scheme 1).^{7,10} Both reactions have shown to be very reliable as well as versatile tools for the functionalization of fullerenes and have thus also been frequently employed in the construction of donor-acceptor nanohybrids which will be presented hereafter.

However, the first specimen of a covalently linked Pc-C₆₀ adduct **1** (Figure 1) was introduced back in 1995 and obtained through Diels-Alder condensation of a previously modified Ni(II)Pc macrocycle serving as diene with pristine C₆₀ playing the part of the dienophile.¹¹ Electrochemical studies indicated almost no effect on the oxidation-reduction potentials with respect to the



Scheme 1. Two main strategies for the construction of functionalized fullerenes by (I) Bingel conditions with malonate derivatives or (II) Prato conditions with aldehydes.

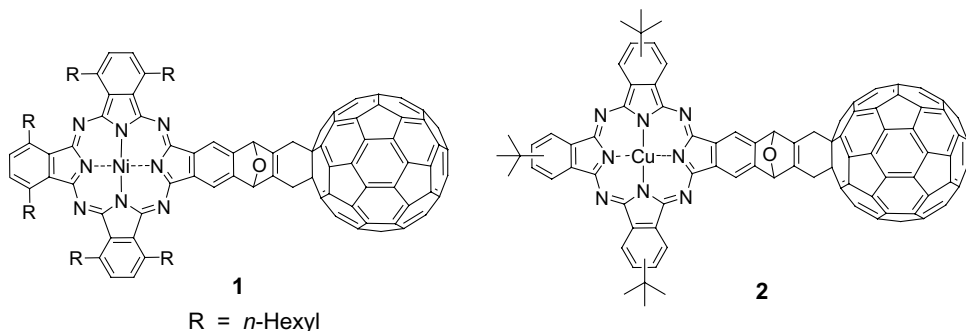


Figure 1. Pc-C₆₀-Dyads **1** and **2** obtained under the use of Diels–Alder reactions for covalent association.

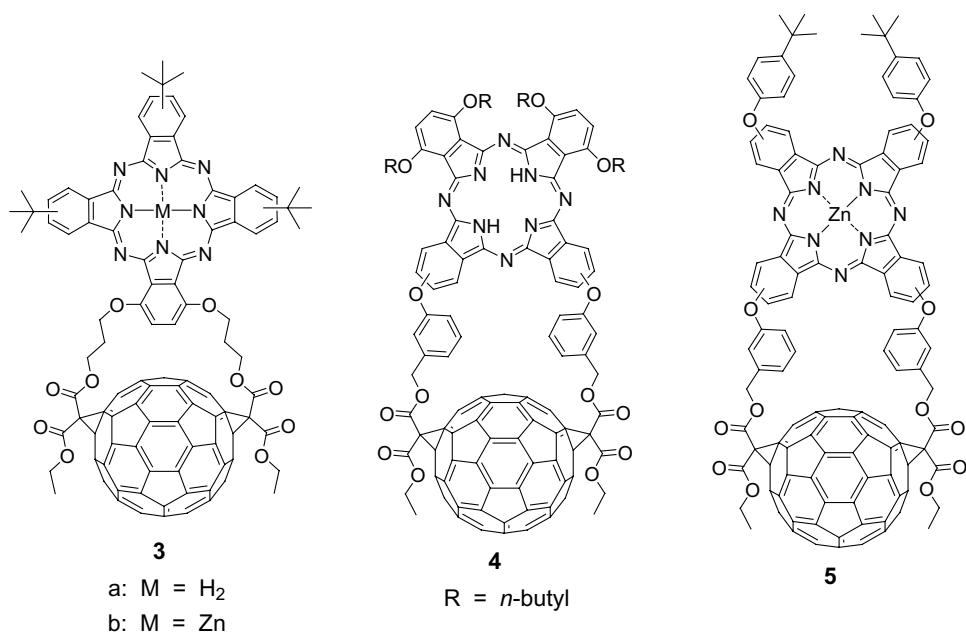


Figure 2. Tethered bis-Bingel adducts **3–5** consisting of spatially close Pcs and fullerene.

single components, the voltammograms showing five reversible reduction peaks, which were assigned by spectroelectrochemistry to be either fullerene- or Pc-based. Similar adducts such as dyad **2** (Figure 2) have been prepared with modified peripheral groups and/or the central metal species in the Pc cavity (Figure 1). These entities have been the subject of non-linear optics investigations, thereby showing high second-order hyperpolarizability values, enhanced optical limiting performances, or non-linear absorption enhancement.¹²

This report inspired the research since then and a plethora of related covalently linked donor-acceptor Pc-fullerene compounds ranging from dyads to more sophisticated examples like triads, tetrads or polymers have been presented. The nature of the appended Pc moiety in these reports has been varied with respect to the metal species in the center as well as to the end groups located at the periphery of the functionalized Pc unit depending on the targeted application.

The approaches using the aforementioned Bingel reaction have been demonstrated to not substantially influence the favorable fullerene properties. The systems presented to date in relation to Pc-fullerene hybrid structures are dominated by either mono- or bis-adducts on the C_{60} sphere giving rise in the latter case to tethered structures. With respect to bis-methano fullerene derivatives, spatially close dyads such as **3–5** have been reported (Figure 2).¹³ Studies by photophysical means showed photoinduced electron transfer (PET) to occur from the excited state of the MPc to the C_{60} in both polar and non-polar environment. Examination of PET energetics revealed that the Pc–fullerene dyads existed mainly in an extended conformation as opposed to a face-to-face orientation common for similar tethered porphyrin–fullerene dyads. Such double-bridged dyads have also been part of Langmuir–Blodgett films.¹⁴ Blending these films with perylene dicarboximide (PDI) led to a rapid quenching process of the fluorescence of the latter followed by a charge separation in the Pc- C_{60} layer, thus yielding a long-lived (a few microseconds) intermolecular charge separated state.^{14b}

Another example of a Bingel C_{60} adduct associated with Pcs has been described by Kim *et al.* (Figure 3).¹⁵ The synthetic sequence started with the preparation of a bis-functionalized fullerene precursor having a free OH group that was conjugated to a Si(IV)Pc. In the first instance, triad **6** was constructed by formation of silicon-oxygen bonds. As a result of the bulky sterically demanding substituents, the core moiety was found to be isolated, hence avoiding the frequently observed Pc aggregation. Electrochemical measurements gave clear indication that the first reduction of the Pc moiety was more anodic than that of a reference compound lacking the C_{60} fullerene axial ligands. On the contrary, the first oxidation of the Pc- C_{60} triad **6** as well as the first reduction potential of the fullerene remained the same when compared to the reference compounds. This observation was rationalized to emanate from the strong electron-withdrawing effect of the two axial fullerene substituents, which led to the stabilization of the first reduced state of the Pc. In continuation of their research, the same group presented similar structures in which the axial fullerene derivatives have been exchanged by dendritic fullerene-rich branches that were also placed as ligands at the axial

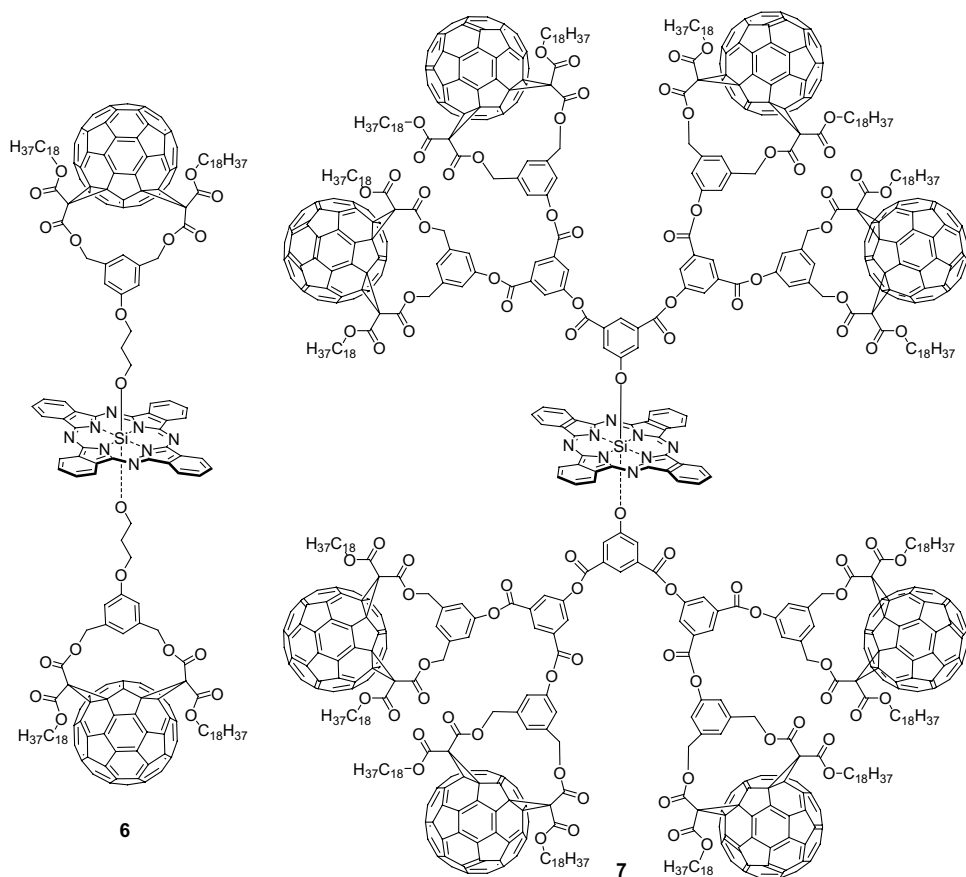


Figure 3. Molecular structures constructed with either two (6) or eight fullerene spheres (7) in the axial positions of SiPc.

positions.¹⁶ For instance, the molecular structure of second generation dendrimer 7 is depicted in Figure 3. Studies by time-resolved fluorescence and transient absorption spectroscopy evidenced the formation of a charge-separation process from the Si(IV)Pc to the C₆₀ subunits with the lifetimes of the radical ion pairs to be prolonged upon going from the pentad (that is, the first generation species carrying four fullerene moieties) to the most voluminous dendrimer of third generation. This was attributed to a possible electron migration among the C₆₀ subunits. The results obtained for such materials were claimed to be particularly interesting in light of exploiting fullerenes in light-harvesting processes.

Another important functionalization of the C₆₀ moiety is the modification under Prato conditions to form *N*-methylpyrrolidine ring structures as

mentioned above.^{7,10} As a result of the relatively high synthetic yield typically observed in this route, it has been used for the preparation of an ample number of Pc-fullerene-derived nanohybrid systems directed towards the generation of charge separated species, which is one of the fundamental principles in the field of photovoltaics. Particularly, the influence of the nature and/or length of the linkage between the two photo- and electrochemically active Pc and C₆₀ moieties has been the object of several studies.

One of the key starting materials for the construction of such donor-acceptor Pc-fullerene entities by covalent linkage is certainly tris(*tert*-butyl) monoiodo Zn(II)Pc that can be rather easily prepared in reasonable yields higher than 20%.¹⁷ Within this building block, pendant *tert*-butyl groups impart high solubility and, in addition, avoid aggregation, which is a phenomenon frequently observed for Pcs. The versatility of the chemistry that can be applied to the iodine functionalization paves the way for coupling with the fullerene sphere through a given spacer moiety.¹⁸ The immediate linkage with a *N*-methylpyrrolidine group between Pc and C₆₀ moieties started with tris(*tert*-butyl)monoiodo Zn(II)Pc whose iodine function was converted first to the corresponding formyl derivative. To this end, the fullerene has been reacted under Prato conditions in the presence of *N*-methylglycine to furnish the spatially-close target dyad molecule **8** having a methylpyrrolidine group (Figure 4). Regardless of the metal atom of the Pc scaffold, a small, ground-state electronic communication between the two photoactive units was found as indicated by UV-vis spectroscopy. On the other hand, electrochemistry resulted in different effects depending on the MPc species, with the oxidation and reduction potentials being positively

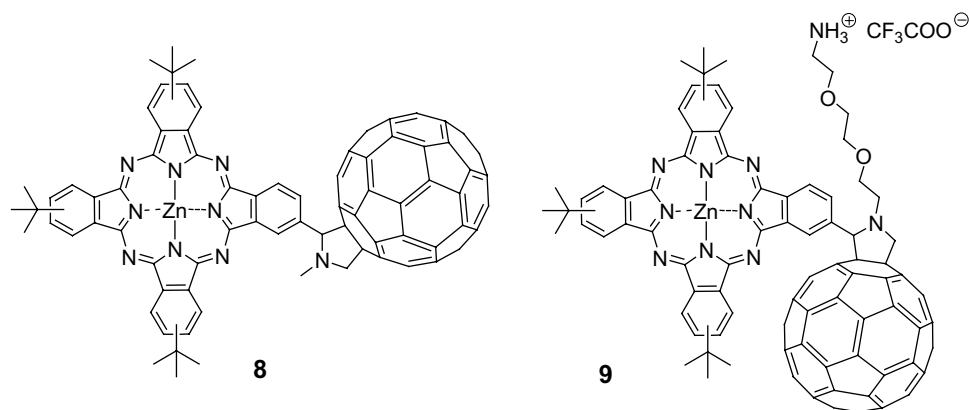


Figure 4. Spatially close Pc-C₆₀ Prato adducts with either a methyl (**8**) or ammonium-terminated oligoethylene glycol chain (**9**) on the pyrrolidine subunit.

shifted for the dyad structures built from free-base derivative H_2Pc or $Zn(II)Pc$, while covalently linking the $Cu(II)Pc$ led to negatively shifted C_{60} -based reduction potentials. The latter results were rationalized with a certain degree of ground-state intra- and/or intermolecular interactions between the electron-donating Pc and the electron accepting fullerene moiety. Importantly, photophysics demonstrated PET events, a phenomenon that has been found to be almost ubiquitous in the covalently-linked $Pc-C_{60}$ systems.

In continuation of the research on $Pc-C_{60}$ dyad structures, the methyl unit present in the pyrrolidine linker has been substituted by an ammonium terminated oligoethylene glycol group (see compound **9**; Figure 4) giving rise to the formation of highly ordered 1-D nanotubes upon dispersion in water as encountered by transmission electron microscopy (TEM).¹⁹

As mentioned before, the spacer unit located in the center between Pc and fullerene has also been subject to modification, thus aiming at studying the influence of the linker unit on the electronic communication between the Pc and fullerene moieties. For instance, either single, double or triple bonds have been implemented in the dyad structures **10–12** (Figure 5).²⁰ The obtained results indicated that, regardless of spacer length and nature, intramolecular electron transfer takes place from the photoexcited Pc

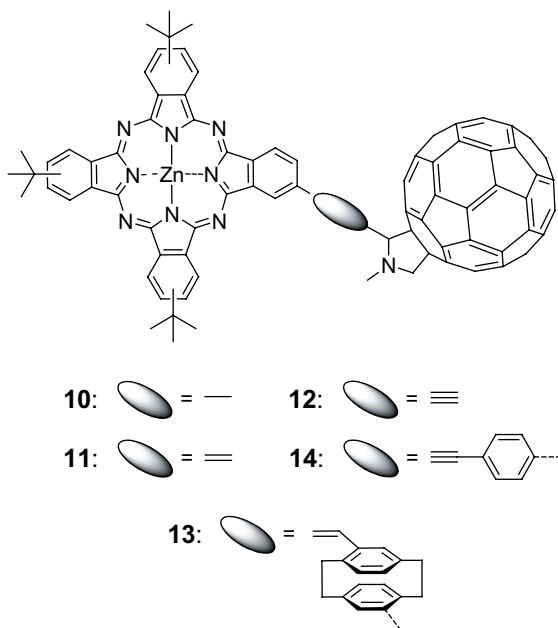


Figure 5. Schematic representation of covalently linked Pc and fullerene moieties **10–14** with linkers of different nature and length.

macrocycle to the electron-accepting carbon cage. Additionally, complementary time-dependent density functional theory calculations supported the spectral assignment seen in the differential absorption spectra for the $\text{ZnPc}^{\bullet+}$ radical cation and the $\text{C}_{60}^{\bullet-}$ radical anion. Similarly, a pseudo-spacer dyad **13** has been presented consisting of the Zn(II)Pc and C_{60} moieties covalently connected through a [2.2]paracyclophane unit (Figure 5). This structurally-rigid dyad also gave rise to a photoinduced dynamic process resulting in the formation of a long-lived charge separated state.

Furthermore, the iodine function of tris(*tert*-butyl)monoiodo Zn(II)Pc served as a starting point for the modification by a palladium-catalyzed Sonogashira coupling reaction with ethynyl benzaldehyde, thus giving rise to a Pc scaffold with terminal aldehyde function. Subsequently, the fullerene was subjected to standard 1,3-dipolar cycloaddition conditions in the presence of *N*-methylglycine to yield the desired dyad structure **14** (Figure 5).²¹ This rigid donor-acceptor system has been studied on highly ordered pyrolytic graphite and graphite-like surfaces by AFM techniques and was found to self-organize with the formation of fibers and films. Importantly, these supramolecularly-assembled nanostructured architectures showed outstanding electrical conductivity values as a result of the extremely high ordered structure within the nanoscopic ensemble.

An ethenyl-bridged dyad consisting of C_{60} and a hexa(*n*-butyloxy)-substituted Zn(II)Pc has been prepared starting from tris(*tert*-butyl)monoiodo Zn(II)Pc carrying an iodine function. The synthetic protocol involved a Heck coupling reaction of this precursor with 4-vinylbenzaldehyde to furnish the formyl-terminated Zn(II)Pc . Conjugation to the fullerene sphere under standard cycloaddition reaction of azomethine ylides with *N*-methylglycine furnished **15** (Figure 6).²² Electrochemical studies evidenced an appreciable electronic communication between Zn(II)Pc and C_{60} in the ground state as indicated by the shifted oxidation potential of the Zn(II)Pc subunit in comparison to the reference compound. In addition, in the excited state, photoexcitation showed the formation of a charge-separated $\text{ZnPc}^{\bullet+}\text{-C}_{60}^{\bullet-}$ state with a lifetime of 130 ns in THF. Mixing this dyad with an electron-deficient octakis(propylsulfonyl) Pd(II)Pc **16a** resulted in a supramolecular triad that has been assessed by different techniques. Heteroassociation thus led to very stable 1:1 conjugates with strong donor-acceptor π - π stacking of the two Pc subunits and, notably, to a substantial stabilization of the radical pair when compared to the covalently linked dyad. Similar ensembles have been investigated with respect to their possible liquid crystallinity.²³ Indeed, blending of different non-mesogenic Pc- C_{60} dyads **15a-c** with mesogenic, symmetrically-substituted octakis(hexadecylthio) Zn(II)Pc **16b** gave rise to hexagonal

columnar mesophases in which the liquid crystalline columns were composed of alternating stacks of the mesogenic Pc and Pc-C₆₀ dyads as suggested by X-ray diffraction studies. The appealing approach of using blends, in which a mesogen induces mesomorphism on a non-mesogenic Pc-based functional material, represents an interesting strategy for the incorporation of photoactive, donor- acceptor Pc-fullerene systems in liquid-crystalline architectures.

Lately, novel nanohybrids **17a-c** have been presented comprising a double-decker lanthanide(III) bis(phthalocyaninato) complex constructed by two different Pcs sandwiched by lanthanide ions (Ln = Sm, Eu, Lu) that were covalently linked to a C₆₀ moiety (Figure 7).²⁴ The final step for the preparation of this rather sophisticated structure involved esterification between the free hydroxyl group of the corresponding lanthanide double-decker complexes and a previously modified C₆₀ species bearing a carboxylic acid function. Accordingly, the three final assemblies have been obtained and characterized subsequently by cyclic voltammetry. This technique showed the superposition of the redox peaks of both components, thus giving clear indication of a lack of ground-state electronic interactions between the two electroactive units.

Apart from using pristine fullerene as a scaffold for the construction of donor-acceptor assemblies, trimetallic nitride templated (TNT) endohedral metallofullerenes (M₃N@C₈₀) have also been used as building blocks in such dyad nanohybrids with Pcs.²⁵ The encapsulation of a trimetallic nitride cluster

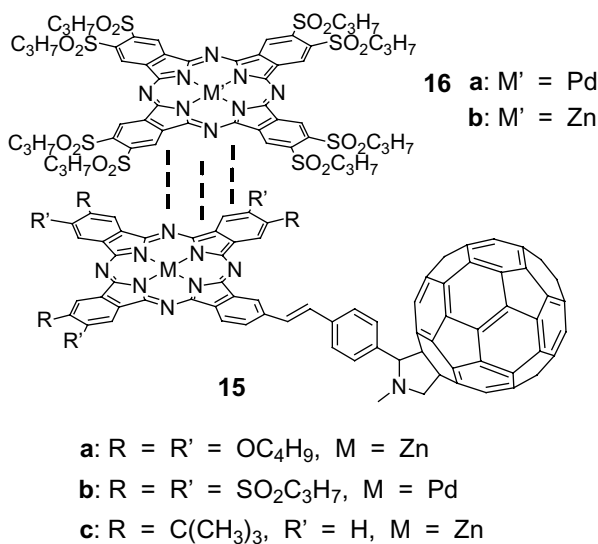


Figure 6. Supramolecular triad consisting of MPc-fullerene dyads **15a-c** and electron-deficient M'Pcs **16a-b**.

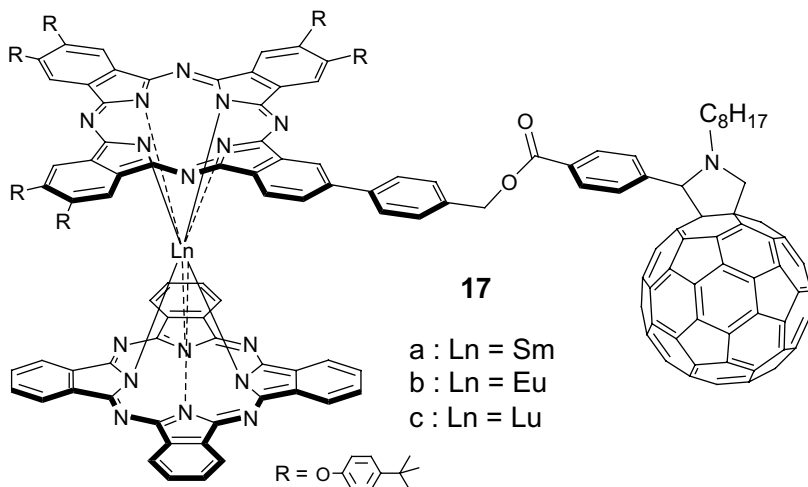


Figure 7. Structure of double-decker lanthanide(III) bis(phthalocyaninato)-C₆₀ dyads **17a–c** (Ln = SM(III), EU(III) or Lu(III)).

within fullerene spheres has been demonstrated to furnish systems with improved material properties.²⁶ Hence, results obtained by fundamental research on these endohedral structures evidenced larger absorptive coefficients in the visible region of the electromagnetic spectrum and lower highest occupied molecular orbital (HOMO)- lowest unoccupied molecular orbital (LUMO) energy gaps, while preserving the remarkable electron-accepting ability of fullerenes. However, the availability in terms of synthesis is still in most cases rather limited and has to be addressed in the coming years in order to support possible future applications. Nonetheless, the TNT fullerene Y₃N@C₈₀ has been successfully subjected to a conjugation reaction with a Zn(II)Pc, though the final structure was obtained in low yields. Accordingly, the 1,3-dipolar cycloaddition reaction of fullerenes with a Zn(II)Pc gave the targeted dyad nanohybrid **18** (Figure 8). Similar attempts have been undertaken to construct dyad **19** under the use of a mono-functionalized Bingel adduct motif (Figure 8).²⁵ However, it turned out that the final assemblies proved to be rather unstable and decomposed during the purification process.

The ease of functionalization by employing the Prato method not only proved to be a reliable tool that has been successfully exploited for the construction of dyads but has also demonstrated its potential for analogue systems comprising either more than one Pc or C₆₀ moiety. For instance, triad **20** consisting of two fullerene cages and one Pc unit has been prepared aiming at a higher stabilization of the photogenerated excited states in order to mimic light harvesting to a higher extent (Figure 9).²⁷ The synthetic

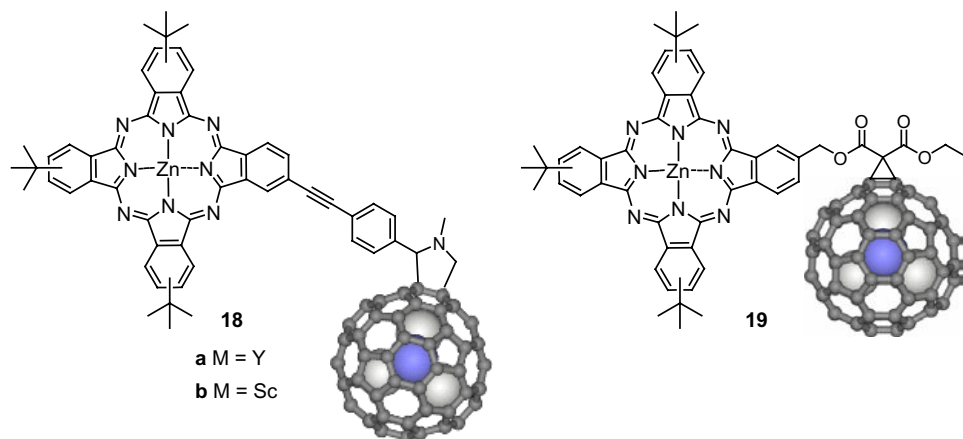


Figure 8. Covalent construction of Pc-containing, $M_3N@C_{80}$ -based ($M = Y, Sc$) dyads by either Prato *N*-methylpyrrolidine addition pattern **18a–b** and as Bingel–Hirsch adduct **19**.

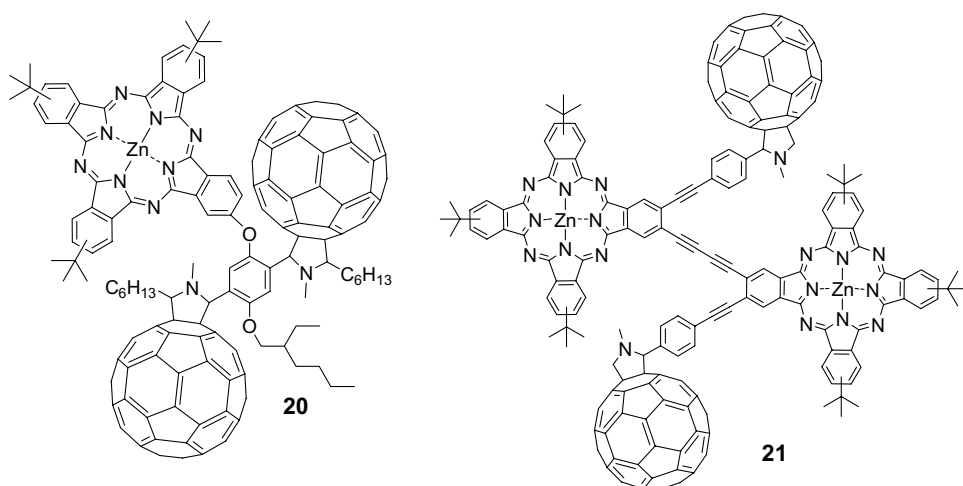


Figure 9. Structures of multicomponent systems: Zn(II)Pc-(C₆₀)₂ triad **20** and Zn(II)Pc₂-(C₆₀)₂ tetrad **21**.

protocol involved the preparation of a Zn(II)Pc substituted by mono-alkylated 2,5-dibromohydroquinone that was then transformed at the two bromo functionalities by means of a double Stille coupling and subsequent oxidation of the resulting terminal alkene moieties yielded the corresponding bisformyl derivative. Each of the aldehyde functions was then subjected to 1,3-dipolar cycloaddition reactions with C₆₀ in the presence of *N*-hexylglycine to give the targeted triad structure **20** (Figure 9). Basic features of this triad are the

harvesting of photons with wavelengths up to the infrared region that could then be efficiently converted into long-lived charge carriers for solar energy conversion. Though in light of possible applications in solar cells, the overall photocurrent and therefore the conversion efficiency was only moderate for such a nanosystem, the fundamental approach in general proved successful, but requires further device optimization in order to improve the transport of charges to the electrodes.

Lately, ensemble **21** comprising two Zn(II)Pc macrocycles and two C₆₀ fullerene units has also been reported (Figure 9).²⁸ The synthetic protocol relied on the preparation of a rigid bis-Zn(II)Pc precursor spacers by two ethynyl groups. Each of the two Zn(II)Pc subunits carried in addition an iodo function. By means of double Sonogashira cross-coupling reactions with 4-ethynylbenzaldehyde the authors were able to introduce the corresponding formyl moieties, allowing for covalent linkage of fullerenes under classical Prato cycloaddition reactions at both functional groups. The resulting tetrad **21** with two terminal C₆₀ units has been studied by photophysical means to evidence relatively short charge separated state lifetimes. This observation was rationalized to have its origin in the close proximity of the Pc and the C₆₀ subunits in the nanohybrid system. The tight contact between the donor and the acceptor moieties could in fact lead to through-space deactivation dynamics, which might prohibit the feasibility of forming long-lived radical ion pairs.

Very recently, Torres and coworkers also described the preparation of another rather sophisticated tetrad **22** comprising three Zn(II)Pc units and a fullerene sphere (Figure 10).²⁹ Tetrakis(4-iodophenyl)methane served as a starting point for the monofunctionalization by means of a Sonogashira cross-coupling reaction with 4-ethynylbenzaldehyde over one of the iodophenyl moieties. The remaining three iodo-functions were then subjected to modification by threefold Pd-assisted coupling with a large excess of monoethynyl-functionalized Zn(II)Pc to provide a formyl-containing tripod. Finally, 1,3-dipolar cycloaddition with pristine fullerene gave the targeted rigid four-component entity **22** by formation of a fulleropyrrolidine moiety. Femtosecond laser photolysis provided spectroscopic evidence for a charge transfer mechanism between photoexcited Zn(II)Pc and C₆₀. In comparison with related multinuclear Pc–fullerene-based systems aiming as well as developing novel electron donor–acceptor conjugates, a significant stabilization of the radical ion pair state lifetime was found. The second order NLO properties of these interesting octupolar systems have been recently reported.³⁰

Appending *p*-formylbenzoic acid in the axial positions of a Si(IV)Pc was the first step of the synthetic protocol to introduce two C₆₀ units perpendicular to the Si(IV)Pc aromatic ring system (Figure 11).³¹ Typical Prato

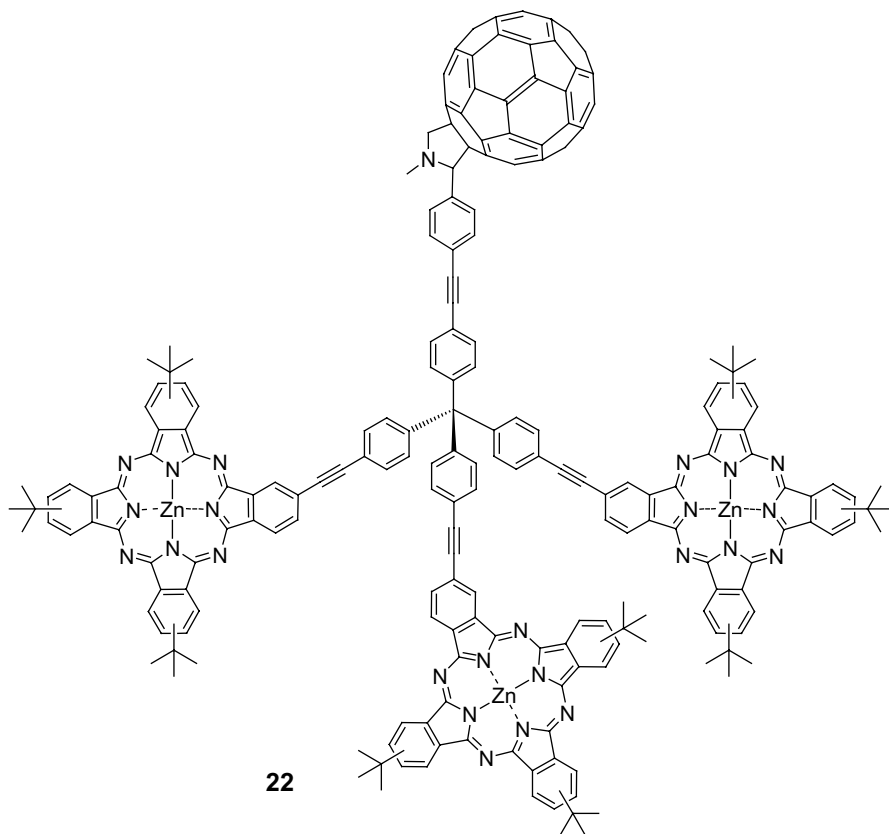


Figure 10. Tripodal structure of a tetrad $\text{Zn(II)Pc}_3\text{-C}_{60}$ **22** built on a tetraphenylmethane centerpiece.

reaction conditions furnished triad structure **23** with very short fullerene-Pc distances. The results observed by photophysical experiments for triad **23** indicated efficient *intramolecular* PET from the fullerene to the Pc subunit. In continuation of this work, the more sophisticated system **24**, built from five components consisting of two terminal C_{60} moieties associated to a central Si(IV)Pc by naphthalenediimide (NDI) spacer units, was synthesized (Figure 11).³² From photophysical studies it could be deduced that the charge-separated state $\text{Si(IV)Pc}^{\bullet+}\text{-(NDI)}_2\text{-(C}_{60}\text{)}^{\bullet-}$ in pentad **24** has a longer lifetime than a Si(IV)Pc substituted in axial positions with only two NDI units as electron acceptors, which underscores the relevance of C_{60} as secondary electron-accepting entity.

The two electroactive fullerene and Pc moieties have also been part of less defined polymer structures **25a–b** (Figure 12).³³ Attaching norbornene to

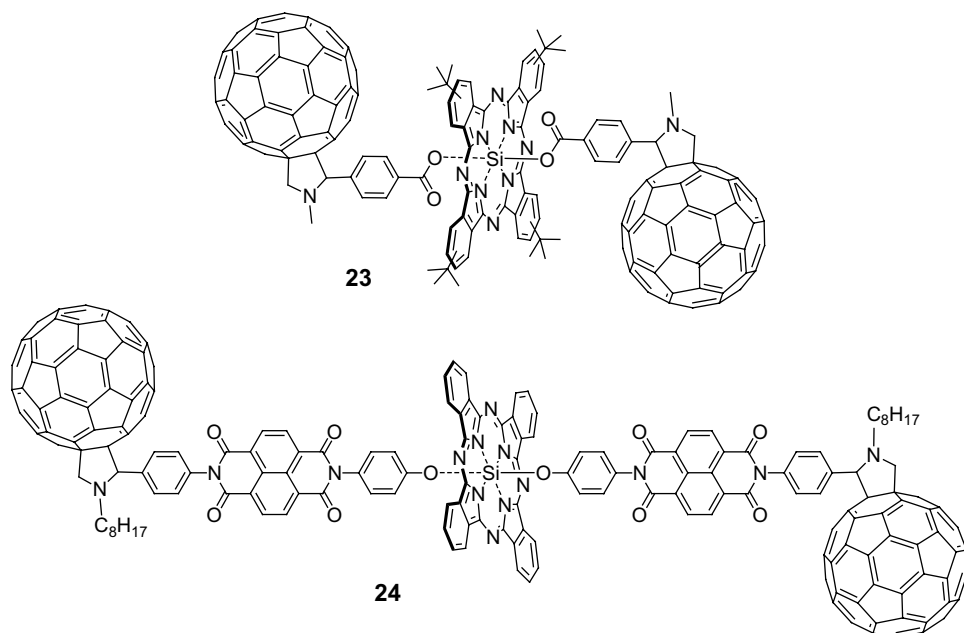


Figure 11. Axially coordinated Si(IV)Pc-triad **23** with two fullerenes and pentad **24** with the C₆₀ moieties spaced by NDI units.

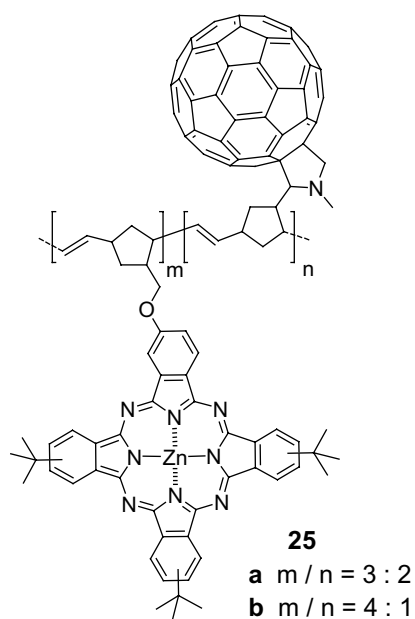


Figure 12. Norbornene-derived polymer **25** synthesized with different ratios (**a**: m/n = 3:2 and **b**: m/n = 4:1) of Zn(II)Pc and C₆₀.

both a *N*-methylfulleropyrrolidine and a Pc *via* an aliphatic ether bond readily provided the precursors for Grubbs ring-opening-metathesis polymerization. Applying different monomer stoichiometries for the polymerization in ratios of either 2:3 or 1:4, respectively, gave the target copolymers, which exhibited long-lived charge-separated states. These could be attributed to PET from the Pc donor units to the C₆₀ acceptor units within the copolymers as has been detected by fluorescence and transient absorption measurements. Attempts to construct preliminary solar cell devices made of one of the copolymers resulted in moderate overall photocurrents and conversion efficiencies.

Apart from the three methods described above consisting of the Diels–Alder, Bingel and Prato reactions for the functionalization of fullerenes, there is also the approach via formation of tosylhydrazones. This method relies on the condensation reaction of the keto function of a given keto-ester with *p*-tosylhydrazine thus obtaining the corresponding tosylhydrazones. *In situ* transformation to diazo compounds allows then for the functionalization of pristine fullerene by cyclopropanation reactions.

However, only a small number of covalently linked donor-acceptor Pc-C₆₀ nanohybrids have been described in the literature based on this technique. All these specimens are closely related to [6,6]-phenyl-C₆₁-butyric acid methyl ester (PCBM). One example is represented by dyad **26** with a flexible azacrown macrocycle as part of the linker between the two photoactive moieties (Figure 13).³⁴ The synthesis of **26** started from [6,6]-phenyl-C₆₁-butyric acid methyl ester (PCBM) as obtained through the tosylhydrazone method. Demethylation of this building block readily provided the carboxylic acid needed for a dicyclohexylcarbodiimide (DCC)-mediated esterification reaction. On the other hand, a Zn(II)Pc building block was prepared and

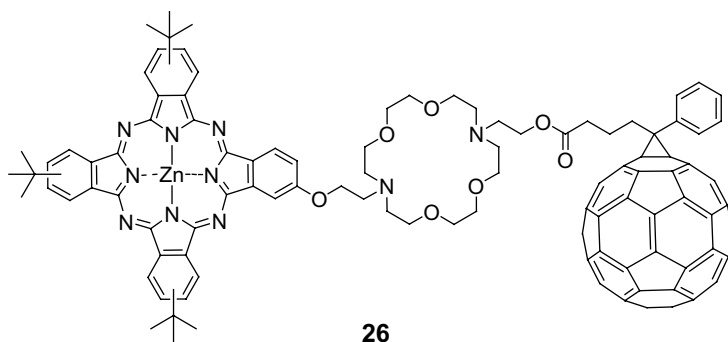


Figure 13. Molecular structure of dyad **26** containing an azacrown linker unit.

modified with a pendant azacrown moiety that carried a free hydroxyl group. Opposite to expected results, the hosting of alkali ions between the Pc and fullerene showed hardly any effect neither on the photophysical nor on the electrochemical properties of the assemblies.

This strategy *via* tosylhydrazone proved to be also successful for the first specimens of mesogenic Pc-C₆₀ dyads. Accordingly, a series of Zn(II)Pcs has been prepared comprising three swallow-tail alkoxy groups and one oligoethylene glycol chain of varying length. The free hydroxyl group located at the end of the glycol chain then allowed for coupling by DCC-mediated esterification with demethylated PCBM to afford targeted dyad structures **27a–d** with spacer groups of different lengths between the two units (Figure 14).³⁵

Similarly, the synthesis of two Pc-C₆₀ dyads **28a–b**, in which a fullerene moiety has been connected covalently to a Zn(II)Pc bearing either *tert*-butyl or trifluoroethoxy groups at its peripheral positions, has been performed (Figure 14). Both dyads were obtained starting from a common fullerene derivative equipped with a terminal phthalonitrile moiety that was then reacted with either 3-*tert*-butyl phthalonitrile or a persubstituted, trifluoroethoxy-coated phthalonitrile, hence leading to Pc-C₆₀ dyads **28a–b**. Electrochemical and spectroscopic studies on both dyad systems evidenced an efficient intramolecular PET process in the case of nanohybrid **28b**, whereas dyad **28a** did not show any sign of electronic communication between Pc and C₆₀.

2.2. Non-covalent phthalocyanine-fullerene systems

The concepts and tools of molecular self-assembly offer an elegant and promising strategy to selectively connect donor and acceptor molecules in a

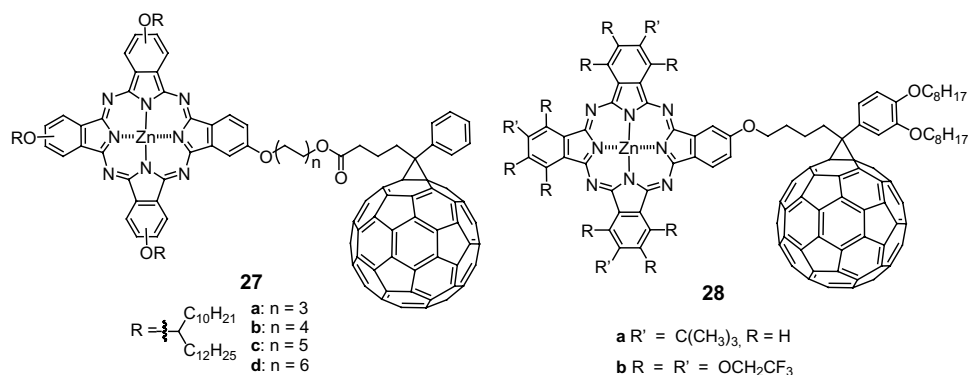


Figure 14. Structures of mesogenic Pc-C₆₀ dyad **27** and bis-component systems with either electron-rich (**28a**) or -deficient Zn(II)Pcs (**28b**).

well-defined conformation. The advantages of using non-covalent interactions to construct D-A systems are manifold: (i) synthetic simplicity and versatility, (ii) the possibility of controlling the association and dissociation of the molecular components as a function of the experimental conditions and, (iii) supramolecular dyads typically exhibit fast energy/electron transfer processes and slow charge recombination rates. To date, several Pc-based supramolecular systems have been prepared using two main approaches: (i) hydrogen-bonding with Pcs that are substituted at the periphery with supramolecular motifs and (ii) axial ligand coordination to the Pc metal center.

In this context, the first examples of Pc- C_{60} pseudorotaxane-like complexes, such as **29a–c** (Figure 15), were reported in 2002.^{36,37} These complexes were formed by spontaneous threading of a dibenzylammonium-fullerene molecule through a dibenzo-24-crown-8-substituted Pc macrocycle, which was prepared by statistical crossover condensation. A similar system, containing two Pc units at both sides of the crown ether was also described.³⁷

^1H NMR experiments confirmed a 1:1 stoichiometry and allowed the determination of the association constant of the complex ($K_a = 1.53 \times 10^4 \text{ M}^{-1}$ for **29b**) by integration of the signals of the species at equilibrium. Whereas electronic absorption and cyclic voltammogram experiments indicated a negligible electronic communication between the two active units in the ground state, excited state photophysical studies revealed an intracomplex

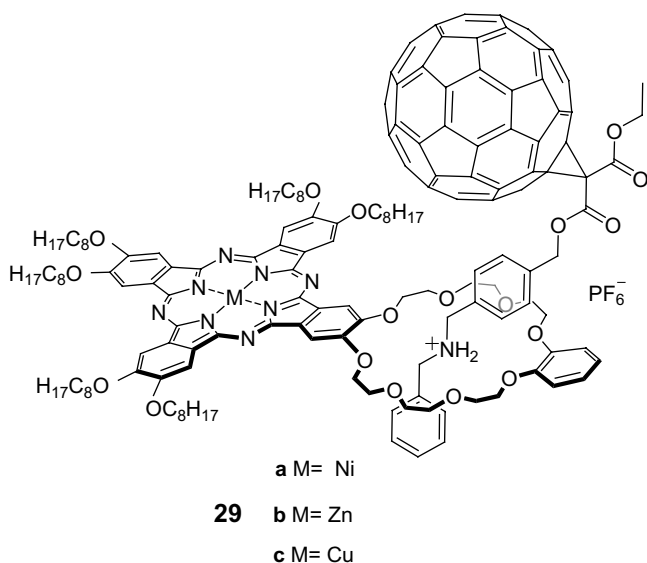


Figure 15. Molecular structure of [2]pseudorotaxane MPc- C_{60} dyads **29a–c**.

deactivation process in the associated species complexes that was ascribed to the formation of the $\text{Pc}^{\bullet+}$ and $\text{C}_{60}^{\bullet-}$ radical ions.³⁷ Remarkably, these supramolecular ensembles exhibited a stabilization of more than two orders of magnitude of their radical ion pair state lifetimes (calculated to be around 1.5 μs), with respect to comparable covalently-linked Zn(II)Pc-C_{60} dyads.

The absence of measurable ground-state electronic interactions between the two components in pseudorotaxane-like systems such as **29** was ascribed to the high flexibility of the dibenzylammonium-crown ether linkage, which can adopt several conformations within the complex as revealed by molecular modeling studies. This conformational flexibility, however, may be avoided by the use of directional hydrogen bonding interactions, which may render the donor and acceptor components in a well-defined orientation. This approach was employed for the assembly of Pc-C_{60} dyad **30**, consisting of a cytidine-substituted Zn(II)Pc and a guanosine-functionalized fulleropyrroline held together *via* Watson–Crick hydrogen bonding interactions between the nucleobases (Figure 16).³⁸

The authors derived for dyad **30** a relatively high binding constant ($2.6 \times 10^6 \text{ M}^{-1}$) from fluorescence titration studies in toluene/dichloromethane mixtures.³⁹ A complete electrochemical study of the supramolecular complex **30** and its constituents revealed significant ground-state interactions between Zn(II)Pc donor and C_{60} fullerene acceptor. For instance, the C_{60} -based reduction potentials were negatively shifted in the complex, while the first

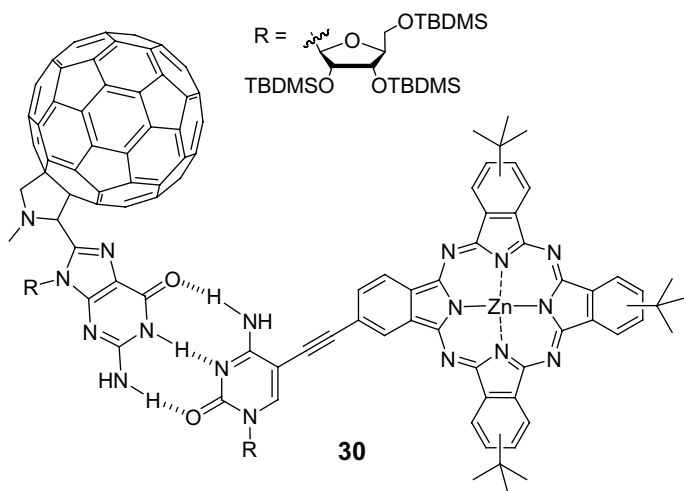


Figure 16. Molecular structure of Zn(II)Pc-C_{60} dyad **30**, assembled through Watson–Crick hydrogen bonding interactions.

and second anodic Pc-based potentials were less positive than those of the cytidine-Pc reference molecules. On the other hand, titration experiments performed by adding the guanosine- C_{60} molecule over a CH_2Cl_2 solution of the cytidine-functionalized Zn(II)Pc led to a non-linear decrease in the fluorescence intensity of the Zn(II)Pc chromophore, suggesting a photoinduced intracomplex charge separation process, which was confirmed by transient absorption experiments. However, spectroscopic and kinetic data revealed a lifetime of 3 ns for the charge-separated state of **30**, which is considerably shorter than those obtained for [2]pseudorotaxane Pc- C_{60} dyads **29b**. This was attributed to a stronger electronic coupling between the Zn(II)Pc and C_{60} moieties in the hydrogen-bonded hybrid **30**.

The possibility of incorporating different metals at the center of Pc or porphyrin macrocycles offers the unique opportunity to exploit another type of non-covalent interaction for the construction of Pc-based D-A supramolecular systems, that is, the use of metal-ligand coordination. In this context, fullerenes derivatized with appropriate ligands (*i.e.*, pyridine, imidazole) have been extensively assembled to porphyrin and Pc macrocycles bearing complementary metal centers (*i.e.*, Zn, Ru).⁴⁰ The idea of using pyridine-substituted fullerene acceptors to complex the metal center of Pcs provides a synthetic simplicity and versatility that is difficult to accomplish with covalent D-A systems. It is therefore not surprising that in recent years these strong metal-ligand interactions have been frequently employed to construct multi-component supramolecular systems.

One of the first examples reported focused on the photophysical study of a series of Zn(II)naphthalocyanine (NPc)- C_{60} systems **31a–d** (Figure 17) in which the fullerene was coordinated to the Zn atom via pyridine or phenylimidazole ligands in non-competing solvents, such as toluene and *o*-DCB.⁴¹ Photophysical studies conducted with **31a** yielded charge recombination rates of $5.3 \times 10^7 \text{ s}^{-1}$ in toluene and $9.2 \times 10^7 \text{ s}^{-1}$ in *o*-DCB. In addition, the fulleropyrrolidine component could be further functionalized with secondary electron-donating moieties, such as ferrocene or *N,N*-dimethylphenylamine, leading to supramolecular triads **31b** and **31c**, respectively (Figure 17).⁴² These secondary electron donor units, in general, assisted in prolonging the radical ion pair state lifetime.

The possibility of incorporating active units at both the peripheral and axial positions of the Pc macrocycle opens the way for the preparation of multicomponent systems. One example is supramolecular triad **32**, in which a covalently-linked, peripherally substituted boron dipyrromethene (Bodipy)-Pc conjugate has been axially coordinated to a C_{60} fullerene derivative bearing a pyridine moiety (Figure 18).⁴³ Electrochemical and electronic absorption

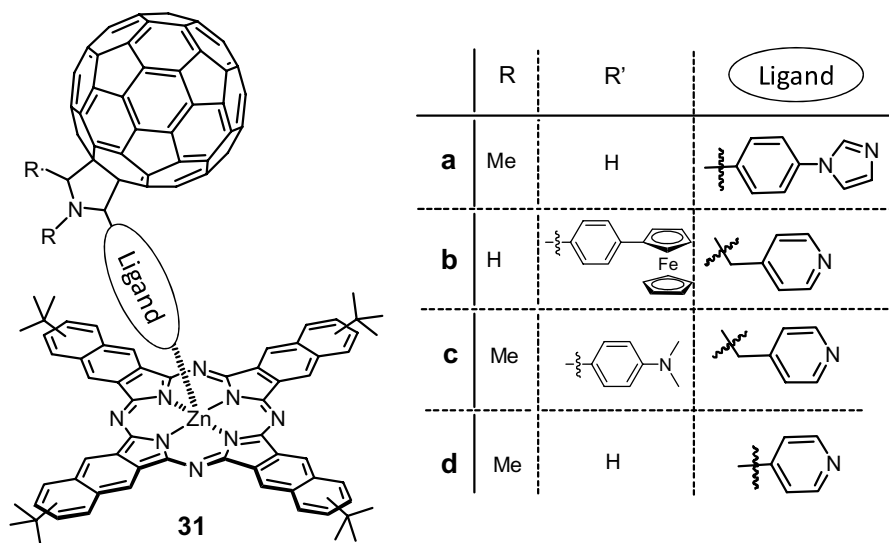


Figure 17. Structures of supramolecular Zn(II)NPC- C_{60} dyads **31a–d**.

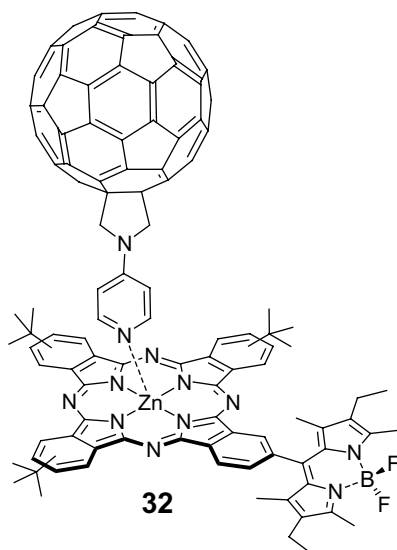


Figure 18. Structure of supramolecular Zn(II)Pc-Bodipy- C_{60} triad **32**.

measurements provided evidence for strong ground-state electronic interactions between the Bodipy and the Zn(II)Pc, which are linked through π -conjugated spacers. Steady-state fluorescence experiments showed a drastic quenching of the Zn(II)Pc emission intensity when the fullerene-derivative

was added to a solution of the Zn(II)Pc-Bodipy in toluene, suggesting that the main deactivation pathway for the photoexcited Pc moiety in **32** was a charge-transfer mechanism, as confirmed by transient absorption spectroscopy. Concretely, irradiation of this supramolecular ensemble within the visible range led to a sequence of energy and charge transfer reactions that ultimately resulted in the charge-separated Bodipy-Pc^{•+}-C₆₀^{•-} radical-ion pairs, which had a lifetime of 39.9 ns in toluene.

It is interesting to note that the substitution of Zn(II) by Ru(II) in the central cavity of MPcs allows the linkage of either one or two ligands (i.e., pyridine or imidazole derivatives) to the axial position of the macrocycle. Furthermore, the strength and stability of the Ru(II)Pc-ligand bond is considerably higher than that of the Zn(II)Pc-ligand bond and can be considered as close to a covalent interaction. Very recently, these appealing features were exploited to prepare a series of Ru(II)Pc-C₆₀ hybrids **33–35** having a linear geometry (Figure 19).⁴⁴ The synthesis of **33** and **34** was carried out by complexation of a Ru(II)Pc derivative, bearing a strongly-coordinated axial carbonyl group at one of the two axial Ru(II) coordination sites, with a *N*-(4-pyridyl)fulleropyrrolidine building block (for **33** and **35**), or a *trans*-1-bis[*N*-(4-pyridyl)fulleropyrrolidine] ligand (for **34**). On the other hand, the preparation of systems in which the Pc was functionalized at both axial Ru(II) coordination sites, such as **35**, started from a Ru(II)Pc derivative equipped with two benzonitrile molecules at the axial positions. These weakly bound ligands were subsequently replaced by the pyridine-functionalized C₆₀.

Arrays **33–35** exhibited electronic coupling between the two electroactive components in the ground state, as demonstrated by electrochemical experiments. A singular characteristic of Ru(II)Pcs is that they present a higher-lying triplet excited state than that of Zn(II)Pcs. This fact seemed to assist in suppressing unwanted charge-recombination process and the radical ion pair state lifetimes generally increase to the order of hundreds of nanoseconds for the Pc-C₆₀ supramolecular adducts (i.e., **33** and **34**). In triad **35**, the radical ion pair state energy raised due to a cathodic shift of the C₆₀ reduction potential, so the triplet excited state, localized on the Ru(II)Pc, offered a very fast deactivation of the radical ion pair state.

The chemical variability of the Pc macrocycle invites to the design and construction of more complex systems that combine diverse supramolecular interactions. Recently, Zn(II)Pc₂-(C₆₀)₂ supramolecular tetrad **36**, comprised of two crown ether-containing Zn(II)Pc units and two pyridine-containing fullerene derivatives, was reported (Figure 20).⁴⁵ In ensemble **36**, multiple cation-dipole interactions between the crown ether substituents on the two Pc rings and four potassium ions led to the formation of a cofacially stacked

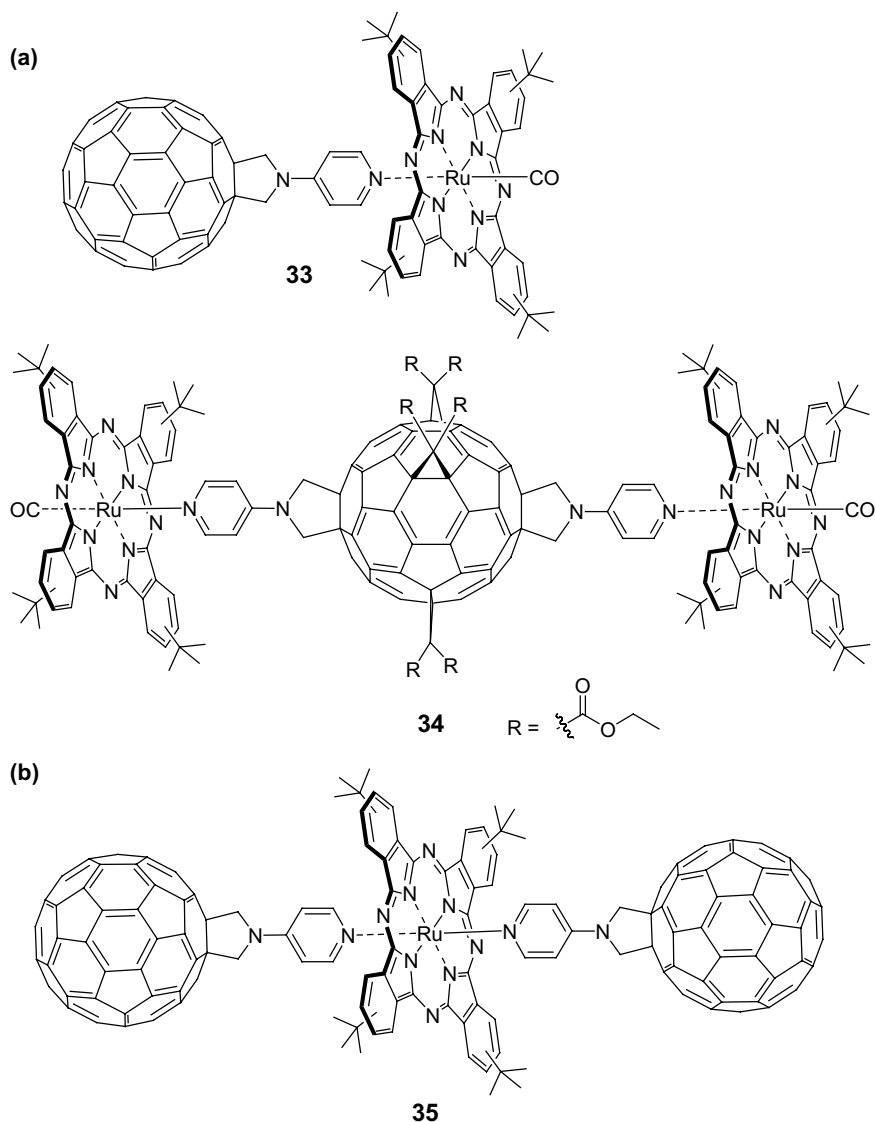


Figure 19. (a) Molecular structures of supramolecular Ru(II)Pc- C_{60} dyad **33** and Ru(II)Pc- C_{60} -Ru(II)Pc triad **34**, coordinated at a single Ru(II)Pc axial site. (b) Molecular structure of supramolecular Ru(II)Pc- $(C_{60})_2$ triad **35**, coordinated at both axial sites.

Pc-Pc dimer, which can also bind to the C_{60} acceptor molecule through Zn-pyridine interactions, as shown in Figure 20. Further stabilization of complex **36** was achieved via hydrogen-bonding interactions of the terminal alkyl ammonium moiety present on the fullerene derivative to one of the crown ether macrocycles.

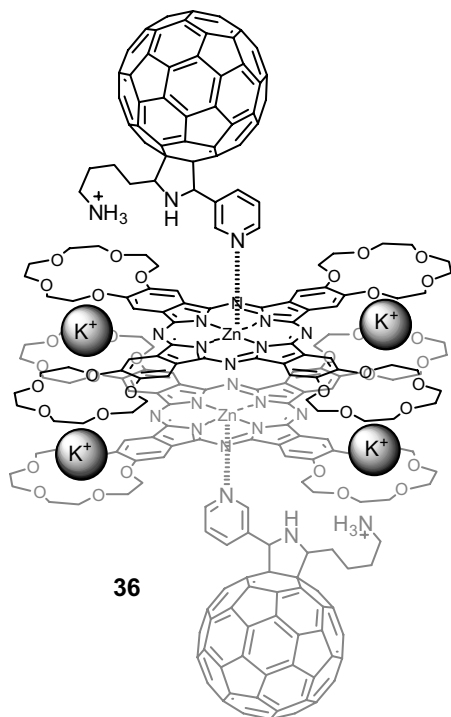
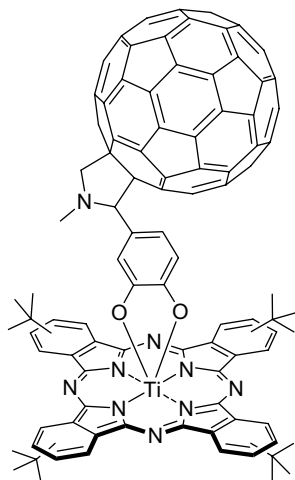


Figure 20. Molecular structure of supramolecular crown-ether Zn(II)Pc₂-(C₆₀)₂ ensemble **36**.

Interestingly, a highly long-lived charge separated state (*i.e.*, 6.7 μ s) was formed upon photoexcitation of **36**. The authors observed that this radical ion pair was formed from the triplet, rather than the singlet, excited state of the Zn(II)Pc, which was attributed to the cofacial Pc-Pc stacking present in this system.

Another kind of metal-ligand bonds that, in terms of their binding strength, can also be compared with typical covalent bonds, are the interactions of catechol with Ti(IV) centers. The use of Ti(IV)Pcs therefore provides a convenient strategy to build D-A metallasupramolecular complexes. This was independently demonstrated by the groups of Ito and Torres, who reported the synthesis of dyad **37**, a catechol-functionalized C₆₀ fullerene coordinated to a Ti-oxide Pc (Ti(IV)OPc) (Figure 21). The two groups prepared dyad **37** following different synthetic pathways. Ito's group followed a route that consisted of: i) axial coordination of 4-formylcatechol to the Ti(IV)OPc and ii) Prato reaction between the axial formyl moiety and C₆₀.⁴⁶ In contrast, the group of Torres explored a route that involved: (i) the preparation of a catechol subunit bearing a C₆₀ moiety and (ii) axial coordination of this derivative to the Ti(IV)OPc.⁴⁷



37

Figure 21. Molecular structure of Ti(IV)OPc-C₆₀ dyad **37**.

In line with most Pc-C₆₀ dyads, photophysical studies demonstrated the occurrence of an electron transfer process from the photoexcited Pc to the fullerene unit. The product was a metastable radical ion pair with lifetimes of 1740 ns and 1230 ns in THF and CH₂Cl₂, respectively. The nonlinear absorptive properties of this dyad, this way aiming at potential applications in the field of optical limiting, have also been studied using the open-aperture Z-scan technique.⁴⁸

3. Phthalocyanine-CNT Assemblies

There exist two main categories of CNTs.⁶ The first are multi-walled carbon nanotubes (MWNTs) which were the first to be discovered in the early 1990s by Iijima⁴⁹ and are made of concentric seamless graphitic cylinders placed around a common central hollow. The second type is called single-walled nanotubes (SWNTs) and their shape is close to an ideal fullerene fiber, having single-layer cylinders extending from end to end. Contrary to MWNTs the analogous SWNTs are rather well-defined systems in terms of structure, with a good uniformity in diameter, that is about 1–2 nm. Furthermore, they present easier handling for chemical manipulation, which makes them ideal targets for functionalization by organic chemistry.⁷ It should also be mentioned here that there exists the end-functionalization of oxidatively etched SWNTs.⁵⁰ Chemical modification leads in most cases to a drastic increase in solubility, which has been a major issue in recent years as CNTs in general

tend to aggregate into bundles and are sparingly soluble in common organic solvents. This way, a plethora of soluble derivatives became accessible with architectures in which the tubular CNT structure was preserved.^{7,51} Aspects of solubilization or dispersion play a crucial role when aiming at investigating the materials properties of given systems. On the other hand, relying on common organic chemistry tools, virtually any additional function can be introduced, thus tailoring or tuning the favorable CNTs materials properties becomes attainable.

The considerable interest in CNTs is closely related to their intriguing properties including electrical and thermal conductivities, chemical stability, and mechanical strength, among others. That is why many scientists and engineers worldwide have focused on such structures throughout recent years. In view of their properties, this relatively novel carbon allotrope has been proposed for applications such as *e.g.*, energy conversion,^{7b,52} sensing,⁵³ actuators,⁵⁴ or biological applications.⁵⁵ Importantly, the efforts to exploit the favorable CNT properties in energy conversion⁵² or electronic devices are fundamentally related to the ease of CNTs playing the role of an electron-acceptor and/or electron donor. A particular feature of SWNTs is that they provide continuous electronic states in their conduction band for collecting electrons from an excited donor molecule and transporting them along the nanotube axis. In recent years, carbon nanotube-based nanohybrids/-conjugates as electron donor acceptor systems have been the focus of attention.⁷⁶ Association with electron-donor or -acceptors thereby permits the modulation of the electronic properties of CNTs. Hence, the combination of SWNTs with light-harvesting/electron donor molecules, such as ferrocene,⁵⁶ tetrathiafulvalene,⁵⁷ or porphyrins⁵⁸ bears great promise for the efficient generation of photocurrent in organic solar cells.⁵⁹ Whereas the first type of nanocylindrical structures consisted of MWNTs, nowadays SWNTs are more in the center of attention in terms of scientific relevance. As for the fullerenes, in the following sections recent advances in the fields of covalent or non-covalent assemblies will be described without aiming at an exhaustive presentation of all architectures described to date and rather highlighting advances made in recent years.

3.1. Covalent phthalocyanine-carbon nanotube systems

The first example of the preparation of a Pc-containing SWNT material was reported by the groups of Torres and Blau.⁶⁰ The raw carbon material was functionalized by using the Smalley procedure⁶¹ to obtain nanotubes capped with carboxylic acid moieties at the open termini, which were then

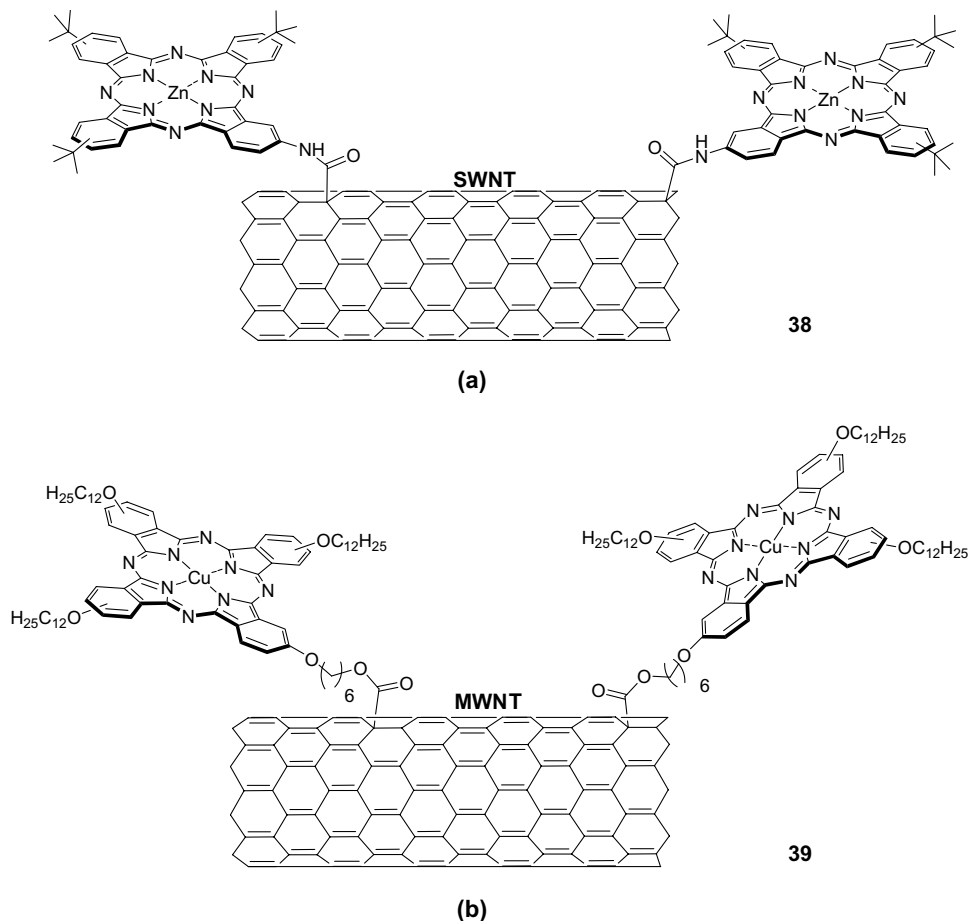


Figure 22. (a) Structure of the covalently-linked Zn(II)Pc-SWNT hybrid **38**. (b) Structure of the covalently-linked Cu(II)Pc-MWNT hybrid **39**.

transformed into the acid chloride by treatment with SOCl_2 .⁵⁰ These activated SWNTs were subsequently reacted in the presence of NEt_3 with an excess of monoaminoZn(II)Pc, to obtain hybrid system **38** with the Zn(II)Pc and the SWNT units covalently connected through amide bonds (Figure 22a). The material was characterized using UV-vis and IR spectroscopies, as well as TEM. The latter technique showed that the nanotubes were no longer aggregated into large bundles. However, the obtained Zn(II)Pc-containing nanotube material proved to be scarcely soluble for an adequate characterization by NMR spectroscopy.

More recently, a similar approach was used to prepare a hybrid free-base H_2Pc -MWNTs system which showed enhanced optical limiting properties.⁶²

Interestingly, the Pc singlet excited state emission intensity was significantly quenched in the covalently-linked MWNTs, suggesting the occurrence of photophysical interactions between both units.

Already from the very first studies it became clear that, similar to the behavior of Pc-fullerene systems, the Pc macrocycle was a good electron donor for nanotubes. For instance, Xu *et al.* managed to prepare SWNTs functionalized with octaamino-substituted Er(III) bisphthalocyaninato (Er(III)Pc₂) sandwich complexes that showed evidences of ground-state charge transfer from the Pc macrocycles to the nanotubes.⁶³ On the other hand, the photoconductivity of a covalently linked tetraaminoMn(II)Pc-MWNT hybrid material in a single-layered device was higher than that of its individual components and non-covalent mixtures, which underscored the importance of covalent bonding to enhance charge transfer between the two components.⁶⁴ These materials were also prepared by reaction of aminoPcs and end-functionalized acylchloride SWNTs.

A different approach to the construction of Pc-MWNT systems lies in the cyclotetramerization reaction of nanotube-substituted phthalonitriles. These can be prepared through reaction of carboxylic-acid-containing MWNTs with 1,6-hexanediol, and subsequent *ipso* substitution of 4-nitrophthalonitrile by the free hydroxyl group attached to the MWNTs. In the presence of a copper salt and an excess of a second phthalonitrile, soluble Cu(II)Pc-MWNT hybrid **39** was obtained (Figure 22b).⁶⁵ Despite the high number of synthetic steps performed with the nanotube material, thermogravimetric analysis led to an estimation of a 10% weight content of Cu(II)Pc within the hybrid system, which showed enhanced photoconductivity properties.

A main drawback of this kind of functionalization at the nanotube termini is that the harsh oxidation conditions employed for the generation of the acidic functions may produce as well a considerable shortening of the tubes, which could ultimately affect their properties. This can be avoided by employing sidewall covalent functionalization methods, which generally involve the use of very reactive species,^{7a,66} such as aryl radicals, aryl cations, nitrenes, carbenes or 1,3-dipoles.

The group of Torres synthesized Zn(II)Pc-SWNT associate **40** (Figure 23) *via* a 1,3-dipolar cycloaddition reaction of azomethine ylides,⁶⁷ a protocol that has been widely utilized in fullerene chemistry as described above.⁷ Two routes were followed to prepare **40**: i) a two-step approach carrying out first a 1,3-dipolar cycloaddition between an azomethine ylide (generated *in situ* by reaction of *N*-octylglycine and *p*-formylbenzoic acid) and the SWNTs, to yield an acid-derivatized nanotube, and then an esterification reaction with a hydroxymethyl-substituted Zn(II)Pc, and, ii) a more

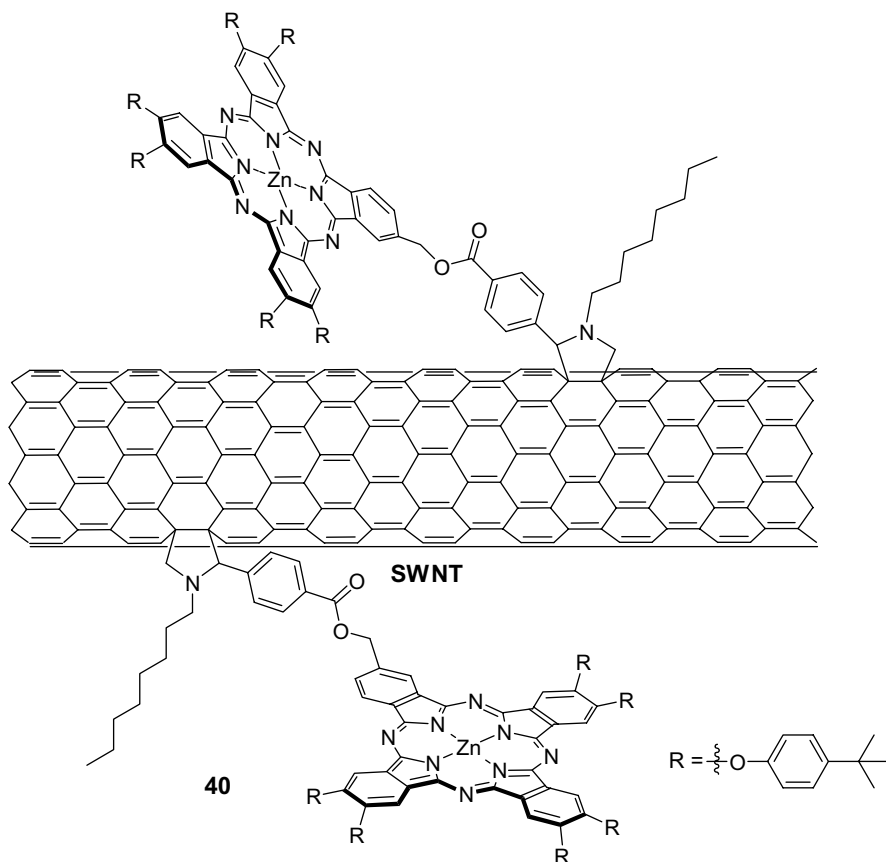


Figure 23. Structure of covalently-linked Zn(II)Pc-SWNT hybrid **40**.

direct route involving the cycloaddition reaction of *N*-octylglycine and a formyl-containing Zn(II)Pc. The combined characterization data of both materials, mainly using spectroscopic (UV-vis, IR, Raman) and microscopy (TEM) techniques, indicated the successful incorporation of the Pcs at the SWNTs walls, which preserved their electronic features to some extent. Despite the second approach being more straightforward, the degree of Pc functionalization of both SWNTs materials, as estimated by thermogravimetric analysis, was higher in the two-step route (an average of one Zn(II)Pc every 300 carbon atoms). On the other hand, photophysical experiments confirmed the occurrence of a PET process from the Zn(II)Pc to the SWNTs. For instance, steady-state fluorescence experiments in DMF solutions of **40** already showed a strong quenching of the Zn(II)Pc fluorescence in the ensemble. Transient absorption studies showed that, after

photoexciting the Zn(II)Pc core, the Pc radical cation (having a transient maximum at 840 nm) was detected together with the bleaching of the van Hove singularities seen in the ground state spectrum. The study of the kinetics of the radical ion pair product yielded a major component lifetime of *ca.* 700 ns in DMF.

An analog of **40**, having metal-free H₂Pcs and nanotubes linked through a flexible spacer was also recently prepared.⁶⁸ The photophysical studies performed on this H₂Pc-SWNT adduct revealed a similar behavior (*i.e.*, PET from the Pc to the nanotube) to that observed for the previous ensembles having a rigid bridge, which suggested that the nature of the spacer or the metal center did not have a notable effect on the photoinduced processes occurring in this type of Pc-SWNT systems.

Other methodologies have been recently employed to increase the number of functionalities covalently attached to the sidewalls of the nanotubes. In 2008, Campidelli *et al.* reported the reaction of azide-functionalized Pcs with SWNTs equipped with ethynylphenyl moieties (Figure 24),⁶⁹ which were prepared following the procedure developed by Tour and coworkers for the addition of aromatic radicals to the CNT sidewalls.⁷⁰ Key to a high yield of functionalization was the use of the Cu(I)-catalyzed, “click” 1,3-dipolar cycloaddition reaction between the azide and the acetylene functions, yielding Zn(II)Pc-SWNT **41**.

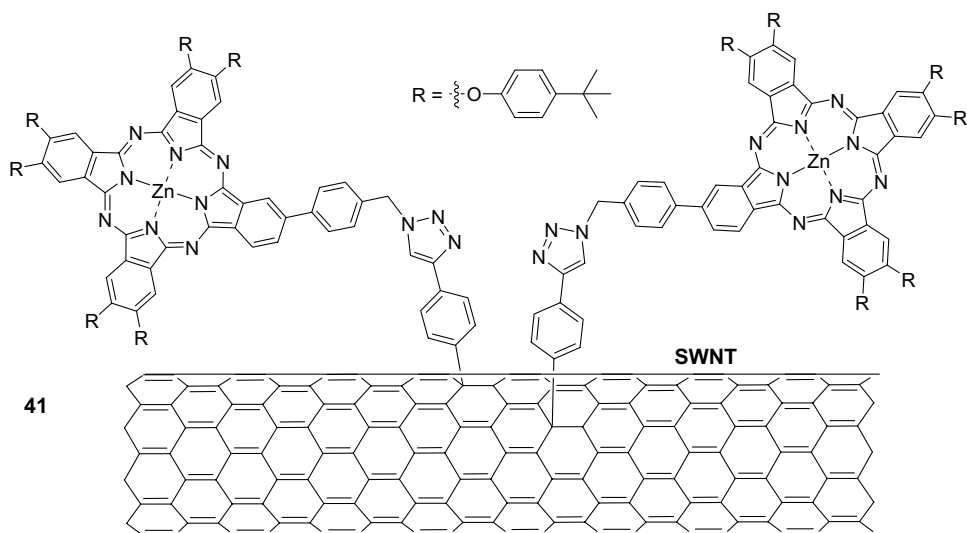


Figure 24. Structure of Zn(II)Pc-SWNT **41**, prepared by “click” Cu(I)-catalyzed reaction between azide-functionalized Zn(II)Pcs and SWNTs equipped with ethynylphenyl moieties.

The number of Pc units introduced after this “click” reaction was estimated to be one for every 165 carbon atoms, which highlights the efficiency of this approach. A photoinduced communication between the two photoactive components took place also in this case, leading to electron injection from the photoexcited Zn(II)Pc to the nanotube. In addition, the photovoltaic potential of this material has been tested by measurement of the photocurrent generated in a photoelectrochemical cell, yielding stable and reproducible monochromatic incident photon-to-current efficiency (IPCE) values as large as 17.3%.

3.2. Non-covalent phthalocyanine-carbon nanotube systems

Preserving the unique CNT properties using the non-covalent modification, while at the same time improving solubility and processability characteristics, is definitely one of the most appealing features offered by this approach. The driving force for the formation of such supramolecular assemblies lies in the favorable π - π interactions with the CNT walls as has been demonstrated for instance for elongated aromatic systems including *e.g.*, pyrene or perylene. It is this extended aromatic system also prevalent in Pc moieties that makes them susceptible to bind to CNT surfaces, hence offering a potent means for the construction of such donor-acceptor systems containing SWNTs. Though the resulting nanohybrids give rise to stable associates, one has to keep in mind that the intermolecular forces involved in the formation of such entities are mainly weaker than in the cases where covalent bonds are responsible for the conjugation.

The first report on non-covalent association of Pcs with CNTs goes back to 2002.⁷¹ Adding Pcs to a previously sonicated solution of CNTs in chloroform provided the target nanoparticles with dimensions of several to tens of nanometers as observed by TEM and AFM. In addition, the resulting dispersion showed color fading upon adsorption of the Pcs onto the CNT surface.

Likewise, nanocomposites consisting of SWNTs and Pcs assembled by non-covalent interactions have been investigated with regards to their non-linear optical behavior.⁷² A significant fluorescence quenching of Zn(II)Pcs was found for the final assemblies with SWNTs. In addition, the dispersions resulting from the mixing of the components gave rise to systems with improved optical limiting capabilities when compared to pure Zn(II)Pc-based materials.

Instead of immediate immobilization of Pcs onto the CNT surfaces, Chitta *et al.* exploited the pyrene motif for the non-covalent linkage of a Zn(II)NPc to the CNT surface.^{58b} On one hand, a Zn(II)NPc with bulky

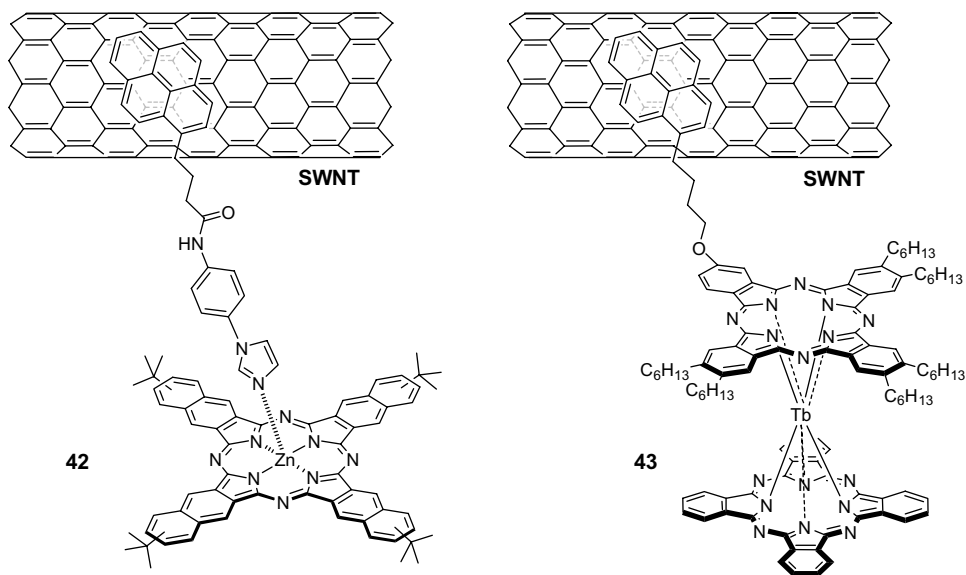


Figure 25. Supramolecular assembly of either Zn(II)NPc (**42**) or double-decker Tb(III)Pc₂-sandwich **43** onto SWNTs by exploiting the pyrene-SWNT interaction motif.

tert-butyl groups at the outer rim was prepared. On the other hand, the synthesis of a pyrene ligand which carried a phenylimidazole function that can strongly coordinate the Zn(II)NPc axial position was accomplished. Association of the pyrene ligand onto the SWNT walls gives the adduct with pendant phenylimidazole units. Upon addition of the Zn(II)NPc the final assembly has been constructed with the pyrene-appended Zn(II)NPc supramolecularly assembled onto the SWNT surface. The resulting donor-acceptor nanohybrid **42** has been assessed by various physicochemical techniques such as TEM, UV-vis and electrochemistry. These results gave evidence for PET from the excited Zn(II)NPc to the carbonaceous SWNT acceptor entity, as indicated by steady-state and time-resolved emission.

More recently, conjugate **43**/SWNT, comprised of a heteroleptic Tb(III)Pc₂ complex bearing a pyrenyl group that can be grafted onto SWNTs using π - π interactions, has been prepared and characterized by high resolution TEM, emission spectroscopy, and AFM.⁷³ An average load of one molecule of **43** per 7–8 nm of SWNT length was obtained. Investigating the magnetic properties of the final ensemble showed a temperature and frequency dependence of ac magnetic susceptibility, typical of single-molecule magnets. Interestingly, magnetization studies revealed that the single molecular magnet behavior of the supramolecular assembly was found to be improved in relation to the non-associated Tb(III)Pc₂ species.

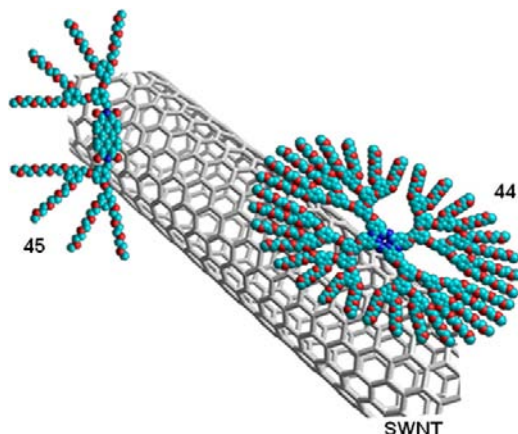


Figure 26. Water-soluble dendritic electron-donating (H_2Pc ; **44**) or electron-accepting (PDI; **45**) structures immobilized onto SWNTs.

Very recently, the groups of Torres and Guldi reported the preparation of new dispersable Pc-SWNT or perylene-SWNT nanohybrids (Figure 26).⁷⁴ The employment of dendritic structures with the hydrophobic H_2Pc (**44**) or perylene (**45**) core moieties surrounded by an increasing number of oligoethylene glycol end groups allowed for their dispersion and study in both common organic solvents and aqueous medium. Selecting either a perylenediimide and/or a H_2Pc offered the incentive of switching from an electron acceptor to an electron donor moiety as a potent means to manipulate the electronic properties of SWNTs. Due to the presence of extended aromatic systems in both H_2Pc as well as perylenediimide centerpiece of the dendrimers, these fractal structures could be successfully immobilized onto the SWNT surfaces by π - π stacking to form stable associates. The complementary use of spectroscopy and microscopy mutual interactions between semiconducting SWNT and these different series of H_2Pc -(**44**) or perylene- (**45**) derived dendrimers confirmed that distinct ground and excited state interactions prevailed and that kinetically and spectroscopically well characterized radical ion pair states were formed. Still ground state interactions were limited to π - π stacking as evidenced by Raman spectroscopy without giving rise to either *p*- or *n*-doping.

Likewise the preparation of adducts consisting of Zn(II)Pc and single-walled-carbon nanohorns (SWNHs) has been accomplished.⁷⁵ Addition of protein bovine serum albumin to the Zn(II)Pc -loaded SWNHs led to a global biocompatible structure with potential in applications such as double photodynamic therapy (PDT) and photohyperthermia (PHT) cancer phototherapy. This double phototherapy effect was confirmed *in vitro* and *in vivo*.

The construction of Pc-CNT nanostructures has also been the object of investigations for possible applications in catalysis or as sensors. These approaches were aimed at the development of hybrid materials with improved catalytic and sensing capabilities. Consequently, CNTs have been immobilized for instance onto carbon or gold electrodes thus promoting electron transfer reactions. When in addition, transition metal Pc complexes were deposited onto such electrodes, an enhanced electrocatalytic activity has been observed.⁷⁶ In these specimens, most often charged Pcs have been employed due to the increased interactions between the CNTs and the Pc units. For instance, a system has been demonstrated to show good responses for the sensing of dopamine.^{76h} In connection with improved sensing properties, also Fe(III)Pcs/MWNTs nanostructures have demonstrated their potential as a tool for the highly sensitive and selective detection of glucose.⁷⁷

Nanohybrids of tetrasulfonated Cu(II)Pcs **46** and oxidized MWNTs have also been at the center of attention (Figure 27).⁷⁸ Opposite to the usual behavior of Pcs, the affinity between the two materials was shown to result in ground-state charge-transfer from the MWNT scaffold to the Pc molecules thanks to the electron withdrawing moieties located at the Pc periphery. The dispersion obtained has then been spin-casted to fabricate uniform thin films. Spectroscopic and morphological studies evidenced that the Pc cores were stacked in columns along the MWNT scaffold, in such a way that the plane of the macrocycle was parallel to the nanotube surface (Figure 27).

MWNTs have also been blended with Ti(IV)OPcs to produce photoconductive devices.⁷⁹ Enhanced photosensitivity was observed in these devices with the composite containing 6 wt% of MWNTs to reach a 5-fold higher value with regard to undoped Ti(IV)OPc devices due to photoinduced charge transfer from the Ti(IV)OPc moiety to the MWNTs. In continuation

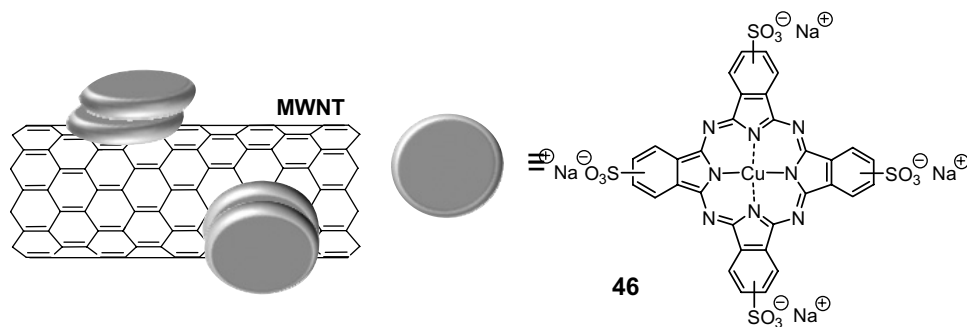


Figure 27. Schematic representation of the columnar stacking of tetrasulfonated Cu(II)Pcs **46** on MWNTs.

of their work, the same group described the MWNT-templated assembly of the reduced form of a sandwich-type Er(III) phthalocyaninate (HEr(III)Pc₂).⁸⁰ TEM images showed MWNTs enrobed with Pc nanoparticles and nanowires. Photoconductivity measurements of the hybrid material indicated again enhanced photosensitivity as a result of the formed charge transfer complex. UV-vis experiments supported this finding and showed that, when increasing the MWNTs content, a new band centered at 770 nm concomitantly raised, which was related with the oxidation of the HEr(III)Pc₂ species.

Supramolecular interactions not only play a key role in the association of molecule to the CNT exterior but have also been presented to be a crucial parameter for the encapsulation of guest molecules in the CNT interior. For instance, the construction of CNT-fullerene peapods has been accomplished. Similar to the external modification described before, such novel nanostructures are anticipated to furnish new materials with improved photophysical and (opto)electronic properties as a result of excitonic interactions between the dyes, as far as a precise control of internal stacking is achieved. In relation to the encapsulation of Pcs inside CNTs, Schulte *et al.* reported the inclusion of Co(II)Pcs inside MWNTs, which were found to show low-order symmetry rather than columnar stacking of the Pcs inside the nanotubes as revealed by near edge X-ray absorption fine structure (NEXAFS) measurements.⁸¹

4. Conclusions and Perspectives

The manipulation of the favorable electronic properties of carbon nanostructures such as fullerenes or carbon nanotubes is at the forefront of current investigations. The combination of these carbonaceous materials with phthalocyanines, that typically present strong electron donating characteristics, but can also behave as acceptor moieties, makes the tailoring of these properties attainable. The preparation in the last few years of a plethora of such multicomponent hybrid arrays, obtained either by covalent or based on supramolecular interactions has already deepened the knowledge of such systems. Likewise, these approaches have contributed significantly to the understanding of such donor-acceptor conjugates, and it is expected and anticipated that the new systems to be developed in the future will also have a tremendous impact on the processes prevalent in such systems. The particular features of the single components present in the photoactive devices have the potential to generate new materials for application in fields such as organic electronics or molecular photovoltaics, just to name a few.

Acknowledgments

We are indebted to Dirk M. Guldi for his continuous and fruitful collaboration with our group in studying the photophysical properties of a large number of phthalocyanine-carbon nanostructures prepared by us and mentioned in this chapter. This work was supported by the ESF-SOHD Program, and the EU Project ROBUST DSC, FP7-Energy-2007-1-RTD, N° 212792. Financial support by the MEC, Spain (CTQ2008-00418/BQU, CONSOLIDER-INGENIO 2010 CDS 2007-00010, PLE2009-0070, PSE-120000-2009-008 FOTOMOL), and CAM (MADRISOLAR-2, S2009/PPQ/1533), is gratefully acknowledged. U.H. thanks the Spanish MEC for a “Ramón y Cajal” contract. D.G.R. would like to acknowledge the European Union for a Marie Curie Reintegration Grant (230964-SOAFNPCM).

References

1. (a) Kadish, K. M.; Smith, K. M.; Guillard, R., Eds.; *The Porphyrin Handbook*; Vols. 15–20, Academic Press: San Diego, **2003**, (b) de la Torre, G.; Nicolau, M.; Torres, T. in *Supramolecular Photosensitive and Electroactive Materials*, Nalwa, H. S. Ed.; Academic Press: New York, **2001**, p. 1–113. (c) de la Torre, G.; Claessens, C. G.; Torres, T. *Chem. Commun.* **2007**, 2000. (d) Claessens, C. G.; Hahn, U.; Torres, T. *Chem. Rec.* **2008**, 8, 75. (e) de la Torre, G.; Bottari, G.; Hahn, U.; Torres, T. *Struct. Bond.* **2010**, 135, 1.
2. Rio, Y.; Rodríguez-Morgade, M. S.; Torres, T. *Org. Biomol. Chem.* **2008**, 6, 1877.
3. (a) Bottari, G.; de la Torre, G.; Guldi, D. M.; Torres, T. *Chem. Rev.* **2010**, DOI: 10.1021/cr900254z. (b) González-Rodríguez, D.; Bottari, G. *J. Porphyrins Phthalocyanines* **2009**, 13, 624. (c) Bottari, G.; González-Rodríguez, D.; Torres, T. in *Fullerenes and Nanotubes: Materials for the New Chemical Frontier*, Kamat, P.; Guldi, D. M.; Kadish, K., Eds.; *Proc. Electrochem. Soc., Fullerenes*, Vol. 14, pp. 282–297, ECS: Pennington, NJ, **2004**. (d) González-Rodríguez, D.; Torres, T. in *The Exciting World of Nanocages and Nanotubes*, Kamat, P.; Guldi, D. M.; Kadish, K., Eds.; *Proc. Electrochem. Soc., Fullerenes*, Vol. 12, pp. 195–210, ECS: Pennington, NJ, **2002**.
4. Delgado, J. L.; Herranz, M. A.; Martín, N. *J. Mater. Chem.* **2008**, 18, 1417.
5. (a) *Fullerenes: From Synthesis to Optoelectronic Properties*, Guldi, D. M.; Martín, N., Eds.; Kluwer Academic Publishers: Dordrecht, **2002**; (b) *The Chemistry of Fullerenes*, Hirsch, A., Ed.; Wiley-VCH: Weinheim, **2005**; (c) *Chemistry of Carbon Nanotubes*, Basiuk, V. A. Ed.; American Scientific Publishers: CA, **2006**; (d) *Fullerenes: Principles and Applications*, Langa de la Puente, F.; Nierengarten, J. F., Eds.; *RSC Nanoscience and Nanotechnology Series*: Cambridge, United Kingdom, **2007**. (e) Martín, N. *Chem. Commun.* **2006**, 2093.
6. (a) Harris, P. J. F. *Carbon Nanotube Science: Synthesis, properties and applications*, Cambridge University Press: Cambridge, **2009**. (b) Reich, S.; Thomsen, C.; Maultzsch, J. *Carbon Nanotubes: Basic Concepts and Physical Properties*, Wiley-VCH: Weinheim, **2004**. (c) *Carbon Nanotubes: Advanced Topics in the Synthesis, Structure, Properties and Applications*, Jorio, A.; Dresselhaus, G.; Dresselhaus, M. S., Eds.; Springer: Berlin, **2008**.

7. (a) Tasis, D.; Tagmatarchis, N.; Bianco, A.; Prato, M. *Chem. Rev.* **2006**, *106*, 1105. (b) Guldi, D. M.; Rahman, G. M. A.; Zerbetto, F.; Prato, M. *Acc. Chem. Res.* **2005**, *38*, 871. (c) Banerjee, S.; Hemraj-Benny, T.; Wong, S. S. *Adv. Mater.* **2005**, *17*, 17. (d) Tasis, D.; Tagmatarchis, N.; Georgakilas, V.; Prato, M. *Chem.-Eur. J.* **2003**, *9*, 4000. (e) Banerjee, S.; Kahn, M. G. C.; Wong, S. S. *Chem.-Eur. J.* **2003**, *9*, 1898. (f) Special issue on carbon nanotubes: *Acc. Chem. Res.* **2002**, *35*, 997.
8. Guldi, D. M.; Rahman, G. M. A.; Sgobba, V.; Ehli, C. *Chem. Soc. Rev.* **2006**, *35*, 471.
9. Bingel, C. *Chem. Ber.* **1993**, *126*, 1957.
10. Prato, M.; Maggini, M. *Acc. Chem. Res.* **1998**, *31*, 519.
11. (a) Linssen, T. G.; Dürr, K.; Hanack, M.; Hirsch, A. *J. Chem. Soc., Chem. Commun.* **1995**, 103. (b) Dürr, K.; Fiedler, S.; Linssen, T.; Hirsch, A.; Hanack, M. *Chem. Ber.* **1997**, *130*, 1375.
12. (a) Tian, Z.; He, C.; Liu, C.; Yang, W.; Yao, J.; Nie, Y.; Gong, Q.; Liu, Y. *Mater. Chem. Phys.* **2005**, *94*, 444. (b) Zhu, P.; Wang, P.; Qiu, W.; Liu, Y.; Ye, C.; Fang, G.; Song, Y. *Appl. Phys. Lett.* **2001**, *78*, 1319. (c) Huang, W.; Wang, S.; Liang, R.; Gong, Q.; Qiu, W.; Liu, Y.; Zhu, D. *Chem. Phys. Lett.* **2000**, *324*, 354.
13. (a) Isosomppi, M.; Tkachenko, N. V.; Efimov, A.; Vahasalo, H.; Jukola, J.; Vainiotalo, P.; Lemmetyinen, H. *Chem. Phys. Lett.* **2006**, *430*, 36. (b) Niemi, M.; Tkachenko, N. V.; Efimov, A.; Lehtivuori, H.; Ohkubo, K.; Fukuzumi, S.; Lemmetyinen, H. *J. Phys. Chem. A* **2008**, *112*, 6884.
14. (a) Lehtivuori, H.; Kumpulainen, T.; Efimov, A.; Lemmetyinen, H.; Kira, A.; Imahori, H.; Tkachenko, N. V. *J. Phys. Chem. C* **2008**, *112*, 9896. (b) Lehtivuori, H.; Kumpulainen, T.; Hietala, M.; Efimov, A.; Lemmetyinen, H.; Kira, A.; Imahori, H.; Tkachenko, N. V. *J. Phys. Chem. C* **2009**, *113*, 1984.
15. Kim, K. N.; Choi, C. S.; Kay, K.-Y. *Tetrahedron Lett.* **2005**, *46*, 6791.
16. El-Khouly, M. E.; Kang, E. S.; Kay, K.-Y.; Choi, C. S.; Aaraki, Y.; Ito, O. *Chem.-Eur. J.* **2007**, *13*, 2854.
17. (a) Maya, E. M.; Vázquez, P.; Torres, T. *Chem. Commun.* **1997**, 1175. (b) Ali, H.; van Lier, J. E. *Tetrahedron Lett.* **1997**, *38*, 1157.
18. Martínez-Díaz, M. V.; Quintiliani, M.; Torres, T. *Synlett* **2008**, 1.
19. Guldi, D. M.; Gouloumis, A.; Vázquez, P.; Torres, T.; Georgakilas, V.; Prato, M. *J. Am. Chem. Soc.* **2005**, *127*, 5811.
20. Quintiliani, M.; Kahnt, A.; Wölflé, T.; Hieringer, W.; Vázquez, P.; Görling, A.; Guldi, D. M.; Torres, T. *Chem.-Eur. J.* **2008**, *14*, 3765.
21. Bottari, G.; Olea, D.; Gómez-Navarro, C.; Zamora, F.; Gómez-Herrero, J.; Torres, T. *Angew. Chem. Int. Ed.* **2008**, *47*, 2026.
22. de la Escosura, A.; Martínez-Díaz, M. V.; Guldi, D. M.; Torres, T. *J. Am. Chem. Soc.* **2006**, *128*, 4112.
23. de la Escosura, A.; Martínez-Díaz, M. V.; Barberá, J.; Torres, T. *J. Org. Chem.* **2008**, *73*, 1475.
24. Ballesteros, B.; de la Torre, G.; Shearer, A.; Hausmann, A.; Herranz, M. Á.; Guldi, D. M.; Torres, T. *Chem.-Eur. J.* **2010**, *16*, 114.
25. Pinzon, J. R.; Cardona, C. M.; Herranz, M. A.; Plonska-Brzezinska, M. E.; Palkar, A.; Athans, A. J.; Martín, N.; Rodríguez-Forteza, A.; Poblet, J. M.; Bottari, G.; Torres, T.; Gayathri, S. S.; Guldi, D. M.; Echegoyen, L. *Chem.-Eur. J.* **2009**, *15*, 864.

26. Chaur, M. N.; Melin, F.; Ortiz, A. L.; Echegoyen, L. *Angew. Chem. Int. Ed.* **2009**, *48*, 7514.
27. Gouloumis, A.; de la Escosura, A.; Vázquez, P.; Torres, T.; Kahnt, A.; Guldi, D. M.; Neugebauer, H.; Winder, C.; Drees, M.; Sariciftci, N. S. *Org. Lett.* **2006**, *8*, 5187.
28. Kahnt, A.; Quintiliani, M.; Vázquez, P.; Guldi, D. M.; Torres, T. *ChemSusChem* **2008**, *1*, 97.
29. Quintiliani, M.; Kahnt, A.; Vázquez, P.; Guldi, D. M.; Torres, T. *J. Mater. Chem.* **2008**, *18*, 1542.
30. Quintiliani, M.; Pérez-Moreno, J.; Asselberghs, I.; Vázquez, P.; Clays, K.; Torres, T.; *J. Phys. Chem. B* **2010**, *114*, 6309.
31. Martín-Gomis, L.; Ohkubo, K.; Fernández-Lazaro, F.; Fukuzumi, S.; Sastre-Santos, A. *Org. Lett.* **2007**, *9*, 3441.
32. El-Khouly, M. E.; Kim, J. H.; Kay, K.-Y.; Choi, C. S.; Ito, O.; Fukuzumi, S. *Chem.-Eur. J.* **2009**, *15*, 5301.
33. de la Escosura, A.; Martínez-Díaz, M. V.; Torres, T.; Grubbs, R. H.; Guldi, D. M.; Neugebauer, H.; Winder, C.; Drees, M.; Sariciftci, N. S. *Chem. -Asian J.* **2006**, *1*, 148.
34. Sastre, A.; Gouloumis, A.; Vázquez, P.; Torres, T.; Doan, V.; Schwartz, B. J.; Wudl, F.; Echegoyen, L.; Rivera, J. *Org. Lett.* **1999**, *1*, 1807.
35. Geerts, Y. H.; Debever, O.; Amato, C.; Sergeyev, S. *Beilstein J. Org. Chem.* **2009**, *5*, No. 49, DOI:10.3762/bjoc.5.49.
36. Martínez-Díaz, M. V.; Fender, N. S.; Rodríguez-Morgade, M. S.; Gomez-Lopez, M.; Diederich, F.; Echegoyen, L.; Stoddart, J. F.; Torres, T. *J. Mater. Chem.* **2002**, *12*, 2095.
37. Guldi, D. M.; Ramey, J.; Martínez-Díaz, M. V.; de la Escosura, A.; Torres, T.; Da Ros, T.; Prato, M. *Chem. Commun.* **2002**, 2774.
38. Sessler, J. L.; Jayawickramarajah, J.; Gouloumis, A.; Pantos, G. D.; Torres, T.; Guldi, D. M. *Tetrahedron* **2006**, *62*, 2123.
39. Torres, T.; Gouloumis, A.; Sánchez-García, D.; Jayawickramarajah, J.; Seitz, W.; Guldi, D. M.; Sessler, J. L. *Chem. Commun.* **2007**, 292.
40. (a) D'Souza, F.; Rath, N. P.; Deviprasad, G. R.; Zandler, M. E. *Chem. Commun.* **2001**, 267. (b) Hauke, F.; Swartz, A.; Guldi, D. M.; Hirsch, A. *J. Mater. Chem.* **2002**, *12*, 2088.
41. El-Khouly, M. E.; Rogers, L. M.; Zandler, M. E.; Suresh, G.; Fujitsuka, M.; Ito, O.; D'Souza, F. *ChemPhysChem* **2003**, *4*, 474.
42. El-Khouly, M. E.; Araki, Y.; Ito, O.; Gadde, S.; Zandler, M. E.; D'Souza, F. *J. Porphyrins Phthalocyanines* **2006**, *10*, 1156.
43. Rio, Y.; Seitz, W.; Gouloumis, A.; Vázquez, P.; Sessler, J. L.; Guldi, D. M.; Torres, T. *Chem.-Eur. J.* **2010**, *16*, 1929.
44. Rodríguez-Morgade, M. S.; Plonska-Brzezinska, M. E.; Athans, A. J.; Carbonell, E.; de Miguel, G.; Guldi, D. M.; Echegoyen, L.; Torres, T. *J. Am. Chem. Soc.* **2009**, *131*, 10484.
45. D'Souza, F.; Maligaspe, E.; Ohkubo, K.; Zandler, M. E.; Subbaiyan, N. K.; Fukuzumi, S. *J. Am. Chem. Soc.* **2009**, *131*, 8787.
46. Chen, Y.; El-Khouly, M. E.; Sasaki, M.; Araki, Y.; Ito, O. *Org. Lett.* **2005**, *7*, 1613.
47. Ballesteros, B.; de la Torre, G.; Torres, T.; Hug, G. L.; Rahman, G. M. A.; Guldi, D. M. *Tetrahedron* **2006**, *62*, 2097.
48. Doyle, J. J.; Ballesteros, B.; de la Torre, G.; McGovern, D. A.; Kelly, J. M.; Torres, T.; Blau, W. J. *Chem. Phys. Lett.* **2006**, *428*, 307.
49. Iijima, S. *Nature* **1991**, *354*, 56.

50. (a) Chen, J.; Rao, A. M.; Lyuksyutov, S.; Itkis, M. E.; Hamon, M. A.; Hu, H.; Cohn, R. W.; Eklund, P. C.; Colbert, D. T.; Smalley, R. E.; Haddon, R. C. *J. Phys. Chem. B* **2001**, *105*, 2525. (b) Chen, J.; Hamon, M. A.; Hu, H.; Chen, Y.; Rao, A. M.; Eklund, P. C.; Haddon, R. C. *Science* **1998**, *282*, 95.
51. (a) Balasubramanian, K.; Burghard, M. *Small* **2005**, *1*, 180. (b) Sun, Y.-P.; Fu, K.; Lin, Y.; Huang, W. *Acc. Chem. Res.* **2002**, *35*, 1096.
52. (a) Fischer, J. E. *Acc. Chem. Res.* **2002**, *35*, 1079. (b) Rahman, G. M. A.; Guldi, D. M.; Cagnoli, R.; Mucci, A.; Schenetti, L.; Vaccari, L.; Prato, M. *J. Am. Chem. Soc.* **2005**, *127*, 10051. (c) Umeyama, T.; Imahori, H. *Energy Environ. Sci.* **2008**, *1*, 120. (d) Guldi, D. M.; Rahman, G. M. A.; Sgobba, V.; Kotov, N. A.; Bonifazi, D.; Prato, M. *J. Am. Chem. Soc.* **2006**, *128*, 2315. (e) Rolison, D. R.; Long, R. W.; Lytle, J. C.; Fischer, A. E.; Rhodes, C. P.; McEvoy, T. M.; Bourga, M. E.; Lubers, A. M. *Chem. Soc. Rev.* **2009**, *38*, 226.
53. (a) Kauffman, D. R.; Star, A. *Angew. Chem., Int. Ed.* **2008**, *47*, 6550. (b) Ahammad, A. J. S.; Lee, J. J.; Rahman, M. A. *Sensors* **2009**, *9*, 2289. (c) Vichchulada, P.; Lipscomb, L. D.; Zhang, Q. H.; Lay, M. D. *J. Nanosci. Nanotechnol.* **2009**, *9*, 2189.
54. (a) Mirfakhrai, T.; Madden, J. D. W.; Baughman, R. H. *Mater. Today* **2007**, *10*, 30. (b) Aliev, A. E.; Oh, J.; Kozlov, M. E.; Kuznetsov, A. A.; Fang, S.; Fonseca, A. F.; Ovalle, R.; Lima, M. D.; Haque, M. H.; Gartstein, Y. N.; Zhang, M.; Zakhidov, A. A.; Baughman, R. H. *Science* **2009**, *323*, 1575. (c) Ahir, S. V.; Terentjev, E. M. *Nat. Mater.* **2005**, *4*, 491. (d) Koerner, H.; Price, G.; Pearce, N. A.; Alexander, M.; Vaia, R. A. *Nat. Mater.* **2004**, *3*, 115. (e) Miaudet, P.; Derré, A.; Maugey, M.; Zakri, C.; Piccione, P. M.; Inoubli, R.; Poulin, P. *Science* **2007**, *318*, 1294.
55. (a) Tran, P. A.; Zhang, L. J.; Webster, T. J. *Adv. Drug Deliv. Rev.* **2009**, *61*, 1097. (b) Saito, N.; Usui, Y.; Aoki, K.; Narita, N.; Shimizu, M.; Hara, K.; Ogiwara, N.; Nakamura, K.; Ishigaki, N.; Kato, H.; Taruta, S.; Endo, M. *Chem. Soc. Rev.* **2009**, *38*, 1897. (c) Prato, M.; Kostarelos, K.; Bianco, A. *Acc. Chem. Res.* **2008**, *41*, 60. (d) Kam, N. W. S.; O'Connell, M.; Wisdom, J. A.; Dai, H. *Proc. Natl. Acad. Sci. U.S.A.* **2005**, *102*, 11600.
56. (a) Yang, X.; Lu, Y.; Ma, Y.; Li, Y.; Du, F.; Chen, Y. *Chem. Phys. Lett.* **2006**, *420*, 416. (b) Guldi, D. M.; Marcaccio, M.; Paolucci, D.; Paolucci, F.; Tagmatarchis, N.; Tasis, D.; Vázquez, E.; Prato, M. *Angew. Chem., Int. Ed.* **2003**, *42*, 4206.
57. (a) Herranz, M. A.; Ehli, C.; Campidelli, S.; Gutierrez, M.; Hug, G. L.; Ohkubo, K.; Fukuzumi, S.; Prato, M.; Martín, N.; Guldi, D. M. *J. Am. Chem. Soc.* **2008**, *130*, 66. (b) Herranz, M. A.; Martín, N.; Campidelli, S.; Prato, M.; Brehm, G.; Guldi, D. M. *Angew. Chem., Int. Ed.* **2006**, *45*, 4478.
58. (a) Yu, J.; Mathew, S.; Flavel, B. S.; Johnston, M. R.; Shapter, J. G. *J. Am. Chem. Soc.* **2008**, *130*, 8788. (b) Chitta, R.; Sandanayaka, A. S. D.; Schumacher, A. L.; D'Souza, L.; Araki, Y.; Ito, O.; D'Souza, F. *J. Phys. Chem. C* **2007**, *111*, 6947. (c) Alvaro, M.; Atienzar, P.; de la Cruz, P.; Delgado, J. L.; Troiani, V.; García, H.; Langa, F.; Palkar, A.; Echegoyen, L. *J. Am. Chem. Soc.* **2006**, *128*, 6626. (d) Ehli, C.; Rahman, G. M. A.; Jux, N.; Balbinot, D.; Guldi, D. M.; Paolucci, F.; Marcaccio, M.; Paolucci, D.; Melle-Franco, M.; Zerbetto, F.; Campidelli, S.; Prato, M. *J. Am. Chem. Soc.* **2006**, *128*, 11222. (e) Guldi, D. M.; Rahman, G. M. A.; Jux, N.; Tagmatarchis, N.; Prato, M. *Angew. Chem., Int. Ed.* **2004**, *43*, 5526.
59. (a) Sgobba, V.; Rahman, G. M. A.; Guldi, D. M.; Jux, N.; Campidelli, S.; Prato, M. *Adv. Mater.* **2006**, *18*, 2264. (b) Hasobe, T.; Fukuzumi, S.; Kamat, P. V. *J. Phys. Chem. B*

- 2006, 110, 25477. (c) Guldi, D. M.; Rahman, G. M. A.; Prato, M.; Jux, N.; Qin, S.; Ford, W. *Angew. Chem. Int. Ed.* **2005**, 44, 2015.
60. de la Torre, G.; Blau, W.; Torres, T. *Nanotechnology* **2003**, 14, 765.
61. Liu, J.; Rinzler, A. G.; Dai, H.; Hafner, J. H.; Bradley, R. K.; Boul, P. J.; Lu, A.; Iverson, T.; Shelimov, K.; Huffman, C. B.; Rodríguez-Macias, F.; Shon, Y. S.; Lee, T.; Colbert, D. T.; Smalley, R. E. *Science* **1998**, 280, 1253.
62. He, N.; Chen, Y.; Bai, J.; Wang, J.; Blau, W. J.; Zhu, J. *J. Phys. Chem. B* **2009**, 113, 13029.
63. Xu, H. B.; Chen, H. Z.; Shi, M. M.; Bai, R.; Wang, M. *Mater. Chem. Phys.* **2005**, 94, 342.
64. Yang, Z.-L.; Chen, H.-Z.; Cao, L.; Li, H.-Y.; Wang M. *Mater. Sci. Eng. B* **2004**, 106, 73.
65. Yang, Z.; Pu, H.; Yuan, J.; Wan, D.; Liu, Y. *Chem. Phys. Lett.* **2008**, 465, 73.
66. Dyke, C.A.; Tour, J. M. *J. Phys. Chem. A* **2004**, 51, 11151.
67. Ballesteros, B.; de la Torre, G.; Ehli, C.; Rahman, G. M. A.; Agulló-Rueda, F.; Guldi, D. M.; Torres, T. *J. Am. Chem. Soc.* **2007**, 129, 5061.
68. Ballesteros, B.; Campidelli, S.; de la Torre, G.; Ehli, C.; Guldi, D. M.; Prato, M.; Torres, T. *Chem. Commun.* **2007**, 2950.
69. Campidelli, S.; Ballesteros, B.; Filoramo, A.; Díaz Díaz, D.; de la Torre, G.; Torres, T.; Rahman, G. M. A.; Ehli, C.; Kiessling, D.; Werner, F.; Sgobba, V.; Guldi, D. M.; Cioffi, C.; Prato, M.; Bourgoign, J. P. *J. Am. Chem. Soc.* **2008**, 130, 11503.
70. Bahr, J.; Tour, J. M. *Chem. Mater.* **2001**, 13, 3823.
71. Wang, B. X.; Liu, Y. Q.; Qiu, W. F.; Zhu, D. B. *J. Mater. Chem.* **2002**, 12, 1636.
72. Wang, J.; Blau, W. J. *Chem. Phys. Lett.* **2008**, 465, 265.
73. Kyatskaya, S.; Mascaros, J. R. G.; Bogani, L.; Hennrich, F.; Kappes, M.; Wernsdorfer, W.; Ruben, M. *J. Am. Chem. Soc.* **2009**, 131, 15143.
74. Hahn, U.; Engmann, S.; Oelsner, C.; Ehli, C.; Guldi, D. M.; Torres, T. *J. Am. Chem. Soc.* **2010**, 132, 6392.
75. Zhang, M.; Murakami, T.; Ajima, K.; Tsuchida, K.; Sandanayaka, A. S. D.; Ito, O.; Iijima, S.; Yudasaka, M. *Proc. Natl. Acad. Sci. U.S.A.* **2008**, 105, 14773.
76. (a) Ozoemena, K. I.; Nyokong, T.; Westbroek, P. *Electroanal.* **2003**, 15, 1762. (b) Siswana, M. P.; Ozoemena, K. I.; Nyokong, T. *Electrochim. Acta* **2006**, 52, 114. (c) Silva, J. F.; Griveau, S.; Richard, C.; Zagal, J. H.; Bedioui, F. *Electrochem. Commun.* **2007**, 9, 1629. (d) Geraldo, D. A.; Chamunorwa, A. T.; Limson, J.; Nyokong, T. *Electrochim. Acta* **2006**, 53, 8051. (e) Porras-Gutierrez, A. G.; Gutierrez-Granados, S.; Alatorre-Ordaz, A.; Griveau, S.; Richard, C.; Zagal, J. H.; Bedioui, F. *ECS Transactions* **2008**, 15, 133. (f) Moraes, F. C.; Cabral, M. F.; Machado, S.A. S.; Mascaró, L. H. *Electroanal.* **2008**, 20, 851. (g) Zagal, J. H.; Griveau, S.; Ozoemena, K. I.; Nyokong, T.; Bedioui, F. *J. Nanosci. Nanotech.* **2009**, 9, 2201. (h) Ozoemena, K. I.; Nyokong, T.; Nkosi, D.; Chambrier, I.; Cook, M. J. *Electrochim. Acta* **2007**, 52, 4132. (i) Siqueira, J. R., Jr.; Gasparotto, L. H. S.; Oliveira, O. N., Jr.; Zucolotto, V. *J. Phys. Chem. C* **2008**, 112, 9050.
77. Ye, J.-S.; Wen, Y.; Zhang, W. D.; Cui, H. F.; Xu, G. Q.; Sheu, F.-S. *Electroanal.* **2005**, 17, 89.
78. Hatton, R. A.; Blanchard N. P.; Stolojan, V.; Miller, A. J.; Silva, S. R. P. *Langmuir* **2007**, 23, 6424.
79. Cao, L.; Chen, H.; Wang, M.; Sun, J.; Zhang, X.; Kong, F. *J. Phys. Chem. B* **2002**, 106, 8971.

80. Cao, L.; Chen, H.-Z.; Zhou, H.-B.; Zhu, L.; Sun, J.-Z.; Zhang, X.-B.; Xu, J. M.; Wang, M.; *Adv. Mater.* **2003**, *15*, 909.
81. Schulte, K.; Swarbrick, J. C.; Smith, N. A.; Bondino, F.; Magnano, E.; Khlobystov, A. N. *Adv. Mater.* **2007**, *19*, 3312.

This page intentionally left blank

Chapter 4

Perfluoroalkylation of Fullerenes

Olga V. Boltalina, Igor V. Kuvrychko, Natalia B. Shustova
and Steven H. Strauss**

Colorado State University, Fort Collins, USA

1. Methods of Synthesis	102
1.1. General remarks	102
1.2. <i>In situ</i> formation of PFAFs in an arc generator or mass spectrometer	103
1.3. Synthesis of PFAFs: reactions with metal trifluoroacetates	105
1.4. Synthesis of PFAFs: reactions with perfluoroalkyl iodides	107
1.4.1. Reactions with CF_3I	108
1.4.2. Reactions with $\text{R}_\text{F}\text{I}$ ($\text{R}_\text{F} = \text{C}_2\text{F}_5, \text{C}_3\text{F}_7, \text{C}_4\text{F}_9, \text{C}_6\text{F}_{13},$ and $\text{C}_{12}\text{F}_{25}$)	112
2. Methods of Isolation and Characterization	115
2.1. Selective syntheses of PFAFs	115
2.2. Purification methods	119
2.3. Characterization	123
2.3.1. Mass spectrometry	123
2.3.2. Vibrational and UV-vis spectroscopy	125
2.3.3. NMR spectroscopy	127
2.3.4. X-ray crystallography	128
3. Physical Properties	134
4. Electrochemical Properties	135

*Corresponding authors. Email: olga.boltalina@colostate.edu; steven.strauss@colostate.edu

5. Chemical Properties	137
6. Conclusions and Perspectives	139
References	139

1. Methods of Synthesis

1.1. General remarks

One of the important properties of fullerenes is their ability to scavenge free radicals.¹ It is therefore not surprising that radical species $C_{60}R_F$, where $R_F = n-C_6F_{13}$ and C_2F_5 , were detected as intermediates in reactions of C_{60} with R_FI in solution.² All reported successful preparations of perfluoroalkylfullerenes (PFAFs) have been achieved by reacting a fullerene with a perfluoroalkyl (R_F) radical precursor. The latter include perfluoroalkyl iodides (R_FI),² perfluorodiacyl peroxides ($(C_3F_7CO_2)_2$ ³ and $(C_2F_5CO_2)_2$),² and metal trifluoroacetates ($M(O_2CCF_3)_n$).⁴ These compounds generate highly reactive R_F radicals under UV or thermal activation. Fullerene perfluoroalkylation has been carried out under a wide variety of experimental conditions (*e.g.*, the nature of the R_F radical precursor, temperature, pressure, reaction medium, and reaction time). Nevertheless, the formation of PFAFs can be divided into several common steps. Figure 1 depicts the main processes that are likely to occur during the high-temperature trifluoromethylation of solid C_{60} using CF_3I gas, but it can be generalized to other fullerenes and other R_FI reagents. It includes the following steps, which may occur simultaneously or consecutively: (i) fullerene sublimation; (ii) trifluoromethylation of fullerene molecules on the surface of the solid fullerene; (iii) sublimation of trifluoromethylfullerenes (TMFs); (iv) trifluoromethylation of fullerene molecules and of TMFs in the gas phase; and (v) condensation of fullerene molecules and TMFs on colder parts of the apparatus.

The use of schemes such as Figure 1 can facilitate the analysis and interpretation of experimental results and can help predict the effects of changing the reaction conditions on the percent conversion of the fullerene substrate and the yields of particular PFAF compositions. For example, a scheme similar to Figure 1 provided the guidance that led to a novel reactor design and the choice of a particular set of reaction parameters that resulted in the large-scale *selective* preparation of a single isomer of $C_{60}(CF_3)_2$ and two isomers each of $C_{60}(CF_3)_4$ and $C_{60}(CF_3)_6$.⁵

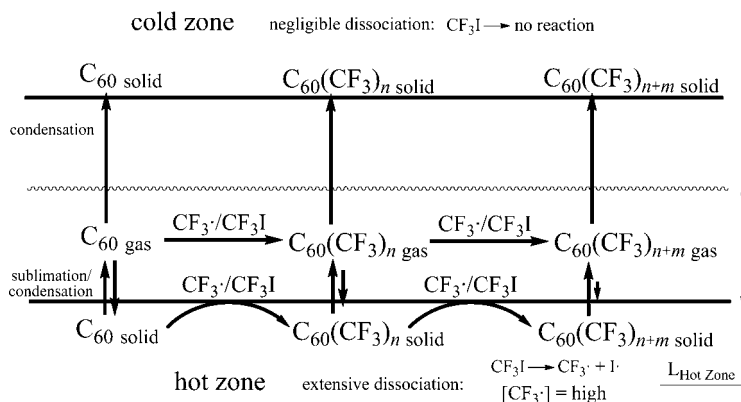


Figure 1. Proposed scheme showing the essential steps in the heterogeneous high-temperature trifluoromethylation of solid C_{60} with CF_3I gas. The subscripts n and m represent even integers.

1.2. *In situ* formation of PFAFs in an arc generator or mass spectrometer

We will first discuss two examples of fullerene perfluoroalkylation that did not result in the isolation of appreciable amounts of PFAFs but were important steps for further development of the field. Interestingly, both were originally designed with the goal of obtaining fluorinated fullerenes (*i.e.*, fullerene(F) $_n$ derivatives). Instead, trifluoromethylated derivatives of fullerenes were unexpectedly formed. In the first study, the idea was to use polytetrafluoroethylene as a source of fluorine atoms for *in situ* fluorination in the fullerene arc generator.⁶ Electron-ionization (EI) mass spectral analysis of the material that was solvent-extracted from the soot resulted in the identification of molecular species with CF_3 groups and H atoms attached to the fullerene (the general formula was $\text{C}_{60}(\text{CF}_3)_n\text{H}_m$). The experiment was repeated with the use of sodium trifluoroacetate as a chemical dopant in the graphite rods in order to boost the concentration of CF_3 radicals. In this case the relative yield of TMFs was slightly higher, thereby confirming the authors' preliminary conclusions about the presence of TMFs in the soot extracts. In addition, species with compositions such as $\text{C}_{70}(\text{CF}_3)_n\text{H}_m$ and $\text{C}_{60}(\text{CF}_3)_n(\text{C}_2\text{F}_5)_k\text{H}_m$ were identified in the mass spectra of the products. This work demonstrated the following: (i) TMFs are thermally robust molecules (*i.e.*, they withstood the high temperature of the arc process); (ii) partial hydrogenation can occur, probably due to the abstraction of H atoms from adventitious moisture; and

(iii) *in situ* synthesis of TMFs in the arc fullerene generator is inefficient, since the soot contained only *ca.* 0.1% by weight TMFs.

The second example was part of an investigation of fullerene fluorination by metal fluorides.⁷⁻⁹ During the HPLC isolation of the numerous minor reaction products, it was discovered that partially trifluoromethylated fluorinated fullerene molecules also formed in the high-temperature fluorination processes. Their formation was rationalized as follows: high temperatures caused partial fragmentation of fluorofullerenes, accompanied by cage rupture, which led to the generation of metastable CF_3 radicals, which attached to other, intact, fullerene molecules, either by replacing F atoms or by adding to already formed fluorofullerenes. Two isomers of $\text{C}_{60}\text{F}_{17}(\text{CF}_3)$ were isolated and characterized by ^{19}F NMR spectroscopy and X-ray crystallography.⁸ A subsequent variable-temperature ^{19}F NMR study of C_s - and C_1 - $\text{C}_{60}\text{F}_{17}(\text{CF}_3)$ and of 1,9- $\text{C}_{60}\text{F}(\text{CF}_3)$ provided rare examples of CF_3 hindered rotation (at the time there were only *ca.* 30 examples in the entire chemical literature).¹⁰ Figure 2 shows the DFT-predicted structure of 1,9- $\text{C}_{60}\text{F}(\text{CF}_3)$ and the X-ray diffraction-determined structures of C_s - and C_1 - $\text{C}_{60}\text{F}_{17}\text{CF}_3$. In all three cases the molecule possesses at least one $\text{C}(sp^3)\text{-F}$ moiety adjacent to the $\text{C}(sp^3)\text{-CF}_3$ moiety. The slow-exchange-limit ^{19}F NMR spectrum of C_1 - $\text{C}_{60}\text{F}_{17}\text{CF}_3$ exhibited 36 resonances due to the CF_3 group alone, and some of these showed signs of additional splitting.¹⁰ In addition to these mixed fluoro/trifluoromethyl derivatives, small amounts of a single isomer of $\text{C}_{60}(\text{CF}_3)_2$ were isolated from the crude product of the reaction of AgF with C_{60} .⁹ Its single-line ^{19}F NMR spectrum indicated that its CF_3 groups are symmetry related. This isomer was later shown to be 1,7- $\text{C}_{60}(\text{CF}_3)_2$.¹¹

To increase the yield of this new compound, which was the first isolated pure TMF, and possibly that of fluorofullerenes (FFs) C_{60}F_n with lower values of n , a different synthetic approach was attempted. The compound AgF was generated *in situ* during the heating of a solid mixture of C_{60} and a large

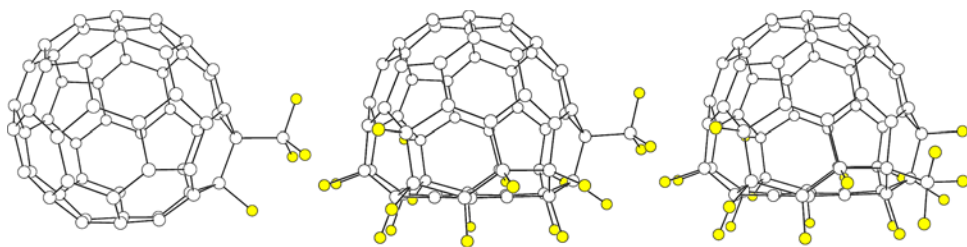


Figure 2. DFT-optimized structure of the proposed isomer 1,9- $\text{C}_{60}\text{F}(\text{CF}_3)$ (left) and X-ray diffraction-determined structures of C_s - $\text{C}_{60}\text{F}_{17}\text{CF}_3$ (middle) and C_1 - $\text{C}_{60}\text{F}_{17}\text{CF}_3$ (right).

excess of AgO_2CCF_3 .⁴ Instead of the expected increase in the yield of FFs and $\text{C}_{60}(\text{CF}_3)_2$, this reaction led (also unintentionally, as in the study reported in reference 6) to the formation of highly trifluoromethylated fullerenes: species with as many as 22 CF_3 groups per cage were identified for both C_{60} and C_{70} by mass spectrometry.⁴ This finding initiated more recent studies of PFAFs because it demonstrated how to prepare mixtures of TMFs that can be separated into pure isomers. (Note that in the original publication on PFAFs only complex, inseparable mixtures of PFAFs were prepared.²)

Another *in situ* study involved the use of a Knudsen cell as a chemical microreactor. The cell was placed inside a mass spectrometer to monitor the volatile products of the reaction between fluorofullerenes and AgO_2CCF_3 .¹² Various species of the general formula $\text{C}_{60}\text{F}_{18-x}(\text{CF}_3)_x$ were detected in that study; this confirmed an earlier hypothesis that the mixed fluoro/trifluoromethyl fullerene derivatives that formed during high-temperature fluorinations originated from the addition of CF_3 radicals. Later, this approach was used on a larger scale with the use of CF_3I as a source of CF_3 radicals. This yielded complex mixtures of $\text{C}_{60}\text{F}_{18-x}(\text{CF}_3)_{x+y}$ compounds, and for some of the HPLC isolated compounds X-ray structures were determined.¹³

There were reports on the use of other metal trifluoroacetates (*e.g.*, $\text{Hg}(\text{O}_2\text{CCF}_3)_2$ ¹⁴) or the persistent Scherer R_F radical¹⁵ as the source of CF_3 radicals in the mass spectrometric studies. TMFs with at least ten CF_3 groups were detected in the gas phase in both of those studies, along with partially hydrogenated TMFs. These studies, however, were not extended to the preparation of macroscopic samples of pure TMFs. Therefore, these reactions cannot be considered practical TMF syntheses.

1.3. Synthesis of PFAFs: reactions with metal trifluoroacetates

Further study of the reaction between C_{60} and AgO_2CCF_3 , first described in reference 4, involved the subsequent sublimation of the crude product.¹⁶ This resulted in the preparation of mixtures which were easily separable by HPLC.^{16,17} A typical experimental setup for the preparation of TMFs using $\text{M}(\text{O}_2\text{CCF}_3)_n$ as the trifluoromethylating agent is shown in Figure 3. The fullerene sample is mixed with the metal trifluoroacetate (usually AgO_2CCF_3) and ground into a fine powder. This mixture is loaded into an open-ended glass ampoule that is sealed inside a metal pipe (typically brass or copper). (The glass ampoule prevents the undesirable reaction between the $\text{M}(\text{O}_2\text{CCF}_3)_n$ reagent and the metal pipe.) After heating the entire apparatus to a fixed temperature in a tube furnace for a given amount of time, the metal

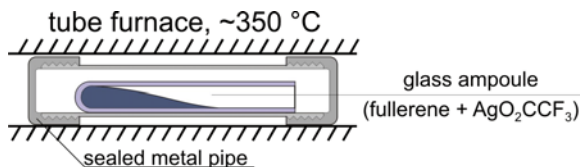


Figure 3. Experimental setup used for fullerene trifluoromethylation using metal trifluoroacetates (AgO_2CCF_3 is shown as an example).

pipe is opened and the fullerene-containing products are separated from insoluble inorganic residues by extracting with an organic solvent.

Since the first report in 2001,⁴ the developments of the synthesis and isolation of TMFs with the use of metal trifluoroacetates have continued in two directions. In one study, crude products of the reaction of C_{60} or C_{70} with AgO_2CCF_3 at 300°C that were extracted by an organic solvent were directly subjected to HPLC separation. Due to the complexity of the mixture, multi-stage HPLC processing was required, which in some cases was still not sufficient to achieve satisfactory purity of the isolated fractions.^{15,18} For example, in the case of C_{60} , as many as 68 different fractions were isolated by HPLC, and their molecular compositions were determined mass spectrometrically.¹⁵ Two types of molecular species were identified, $\text{C}_{60}(\text{CF}_3)_n$ and $\text{C}_{60}(\text{CF}_3)_n\text{H}_m$. The latter were more difficult to isolate because of the presence of a large number of isomers with similar retention times. The large number of compounds meant that the amount of each compound in the mixture was very small. Only a few of them were isolated in sufficient quantity to be characterized by ^{19}F NMR spectroscopy.¹⁹ The complexity of the TMF mixtures, especially the presence of numerous hydrogenated species, and the low yields of individual TMFs limited the practical use of this synthetic method.

The other direction involved the synthesis of crude TMF product mixtures as depicted in Figure 3 followed by an additional thermal treatment (*i.e.*, vacuum sublimation).^{11,16,17} The latter procedure proved beneficial because (i) it completely removed partially hydrogenated products that interfere with HPLC purification and (ii) it significantly reduced the number of isomers of a given composition (probably by either decomposition reactions or by the rearrangement of less stable isomers into more stable ones). Experiments with C_{70} led to even more dramatic changes in the distribution of TMFs, as shown in Figure 4. A very complex crude mixture of $\text{C}_{70}(\text{CF}_3)_n\text{H}_m$ products was vacuum sublimed at 480°C , producing a sublimate considerably enriched in the single isomer $\text{C}_s\text{-C}_{70}(\text{CF}_3)_8$. This compound was relatively easy to isolate in pure form, along with several other $\text{C}_{70}(\text{CF}_3)_n$ derivatives with $n = 2, 4, 6$, and 10 .¹⁷

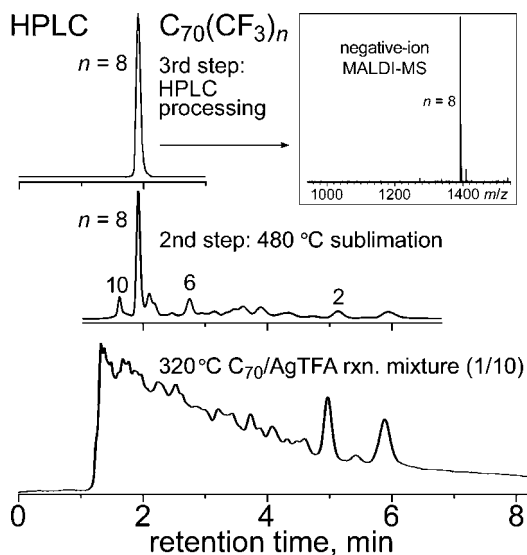


Figure 4. HPLC traces of the crude products from the reaction of C_{70} with AgO_2CCF_3 before (bottom) and after (middle) vacuum sublimation. The HPLC trace and MALDI mass spectrum of pure $C_{70}(CF_3)_8$ are shown at the top.

The reactions of AgO_2CCF_3 with the endometallofullerenes $Y@C_{82}-C_{2v}(9)$ and $Sc_3N@C_{80}-I_h(7)$ were also studied.^{20–24} The addition of an odd number of CF_3 groups to paramagnetic $Y@C_{82}-C_{2v}(9)$ resulted in diamagnetic trifluoromethylated products, including three isomers of $Y@(C_{82}-C_{2v}(9))(CF_3)_5$.²⁰ In the case of $Sc_3N@C_{80}-I_h(7)$, trifluoromethylated products $Sc_3N@(C_{80}-I_h(7))(CF_3)_n$ were prepared and isolated in sufficient amounts for spectroscopic ($n = 2, 4, 8, 10, 12, 14$, and 16) and structural studies ($n = 10, 12, 14$, and 16).^{21–24}

In conclusion, even with the use of the additional step of vacuum sublimation of the crude product, several major drawbacks of the synthetic approach based on $M(O_2CCF_3)_n$ remain: (i) generally low-to-very low yields of TMFs; (ii) low conversion of the fullerene substrate; (iii) insignificant variability of available TMF compositions; and (iv) complications due to the formation of hydrogenated by-products.

1.4. Synthesis of PFAFs: reactions with perfluoroalkyl iodides

Perfluoroalkyl iodides represent a family of common fluoroalkylating agents. Although CF_3I is a gas above $-22^\circ C$, other homologues R_FI are liquids (and their boiling point increases as the size of R_F chain increases). The weak C–I bond can be readily cleaved, by thermal or photochemical activation, releasing

iodine atoms and R_F radicals. Perfluoroalkyl iodides were the first reagents used in the perfluoroalkylation of fullerenes; both photochemical and thermal reactions yielded PFAFs.²

1.4.1. Reactions CF_3I

The reaction of C_{60} and C_{70} with CF_3I was first studied in 1993.² Fullerenes were treated with a large excess of CF_3I in benzene or perfluorobenzene, either at elevated temperature or under UV irradiation. The products were analyzed by negative-ion electron-capture mass spectrometry, which showed that TMF products were formed with up to 14 CF_3 groups per cage in high-temperature reactions or up to 13 CF_3 groups per cage in UV-activated reactions. In the latter case, species with H atoms attached to the fullerene cage were also formed when benzene was used as the solvent. When C_6F_6 was the solvent, hydrogenated products were not formed, demonstrating that H-atom abstraction from benzene was responsible for the previously-observed hydrogenated products. Spectroscopic data showed that multiple TMF components were present. Therefore, these reactions cannot be considered as selective syntheses of TMFs.

More than a decade later, a different approach to the trifluoromethylation of fullerenes with CF_3I was introduced.²⁵ This method employed heterogeneous reactions between heated solid fullerenes and gaseous CF_3I . These reactions were typically carried out at significantly higher temperatures than those used for AgO_2CCF_3 -based reactions or in reactions between CF_3I and fullerenes in solution. Below we will discuss three types of reaction vessels that were used: (i) flow-tube reactors, (ii) sealed glass ampoules; and (iii) gradient-temperature gas-solid (GTGS) reactors.

In a reaction using a flow-tube reactor, an example of which is shown in Figure 5, a finely ground solid fullerene sample is loaded in a glass tube, placed in a tube furnace, heated to 400–600°C, and allowed to react with a

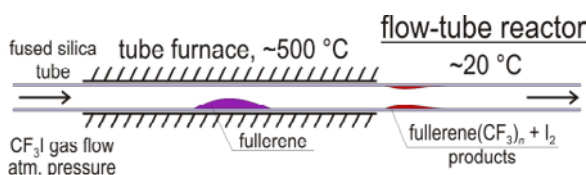


Figure 5. High-temperature flow-tube experimental setup used for fullerene trifluoromethylations using gaseous CF_3I .

stream of CF_3I at 1 atm. Volatile TMFs and I_2 sublime from the hot zone and condense in the colder parts of the flow tube.

Depending on the temperature used, flow-tube syntheses yielded fullerene(CF_3) $_n$ products with even n values from 2 to 18. The distribution of product compositions at a given temperature was found to be relatively narrow but varied as a function of reaction temperature. For example, C_{60} trifluoromethylation performed at 460°C afforded mostly $\text{C}_{60}(\text{CF}_3)_{8-12}$, while at a *higher* temperature the *lower* n -value compounds $\text{C}_{60}(\text{CF}_3)_{2-6}$ were the predominant products.^{25,26} This counterintuitive result is due to the fact that the accumulation of CF_3 groups on the fullerene and the sublimation of the fullerene(CF_3) $_n$ products are competing kinetic phenomena, and fullerene(CF_3) $_n$ volatility increases as n increases.^{25,26}

A typical setup for a sealed-ampoule syntheses is shown in Figure 6. The end of the ampoule containing the fullerene powder is placed in the furnace while the other end, containing a large excess of liquefied CF_3I , is kept at room temperature. These reactions are typically carried out from 48 hours to several days. The results reported to date indicate a high conversion of the fullerene starting material and the production of fullerene(CF_3) $_n$ products with relatively high n values. In one case, the selective preparation of $\text{S}_6\text{-C}_{60}(\text{CF}_3)_{12}$ was described.²⁷ However, the description of the reaction conditions leads one to the conclusion that the particular reaction conditions used for the selective formation of this TMF may be hard to reproduce: the report described the formation of an I_2 “plug” inside the ampoule that prevented further access of CF_3I vapor to the product.²⁷ In fact, in our hands the originally-reported selectivity of this reaction has not been reproduced.²⁸ Furthermore, synthetic procedures that make use of pressurized glass ampoules are extremely difficult to scale up because the size (*i.e.*, the radius) of the ampoule cannot be increased significantly without the risk of compromising its strength, which makes this methodology impractical for larger-scale preparatory work. Taking into account the high vapor pressure of liquefied CF_3I at room temperature (*ca.* 5 bar), these reactions are potentially explosive and should only be performed by trained personnel.

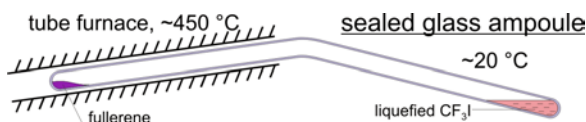


Figure 6. Experimental setup used for trifluoromethylations with CF_3I in a sealed glass ampoule reactor.

Comparison of the two reactor types shows that the flow-tube reactor method should be preferred: it is simpler, scalable, and gives a wider range of TMFs with high yields and good conversion. The advantages of the sealed-ampoule reactor, on the other hand, are a more economical use of CF_3I gas and the possibility of producing a specific TMF more selectively.

One of the common drawbacks of both methods, however, is that they do not allow one to use varying pressures of the CF_3I reagent and/or varying pressures of an inert buffer gas, both of which are potentially important parameters. (For example, the various kinetic processes shown in Figure 1 should clearly depend on the partial pressure of CF_3I and the total pressure in the apparatus.) For sealed ampoules the pressure is determined by the vapor pressure of CF_3I at a given temperature; for the flow-tube reactor, the partial pressure of CF_3I is equal to 1 atm unless an elaborate gas-mixing and flow-control system is used, and even then the total pressure is fixed at 1 atm. Another drawback is that neither of the two methods affords significant amounts of TMFs with low n values (*i.e.*, $n = 2$ and 4). These shortcomings were addressed by designing a third type of reactor for high-temperature heterogeneous fullerene trifluoromethylation, the gradient-temperature gas-solid (GTGS) reactor, which is shown schematically in Figure 7.⁵

The GTGS reactor has two key components in its design: a gas-handling/vacuum manifold and a small hot (reaction) zone. It allows a wide range of experimental conditions to be used, including varying the pressure of CF_3I and the total pressure in the apparatus. Significantly, this reactor reduces the residence time of the TMF products in the hot zone, an important factor in limiting the n value to small numbers.

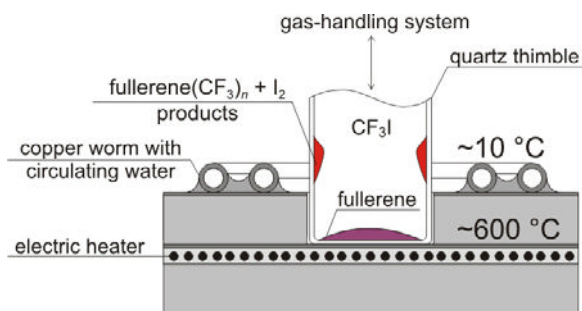


Figure 7. A gradient-temperature gas-solid (GTGS) reactor used for the high-temperature heterogeneous trifluoromethylation of fullerenes with CF_3I gas.

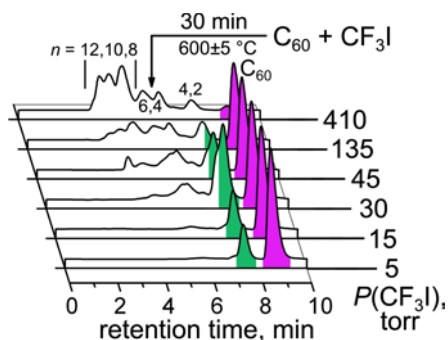


Figure 8. HPLC traces of the fullerenes present (*i.e.*, C_{60} and $C_{60}(CF_3)_n$) after the trifluoromethylation of C_{60} with different partial pressures of CF_3I in a GTGS reactor.

The trifluoromethylation of C_{60} and C_{70} under a variety of different reaction conditions (temperature, CF_3I partial pressure, reaction time, amount of fullerene, radius of the quartz thimble, depth of the hot zone, etc.) was recently carried out using a number of GTGS reactors.⁵ This study demonstrated, in particular, the importance of CF_3I pressure as a reaction parameter. For example, Figure 8 shows that a low pressure of CF_3I (*e.g.*, 5 or 15 torr) can result in a 90+ mol% yield of the single isomer 1,7- $C_{60}(CF_3)_2$ based on converted C_{60} , albeit at a very low conversion of C_{60} to TMF products. This result can be rationalized using the scheme shown in Figure 1. Scaling-up this reaction led to the preparation (and subsequent HPLC separation) of pure isomers of $C_{60}(CF_3)_{2,4,6}$ in 300+ mg quantities.⁵

In conclusion, fullerene reactions with CF_3I generally yield mixtures of TMFs that require subsequent separation by HPLC into compositionally and isomerically pure products (in this way such reactions are similar to reactions involving $M(O_2CCF_3)_n$ reagents). Nevertheless, both the flow-tube method and the GTGS method have some significant advantages over the use of metal trifluoroacetates: (i) no additional sublimation step is required (because no partially hydrogenated products are produced and because the use of higher temperatures in both the flow-tube and GTGS reactors appears to favor the formation of fewer, presumably more stable, isomers; (ii) higher fullerene conversion can be achieved; (iii) higher TMF yields are possible; and (iv) ease of scale-up (some TMFs were prepared in 300–500 mg quantities using a GTGS or flow-tube reactor²⁹ (in contrast, the largest sample sizes possible using sealed ampoules were a few tens of milligrams²⁷)).

1.4.2. Reactions with perfluoroalkyl iodides R_FI ($R_F = C_2F_5, C_3F_7, C_4F_9, C_6F_{13},$ and $C_{12}F_{25}$)

The second simplest homologue in the series of R_FI is perfluoroethyl iodide. It is a low-boiling colorless liquid (bp = 14°C). Therefore, it can be used as a perfluoroalkylating reagent in much the same ways as described above for CF_3I . However, it was found that lower temperatures are necessary for C_2F_5I reactions to avoid cleavage of the F_3C-CF_2 bond and the concomitant formation of CF_3 radicals and CF_2 moieties.²⁸ In fact, the use of higher temperature with pure C_2F_5I did lead to the formation of the mixed C_2F_5/CF_3 derivatives.²⁸ The dependence between the temperature used for fullerene perfluoroethylation and the resulting PFAF composition was studied for C_{60} and C_{70} fullerenes. Figure 9 shows the shift in the product distribution towards fullerene(C_2F_5)_{*n*} derivatives with lower *n* values as the temperature increases.

Figure 9 also shows that the highest reaction temperature used, 500°C, resulted in the formation of fullerene(CF_3)_{*n*} derivatives instead of fullerene(C_2F_5)_{*n*} derivatives. Furthermore, product mixtures formed in perfluoroethylation reactions were found to be more complex than the TMF product mixtures formed under analogous conditions with CF_3I . This conclusion is supported by the number of PFAF isomers observed; there were many more isomers for *n* = 8 and 10 for fullerene(C_2F_5)_{*n*} product mixtures than for fullerene(CF_3)_{*n*} product mixtures.

The reaction between C_{60} and perfluoro-*n*-hexyl iodide in 1,2,4-trichlorobenzene at 200°C led to the formation of a compound with ten C_6F_{13} groups as the major product.² Furthermore, even for the longer-chain R_F group *n*- $C_{12}F_{25}$, the composition $C_{60}(R_F)_{10}$ was dominant.^{2,30} Figure 10 shows the EI mass spectra of the products obtained in the reactions of C_{60} with *n*- C_3F_7I , *n*- C_4F_9I , and *n*- $C_6F_{13}I$.²⁸ All three reactions were performed at 320–350°C in a flow-tube reactor in the presence of copper powder as a promoter (a stream of dinitrogen was bubbled through the liquid R_FI reagent before passing through the hot zone). Note that the products all have similar ranges of *n* values, with $C_{60}(R_F)_{10}$ being the most abundant composition. Significantly, a similar result was obtained for the reaction of C_{60} with *n*- C_3F_7I vapor in a sealed glass ampoule (290°C; 24 h).

The reaction of C_{70} with *n*- C_3F_7I was carried out in a flow-tube reactor (350–380°C; 7 h; copper powder promoter; dinitrogen gas bubbled through neat *n*- C_3F_7I), giving a product that was predominantly $C_{70}(n-C_3F_7)_{10}$.²⁸ Similar reactions between C_{70} and *n*- C_3F_7I vapor carried out in sealed glass ampoules at lower temperatures and for longer times produced mixtures in

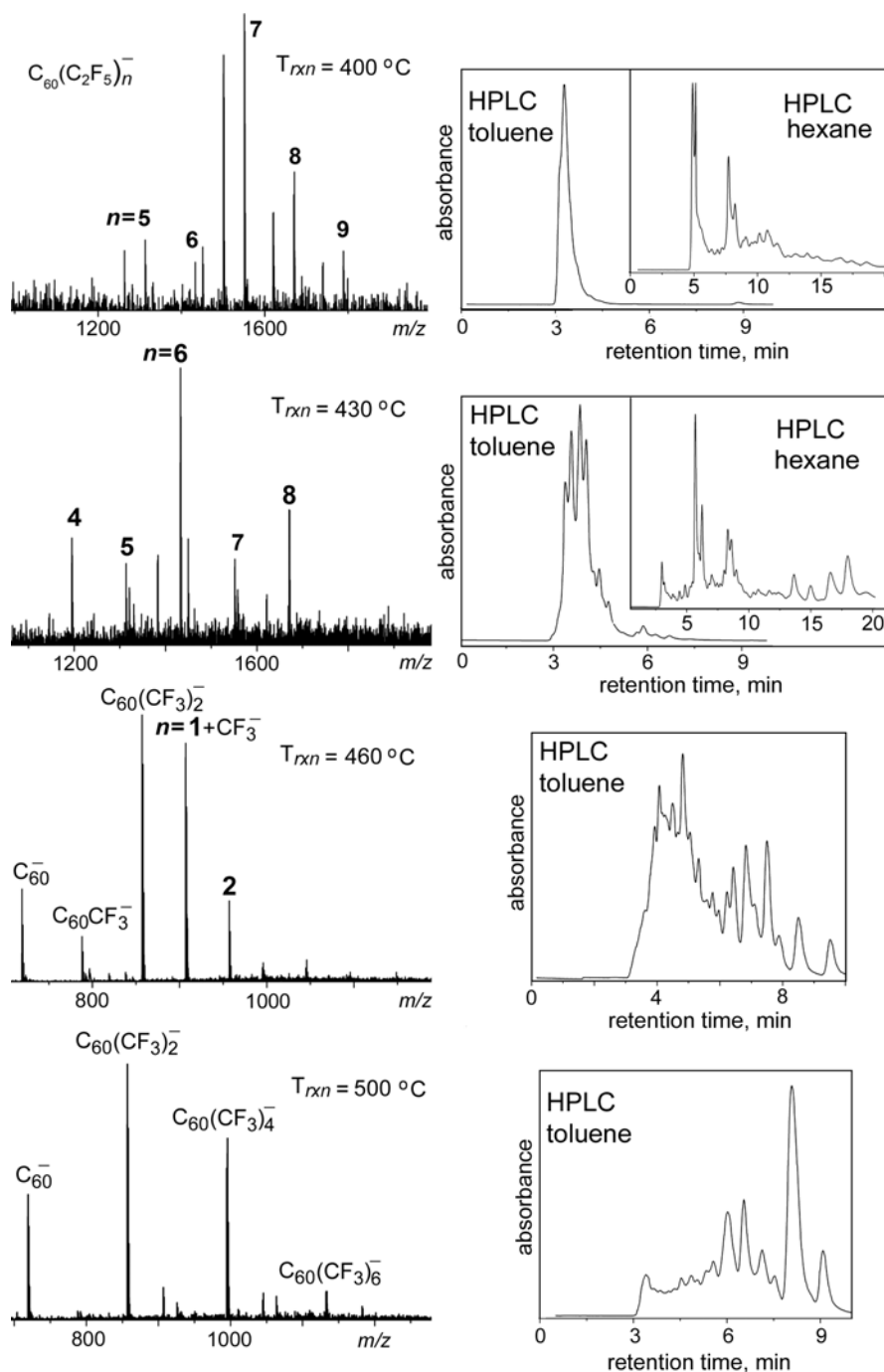


Figure 9. MALDI mass spectra and HPLC traces for the crude reaction products of C_{60} perfluoroethylation using C_2F_5I at 400, 430, 460, and 500 °C.

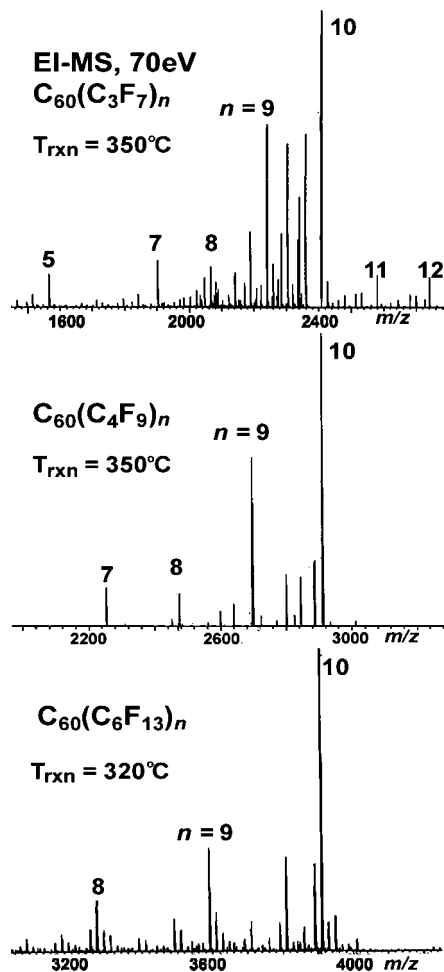


Figure 10. Electron-ionization mass spectra of the crude products of the perfluoroalkylation of C_{60} in a high-temperature flow-tube reactor.

which $C_{70}(n-C_3F_7)_8$ was the dominant composition (other $C_{70}(n-C_3F_7)_{2-10}$ species were also observed by mass spectrometry).³¹ These results clearly indicate that reaction temperatures higher than $300^\circ C$ lead to the formation of fullerene(R_F) $_n$ products with $n \leq 10$ for $R_F = n-C_3F_7$, $n-C_4F_9$, and $n-C_6F_{13}$.²⁸ Note that fullerene($n-C_6F_{13}$) $_n$ compounds with $n > 10$ were only observed in crude PFAF mixtures prepared at $175^\circ C$. The absence of PFAFs with $n > 10$ in the high-temperature reaction products suggests that these derivatives may have limited thermal stability. In agreement with this, TGA measurements indicated that perfluoro-*n*-hexylfullerenes decompose above $270^\circ C$.²

2. Methods of Isolation and Characterization

In view of the potential applications of fullerene derivatives, including PFAFs, it is important to evaluate not only the efficiencies of the synthetic reactions and the cost of the reagents, but also the efficiencies of purification methods needed. For example, the current price of [6,6]-phenyl- C_{61} -butyric acid methyl ester (PCBM), a fullerene derivative widely used in the active layers of organic photovoltaic devices,^{32,33} is in the range of one thousand U.S. dollars per gram. Such a high price is partially due to the fact that its purification from the crude reaction product involves a laborious chromatographic procedure. It would be advantageous, therefore, to develop, whenever possible, synthetic methods that would require fewer purification steps for the isolation of the target compound. These synthetic methods would be especially useful if they obviate time- and labor-intensive chromatographic separations. The purification stage is especially challenging for fullerene polyadditions, which typically yield multiple isomers of multiple compositions with similar retention times. In this section, procedures for the selective synthesis of PFAFs will be discussed. These will include the methods of isolation of many PFAFs from the mixtures.

2.1. Selective syntheses of PFAFs

The isolation of pure PFAF compounds generally necessitates chromatographic purification procedures, which will be discussed in the next section. However, there are a few reports that describe a relatively high-yield one-step synthesis of a relatively pure single isomer of a single PFAF composition. The first such report described the preparation of a single asymmetric isomer of a decakis(trifluoromethyl) derivative of C_{70} , 1,4,10,19,25,41,49,60,66,69- $C_{70}(CF_3)_{10}$. The original method afforded a 27% isolated yield of this compound (hereinafter referred to as C_1 - $C_{70}(CF_3)_{10}$) based on converted C_{70} , which at the time was by far the highest yield for any single-isomer fullerene derivative with exactly ten addends.³⁴ This selective synthesis was subsequently further optimized to increase the scale of the reaction and to increase the isolated yield to *ca.* 70% based on converted C_{70} .^{35,29}

Figure 11 shows the ^{19}F NMR spectrum and the HPLC trace of the crude product from a 90-min 530°C flow-tube reaction of C_{70} and CF_3I .³⁵ These data demonstrated that 89 mol% of the crude TMF reaction products obtained in this one-step reaction was the single isomer C_1 - $C_{70}(CF_3)_{10}$ (the X-ray structure and Schlegel diagram of this compound are also shown in Figure 11; note that C_1 - $C_{70}(CF_3)_{10}$ is abbreviated as **70-10-1** in Table 2).

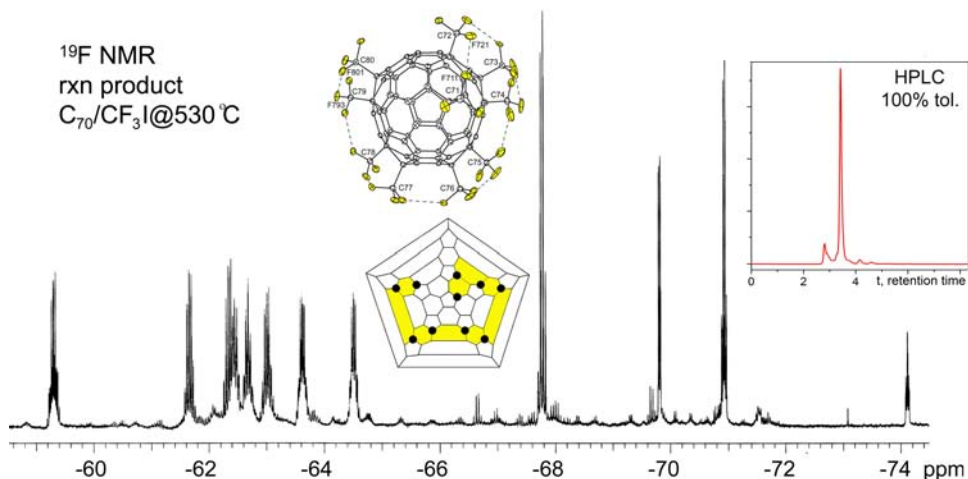
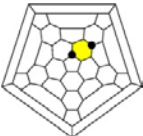

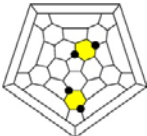

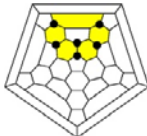

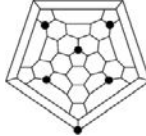
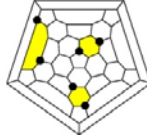
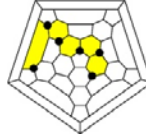





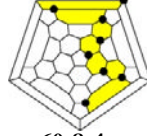

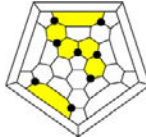
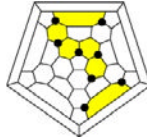
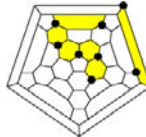
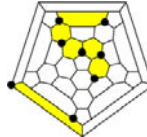


Figure 11. The ^{19}F NMR spectrum and HPLC trace of the crude product from a 90-minute reaction between C_{70} and CF_3I at 530°C in an 80-cm long flow tube. The data show that the sample contains 89 mol% $\text{C}_1\text{-C}_{70}(\text{CF}_3)_{10}$. A thermal-ellipsoid plot (50% probability ellipsoids) and the Schlegel diagram of $\text{C}_1\text{-C}_{70}(\text{CF}_3)_{10}$ are also shown.

Similar procedures with larger amounts of C_{70} afforded 450+ mg of 98 mol% $\text{C}_1\text{-C}_{70}(\text{CF}_3)_{10}$ (two-stage HPLC processing was used to purify the crude product).²⁹ Such high selectivity and yield are quite remarkable for a radical polyaddition reaction (over 19 billion isomers are theoretically possible for the composition $\text{C}_{70}\text{X}_{10}$ ³⁶). This compound has recently been proven to be a useful synthon for further derivatizations and for the preparation of donor-acceptor molecular assemblies.^{29,37,38}

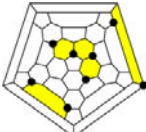
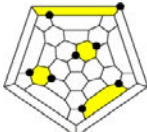
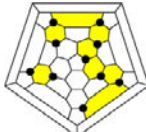
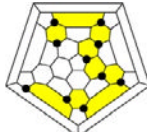
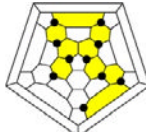
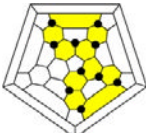



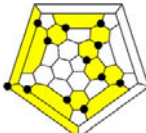


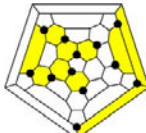
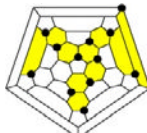
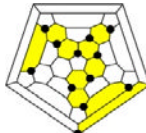


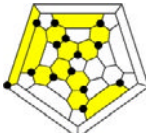
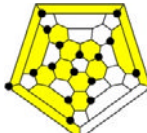
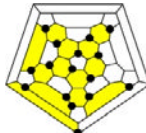
The other example of a selective PFAF synthesis is the single-isomer of $\text{C}_{60}(\text{CF}_3)_{12}$ prepared in a sealed glass ampoule at 440°C .²⁷ The crystals of the product were examined by X-ray crystallography and were shown to be $S_6\text{-C}_{60}(\text{CF}_3)_{12}$ (**60-12-1** in Table 1). The authors' conclusions about the high compositional and isomeric purity of the crude product were based solely on the single-crystal X-ray structure. However, the results of an X-ray diffraction study of a single crystal provides no information on the composition of the bulk sample. A recent study has shown the deficiencies of some analytical methods for the determination of the compositional purity of bulk samples of poly-adducts of fullerenes.³⁹ The selectivity of a PFAF synthesis can only be judged if the bulk material is examined by methods such as HPLC and ^{19}F NMR spectroscopy. In the case of $S_6\text{-C}_{60}(\text{CF}_3)_{12}$, a subsequent study by the original authors revealed that the high selectivity was strongly dependant on the reaction parameters; in particular, the selectivity was high only when the

Table 1. Schlegel diagrams, abbreviations, and IUPAC numbering for C₆₀ PFAFs.^a

				
60-2-1	60-4-1	60-4-2	60-6-1	60-6-2
60-2-1-R_F	1,7-C ₆₀ (R _F) ₂		R _F = CF ₃ , ^{11,16} <i>i</i> -C ₃ F ₇ ⁶⁸	
60-4-1	1,6,11,18-C ₆₀ (CF ₃) ₄ ^{11,16}			
60-4-2	1,7,16,36-C ₆₀ (CF ₃) ₄			
60-6-1	1,6,11,18,24,27-C ₆₀ (CF ₃) ₆ ^{11,16}			
60-6-2	1,6,9,12,15,18-C ₆₀ (CF ₃) ₆ ²⁶			
				
60-6-3	60-6-4	60-6-5	60-6-6	60-6-7
60-6-3-C₂F₅	1,7,16,36,46,49-C ₆₀ (C ₂ F ₅) ₆ ⁸⁰			
60-6-4	1,23,28,33,38,60-C ₆₀ (CF ₃) ₆ ⁵⁷			
60-6-5-<i>i</i>-C₃F₇	1,7,16,30,36,47-C ₆₀ (<i>i</i> -C ₃ F ₇) ₆ ⁸¹			
60-6-6	1,6,11,18,28,31-C ₆₀ (CF ₃) ₆ ¹¹			
60-6-7	1,6,11,18,33,51-C ₆₀ (CF ₃) ₆ ^{11,82}			
				
60-6-8	60-8-1	60-8-2	60-8-3	60-8-4
60-6-8-R_F	1,7,16,36,45,57-C ₆₀ (R _F) ₆		R _F = C ₂ F ₅ , ⁸² <i>i</i> -C ₃ F ₇ ⁸³	
60-8-1-R_F	1,6,11,16,18,24,27,36-C ₆₀ (R _F) ₈		R _F = CF ₃ , ⁸⁴ C ₂ F ₅ ²⁸	
60-8-2	1,6,11,18,24,27,52,55-C ₆₀ (CF ₃) ₈ ⁸⁵			
60-8-3-R_F	1,6,11,18,24,27,53,56-C ₆₀ (R _F) ₈		R _F = CF ₃ , ⁵⁷ C ₂ F ₅ ²⁸	
60-8-4	1,6,11,16,18,28,31,36-C ₆₀ (CF ₃) ₈ ⁵⁷			
				
60-8-5	60-8-6	60-8-7	60-8-8	60-8-9
60-8-5	1,6,11,18,24,27,33,51-C ₆₀ (CF ₃) ₈ ⁵⁷			
60-8-6-C₂F₅	1,6,11,18,24,27,32,35-C ₆₀ (C ₂ F ₅) ₈ ⁸⁰			
60-8-7-C₂F₅	1,6,11,18,24,27,36,39-C ₆₀ (C ₂ F ₅) ₈ ²⁸			
60-8-8-C₂F₅	1,6,11,18,24,27,41,57-C ₆₀ (C ₂ F ₅) ₈ ⁸²			
60-8-9-C₂F₅	1,6,11,18,24,27,51,59-C ₆₀ (C ₂ F ₅) ₈ ⁸²			

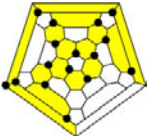


(Continued)

Table 1. (Continued)

				
60-8-10	60-8-11	60-10-1	60-10-2	60-10-3
60-8-10-C₂F₅	1,6,11,18,32,35,42,56-C ₆₀ (C ₂ F ₅) ₈ ⁸²			
60-8-11-<i>i</i>-C₃F₇	1,7,14,31,36,39,45,57-C ₆₀ (<i>i</i> -C ₃ F ₇) ₈ ⁸³			
60-10-1	1,6,11,16,18,24,27,36,41,57-C ₆₀ (CF ₃) ₁₀ ⁵⁷			
60-10-2	1,6,11,16,18,24,27,36,54,60-C ₆₀ (CF ₃) ₁₀ ⁶⁵			
60-10-3	1,3,7,10,14,17,23,28,31,40-C ₆₀ (CF ₃) ₁₀ ²⁵			
				
60-10-4	60-10-5	60-10-6	60-10-7	60-12-1
60-10-4	1,6,12,15,18,23,25,41,45,57-C ₆₀ (CF ₃) ₁₀ ⁸⁶			
60-10-5	1,6,11,16,18,26,36,41,44,57-C ₆₀ (CF ₃) ₁₀ ⁵⁷			
60-10-6-R_F	1,6,11,18,24,27,33,51,54,60-C ₆₀ (R _F) ₁₀ R _F = CF ₃ , ⁸⁷ C ₂ F ₅ ^{28,82}			
60-10-7-C₂F₅	1,6,11,16,18,28,31,36,42,56-C ₆₀ (C ₂ F ₅) ₁₀ ⁸²			
60-12-1	1,6,11,16,18,26,36,44,46,49,54,60-C ₆₀ (CF ₃) ₁₂ ²⁷			
				
60-12-2	60-12-3	60-12-4	60-12-5	60-12-6
60-12-2	1,3,6,11,13,18,26,32,35,41,44,57-C ₆₀ (CF ₃) ₁₂ ⁴²			
60-12-3	1,6,9,12,15,18,43,46,49,52,55,60-C ₆₀ (CF ₃) ₁₂ ^{57,88}			
60-12-4	1,3,7,10,14,17,21,28,31,42,52,55-C ₆₀ (CF ₃) ₁₂ ⁸⁹			
60-12-5	1,6,8,11,16,18,23,28,31,36,41,57-C ₆₀ (CF ₃) ₁₂ ⁴⁰			
60-12-6	1,6,8,11,16,18,23,28,31,36,54,60-C ₆₀ (CF ₃) ₁₂ ⁴⁰			
				
60-14-1	60-14-2	60-14-3	60-16-1	60-16-2
60-14-1	1,3,6,8,11,13,18,23,33,41,46,49,51,57-C ₆₀ (CF ₃) ₁₄ ⁸⁸			
60-14-2	1,3,6,11,13,18,26,33,41,44,46,49,51,57-C ₆₀ (CF ₃) ₁₄ ⁸⁸			
60-14-3	1,3,7,10,11,14,17,24,27,31,36,39,47,59-C ₆₀ (CF ₃) ₁₄ ⁴⁰			
60-16-1	1,3,6,11,13,18,22,28,31,34,37,41,43,46,51,59-C ₆₀ (CF ₃) ₁₆ ⁹⁰			
60-16-2	1,3,6,8,11,13,18,23,28,31,34,35,37,50,54,60-C ₆₀ (CF ₃) ₁₆ ⁹⁰			

(Continued)

Table 1. (Continued)

			
60-16-3	1,3,6,11,13,18,22,24,27,33,41,43,46,49,51,59-C ₆₀ (CF ₃) ₁₆ ⁹⁰		
60-18-1	1,3,6,8,11,13,18,23,28,31,34,37,43,46,51,53,56,59-C ₆₀ (CF ₃) ₁₈ ⁹⁰		
60-18-2	1,3,6,11,13,18,22,24,27,32,35,37,41,43,46,49,52,54-C ₆₀ (CF ₃) ₁₈ ⁴¹		

^a The abbreviations can refer to a particular compound or a particular addition pattern. When only the CF₃ derivative is known, as in, for example, **60-6-7**, the abbreviation alone refers to the compound 1,6,11,18,33,51-C₆₀(CF₃)₆ and reference to the addition pattern of this compound would be in statements such as “The **60-6-7** addition pattern...” When more than one PFAF is known with a given addition pattern, as in **60-6-8-RF**, the abbreviation **60-6-8** refers to the addition pattern itself and to the (as yet unknown) compound 1,7,16,36,45,57-C₆₀(CF₃)₆, the abbreviation **60-6-8-C₂F₅** refers to the known compound 1,7,16,36,45,57-C₆₀(C₂F₅)₆, and the abbreviation **60-6-8-i-C₃F₇** refers to the known compound 1,7,16,36,45,57-C₆₀(i-C₃F₇)₆. This also allows other known and hypothetical compounds to be readily abbreviated, such as **60-6-2-Cl** for the known compound 1,6,9,12,15,18-C₆₀Cl₆ and **60-8-1-H** for the hypothetical compound 1,6,11,16,18,24,27,36-C₆₀H₈.

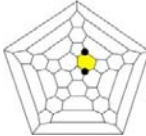
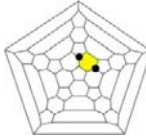
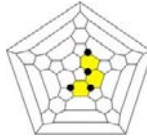
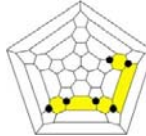
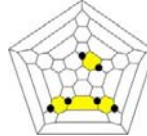
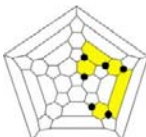
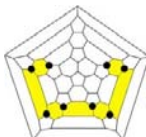

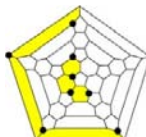
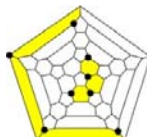
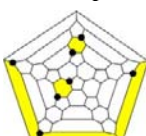
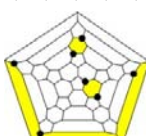
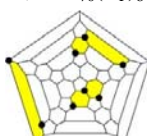
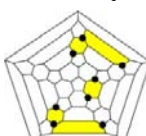

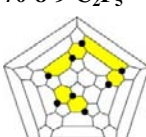


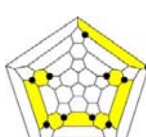

ampoule was almost completely clogged with I₂ crystals.⁴⁰ In another study, the same reaction conditions yielded mixtures of C₆₀(CF₃)_n compounds with even *n* = 12–18.²⁸ Additional work will be needed to develop a reliable and reproducible procedure for the large-scale selective synthesis of S₆-C₆₀(CF₃)₁₂.

The third example involves the selective synthesis of 1,7-C₆₀(CF₃)₂ that was achieved using a GTGS reactor. When the trifluoromethylation was performed under a low partial pressure of CF₃I (5–15 torr) in a reactor with a small hot zone, 1,7-C₆₀(CF₃)₂ was produced with a relatively high purity (80–90%) and a reasonable yield (20–30%). The selectivity of this procedure was due to the hypothesis that a low-conversion reaction (*i.e.*, 20–40%) would result in a mixture of TMF products highly enriched in the composition C₆₀(CF₃)₂.⁵

2.2. Purification methods





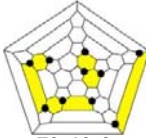


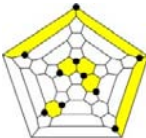







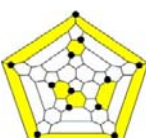



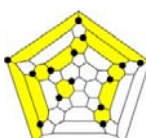
Complex mixtures of PFAFs are usually separated into their individual components, when possible, by HPLC using Cosmosil BuckyPrep columns, which were specifically designed for fullerene separations. In many cases, multi-stage HPLC separations employing different eluents are necessary in order to achieve 99+ mol% purity of individual PFAFs. The most commonly

Table 2. Schlegel diagrams, abbreviations, and IUPAC numbering for C₇₀ PFAFs.^a

				
70-2-1	70-2-2	70-4-1	70-6-1	70-6-2
70-2-1-R_F	7,24-C ₇₀ (R _F) ₂			$R_F = CF_3^{17,44,91}, C_2F_5^{44}$
70-2-2	8,23-C ₇₀ (CF ₃) ₂ ³⁵			
70-4-1	7,24,44,47-C ₇₀ (CF ₃) ₄ ¹⁷			
70-6-1	1,4,11,19,31,41-C ₇₀ (CF ₃) ₆ ¹⁷			
70-6-2	1,4,11,23,31,44-C ₇₀ (CF ₃) ₆ ³⁵			
				
70-6-3	70-8-1	70-8-2	70-8-3	70-8-4
70-6-3	1,4,10,19,25,41-C ₇₀ (CF ₃) ₆ ¹⁷			$R_F = CF_3^{17,55}, C_2F_5^{46}$
70-8-1-R_F	1,4,11,19,31,41,51,64-C ₇₀ (R _F) ₈			
70-8-2	1,4,11,19,31,41,51,60-C ₇₀ (CF ₃) ₈ ^{17,35,56}			$R_F = C_2F_5^{46}, n-C_3F_7^{31}$ $R_F = C_nF_{2n+1} (n = 1-3)^{31,46}$
70-8-3-R_F	7,17,24,36,44,47,53,56-C ₇₀ (R _F) ₈			
70-8-4-R_F	7,15,24,34,44,47,53,56-C ₇₀ (R _F) ₈			
				
70-8-5	70-8-6	70-8-7	70-8-8	70-8-9
70-8-5-R_F	1,4,23,28,36,44,46,57-C ₇₀ (R _F) ₈			$R_F = C_2F_5^{46}, n-C_3F_7^{31}$ $R_F = C_2F_5^{46}, n-C_3F_7^{31}$
70-8-6-R_F	1,4,23,28,34,44,46,52-C ₇₀ (R _F) ₈			
70-8-7-C₂F₅	1,4,11,24,43,52,54,68-C ₇₀ (C ₂ F ₅) ₈ ⁴⁶			
70-8-8-C₂F₅	1,4,11,33,53,58,61,64-C ₇₀ (C ₂ F ₅) ₈ ⁴⁶			
70-8-9-C₂F₅	1,4,23,28,44,46,55,67-C ₇₀ (C ₂ F ₅) ₈ ⁴⁶			
				
70-8-10	70-10-1	70-10-2	70-10-3	70-10-4
70-8-10-C₂F₅	1,4,11,19,31,55,57,67-C ₇₀ (C ₂ F ₅) ₈ ⁴⁶			$R_F = CF_3^{34}, C_2F_5^{46}$
70-10-1-R_F	1,4,10,19,25,41,49,60,66,69-C ₇₀ (R _F) ₁₀			
70-10-2	1,4,11,19,31,41,49,60,66,69-C ₇₀ (CF ₃) ₁₀ ³⁵			
70-10-3	1,4,11,19,26,31,41,48,60,69-C ₇₀ (CF ₃) ₁₀ ³⁵			
70-10-4	1,4,10,19,23,25,44,49,66,69-C ₇₀ (CF ₃) ₁₀ ³⁵			




(Continued)

Table 2. (Continued)

				
70-10-5	70-10-6	70-10-7	70-10-8	70-10-9
70-10-5	1,4,11,19,24,31,41,51,61,64- $C_{70}(CF_3)_{10}^{35}$			
70-10-6	1,4,10,19,25,41,55,60,67,69- $C_{70}(CF_3)_{10}^{92}$			
70-10-7	1,4,10,19,25,32,41,54,60,67- $C_{70}(CF_3)_{10}^{93}$			
70-10-8- C_2F_5	1,4,11,19,31,41,46,55,62,67- $C_{70}(C_2F_5)_{10}^{45}$			
70-10-9- C_2F_5	1,4,11,19,23,31,44,55,57,67- $C_{70}(C_2F_5)_{10}^{45}$			
				
70-10-10	70-10-11	70-10-12	70-10-13	70-10-14
70-10-10- C_2F_5	1,4,11,33,38,46,53,55,62,64- $C_{70}(C_2F_5)_{10}^{45}$			
70-10-11- C_2F_5	1,4,11,24,33,38,43,48,53,55- $C_{70}(C_2F_5)_{10}^{45}$			
70-10-12- C_2F_5	1,4,23,28,33,38,44,46,53,55- $C_{70}(C_2F_5)_{10}^{45}$			
70-10-13- C_2F_5	1,4,11,33,38,46,48,53,55,62- $C_{70}(C_2F_5)_{10}^{45}$			
70-10-14- C_2F_5	1,4,11,24,33,38,43,53,55,64- $C_{70}(C_2F_5)_{10}^{46}$			
				
70-10-15	70-12-1	70-12-2	70-12-3	70-12-4
70-10-15- C_2F_5	1,11,16,18,33,46,48,54,62,68- $C_{70}(C_2F_5)_{10}^{46}$			
70-12-1	1,4,10,19,25,32,41,49,54,60,66,69- $C_{70}(CF_3)_{12}^{94}$			
70-12-2	1,4,10,14,19,25,35,41,49,60,66,69- $C_{70}(CF_3)_{12}^{95}$			
70-12-3	1,4,8,11,18,23,31,35,51,58,61,64- $C_{70}(CF_3)_{12}^{35}$			
70-12-4	1,4,8,11,23,31,38,51,55,58,61,64- $C_{70}(CF_3)_{12}^{35}$			
				
70-12-5	70-14-1	70-14-2	70-14-3	70-14-4
70-12-5- C_2F_5	1,4,23,25,27,31,38,44,47,51,55,68- $C_{70}(C_2F_5)_{12}^{28}$			
70-14-1	1,4,7,11,18,21,24,31,35,39,51,58,61,64- $C_{70}(CF_3)_{14}^{96}$			
70-14-2	1,4,8,11,19,24,27,31,41,43,51,54,64,68- $C_{70}(CF_3)_{14}^{97}$			
70-14-3	1,4,8,11,19,23,26,31,41,48,55,60,67,69- $C_{70}(CF_3)_{14}^{97}$			
70-14-4	1,4,8,11,19,24,27,31,36,41,43,51,57,64- $C_{60}(CF_3)_{14}^{97}$			

(Continued)

Table 2. (Continued)

			
	70-14-5	70-16-1	70-18-1
70-14-5	1,4,8,11,19,24,27,31,41,43,51,53,56,64-C ₇₀ (CF ₃) ₁₄ ⁹¹		
70-16-1	1,4,8,11,18,23,24,27,31,35,44,47,51,58,61,64-C ₇₀ (CF ₃) ₁₆ ⁹⁸		
70-18-1	1,4,8,11,16,19,23,27,31,34,37,41,44,46,47,52,60,69-C ₇₀ (CF ₃) ₁₈ ⁹⁸		

^a See footnote a in Table 1 for an explanation of the abbreviations.

used eluents are toluene, heptanes, hexanes, and their mixtures. PFAFs are not very soluble in polar solvents, and this has limited the use of such solvents in HPLC-based PFAF purifications.

There are only a few PFAFs for which a 99 mol% purity could be achieved with a single-stage HPLC separation. All of them had either two, four, of six R_F groups and therefore relatively long retention times.¹⁷ Perfluoroalkylfullerenes with 8–18 R_F groups have significantly shorter retention times, and short retention times lead to extensive peak overlap and greatly diminished separation efficiency. Therefore, large-scale purifications of C₆₀(CF₃)_n compounds are difficult for $n \geq 12$; even with the use of the “weakest” eluents, heptanes or hexanes, the bands for different isomers overlap significantly. HPLC purifications of C₆₀(CF₃)_n derivatives with even $n = 14$ –18 were done on very small scales, and in some cases even laborious multi-stage HPLC processing did not result in high purity.^{40,41} The purification of PFAFs with high n values continues to be a challenge, and only a few of the many isomers of C₆₀(CF₃)_{12–18} have been isolated, and even fewer can be said to be well-characterized.^{40–43}

For a given value of n , PFAFs with C₂F₅ groups have shorter retention times than PFAFs with CF₃ groups. Therefore, HPLC processing of fullerene(C₂F₅)_n derivatives is difficult for $n \geq 10$. Despite the fact that eleven isomers of C₇₀(C₂F₅)₁₀ have had their structures determined by X-ray crystallography, many more isomers of C₇₀(C₂F₅)₁₀ are known to exist and have unknown addition patterns.

Following this trend, PFAFs with R_F groups larger than C₂F₅ are even more difficult to purify, because HPLC retention times continue to decrease as the size of the R_F group increases for a given value of n .^{28,44} For example, under similar HPLC conditions, C₇₀(n -C₃F₇)₁₀ isomers elute in 2.7–3.5 min

whereas $C_{70}(C_2F_5)_{10}$ isomers elute in 2.7–7.0 min.^{31,45} In the case of $C_{70}(n-C_3F_7)_8$ and $C_{70}(C_2F_5)_8$ isomers, the respective ranges of retention times in neat heptane are 3.5–13 min and 7–42 min, respectively.^{31,46} Therefore, even the best possible HPLC configuration (a Cosmosil Buckyprep column and heptane as the eluent) does not allow practical amounts of highly-purified fullerene(R_F) $_n$ compounds with $n \geq 10$ and R_F groups larger than C_2F_5 to be isolated.

These results demonstrate the limitations of existing PFAF purification techniques. At present, only a limited range of PFAF compositions can be separated into all of the most abundant individual isomers with satisfactory purity and in quantities necessary for detailed physicochemical studies or further derivatization. The most comprehensive studies to date were carried out with the $C_{60}(CF_3)_{2-10}$ and $C_{70}(CF_3)_{2-12}$ series of compounds. With larger R_F groups, only isomers of $C_{60}(C_2F_5)_{6-8}$ and $C_{60}(i-C_3F_7)_6$ have been adequately purified; for other PFAF mixtures only a few of the many compounds present could be isolated and characterized. Such a situation calls for the development of new and unconventional separation techniques to provide access to new PFAF derivatives and to known PFAFs in practical amounts.

2.3. Characterization

2.3.1. Mass spectrometry

Due to the presence of electron-withdrawing R_F groups on PFAFs, their mass spectrometry (MS) analysis is straightforward when one uses the negative-ion mode of the MS instrument. A number of ionization methods have been used for PFAFs. For example, in the original paper on the synthesis of fullerene(R_F) $_n$ derivatives, electron-capture mass spectra were presented in which a wide distribution of the ionic species with both odd and even n values could be seen. Since the samples were proven to be mixtures of different compounds, and most likely different compositions, it was not clear at the time to what extent ions with even n values represented molecular species or fragments.² Similar results were obtained using negative-ion Fourier transform mass spectrometry. In the positive-ion mode, TMF^+ species with even n values were more intense than those with odd n values in EI mass spectra.^{6,14}

When pure samples of TMFs became available, it was found that fragmentation under electron-ionization conditions could be almost completely suppressed by lowering the electron energy (U_e) from 70 eV to 20 eV, as shown in Figure 12.¹⁶ This technique was subsequently used for the analysis of TMF mixtures because the peaks in EI mass spectra could be assumed to

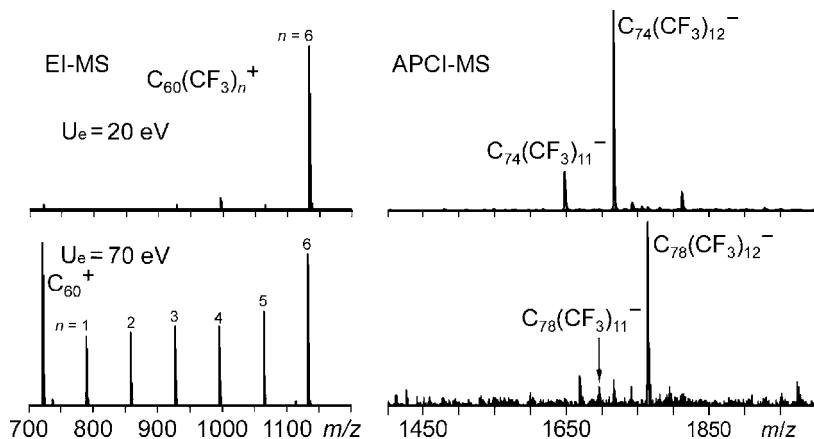


Figure 12. Left: Electron ionization mass spectra of $C_{60}(CF_3)_6$ recorded at $U_e = 20$ eV (top) and at $U_e = 70$ eV (bottom). Right: Negative-ion APCI mass spectra of TMFs of the small-bandgap fullerenes $C_{74}-D_{3h}(1)$ and $C_{78}-D_{3h}(5)$.

represent molecular species when U_e was 20 eV. Thermal desorption of the samples may cause some distortions in the relative distribution of the components due to differences in their volatilities; compounds with high n values would be more abundant in mass spectra at lower evaporator temperatures, while species with low n values would be only observed at higher temperatures.

Fragmentation-free mass spectra can be easily obtained using soft-ionization methods such as electrospray, atmospheric-pressure photoionization, or atmospheric-pressure chemical ionization.⁴⁷ These methods require that the PFAF samples be soluble in polar organic solvents because these MS methods are based on spraying solutions of analytes dissolved in polar solvents. Laser-desorption MS can be used for the analysis of solid samples, but it is also accompanied by severe fragmentation of PFAFs (in some cases down to the parent bare-cage fullerene).⁴⁸ Use of matrix-assisted laser-desorption (MALDI) MS makes it less destructive, but in order to obtain good results with this method it is preferable that the analytes are soluble in solvents that also dissolve the matrix compounds. Matrices such as elemental sulfur and *trans*-2-[3-(4-*tert*-butylphenyl)-2-methyl-2-propenylidene]malononitrile (DCTB), which were earlier shown to be well-suited for the analysis of fluoro- and chlorofullerenes,^{49,50} have also performed well for PFAF analysis.^{17,20,28} These methods usually yield mass spectra with molecular anions; for PFAFs with higher n values fragmentation due to the cleavage of R_F groups

was appreciable. Furthermore, ions due to the addition of adventitious oxygen atoms can be formed during MALDI-MS analysis.^{40,41}

2.3.2. Vibrational and UV-vis spectroscopy

Electronic (UV-vis) spectroscopy is a common technique used extensively for the characterization of fullerenes and their derivatives. In many cases it can assist in the identification of common addition patterns for derivatives with different substituents. For example, derivatives of C_{60} with the common skew-pentagonal-pyramid (SPP) addition pattern have characteristic absorption bands in their UV-vis spectra. Figure 13 shows that the spectra of SPP- $C_{60}(R_F)_4O$ ($R_F = CF_3$ and C_2F_5), SPP- $C_{60}(CF_3)_6$ (**60-6-2** in Table 1), and SPP- $C_{60}Cl_6$ are virtually identical.

In favorable cases it is possible to distinguish between addition patterns by comparing UV-vis spectra; examples include the 1,4 (*i.e.*, *para*) and 1,2 (*i.e.*, *ortho*) addition patterns in bis-adducts of C_{60} or isomers of bis-adducts of C_{70} .^{51,52} Further elucidations of the structures should, however, be done with NMR spectroscopy or X-ray crystallography.

Vibrational spectroscopy has been useful for the characterization of polyadducts of fullerenes. In particular, experimental and theoretical studies of the IR and Raman spectra of halofullerenes have provided valuable

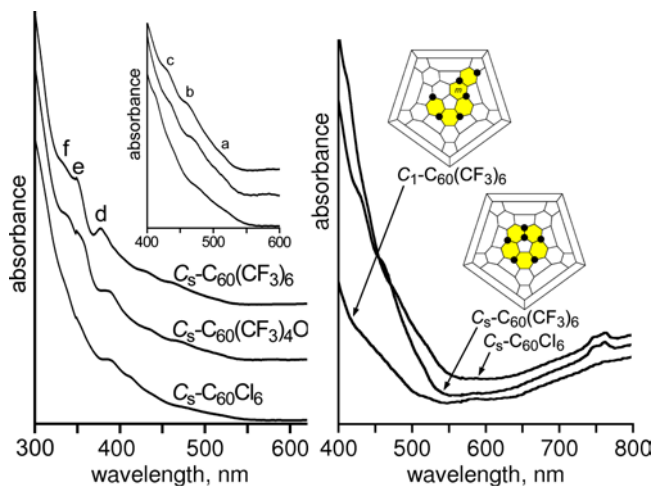


Figure 13. Left: UV-vis spectra of $C_{60}X_6$ and $C_{60}X_4O$ compounds with the common skew-pentagonal-pyramid addition pattern. Right: Comparison of the UV-vis spectra of SPP- $C_{60}X_6$ and $C_1-C_{60}(CF_3)_6$ (**60-6-1** in Table 1).

structural information.^{53,54} In fact, when other physicochemical methods do not afford an unambiguous structure elucidation, Raman and IR spectra combined with theoretical calculations can help to narrow down the possibilities.

An example of this was a study of $C_{70}(CF_3)_8$ isomers.¹⁷ The ^{19}F NMR spectrum of the major isomer suggested that it could have either C_s or C_2 symmetry (the difference is in the position of a single CF_3 group). The Raman spectrum of the major isomer was compared with the DFT-predicted Raman spectra of the two most-probable isomers, as shown in Figure 14 (note that the positions and intensities of bands in the 140–280 cm^{-1} region are sensitive to the addition pattern). This comparison allowed the authors to propose that the major isomer had C_s symmetry.¹⁷ Subsequent X-ray diffraction studies of both isomers confirmed the structural assignments made by analyzing the Raman spectra.^{55,56}

Many TMF structures determined by single-crystal X-ray diffraction provided ample opportunity for the validation of the structural predictions based on the combined analysis of NMR spectra, vibrational spectroscopy, and DFT calculations. In all cases reported to date, the predictions of these “sporting” methods for the determination of PFAF addition patterns were confirmed by X-ray crystallography. Therefore, sufficient data have now been accumulated to warrant the inclusion of these methods in the arsenal of indispensable complementary techniques for the elucidation of fullerene(X)_n structures, including those of PFAFs.

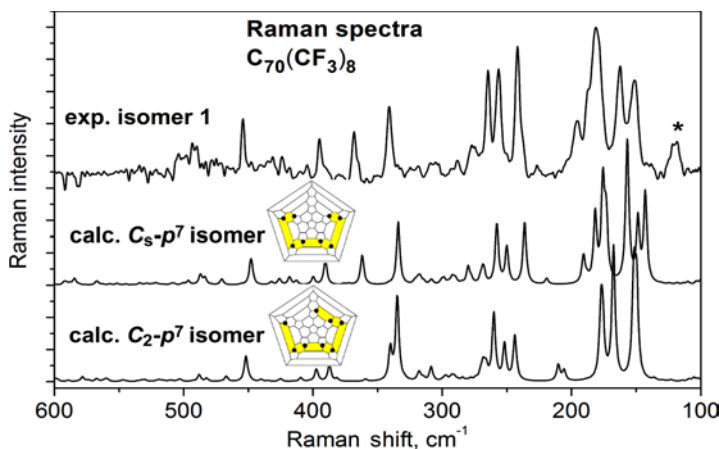


Figure 14. Experimental Raman spectrum of a sample of $C_{70}(CF_3)_8$ and the DFT-predicted Raman spectra of C_s - and C_2 - $C_{70}(CF_3)_8$ isomers (their Schlegel diagrams are also shown).

2.3.3. NMR spectroscopy

Carbon-13 NMR spectroscopy is, in general, difficult to use for the analysis and characterization of fullerene derivatives because of the relatively low receptivity of ^{13}C as an NMR nucleus (*ca.* 5,500 times lower than ^1H) and the high molar masses of fullerene compounds (and their concomitant relatively low solubilities). In order to record a ^{13}C NMR spectrum with an acceptable signal-to-noise ratio (*e.g.*, $S/N > 6$), acquisition times ranging from many hours to days are typically required even for multi-milligram samples, especially when the compounds are asymmetric, as are most PFAFs with four or more R_F groups (see Tables 1 and 2). These reasons have precluded the extensive use of ^{13}C NMR spectroscopy for the characterization of PFAFs. In fact, PFAF ^{13}C NMR spectra are only known for $\text{C}_s\text{-1,7-C}_{60}(\text{CF}_3)_2$ ⁹ and $\text{C}_1\text{-C}_{70}(\text{CF}_3)_{10}$.³⁹

On the other hand, the presence of F atoms on R_F groups that are on *meta*- or *para*- $\text{C}_6(\text{CF}_3)_2$ hexagons, 1,3- $\text{C}_5(\text{CF}_3)_2$ pentagons, or, in the case of **60-6-2** and **60-12-3** (see Table 1), on adjacent cage $\text{C}(sp^3)$ atoms makes ^{19}F NMR spectroscopy especially well-suited to help elucidate the addition patterns of PFAFs (additional advantageous features of ^{19}F NMR are 100% natural abundance, a wide chemical-shift range, and a high receptivity relative to ^1H (0.83)). The α -F atoms on R_F groups on adjacent cage $\text{C}(sp^3)$ atoms or that share a common hexagon or pentagon (*i.e.*, nearest-neighbor R_F groups) have inter- R_F -group $\text{F}\cdots\text{F}$ distances of 2.4–2.9 Å and exhibit instantaneous ^6J_FF or ^7J_FF values as high as 180 Hz (the time-averaged coupling constants for nearest-neighbor CF_3 groups are nine times smaller and range from 8 to 20 Hz).^{16,17,20,47,57} The dominant coupling mechanism is Fermi-contact through-space coupling (*i.e.*, the direct overlap of F atom lone-pair orbitals) rather than through-bond coupling;¹⁰ this mechanism for ^{19}F – ^{19}F coupling between proximate F atoms separated by four or more bonds has been verified in many other fluorinated organic molecules^{58–64}).

From detailed analyses of the number of multiplets, the multiplet splitting patterns, the δ and ^6J_FF values, and 2D COSY correlations, addition patterns can be determined for PFAFs by ^{19}F NMR spectroscopy, especially for TMF derivatives of C_{60} , C_{70} , hollow higher fullerenes, and endometallofullerenes.^{16,17,20,47,57} These ^{19}F NMR addition-pattern investigations were always performed in conjunction with DFT calculations of the most stable structures that were consistent with the experimental 1D and 2D ^{19}F NMR spectra.

For $n \leq 12$, some consistently observed $\text{C}_{60,70}(\text{CF}_3)_n$ addition-pattern tendencies based on published NMR and DFT studies (many but not all confirmed later by X-ray crystallography) are as follows (see Table 1 for references). Pairs of CF_3 radicals tend to add to *para* positions on fullerene

hexagons, and these hexagons tend to form ribbons and/or loops of edge-sharing *meta*- and/or *para*-C₆₀(CF₃)₂ hexagons (an early interpretation^{15,19} that the CF₃ groups are arranged on strings of adjacent C(*sp*³) atoms proved to be incorrect). Note that the shared edges are C(*sp*³)-C(*sp*²) edges. The CF₃ groups at either terminus of a ribbon, which give rise to quartets in ¹⁹F NMR spectra, are almost always *para* to their nearest-neighbor CF₃ group (the only exception is **70-10-7**) and have higher $-\delta$ values relative to the CF₃ groups on the interior of the ribbon, which give rise to quartets-of-quartets (or apparent septets when the two ^{6,7}J_{FF} values are nearly the same). Also common are two ribbons (**60-10-6**, **70-8-4**, **70-10-4**, and **70-10-7**) or a ribbon plus an isolated *p*-C₆(CF₃)₂ hexagon (**60-6-7**, **60-8-2**, **60-8-3**, **60-8-5**, **60-10-1**, **70-12-1**, and **70-12-2**). These have ¹⁹F NMR spectra with four quartets instead of only two for a single ribbon. Furthermore, 2D COSY spectra readily indicate the presence of an isolated *p*-C₆₀(CF₃)₂ hexagon when two quartets are correlated. Isolated CF₃ groups, which would give rise to ¹⁹F singlets, is a rare occurrence, having only been observed in the NMR spectrum of **70-10-5**. Three quartets in the ¹⁹F NMR spectrum indicate a branching pattern, with a 1,3,5-C₆(CF₃)₃ hexagon at the branch point, as in **60-12-5** and **60-12-6**. Finally, the absence of quartets in the ¹⁹F NMR spectrum indicates an addition pattern with one or more loops of edge-sharing C₆(CF₃)₂ hexagons, as in **60-10-4** and **60-12-1**.

Figure 15 shows the 1D and 2D COSY ¹⁹F NMR spectrum reported in 2005 for the isomer of C₆₀(CF₃)₁₀ abbreviated **60-10-2**.²⁵ The presence of two quartets indicated a singlet ribbon. The magnitude of the J_{FF} values for the quartets indicated which one was due to the CF₃ group at the *pmp* terminus of the ribbon (quartet **j**) and which one was due to the CF₃ group at the *p*³ terminus (quartet **i**). The absence of $-\delta$ values lower than 60 indicated the lack of eclipsed or nearly-eclipsed CF₃ groups, which ruled out the presence of a 1,3-C₅(CF₃)₂ pentagon. Taken together, these observations indicated that this isomer almost certainly had a *p*³*mmpmpmp* addition pattern, and this was subsequently proved by X-ray crystallography in 2006.⁶⁵ The F...F distances involving CF₃ groups that gave rise to quartets **i** and **j** were found to be nearly the same, but the F-C...C-F torsion angles were different, 2.1° for the CF₃(**j**) group and 23.6° for the CF₃(**i**) group. Larger F-C...C-F torsion angles are correlated with larger ⁷J_{FF} values.¹⁰

2.3.4. X-ray crystallography

More than 100 single-crystal X-ray structures of fullerene(R_F)_n compounds with even *n* = 2–18 have been reported to date. This constitutes over 10% of

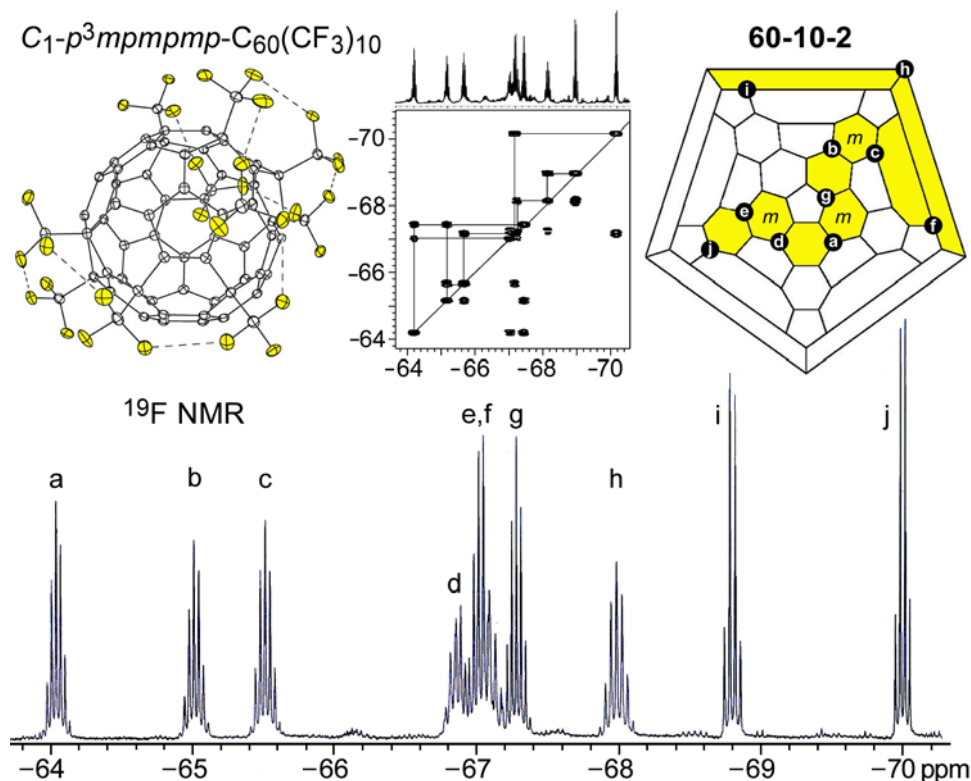


Figure 15. The 1D and 2D COSY ^{19}F NMR spectra of the isomer 60-10-2 (see Table 1 for a list of abbreviations and references). Also included are a thermal ellipsoid plot of the X-ray structure of this compound (50% probability ellipsoids) and the Schlegel diagram showing the *para*³-*meta*-*para*-*meta*-*para*-*meta*-*para* (p^3mp) ribbon of edge-sharing $C_6(CF_3)_2$ hexagons. The $F_2CF \cdots FCF_2$ interactions shown as dotted lines in the thermal ellipsoid plot range from 2.565(1) to 2.727(1) Å. Significantly, the F–C \cdots C–F torsion angles that involve the terminal CF_3 groups on the ribbon are 2.1° for the CF_3 group at the *pmp* terminus and 23.6° for the CF_3 groups at the p^3 terminus.

all reported X-ray structures of fullerenes and their derivatives. Slow solvent evaporation of solvent from a saturated solution and vapor diffusion of a co-solvent into a solution are the most common techniques used for the growth of single crystals of PFAFs suitable for X-ray diffraction. These methods work well for the majority of the perfluoroalkylated compounds, even for sub-milligram samples, which are often the only pure samples available for crystallization.^{21,28,41,46,66} Since PFAFs are composed of atoms with low X-ray scattering factors (*i.e.*, C and F) and since the size of the single crystals grown are frequently small (*e.g.*, the smallest dimension can be only 10–80 μm),

synchrotron radiation sources are often employed for the data collection. Structural information provided by crystallographic studies is usually used for (i) determination of fullerene(R_F) $_n$ addition patterns (especially for compounds with C_mF_{2m+1} groups ($m > 1$)); (ii) mapping the remaining cage $C(sp^2)-C(sp^2)$ bonds to distinguish between the bonds that are essentially single-bond or double-bond in character; and (iii) validation of theoretical calculations. For the visualization of such validations, it is convenient to plot the DFT-predicted cage C–C bond distances *vs.* the X-ray determined distances. Figure 16 shows such a plot for the isomer **60-10-2**.

For such validations to be meaningful, it is imperative that the crystallographic results (bond distances and angles) are known with high precision. In most cases, some crystallographic problems have to be overcome to improve the quality of the structural model. First, one or more of the R_F groups can exhibit rotational disorder about the $R_F-C(\text{cage})$ bond.^{21,42} A simple example of this type of disorder for a CF_3 group is shown in Figure 17. Increasing of the length of the perfluoroalkyl chains in PFAFs leads to many more possible conformations due to rotations about F_2C-CF_2 bonds as well as the $R_F-C(\text{cage})$ bond.^{31,45,46,67}

Positional disorder of the fullerene cage is often observed for PFAFs with only a few R_F groups. In such cases, different fullerene cage orientations are observed but the perfluoroalkyl groups may or may not be disordered. The X-ray structure of C_s -1,7- $C_{60}(i-C_3F_7)_2$,⁶⁸ which is an example of this type of

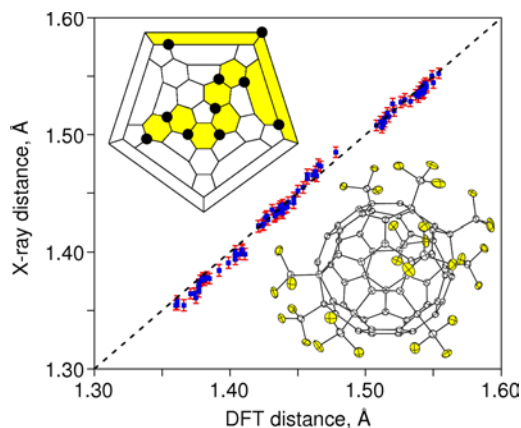


Figure 16. The excellent correlation between the 90 X-ray-determined cage C–C distances ($\pm 3\sigma$ error bars) and the DFT-predicted distances in the structure of **60-10-2** (see Table 1 for a list of PFAF abbreviations). A thermal ellipsoid plot (50% probability ellipsoids) and the Schlegel diagram of this compound are also shown.

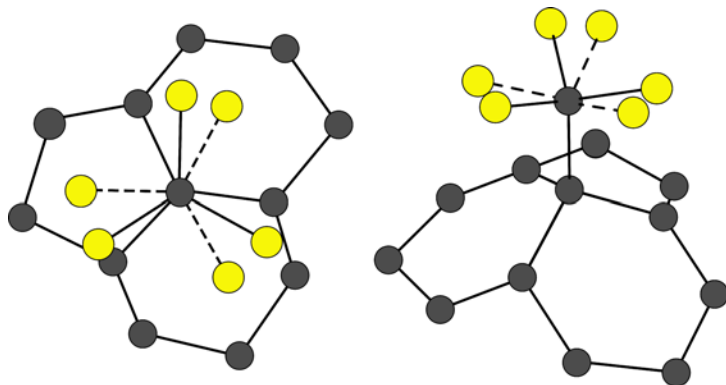


Figure 17. A two-fold conformation disorder of a CF_3 group in a PFAF X-ray structure. The C–F distances in the disordered components must often be restrained to be similar during structure refinement.

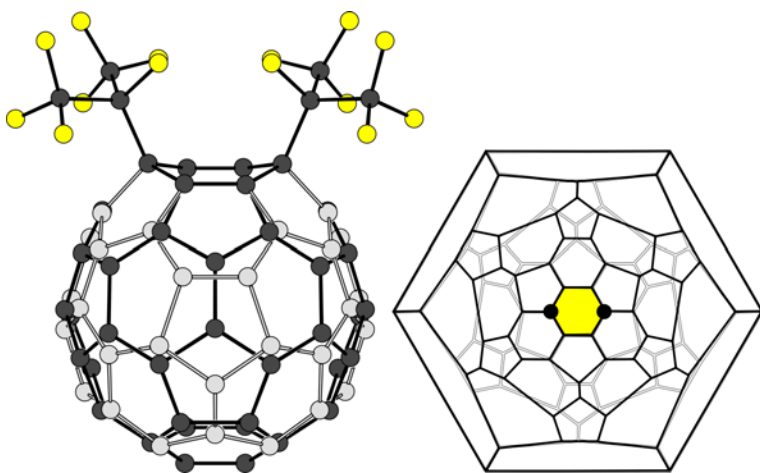


Figure 18. An example of positional cage disorder in the X-ray structure of $\text{C}_5\text{-1,7-C}_{60}(\textit{i}\text{-C}_3\text{F}_7)_2$. There are two observed orientations of the C_{60} cage rotated 180° relative to one another. The superposition of the two orientations is shown as a Schlegel diagram (right) and a ball-and-stick plot (left). The presence of a crystallographic mirror plane and the absence of a crystallographic two-fold axis lead to two possible orientations of the C_{60} cage with identical positions of the $\textit{i}\text{-C}_3\text{F}_7$ groups.

disorder, is shown in Figure 18. Rigid-group constraints (*e.g.*, the FRAG instruction in SHELXL) are normally required to locate the positions of the disordered cage C atoms, especially during the early stages of structure refinement.

The design of the molecular assemblies in which fullerene molecules are surrounded by solvent molecules in an orderly fashion can lead to a decrease in the conformational or positional disorder and improvement of the precision of the structure. There are many examples in which large flat or bowl-shaped molecules, including metal complexes of octaethylporphyrin (OEP),⁶⁹ calixarenes,⁷⁰ cyclodextrins⁷¹ or cyclotrimeratrylene,⁷² were co-crystallized with underivatized hollow fullerenes and with endometallofullerenes, resulting in ordered (or at least less disordered) structures (*e.g.*, $C_{60} \cdot 2Co(OEP) \cdot CHCl_3$ ⁶⁹ shown in Figure 19).

This use of large flat or bowl-shaped molecules to avoid disorder may not work for PFAFs with many R_F groups because the remaining fullerene π system may be a collection of small patches. Instead, small aromatic solvents such as benzene, toluene, and *p*-xylene have been found to produce ordered structures by forming π - π interactions with “bare” patches of the fullerene cage. One such example is the X-ray structure of $Sc_3N@C_{80}(CF_3)_{10} \cdot 1.5(p\text{-xylene})$,⁷³ also shown in Figure 19. In the X-ray structures of $C_{74}(CF_3)_{12} \cdot 3(p\text{-xylene})$,⁷⁴ $Sc_3N@C_{80}(CF_3)_{10} \cdot 1.5(p\text{-xylene})$,⁷³ and $Sc_3N@C_{80}(CF_3)_{14} \cdot 0.5(p\text{-xylene})$,²¹ the *p*-xylene molecules form channels, as shown in Figure 20, which may also help prevent positional cage disorder.

However, co-crystallized solvent molecules themselves can exhibit positional disorder, and when this occurs it leads to a decrease in the quality of the structure. In some cases, the solvent molecules are severely disordered and it is not possible to resolve their distinct orientations or conformations.

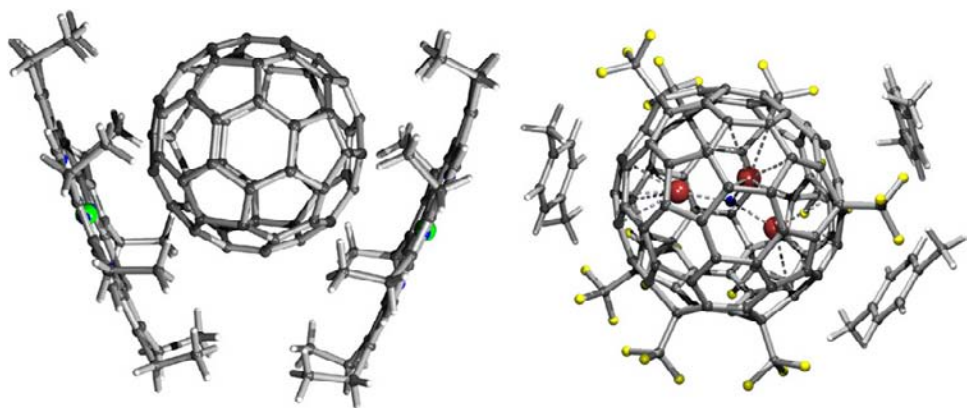


Figure 19. Left: X-ray structure of $C_{60} \cdot 2Co(OEP) \cdot CHCl_3$. The C_{60} molecules are surrounded by porphyrin molecules. Right: X-ray structure of $Sc_3N@C_{80}(CF_3)_{10} \cdot 1.5 C_8H_{10}$. The $Sc_3N@C_{80}(CF_3)_{10}$ molecules are surrounded by *p*-xylene solvent molecules.

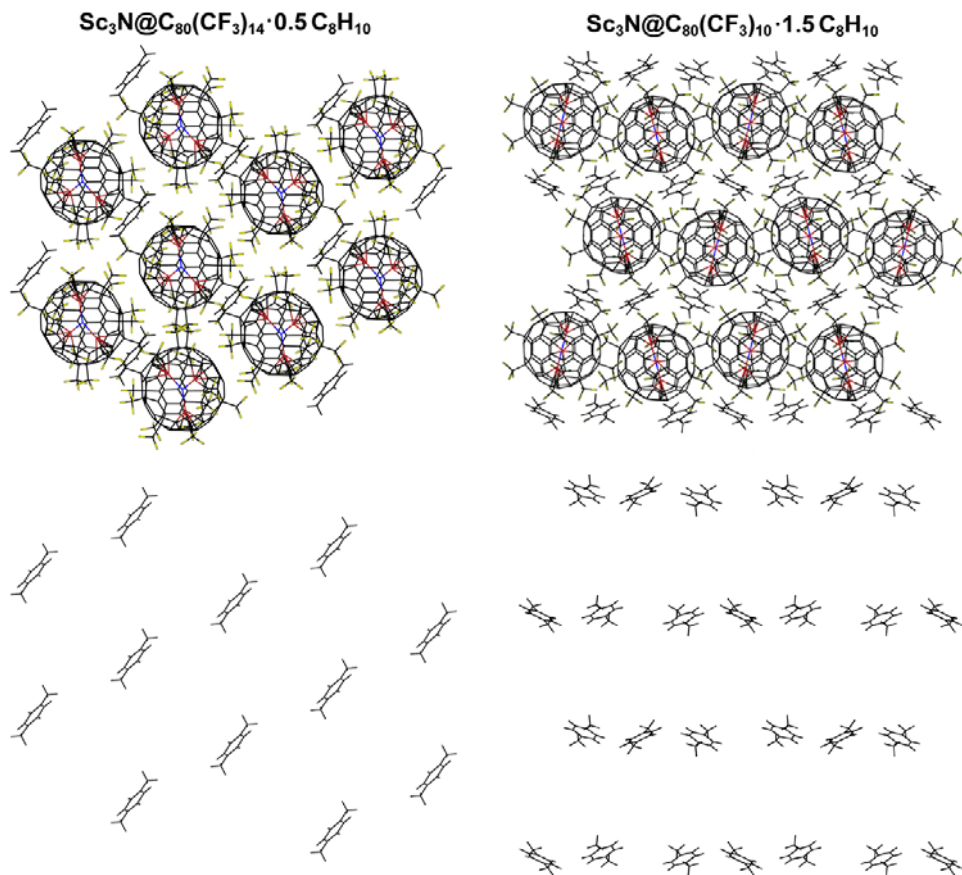


Figure 20. The packing of $\text{Sc}_3\text{N}@C_{80}(\text{CF}_3)_{10}$ and $\text{Sc}_3\text{N}@C_{80}(\text{CF}_3)_{14}$ molecules in the structures of $\text{Sc}_3\text{N}@C_{80}(\text{CF}_3)_{10} \cdot 1.5(p\text{-xylene})$ and $\text{Sc}_3\text{N}@C_{80}(\text{CF}_3)_{14} \cdot 0.5(p\text{-xylene})$. The p -xylene solvent molecules form channels which may help prevent the positional disorder of the fullerene cage.

The contribution of the disordered solvent to the structure can be estimated and accounted for using the SQUEEZE protocol.^{74–76} In the X-ray crystal structures of endometallofullerenes and their derivatives, a disorder in the positions of the endohedral metal atoms or metal cluster is often observed. For example, up to five different orientations of the Sc_3N cluster were reported in the structure of $\text{Sc}_3\text{N}@C_{80}\text{-}I_h(7)$.⁷⁷ The attachment of a large number of the CF_3 groups to this compound resulted in electron-rich and electron-poor regions on the fullerene cage, and this resulted in no Sc_3N disorder in the structures of $\text{Sc}_3\text{N}@C_{80}(\text{CF}_3)_{10}$,⁷³ $\text{Sc}_3\text{N}@C_{80}(\text{CF}_3)_{12}$,⁷³ and $\text{Sc}_3\text{N}@C_{80}(\text{CF}_3)_{14}$.⁷⁸

3. Physical Properties

Crude products of perfluoroalkylation reactions are solid polycrystalline materials, with colors ranging from dark-brown to light lemon-yellow. In the case of TMFs, the color of a purified isomer changes in an understandable way as the number of CF_3 groups increases. For example, $\text{C}_{60}(\text{CF}_3)_n$ compounds with $n = 2$ and 4 are dark brown or deep red in color, both in the solid state and in solution. With even $n = 8\text{--}18$, the colors are orange and light lemon-yellow. These observations are in general agreement with the decrease of the size of the conjugated π -system in fullerene derivatives as more R_F groups are added. At the same time, a wide variation of colors has been observed for different isomers of the same composition. Therefore, it appears that the optical gaps and visible-light absorption properties of PFAFs are also determined by the addition pattern and not only by the number of substituents.⁵⁷

PFAFs are soluble in a variety of organic solvents, and in general they have higher solubilities than the bare-cage parent fullerene. The presence of multiple R_F groups makes some PFAFs soluble in perfluorinated solvents (the solubility increases with increasing n values and with an increase in the size of the R_F group). On the other hand, PFAF solubilities in hydrocarbon solvents generally decrease as the number of R_F groups increases.

PFAFs were found to be stable for years when stored as solids in the presence of air and under ambient laboratory light. In addition, PFAFs were found to be stable for many months when dissolved in organic solvents in the presence of air and light, in sharp contrast to some halogenated fullerenes.³⁹

The outstanding thermal stability of PFAFs is notable. The majority of stable PFAF isomers characterized to date were prepared at temperatures ranging from 300 to 600°C. Strong $\text{R}_\text{F}\text{--C}(\text{cage})$ bonds are apparently the reason that most PFAFs can be sublimed without degradation. The sublimation temperatures of TMFs depend on the number of CF_3 groups: the higher the n value, the lower the sublimation temperature.^{26,35} This seemingly counter-intuitive trend is due to weaker intermolecular interactions between high- n PFAF molecules that have a significant portion of their surface covered with a “Teflon-like” coating compared with PFAF molecules that have only two or four R_F groups. These experimental observations were supported by the recently measured enthalpy of sublimation of $\text{S}_6\text{--C}_{60}(\text{CF}_3)_{12}$, 140 kJ mol^{−1} (*cf.* C_{60} , 175 kJ mol^{−1}). The sublimation temperature of $\text{S}_6\text{--C}_{60}(\text{CF}_3)_{12}$ (**60-12-1**) is close to that of the highly-fluorinated fullerene $\text{C}_{60}\text{F}_{36}$.

The volatility of PFAFs with longer R_F chains is lower than that of TMFs with the n value. Furthermore, some mixtures of $\text{C}_{60}(\text{C}_2\text{F}_5)_n$ and $\text{C}_{60}(\text{CF}_3)_n$

compounds melt at 290 and 400°C, respectively, a behavior that has not, to our knowledge, been reported for other mixtures of fullerene derivatives. Such diverse physical properties, in addition to their outstanding stability, expands the potential uses and the options for processing these promising electron acceptors.

4. Electrochemical Properties

The preparation of many dozens of highly-stable pure isomers of PFAFs and the determination of their addition patterns by spectroscopic methods and X-ray crystallography created an opportunity to study their physicochemical properties in much greater detail, and in a more systematic way, than was previously possible for any other class of fullerene derivatives. Two major electrochemical studies of C_{60} and C_{70} TMFs were published in 2007 and 2008, respectively.^{35,57} Combined, these two studies reported cyclic voltammetry data and a comprehensive theoretical study of the frontier orbitals of 35 TMFs with a wide range of compositions and with up to six isomers for a given composition.

With one exception,³⁵ all PFAFs exhibited reversible first reductions; many also exhibited reversible second reductions and some exhibited reversible third reductions.^{35,57} Cyclic voltammograms for five isomers of $C_{60}(CF_3)_{10}$ are shown in Figure 21.⁵⁷ The majority of $C_{60}(CF_3)_n$ derivatives exhibited $E_{1/2}(0/-)$ values anodically shifted relative to C_{60} , as shown in

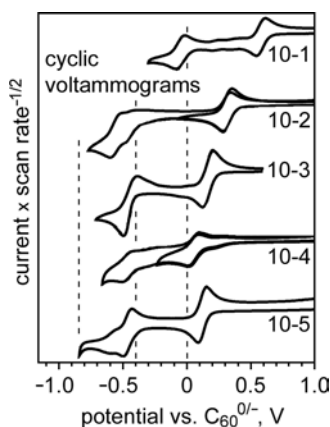


Figure 21. Representative cyclic voltammograms for $C_{60}(CF_3)_{10}$ derivatives (0.1M $TBA^+BF_4^-$ in CH_2Cl_2 , glassy carbon or Pt working electrode, 20 $mV\ s^{-1}$ scan rate). The vertical dotted lines denote the first, second, and third reduction potentials for C_{60} .

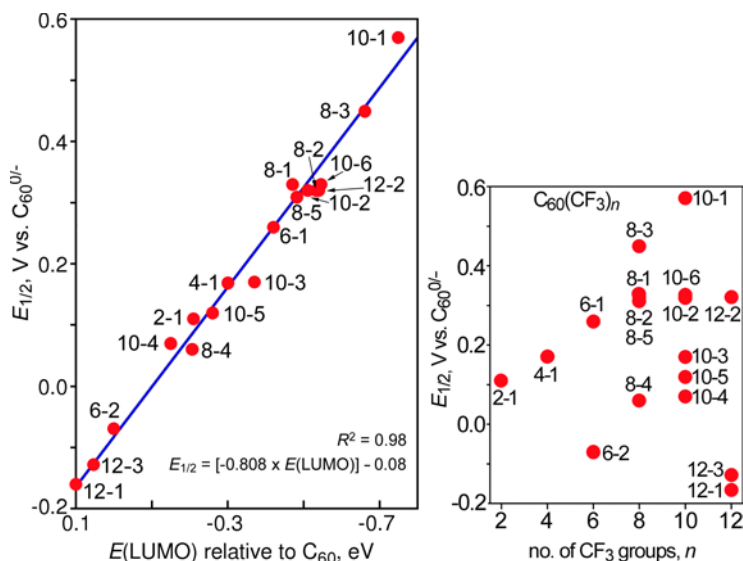


Figure 22. Left: Plot of $E_{1/2}$ values for $C_{60}(CF_3)_n^{0/-}$ couple *vs.* the DFT-predicted LUMO energy. Right: Plot of $E_{1/2}$ values for $C_{60}(CF_3)_n^{0/-}$ couple *vs.* n , the number of CF_3 groups.⁵⁷ In both plots 0.0 V is the $E_{1/2}$ value for the $C_{60}^{0/-}$ couple under the same experimental conditions.

Figure 22.⁵⁷ The largest $E_{1/2}$ difference observed to date for any PFAF is 570 mV between the isomer **60-10-1** and C_{60} . However, Figure 22 also shows that three PFAFs, **60-6-2**, **60-12-1**, and **60-12-3** have first reduction potentials that are *cathodically* shifted relative to the first reduction potential of C_{60} . The entire range of $E_{1/2}(0/-)$ values for these compounds is 0.73 V.

Figure 22 also shows that isomers of $C_{60}(CF_3)_8$, $C_{60}(CF_3)_{10}$, and $C_{60}(CF_3)_{12}$ exhibit wide ranges of $E_{1/2}(0/-)$ values, up to 0.5 V for the $C_{60}(CF_3)_{10}$ and $C_{60}(CF_3)_{12}$ isomers. Along with the negative $E_{1/2}(0/-)$ values (relative to $C_{60}^{0/-}$) for **60-6-2**, **60-12-1**, and **60-12-3**, these results demonstrated that the addition pattern is as important, if not more important in some cases, than the number of substituents or the electron-withdrawing or -donating nature of the substituent.⁵⁷ A detailed analysis of the addition patterns, DFT-predicted LUMOs and LUMO energies, and experimental $E_{1/2}$ values led to the conclusion that the best electron acceptors are those TMF isomers that have addition patterns with the most delocalized LUMOs *and* the greatest number of non-terminal double bonds in pentagons.⁵⁷

The electrochemical properties of bis-adducts $Sc_3N@C_{80}(CF_3)_2$ ^{22,23} and $C_{70}(C_2F_5)_2$,⁴⁴ some perfluorinated cycloadducts of C_{60} , and several fullerene $(C_2F_5)_n$ isomers²⁸ were recently reported. Only one PFAF, $Sc_3N@C_{80}(CF_3)_2$, exhibited a reversible oxidation (in addition to three reversible reductions).^{22,23}

5. Chemical Properties

The further derivatization of PFAFs is an important endeavor, both in view of potential applications and from the standpoint of fundamental knowledge (*e.g.*, which of the remaining double bonds in PFAFs are the most susceptible to further addition, and why?). Development of PFAF-based materials for various applications may require modification of their physical, chemical, optical, or magnetic properties, any of which might be accomplished by adding other functional groups to PFAFs.

One of the best tools developed in synthetic fullerene chemistry is cycloaddition chemistry.⁷⁹ There is a considerably broad range of PFAF compositions that may be attractive synthons for further elaboration. For PFAFs with $n = 2$ and 4, a large part of the fullerene sphere remains accessible for further additions. No chemical-reactivity studies of low- n -value PFAFs have been published to date. The PFAF compounds with higher n values could be useful synthons for selective syntheses if one or two particularly reactive double bonds are present in their structures. The chemical reactivity of one such PFAF compound, **70-10-1**, has been recently studied and will be discussed below.^{29,37,38}

The thermodynamically most stable and most abundant isomer of $C_{70}(CF_3)_{10}$ is **70-10-1**. It is the only PFAF that can be prepared selectively and in quantities of hundreds of milligrams.²⁹ Its molecular structure was determined by ^{19}F NMR spectroscopy combined with the DFT calculations and confirmed by X-ray crystallography (see Figure 11). The two remaining $C(sp^2)_5$ pentagons in this isomer are involved in the further addition of two CF_3 groups, and all four known isomers of $C_{70}(CF_3)_{12}$, which have the substructure of **70-10-1**, have the two additional CF_3 groups on one or both of these pentagons. The [6,6] double bond between these $C(sp^2)_5$ pentagons in **70-10-1** (the C33–C34 bond in Figure 23) should be the most reactive bond for cycloadditions, and indeed, recent studies have demonstrated that this is the case for Bingel-Hirsch and Diels-Alder cycloaddition reactions, as shown in Figure 23.

Under Bingel-Hirsch conditions, the reaction of **70-10-1** (**1**) with diethyl malonate yielded 48% of a single product, Bingel adduct **2**.^{29,37} Another example of such reaction is a successful preparation of an electroactive dyad **4**: **70-10-1** reacted with di[9,10-bis(1,3-dithiol-2-ylidene)-9,10-dihydro-2-anthracenylhydroxymethyl] malonate **3**, in the presence of CBr_4 and DBU. The yield was even higher: 80% based on converted $C_1-C_{70}(CF_3)_{10}$.²⁹ In a Diels-Alder cycloaddition, the reaction of $C_1-C_{70}(CF_3)_{10}$ with 3,6-dimethoxy-1,2-quinodimethane resulted in the regioselective synthesis of a single monoadduct with a yield of 73% based on converted

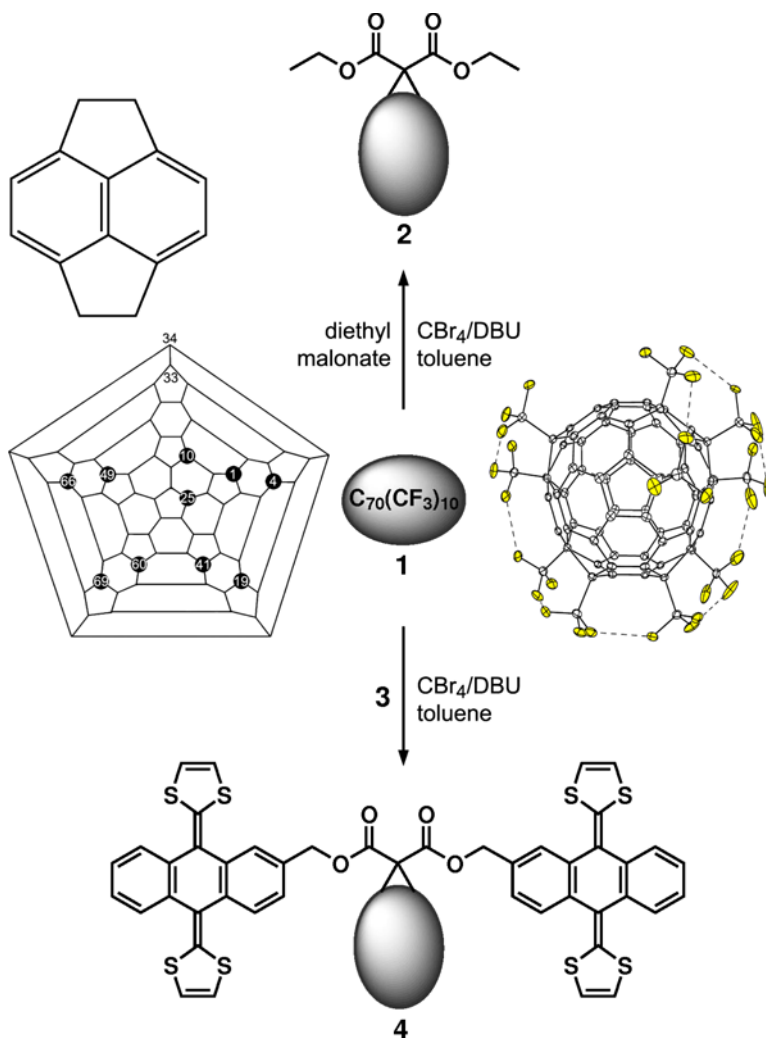


Figure 23. The transformations of **1** into Bingel-Hirsch cycloadducts **2** and **4** (compound **3** is di[9,10-bis(1,3-dithiol-2-ylidene)-9,10-dihydro-2-anthracenylmethyl] malonate). Also shown are the X-ray structure and IUPAC-numbered Schlegel diagram of **1** (**70-10-1**) and a pyracene-like fullerene fragment showing a [6,6] double bond in the center (such as the reactive bond C33–C34 in **1**).²⁹

$C_1-C_{70}(CF_3)_{10}$. Similar to the Bingel-Hirsch adducts, the same short double bond between C33 and C34 was attacked to form a [4+2] cycloadduct. Electrochemical studies of the Diels-Alder adduct demonstrated a significant cathodic shift (*ca.* 250 mV) of the reduction potentials relative to **70-10-1**, possibly due to the additional loss of a cage double bond and the formation of a compound with a new addition pattern (which was shown to have a

higher LUMO energy than that of **70-10-1**).³⁸ These initial successful studies of cycloaddition chemistry with a PFAF starting material open up a wide avenue for further explorations and ultimately the preparation of targeted compounds with specific properties for practical applications, including covalently-bonded and supramolecular assemblies.

6. Conclusions and Perspectives

Several efficient synthetic procedures for the preparation of air- and thermally-stable PFAFs with the variety of R_F radicals have been developed in recent years. These reactions occur at elevated temperatures and with good-to-quantitative fullerene conversion. Most of the crude product mixtures require HPLC separation. Nevertheless, many dozens of pure PFAF isomers have been isolated and characterized. Future developments in their synthesis and purification should be directed towards improving selectivity and searching for alternative separation methods for PFAFs with many R_F groups, which cannot be separated into pure compounds using currently available HPLC procedures.

Two important areas for future study include (i) the electrochemical properties of PFAFs other than fullerene(CF_3)_n derivatives and (ii) the chemical properties of different PFAFs. Knowledge of the reduction potentials of new PFAFs and their derivatives, with unprecedented addition patterns that can be expected with very bulky R_F groups, will significantly increase our fundamental understanding of the correlations between addition patterns and various physicochemical properties and will open up new areas for their application as components in organic electronics and photonics. Advancements in the further functionalization of PFAFs will allow one to develop new generations of PFAF-based materials that are designed from first principles to have specific physical, chemical, optical, magnetic, and/or electronic properties.

References

1. Krusic, P. J.; Wasserman, E.; N., K. P.; Morton, J. R.; Preston, K. F. *Science* **1991**, *254*, 1183–1186.
2. Fagan, P. J.; Krusic, P. J.; McEwen, C. N.; Lazar, J.; Parker, D. H.; Herron, N.; Wasserman, E. *Science* **1993**, *262*, 404–407.
3. Yoshida, M.; Sultana, F.; Uchiyama, N.; Yamada, Y.; Iyoda, M. *Tetrahedron Lett.* **1999**, *40*, 735–736.
4. Uzkikh, I. S.; Dorozhkin, E. I.; Boltalina, O. V.; Boltalin, A. I. *Dokl. Akad. Nauk* **2001**, *379*, 344–347.
5. Kuvychko, I. V.; Whitaker, J. B.; Larson, B. W.; Shustova, N. B.; Raguindin, R. S.; Suhr, K. J.; Strauss, S. H.; Boltalina, O. V. **2010**, submitted for publication.

6. Fritz, H. P.; Hiemeyer, R. *Carbon* **1995**, 33, 1601–1609.
7. Boltalina, O. V.; Darwish, A. D.; Street, J. M.; Taylor, R.; Wei, X.-W. *Perkin Trans.* **2002**, 2, 251–256.
8. Boltalina, O. V.; Hitchcock, P. B.; Troshin, P. A.; Street, J. M.; Taylor, R. *J. Chem. Soc., Perkin Trans.* **2000**, 2, 2410–2414.
9. Avent, A. G.; Boltalina, O. V.; Goryunkov, A. V.; Darwish, A. D.; Markov, V. Y.; Taylor, R. *Fullerenes Nanotubes Carbon Nanostruct.* **2002**, 10, 235–241.
10. Kareev, I. E.; Santiso-Quinones, G.; Kuvychko, I. V.; Ioffe, I. N.; Goldt, I. V.; Lebedkin, S. F.; Seppelt, K.; Strauss, S. H.; Boltalina, O. V. *J. Am. Chem. Soc.* **2005**, 127, 11497–11504.
11. Dorozhkin, E. I.; Goryunkov, A. A.; Ioffe, I. N.; Avdoshenko, S. M.; Markov, V. Y.; Tamm, N. B.; Ignat'eva, D. V.; Sidorov, L. N.; Troyanov, S. I. *Eur. J. Org. Chem.* **2007**, 5082–5094.
12. Boltalina, O. V.; Goryunkov, A. A.; Markov, V. Y.; Ioffe, I. N.; Sidorov, L. N. *Int. J. Mass Spectrom.* **2003**, 228, 807–824.
13. Troyanov, S. I.; Goryunkov, A. A.; Tamm, N. B.; Markov, V. Y.; Ioffe, I. N.; Sidorov, L. N. *Dalton Trans.* **2008**, 2627–2632.
14. Lyakhovetsky, Y. I.; Shilova, E. A.; Tumanskii, B. L.; Usatov, A. V.; Avetisyan, E. A.; Sterlin, S. R.; Pleshkova, A. P.; Novikov, Y. N.; Nekrasov, Y. S.; Taylor, R. *Fullerene Sci. Technol.* **1999**, 7, 263–287.
15. Darwish, A. D.; Abdul-Sada, A. K.; Avent, A. G.; Lyakhovetsky, V. I.; Shilova, E. A.; Taylor, R. *Org. Biomol. Chem.* **2003**, 1, 3102–3110.
16. Goryunkov, A. A.; Kuvychko, I. V.; Ioffe, I. N.; Dick, D. L.; Sidorov, L. N.; Strauss, S. H.; Boltalina, O. V. *J. Fluorine Chem.* **2003**, 124, 61–64.
17. Dorozhkin, E. I.; Ignat'eva, D. V.; Tamm, N. B.; Goryunkov, A. A.; Khavrel, P. A.; Ioffe, I. N.; Popov, A. A.; Kuvychko, I. V.; Streletskiy, A. V.; Markov, V. Y.; Spandl, J.; Strauss, S. H.; Boltalina, O. V. *Chem.-Eur. J.* **2006**, 12, 3876–3889.
18. Darwish, A. D.; Abdul-Sada, A. K.; Avent, A. G.; Martsinovich, N.; Street, J. M.; Taylor, R. *J. Fluorine Chem.* **2004**, 125, 1383–1391.
19. Darwish, A. D.; Avent, A. G.; Abdul-Sada, A. K.; Taylor, R. *Chem. Commun.* **2003**, 1374–1375.
20. Kareev, I. E.; Lebedkin, S. F.; Bubnov, V. P.; Yagubskii, E. B.; Ioffe, I. N.; Khavrel, P. A.; Kuvychko, I. V.; Strauss, S. H.; Boltalina, O. V. *Angew. Chem. Int. Ed.* **2005**, 44, 1846–1849.
21. Shustova, N. B.; Chen, Y. S.; Mackey, M. A.; Coumbe, C. E.; Phillips, J. P.; Stevenson, S.; Popov, A. A.; Boltalina, O. V.; Strauss, S. H. *J. Am. Chem. Soc.* **2009**, 131, 17630–17637.
22. Shustova, N. B.; Popov, A. A.; Mackey, M. A.; Coumbe, C. E.; Phillips, J. P.; Stevenson, S.; Strauss, S. H.; Boltalina, O. V. *J. Am. Chem. Soc.* **2007**, 129, 11676–11677.
23. Popov, A. A.; Shustova, N. B.; Svitova, A. L.; Mackey, M. A.; Coumbe, C. E.; Phillips, J. P.; Stevenson, S.; Strauss, S. H.; Boltalina, O. V.; Dunsch, L. *Chem.-Eur. J.* **2010**, 16, 4721–4724.
24. Shustova, N. B.; Peryshkov, D. V.; Kuvychko, I. V.; Chen, Y.-S.; Mackey, M. A.; Coumbe, C. E.; Heaps, D. T.; Confait, B. S.; Heine, T.; Phillips, J. P.; Stevenson, S.; Dunsch, L.; Popov, A. A.; Strauss, S. H.; Boltalina, O. V. **2010**, submitted for publication.
25. Kareev, I. E.; Kuvychko, I. V.; Lebedkin, S. F.; Miller, S. M.; Anderson, O. P.; Seppelt, K.; Strauss, S. H.; Boltalina, O. V. *J. Am. Chem. Soc.* **2005**, 127, 8362–8375.
26. Kareev, I. E.; Shustova, N. B.; Kuvychko, I. V.; Lebedkin, S. F.; Miller, S. M.; Anderson, O. P.; Popov, A. A.; Strauss, S. H.; Boltalina, O. V. *J. Am. Chem. Soc.* **2006**, 128, 12268–12280.
27. Troyanov, S. I.; Dimitrov, A.; Kemnitz, E. *Angew. Chem. Int. Ed.* **2006**, 45, 1971–1974.

28. Shustova, N. B.; Kareev, I. E.; Kuvychko, I. V.; Whitaker, J. B.; Lebedkin, S. F.; Popov, A. A.; Chen, Y. S.; Seppelt, K.; H., S. S.; Boltalina, O. V. *J. Fluorine Chem.* **2010**, *131*, 1198–1212.
29. Takano, Y.; Ángeles Herranz, M.; Martín, N.; de Miguel Rojas, G.; Guldi, D. M.; Kareev, I. E.; Strauss, S. H.; Boltalina, O. V.; Tsuchiya, T.; Akasaka, T. *Chem.–Eur. J.* **2010**, *16*, 5343–5353.
30. McEwen, C. N.; Fagan, P. J.; Krusic, P. J. *Int. J. Mass Spectrom.* **1995**, *146*, 297–304.
31. Mutig, T.; Kemnitz, E.; Troyanov, S. I. *Eur. J. Org. Chem.* **2008**, 3256–3259.
32. Svensson, M.; Zhang, F.; Veenstra, S. C.; Verhees, W. J. H.; Hummelen, J. C.; Kroon, J. M.; Inganaes, O.; Andersson, M. R. *Adv. Mater. (Weinheim, Ger.)* **2003**, *15*, 988–991.
33. Chidichimo, G.; Filippelli, L. *Int. J. Photoenergy* **2010**, *2010*, 123534–1–11.
34. Kareev, I. E.; Kuvychko, I. V.; Popov, A. A.; Lebedkin, S. F.; Miller, S. M.; Anderson, O. P.; Strauss, S. H.; Boltalina, O. V. *Angew. Chem. Int. Ed.* **2005**, *44*, 7984–7987.
35. Popov, A. A.; Kareev, I. E.; Shustova, N. B.; Lebedkin, S. F.; Strauss, S. H.; Boltalina, O. V.; Dunsch, L. *Chem.–Eur. J.* **2008**, *14*, 107–121.
36. Fowler, P. W.; Redmond, D. B.; Sandall, J. P. B. *J. Chem. Soc. Faraday Trans.* **1998**, *94*, 2883–2887.
37. Ovchinnikova, N. S.; Ignat'eva, D. V.; Tamm, N. B.; Avdoshenko, S. M.; Goryunkov, A. A.; Loffe, I. N.; Markov, V. Y.; Troyanov, S. I.; Sidorov, L. N.; Yurovskaya, M. A.; Kemnitz, E. *New J. Chem.* **2008**, *32*, 89–93.
38. Takano, Y.; Herranz, M. A.; Kareev, I. E.; Strauss, S. H.; Boltalina, O. V.; Akasaka, T.; Martín, N. *J. Org. Chem.* **2009**, *74*, 6902–6905.
39. Kuvychko, I. V.; Streletskii, A. A.; Shustova, N. B.; Seppelt, K.; Drewello, T.; Popov, A. A.; Strauss, S. H.; Boltalina, O. V. *J. Am. Chem. Soc.* **2010**, *132*, 6443–6462.
40. Samokhvalova, N. A.; Khavrel, P. A.; Goryunkov, A. A.; Ioffe, I. N.; Karnatsevich, V. L.; Sidorov, L. N.; Kemnitz, E.; Troyanov, S. I. *Rus. Chem. Bull.* **2008**, *57*, 2526–2534.
41. Samokhvalova, N. A.; Khavrel, P. A.; Markov, V. Y.; Samokhvalov, P. S.; Goryunkov, A. A.; Kemnitz, E.; Sidorov, L. N.; Troyanov, S. I. *Eur. J. Org. Chem.* **2009**, 2935–2938.
42. Kareev, I. E.; Shustova, N. B.; Peryshkov, D. V.; Lebedkin, S. F.; Miller, S. M.; Anderson, O. P.; Popov, A. A.; Boltalina, O. V.; Strauss, S. H. *Chem. Commun.* **2007**, 1650–1652.
43. Troyanov, S. I.; Goryunkov, A. A.; Dorozhkin, E. I.; Ignat'eva, D. V.; Tamm, N. B.; Avdoshenko, S. M.; Ioffe, I. N.; Markov, V. Y.; Sidorov, L. N.; Scheural, K.; Kemnitz, E. *J. Fluorine Chem.* **2007**, *128*, 545–551.
44. Popov, A. A.; Shustova, N. B.; Boltalina, O. V.; Strauss, S. H.; Dunsch, L. *Chem. Phys. Chem.* **2008**, *9*, 431–438.
45. Tamm, N. B.; Troyanov, S. I. *Mendeleev Commun.* **2007**, *17*, 172–174.
46. Tamm, N. B.; Ioffe, I. N.; Kemnitz, E.; Troyanov, S. I. *Dalton Trans.* **2009**, 2740–2745.
47. Shustova, N. B.; Kuvychko, I. V.; Bolskar, R. D.; Seppelt, K.; Strauss, S. H.; Popov, A. A.; Boltalina, O. V. *J. Am. Chem. Soc.* **2006**, *128*, 15793–15798.
48. Tagmatarchis, N.; Taninaka, A.; Shinohara, H. *Chem. Phys. Lett.* **2002**, *355*, 226–232.
49. Streletskiy, A. V.; Kouvitchko, I. V.; Esipov, S. E.; Boltalina, O. V. *Rapid Commun. Mass Spectr.* **2001**, *16*, 99–102.
50. Streletskii, A. V.; Ioffe, I. N.; Kotsiris, S. G.; Barrow, M. P.; Drewello, T.; Strauss, S. H.; Boltalina, O. V. *J. Phys. Chem. A* **2005**, *109*, 714–719.
51. Kadish, K. M.; Gao, X.; Van Caemelbecke, E.; Hirasaka, T.; Suenobu, T.; Fukuzumi, S. *J. Phys. Chem.* **1998**, *100*, 3898–3906.

52. Kadish, K.; Gao, X.; Gorelik, O.; Van Caemelbecke, E.; Suenobu, T.; Fukuzumi, S. *J. Phys. Chem. A* **2000**, *104*, 2902–2907.
53. Popov, A. A.; Goryunkov, A. A.; Goldt, I. V.; Kareev, I. E.; Kuvychko, I. V.; Hunnius, W.-D.; Seppelt, K.; Strauss, S. H.; Boltalina, O. V. *J. Phys. Chem. A* **2004**, *108*, 11449–11456.
54. Popov, A. A.; Senyavin, V. M.; Boltalina, O. V.; Seppelt, K.; Spandl, J.; Feigerle, C. S.; Compton, R. N. *J. Phys. Chem. A* **2006**, *110*, 8645–8652.
55. Goryunkov, A. A.; Dorozhkin, E. I.; Ignat'eva, D. V.; Sidorov, L. N.; Kemnitz, E.; Sheldrick, G. M.; Troyanov, S. I. *Mendeleev Commun.* **2005**, 225–227.
56. Mutig, T.; Ioffe, I. N.; Kemnitz, E.; Troyanov, S. I. *Mendeleev Commun.* **2008**, *18*, 73–75.
57. Popov, A. A.; Kareev, I. E.; Shustova, N. B.; Stukalin, E. B.; Lebedkin, S. F.; Seppelt, K.; Strauss, S. H.; Boltalina, O. V.; Dunsch, L. *J. Am. Chem. Soc.* **2007**, *129*, 11551–11568.
58. Barbarich, T. J.; Rithner, C. D.; Miller, S. M.; Anderson, O. P.; Strauss, S. H. *J. Am. Chem. Soc.* **1999**, *121*, 4280–4281.
59. Barbarich, T. J.; Nolan, B. G.; Tsujioka, S.; Miller, S. M.; Anderson, O. P.; Strauss, S. H. *J. Fluorine Chem.* **2001**, *112*, 335–342.
60. Arnold, W. D.; Mao, J.; Sun, H.; Oldfield, E. *J. Am. Chem. Soc.* **2000**, *122*, 12164–12168.
61. Peralta, J. E.; Barone, V.; Contreras, R. H.; Zaccari, D. G.; Snyder, J. P. *J. Am. Chem. Soc.* **2001**, *123*, 9162–9163.
62. Alkorta, I.; Elguero, J. E. *Struct. Chem.* **2004**, *15*, 117–120.
63. Tuttle, T.; Grafenstein, J.; Cremer, D. *Chem. Phys. Lett.* **2004**, *394*, 5–13.
64. San Fabian, J.; Westra Hoekzema, A. J. A. *J. Chem. Phys.* **2004**, *121*, 6268–6276.
65. Kareev, I. E.; Lebedkin, S. F.; Miller, S. M.; Anderson, O. P.; Strauss, S. H.; Boltalina, O. V. *Acta Crystallogr.* **2006**, *E62*, o1498–o1500.
66. Troyanov, S. I.; Tamm, N. B. *Crystallogr. Rep.* **2009**, *54*, 598–602.
67. Deya, A.; Metrangolo, P.; Pilati, T.; Resnati, G.; Terraneo, G.; Wlassics, I. *J. Fluorine Chem.* **2009**, *130*, 816–823.
68. Shustova, N. B.; Kuvychko, I. V.; Peryshkov, D. V.; Whitaker, J. B.; Larson, B. W.; Chen, Y. S.; Dunsch, L.; Seppelt, K.; Popov, A. A.; Strauss, S. H.; Boltalina, O. V. *Chem. Commun.* **2010**, in press (doi 10.1039/c0cc03247f).
69. Olmstead, M. M.; Costa, D. A.; Maitra, K.; Noll, B. C.; Phillips, S. L.; Van Calcar, P. M.; Balch, A. L. *J. Am. Chem. Soc.* **1999**, *121*, 7090–7097.
70. Atwood, J. L.; Koutsantonis, G. A.; Raston, C. L. *Nature* **1994**, *368*, 229–231.
71. Yoshida, Z. *Angew. Chem. Int. Ed.* **1994**, *33*, 1597–1599.
72. Steed, J. W.; Junk, P. C.; Atwood, J. L.; Barnes, M. J.; Raston, C. L.; Burkhalter, R. S. *J. Am. Chem. Soc.* **1994**, *116*, 10346–10347.
73. Shustova, N. B.; Peryshkov, D. V.; Kuvychko, I. V.; Chen, Y.-S.; Mackey, M. A.; Coumbe, C. E.; Heaps, D. T.; Confait, B. S.; Heine, T.; Phillips, J. P.; Stevenson, S.; Dunsch, L.; Popov, A. A.; Strauss, S. H.; Boltalina, O. V. **2010**, submitted for publication.
74. Shustova, N. B.; Popov, A. A.; Newell, B. S.; Miller, S. M.; Anderson, O. P.; Seppelt, K.; Bolskar, R. D.; Boltalina, O. V.; Strauss, S. H. *Angew. Chem. Int. Ed.* **2007**, *46*, 4111–4114.
75. Spek, A. L. *J. Appl. Crystallogr.* **2003**, *36*, 7–13.
76. van der Sluis, P.; Spek, A. L. *Acta Crystallogr.* **1990**, *A46*, 194–201.
77. Cai, T.; Slebonick, C.; Xu, L.; Harich, K.; Glass, T. E.; Chancellor, C.; Fettingner, J. C.; Olmstead, M. M.; Balch, A. L.; Gibson, H. W.; Dorn, H. C. *J. Am. Chem. Soc.* **2006**, *128*, 6486–6492.
78. Shustova, N. B.; Chen, Y.-S.; Mackey, M. A.; Coumbe, C. E.; Phillips, J. P.; Stevenson, S.; Popov, A. A.; Boltalina, O. V.; Strauss, S. H. *J. Am. Chem. Soc.* **2009**, *131*, 17630–17637.

79. Hirsch, A.; Brettreich, M. *Fullerenes — Chemistry and Reactions*; Wiley-VCH: Weinheim, **2005**.
80. Kareev, I. E.; Kuvychko, I. V.; Lebedkin, S. F.; Miller, S. M.; Anderson, O. P.; Strauss, S. H.; Boltalina, O. V. *Chem. Commun.* **2006**, 308–310.
81. Shustova, N. B.; Kuvychko, I. V.; Boltalina, O. V.; Strauss, S. H. *Acta Crystallogr.* **2007**, E63, o4575.
82. Tamm, N. B.; Avdoshenko, S. M.; Kemnitz, E.; Troyanov, S. I. *Russ. Chem. Bull. Int. Ed.* **2007**, 56, 915–921.
83. Mutig, T.; Avdoshenko, S. M.; Kemnitz, E.; Troyanov, S. I. *J. Fluorine Chem.* **2009**, 130, 241–247.
84. Shustova, N. B.; Peryshkov, D. V.; Kareev, I. E.; Boltalina, O. V.; Strauss, S. H. *Acta Crystallogr.* **2007**, E63, o3398.
85. Kareev, I. E.; Shustova, N. B.; Newell, B. S.; Miller, S. M.; Anderson, O. P.; Strauss, S. H.; Boltalina, O. V. *Acta Crystallogr.* **2006**, E62, o3154–o3156.
86. Kareev, I. E.; Lebedkin, S. F.; Popov, A. A.; Miller, S. M.; Anderson, O. P.; Strauss, S. H.; Boltalina, O. V. *Acta Crystallogr.* **2006**, E62, o1501–o1503.
87. Shustova, N. B.; Peryshkov, D. V.; Popov, A. A.; Boltalina, O. V.; Strauss, S. H. *Acta Crystallogr.* **2007**, E62, o3129.
88. Omelyanyuk, N. A.; Goryunkov, A. A.; Tamm, N. B.; Avdoshenko, S. M.; Ioffe, I. N.; Sidorov, L. N.; Kemnitz, E.; Troyanov, S., I. *Chem. Commun.* **2007**, 4794–4796.
89. Shustova, N. B.; Anderson, O. P.; Boltalina, O. V.; Strauss, S. H.; Kareev, I. E. *Acta Crystallogr.* **2008**, E64, o0159.
90. Troyanov, S. I.; Goryunkov, A. A.; Dorozhkin, E. I.; Ignat'eva, D. V.; Tamm, N. B.; Avdoshenko, S. M.; Ioffe, I. N.; Markov, V. Y.; Sidorov, L. N.; Scheurel, K.; Kemnitz, E. *J. Fluorine Chem.* **2007**, 128, 545–551.
91. Mutig, T.; Kemnitz, E.; Troyanov, S. I. *Mendeleev Commun.* **2009**, 19, 30–31.
92. Shustova, N. B.; Kareev, I. E.; Popov, A. A.; Boltalina, O. V.; Strauss, S. H. *Acta Crystallogr.* **2007**, E62, 4073.
93. Kareev, I. E.; Boltalina, O. V.; Strauss, S. H.; Popov, A. A. **2010**, Unpublished prediction based on ^{19}F NMR data and DFT calculations.
94. Kareev, I. E.; Lebedkin, S. F.; Miller, S. M.; Anderson, O. P.; Strauss, S. H.; Boltalina, O. V. *Acta Crystallogr.* **2006**, E62, o617–o619.
95. Kareev, I. E.; Lebedkin, S. F.; Miller, S. M.; Anderson, O. P.; Strauss, S. H.; Boltalina, O. V. *Acta Crystallogr.* **2006**, E62, o620–o622.
96. Shustova, N. B.; Kareev, I. E.; Popov, A. A.; Boltalina, O. V.; Strauss, S. H. *Acta Crystallogr.* **2007**, E62, o3928.
97. Goryunkov, A. A.; Ignat'eva, D. V.; Tamm, N. B.; Moiseeva, N. N.; Ioffe, I. N.; Avdoshenko, S. M.; Markov, V. Y.; Sidorov, L. N.; Kemnitz, E.; Troyanov, S., I. *Eur. J. Org. Chem.* **2006**, 2508–2512.
98. Avdoshenko, S. M.; Goryunkov, A. A.; Ioffe, I. N.; Ignat'eva, D. V.; Sidorov, L. N.; Pattison, P.; Kemnitz, E.; Troyanov, S., I. *Chem. Commun.* **2006**, 2463–2465.

This page intentionally left blank

Chapter 5

New Vistas in Endohedral Metallofullerenes

Michio Yamada^{}, Takeshi Akasaka^{†,§} and Shigeru Nagase^{‡,¶}*

^{}Department of Chemistry, Tokyo Gakugei University,
Koganei, Tokyo 184-8501, Japan*

*[†]Life Science Center of Tsukuba Advanced Research Alliance,
Tsukuba, Ibaraki 305-8577, Japan*

*[‡]Department of Theoretical and Computational Molecular Science,
Institute for Molecular Science, Okazaki, Aichi 444-8585, Japan*

1. Introduction	146
2. Cage Frameworks, Positions, and Movements of Encaged Species	147
2.1. Monometallofullerenes	147
2.2. Dimetallofullerenes	149
2.3. Clusterfullerenes	153
3. Electronic Properties of Pristine Endohedral Metallofullerenes	154
4. Chemistry of Endohedral Metallofullerenes	156
4.1. Bis-silylation	156
4.2. Electrophilic carbene addition	160
4.3. 1,3-Dipolar cycloaddition	165
4.4. Nucleophilic addition	168
4.5. Diels–Alder reaction	170
4.6. Radical reaction	173
5. Electronic Tuning by Chemical Functionalization	175

Corresponding authors. E-mail: [§]akasaka@tara.tsukuba.ac.jp (Takeshi Akasaka); [¶]nagase@ims.ac.jp (Shigeru Nagase)

6. Conclusions and Perspectives	180
Acknowledgments	180
References	180

1. Introduction

The first experimental evidence for fullerene C_{60} formation was reported by Smalley, Kroto, Curl and coworkers in 1985.¹ Since then, numerous studies have conceptualized and developed future applications of that new carbon nanomaterial. In the field of material science, atom-doping is a powerful methodology to modulate electronic properties and has been applied to fullerene chemistry as well. A pronounced breakthrough in the course of these studies was successful endohedral atom-doping in fullerenes, which was first reported in 1991.² In particular, endohedral doping of metal atoms produces unique hybrid molecules, in which metal atoms are isolated from the outside world by the carbon sphere.^{3,4} Because several endohedral metallofullerenes are soluble in organic solvents and isolable using chromatographic techniques as usual organic molecules, their use has been extended widely into research areas of chemistry, physics, materials science, and medical science. These days, fullerenes are known to be capable of encapsulating not only metal atoms but also clusters such as metal nitrides,⁵ carbides,⁶ oxides,⁷ and sulfides.⁸ In such endohedral metallofullerenes, electron transfer takes place from encapsulated species to the fullerene cage to stabilize them energetically. Therefore, the encaged metal atoms are cationic, whereas the fullerene itself is anionic. This unique feature lends them fascinating electronic structures and properties that hollow fullerenes never have.⁹ Consequently, endohedral metallofullerenes are in great demand for further exploitation of their fundamental features and for exploration of their potential applications as new carbon materials designed at the nanoscale. Even so, many potentially important and intriguing problems remain that must be clarified in the near future. In this regard, determination of cage structures and positions of metal atoms is currently of central interest because they play important roles in the determination of their electronic and magnetic properties. Definitive proof for structures must be produced for each endohedral metallofullerene. It is also of current interest whether metal atoms are rigidly attached to fullerene cages or move around because controlling the movement and orientation would help in designing functional devices for molecular electronics.¹⁰ Organic functionalization will also be an important direction for the synthesis of further novel materials based on endohedral metallofullerenes. Furthermore, functionalization is sometimes useful in

characterizing molecular structures by X-ray crystallography because addition of organic groups promotes crystal growth of fullerenes. In this chapter, we summarize ongoing efforts to elucidate the molecular structures of endohedral metallofullerenes, including the positions and movements of encaged species, electronic properties, and development of strategies to functionalize them.

Hereinafter, the symbol of @ is used to signify the endohedral nature of endohedral metallofullerenes conventionally. To designate isomers of hollow fullerenes, carbon cages are labeled by their symmetry and number in accordance with the Fowler–Monolopoulos spiral algorithm.¹¹ Usually, a short form of numbering system is used, in which only isolated pentagon rule (IPR) isomers are numbered. In this chapter, a short form of the numbering system is used for IPR isomers, as given in “*An Atlas of Fullerenes*,” whereas a full numbering system is adopted for non-IPR isomers to simplify comparison of the discussion in this paper with previous literature.¹² Furthermore, for additional simplification, the numbers are not shown when a cage with the same symmetry is not plural for IPR isomers.

2. Cage Frameworks, Positions, and Movements of Encaged Species

2.1. Monometallofullerenes

Representative monometallofullerenes, $M@C_{2v}\text{-}C_{82}s$ (M = Group 3 metals and lanthanides), are generally produced in the highest yields using typical arc-discharge method. The electron transfer of three valence electrons creates an open-shell electronic structure, formally described as $M^{3+}(C_{2v}\text{-}C_{82})^{3-}$. Their paramagnetic nature has obstructed NMR spectroscopic studies of them. To solve this problem, electrochemical or chemical reduction of these paramagnetic species has been applied for measurements of the ^{13}C -NMR spectra of their anions to determine the frameworks of the fullerene cages. In theory, the C_{82} cage has nine distinct isomers ($C_2(1)$, $C_3(2)$, $C_2(3)$, $C_3(4)$, $C_2(5)$, $C_3(6)$, $C_{3v}(7)$, $C_{3v}(8)$, and C_{2v}) that satisfy the IPR. The ^{13}C -NMR spectrum of the most abundant isomer of $\text{La}@C_{82}$ anion exhibits 17 distinct lines with full intensity and 7 lines with half intensity, verifying clearly that the major isomer of $\text{La}@C_{82}$ has C_{2v} symmetry.¹³ To date, the most abundant isomers of $M@C_{82}s$ (M = La,¹³ Ce,¹⁴ Pr,¹⁵ and Y¹⁶) have been identified as having the same C_{2v} symmetric cages and therefore expressed as $M@C_{2v}\text{-}C_{82}s$.

The determination of the metal atoms' positions and movements is a crucial issue to clarify the physical and chemical properties of endohedral

metallofullerenes because molecular properties such as charge densities and dipole moments are highly dependent on them. Single-crystal X-ray crystallography is a powerful tool to elucidate organic molecules' structures. However, most X-ray crystallographic analyses of pristine fullerenes are difficult because molecules in the lattices rotate freely even at low temperatures as a result of their round structures. In this context, NMR study is an alternative method to elucidate positions of metal atoms in pristine endohedral metallofullerenes in solution. To verify the position of the metal atom in $M@C_{2v}-C_{82}$, NMR spectroscopic analysis of the paramagnetic effects caused by an f electron on the Ce atom in $Ce@C_{2v}-C_{82}$ was conducted, which yielded information related to the position of the Ce atom by measuring ^{13}C -NMR shifts of its anion.¹⁷

First, the bond connectivity in $Ce@C_{2v}-C_{82}$ anion was determined and all the ^{13}C -NMR signals were assigned absolutely using 2D Incredible Natural Abundance Double Quantum Transfer Experiment (INADEQUATE) NMR. This complete assignment enabled the authors to conduct the following paramagnetic NMR shift analysis. The f electron spin on the Ce atom interacts with nucleus spins on the carbons of the cage. Therefore, all carbon chemical shifts (δ) of the carbon atoms exhibit considerable temperature dependence. In general, the chemical shifts of paramagnetic molecules in solution are expressed as a sum of three contributions from diamagnetic (δ_{dia}), Fermi contact (δ_{fc}), and pseudocontact (δ_{pc}) shifts, in which the paramagnetic δ_{fc} and δ_{pc} are, respectively, proportional to T^{-1} and T^{-2} (T = absolute temperature).¹⁸ Constants c_{fc} and c_{pc} signify characteristic values of individual carbon signals. The δ_{dia} values correspond to chemical shifts of the diamagnetic $La@C_{2v}-C_{82}$ anion.¹⁹ Regarding endohedral metallofullerenes, anisotropic pseudocontact interaction shows a more dominant contribution than isotropic Fermi contact interaction because no meaningful connection exists between the Ce atom and carbon atoms of the cage. This consideration was confirmed through analysis of line-fitting plots for the carbon signals. Therefore, the chemical shifts of cerium-encapsulated metallofullerenes are expressed briefly as Equation 1, in which r represents the distance between Ce and cage carbons, θ denotes the angle between the r vector and the C_2 axis of $Ce@C_{2v}-C_{82}$, C is a common constant with a negative value for all carbon atoms of the cage (see Figure 1).

$$\delta = \delta_{\text{dia}} + C(3\cos^2\theta - 1)/r^3T^2 \quad (1)$$

It is noteworthy that c_{pc} includes geometrical information (r and θ) related to the encapsulated Ce atoms. Variable-temperature (VT) ^{13}C -NMR measurements of $Ce@C_{2v}-C_{82}$ anion were conducted to obtain the experimental c_{pc}

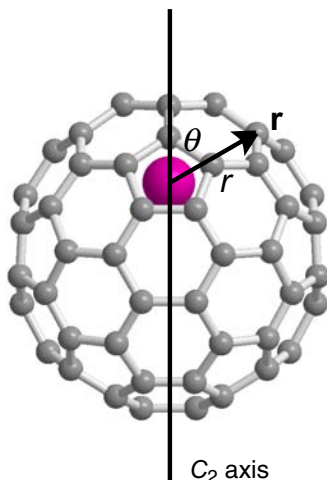


Figure 1. Definition of r , r' , and θ for $\text{Ce}@C_{2v}\text{-C}_{82}$ anion.

values. Use of the least squares method revealed the distance between the Ce atom and the center of the hexagonal ring along the C_2 axis as 2.1–2.8 Å. This Ce atom position corresponds to the minimum of the electrostatic potential of $C_{2v}\text{-C}_{82}^{3-}$.²⁰ This agreement is important evidence that the electrostatic metal–cage interaction plays a dominant role in determining the position of the encaged metal atoms.

2.2. Dimetallofullerenes

As for diamagnetic molecules such as dimetallofullerenes, ^{13}C -NMR measurements can be made to elucidate the frameworks of carbon cages in a neutral state. The ^{13}C -NMR spectrum of $\text{La}_2@D_2(10611)\text{-C}_{72}$ presents 18 lines of equal intensity in a diamagnetic shift range of 130–160 ppm.²¹ Despite the fact that only one cage of D_{6d} symmetry satisfies the IPR, the observed pattern of the ^{13}C -NMR spectrum does not correspond to that of the $D_{6d}\text{-C}_{72}$. Instead, $\text{La}_2@D_2(10611)\text{-C}_{72}$ has the non-IPR cage of $D_2(10611)$ symmetry,²² which was ascertained using subsequent X-ray crystallographic analysis of its carbene adducts.²³ Recent calculations revealed that the $D_2(10611)\text{-C}_{72}^{6-}$ has the lowest energy among the 39 C_{72} hexaanions including 24 $D_2\text{-C}_{72}$ cages and 15 C_{72} cages having higher symmetries.²⁴ This result confirms that $\text{La}_2@D_2(10611)\text{-C}_{72}$ is energetically the most stable isomer; the electronic structure is formally described as $\text{La}_2^{3+}\text{C}_{72}^{6-}$. The ^{139}La -NMR spectrum of $\text{La}_2@D_2(10611)\text{-C}_{72}$ at 334 K shows a broad signal at –575.6 ppm, indicating that the two metal atoms are magnetically equivalent inside the

cage.²¹ The metal atoms are believed to stabilize the non-IPR cage possessing two fused pentagons. Indeed, paramagnetic NMR shift analysis of $\text{Ce}_2@D_2(10611)\text{-C}_{72}$ showed that the Ce atoms face the two fused pentagons on the two poles of the $D_2(10611)\text{-C}_{72}$ cage.²⁵ The ^{13}C -NMR signals of the fused pentagons of $\text{Ce}_2@D_2(10611)\text{-C}_{72}$ are shifted strongly with decreasing temperature because of the paramagnetic effects of the facing Ce atoms. Paramagnetic NMR shift analysis is also applicable to dimetallofullerenes. The fundamental assumption in the analysis is that the pseudocontact shifts are produced using a sum of the individual contributions from the two Ce cations. The results obtained from the paramagnetic NMR shift analysis agree well with those of the theoretical calculations (see Figure 2(a)).

Actually, $\text{La}_2@D_{3b}(5)\text{-C}_{78}$ was first reported in 2004.²⁶ The ^{13}C -NMR spectrum presented five lines with full intensity and three lines with half intensity, indicating that $\text{La}_2@D_{3b}(5)\text{-C}_{78}$ is D_{3b} symmetric in solution. In theory, the C_{78} cage has five IPR-isomers having D_3 , $C_{2v}(2)$, $C_{2v}(3)$, $D_{3b}(4)$, and $D_{3b}(5)$ symmetries. Therefore, ^{13}C -NMR spectroscopy is unable to determine the framework of $\text{La}_2@D_{3b}(5)\text{-C}_{78}$. The framework of the cage was clarified as $D_{3b}(5)$ symmetric by subsequent X-ray crystallographic analysis of its carbene

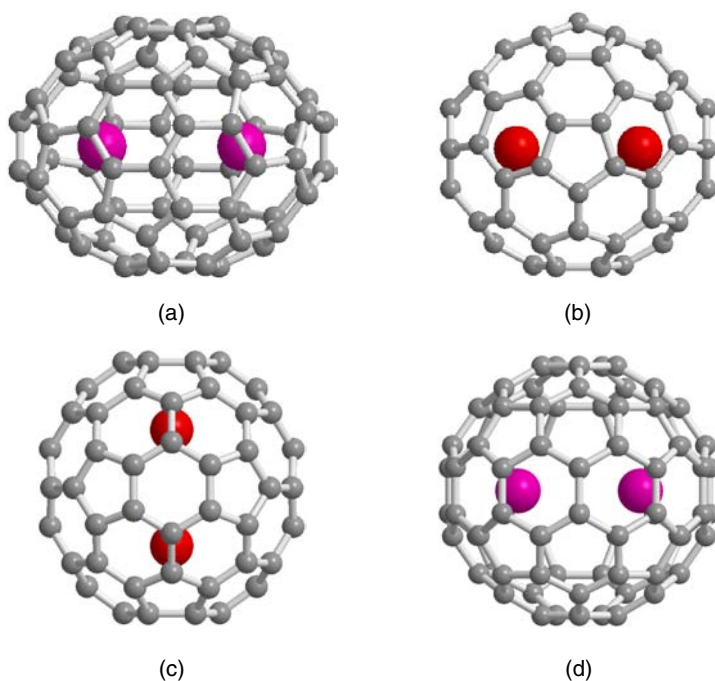


Figure 2. Optimized structures of (a) $\text{Ce}_2@D_2(10611)\text{-C}_{72}$, (b) $\text{La}_2@D_{3b}(5)\text{-C}_{78}$, (c) $\text{La}_2@I_h\text{-C}_{80}$, and (d) $\text{Ce}_2@D_{5b}\text{-C}_{80}$.

adduct.²⁷ Also, $\text{Ce}_2@D_{3h}(5)\text{-C}_{78}$ has the same cage framework as that of $\text{La}_2@D_{3h}(5)\text{-C}_{78}$.²⁸ In fact, the absorption spectrum of $\text{Ce}_2@D_{3h}(5)\text{-C}_{78}$ shows characteristic absorptions at 644, 553, and 526 nm, which resemble those of $\text{La}_2@D_{3h}(5)\text{-C}_{78}$. The ^{13}C -NMR signals show considerable temperature dependence, as observed in $\text{Ce}_2@D_2(10611)\text{-C}_{72}$.²⁵ The paramagnetic NMR shift analysis disclosed that the metal atoms in $\text{Ce}_2@D_{3h}(5)\text{-C}_{78}$ are localized on the C_3 axis of the ellipsoidal cage. This result agrees well with the optimized structure of $\text{La}_2@D_{3h}(5)\text{-C}_{78}$, as calculated using the density functional theory (DFT) method (see Figure 2(b)).

Among endohedral metallofullerenes, $\text{La}_2@I_h\text{-C}_{80}$ is a fascinating molecule because the encaged metal atoms show three-dimensional movement inside the icosahedral cage. The evidence for the circular motion of metal atoms was given by results of ^{13}C and ^{139}La -NMR spectroscopy.²⁹ It is interesting that the overall symmetry of the molecule is altered by the placement of metal atoms. However, no placement can explain the ^{13}C -NMR spectrum of $\text{La}_2@I_h\text{-C}_{80}$, in which only two signals were observed at 298 K.³⁰ Therefore, it was concluded that the random circulation of the two La atoms reduces the symmetry of the molecule to one that is icosahedral. Moreover, the ^{139}La -NMR spectrum of $\text{La}_2@I_h\text{-C}_{80}$ exhibited a single signal at -402.6 ppm with a linewidth of 113 Hz, suggesting that the two La atoms are magnetically equivalent inside the $I_h\text{-C}_{80}$ cage. It is noteworthy that large broadening of the ^{139}La NMR line width was observed with increasing temperature from 305 to 363 K. This observation is explainable by the existence of dynamic circulation of the La^{3+} cations. This circulation of the positively charged species produces a new magnetic field at the La position. Ordinarily, the interaction between the nuclear spins of atoms and the induced magnetic field (the spin-rotation interaction) does not contribute significantly to the relaxation time because effects of molecular rotation are predominantly quenched by neighbors in solution. For $\text{La}_2@I_h\text{-C}_{80}$, however, the rotation of the La atoms can be preserved because of the unique protection with the carbon cage. Consequently, the spin-rotation interaction produces an extremely strong effect on the relaxation process. This relaxation caused by the spin-rotation interaction engenders an increase in the linewidth with increasing temperature. On the other hand, narrowing of the linewidth with increasing temperature from 258 to 305 K is a typical situation because of the overall rotation of the molecule (quadrupole-dominated relaxation). In addition, theoretical calculations suggest that the electrostatic potential map of $I_h\text{-C}_{80}^{6-}$ shows almost concentric circles with no clear minima, reflecting the round structure of the cage.³¹ The calculated rotational barrier of the La atoms is 4.9 kcal/mol. The recent computational study proposed that the most stable configuration for

$\text{La}_2@I_h\text{-C}_{80}$ is D_{2b} symmetry (see Figure 2(c)). Nevertheless, the detailed trajectory remains controversial.^{32,33}

Similar dynamic movement of metal atoms is also apparent in the analog, $\text{Ce}_2@I_h\text{-C}_{80}$. The presence of only two signals with a 3:1 intensity ratio in the ^{13}C -NMR spectrum of $\text{Ce}_2@I_h\text{-C}_{80}$ indicates that the Ce atoms circulate randomly, as La does in $\text{La}_2@I_h\text{-C}_{80}$.³⁴ The ^{13}C -NMR signals show very slight temperature dependence compared to those of $\text{Ce}_2@D_2(10611)\text{-C}_{72}$ ²⁵ and $\text{Ce}_2@D_{3h}(5)\text{-C}_{78}$,²⁸ despite the fact that two Ce atoms having f electrons are included as well. This observation results is attributable to the three-dimensional circulation of the Ce atoms, which causes delocalization of the f electrons, thereby reducing the paramagnetic effects. It is particularly interesting that recent calculations suggest a D_{3d} symmetric ground state structure for $\text{Ce}_2@I_h\text{-C}_{80}$, which is in marked contrast to the D_{2b} ground state for $\text{La}_2@I_h\text{-C}_{80}$.³⁵

The second isomer of $\text{La}_2@C_{80}$ was first isolated in 1997.³⁶ However, no information about the cage symmetry and the motion of the La atoms in the second isomer has been reported as caused by the much lower yield of the second isomer than that of $\text{La}_2@I_h\text{-C}_{80}$. Seven C_{80} isomers satisfy the IPR (D_{5d} , D_2 , $C_{2v}(3)$, D_3 , $C_{2v}(5)$, D_{5h} , and I_h). Meanwhile, a substantial amount of the second $\text{Ce}_2@C_{80}$ isomer was obtained; the structure of the cage was elucidated as D_{5h} symmetric.³⁷ At 467 nm, $\text{Ce}_2@D_{5h}\text{-C}_{80}$ has a characteristic absorption peak resembling that of the second isomer of $\text{La}_2@C_{80}$. On the other hand, featureless absorption was observed for $\text{Ce}_2@I_h\text{-C}_{80}$, which resembles the absorption spectrum of $\text{La}_2@I_h\text{-C}_{80}$. Therefore, it is reasonable to regard the cage symmetry of $\text{Ce}_2@D_{5h}\text{-C}_{80}$ as identical to that of the second isomer of $\text{La}_2@C_{80}$ based on the similarity between their absorption spectra. It is particularly interesting that the observed ϵ_{pc} values of the carbon signals are larger than those of $\text{Ce}_2@D_{3h}(5)\text{-C}_{78}$,²⁸ in which the two Ce atoms are stationary at specific positions. The strong temperature dependence of the carbon signals indicates that the two Ce atoms in $\text{Ce}_2@D_{5h}\text{-C}_{80}$ do not circulate three-dimensionally. Instead, they move in a restricted manner. The paramagnetic NMR shift analysis, together with theoretical calculations, led us to conclude that the Ce atoms in $\text{Ce}_2@D_{5h}\text{-C}_{80}$ circulate two-dimensionally along a band of 10 contiguous hexagons (see Figure 2(d)), which contrasts sharply with the three-dimensional movement of two Ce atoms in $\text{Ce}_2@I_h\text{-C}_{80}$.³⁴ In fact, the ^{13}C -NMR signals of $\text{Ce}_2@D_{5h}\text{-C}_{80}$ displayed greater temperature dependence than those of $\text{Ce}_2@I_h\text{-C}_{80}$, reflecting the restricted circulation of the Ce atoms in $\text{Ce}_2@D_{5h}\text{-C}_{80}$. This finding emphasizes that the dynamic movement of the metal atoms depends not only on the cage size, but also on the cage symmetry.

2.3. Clusterfullerenes

The most representative clusterfullerene, $\text{Sc}_3\text{N}@I_h\text{-C}_{80}$, was discovered by Dorn and coworkers in 1999.⁵ As in the case of $\text{La}_2@I_h\text{-C}_{80}$ and $\text{Ce}_2@I_h\text{-C}_{80}$, the encaged moiety in $\text{Sc}_3\text{N}@I_h\text{-C}_{80}$ rotates randomly inside the $I_h\text{-C}_{80}$ cage. The ^{13}C -NMR spectrum consists of only two resolved lines, showing that internal motion of the Sc_3N cluster preserves overall I_h symmetry for the carbon cage (see Figure 3(a)). The ^{45}Sc -NMR spectrum for $\text{Sc}_3\text{N}@I_h\text{-C}_{80}$ exhibits a single symmetric line, which is also indicative of a dynamic movement of the cluster. Based on the similarity of the absorption spectra of $\text{Sc}_3\text{N}@I_h\text{-C}_{80}$ and $\text{M}_2@I_h\text{-C}_{80}$ s ($\text{M} = \text{La}, \text{Ce}$), the electronic structure of $\text{Sc}_3\text{N}@I_h\text{-C}_{80}$ is considered to be described formally as $(\text{Sc}_3\text{N})^{6+}(I_h\text{-C}_{80})^{6-}$. Similarly, paramagnetic NMR shift analysis was adopted for $\text{CeSc}_2\text{N}@I_h\text{-C}_{80}$.³⁸ The ^{45}Sc -NMR signal of $\text{CeSc}_2\text{N}@I_h\text{-C}_{80}$ exhibited a temperature-dependent chemical shift that originates from the buried f electron spin remaining on the Ce^{3+} ion. A temperature increase from 313 K to 383 K yields an upfield shift in the resonance frequency of the ^{45}Sc signal from 257.3 to 235.7 ppm. The observed temperature dependence suggests that the pseudocontact interaction dominates the chemical shift in a fashion similar to that of $\text{Ce}@C_{2v}\text{-C}_{82}$. Another technique that is available to evaluate cluster movements inside fullerene cages is ^{89}Y -NMR. The ^{89}Y -NMR spectrum for $\text{Y}_3\text{N}@I_h\text{-C}_{80}$ exhibits a single sharp resonance at 191.63 ppm, confirming isotropic motional averaging of the Y_3N cluster.³⁹ This characteristic is also consistent with the ^{13}C -NMR spectrum, in which two lines with a 3:1 ratio were observed.

Movements of encaged metal carbides have also been reported. The ^{13}C -NMR spectrum of $\text{Sc}_2\text{C}_2@C_{3v}(8)\text{-C}_{82}$ showed 17 signals for the carbon atoms of the cage (see Figure 3(b)).⁴⁰ In addition, one signal was observed at 253.2 ppm that originates from the encaged C_2 unit because of ^{13}C -enrichment.⁴¹

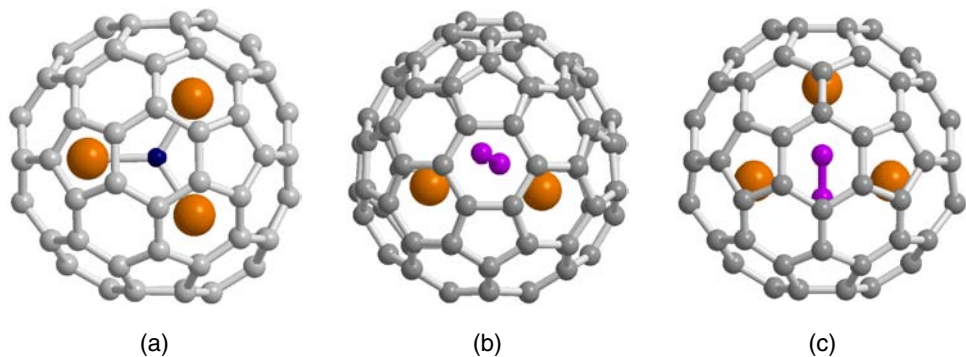


Figure 3. Optimized structures of (a) $\text{Sc}_3\text{N}@I_h\text{-C}_{80}$, (b) $\text{Sc}_2\text{C}_2@C_{3v}(8)\text{-C}_{82}$, and (c) $\text{Sc}_3\text{C}_2@I_h\text{-C}_{80}$.

The extreme downfield shift results from the dianion character of the C_2 unit. Theoretical calculations exhibited that the electronic structure of $Sc_2C_2@C_{3v}(8)-C_{82}$ is formally described as $Sc_2^{6+}C_2^{2-}(C_{3v}(8)-C_{82})^{4-}$. The linewidth for the C_2 unit is five times broader than those for the carbon atoms of the cage. It is particularly interesting that broadening of the ^{13}C -NMR linewidth for the C_2 unit was observed with increasing temperature from 253 to 303 K because of spin-rotation relaxation, as found in the VT ^{139}La -NMR spectra of $La_2@I_h-C_{80}$.²⁸ In contrast, such broadening was not observed for the cage carbon atoms with increasing temperature. This observation proves that the C_2 unit rotates inside the $C_{3v}(8)-C_{82}$ cage.

The ^{13}C -NMR spectrum of $Sc_3C_2@I_h-C_{80}$ anion showed two signals with the integral ratio of 3:1 for the I_h-C_{80} cage and one signal at 328.3 ppm for the C_2 unit.^{41,42} This finding clearly signifies that the encaged cluster is allowed to rotate inside the I_h-C_{80} cage (see Figure 3(c)). This rotation makes three Sc atoms magnetically equivalent on the EPR timescale. Accordingly, the symmetrical hyperfine splitting of 22 lines is observed in the EPR spectrum of neutral $Sc_3C_2@I_h-C_{80}$. DFT calculations corroborated that the electronic structure of $Sc_3C_2@I_h-C_{80}$ can be described as $(Sc^{3+})_3(C_2)^{3-}(I_h-C_{80})^{6-}$.

3. Electronic Properties of Pristine Endohedral Metallofullerenes

Electronic properties of endohedral metallofullerenes are fascinating features because they possess unique properties featuring internal electron transfer. Electrochemical potentials provide valuable information related to the interaction between the encaged species and the fullerene cages. The redox potentials of the representative endohedral metallofullerenes determined by electrochemical measurements are presented in Table 1. The redox potentials depend strongly on the frameworks of carbon cages and the numbers of metal atoms.

The potential gap separating the first reduction potential and the first oxidation potential of $La@C_5(6)-C_{82}$ is smaller than that of $La@C_{2v}-C_{82}$, in which their only difference is the cage symmetry.⁴³ The smaller gap of $La@C_5-C_{82}$ is associated with the fact that $La@C_5(6)-C_{82}$ is less stable than $La@C_{2v}-C_{82}$ in air. In contrast, the redox potentials of $M@C_{2v}-C_{82}$ s are similar when the metal atom shown as M is replaced by La,⁴³ Ce,¹⁴ Gd,⁴⁴ and Y.⁴⁴ This observation shows that these encaged metal atoms have the same formal charge of 3+. The minor deviation in their redox potentials might be caused by different contributions of back donation from the cages to the metal atoms. The first reduction and oxidation potentials of the monometallofullerenes are

Table 1. Redox Potentials^a of Pristine Endohedral Metallofullerenes

Compound	^{ox} E_3	^{ox} E_2	^{ox} E_1	^{red} E_1	^{red} E_2	^{red} E_3	Refs.
La@C _{2v} -C ₈₂		+1.07 ^{b,c}	+0.07	-0.42	-1.37	-1.53	43
La@C _s (6)-C ₈₂		+1.08 ^{b,c}	-0.07	-0.47	-1.40	-1.40	43
Ce@C _{2v} -C ₈₂		+1.08 ^{b,c}	+0.08	-0.41	-1.41	-1.53	14
Gd@C _{2v} -C ₈₂		+1.08 ^{b,c}	+0.09	-0.39	-1.38	-1.38	44
Y@C _{2v} -C ₈₂		+1.07 ^{b,c}	+0.10	-0.37	-1.34	-1.34	44
La ₂ @D ₂ (10611)-C ₇₂		+0.75 ^{b,c}	+0.24	-0.68	-1.92		23
Ce ₂ @D ₂ (10611)-C ₇₂		+0.82 ^{b,c}	+0.18	-0.81	-1.86		25
La ₂ @D _{3h} (5)-C ₇₈	+1.11 ^b	+0.62 ^b	+0.26 ^b	-0.40 ^b	-1.84 ^b	-2.28 ^b	26
Ce ₂ @D _{3h} (5)-C ₇₈		+0.79 ^{b,c}	+0.25 ^b	-0.52 ^b	-1.86 ^b	-2.23 ^b	28
La ₂ @I _h -C ₈₀		+0.95	+0.56	-0.31	-1.71	-2.13 ^{b,c}	45
Ce ₂ @I _h -C ₈₀		+0.95	+0.57	-0.39	-1.71		34
La ₂ @D _{5h} -C ₈₀		+0.78	+0.22	-0.36	-1.72		36
Ce ₂ @D _{5h} -C ₈₀	+0.86 ^b	+0.66 ^b	+0.20	-0.40	-1.76	-2.16	37
Sc ₃ N@I _h -C ₈₀			+0.62	-1.22	-1.59	-1.90	46
Sc ₂ C ₂ @C _{3v} (8)-C ₈₂		+0.93 ^{b,c}	+0.47	-0.94 ^{b,c}	-1.15	-1.60	47
Sc ₃ C ₂ @I _h -C ₈₀			-0.03	-0.50	-1.64	-1.84	42
C ₆₀			+1.21 ^{b,c}	-1.12	-1.50	-1.95	43

^aHalf-cell potentials unless otherwise stated. Values are in volts relative to the ferrocene/ferrocenium couple. ^bValues are obtained using DPV. ^cIrreversible.

much lower than those of other endohedral metallofullerenes. The narrow potential gaps of the monometallofullerenes are attributable to their open-shell electronic structures. In fact, M@C_{2v}-C₈₂s (M = La, Ce, Y, and Gd) can be reduced or oxidized easily using electrochemical electrolysis or chemical treatment, yielding diamagnetic anions or cations. Similarity in the redox potentials of La₂@D₂(10611)-C₇₂²³ and Ce₂@D₂(10611)-C₇₂²⁵ is also apparent. The same applies to La₂@D_{3h}(5)-C₇₈²⁶ and Ce₂@D_{3h}(5)-C₇₈,²⁸ La₂@I_h-C₈₀⁴⁵ and Ce₂@I_h-C₈₀,³⁴ as well as La₂@D_{5h}-C₈₀³⁶ and Ce₂@D_{5h}-C₈₀.³⁷ It is particularly interesting that the dimetallofullerenes also have lower electrochemical potential gaps than those of C₆₀ despite their closed-shell electronic structures. Computational studies have revealed that the lowest unoccupied molecular orbitals (LUMOs) of the dimetallofullerenes are localized on the two metal cations, which contrasts sharply to the case of the monometallofullerenes, in which the LUMOs are distributed not only to the metal cations but also to the carbon atoms of the cage. In the case of M₂@D₂(10611)-C₇₂s (M = La and Ce), two reversible reductions, one reversible oxidation, and one irreversible oxidation processes were observed.^{23,25} The reversibility at the first oxidation as well as two-step reduction is consistent with the fact that M₂@D₂(10611)-C₇₂ molecules are stable under ambient conditions despite

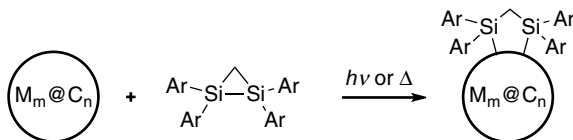
their non-IPR structures. In addition, $M_2@D_2(10611)-C_{72}$ s have much lower oxidation and higher reduction potentials than $M_2@I_h-C_{80}$ s have. Indeed, the highest occupied molecular orbital (HOMO)–LUMO gaps of $M_2@D_2(10611)-C_{72}$ s are larger than those of the previously reported dimetallofullerenes such as $La_2@I_h-C_{80}$.⁴⁵ These results are consistent with theoretical calculations. Based on differential pulse voltammetry (DPV) measurements, the first reduction and oxidation potentials of $La_2@D_{3h}(5)-C_{78}$ are positively and negatively shifted, respectively, with respect to those of the empty D_3-C_{78} , suggesting that the capabilities of $La_2@D_{3h}(5)-C_{78}$ as an electron acceptor or donor are stronger than those of D_3-C_{78} .²⁶ In $Ce_2@D_{3h}(5)-C_{78}$, three reversible reductions, one reversible oxidation, and one irreversible oxidation potentials were observed.²⁸ The first reduction potential of $Ce_2@D_{3h}(5)-C_{78}$ is lower than that of $Ce_2@D_2(10611)-C_{72}$. It is particularly interesting that the I_h -symmetric dimetallofullerene, $Ce_2@I_h-C_{80}$, has higher oxidation potentials and lower reduction potentials than those of smaller dimetallofullerenes.³⁴ Remarkably, $M_2@I_h-C_{80}$ s ($M = La$ and Ce) are easier to reduce than $M@C_{2v}-C_{82}$ s. Moreover, the electrochemical reduction processes of $M_2@D_{5h}-C_{80}$ s ($M = La$ and Ce) closely resemble those of $M_2@I_h-C_{80}$ s.^{36,37} On the other hand, the first oxidation potentials of $M_2@D_{5h}-C_{80}$ s are lower than those of $M_2@I_h-C_{80}$ s. In fact, $M_2@D_{5h}-C_{80}$ s possess the lowest HOMO–LUMO gaps reported to date for endohedral metallofullerenes having closed-shell electronic structures.

It is particularly interesting that clusterfullerenes of the two types, $Sc_3N@I_h-C_{80}$ ⁴⁶ and $Sc_3C_2@I_h-C_{80}$ ⁴² displayed contrasting redox properties. The first oxidation potential of $Sc_3N@I_h-C_{80}$ is similar to that of $La_2@I_h-C_{80}$,⁴⁵ however, the first reduction potential (−1.22 V) is much more negative than that of C_{60} (−1.12 V).⁴³ On the other hand, $Sc_3C_2@I_h-C_{80}$ exhibited much smaller potential gap than that of $Sc_3N@I_h-C_{80}$. In particular, the first oxidation potential (−0.03 V) of $Sc_3C_2@I_h-C_{80}$ is comparable to those of $M@C_{2v}-C_{82}$ s (+0.10–0.07 V). Apparently, the paramagnetic nature of $Sc_3C_2@I_h-C_{80}$ is attributed to the extremely low redox potentials. In fact, the redox potentials of diamagnetic $Sc_2C_2@C_{3v}(8)-C_{82}$ are much higher than those of $Sc_3C_2@I_h-C_{80}$.⁴⁷

4. Chemistry of Endohedral Metallofullerenes

4.1. Bis-silylation

The first exohedral adducts of endohedral metallofullerenes were reported in 1995, when the formation of the bis-silylated $La@C_{2v}-C_{82}$ was detected using laser-desorption time-of-flight (LD-TOF) mass spectrometry and electron



Scheme 1. Bis-silylation of endohedral metallofullerenes. $M_m@C_n$ = $\text{La}@C_{2v}\text{-C}_{82}$, $\text{Ce}@C_{2v}\text{-C}_{82}$, $\text{Pr}@C_{2v}\text{-C}_{82}$, $\text{Gd}@C_{2v}\text{-C}_{82}$, $\text{Y}@C_{2v}\text{-C}_{82}$, $\text{Ce}_2@D_{3h}(5)\text{-C}_{78}$, $\text{La}_2@I_h\text{-C}_{80}$, $\text{Ce}_2@I_h\text{-C}_{80}$, and $\text{Sc}_3\text{N}@I_h\text{-C}_{80}$. Ar = mesityl (Mes), 2,6-diethylphenyl (Dep).

paramagnetic resonance spectroscopy (EPR) as depicted in Scheme 1.⁴⁸ The EPR spectrum of the mixture of the reaction suggested that at least two product species with different La isotropic splitting were formed.⁴⁹ However, isolation of the adducts was not achieved at that time. Later, one isomer of the bis-silylated $\text{La}@C_{2v}\text{-C}_{82}$ derivatives and two isomers of bis-silylated $\text{Y}@C_{2v}\text{-C}_{82}$ derivatives were isolated and characterized, respectively.⁵⁰ The absorption spectrum of the bis-silylated $\text{La}@C_{2v}\text{-C}_{82}$ showed an absorption maximum at 1146 nm, whereas that of $\text{La}@C_{2v}\text{-C}_{82}$ was at 1003 nm. This difference demonstrates that the π -electronic state of the cage is altered by bis-silylation. In this context, bis-silylation is effective to tune the electronic character of endohedral metallofullerenes.

It is also noteworthy that $\text{La}@C_{2v}\text{-C}_{82}$ undergoes both photochemical and thermal reactions with 1,1,2,2-tetramesityl-1,2-disilirane to form bis-silylated adducts, whereas the bis-silylation of C_{60} proceeds only under photochemical conditions. The high thermal reactivity of $\text{La}@C_{2v}\text{-C}_{82}$ toward disilirane can be rationalized based on its stronger electron acceptor property relative to C_{60} , as described earlier. The reactivity of a fullerene toward disilirane is strikingly distinctive of its first reduction potential. Therefore, bis-silylation can be useful as mechanistic probe to clarify the electronic properties of fullerene species. To date, the respective reactivities of $M@C_{2v}\text{-C}_{82}$ ($M = \text{La}$,^{48,50} Ce ,¹⁴ Pr ,⁵¹ Gd ,⁵² and Y ⁵⁰), $M_2@I_h\text{-C}_{80}$ ($M = \text{La}$ ³⁰ and Ce ³⁴), $\text{Sc}_3\text{N}@I_h\text{-C}_{80}$,⁴⁶ $\text{Sc}_3\text{C}_2@I_h\text{-C}_{80}$,⁵³ and $\text{Sc}_2\text{C}_2@C_{3v}(8)\text{-C}_{82}$ ⁵⁴ have been investigated, among which $\text{Sc}_3\text{N}@I_h\text{-C}_{80}$ and $\text{Sc}_2\text{C}_2@C_{3v}(8)\text{-C}_{82}$ do not react thermally with disilirane, although the others do so smoothly at 80°C. This reactivity is perfectly comparable to the trend of the first reduction potentials of the endohedral metallofullerenes.

The reactivity of endohedral metallofullerenes can be tuned by one-electron uptake or release on the cages.⁵⁵ Chemically prepared $M@C_{2v}\text{-C}_{82}$ cations react with disilirane even at room temperature to form the corresponding adducts, as confirmed based on fast atom bombardment (FAB) mass spectroscopy. In contrast, $M@C_{2v}\text{-C}_{82}$ anions do not react with disilirane even at elevated temperatures (80 °C). This result is reasonable because the enhanced electron

affinity of the $M@C_{2v}-C_{82}$ cations promotes bis-silylation, whereas the anions lose reactivity with disilirane because of their much lower electron affinity.

Although bis-silylation of $La@C_{2v}-C_{82}$ is not stereoselective, thermal reaction of $M_2@I_h-C_{80}$ s ($M = La^{30}$ and Ce^{34}) with 1,1,2,2-tetrakisaryl-1,2-disilirane yielded single products. The bis-silylated $La_2@I_h-C_{80}$ in which mesityl groups are attached on the silicon atoms is thermally unstable; retrocycloaddition took place gradually at room temperature. The stability can be improved by the replacement of the mesityl (Mes) groups by 2,6-diethylphenyl (Dep) groups. The X-ray structure of $La_2@I_h-C_{80}(Dep_2Si)_2CH_2$ shows that the two silicon atoms are attached on the 1,4-position of a hexagonal ring (see Figure 4(a)). It is noteworthy that the two La atoms are located at two positions directed toward the hexagonal ring along the equatorial plane of the I_h-C_{80} sphere, reflecting that these positions are energetically the most favorable. A VT ^{139}La -NMR study showed that the dynamic movement of the La atoms exists in the bis-silylated I_h-C_{80} cage, resulting in large broadening of the ^{139}La -NMR linewidth with increasing temperature from 183 K to 363 K. Further information concerning the dynamic movement in a bis-silylated I_h-C_{80} cage was obtained from the paramagnetic NMR shift analysis of $Ce_2@C_{80}(Mes_2Si)_2CH_2$.³⁴ In fact, six ^{13}C signals are highly shifted by decreasing temperatures from 303 K to 253 K in the VT ^{13}C -NMR measurements. This result is explainable by the fact that each Ce atom is delocalized and

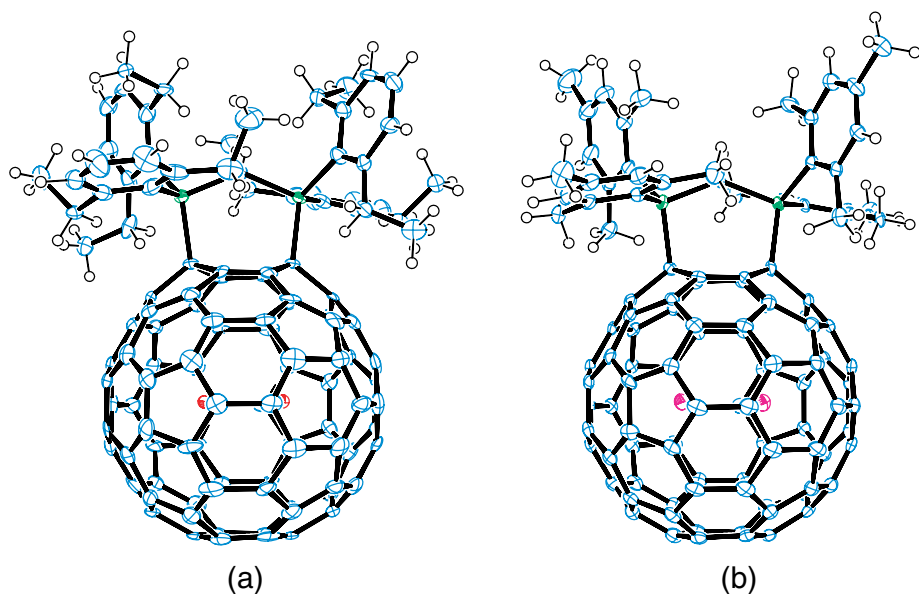


Figure 4. ORTEP plots of (a) bis-silylated $La_2@I_h-C_{80}$ and (b) bis-silylated $Ce_2@I_h-C_{80}$.

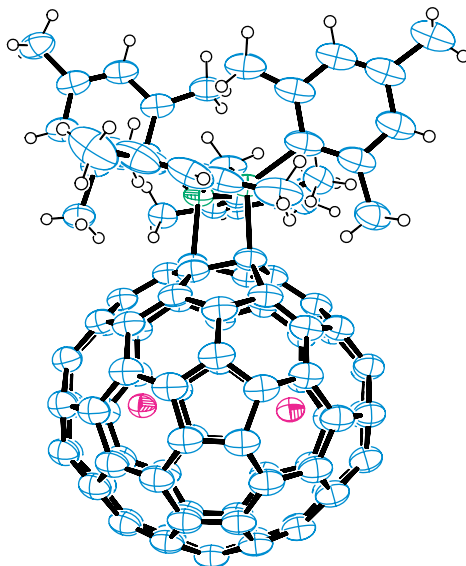


Figure 5. ORTEP plot of bis-silylated $\text{Ce}_2@D_{3h}(5)\text{-C}_{78}$.

directed toward a hexagonal ring at the equator of the cage, as revealed in the X-ray structure (see Figure 5(b)). On the other hand, the ^{13}C signal of the sp^3 carbon atoms on the cage are not shifted considerably by the paramagnetic effects, indicating that the metal position facing the addend is not favorable. Therefore, it is concluded that the two metal atoms in a bis-silylated $I_h\text{-C}_{80}$ hop two-dimensionally along the equator of the cage. In this context, the dynamic movement of metal atoms inside a fullerene cage can be altered by exohedral chemical functionalization. This hopping motion is supported by results of theoretical studies that preceded the experimental observations.⁵⁶ The strong electron-donating character of the silyl group gives *ca.* 0.9 electron to the cage, where the electrostatic potential is transformed. It is particularly interesting that the X-ray structure of $\text{Ce}_2@I_h\text{-C}_{80}(\text{Mes}_2\text{Si})_2\text{CH}_2$ consists of two conformers, which are caused by the two possible twist modes on conformation of the addend. The two conformers are also observable in the NMR timescale. The ^1H and 2D EXSY NMR experiments revealed that the Gibbs free energy of activation ΔG^\ddagger for the interconversion and the energy difference ΔG between the two conformers are, respectively, 12 kcal/mol and 0.8 kcal/mol.

Bis-silylation reaction of $\text{Ce}_2@D_{3h}(5)\text{-C}_{78}$ also proceeded smoothly to form a single isomer of $\text{Ce}_2@D_{3h}(5)\text{-C}_{78}(\text{Mes}_2\text{Si})_2\text{CH}_2$.²⁸ The adduct results from the 1,4-addition of the disilirane to the cage (see Figure 5), as found in $\text{Ce}_2@I_h\text{-C}_{80}(\text{Mes}_2\text{Si})_2\text{CH}_2$.³⁴ The Ce atoms are located at two positions

directed toward the hexagonal ring at the C_3 axis of the ellipsoidal cage. The considerably long Ce–Ce distance of 4.036 Å in the derivative results from the electrostatic repulsion between the Ce atoms at the C_3 axis, where the repulsion is minimized. For the bis-silylated adduct, the observed ^{13}C signals show large temperature dependence, as compared to the pristine $\text{Ce}_2@D_{3h}(5)\text{-C}_{78}$ case, which indicates that the two Ce atoms are more tightly localized in the bis-silylated adduct than in pristine $\text{Ce}_2@D_{3h}(5)\text{-C}_{78}$. On the other hand, $\text{Ce}_2@D_2(10611)\text{-C}_{72}$ does not react with disilane thermally because the reduction potential is much higher than that of $\text{Ce}_2@D_{3h}(5)\text{-C}_{78}$.²⁵

Photochemical reaction of $\text{Sc}_3\text{N}@I_h\text{-C}_{80}$ with 1,1,2,2-tetramesityl-1,2-disilane engendered the formation of two regioisomers of the bis-silylated adducts in the ratio of 3:2.⁵⁷ The major isomer results from the addition of disilane on the [5,6]-bond junction that bisects pentagonal and hexagonal rings ([5,6]-closed). The NMR study suggested that the 1,3-disilolane ring in the major isomer has a bent conformation. On the other hand, the minor isomer results from the addition of disilane on the 1,4-position of a hexagonal ring, as found in the bis-silylated $\text{M}_2@I_h\text{-C}_{80}$ ($\text{M} = \text{La}, \text{Ce}$). The 1,4-isomer of the bis-silylated $\text{Sc}_3\text{N}@I_h\text{-C}_{80}$ has two conformers derived from the twist modes on conformation of the addend as well. The estimated values of ΔG^\ddagger for the interconversion and ΔG between the two conformers are, respectively, 14 kcal/mol and 0.2 kcal/mol. It is noteworthy that the [5,6]-closed 1,2-isomer converts into the 1,4-isomer thermally because the 1,2-isomer is thermodynamically less stable than the 1,4-isomer. The X-ray structure of the 1,4-isomer of $\text{Sc}_3\text{N}@I_h\text{-C}_{80}(\text{Mes}_2\text{Si})_2\text{CH}_2$ exhibited that the Sc_3N cluster is located at a single site, in which one Sc atom is located at the bottom of the cage and far away from the addend; the other two Sc atoms repulse each other to minimize the energy (see Figure 6).

4.2. Electrophilic carbene addition

Because 24 non-equivalent carbons exist in $\text{M}@C_{2v}\text{-C}_{82}$, addition might take place at several sites to yield several possible isomers of mono-adducts. In contrast, the addition reaction of $\text{M}@C_{2v}\text{-C}_{82}$ ($\text{M} = \text{La}$,^{58,59} Ce ,⁶⁰ Gd ,⁶¹ and Y^{62}) with adamantylidene (Ad) carbene affords one dominant isomer of $\text{M}@C_{2v}\text{-C}_{82}(\text{Ad})\text{-I}$ together with a minor regioisomer of $\text{M}@C_{2v}\text{-C}_{82}(\text{Ad})\text{-II}$, as shown in Scheme 2.

The X-ray crystallographic analyses of $\text{La}@C_{2v}\text{-C}_{82}(\text{Ad})\text{-I}$ and $[\text{Ce}@C_{2v}\text{-C}_{82}(\text{Ad})\text{-II}]^-$ revealed that the C–C bond on the sites of addition are cleaved by adding the electrophilic carbene to form [6,6]-open structures in both cases (see Figure 7). The absorption features of the carbene adducts are

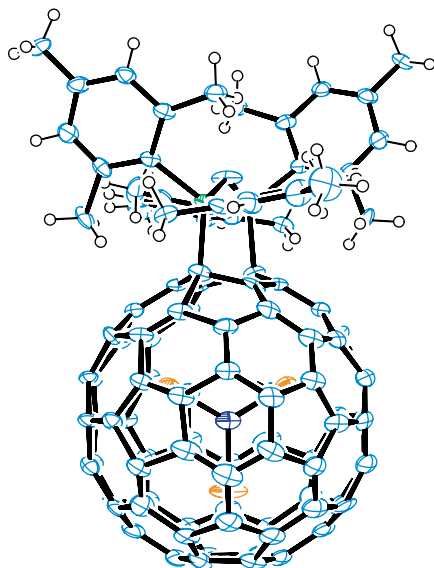
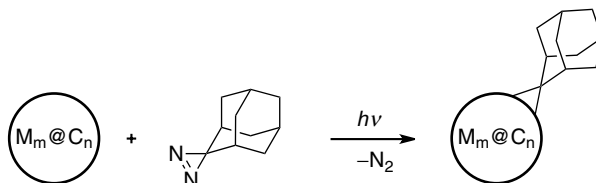


Figure 6. ORTEP plot of bis-silylated $\text{Sc}_3\text{N}@I_h\text{-C}_{80}$.



Scheme 2. Carbene addition of endohedral metallofullerenes. $M_m@C_n = \text{La}@C_{2v}\text{-C}_{82}$, $\text{Ce}@C_{2v}\text{-C}_{82}$, $\text{Gd}@C_{2v}\text{-C}_{82}$, $\text{Y}@C_{2v}\text{-C}_{82}$, $\text{La}_2@D_2(10611)\text{-C}_{72}$, $\text{La}_2@D_{3h}(5)\text{-C}_{78}$, $\text{La}_2@I_h\text{-C}_{80}$, $\text{Ce}_2@I_h\text{-C}_{80}$, $\text{Sc}_3\text{C}_2@I_h\text{-C}_{80}$, and $\text{Sc}_2\text{C}_2@C_{3v}(8)\text{-C}_{82}$.

almost identical to those of pristine $M@C_{2v}\text{-C}_{82}$. This strong similarity suggests that the carbene addition scarcely changes the π -electron system of the cage because the sp^2 -character of the carbon atoms at the site of addition is retained. The Mulliken charge densities and π orbital axis vector (POAV)⁶³ values are found to be large for the carbons in the hexagonal ring nearest the metal atom. We consider that the carbene selectively attacks one of the six electron-rich strained carbons to form the two regioisomers of [6,6]-open adducts. The position of the metal atom is changed slightly by the carbene addition and is located at a single site nearest the site of addition. It is considered that $M@C_{2v}\text{-C}_{82}(\text{Ad})\text{-I}$ is a kinetic product whereas $M@C_{2v}\text{-C}_{82}(\text{Ad})\text{-II}$ is a thermodynamic product. In fact, $\text{La}@C_{2v}\text{-C}_{82}(\text{Ad})\text{-I}$ isomerizes thermally to $\text{La}@C_{2v}\text{-C}_{82}(\text{Ad})\text{-II}$. Theoretical calculations showed that $\text{La}@C_{2v}\text{-C}_{82}(\text{Ad})\text{-I}$

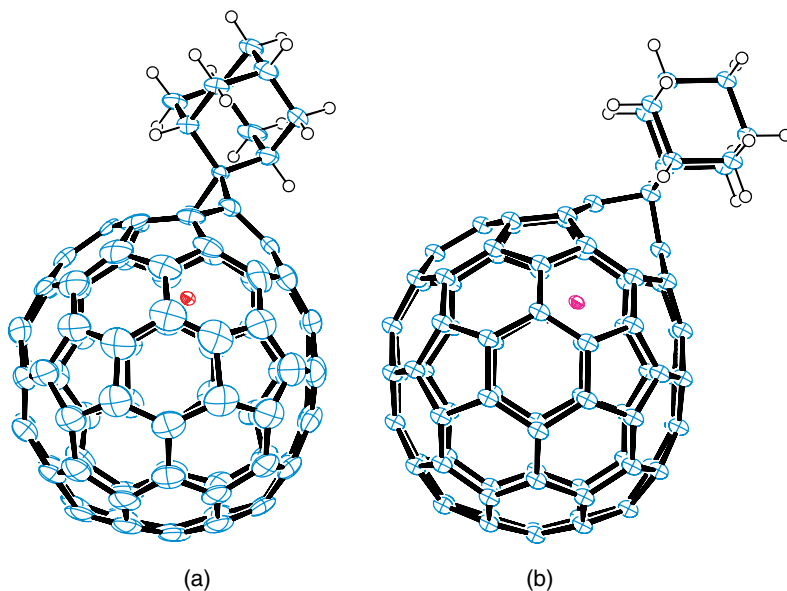


Figure 7. ORTEP plots of (a) $\text{La@C}_{2v}\text{-C}_{82}(\text{Ad})\text{-I}$ and (b) $[\text{Ce@C}_{2v}\text{-C}_{82}(\text{Ad})\text{-II}]^-$.

is 2.5 kcal/mol less stable than $\text{La@C}_{2v}\text{-C}_{82}(\text{Ad})\text{-II}$ is. Moreover, recent crystallographic analyses have revealed that the molecular structures of $\text{Gd@C}_{2v}\text{-C}_{82}(\text{Ad})\text{-I}^{61}$ and $\text{Y@C}_{2v}\text{-C}_{82}(\text{Ad})\text{-I}^{62}$ are almost identical to that of $\text{La@C}_{2v}\text{-C}_{82}(\text{Ad})\text{-I}$.

The use of ^{13}C -NMR measurements of $\text{Ce@C}_{2v}\text{-C}_{82}(\text{Ad})\text{-I}$ and $\text{Ce@C}_{2v}\text{-C}_{82}(\text{Ad})\text{-II}$ anions for paramagnetic NMR shift analyses was made possible by electrochemical reduction.⁶⁰ Surprisingly, the observed paramagnetic NMR shifts of both show good agreement with the calculated values of the optimized structures based on Equation 1, despite their lower symmetries.

A non-IPR fullerene, $\text{La}_2@\text{D}_2(10611)\text{-C}_{72}$, was subjected to reaction with Ad carbene.²³ Six isomers of $\text{La}_2@\text{D}_2(10611)\text{-C}_{72}(\text{Ad})$ were isolated and characterized, among which the structures of the three most abundant isomers (designated as isomer B, isomer C, and isomer D) were elucidated using X-ray crystallography (see Figure 8). The hemisphere on which Ad is not attached seems to remain unchanged in the three isomers, indicating that the addition to a bond far from the [5,5]-bond junction has little effect on the strong interaction between the metal atoms and the fused pentagon bond. It is particularly interesting that the La atoms close to the Ad moieties in the three isomers move from positions on the [5,5]-bonds to the cavities of the broken pentagons. These results suggest that the breaking of a bond close to the [5,5]-junction affects the position of the adjacent metal atoms.

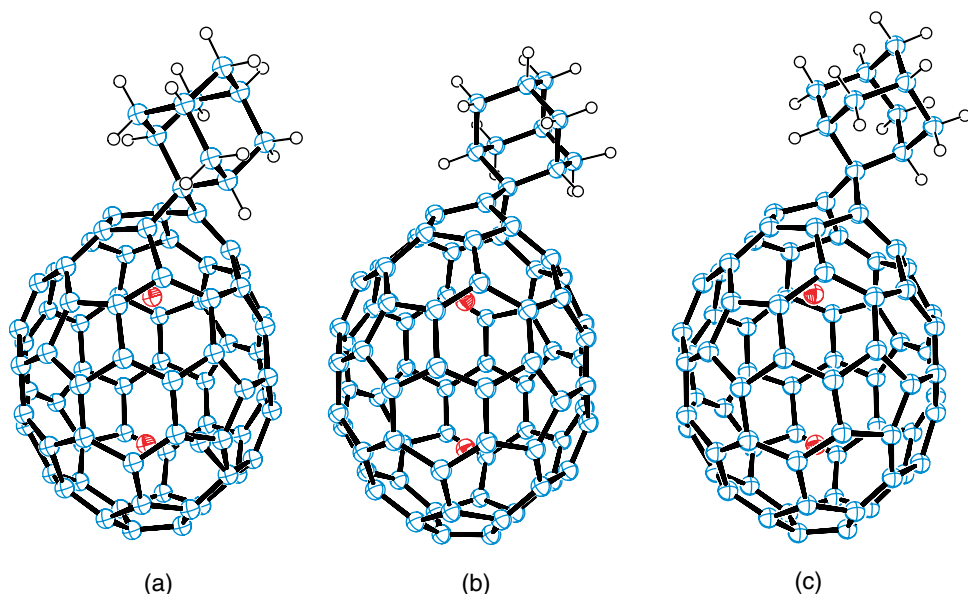


Figure 8. ORTEP plots of $\text{La}_2@D_2(10611)\text{-C}_{72}(\text{Ad})$ isomers. (a) isomer-B, (b) isomer-C, and (c) isomer-D.

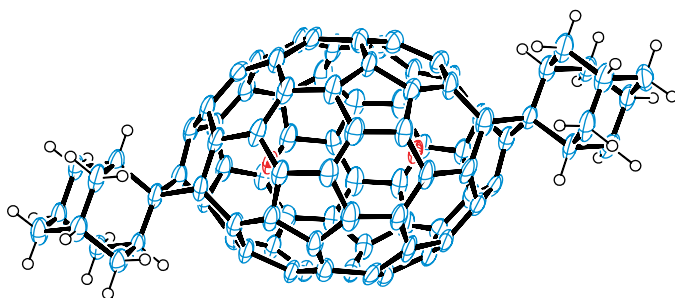


Figure 9. ORTEP plot of $\text{La}_2@D_2(10611)\text{-C}_{72}(\text{Ad})_2$.

By modifying the condition of the reaction, seven isomers of bis-carbene adducts, $\text{La}_2@D_2(10611)\text{-C}_{72}(\text{Ad})_2$, were synthesized.⁶⁴ Among these, the structure of the most abundant isomer was clarified using X-ray crystallography (see Figure 9). The La atoms are situated close to the cavities of the broken pentagons. The La–La distance of 4.300 Å is longer than those for the mono-adducts (4.171–4.178 Å), which indicates that the two open parts help to relieve the strong repulsion between the two La atoms.

The electrophilic addition of $\text{La}_2@D_{3h}(5)\text{-C}_{78}$ with Ad carbene afforded four isomers of the mono-adducts $\text{La}_2@D_{3h}(5)\text{-C}_{78}(\text{Ad})$.²⁷ The X-ray study shows that one mono-adduct has an [5,6]-open structure with the La–La

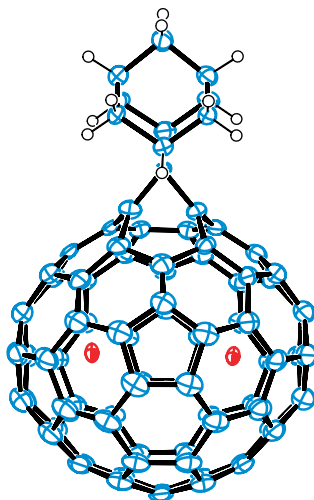


Figure 10. ORTEP plot of $\text{La}_2@D_{3h}(5)\text{-C}_{78}(\text{Ad})$.

distance of 4.081 Å (see Figure 10). The metal positions are almost identical to those in pristine $\text{La}_2@D_{3h}(5)\text{-C}_{78}$, although the C–C bond on the cage is cleaved by the reaction. In this respect, the C–C bond cleavage far from the metal atoms has little effect on the metal position.

To form the [6,6]-open adduct, $\text{Ce}_2@I_h\text{-C}_{80}(\text{Ad})$, $\text{Ce}_2@I_h\text{-C}_{80}$ reacted with Ad carbene, in which the [6,6]-bond is broken by its addition.⁶⁵ Subsequent X-ray crystallographic analysis of the $\text{La}_2@I_h\text{-C}_{80}$ analog, $\text{La}_2@I_h\text{-C}_{80}(\text{Ad})$, revealed that the metal atoms are collinear with the spiro carbon of the carbene adduct, unlike the 3D random movement in $\text{La}_2@I_h\text{-C}_{80}$ (see Figure 11). It is noteworthy that the La–La distance is highly elongated to 4.031 Å. The remarkable metal–metal elongation in the carbene adduct results from the expansion of the cage’s inner space caused by the bond cleavage, which reduces the electrostatic repulsion between the metal cations. This elongation engenders the regulation of metal atoms from 3D movement to the restricted behavior. In addition, the paramagnetic NMR shift analysis of $\text{Ce}_2@I_h\text{-C}_{80}(\text{Ad})$ indicates that the Ce positions are also regulated and that they stand still at specific positions that are collinear with the spiro carbon of the Ad carbene at room temperature in solution, as found for $\text{La}_2@I_h\text{-C}_{80}(\text{Ad})$. The absorption spectra of $\text{La}_2@I_h\text{-C}_{80}(\text{Ad})$ and $\text{Ce}_2@I_h\text{-C}_{80}(\text{Ad})$ respectively resemble those of the pristine $\text{La}_2@I_h\text{-C}_{80}$ and $\text{Ce}_2@I_h\text{-C}_{80}$. These facts indicate that the π -electronic state of the $I_h\text{-C}_{80}$ cage is little changed by the carbene addition because the sp^2 -character of the carbon atoms at the site of addition is retained.

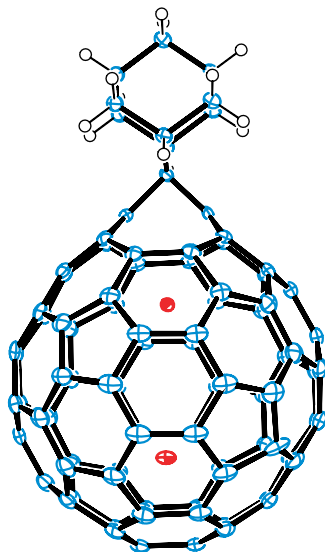


Figure 11. ORTEP plot of $\text{La}_2@I_h\text{-C}_{80}(\text{Ad})$.

The $\text{Sc}_2\text{C}_2@C_{3v}(8)\text{-C}_{82}$ reacted with Ad carbene to form several $\text{Sc}_2\text{C}_2@C_{3v}(8)\text{-C}_{82}(\text{Ad})$ isomers, among which the major isomer of $\text{Sc}_2\text{C}_2@C_{3v}(8)\text{-C}_{82}(\text{Ad})$ was isolated and characterized.⁴⁷ Results of X-ray crystallographic analysis showed that the adduct has the [5,6]-open structure (see Figure 12(a)). At 90 K, three Sc_2 pairs with occupancies of 0.51, 0.40, and 0.09 are observed inside the cage, suggesting rotational movement of the encaged cluster. Because of this rotation, $\text{Sc}_2\text{C}_2@C_{3v}(8)\text{-C}_{82}(\text{Ad})$ has C_s symmetry in the ^{13}C -NMR spectrum; a single signal is observed in the ^{45}Sc -NMR spectrum.

The electrophilic addition of $\text{Sc}_3\text{C}_2@I_h\text{-C}_{80}$ with Ad carbene yielded a single product of $\text{Sc}_3\text{C}_2@I_h\text{-C}_{80}(\text{Ad})$.⁴² Subsequent X-ray crystallographic analysis showed that $\text{Sc}_3\text{C}_2@I_h\text{-C}_{80}(\text{Ad})$ has a [6,6]-open structure, in which one Sc atom is close to the cavity of the addition site and the two encaged carbon atoms are collinear with the Ad group (see Figure 12(b)). Because the two carbon atoms are non-equivalent, the ^{13}C -NMR chemical shifts of the C_2 unit were observed at 257.2 and 384.4 ppm, which agree well with the calculated values of 275.4 and 380.9 ppm.⁴¹ Therefore, the rotation of the encaged cluster is slower than the NMR timescale.

4.3. 1,3-Dipolar cycloaddition

The 1,3-dipolar cycloaddition of $\text{M}_2@I_h\text{-C}_{80}$ with *in situ* generated azomethine ylide afforded [6,6]-closed and [5,6]-closed adducts of

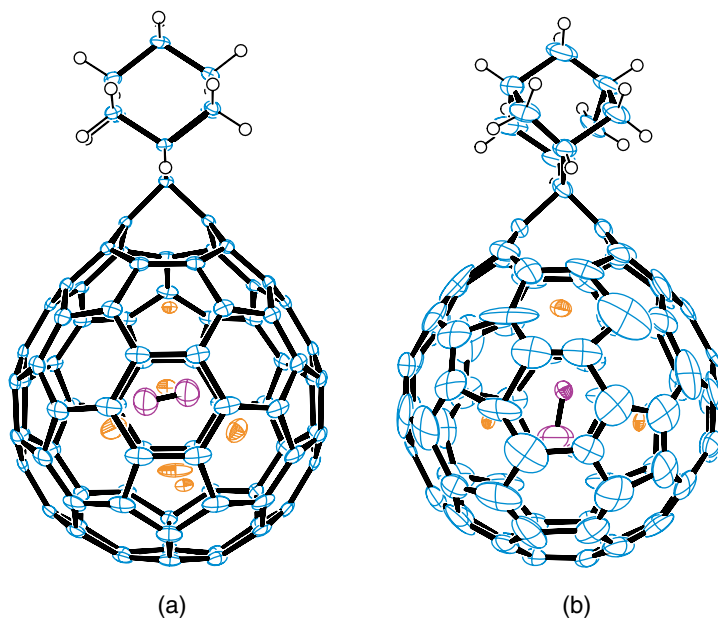
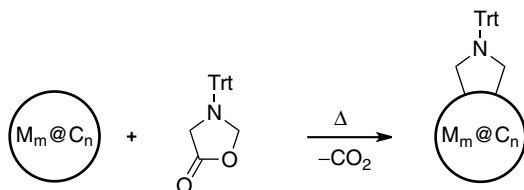


Figure 12. ORTEP plots of (a) $\text{Sc}_2\text{C}_2@C_{3v}(8)\text{-C}_{82}(\text{Ad})$ and (b) $\text{Sc}_3\text{C}_2@I_h\text{-C}_{80}(\text{Ad})$.



Scheme 3. 1,3-Dipolar cycloaddition of endohedral metallofullerenes. $M_m@C_n = \text{La}_2@I_h\text{-C}_{80}$, $\text{Ce}_2@I_h\text{-C}_{80}$ and $\text{Sc}_3\text{N}@I_h\text{-C}_{80}$. Trt = trityl.

pyrrolidinodimetallofullerene $M_2@I_h\text{-C}_{80}(\text{CH}_2)_2\text{NTrt}$ ($M = \text{La}^{66}$ and Ce ,⁶⁷ Trt = trityl) as depicted in Scheme 3.

In particular, the structures of the [6,6]-closed derivatives of $\text{La}_2@I_h\text{-C}_{80}$ and $\text{Ce}_2@I_h\text{-C}_{80}$ were elucidated unambiguously using X-ray crystallography (see Figure 13). The metal positions in the pyrrolidinodimetallofullerenes were determined using paramagnetic NMR shift analyses. The two metal atoms are fixed at slantwise positions on the mirror plane in the [6,6]-closed isomers, whereas the metal atoms are collinear with the pyrrolidine ring in the [5,6]-closed isomers. The metal positions in [6,6]-closed and [5,6]-closed adducts are explainable by the electrostatic potential maps inside the corresponding pyrrolidino cages. This finding indicates that the metal positions

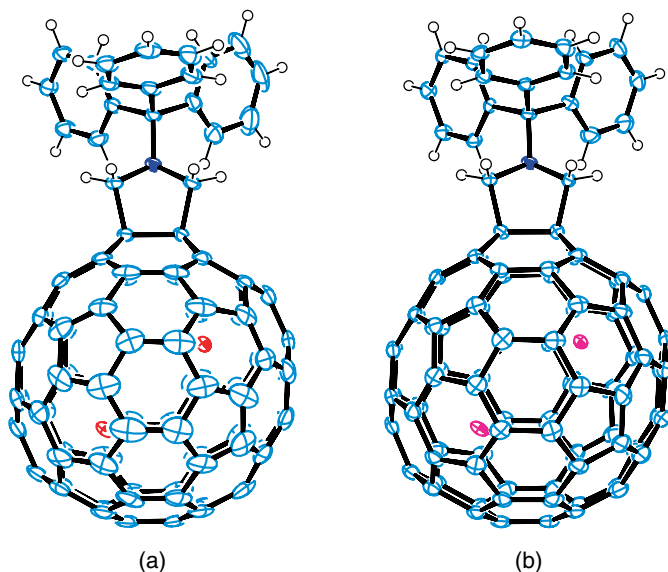


Figure 13. ORTEP plots of (a) $[6,6]\text{-La}_2@I_h\text{-C}_{80}(\text{CH}_2)_2\text{NTrt}$ and (b) $[6,6]\text{-Ce}_2@I_h\text{-C}_{80}(\text{CH}_2)_2\text{NTrt}$.

can be controlled by the addition positions of the addends. The metal distance in $[6,6]\text{-closed La}_2@I_h\text{-C}_{80}(\text{CH}_2)_2\text{NTrt}$ ($\text{La-La} = 3.823 \text{ \AA}$) is shorter than that in $[6,6]\text{-closed Ce}_2@I_h\text{-C}_{80}(\text{CH}_2)_2\text{NTrt}$ ($\text{Ce-Ce} = 3.900 \text{ \AA}$).

In fact, $\text{M}_3\text{N}@I_h\text{-C}_{80}\text{s}$ ($\text{M} = \text{Sc}$ and Y) also reacted with azomethine ylide to form $[6,6]\text{-closed}$ and $[5,6]\text{-closed}$ pyrrolidino adducts.^{68–74} It is noteworthy that the $[6,6]\text{-closed}$ adduct is the kinetic product and the $[5,6]\text{-closed}$ adduct is the thermodynamic product. Indeed, interconversion from $[6,6]\text{-closed}$ adducts to $[5,6]\text{-closed}$ ones was observed for pyrrolidino $\text{M}_3\text{N}@I_h\text{-C}_{80}$ derivatives ($\text{M} = \text{Sc}$ and Y). In contrast, similar interconversion was not observed for $[6,6]\text{-closed La}_2@I_h\text{-C}_{80}(\text{CH}_2)_2\text{NTrt}$. It is also interesting that the presence of 15 sites for scandium atoms is observed in the X-ray structure of $[6,6]\text{-closed Sc}_3\text{N}@I_h\text{-C}_{80}(\text{CH}_2)_2\text{NTrt}$.⁷³ In contrast, only two sets of the cluster are observed in the X-ray structures of $[5,6]\text{-closed Sc}_3\text{N}@I_h\text{-C}_{80}(\text{CH}_2)_2\text{NTrt}$. This finding shows that the cluster movement is not always consistent with that of metal atoms in the corresponding functionalized dimetallofullerenes. That inconsistency results from the difference in the electronic structures and charge distributions of whole molecules between clusterfullerenes and dimetallofullerenes. In addition, the electrostatic interactions inside the cages differ. With regard to dimetallofullerenes, two metal cations are not bonded and are repulsive towards each other. In contrast, clusters such as metal nitrides

have a complicated charge distribution. For that reason, it is difficult to explain the positions of the clusters in clusterfullerenes using the electrostatic potential maps inside the anionic cage.

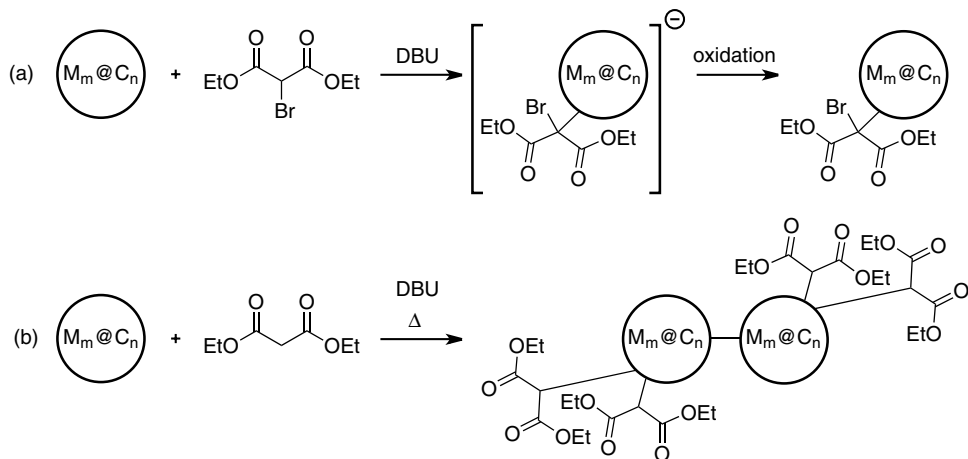
Two regioisomers of pyrrolidino $\text{Sc}_3\text{N}@D_{3h}(5)\text{-C}_{78}$ were synthesized; the molecular structure of one was elucidated using X-ray crystallography.⁷⁵ The X-ray structure disclosed that the addition occurred at a [6,6]-junction bond on the ellipsoidal cage. The Sc_3N cluster remains in the horizontal plane of the $D_{3h}(5)$ cage after the addition and does not interact directly with the addition site.

Recently, a pyrrolidino adduct of $\text{Sc}_3\text{C}_2@I_h\text{-C}_{80}$ was synthesized and characterized.⁷⁶ Although the adduct is paramagnetic, the ^{13}C -NMR spectrum showed a singlet at 71.62 ppm for the ^{13}C -labeled methylene carbon in the pyrrolidine ring, indicating the possession of the [5,6]-closed structure. The splitting EPR signal for the adduct suggests that the free rotation of the cluster is hindered by the exohedral addition, which engenders inhomogeneous spin density distributions on the internal cluster.

The base-induced decomposition of tosylhydrazone led to *in situ* generation of the diazoalkane, which underwent 1,3-dipolar addition with $\text{M}_3\text{N}@I_h\text{-C}_{80}$ ($\text{M} = \text{Sc}$ and Y) followed by the elimination of N_2 to form [6,6]-open adducts as phenyl butyric acid methyl ester (PCBM) analogues.⁷⁷

4.4. Nucleophilic addition

The Bingel–Hirsch reaction is widely applied in fullerene chemistry. The reaction to $\text{La}@C_{2v}\text{-C}_{82}$ with bromomalonate yields a mono-adduct $\text{La}@C_{2v}\text{-C}_{82}\text{CBr}(\text{COOEt})_2$ as the major product (see Scheme 4(a) and Figure 14(a)).^{78,79} Because the reaction takes place at room temperature, formation of the products is believed to be controlled kinetically. The bromomalonate group is singly bonded to the carbon atom on the cage, which is far from the La atom. It is assumed that the carbanion attacked the most positively charged and second-most strained carbon atom on the cage, with subsequent oxidation to afford the diamagnetic product. The metal position in $\text{La}@C_{2v}\text{-C}_{82}\text{CBr}(\text{COOEt})_2$ is almost identical to that in $\text{La}@C_{2v}\text{-C}_{82}$. This finding is acceptable because the site of addition is distant from the metal atom, which causes little change of circumstances near the metal atom. When malonate was subjected to the reaction instead of bromomalonate, bis-addition proceeded in a highly regioselective way and engendered the dominant formation of a single bis-adduct isomer, $\text{La}@C_{2v}\text{-C}_{82}[\text{CH}(\text{COOEt})_2]_2$ as shown in Scheme 4(b).⁸⁰ The bis-adduct retains an open-shell electronic structure and crystallizes to form



Scheme 4. Bingel–Hirsch reactions of endohedral metallofullerenes. $M_m@C_n = \text{La}@C_{2v}\text{-C}_{82}$.

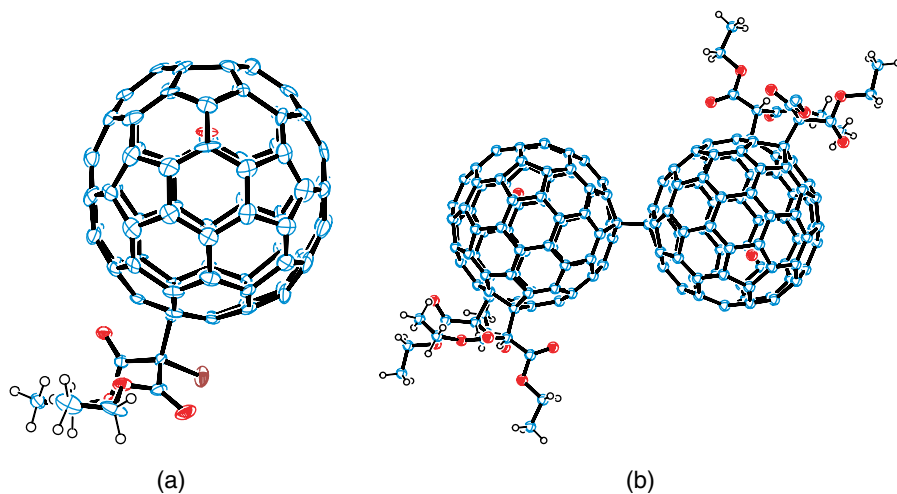
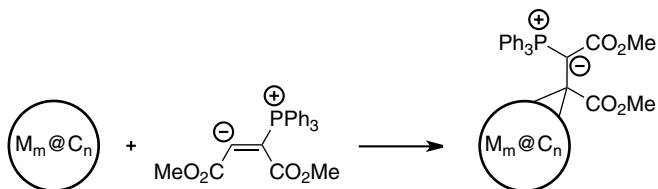


Figure 14. ORTEP plots of (a) $\text{La}@C_{2v}\text{-C}_{82}\text{CBr}(\text{COOEt})_2$ and (b) $\text{La}@C_{2v}\text{-C}_{82}[\text{CH}(\text{COOEt})_2]_2$ dimer.

a dimer. The La positions are off the C_2 axis and move slightly toward the hemisphere that undergoes bis-addition (see Figure 14(b)).

The Bingel–Hirsch reaction of $\text{Y}_3\text{N}@I_h\text{-C}_{80}$ and $\text{Er}_3\text{N}@I_h\text{-C}_{80}$ with bromodiethylmalonate in the presence of DBU produced stable adducts, although $\text{Sc}_3\text{N}@I_h\text{-C}_{80}$ did not react under the same condition.⁸¹ This result implies that intramolecular interaction between the trimetallic nitride cluster and the cage affects the reactivity of endohedral metallofullerenes. The X-ray crystal structure



Scheme 5. Regioselective reaction of endohedral metallofullerenes with DMAD and triphenylphosphine. $M_m@C_n = Dy@C_{2v}-C_{82}$.

of $Y_3N@I_h-C_{80}C(CO_2CH_2Ph)_2$ revealed that the Bingel–Hirsch adduct has a [6,6]-open structure, where the C–C bond at the site of addition on the fullerene is broken. In contrast, the Bingel–Hirsch reaction of $Sc_3N@D_{3h}(5)-C_{78}$ afforded mono- and bis-adducts.⁸² This result clearly indicates that $Sc_3N@D_{3h}(5)-C_{78}$ has significantly higher reactivity than $Sc_3N@I_h-C_{80}$. The ^{13}C -NMR spectrum of the mono-adduct exhibits two signals at 45.54 and 52.49 ppm, which are assignable to the sp^3 -hybridized carbon atoms in the cyclopropane ring. Therefore, it is proposed that the mono-adduct has a closed cyclopropyl structure, as opposed to the ring-opened structure found for the Bingel–Hirsch adduct of $Y_3N@I_h-C_{80}$. It is particularly interesting that the bis-adduct has C_{2v} symmetry, as determined using NMR spectroscopy, which suggests that the second addition occurred in a highly regioselective manner.

A $Dy@C_{2v}-C_{82}$ derivative bearing a single phosphorous substituent was synthesized by the regioselective reaction of $Dy@C_{2v}-C_{82}$ with dimethyl acetylenedicarboxylate (DMAD) and triphenylphosphine as depicted in Scheme 5.⁸³ It is considered that the attack of triphenylphosphine at the activated acetylene carbon first generated the zwitterion intermediate *in situ*, which was then added onto $Dy@C_{2v}-C_{82}$. Theoretical calculations suggest that the addition preferentially gives rise to an [6,6]-open adduct, as found in the X-ray structure, not a [6,6]-closed adduct. As might be readily apparent, the [6,6]-open structure of the $Dy@C_{2v}-C_{82}$ derivative was confirmed using X-ray crystallography (see Figure 15).

4.5. Diels–Alder reaction

The Diels–Alder reaction of $La@C_{2v}-C_{82}$ with cyclopentadiene (Cp) was found to be reversible and regioselective.⁸⁴ The EPR spectrum of the adduct, $La@C_{2v}-C_{82}(Cp)$ exhibits a distinctive octet signal. However, the retrocycloaddition of $La@C_{2v}-C_{82}(Cp)$ proceeded rapidly even at room temperature. Meanwhile, the cycloadduct of $La@C_{2v}-C_{82}$ with 1,2,3,4,5-pentamethylcyclopentadiene (Cp*) is stable to accomplish X-ray crystallography (see

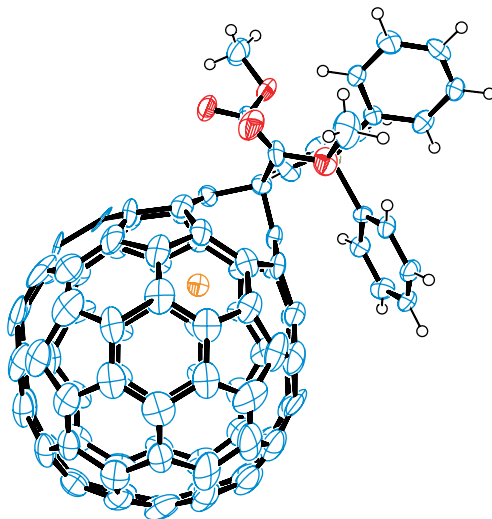
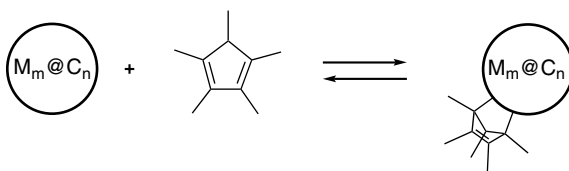


Figure 15. ORTEP plots of $\text{Dy}@C_{2v}\text{-C}_{82}$ bearing a single phosphorus substituent.



Scheme 6. Reversible Diels–Alder reaction of endohedral metallofullerenes. $M_m@C_n = \text{La}@C_{2v}\text{-C}_{82}$.

Scheme 6 and Figure 16).⁸⁵ Results of X-ray analysis show that $\text{La}@C_{2v}\text{-C}_{82}(\text{Cp}^*)$ takes two orientations in the crystal structure and that 60% of the molecule is found to have dimer formation. It is particularly interesting that not only the site of addition but also formation of dimers in the crystal structures show the same situation with those of $\text{La}@C_{2v}\text{-C}_{82}[\text{CH}(\text{COOEt})_2]$.⁸⁰ The formation of dimers is explainable by high POAV angles (11.0°) and high spin density (0.028) of the bonded carbon atoms. The carbon atoms at the attached site of the Cp^* moiety have no LUMO and SOMO coefficient sufficient to overlap with the HOMO of Cp^* . Instead, they have the highest positive charge density and the 5th and 7th highest POAV values among the 24 nonequivalent carbon atoms. This result implies that the reaction mechanism proceeds not in a concerted but a stepwise manner.

Reactivity of $\text{La}@C_{2v}\text{-C}_{82}$ with benzyne was also studied. *In situ* generated benzyne by the diazotization of anthranilic acid with isoamyl nitrite reacts

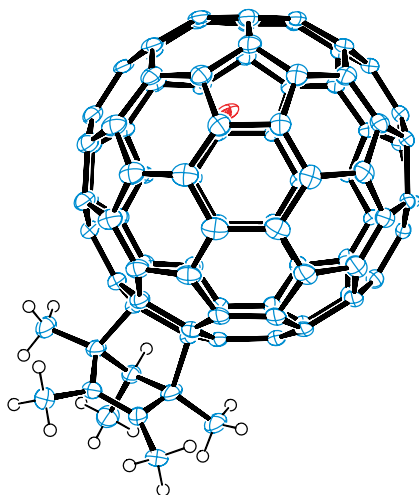


Figure 16. ORTEP plot of La@C_{2v}-C₈₂(Cp*) monomer.

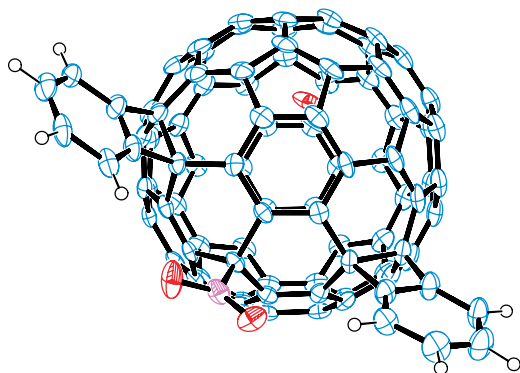
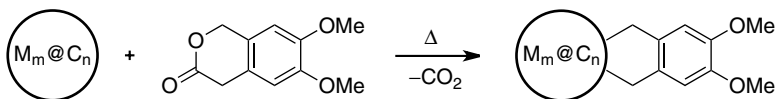


Figure 17. ORTEP plot of La@C_{2v}-C₈₂(C₆H₄)₂NO₂.

smoothly with $\text{La}@C_{2v}\text{-C}_{82}$, giving complexed products, among which $\text{La}@C_{2v}\text{-C}_{82}(\text{C}_6\text{H}_4)_2\text{NO}_2$ was isolated eventually (see Figure 17).⁸⁶ It is proposed that a radical coupling reaction of $\text{La}@C_{2v}\text{-C}_{82}$ with trace NO_2 radicals first produces $\text{La}@C_{2v}\text{-C}_{82}\text{NO}_2$, followed by the bis-addition of benzyne.

An irreversible Diels–Alder reaction was first subjected to $\text{Sc}_3\text{N}@I_b\text{-C}_{80}$, in which $\text{Sc}_3\text{N}@I_b\text{-C}_{80}$ reacts with *in situ* generated *o*-quinodimethane to form the corresponding [5,6]-closed cycloadduct (see Scheme 7).^{87,88} The Sc_3N units are positioned away from the site of addition, causing carbon atoms immediately neighboring the scandium atoms to protrude slightly from the fullerene cage surface.

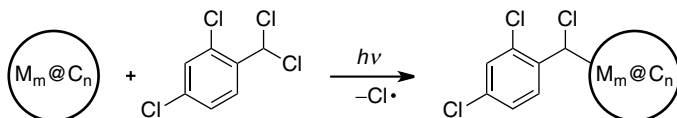


Scheme 7. Irreversible Diels–Alder reaction of endohedral metallofullerenes. $M_m@C_n = \text{Sc}_3\text{N}@I_h\text{-C}_{80}$.

4.6. Radical reaction

Photoirradiation of $\text{La}@C_{2v}\text{-C}_{82}$ with $\alpha,\alpha,2,4$ -tetrachlorotoluene afforded two regioisomers of the radical coupling products, $\text{La}@C_{2v}\text{-C}_{82}\text{CHClC}_6\text{H}_3\text{Cl}_2$.⁸⁹ The products have closed-shell electronic structures because a single benzyl radical bonded to paramagnetic $\text{La}@C_{2v}\text{-C}_{82}$. The X-ray crystallographic analysis was performed for one isomer to disclose its structure (see Scheme 8 and Figure 18). The La position in the isomer is off the C_2 axis and moves slightly against the hemisphere that undergoes a coupling reaction. This trend contrasts with the case of $\text{La}@C_{2v}\text{-C}_{82}\text{CBr}(\text{COOEt})_2$.^{78,79} In contrast, photoirradiation of $\text{Sc}_3\text{N}@I_h\text{-C}_{80}$ in the presence of benzyl bromide produced the dibenzyl adduct of $\text{Sc}_3\text{N}@I_h\text{-C}_{80}$ in high yield and high selectivity.⁹⁰ The X-ray crystallographic analysis disclosed that the product has a 1,4-addition pattern.

Some monometallofullerenes, such as $\text{La}@C_{72}$, $\text{La}@C_{74}$, and $\text{La}@C_{80}$, are known to be insoluble and are not extractable despite the fact that their existence was detected in raw soot using mass spectrometry.² It is proposed that such monometallofullerenes bind strongly with amorphous carbons and/or other metallofullerenes to form insoluble aggregates because of their high radical characters and small band gaps. Actually, $\text{La}@C_2(10612)\text{-C}_{72}$, $\text{La}@D_{3h}\text{-C}_{74}$, and $\text{La}@C_{2v}(3)\text{-C}_{80}$ are soluble and isolable because of the addition of dichlorophenyl radicals, which takes place during the extraction of raw soot using 1,2,4-trichlorobenzene. To date, three isomers of $\text{La}@C_2(10612)\text{-C}_{72}\text{C}_6\text{H}_3\text{Cl}_2$,⁹¹ three isomers of $\text{La}@D_{3h}\text{-C}_{74}$,⁹² and three isomers of $\text{La}@C_{2v}(3)\text{-C}_{80}\text{C}_6\text{H}_3\text{Cl}_2$ ⁹³ derivatives have been isolated and characterized. The dichlorophenyl radicals reacted with carbon atoms that have high spin densities and high POAV values in the pristine cages, as disclosed by X-ray crystallography (see Figure 19). Among these, it is



Scheme 8. Radical coupling reaction of endohedral metallofullerenes with $\alpha, \alpha,2,4$ -tetrachlorotoluene. $M_m@C_n = \text{La}@C_{2v}\text{-C}_{82}$.

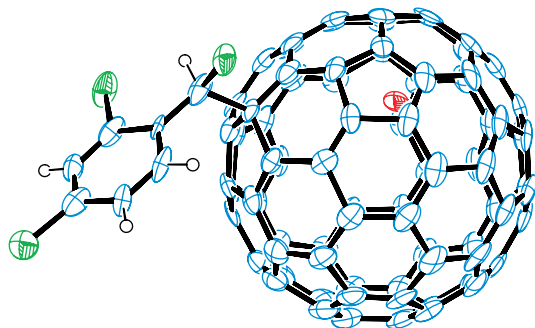


Figure 18. ORTEP plot of $\text{La@C}_{2v}\text{-C}_{82}\text{CHClC}_6\text{H}_3\text{Cl}_2$.

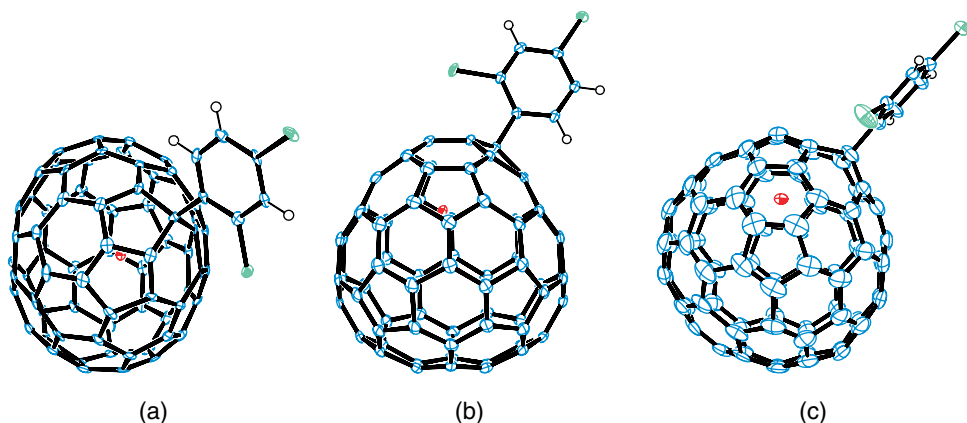


Figure 19. ORTEP plots of (a) $\text{La@C}_2(10612)\text{-C}_{72}\text{C}_6\text{H}_3\text{Cl}_2$, (b) $\text{La@D}_{3h}\text{-C}_{74}\text{C}_6\text{H}_3\text{Cl}_2$, and (c) $\text{La@C}_{2v}(3)\text{-C}_{80}\text{C}_6\text{H}_3\text{Cl}_2$.

noteworthy that the encaged La atoms in the X-ray structure of a $\text{La@C}_2(10612)\text{-C}_{72}\text{C}_6\text{H}_3\text{Cl}_2$ isomer were found to be located in the fold of the fused pentagons. The radical coupling reactions cause monometallofullerenes to be diamagnetic and stable. The results suggest that many other insoluble and unknown endohedral metallofullerenes exist in raw soot produced by arc-discharging.

Radical trifluoromethylation of $\text{Y@C}_{2v}\text{-C}_{82}$ was conducted by heating the mixture of Y@C_{82} -enriched extract and silver(I) trifluoroacetate at 400°C under dynamic vacuum.⁹⁴ The addition of an odd number of CF_3 groups to paramagnetic $\text{Y@C}_{2v}\text{-C}_{82}$ rendered the two isolable isomers of $\text{Y@C}_{2v}\text{-C}_{82}(\text{CF}_3)_5$ diamagnetic. The combination of ^{19}F NMR spectroscopy and DFT calculations suggested that both the isomers have 1,4-addition structures. Similarly, $\text{Sc}_3\text{N@I}_h\text{-C}_{80}$ and $\text{Sc}_3\text{N@D}_{5h}\text{-C}_{80}$ can be transformed into trifluoromethylated

derivatives, among which the structures of $\text{Sc}_3\text{N}@I_h\text{-C}_{80}(\text{CF}_3)_{14}$ and $\text{Sc}_3\text{N}@I_h\text{-C}_{80}(\text{CF}_3)_{16}$ were elucidated using X-ray crystallography.^{95,96}

Manganese(III) acetate can abstract a hydrogen radical from diethyl malonate to form the corresponding free radical that can add to alkenes and alkynes. This free radical reaction was applied to functionalization of $\text{Sc}_3\text{N}@I_h\text{-C}_{80}$ and $\text{Lu}_3\text{N}@I_h\text{-C}_{80}$, producing [6,6]-open derivatives.⁹⁷

5. Electronic Tuning by Chemical Functionalization

Another intriguing issue is whether the electronic properties of endohedral metallofullerenes can be modulated by exohedral chemical functionalization. Functionalized endohedral metallofullerenes with desired HOMO–LUMO levels would be useful as a component in organic electronic devices such as photovoltaics.⁹⁸ Redox potentials of functionalized endohedral metallofullerenes obtained by electrochemical measurements are presented in Tables 2–4, in which those of pristine molecules are also given to show effects by functionalization.

Table 2 presents redox potentials of functionalized monometallofullerenes. As compared to pristine $\text{M}@C_{2v}\text{-C}_{82}$ ($\text{M} = \text{La}$ and Y), the reduction and oxidation potentials of the bis-silylated monometallofullerenes were shifted cathodically to 80–210 and 130–200 mV, respectively.⁵⁰ The bis-silylated cages are electron-rich as a result of electron donation from the silyl substituent. Therefore, they are reluctant to undergo reduction and instead prefer oxidation. In contrast, the reduction and oxidation potentials of $\text{M}@C_{2v}\text{-C}_{82}(\text{Ad})$ derivatives, which possess carbon substituents, are only shifted cathodically to 70–80 and 60–80 mV, respectively.^{58–62} Introduction of an Ad group decreases the electron-accepting property because of the inductive effect, as confirmed by the calculated electron affinities. It is also notable that the difference between the sites of addition in the major isomer and the minor one does not influence the electronic properties, which is in good agreement with results of the absorption spectra. The large difference between the bis-silylated derivative and the carbene adducts suggests that the silylated $\text{M}@C_{2v}\text{-C}_{82}$ has a considerably higher-lying HOMO level than the carbene adducts. It is noteworthy that the silylated $\text{M}@C_{2v}\text{-C}_{82}$ s have smaller HOMO–LUMO gaps than those of the pristine species.

The singly bonded Bingel adduct, $\text{La}@C_{2v}\text{-C}_{82}\text{CBr}(\text{COOEt})_2$, has a much larger potential gap of 1.04 V than that for $\text{La}@C_{2v}\text{-C}_{82}$ (0.49 V), because the first oxidation wave is shifted anodically by 310 mV whereas the first reduction wave is shifted cathodically by 240 mV relative to the values for $\text{La}@C_{2v}\text{-C}_{82}$.⁷⁸ Therefore, the singly bonded adduct possesses a larger

Table 2. Redox Potentials^a of Functionalized Monometallofullerenes

Compound	^{ox} E_2	^{ox} E_1	^{red} E_1	^{red} E_2	^{red} E_3	Refs.
La@C _{2v} -C ₈₂	+1.07 ^{b,c}	+0.07	-0.42	-1.37	-1.53	43
La@C _{2v} -C ₈₂ (Mes ₂ Si) ₂ CH ₂ -I		-0.07 ^b	-0.50 ^b	-1.71 ^b	-1.75 ^b	50
La@C _{2v} -C ₈₂ (Ad)-I	+1.01 ^b	-0.01	-0.49	-1.44	-1.79	58
La@C _{2v} -C ₈₂ (Ad)-II		+0.01 ^b	-0.48	-1.40	-1.76	59
La@C _{2v} -C ₈₂ CBr(COOEt) ₂	+0.85 ^b	+0.38 ^b	-0.66 ^{b,c}	-1.31 ^b	-1.47 ^b	78
La@C _{2v} -C ₈₂ [CH(COOEt) ₂] ₂		+0.08 ^b	-0.32 ^b	-1.57 ^b		80
La@C _{2v} -C ₈₂ (Cp*)		+0.02	-0.45	-1.71	-2.22	85
La@C _{2v} -C ₈₂ CHClC ₆ H ₃ Cl ₂		+0.25 ^b	-0.98 ^{b,c}	-1.07 ^{b,c}	-1.34 ^{b,c}	89
La@C _{2v} -C ₈₂ (C ₆ H ₄) ₂ NO ₂		+0.25 ^b	-0.39 ^b	-1.39 ^b		86
Ce@C _{2v} -C ₈₂	+1.08 ^{b,c}	+0.08	-0.41	-1.41	-1.53	14
Ce@C _{2v} -C ₈₂ (Ad)-I		+0.01 ^b	-0.41 ^b	-1.36 ^b	-1.72 ^b	60
Ce@C _{2v} -C ₈₂ (Ad)-II		+0.02 ^b	-0.42 ^b	-1.35 ^b	-1.74 ^b	60
Gd@C _{2v} -C ₈₂	+1.08 ^{b,c}	+0.09	-0.39	-1.38	-1.38	44
Gd@C _{2v} -C ₈₂ (Ad)-I		+0.06	-0.62	-1.48	-1.76	61
Y@C _{2v} -C ₈₂	+1.07 ^{b,c}	+0.10	-0.37	-1.34	-1.34	44
Y@C _{2v} -C ₈₂ (Mes ₂ Si) ₂ CH ₂ -I	+0.10 ^b	-0.10 ^b	-0.55 ^b	-1.36 ^b		50
Y@C _{2v} -C ₈₂ (Mes ₂ Si) ₂ CH ₂ -II		-0.03 ^b	-0.42 ^b			50
Y@C _{2v} -C ₈₂ (Ad)-I		-0.02	-0.54	-1.51	-1.84 ^c	62
Y@C _{2v} -C ₈₂ (Ad)-II		+0.05	-0.43	-1.37	-1.70	62

^aHalf-cell potentials unless otherwise stated. Values are in volts relative to the ferrocene/ferrocenium couple. ^bValues are obtained using DPV. ^cIrreversible.

HOMO–LUMO energy gap because of its higher-lying LUMO level and lower-lying HOMO level, as compared with those of La@C_{2v}-C₈₂. The results agree well with the EPR study, in which the singly bonded adducts are silent because of their closed-shell electronic structure. It is particularly interesting that the first reduction of the singly bonded adduct was irreversible, indicating that the radical anion of the adduct is unstable under the condition. In contrast, electrochemical measurements of the Bingel bis-adduct, La@C_{2v}-C₈₂[CH(COOEt)₂]₂, showed that the first oxidation potential of 0.08 V is very close to the value of 0.07 V for La@C_{2v}-C₈₂, although its first reduction potential shifted positively by 100 mV relative to the value for La@C_{2v}-C₈₂.⁸⁰ In fact, the bis-adduct is EPR-active and gives an octet signal, confirming its open-shell electronic structure. Furthermore, the bis-adduct exhibited perfectly reversible behaviors for its first redox processes.

The Diels–Alder adduct, La@C_{2v}-C₈₂(Cp*), exhibited one reversible oxidation and three reversible reduction processes.⁸⁵ First reduction and oxidation potentials of the Diels–Alder adduct were slightly lower than those of La@C_{2v}-C₈₂. In fact, the absorption spectrum of La@C_{2v}-C₈₂(Cp*) resembles

Table 3. Redox Potentials^a of Functionalized Dimetallofullerenes

Compound	ox E_2	ox E_1	red E_1	red E_2	red E_3	Refs.
La ₂ @D ₂ (10611)-C ₇₂	+0.75 ^{b,c}	+0.24	-0.68	-1.92		23
La ₂ @D ₂ (10611)-C ₇₂ (Ad)-B	+0.64	+0.12	-0.80			23
La ₂ @D ₂ (10611)-C ₇₂ (Ad)-C	+0.67	+0.15	-0.76	-2.00 ^{b,c}		23
La ₂ @D ₂ (10611)-C ₇₂ (Ad)-D	+0.60	+0.10	-0.79	-2.06 ^{b,c}		23
La ₂ @D ₂ (10611)-C ₇₂ (Ad) ₂	+0.57	+0.02	-0.86	-2.08		64
La ₂ @D _{3h} (5)-C ₇₈	+0.62 ^b	+0.26 ^b	-0.40 ^b	-1.84 ^b	-2.28 ^b	26
La ₂ @D _{3h} (5)-C ₇₈ (Ad)	+0.63 ^b	+0.23 ^b	-0.43 ^b	-1.82 ^b		27
Ce ₂ @D _{3h} (5)-C ₇₈	+0.79 ^{b,c}	+0.25 ^b	-0.52 ^b	-1.86 ^b	-2.23 ^b	28
Ce ₂ @D _{3h} (5)-C ₇₈ (Mes ₂ Si) ₂ CH ₂	+0.50 ^{b,c}	-0.04 ^b	-0.81 ^b			28
La ₂ @I _h -C ₈₀	+0.95	+0.56	-0.31	-1.71	-2.13 ^{b,c}	45
La ₂ @I _h -C ₈₀ (Mes ₂ Si) ₂ CH ₂		-0.06 ^{b,c}	-0.76 ^b			30
La ₂ @I _h -C ₈₀ (Dep ₂ Si) ₂ CH ₂		-0.03 ^{b,c}	-0.70 ^b			30
La ₂ @I _h -C ₈₀ (Ad)	+0.86 ^b	+0.49	-0.36	-1.78	-2.33 ^b	65
6,6-La ₂ @I _h -C ₈₀ (CH ₂) ₂ NTrt	+0.95 ^{b,c}	+0.55	-0.51	-1.65	-2.19	67
5,6-La ₂ @I _h -C ₈₀ (CH ₂) ₂ NTrt	+0.63	+0.23	-0.45	-1.71	-2.30	67
Ce ₂ @I _h -C ₈₀	+0.95	+0.57	-0.39	-1.71		34
Ce ₂ @I _h -C ₈₀ (Mes ₂ Si) ₂ CH ₂		-0.07 ^{b,c}	-0.73			34
Ce ₂ @I _h -C ₈₀ (Ad)	+0.89 ^b	+0.47	-0.43			65
6,6-Ce ₂ @I _h -C ₈₀ (CH ₂) ₂ NTrt	+0.99 ^{b,c}	+0.56 ^b	-0.55 ^b	-1.75 ^b	-2.34 ^b	67
5,6-Ce ₂ @I _h -C ₈₀ (CH ₂) ₂ NTrt	+0.62 ^b	+0.22 ^b	-0.51 ^b	-1.76 ^b	-2.25 ^b	67

^aHalf-cell potentials unless otherwise stated. Values are in volts relative to the ferrocene/ferrocenium couple. ^bValues are obtained using DPV. ^cIrreversible.

Table 4. Redox Potentials^a of Functionalized Clusterfullerenes

Compound	ox E_2	ox E_1	red E_1	red E_2	red E_3	Refs.
Sc ₃ N@I _h -C ₈₀		+0.62	-1.22	-1.59	-1.90	46
Sc ₃ N@I _h -C ₈₀ (Mes ₂ Si) ₂ CH ₂		+0.08 ^{b,c}	-1.45			57
Sc ₂ C ₂ @C _{3v} (8)-C ₈₂	+0.93 ^{b,c}	+0.47	-0.94 ^{b,c}	-1.15	-1.60	47
Sc ₂ C ₂ @C _{3v} (8)-C ₈₂ (Ad)	+0.72	+0.38 ^{b,c}	-0.79	-1.12	-1.63	47
Sc ₃ C ₂ @I _h -C ₈₀		-0.03	-0.50	-1.64	-1.84	42
Sc ₃ C ₂ @I _h -C ₈₀ (Ad)		-0.11	-0.55	-1.74		42

^aHalf-cell potentials unless otherwise stated. Values are in volts relative to the ferrocene/ferrocenium couple. ^bValues are obtained using DPV. ^cIrreversible.

that of La@C_{2v}-C₈₂. Repeated scanning during CV measurements showed no degradation, suggesting that the electrochemical reduction and oxidation states of La@C_{2v}-C₈₂(Cp*) are stable.

Addition of a benzyl radical produces singly bonded derivatives with large potential gaps, as found in the Bingel reaction. The major isomer of

$\text{La@C}_{2v}\text{-C}_{82}\text{CHClC}_6\text{H}_3\text{Cl}_2$ derivatives displayed one reversible oxidation and three irreversible reduction potentials.⁸⁹ The electrochemical potential gap separating the first oxidation and reduction potentials of 1.23 V is larger than that of $\text{La@C}_{2v}\text{-C}_{82}\text{CBr}(\text{COOEt})_2$. However, the benzyl adduct is unstable under the reduction steps.

The electrochemical reduction processes of the nitrated bis-benzene derivative of $\text{La@C}_{2v}\text{-C}_{82}$, $\text{La@C}_{2v}\text{-C}_{82}(\text{C}_6\text{H}_4)_2\text{NO}_2$, show less difference with those of $\text{La@C}_{2v}\text{-C}_{82}$ despite the fact that the molecule has a closed-shell electronic structure.⁸⁶ The first and the second reduction potentials of $\text{La@C}_{2v}\text{-C}_{82}(\text{C}_6\text{H}_4)_2\text{NO}_2$ of -0.39 V and -1.39 V respectively resemble the corresponding values of -0.42 V and -1.34 V for $\text{La@C}_{2v}\text{-C}_{82}$. On the other hand, the oxidation potential of $\text{La@C}_{2v}\text{-C}_{82}(\text{C}_6\text{H}_4)_2\text{NO}_2$ is 180 mV more positive than the value of $\text{La@C}_{2v}\text{-C}_{82}$. Because a nitro group is known to be highly electron-withdrawing, it is reasonable to speculate that the electron-accepting ability of the diamagnetic molecule is comparable with that of $\text{La@C}_{2v}\text{-C}_{82}$, having a paramagnetic nature by exohedral nitration.

The redox potentials of functionalized dimetallofullerenes are shown in Table 3. As found for functionalized monometallofullerenes, addition of an Ad group results in a slight increase of the HOMO and LUMO levels because it has a mild electron-donating character.^{23,27,65} When a second Ad group is introduced on the carbon cage, the HOMO and LUMO levels rise slightly further.⁶⁴ The redox potentials are rarely affected by the position of the attached Ad group. The small shifts of the redox potentials reflect the fact that the HOMO–LUMO energy gaps of the Ad carbene adducts resemble those of pristine dimetallofullerenes.

In contrast to addition of Ad carbene, bis-silylation of dimetallofullerenes is strongly effective for tuning electronic properties. The bis-silylated adduct of $\text{Ce}_2@D_{3h}(5)\text{-C}_{78}$ exhibited one irreversible and one reversible oxidation wave as well as one reversible reduction wave in the cyclic voltammograms.²⁸ Compared to $\text{Ce}_2@D_{3h}(5)\text{-C}_{78}$, all the oxidation and reduction potentials of the bis-silylated derivative are shifted cathodically by 290 mV. This observation reflects that the cage was negatively charged to a considerable extent by bis-silylation, which leads to the rise of the HOMO and LUMO levels. The result is reasonable because the silyl group on carbon cages can act as a strong electron-donor as the result of a kind of hyperconjugation, the so-called beta-silicon effect. The electronic effect in bis-silylation is much more pronounced when $\text{M}_2@I_h\text{-C}_{80}\text{s}$ ($\text{M} = \text{La}^{30}$ and Ce^{34}) are subjected. Both the oxidation and reduction potentials of the bis-silylated $\text{M}_2@I_h\text{-C}_{80}\text{s}$ ($\text{M} = \text{La}$ and Ce) were shifted cathodically to 590–640 mV and 340–450 mV, respectively, relative to those of pristine $\text{M}_2@I_h\text{-C}_{80}\text{s}$. It is particularly interesting that the first

oxidation of the bis-silylated $M_2@I_b-C_{80}$ s led to removal of the silyl substituents from the carbon cage. The bis-silylated $Ce_2@D_{3h}(5)-C_{78}$ is stable at the first oxidation potential,²⁸ but the quantitative retrocycloaddition takes place at the second oxidation potential.

The redox potentials of two regioisomers of endohedral pyrrolidinodimetallfullerenes were also investigated.⁶⁷ The [6,6]-pyrrolidino adducts, [6,6]- $M_2@I_b-C_{80}(CH_2)_2NTrt$ ($M = La$ and Ce) showed three reversible reductions, one reversible oxidation, and one irreversible oxidation processes, whereas the [5,6]-pyrrolidino adducts, [5,6]- $M_2@I_b-C_{80}(CH_2)_2NTrt$ exhibited three reversible reductions, two reversible oxidations and one irreversible oxidation processes (the third oxidation potentials are not shown in Table 3). Compared to $M_2@I_b-C_{80}$, the first oxidation and reduction potentials of the [6,6]-pyrrolidino adducts are shifted cathodically to 10 and 160–200 mV, respectively, whereas the corresponding potentials of the [5,6]-pyrrolidino adducts are shifted cathodically to 330–350 mV and 120–140 mV, respectively. Such a striking difference in the redox potentials of the two regioisomers indicates that the electronic states of the fullerene cages in the [6,6]- and [5,6]-pyrrolidinodimetallfullerenes differ greatly. That difference can be rationalized using computational calculations, displaying that the distribution of the electrostatic potentials inside [6,6]-pyrrolidino and [5,6]-pyrrolidino adducts of $[I_b-C_{80}(CH_2)_2NH]^{6-}$ differ greatly. For the [6,6]-pyrrolidino adduct, the electrostatic potential map portrays a clear minimum on the mirror plane inside the cage. However, the electrostatic potentials of the [5,6]-pyrrolidino adduct are flat and located on the opposite side from the position of addition. It is reasonable to infer that the difference engenders the different movements of the encaged metal atoms inside the pyrrolidino-functionalized carbon cages.

Table 4 presents the redox potentials of functionalized clusterfullerenes. Regarding clusterfullerenes $Sc_2C_2@C_{3v}(8)-C_{82}$ and $Sc_3C_2@I_b-C_{80}$, addition of an Ad carbene engenders slight cathodic shifts of their redox potentials, as found in the case of monometallofullerenes and dimetallofullerenes.^{42,47} Bis-silylation is also effective to modulate electronic properties of clusterfullerenes.⁵⁷ The first oxidation and reduction potentials of the bis-silylated $Sc_3N@I_b-C_{80}$ were shifted cathodically to 540 mV and 230 mV, respectively. Apparently, the electronic tuning is derived from the electron-donating character of the silyl group. It is noteworthy that the bis-silylated $Sc_3N@I_b-C_{80}$ has a smaller HOMO–LUMO gap than that of the pristine $Sc_3N@I_b-C_{80}$. It was calculated that a considerable charge transfer takes place from the silyl group to the clusterfullerene, giving an electronic structure of $(Sc_3N@I_b-C_{80})^{1.2-}((Mes_2Si)_2CH_2)^{1.2+}$. In addition, retrocycloaddition occurred at the first oxidation potential.

6. Conclusions and Perspectives

In-depth understanding of molecular structures and electronic properties of various endohedral metallofullerenes has been achieved through numerous careful and systematic investigations. In particular, successful X-ray crystallographic analyses have provided large amounts of useful information including addition patterns of functionalized endohedral metallofullerenes and dynamic behavior of the engaged species. Recent advances in endohedral metallofullerenes have clearly demonstrated appealing possibilities for future applications as redox-active components in organic devices. We believe that the diversity of molecular structures and their structural tunability make these molecules particularly promising candidates because of their desired functionality.

Acknowledgments

This work was supported in part by a Grant-in-Aid for Scientific Research on Innovative Areas (No. 20108001, “pi-Space”), a Grant-in-Aid for Scientific Research (A)(No. 20245006), The Next Generation Super Computing Project (Nanoscience Project), Nanotechnology Support Project, and a Grant-in Aid for Scientific Research on Priority Area (Nos. 20036008, 20038007) from the Ministry of Education, Culture, Sports, Science, and Technology of Japan. M. Y. acknowledges the receipt of a JSPS Research Fellowship for Young Scientists.

References

1. Kroto, H. W.; Heath, J. R.; O'Brien, S. C.; Curl, R. F.; Smalley, R. E. *Nature* **1985**, *318*, 162.
2. Chai, Y.; Guo, T.; Jin, C.; Haufler, R. E.; Chibante, L. P. F.; Fure, J.; Wang, L.; Alford, J. M.; Smalley, R. E. *J. Phys. Chem.* **1991**, *95*, 7564.
3. Akasaka, T.; Nagase, S., Eds.; *Fullerenes: A New Family of Carbon Clusters*, Kluwer: Dordrecht, **2002**.
4. Chaur, M. N.; Melin, F.; Ortiz, A. L.; Echegoyen, L. *Angew. Chem. Int. Ed.* **2009**, *48*, 7514.
5. Stevenson, S.; Rice, G.; Glass, T.; Harish, K.; Cromer, F.; Jordan, M. R.; Kraft, J.; Hadju, E.; Bible, R.; Olmstead, M. M.; Maitra, K.; Fisher, A. J.; Balch, A. L. Dorn, H. C. *Nature* **1999**, *401*, 55.
6. Wang, C. R.; Kai, T.; Tomiyama, T.; Yoshida, T.; Kobayashi, Y.; Nishibori, E.; Takata, M.; Sakata, M. Shinohara, H. *Angew. Chem. Int. Ed.* **2001**, *40*, 397.
7. Stevenson, S.; Mackey, M. A.; Stuart, M. A.; Phillips, J. P.; Easterling, M. L.; Chancellor, C. J.; Olmstead, M. M.; Balch, A. L. *J. Am. Chem. Soc.* **2008**, *130*, 11844.
8. Dunsch, L.; Yang, S.; Zhang, L.; Svitova, A.; Oswald, S.; Popov, A. A. *J. Am. Chem. Soc.* **2010**, *132*, 5413.

9. Yamada, M.; Tsuchiya, T.; Akasaka, T.; Nagase, S. *Pure Appl. Chem.* **2010**, *82*, 757.
10. Yamada, M.; Akasaka, T.; Nagase, S. *Acc. Chem. Res.* **2010**, *43*, 92.
11. Fowler, P.; Manolopoulos, D. E. *An Atlas of Fullerenes*, Clarendon Press: Oxford, **1995**.
12. Popov, A. A. *J. Comput. Theor. Nanosci.* **2008**, *6*, 1.
13. Akasaka, T.; Wakahara, T.; Nagase, S.; Kobayashi, K.; Waelchli, M.; Yamamoto, K.; Kondo, M.; Shirakura, S.; Okubo, S.; Maeda, Y.; Kato, T.; Kako, M.; Nakadaira, Y.; Nagahata, R.; Gao, X.; Van Caemelbecke, E.; Kadish, K. M. *J. Am. Chem. Soc.* **2000**, *122*, 9316.
14. Wakahara, T.; Kobayashi, J.-i.; Yamada, M.; Maeda, Y.; Tsuchiya, T.; Okamura, M.; Akasaka, T.; Waelchli, M.; Kobayashi, K.; Nagase, S.; Kato, T.; Kako, M.; Yamamoto, K.; Kadish, K. M. *J. Am. Chem. Soc.* **2004**, *126*, 4883.
15. Wakahara, T.; Okubo, S.; Kondo, M.; Maeda, Y.; Akasaka, T.; Waelchli, M.; Kako, M.; Kobayashi, K.; Nagase, S.; Kato, T.; Yamamoto, K.; Gao, X.; Van Caemelbecke, E.; Kadish, K. M. *Chem. Phys. Lett.* **2002**, *360*, 235.
16. Feng, L.; Wakahara, T.; Tsuchiya, T.; Maeda, Y.; Lian, Y.; Akasaka, T.; Mizorogi, N.; Kobayashi, K.; Nagase, S. *Chem. Phys. Lett.* **2005**, *405*, 274.
17. Yamada, M.; Wakahara, T.; Lian, Y.; Tsuchiya, T.; Akasaka, T.; Waelchli, M.; Mizorogi, N.; Nagase, S.; Kadish, K. M. *J. Am. Chem. Soc.* **2006**, *128*, 1400.
18. Bleaney, B. *J. Magn. Reson.* **1972**, *8*, 91.
19. Tsuchiya, T.; Wakahara, T.; Maeda, Y.; Akasaka, T.; Waelchli, M.; Kato, T.; Okubo, H.; Mizorogi, N.; Kobayashi, K.; Nagase, S. *Angew. Chem. Int. Ed.* **2005**, *44*, 3282.
20. Kobayashi, K.; Nagase, S. *Chem. Phys. Lett.* **1998**, *282*, 325.
21. Kato, H.; Taninaka, A.; Sugai, T.; Shinohara, H. *J. Am. Chem. Soc.* **2003**, *125*, 7782.
22. Tan, Y.-Z.; Xie, S.-Y.; Huang, R.-B.; Zheng, L.-S. *Nat. Chem.* **2009**, *1*, 450.
23. Lu, X.; Nikawa, H.; Nakahodo, T.; Tsuchiya, T.; Ishitsuka, M. O.; Maeda, Y.; Akasaka, T.; Toki, M.; Sawa, H.; Slanina, Z.; Mizorogi, N.; Nagase, S. *J. Am. Chem. Soc.* **2008**, *130*, 9129.
24. Slanina, Z.; Chen, Z.; Schleyer, P. v. R.; Uhlik, F.; Lu, X.; Nagase, S. *J. Phys. Chem. A* **2006**, *110*, 2231.
25. Yamada, M.; Wakahara, T.; Tsuchiya, T.; Maeda, Y.; Akasaka, T.; Mizorogi, N.; Nagase, S. *J. Phys. Chem. A* **2008**, *112*, 7627.
26. Cao, B.; Wakahara, T.; Tsuchiya, T.; Kondo, M.; Maeda, Y.; Rahman, G. M. A.; Akasaka, T.; Kobayashi, K.; Nagase, S.; Yamamoto, K. *J. Am. Chem. Soc.* **2004**, *126*, 9164.
27. Cao, B.; Nikawa, H.; Nakahodo, T.; Tsuchiya, T.; Maeda, Y.; Akasaka, T.; Sawa, H.; Slanina, Z.; Mizorogi, N.; Nagase, S. *J. Am. Chem. Soc.* **2008**, *130*, 983.
28. Yamada, M.; Wakahara, T.; Tsuchiya, T.; Maeda, Y.; Kako, M.; Akasaka, T.; Yoza, K.; Horn, E.; Mizorogi, N.; Nagase, S. *Chem. Commun.* **2008**, 558.
29. Akasaka, T.; Nagase, S.; Kobayashi, K.; Wälchli, M.; Yamamoto, K.; Funasaka, H.; Kako, M.; Hoshino, T.; Erata, T. *Angew. Chem. Int. Ed. Engl.* **1997**, *36*, 1643.
30. Wakahara, T.; Yamada, M.; Takahashi, S.; Nakahodo, T.; Tsuchiya, T.; Maeda, Y.; Akasaka, T.; Kako, M.; Yoza, K.; Horn, E.; Mizorogi, N.; Nagase, S. *Chem. Commun.* **2007**, 2680.
31. Kobayashi, K.; Nagase, S.; Akasaka, T. *Chem. Phys. Lett.* **1996**, *261*, 502.
32. Shimotani, H.; Ito, T.; Taninaka, A.; Shinohara, H.; Nishibori, E.; Takata, M.; Sakata, M. *J. Am. Chem. Soc.* **2004**, *126*, 364.
33. Zhang, J.; Hao, C.; Li, S.; Mi, W.; Jin, P. *J. Phys. Chem. C* **2007**, *111*, 7862.
34. Yamada, M.; Nakahodo, T.; Wakahara, T.; Tsuchiya, T.; Maeda, Y.; Akasaka, T.; Kako, M.; Yoza, K.; Horn, E.; Mizorogi, N.; Kobayashi, K. Nagase, S. *J. Am. Chem. Soc.* **2005**, *127*, 14570.

35. Muthukumar, K. Larsson, J. A. *J. Mater. Chem.* **2008**, *18*, 3347.
36. Yamamoto, K.; Ishiguro, T.; Sakurai, K.; Funasaka, H.; Akasaka, T. in *Fullerenes: Recent Advances in the Chemistry and Physics of Fullerenes and Related Materials*, Vol. 5, The Electrochemical Society, Pennington, **1997**, p. 743.
37. Yamada, M.; Mizorogi, N.; Tsuchiya, T.; Akasaka, T.; Nagase, S. *Chem.-Eur. J.* **2009**, *15*, 9486.
38. Wang, X.; Zuo, T.; Olmstead, M. M.; Duchamp, J. C.; Glass, T. E.; Cromer, F.; Balch, A. L. Dorn, H. C. *J. Am. Chem. Soc.* **2006**, *128*, 8884.
39. Fu, W.; Xu, L.; Azurmendi, H.; Ge, J.; Fuhrer, T.; Zuo, T.; Reid, J.; Shu, C.; Harich, K.; Dorn, H. C. *J. Am. Chem. Soc.* **2009**, *131*, 11762.
40. Iiduka, Y.; Wakahara, T.; Nakajima, K.; Tsuchiya, T.; Nakahodo, T.; Maeda, Y.; Akasaka, T.; Mizorogi, N.; Nagase, S. *Chem. Commun.* **2006**, 2057.
41. Yamazaki, Y.; Nakajima, K.; Wakahara, T.; Tsuchiya, T.; Ishitsuka, M. O.; Maeda, Y.; Akasaka, T.; Waelchli, M.; Mizorogi, N.; Nagase, S. *Angew. Chem. Int. Ed.* **2008**, *47*, 7905.
42. Iiduka, Y.; Wakahara, T.; Nakahodo, T.; Tsuchiya, T.; Sakuraba, A.; Maeda, Y.; Akasaka, T.; Yoza, K.; Horn, E.; Kato, T.; Liu, M. T. H.; Mizorogi, N.; Kobayashi, K.; Nagase, S. *J. Am. Chem. Soc.* **2005**, *127*, 12500.
43. Suzuki, T.; Maruyama, Y.; Kato, T.; Kikuchi, K.; Nakao, Y.; Suzuki, S.; Achiba, Y.; Yamamoto, K.; Funasaka, H.; Takahashi, T. *Synth. Met.* **1995**, *70*, 1443.
44. Suzuki, T.; Kikuchi, K.; Oguri, F.; Nakao, Y.; Suzuki, S.; Achiba, Y.; Yamamoto, K.; Funasaka, H.; Takahashi, T. *Tetrahedron* **1996**, *52*, 4973.
45. Suzuki, T.; Maruyama, Y.; Kato, T.; Kikuchi, K.; Nakao, Y.; Achiba, Y.; Kobayashi, K.; Nagase, S. *Angew. Chem. Int. Ed. Engl.* **1995**, *34*, 1094.
46. Iiduka, Y.; Ikenaga, O.; Sakuraba, A.; Wakahara, T.; Tsuchiya, T.; Maeda, Y.; Nakahodo, T.; Akasaka, T.; Kako, M.; Mizorogi, N.; Nagase, S. *J. Am. Chem. Soc.* **2005**, *127*, 9956.
47. Iiduka, Y.; Wakahara, T.; Nakajima, K.; Nakahodo, T.; Tsuchiya, T.; Maeda, Y.; Akasaka, T.; Yoza, K.; Liu, M. T. H.; Mizorogi, N.; Nagase, S. *Angew. Chem. Int. Ed.* **2007**, *46*, 5562.
48. Akasaka, T.; Kato, T.; Kobayashi, K.; Nagase, S.; Yamamoto, K.; Funasaka, H. Takahashi, T.; *Nature* **1995**, *374*, 600.
49. Kato, T.; Akasaka, T.; Kobayashi, K.; Nagase, S.; Kikuchi, K.; Achiba, Y.; Suzuki, T.; Yamamoto, K. *J. Phys. Chem. Solids*, **1997**, *58*, 1779.
50. Yamada, M.; Feng, L.; Wakahara, T.; Tsuchiya, T.; Maeda, Y.; Lian, Y.; Kako, M.; Akasaka, T.; Kato, T.; Kobayashi, K.; Nagase, S. *J. Phys. Chem. B*, **2005**, *109*, 6049.
51. Akasaka, T.; Okubo, S.; Kondo, M.; Maeda, Y.; Wakahara, T.; Kato, T. Suzuki, T.; Yamamoto, K.; Kobayashi, K.; Nagase, S. *Chem. Phys. Lett.* **2000**, *319*, 153.
52. Akasaka, T.; Nagase, S.; Kobayashi, K.; Suzuki, T.; Kato, T.; Yamamoto, K.; Funasaka, H. Takahashi, T. *J. Chem. Soc., Chem. Commun.* **1995**, 1343.
53. Wakahara, T.; Sakuraba, A.; Iiduka, Y.; Okamura, M.; Tsuchiya, T.; Maeda, Y.; Akasaka, T.; Okubo, S.; Kato, T.; Kobayashi, K.; Nagase, S. Kadish, K. M. *Chem. Phys. Lett.* **2004**, *398*, 553.
54. Akasaka, T.; Nagase, S.; Kobayashi, K.; Suzuki, T.; Kato, T.; Kikuchi, K.; Achiba, Y.; Yamamoto, K.; Funasaka, H.; Takahashi, T. *Angew. Chem. Int. Ed. Engl.* **1995**, *34*, 2139.
55. Maeda, Y.; Miyashita, J.; Hasegawa, T.; Wakahara, T.; Tsuchiya, T.; Feng, L.; Lian, Y.; Akasaka, T.; Kobayashi, K.; Nagase, S.; Kako, M.; Yamamoto, K.; Kadish, K. M. *J. Am. Chem. Soc.* **2005**, *127*, 2143.
56. Kobayashi, K.; Nagase, S.; Maeda, Y.; Wakahara, T.; Akasaka, T. *Chem. Phys. Lett.* **2003**, *374*, 562.

57. Wakahara, T.; Iiduka, Y.; Ikenaga, O.; Nakahodo, T.; Sakuraba, A.; Tsuchiya, T.; Maeda, Y.; Kako, M.; Akasaka, T.; Yoza, K.; Horn, E.; Mizorogi, N.; Nagase, S. *J. Am. Chem. Soc.* **2006**, *128*, 9919.
58. Maeda, Y.; Matsunaga, Y.; Wakahara, T.; Takahashi, S.; Tsuchiya, T.; Ishitsuka, M. O.; Hasegawa, T.; Akasaka, T.; Liu, M. T. H.; Kokura, K.; Horn, E.; Yoza, K.; Kato, T.; Okubo, S.; Kobayashi, K.; Nagase, S.; Yamamoto, K. *J. Am. Chem. Soc.* **2004**, *126*, 6858.
59. Matsunaga, Y.; Maeda, Y.; Wakahara, T.; Tsuchiya, T.; Ishitsuka, M. O.; Akasaka, T.; Mizorogi, N.; Kobayashi, K.; Nagase, S.; Kadish, K. M. *ITE Lett. Batteries New Technol. Med.* **2006**, *7*, 43.
60. Takano, Y.; Aoyagi, M.; Yamada, M.; Nikawa, H.; Slanina, Z.; Mizorogi, N.; Ishitsuka, M. O.; Tsuchiya, T.; Maeda, Y.; Akasaka, T.; Kato, T.; Nagase, S. *J. Am. Chem. Soc.* **2009**, *131*, 9340.
61. Akasaka, T.; Kono, T.; Takematsu, Y.; Nikawa, T.; Nakahodo, H.; Wakahara, T.; Ishitsuka, M. O.; Tsuchiya, T.; Maeda, Y.; Liu, M. T. H.; Yoza, K.; Kato, T.; Yamamoto, K.; Mizorogi, N.; Slanina, Z.; Nagase, S. *J. Am. Chem. Soc.* **2008**, *130*, 12840.
62. Lu, X.; Nikawa, H.; Feng, L.; Tsuchiya, T.; Maeda, Y.; Akasaka, T.; Mizorogi, N.; Slanina, Z.; Nagase, S. *J. Am. Chem. Soc.* **2009**, *131*, 12066.
63. Haddon, R. C. *Science* **1993**, *261*, 1545.
64. Lu, X.; Nikawa, H.; Tsuchiya, T.; Maeda, Y.; Ishitsuka, M. O.; Akasaka, T.; Toki, M.; Sawa, H.; Slanina, Z.; Mizorogi, N.; Nagase, S. *Angew. Chem. Int. Ed.* **2008**, *47*, 8642.
65. Yamada, M.; Someya, C.; Wakahara, T.; Tsuchiya, T.; Maeda, Y.; Akasaka, T.; Yoza, K.; Horn, E.; Liu, M. T. H.; Mizorogi, N.; Nagase, S. *J. Am. Chem. Soc.* **2008**, *130*, 1171.
66. Yamada, M.; Wakahara, T.; Nakahodo, T.; Tsuchiya, T.; Maeda, Y.; Akasaka, T.; Yoza, K.; Horn, E.; Mizorogi, N.; Nagase, S. *J. Am. Chem. Soc.* **2006**, *128*, 1402.
67. Yamada, M.; Okamura, M.; Sato, S.; Someya, C. I.; Mizorogi, N.; Tsuchiya, T.; Akasaka, T.; Kato, T.; Nagase, S. *Chem.-Eur. J.* **2009**, *15*, 10533.
68. Cardona, C. M.; Kitaygorodskiy, A.; Ortiz, A.; Ángeles Herranz, M.; Echegoyen, L. *J. Org. Chem.* **2005**, *70*, 5092.
69. Cai, T.; Ge, Z. X.; Iezzi, E. B.; Glass, T. E.; Harich, K.; Gibson, H. W.; Dorn, H. C. *Chem. Commun.* **2005**, 3594.
70. Cardona, C. M.; Kitaygorodskiy, A.; Echegoyen, L. *J. Am. Chem. Soc.* **2005**, *127*, 10448.
71. Echegoyen, L.; Chancellor, C. J.; Cardona, C. M.; Elliott, B.; Rivera, J.; Olmstead, M. M.; Balch, A. L. *Chem. Commun.* **2006**, 2653.
72. Cardona, C. M.; Elliott, B.; Echegoyen, L. *J. Am. Chem. Soc.* **2006**, *128*, 6480.
73. Cai, T.; Slebodnick, C.; Xu, L.; Harich, K.; Glass, T. E.; Chancellor, C.; Fettinger, J. C.; Olmstead, M. M.; Balch, A. L.; Gibson, H. W.; Dorn, H. C. *J. Am. Chem. Soc.* **2006**, *128*, 6486.
74. Chen, N.; Zhang, E.-Y.; Tan, K.; Wang, C.-R.; Lu, X. *Org. Lett.* **2007**, *9*, 2011.
75. Cai, T.; Xu, L.; Gibson, H. W.; Dorn, H. C.; Chancellor, C. J.; Olmstead, M. M.; Balch, A. L. *J. Am. Chem. Soc.* **2007**, *129*, 10795.
76. Wang, T.; Wu, J.; Xu, W.; Xiang, J.; Lu, X. Li, B.; Jiang, L.; Shu, C.; Wang, C. *Angew. Chem. Int. Ed.* **2010**, *49*, 1786.
77. Shu, C.; Xu, W.; Slebodnick, C.; Champion, H.; Fu, W.; Reid, J. E.; Azurmendi, H.; Wang, C.; Harich, K.; Dorn, H. C.; Gibson, H. W. *Org. Lett.* **2009**, *11*, 1753.
78. Feng, L.; Nakahodo, T.; Wakahara, T.; Tsuchiya, T.; Maeda, Y.; Akasaka, T.; Kato, T.; Horn, E.; Yoza, K.; Mizorogi, N.; Nagase, S. *J. Am. Chem. Soc.* **2005**, *127*, 17136.
79. Feng, L.; Wakahara, T.; Nakahodo, T.; Tsuchiya, T.; Piao, Q.; Maeda, Y.; Lian, Y.; Akasaka, T.; Horn, E.; Yoza, K.; Kato, T.; Mizorogi, N.; Nagase, S. *Chem.-Eur. J.* **2006**, *12*, 5578.

80. Feng, L.; Tsuchiya, T.; Wakahara, T.; Nakahodo, T.; Piao, Q.; Maeda, Y.; Akasaka, T.; Kato, T.; Yoza, K.; Horn, E.; Mizorogi, N.; Nagase, S. *J. Am. Chem. Soc.* **2006**, *128*, 5990.
81. Lukoyanova, O.; Cardona, C. M.; Rivera, J.; Lugo-Morales, L. Z.; Chancellor, C. J.; Olmstead, M. M.; Rodríguez-Fortea, A.; Poblet, J. M.; Balch, A. L.; Echegoyen, L. *J. Am. Chem. Soc.* **2007**, *129*, 10423.
82. Cai, T.; Xu, L.; Shu, C.; Champion, H. A.; Reid, J. E.; Anklin, C.; Anderson, M. R.; Gibson, H. W.; Dorn, H. C. *J. Am. Chem. Soc.* **2008**, *130*, 2136.
83. Li, X.; Fan, L.; Liu, D.; Sung, H. H. Y.; Williams, I. D.; Yang, S.; Tan, K.; Lu, X. *J. Am. Chem. Soc.* **2007**, *129*, 10636.
84. Maeda, Y.; Miyashita, J.; Hasegawa, T.; Wakahara, T.; Tsuchiya, T.; Nakahodo, T.; Akasaka, T.; Mizorogi, N.; Kobayashi, K.; Nagase, S.; Kato, T.; Ban, N.; Nakajima, H.; Watanabe, Y. *J. Am. Chem. Soc.* **2005**, *127*, 12190.
85. Maeda, Y.; Sato, S.; Inada, K.; Nikawa, H.; Yamada, M.; Mizorogi, N.; Hasegawa, T.; Tsuchiya, T.; Akasaka, T.; Kato, T.; Slanina, Z.; Nagase, S. *Chem.-Eur. J.* **2010**, *16*, 2193.
86. Lu, X.; Nikawa, H.; Tsuchiya, T.; Akasaka, T.; Toki, M.; Sawa, H.; Mizorogi, N.; Nagase, S. *Angew. Chem. Int. Ed.* **2010**, *49*, 594.
87. Iezzi, E. B.; Duchamp, J. C.; Harich, K.; Glass, T. E.; Lee, H. M.; Olmstead, M. M.; Balch, A. L.; Dorn, H. C. *J. Am. Chem. Soc.* **2002**, *124*, 524.
88. Lee, H. M.; Olmstead, M. M.; Iezzi, E.; Duchamp, J. C.; Dorn, H. C.; Balch, A. L. *J. Am. Chem. Soc.* **2002**, *124*, 3494.
89. Takano, Y.; Yomogida, A.; Nikawa, H.; Yamada, M.; Wakahara, T.; Tsuchiya, T.; Ishitsuka, M. O.; Maeda, Y.; Akasaka, T.; Kato, T.; Slanina, Z.; Mizorogi, N.; Nagase, S. *J. Am. Chem. Soc.* **2008**, *130*, 16224.
90. Shu, C.; Sleboznick, C.; Xu, L.; Champion, H.; Fuhrer, T.; Cai, T.; Reid, J. E.; Fu, W.; Harich, K.; Dorn, H. C.; Gibson, H. W. *J. Am. Chem. Soc.* **2008**, *130*, 17755.
91. Wakahara, T.; Nikawa, H.; Kikuchi, T.; Nakahodo, T.; Rahman, G. M. A.; Tsuchiya, T.; Maeda, Y.; Akasaka, T.; Yoza, K.; Horn, E.; Yamamoto, K.; Mizorogi, N.; Skanina, Z.; Nagase, S. *J. Am. Chem. Soc.* **2006**, *128*, 14228.
92. Nikawa, H.; Kikuchi, T.; Wakahara, T.; Nakahodo, T.; Tsuchiya, T.; Rahman, G. M. A.; Akasaka, T.; Maeda, Y.; Yoza, K.; Horn, E.; Yamamoto, K.; Mizorogi, N.; Nagase, S. *J. Am. Chem. Soc.* **2005**, *127*, 9684.
93. Nikawa, H.; Yamada, T.; Cao, B.; Mizorogi, N.; Slanina, Z.; Tsuchiya, T.; Akasaka, T.; Yoza, K.; Nagase, S. *J. Am. Chem. Soc.* **2009**, *131*, 10950.
94. Kareev, I. E.; Lebedkin, S. F.; Bubnov, V. P.; Yagubskii, E. B.; Ioffe, I. N.; Khavrel, P. A.; Kuvychko, I. V.; Strauss, S. H.; Boltalina, O. V. *Angew. Chem. Int. Ed.* **2005**, *44*, 1846.
95. Shustova, N. B.; Popov, A. A.; Mackey, M. A.; Coumbe, C. E.; Paige Phillips, J.; Stevenson, S.; Strauss, S. H.; Boltalina, O. V. *J. Am. Chem. Soc.* **2007**, *129*, 11676.
96. Shustova, N. B.; Chen, Y.-S.; Mackey, M. A.; Coumbe, C. E.; Paige Phillips, J.; Stevenson, S.; Popov, A. A.; Boltalina, O. V.; Strauss, S. H. *J. Am. Chem. Soc.* **2009**, *131*, 17630.
97. Shu, C.; Cai, T.; Xu, L.; Zuo, T.; Reid, J.; Harich, K.; Dorn, H. C.; Gibson, H. W. *J. Am. Chem. Soc.* **2007**, *129*, 15710.
98. Ross, R. B.; Cardona, C. M.; Guldi, D. M.; Sankaranarayanan, S. G.; Reese, M. O.; Kopidakis, N.; Peet, J.; Walker, B.; Bazan, G. C.; Van Keuren, E.; Holloway, B. C.; Drees, M. *Nat. Chem.* **2009**, *8*, 208.

Chapter 6

Metallic Oxide Clusters in Fullerene Cages

*Steven Stevenson**

*Department of Chemistry and Biochemistry,
University of Southern Mississippi, Hattiesburg, MS, 39406 USA*

1. Introduction	186
2. Synthesis	188
2.1. Historical perspective on oxometallic fullerene (OMF) and metallic nitride fullerene (MNF) synthesis	188
2.2. Electric-arc synthesis of OMFs	189
3. Isolation	191
3.1. Stir and Filter Approach (SAFA) for $\text{Sc}_4\text{O}_2@\text{C}_{80}$ and $\text{Sc}_4\text{O}_3@\text{C}_{80}$	192
3.2. Selective precipitation method using Lewis acids	196
3.2.1. Isolation of a Stage 1 metallofullerene (e.g., $\text{Sc}_4\text{O}_3@\text{C}_{80}$)	198
3.2.2. Isolation of a Stage 2 metallofullerene (e.g., $\text{Sc}_2\text{O}@\text{C}_{82}$)	199
4. Reactivity	200
4.1. Reactivity comparison with other fullerenes	200
4.2. Reactivity comparison to electrochemical band gap	201
5. UV Characterization	203
6. Conclusions and Perspectives	203
Acknowledgments	203
References	203

*Corresponding author. Email: Steven.Stevenson@usm.edu

1. Introduction

Since 1999, there has been much excitement generated from metallofullerenes containing trimetallic nitride clusters encapsulated within fullerene cages.¹ Containing a Group V element, these metallic nitride fullerenes (MNFs) include $\text{Sc}_3\text{N@C}_{68}$,^{2–8} $\text{Sc}_3\text{N@C}_{78}$,^{9–13} and $\text{Sc}_3\text{N@C}_{80}$ ^{1,9, 14–24} as dominant species. A decade later, Stevenson *et al.* reported in 2008 a new family²⁵ of metallofullerene compounds, in which a Group VI element is entrapped for the first time as an oxometallic cluster entrapped within a carbon cage. Family members for these oxometallic fullerenes (OMFs) include $\text{Sc}_2\text{O@C}_{82}$,²⁶ $\text{Sc}_4\text{O}_2\text{@C}_{80}$,^{25,27} and $\text{Sc}_4\text{O}_3\text{@C}_{80}$,^{25,27,28} of which the latter represents the largest cluster (*e.g.*, 7 atoms) ever entrapped within a fullerene cage.

An obvious curiosity is the peculiar nature of the encapsulated metallic oxide moiety because these Sc_4O_3 and Sc_4O_2 clusters have no precedence in the literature for their chemical behavior.²⁸ Unlike the stable form of scandium oxide, Sc_2O_3 , these Sc_4O_3 and Sc_4O_2 clusters^{25,27,28} are stable in the charged state²⁷ as $(\text{Sc}_4\text{O}_3)^{6+}$ and $(\text{Sc}_4\text{O}_2)^{6+}$. As the icosahedral C_{80}^{6-} cage is highly stable with a formal charge of +6, the symbiotic nature of the cluster and cage sparks the debate of whether the cluster inside controls which fullerene cage is used or whether the cage's formal charge dictates which cluster can be encapsulated.

For example, the icosahedral C_{80}^{6-} cage²⁹ is the prototypical cage within metallic nitride clusters Sc_3N^{6+} to form MNFs. This C_{80}^{6-} cage²⁹ is also used to encapsulate the oxometallic clusters of $(\text{Sc}_4\text{O}_3)^{6+}$ and $(\text{Sc}_4\text{O}_2)^{6+}$ to form OMFs.²⁷ In a similar manner, a $(\text{Sc}_2\text{O})^{4+}$ cluster requires a tetra-anion C_{82}^{4-} cage,^{26,30,31} (C_{82}^{4-}) to accommodate its oxometallic cluster with a formal charge of +4. Experimentally, this occurs when a $(\text{Sc}_2\text{O})^{4+}$ cluster is paired with a C_{82}^{4-} cage to create $\text{Sc}_2\text{O@C}_{82}$.

Note that within this balance of matching formal charges of the cluster with the cage, nature can create atypical oxidation states. For example, in $\text{Sc}_4\text{O}_2\text{@C}_{80}$ the $(\text{Sc}_4\text{O}_2)^{6+}$ cluster forces mixed oxidation states for the Sc atoms, with half the atoms in the +3 state and the other two Sc atoms in a +2 oxidation state.^{25,27}

Given the very recent timeline since these OMFs were reported,²⁵ much of the experimental work described in the literature has been isolating sufficient material for determination of X-Ray crystallographic structures,^{25,28} which has been successfully performed on sub-milligram quantities of isolated samples. Much of the theoretical work involves density functional theory computations.²⁷ The crystal structures (Figure 16) and computational discussions are described elsewhere.^{25,27,28}

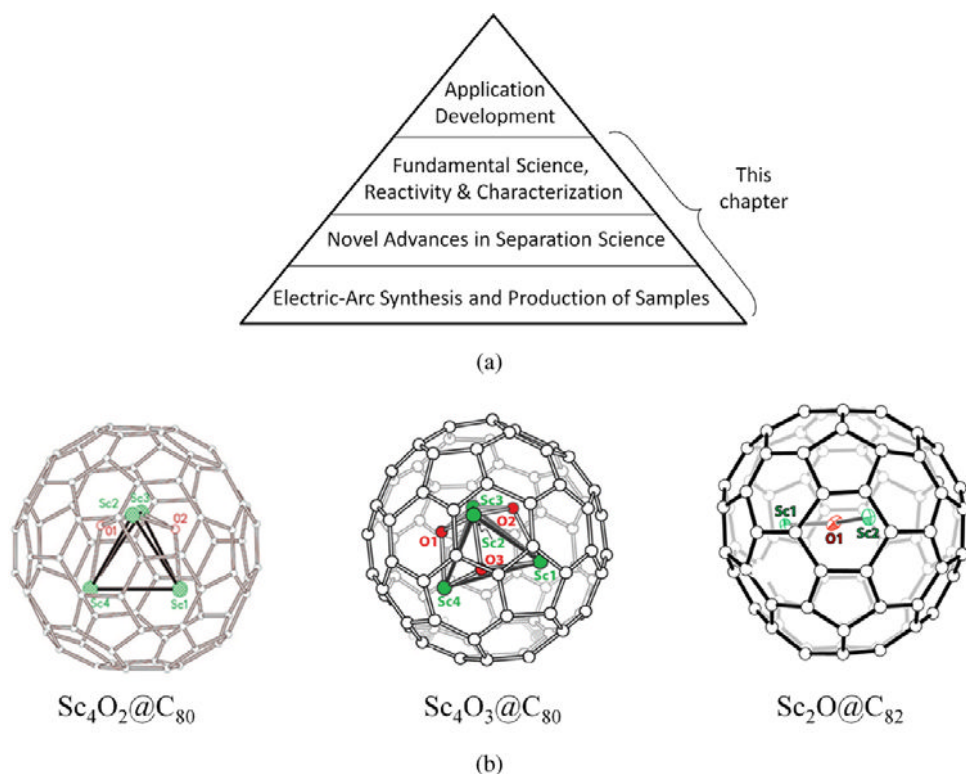


Figure 1. (a) Pyramid demonstrating the foundation and importance of research investments into OMF synthesis, their separation science, and seminal reactivity investigations. (b) X-ray structures (Modified, left to right, from Refs. 25, 26 and 28).

The goal of this writing is addressing sample availability and technical challenges. How can OMF yields be improved in the electric-arc synthesis? Can we develop new separation paradigms so OMF samples can be more readily isolated? Can we learn about OMF reactivity versus other fullerene types and manipulate those differences in a chemically based separation scheme?

Figure 1a shows an overview of this chapter's content and conveys the importance of investing research time and dollars into OMF synthesis and purification. With application development of OMFs (and MNFs) as an eventual motivation, the extent of sample availability to researchers depends ultimately on the ability to overcome hurdles associated with their production and separation.

Herein, we specifically address these issues and provide solutions to these questions. From the production end, we reveal a synthetic method which uses the CAPTEAR³² approach, *i.e.*, Chemically Adjusting Plasma Temperature,

Energy, and Reactivity. Using an electric-arc reactor, optimal OMF yields^{25,28,32} are readily achieved with an “oxidizing” atmosphere created from this method.³²

Upon production of OMF fullerene extracts, separation choices for isolating these compounds include (1) a “Stir and Filter Approach” (SAFA)^{33,34} technique or (2) a selective complexation and precipitation method³⁵ with Lewis acids. These pre-cleanup stages permit enriched samples of OMFs, which are then readily isolated with routine HPLC fraction collection.

Reactivity data of OMFs³⁵ relative to other fullerene types (*e.g.*, empty-cage fullerenes and MNF metallofullerenes) is also presented. Although initial characterization of OMFs includes UV-vis spectra, other research into OMF properties and characterization is forthcoming as scientists are now performing experiments with these purified samples.

2. Synthesis

2.1. Historical perspective on oxometallic fullerene (OMF) and metallic nitride fullerene (MNF) synthesis

Note the discovery of OMFs²⁵ occurred 20-over years after the discovery of metallofullerenes. This delay was due to the fear of other scientists to intentionally add air to their reactors. Original levels of OMF prior to CAPTEAR optimization were 0.001%, *i.e.*, 99.999% of the fullerene content in extracts were not from OMFs. This paucity of OMF production made their detection and separation especially challenging.

Because efforts for characterization, functionalization, and application development for OMFs are so dependent on sample availability, we have invested resources toward reactor R&D, *i.e.*, understanding their formation and increasing their yield. Advances in their synthesis would, in turn, permit fullerene extracts of sufficient OMF quantities for subsequent separation science R&D experiments.

The traditional route for producing endohedral metallofullerenes (EMFs) uses the electric-arc plasma approach.³⁶ Typical reactor parameters include He as the buffer gas. For the synthesis of metallic nitride fullerenes (MNFs), addition of nitrogen as a gaseous source varies from N₂ (Dorn method),¹ NH₃ (Dunsch method)³⁷ or a CAPTEAR combustible gas (Stevenson method)³² such as NO_x which is readily available in the reactor as the decomposition byproduct of copper nitrate hydrate. Addition of copper nitrate to the metal oxide powder and subsequent packing of the mixture into cored graphite rods for vaporization is previously described.³² For OMF synthesis, an oxidizing environment and addition of an oxygen source is necessary.^{25,28,32}

CAPTEAR conditions can be attained *via* addition of air and/or copper nitrate to the reaction chamber.³²

It is well-known that air introduced into the electric-arc chamber reduces overall fullerene yield. Whereas EMF and MNF synthesis *via* the Dorn¹ and Dunsch³⁷ methods do not introduce air into the reactor, air in the appropriate amount is, ironically and serendipitously, a key component of the CAPTEAR process.³² With CAPTEAR, new fullerene types are selectively synthesized by “tuning” the plasma to optimal formation parameters (*e.g.*, a plasma’s exothermicity, energy, reactivity and size). For example, metallic nitride clusters in azafullerene cages (MNAFs)³⁸ such as $\text{Sc}_3\text{N}@C_{79}\text{N}$, $\text{LaSc}_2\text{N}@C_{79}\text{N}$ and $\text{La}_3\text{N}@C_{79}\text{N}$, are readily formed under CAPTEAR conditions in addition to empty-cage fullerenes, MNFs and OMFs. With inclusion of MNAFs and classical EMFs, *e.g.*, $\text{Sc}_2\text{O}@C_{82}$, five different classes of fullerenes are synthesized simultaneously using the CAPTEAR process.

Using CAPTEAR, scandium-based OMFs produced include $\text{Sc}_4\text{O}_2@\text{I}_h\text{-C}_{80}$, $\text{Sc}_4\text{O}_3@\text{I}_h\text{-C}_{80}$, and now $\text{Sc}_2\text{O}@C_{82}$. As scandium oxide is an expensive raw material, it is noteworthy that these OMF compounds are also synthesized using recovered Sc_2O_3 powder obtained from a recycling process.^{39,40}

Of particular significance to $\text{Sc}_4\text{O}_2@\text{I}_h\text{-C}_{80}$ and $\text{Sc}_4\text{O}_2@\text{I}_h\text{-C}_{80}$ OMFs is the encapsulation of such a large number of atoms (six and seven, respectively). All oxygen atoms are bonded to separate faces of a four-atom Sc_4 pyramid encapsulated within the fullerene cage.^{25,28} X-Ray crystallographic data^{25,28} confirms the encapsulation (endohedral) of oxygen in lieu of epoxide formation on the cage surface (exohedral). The endohedral nature of the oxygen encapsulation in OMFs is an important discovery as oxygen attachment exohedral to fullerene cages has been reported on the outside of the cage surface, *e.g.*, epoxide formation (*e.g.*, C_{60}O)⁴¹ or as an oxygen atom linking two fullerenes (*e.g.*, $\text{C}_{60}\text{OC}_{60}$).⁴²

Reports of other large, endohedral clusters in C_{80} cages include a five-atom Sc_3CH cluster⁴³ synthesized in a reactor using a CH_4 reactive gas atmosphere. A four-atom ScYErN cluster⁴⁴ in a C_{80} cage (*i.e.*, $\text{ScYErN}@C_{80}$) has also been prepared and isolated.

2.2. Electric-arc synthesis of OMFs

Graphite rods, six inches in length, are core-drilled with either a $3/4$ or $5/16$ inch drill bit to a depth of 4 inches (10 cm) as previously described^{32,45} and packed with Sc_2O_3 for subsequent vaporization. The reactor chamber is vacuum pumped with subsequent backfilling of He to a reactor pressure of 300 Torr. Air flow rates vary from 0.1 to 18 torr/min, and experiments are conducted under a dynamic flow of He/air at 300 torr. Typical reactor parameters are

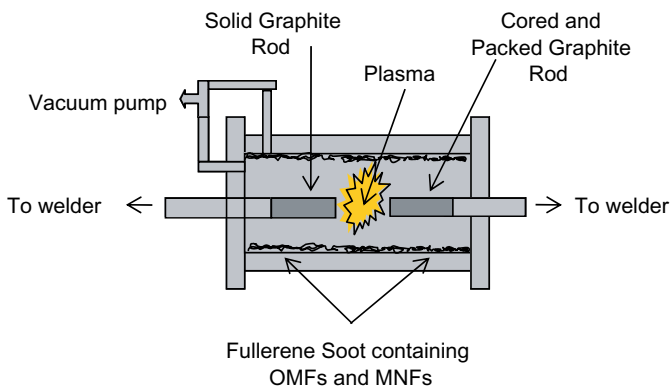


Figure 2. Schematic of an electric-arc reactor used in OMF synthesis (Modified from Ref. 45).

220 A for $\frac{3}{4}$ inch cored rods or 320 A for $\frac{5}{8}$ inch cored rods. The cathode/anode gap voltage is 38 V. A schematic of our electric arc reactor used for OMF production is shown in Figure 2. CAPTEAR conditions and other experimental details of our synthesis with copper and copper nitrate are reported elsewhere.^{32,45}

After vaporization of packed rods, the chamber is opened for soot collection. The harvested material is extracted with carbon disulfide or *o*-xylene and subsequently filtered using a PTFE membrane filter to remove insoluble carbonaceous material and residual metal precursors. Solvent removal under reduced pressure yields a dried extract, which is washed with a polar solvent (*e.g.*, diethyl ether) to remove non-fullerene hydrocarbon material. Soot extracts are weighed and characterized by HPLC and MALDI mass spectrometry to determine the amount and type of fullerene produced.

To demonstrate the usefulness of the CAPTEAR method³² for OMF synthesis,^{25,28} experiments are conducted at 0.6 torr/min of air with various amounts of copper nitrate hydrate mixed with scandium oxide and packed in graphite rods. Their corresponding MALDI spectra are shown in Figure 3. As reported previously,³² the copper nitrate hydrate decomposes to generate NO_x vapor in the reactor during vaporization. One can control the amount of NO_x vapor by varying stoichiometric amounts of $\text{Cu}(\text{NO}_3)_2$ packed into cored graphite rods prior to vaporization.

The fullerene composition of the control experiment (*i.e.*, Figure 3a, no added copper nitrate) indicates only a small amount of $\text{Sc}_2\text{O}@C_{82}$ with no detectable $\text{Sc}_4\text{O}_2@C_{80}$ or $\text{Sc}_4\text{O}_3@C_{80}$. Data in Figure 3b suggests that increasing the amount of copper nitrate content to 33% $\text{Cu}(\text{NO}_3)_2$ / 67% Sc_2O_3 wt-wt%

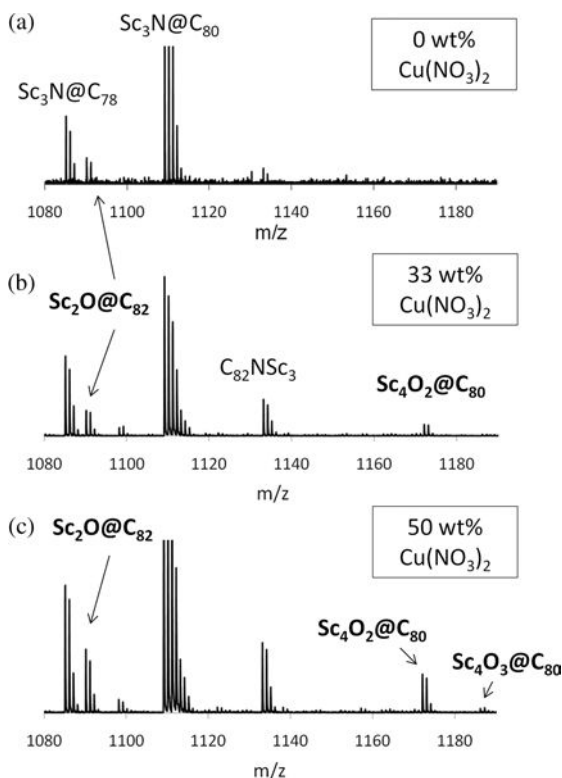


Figure 3. MALDI data for fullerene extracts prepared from CAPTEAR experiments performed at 0.6 torr/min air flow with increasing amounts of copper nitrate mixed with Sc_2O_3 packing material (wt-wt %). Weight percentages are (a) 0% $\text{Cu}(\text{NO}_3)_2$ (b) 33% $\text{Cu}(\text{NO}_3)_2$, and (c) 50% $\text{Cu}(\text{NO}_3)_2$.

results in a fullerene extract in which the $\text{Sc}_4\text{O}_2@C_{80}$ compound is now present along with $\text{Sc}_2\text{O}@C_{82}$. At 50% $\text{Cu}(\text{NO}_3)_2$, the yields of $\text{Sc}_2\text{O}@C_{82}$ and $\text{Sc}_4\text{O}_2@C_{80}$ increase further, along with the emergence of the lowest yielding OMF, $\text{Sc}_4\text{O}_3@C_{80}$ (Figure 3c).

3. Isolation

Typical metallofullerene extracts contain predominantly (1) non-OMF fullerene types (*e.g.*, C_{60} , C_{70} , C_{76} , C_{78} , C_{82} , C_{84} , C_{86} , C_{88} , C_{90}), (2) classical metallofullerenes,^{46,47} *e.g.*, $\text{Sc}_2@C_{82}$ and (3) MNFs, *e.g.*, $\text{Sc}_3\text{N}@C_{68}$, $\text{Sc}_3\text{N}@C_{78}$, $\text{Sc}_3\text{N}@I_h-C_{80}$ and $\text{Sc}_3\text{N}@D_{5h}-C_{80}$.^{17,21,34,48} OMF fullerene extracts obtained under optimized CAPTEAR conditions are at best 10% of the sample. Clearly, advances in separation science are needed to purify these low-levels of OMFs.

Traditional HPLC separation methods for OMFs and MNFs are unfavorable due to (1) expense of equipment, solvents, and specialty columns, (2) poor throughput from a low solubility of OMFs and MNFs in mobile phases and (3) co-elution of fullerenes and metallofullerenes. To address these problems, researchers have pursued new separation strategies to remove these contaminant fullerenes. Approaches for isolating MNF-enriched samples include selective chemical oxidation,¹⁸ eutectic points,⁴⁹ reactive solid supports,^{33,34,50} and selective precipitation with Lewis acids.³⁵

These advances in MNF separation science include the use of cyclopentadiene immobilized on an insoluble resin (Merrifield) as a flash chromatographic medium for room temperature MNF separations.⁵⁰ Due, in part, to the time and expense of synthesizing the cyclopentadienyl-resin, an alternative approach which implements a reactive moiety (*e.g.*, amino groups) onto silica has been reported.^{33,34}

3.1. Stir and Filter Approach (SAFA) for $\text{Sc}_4\text{O}_2@\text{C}_{80}$ and $\text{Sc}_4\text{O}_3@\text{C}_{80}$

The “Stir and Filter Approach” (SAFA) successfully isolates MNFs.^{33,34} For SAFA experiments with aminosilica, the amino groups on silica readily react and immobilize contaminant empty-cage fullerenes (*e.g.*, C_{60} , C_{70}) and classical metallofullerenes (*e.g.*, $\text{Sc}_2@\text{C}_{82}$). The OMFs and MNFs are much more resistant to reaction with aminosilica and remain in solution. As illustrated in Figure 4, the filtrate of a reaction mixture represents a sample of purified MNFs^{33,34} or enriched in OMFs.³⁵

Advantages of SAFA over traditional OMF or MNF separation methods are as follows: (1) nonchromatographic separation (2) no flowing solvent, (3) rapid separation time (4) no electrochemical equipment, (5) room temperature separations, (6) isolation in aerobic environments, (7) inexpensive chemicals to make functionalized silica, (8) unattended purification, (9) scalable process for industry and (10) no HPLC fraction collection.

The metallofullerene distribution remaining in solution is controlled by judiciously monitoring the loss of fullerene type from solution. Withdrawn aliquots are filtered and analyzed by HPLC. At lengthy SAFA reaction times, only $\text{Sc}_3\text{N}@\text{I}_h\text{-C}_{80}$ remains. At moderate SAFA reaction times, the filtrate contains only OMF and MNFs. In contrast, short SAFA reaction times result in a filtrate containing OMFs, MNFs, and small size fullerenes (*e.g.*, C_{60} , C_{70}), but with uptake of the very reactive, higher empty-cage fullerenes (*e.g.*, C_{78} - C_{90}) and classical metallofullerenes.

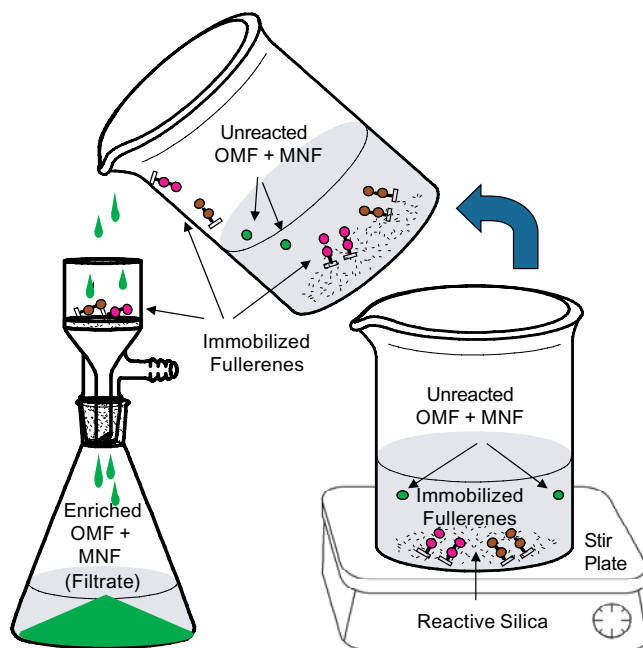


Figure 4. Overview of the Stir and Filter Approach (SAFA) (Modified from Ref. 33).

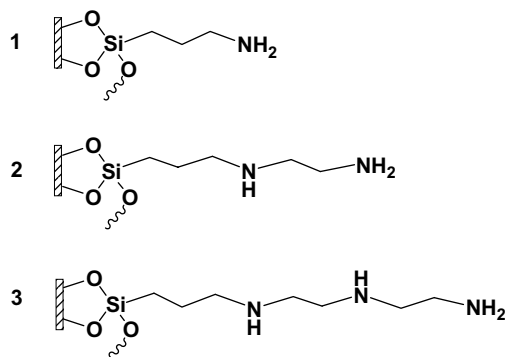


Figure 5. Examples of functionalized silica used in SAFA-based separation schemes for OMFs and MNFs compounds. (1) aminosilica, (2) diaminosilica, and (3) triaminosilica.

To demonstrate the usefulness of SAFA as an OMF pre-cleanup step, an experiment is performed with 954 mg of fullerene extract dissolved in 1 L anhydrous ODCB. To this solution was added 200 g of diaminosilica gel (Figure 5) dried in a vacuum oven.

The HPLC chromatogram for fullerene extract before addition of diaminosilica is shown in Figure 6a. After only 2 minutes of SAFA reaction

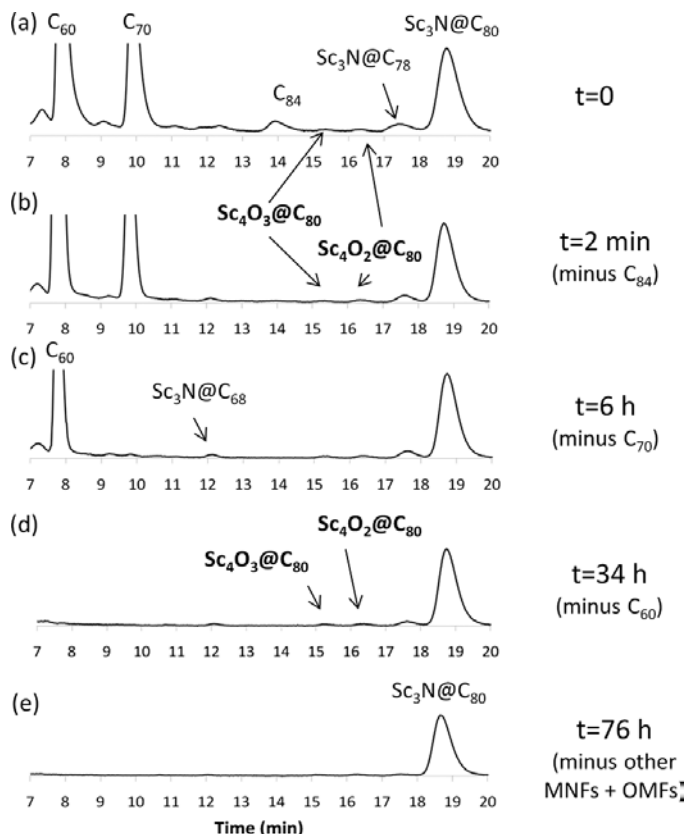


Figure 6. (a) HPLC chromatogram of Sc fullerene stock extract, (b–e) HPLC data for aliquots of fullerenes remaining in solution from the SAFA reaction mixture (a–e) HPLC conditions are 0.5mL/min xylenes, PYE column, and 360 nm UV detection.

time, higher empty-cage fullerenes (*i.e.*, C_{76} , C_{78} , C_{82} , C_{84}) are removed from solution and immobilized onto diaminosilica as shown by the HPLC analysis of an aliquot of the filtrate (Figure 6b).

Continued monitoring of the fullerenes remaining in solution indicates that by 6 hours, C_{70} has been removed from solution (Figure 6c). The loss of C_{60} occurs by 34 hours (Figure 6d), at which time only OMF and MNF compounds remain in solution. At 34 hours, this is an ideal time to stop the SAFA experiment for subsequent HPLC fraction collection because the filtrate now contains only OMFs and MNFs. Purified OMFs have been isolated in this manner. If purified $Sc_3N@I_h-C_{80}$ is desired in lieu of OMFs, then an increased SAFA reaction time to 76 hours is needed (Figure 6e). OMF uptake from 34 h to 76 h is a slow process as OMFs are only slightly reactive to diaminosilica.

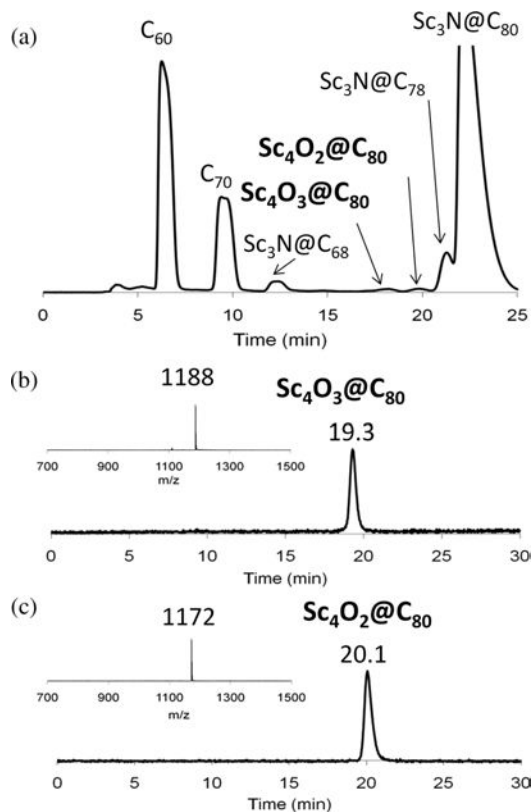


Figure 7. (a) HPLC chromatogram of the SAFA filtrate after 2 hours of SAFA reaction with o-xylene (b,c) HPLC and corresponding MALDI of purified $\text{Sc}_4\text{O}_3@I_h\text{-C}_{80}$ and $\text{Sc}_4\text{O}_2@I_h\text{-C}_{80}$ OMFs (a–c) HPLC conditions are 1.5 mL/min o-xylene, PYE column, and 360 nm UV detection (Modified from Ref. 25).

To demonstrate the isolation of OMFs using this SAFA pre-cleanup step, an experiment is performed using 100 mg of fullerene extract dissolved in 100 mL o-xylene.²⁵ While stirring, 1.7 g vacuum-oven dried diaminosilica is added. Aliquots are removed from the reaction mixture, filtered, and analyzed *via* HPLC to monitor loss of fullerenes from solution. The HPLC chromatogram of the SAFA filtrate after 2 hours is shown in Figure 7a. After 2 hours, contaminant higher empty-cage fullerenes and classical metallofullerenes are removed from solution. The HPLC chromatogram of the filtrate (Figure 7a) indicates a sample containing four dominant MNFs (*i.e.*, $\text{Sc}_3\text{N}@C_{68}$, $\text{Sc}_3\text{N}@C_{78}$, $\text{Sc}_3\text{N}@D_{5h}\text{-C}_{80}$, and $\text{Sc}_3\text{N}@I_h\text{-C}_{80}$) in addition to $\text{Sc}_4\text{O}_3@C_{80}$ and $\text{Sc}_4\text{O}_2@C_{80}$ OMFs. Fraction collection is initiated at this early SAFA time because isolation of all six compounds (*i.e.*, 4 MNFs

and 2 OMFs) is desired. After HPLC fraction collection, samples of purified $\text{Sc}_4\text{O}_3@\text{C}_{80}$ and $\text{Sc}_4\text{O}_2@\text{C}_{80}$ are readily obtained. Their chromatograms and corresponding MALDI mass spectra are shown in Figures 7b and 7c, respectively.

3.2. Selective precipitation method using Lewis acids

Recently, a new separation method has been developed for isolating OMF and MNF metallofullerenes.³⁵ This approach utilizes Lewis acids for reaction with fullerene cages to selectively complex and precipitate (*i.e.*, remove from solution) metallofullerenes. Possessing negative formal charges on their cage, (*i.e.*, C_{82}^{4-} , C_{80}^{6-}), the electron rich cage surface of metallofullerenes is ideal for reactions with Lewis acids. MNFs and OMFs react easily and their extent of precipitation can be manipulated with stoichiometric amounts of Lewis acids (*e.g.*, AlCl_3 , FeCl_3).³⁵

In contrast to the SAFA process, which utilizes a reactive functional group on a support (*e.g.*, resin or silica), the Lewis acid approach is a support-free separation method. Unlike the SAFA process, in which some fullerenes are lost to irreversible adsorption to the support, the selective precipitation scheme with Lewis acids (1) circumvents sample loss to the support matrix and (2) yields a precipitate which is easily filterable and handled.

Manipulation of Lewis acids, molar ratios, and kinetic differences within OMF and MNF compounds can be leveraged into a separation scheme to obtain enriched metallofullerene samples for subsequent HPLC fraction collection.³⁵ Alternatively, the Lewis acid separation approach can be used in its entirety (*i.e.*, no HPLC) to obtain purified samples, such as $\text{Sc}_3\text{N}@\text{I}_h\text{-C}_{80}$.³⁵

To demonstrate the Lewis acid approach as a separation method, 1.3 g of fullerene extract containing OMFs and MNFs is dissolved in 1 L of carbon disulfide.³⁵ The fullerene composition of the extract is analyzed by HPLC and MALDI mass spectrometry (Figure 8a,e). As the sample is stirring, 250 mg AlCl_3 is added with aliquots taken to monitor the loss of metallofullerenes from solution. After 16.5 hours of reaction time, the most reactive metallofullerenes are complexed and precipitated from solution. Upon filtration of the reaction mixture, the precipitate/filter cake consists of complexed OMFs and MNFs, and placed in a separatory funnel containing a saturated NaHCO_3 solution, ice chips, and ice water (10% vol) along with CS_2 (90% vol) for the subsequent decomplexation of metallofullerenes and transfer of OMFs and MNFs to the CS_2 layer.

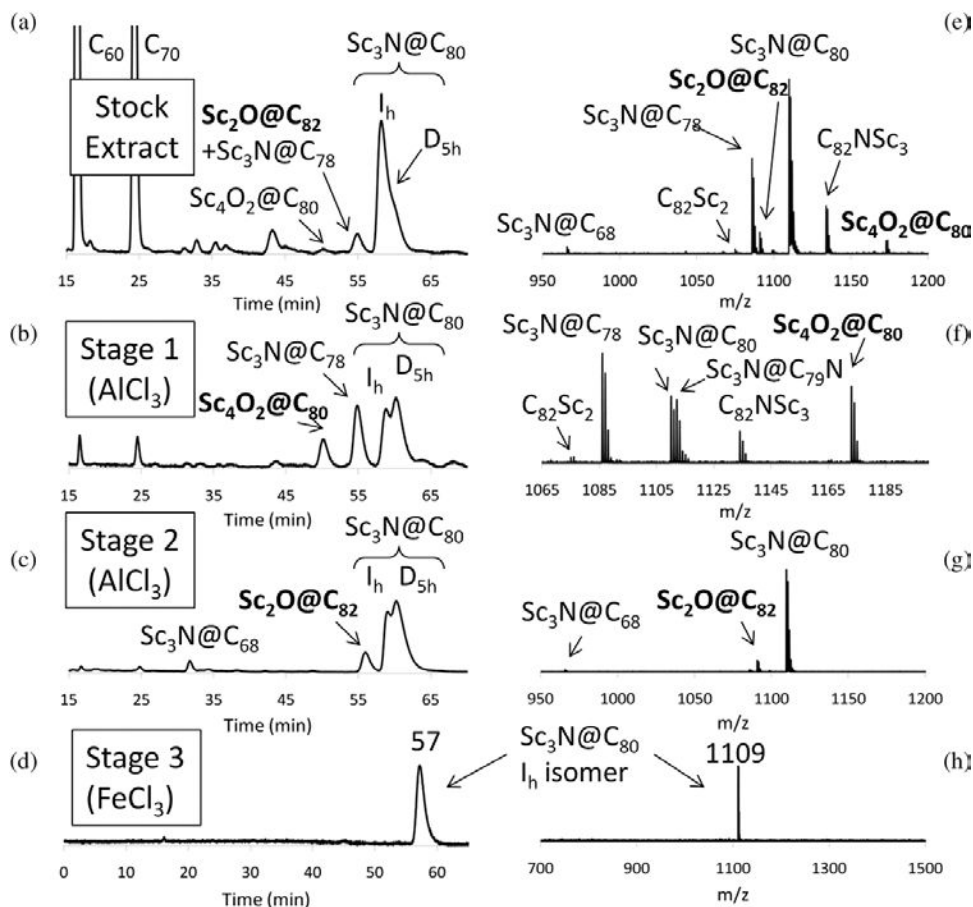


Figure 8. (a–d) HPLC chromatograms and corresponding (e–g) MALDI mass spectra for separation experiments of Sc fullerene extract with Lewis acids. (a,e) Sc fullerene extract, (b,f) fullerenes after precipitation and decomplexation, Stage 1, 1st $AlCl_3$ treatment, (c,g) fullerenes obtained after precipitation and decomplexation, Stage 2, 2nd $AlCl_3$ treatment, and (d,h) purified $Sc_3N@I_h-C_{80}$ after precipitation and decomplexation, Stage 3, $FeCl_3$ treatment. HPLC conditions are 0.3mL/min toluene, PYE column, and 360 nm UV detection (Modified from Ref. 26).

After 2 further washes with distilled water, this CS_2 solution is membrane filtered. Upon solvent removal and washing with diethyl ether, 75 mg of metallofullerene sample is obtained after this 1st Lewis acid stage, and the corresponding HPLC and MALDI data (Figure 8b,f) indicate that a sample highly enriched in metallofullerenes (>90%) can be obtained after this decomplexation step with $AlCl_3$ (Stage 1). This initial step also permits the separation of $Sc_3N@C_{78}$, which precipitates, from $Sc_2O@C_{82}$, which remains in solution.

Also of significance are the many types of fullerenes precipitated in this Stage 1 process. The types of fullerenes recovered from the precipitate include the following metallofullerenes (1) metallic nitride azafullerenes (MNAFs) *e.g.*, $\text{Sc}_3\text{N@C}_{79}\text{N}$, (2) the most reactive MNFs *e.g.*, $\text{Sc}_3\text{N@C}_{78}$, $\text{NSc}_3\text{C}_{82}$, $\text{Sc}_3\text{N@D}_{5h}\text{-C}_{80}$ and (3) OMFs, *e.g.*, $\text{Sc}_4\text{O}_2\text{@C}_{80}$.

Depleted of the more reactive metallofullerenes, the filtrate remaining from this 1st stage is now the starting point for a subsequent Lewis acid reaction (Stage 2). To this stirring filtrate is added an additional 250 mg of AlCl_3 . After 6.5 h, the reaction mixture is filtered to obtain a precipitate which is decomplexed as described above to obtain a new set of metallofullerenes. HPLC analysis (Figure 8c) and MALDI mass spectra (Figure 8g) indicate a sample enriched in Stage 2 OMF ($\text{Sc}_2\text{O@C}_{82}$) and MNF metallofullerenes ($\text{Sc}_3\text{N@C}_{68}$, more $\text{Sc}_3\text{N@D}_{5h}\text{-C}_{80}$). Note the separation of $\text{Sc}_3\text{N@C}_{78}$ from $\text{Sc}_2\text{O@C}_{82}$ (Figure 8a) into two fractions. $\text{Sc}_3\text{N@C}_{78}$, a Stage 1 metallofullerene (Figure 8b,f) is in one container. $\text{Sc}_2\text{O@C}_{82}$, a Stage 2 metallofullerene (Figure 8c,g) is now in a separate fraction.

The filtrate after Stage 2, consists of empty-cage fullerenes (95%) and predominantly the least reactive metallofullerene, $\text{Sc}_3\text{N@I}_h\text{-C}_{80}$. To quickly precipitate $\text{Sc}_3\text{N@I}_h\text{-C}_{80}$, a more reactive Lewis acid (FeCl_3) to metallofullerenes is used (Stage 3). To the filtrate from Stage 2 is added 150 mg of FeCl_3 to a stirring solution. After only 1 hour of reaction time, the mixture is filtered. Isomerically purified $\text{Sc}_3\text{N@I}_h\text{-C}_{80}$ is obtained upon decomplexation of the precipitate. The HPLC and MALDI mass spectrum (Figure 8d,h) indicate a highly purified sample of the icosahedral isomer of $\text{Sc}_3\text{N@C}_{80}$.³⁵

3.2.1. Isolation of a Stage 1 metallofullerene (*e.g.*, $\text{Sc}_4\text{O}_3\text{@C}_{80}$)

To demonstrate the Lewis acid approach to isolating a Stage 1 metallofullerene, the $\text{Sc}_4\text{O}_3\text{@C}_{80}$ OMF is selected.²⁸ To speed up the reaction, the AlCl_3 is increased from 250 mg to 4 g. The amount of CS_2 is decreased from 1 L to 500 mL to furnish a more concentrated solution. Shown in Figure 9a is the HPLC chromatogram corresponding to this fullerene extract. After only 5 minutes, the reaction is stopped, and the mixture is filtered. The recovered precipitate is treated to release the fullerenes, whose HPLC chromatogram is shown in Figure 9b. Chromatographic analysis of this sample indicates an order of magnitude decrease in contaminant empty-cage fullerenes.

The $\text{Sc}_4\text{O}_3\text{@C}_{80}$ OMF compound eluting at 15 minutes is injected for HPLC fraction collection until a single peak is obtained (Figure 9c). The corresponding MALDI mass spectrum (Figure 9d) confirms a highly purified sample of $\text{Sc}_4\text{O}_3\text{@C}_{80}$. Its X-Ray crystal structure is published.²⁸

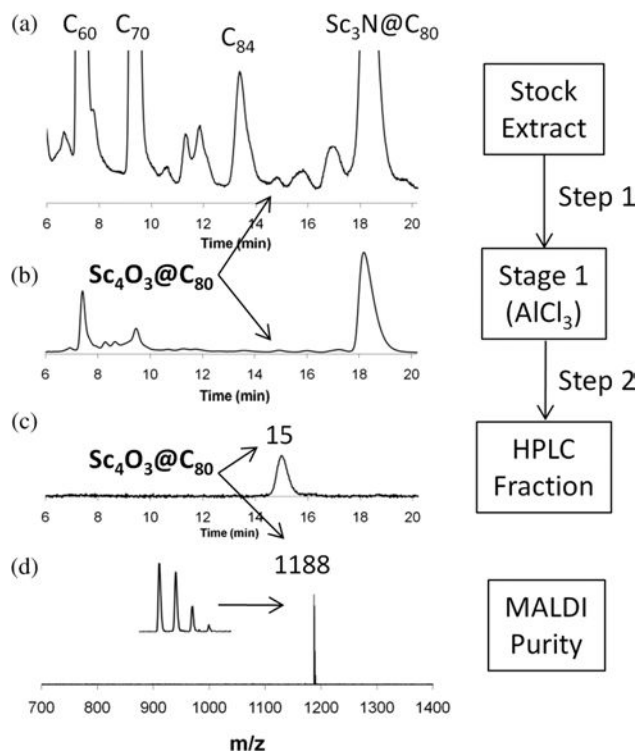


Figure 9. (a–c) HPLC chromatograms for separation experiments of Sc fullerene extract with Lewis acids in the isolation of $Sc_4O_3@I_h-C_{80}$. (a) Sc fullerene extract before addition of $AlCl_3$, (b) fullerenes recovered after precipitation and decomplexation, Stage 1, 1st $AlCl_3$ treatment, (c) purified $Sc_4O_3@I_h-C_{80}$ obtained upon HPLC fraction collection and (d) corresponding MALDI mass spectrum. HPLC conditions are 0.5 mL/min xylenes, PYE column, and 360 nm UV detection.

3.2.2. Isolation of a Stage 2 metallofullerene (e.g., $Sc_2O@C_{82}$)

The direct isolation of $Sc_2O@C_{82}$ from fullerene extract is not feasible due to (1) the poor abundance of $Sc_2O@C_{82}$ (<0.5%) in the sample and (2) co-elution of $Sc_2O@C_{82}$ with $Sc_3N@C_{78}$. With the Lewis acid approach,³⁵ we have separated $Sc_3N@C_{78}$ (Stage 1) from $Sc_2O@C_{82}$ (Stage 2). A typical HPLC chromatogram for Stage 2 metallofullerenes is shown in Figure 10a.

Although fraction collection focuses here on the $Sc_2O@C_{82}$ OMF, other compounds (e.g., $Sc_3N@C_{68}$) are also purified simultaneously during fraction collection. Repeated injection of Stage 2 sample (Figure 10a) is performed until a single peak is obtained at 58 min (Figure 10b). The corresponding MALDI mass spectrum (Figure 10c) confirms an isolated $Sc_2O@C_{82}$ sample of high purity.

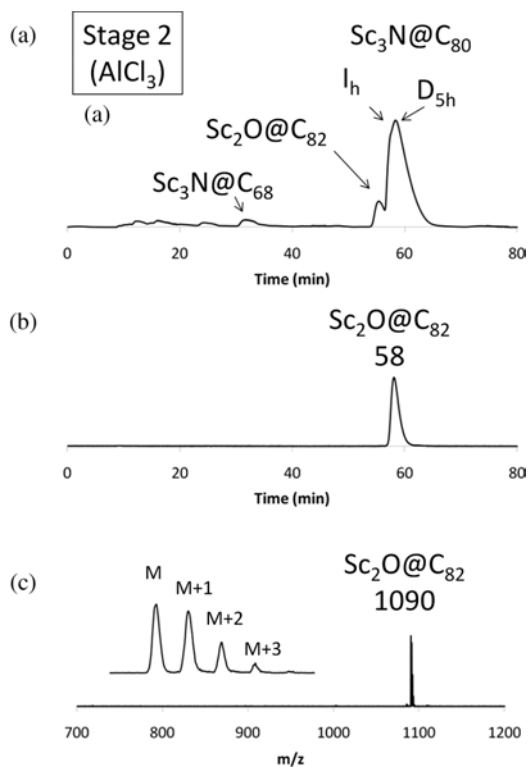


Figure 10. (a,b) HPLC chromatograms for the isolation of Sc₂O@C₈₂ using Lewis acids. (a) HPLC chromatogram of fullerenes obtained after the precipitation step (Stage 2, AlCl₃). Repeated HPLC fraction collection of leads to (b) HPLC chromatogram of purified Sc₂O@C₈₂ and (c) its MALDI mass spectrum. HPLC conditions are 0.3 mL/min toluene, PYE column, and 360 nm UV detection.

4. Reactivity

The Lewis acid reactivity for metallofullerenes can be qualitatively compared as shown in Table 1.³⁵ The class of metallofullerenes being the most reactive to Lewis acids precipitates first in Stage 1; whereas the less reactive metallofullerenes precipitate in Stage 2. The most chemically inert Sc₃N@I_h-C₈₀ precipitates last (Stage 3) with a more reactive Lewis acid, FeCl₃.

4.1. Reactivity comparison with other fullerenes

To obtain quantitative data, experiments are performed to investigate their kinetics. The goal is a comparison of OMF and MNF reactivities.³⁵ In lieu of FeCl₃, AlCl₃ is selected based on slower reaction kinetics with OMFs and

Table 1. Summary table correlating the type of metallofullerene precipitated versus the Lewis acid stage in which precipitation occurs.

	Oxo Metallic Fullerene (OMF)	Metallic Nitride Fullerene (MNF)	Metallic Nitride AzaFullerene (MNAF)	Classical Metallo- Fullerene (MF)
Stage 1 (AlCl₃)	Sc ₄ O ₂ @C ₈₀ Sc ₄ O ₃ @C ₈₀	Sc ₃ N@C ₇₈ Sc ₃ N@D _{5h} -C ₈₀ C ₈₂ Sc ₃ N	Sc ₃ N@C ₇₉ N	C ₈₂ Sc ₂
Stage 2 (AlCl₃)	Sc ₂ O@C ₈₂	Sc ₃ N@C ₆₈ Sc ₃ N@D _{5h} -C ₈₀	—	C ₈₄ Sc ₂
Stage 3 (FeCl₃)	—	Sc ₃ N@I _h -C ₈₀	—	—

Table 2. Kinetic data for Lewis acid reactions with OMFs and MNFs.

	k _{obs} (min ⁻¹)	Relative rate (I _h)
Sc ₄ O ₂ @I _h -C ₈₀	0.037	3.7
Sc ₃ N@C ₇₈	0.031	3.1
Sc ₃ N@D _{5h} -C ₈₀	0.018	1.8
Sc ₃ N@C ₆₈	0.016	1.6
Sc ₃ N@I _h -C ₈₀	0.010	1.0

MNFs. Of particular interest is comparing the reactivity of the OMF species (*e.g.*, Sc₂O@C₈₂, Sc₄O₂@I_h-C₈₀) with MNF compounds such as Sc₃N@C₆₈, Sc₃N@C₇₈, Sc₃N@D_{5h}-C₈₀, and Sc₃N@I_h-C₈₀.

For these experiments,³⁵ a 2 mg sample containing OMFs and MNFs is dissolved in 15 mL of CS₂. While stirring, 10 mg of AlCl₃ is added. Aliquots from this reaction mixture are analyzed by HPLC to monitor the loss of HPLC peak area, *i.e.*, loss of fullerene type from solution to precipitation. Under these conditions, C₆₀ and C₇₀ are unreactive and remain in solution. Plotting the logarithm of fullerene concentration as a function of time reveals that 1st order kinetics are observed. Table 2 summarizes the kinetic data and compares their reactivities.

4.2. Reactivity comparison to electrochemical band gap

The reactivity of these metallofullerenes and kinetic data (Table 2) may be related to the electrochemical EC band gap.³⁵ When our experimental kinetic data (*i.e.*, k_{obs}) from Table 2 is plotted with published electrochemical data

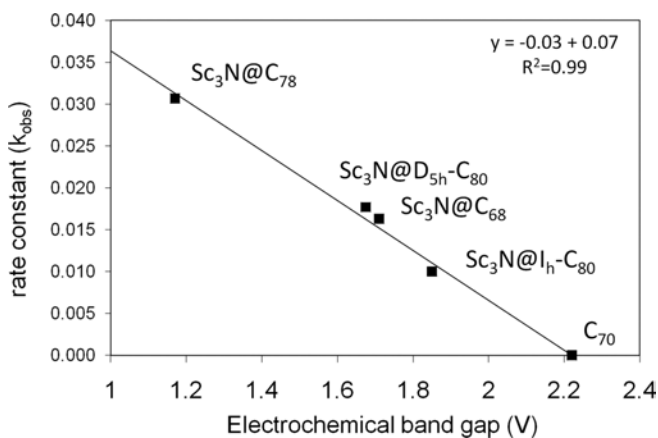


Figure 11. Plot correlating rate constants versus EC band gaps (Modified from Ref. 35).

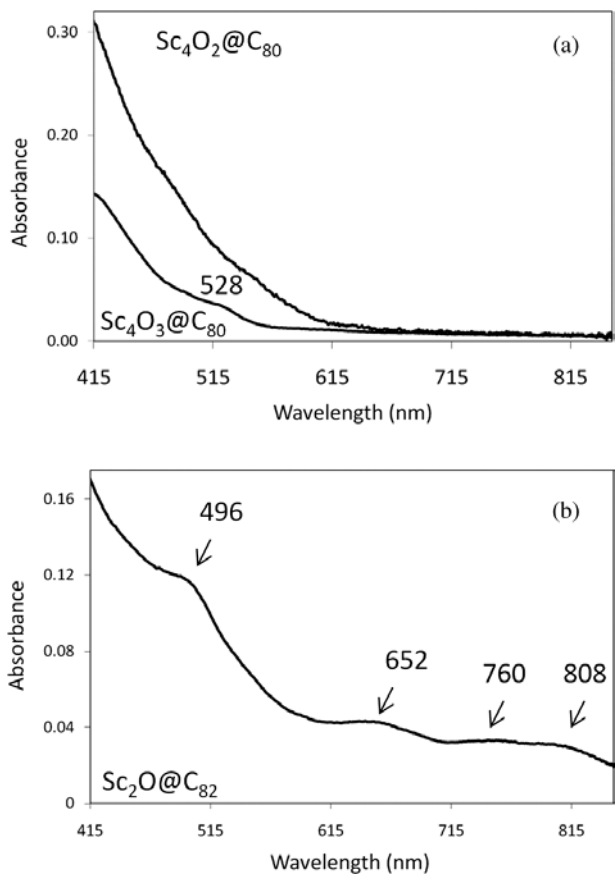


Figure 12. UV-vis spectra in CS_2 for Sc-based OMF metallofullerenes (a) $\text{Sc}_4\text{O}_2@\text{C}_{80}$, $\text{Sc}_4\text{O}_3@\text{C}_{80}$ and (b) $\text{Sc}_2\text{O}@C_{82}$.

for C_{70} ,^{51,52} $Sc_3N@I_h-C_{80}$,^{18,21,48} $Sc_3N@D_{5h}-C_{80}$,⁴⁸ $Sc_3N@C_{68}$,⁸ and $Sc_3N@C_{78}$,¹³ a straight line is obtained, and a correlation can be made (Figure 11). Using the data in Table 2, a predicted EC band gap for $Sc_4O_2@I_h-C_{80}$ of ~1 V can be made.

5. UV Characterization

Purified OMF samples are readily dissolved in CS_2 . UV-vis spectra for purified $Sc_4O_2@C_{80}$ and $Sc_4O_3@C_{80}$ are shown in Figure 12a.²⁵ $Sc_4O_3@C_{80}$ has a peak at 528 nm; whereas the spectrum for $Sc_4O_2@C_{80}$ has little definition. In contrast, the UV-vis spectrum for the C_{82} OMF, $Sc_2O@C_{82}$, possesses clear peak maxima at 496 nm, 652 nm, 760 nm, and 808 nm (Figure 12b).

6. Conclusions and Perspectives

Given the small quantities of OMFs obtained during their discovery, experimental characterization was limited to X-Ray crystallography and UV-vis spectroscopy. X-Ray crystallographic structures are obtained for all three scandium OMFs, $Sc_4O_2@I_h-C_{80}$, $Sc_4O_3@I_h-C_{80}$, and now $Sc_2O@C_{82}$. Amazingly, in each case, the crystal structure was resolved with less than a milligram of purified OMF sample. The objective of this writing is to provide information regarding their synthesis and separation such that others can independently obtain samples for their experiments.

Additional experiments to (1) probe their fundamental properties, (2) explore their chemical reactivity and functionalization, and (3) evaluate their use in applications depend on sufficient quantities of purified OMFs. Upcoming experiments to expand the OMF family by replacing scandium with other metals (*e.g.*, Y, rare-earths) are underway.

Acknowledgments

The author thanks the NSF CAREER grant (CHE-0547988), the Lucas Foundation for financial assistance.

References

1. Stevenson, S.; Rice, G.; Glass, T.; Harich, K.; Cromer, F.; Jordan, M. R.; Craft, J.; Hadju, E.; Bible, R.; Olmstead, M. M.; Maitra, K.; Fisher, A. J.; Balch, A. L.; Dorn, H. C. *Nature* **1999**, *401*, 55–57.

2. Olmstead, M. M.; Lee, H. M.; Duchamp, J. C.; Stevenson, S.; Marciu, D.; Dorn, H. C.; Balch, A. L. *Angew. Chem. Int. Ed.* **2003**, *42*, 900–903.
3. Park, S. S.; Liu, D.; Hagelberg, F. *J. Phys. Chem. A* **2005**, *109*, 8865–8873.
4. Rapta, P.; Popov, A. A.; Yang, S.; Dunsch, L. *J. Phys. Chem. A* **2008**, *112*, 5858–5865.
5. Reveles, J. U.; Heine, T.; Koster, A. M. *J. Phys. Chem. A* **2005**, *109*, 7068–7072.
6. Wang, D. L.; Sun, X. P.; Zhai, Y. C. *Chin. J. Struct. Chem.* **2007**, *26*, 321–327.
7. Yang, S. F.; Kalbac, M.; Popov, A.; Dunsch, L. *Chem.–Eur. J.* **2006**, *12*, 7856–7863.
8. Yang, S. F.; Rapta, P.; Dunsch, L. *Chem. Commun.* **2007**, 189–191.
9. Campanera, J. M.; Bo, C.; Olmstead, M. M.; Balch, A. L.; Poblet, J. M. *J. Phys. Chem. A* **2002**, *106*, 12356–12364.
10. Krause, M.; Popov, A.; Dunsch, L. *Chemphyschem* **2006**, *7*, 1734–1740.
11. Olmstead, M. H.; de Bettencourt-Dias, A.; Duchamp, J. C.; Stevenson, S.; Marciu, D.; Dorn, H. C.; Balch, A. L. *Angew. Chem. Int. Ed.* **2001**, *40*, 1223–1225.
12. Popov, A. A.; Krause, M.; Yang, S. F.; Wong, J.; Dunsch, L. *J. Phys. Chem. B* **2007**, *111*, 3363–3369.
13. Zhang, L.; Chen, N.; Fan, L. Z.; Wang, C. R.; Yang, S. H. *J. Electroanal. Chem.* **2007**, *608*, 15–21.
14. Alvarez, L.; Pichler, T.; Georgi, P.; Schwieger, T.; Peisert, H.; Dunsch, L.; Hu, Z.; Knupfer, M.; Fink, J.; Bressler, P.; Mast, M.; Golden, M. S. *Phys. Rev. B* **2002**, *66*, 035107.
15. Cardona, C. M.; Elliott, B.; Echegoyen, L. *J. Am. Chem. Soc.* **2006**, *128*, 6480–6485.
16. Chen, N.; Fan, L. Z.; Tan, K.; Wu, Y. Q.; Shu, C. Y.; Lu, X.; Wang, C. R. *J. Phys. Chem. C* **2007**, *111*, 11823–11828.
17. Duchamp, J. C.; Demortier, A.; Fletcher, K. R.; Dorn, D.; Iezzi, E. B.; Glass, T.; Dorn, H. C. *Chem. Phys. Lett.* **2003**, *375*, 655–659.
18. Elliott, B.; Yu, L.; Echegoyen, L. *J. Am. Chem. Soc.* **2005**, *127*, 10885–10888.
19. Gan, L. H.; Yuan, R. *Chemphyschem* **2006**, *7*, 1306–1310.
20. Iiduka, Y.; Ikenaga, O.; Sakuraba, A.; Wakahara, T.; Tsuchiya, T.; Maeda, Y.; Nakahodo, T.; Akasaka, T.; Kako, M.; Mizorogi, N.; Nagase, S. *J. Am. Chem. Soc.* **2005**, *127*, 9956–9957.
21. Krause, M.; Dunsch, L. *Chemphyschem* **2004**, *5*, 1445–1449.
22. Krause, M.; Kuzmany, H.; Georgi, P.; Dunsch, L.; Vietze, K.; Seifert, G. *J. Chem. Phys.* **2001**, *115*, 6596–6605.
23. Plonska-Brzezinska, M. E.; Athans, A. J.; Phillips, J. P.; Stevenson, S.; Echegoyen, L. *J. Electroanal. Chem.* **2008**, *614*, 171–174.
24. Slanina, Z.; Nagase, S. *Chemphyschem* **2005**, *6*, 2060–2063.
25. Stevenson, S.; Mackey, M. A.; Stuart, M. A.; Phillips, J. P.; Easterling, M. L.; Chancellor, C. J.; Olmstead, M. M.; Balch, A. L. *J. Am. Chem. Soc.* **2008**, *130*, 11844–11845.
26. Mercado, B. Q.; Stuart, M. A.; Mackey, M. A.; Pickens, J. E.; Confait, B. S.; Stevenson, S.; Easterling, M. L.; Valencia, R.; Rodríguez-Forte, A.; Poblet, J. M.; Olmstead, M. M.; Balch, A. L. *J. Am. Chem. Soc.* **2010**, *132*, 12098–12105.
27. Valencia, R.; Rodríguez-Forte, A.; Stevenson, S.; Balch, A. L.; Poblet, J. M. *Inorg. Chem.* **2009**, *48*, 5957–5961.
28. Mercado, B.; Olmstead, M. M.; Beavers, C. M.; Easterling, M. L.; Stevenson, S.; Mackey, M. A.; Coumbe, C. E.; Phillips, J. D.; Phillips, J. P.; Balch, A. L. *Chem. Commun.* **2010**, *46*, 279–281.
29. Kobayashi, K.; Sano, Y.; Nagase, S. *J. Comput. Chem.* **2001**, *22*, 1353–1358.
30. Aihara, J. *Phys. Chem. Chem. Phys.* **2001**, *3*, 1427–1431.

31. Wang, C. R.; Inakuma, M.; Shinohara, H. *Chem. Phys. Lett.* **1999**, *300*, 379–384.
32. Stevenson, S.; Thompson, M. C.; Coumbe, H. L.; Mackey, M. A.; Coumbe, C. E.; Phillips, J. P. *J. Am. Chem. Soc.* **2007**, *129*, 16257–16262.
33. Stevenson, S.; Harich, K.; Yu, H.; Stephen, R. R.; Heaps, D.; Coumbe, C.; Phillips, J. P. *J. Am. Chem. Soc.* **2006**, *128*, 8829–8835.
34. Stevenson, S.; Mackey, M. A.; Coumbe, C. E.; Phillips, J. P.; Elliott, B.; Echegoyen, L. *J. Am. Chem. Soc.* **2007**, *129*, 6072–6073.
35. Stevenson, S.; Mackey, M. A.; Pickens, J. E.; Stuart, M. A.; Confait, B. S.; Phillips, J. P. *Inorg. Chem.* **2009**, *48*, 11685–11690.
36. Kratschmer, W.; Lamb, L. D.; Fostiropoulos, K.; Huffman, D. R. *Nature* **1990**, *347*, 354–358.
37. Dunsch, L.; Krause, M.; Noack, J.; Georgi, P. *J. Phys. Chem. Solids* **2004**, *65*, 309–315.
38. Stevenson, S.; Ling, Y.; Coumbe, C. E.; Mackey, M. A.; Confait, B. S.; Phillips, J. P.; Dorn, H. C.; Zhang, Y. *J. Am. Chem. Soc.* **2009**, *131*, 17780–17782.
39. Stevenson, S.; Coumbe, C. E.; Thompson, M. C.; Coumbe, H. L.; Phillips, J. P.; Buckley, J. L.; Wynne, J. H. *Ind. Eng. Chem. Res.* **2008**, *47*, 2096–2099.
40. Wynne, J. H.; Buckley, J. L.; Coumbe, C. E.; Phillips, J. P.; Stevenson, S. *J. Environ. Sci. Health, Part A: Toxic/Hazard. Subst. Environ. Eng.* **2008**, *43*, 357–360.
41. Creggan, K. M.; Robbins, J. L.; Robbins, W. K.; Millar, J. M.; Sherwood, R. D.; Tindall, P. J.; Cox, D. M. *J. Am. Chem. Soc.* **1992**, *114*, 1103–1105.
42. Lebedkin, S.; Ballenweg, S.; Gross, J.; Taylor, R.; Kratschmer, W. *Tetrahedron Lett.* **1995**, *36*, 4971–4974.
43. Krause, M.; Ziegs, F.; Popov, A. A.; Dunsch, L. *Chemphyschem* **2007**, *8*, 537–540.
44. Chen, N.; Zhang, E. Y.; Wang, C. R. *J. Phys. Chem. B* **2006**, *110*, 13322–13325.
45. Stevenson, S.; Mackey, M. A.; Thompson, M. C.; Coumbe, H. L.; Madasu, P. K.; Coumbe, C. E.; Phillips, J. P. *Chem. Commun.* **2007**, 4263–4265.
46. Shinohara, H.; Takata, M.; Sakata, M.; Hashizume, T.; Sakurai, T. **1996**, *232*, 207–232.
47. Shinohara, H. *Rep. Prog. Phys.* **2000**, *63*, 843–892.
48. Cai, T.; Xu, L. S.; Anderson, M. R.; Ge, Z. X.; Zuo, T. M.; Wang, X. L.; Olmstead, M. M.; Balch, A. L.; Gibson, H. W.; Dorn, H. C. *J. Am. Chem. Soc.* **2006**, *128*, 8581–8589.
49. Angeli, C. D.; Cai, T.; Duchamp, J. C.; Reid, J. E.; Singer, E. S.; Gibson, H. W.; Dorn, H. C. *Chem. Mater.* **2008**, *20*, 4993–4997.
50. Ge, Z. X.; Duchamp, J. C.; Cai, T.; Gibson, H. W.; Dorn, H. C. *J. Am. Chem. Soc.* **2005**, *127*, 16292–16298.
51. Xie, Q.; Arias, F.; Echegoyen, L. *J. Am. Chem. Soc.* **1993**, *115*, 9818–9819.
52. Yang, Y. F.; Arias, F.; Echegoyen, L.; Chibante, L. P. F.; Flanagan, S.; Robertson, A.; Wilson, L. J. *J. Am. Chem. Soc.* **1995**, *117*, 7801–7804.

This page intentionally left blank

Chapter 7

Synthesis of Electron Donor-[60]Fullerene Multi-Ring Interlocked Systems

Jackson D. Megiatto, Jr. and David I. Schuster**

*Department of Chemistry, New York University,
New York, 1000, USA*

1. Introduction	207
2. Electron Transfer Reactions in Artificial Photosynthetic Systems	209
3. Supramolecular Artificial Photosynthesis — Catenanes and Rotaxanes	210
4. Synthesis of Ferrocene-C ₆₀ -Rotaxane	216
5. Synthesis of Zn(II)-Porphyrin-“Stoppered”-C ₆₀ -Rotaxane	221
6. Synthesis of Zn(II)-Porphyrin-C ₆₀ -[2]Catenates	224
7. Structural Characterization	226
8. Synthesis of [3]Catenates	228
9. Conclusion and Perspectives	238
References	240

1. Introduction

It has been amply demonstrated that world demand for energy is projected to more than double by 2050 and more than triple by the end of the century. Finding sufficient supplies of clean energy to satisfy the increasing worldwide energy demand is one of society's most urgent challenges.

*Corresponding authors. Email: jackson.megiatto@nyu.edu (Jackson D. Megiatto, Jr.); david.schuster@nyu.edu (David I. Schuster)

Sunlight is a compelling solution to our need for a clean, abundant source of energy in the future. It is readily available, secure from geopolitical tension, and poses no threat to our environment through pollution or to our climate through greenhouse gases. The possibility of harvesting, storing and distributing the energy coming from the sky has fascinated scientists for centuries. Much effort in many different scientific disciplines has been devoted to better understanding the fundamental steps of the conversion of sunlight into fuel. One obvious route to achieve this long-term goal involves better understanding of the fundamental steps of natural photosynthesis.¹⁻¹⁰

Nature has taught us that solar light can be harnessed and stored in chemically useful products, which represent the fuel that fundamentally sustains life on earth. Purple bacterial photosynthesis, the best understood system to date, demonstrates the basic route chosen by Nature to transform sunlight into chemical energy: absorption, conversion, processing and storage. The absorption of sunlight is executed by an antenna device composed of several organic pigments (chiefly chlorophyll) that capture light in the solar spectral region and convert it into electronic energy *via* generation of electronic excited states of the pigment molecules. The electronic energy gathered in the antenna device is then transferred (EnT) to another component of the system called the reaction center. The reaction center is basically composed of electron donor and acceptor assemblies, specially organized through non-covalent interactions in a protein matrix, that efficiently uses the captured electronic energy to produce and to separate charges through a series of electron transfer reactions. These separated charges are then used as redox potential energy to produce carbohydrates and oxygen from water and atmospheric carbon dioxide.¹¹⁻¹⁸

Although the basic processes involved in natural photosynthesis are understood in principle, Nature's design together with evolution have resulted in biological photosynthetic systems composed of highly complex and organized structures, which are made of intricate protein assemblies that are as yet beyond complete human comprehension.¹⁹ As a result, many important details of the mechanisms involved in solar light-induced photochemical conversion processes still remain to be resolved. Investigation of much simpler artificial photosynthetic systems that mimic the behavior of the natural system has emerged as an alternative approach to improve our understanding of the secrets behind the natural light conversion process. Much progress in this area has been made, and some commercial dye-sensitized photovoltaic cells have been developed, but these have had only limited practical application to date.⁷

2. Electron Transfer Reactions in Artificial Photosynthetic Systems

The conversion of light into species where charge is separated often by long distances has been reproduced on the laboratory scale by carefully designed artificial systems composed of electron donor (D) and electron acceptor (A) subunits.^{18,20–30} The dependence of the rates of intramolecular electron transfer (ET) reactions within covalently linked D-A molecules depends on the free energy of the ET process and the extent of electronic interaction between the D and A subunits, and has been theoretically and experimentally well described.^{31–40} Both theory and experiment show that there is an optimal value of the free energy change for achieving the maximum ET rate, and therefore the maximum efficiency, for this process. A key prediction of the theory proposed originally by Marcus is that the rate of an ET reaction will slow down when the free energy of the process becomes increasingly exergonic. The design and synthesis of organic systems which possess large free energies for charge recombination is key to achieving the long charge-separated state lifetimes essential for driving chemical reactions for fuel formation in organic solar cells. There seems to be general agreement that the ultimate goal is to produce efficient and stable solar cells constructed from cheap organic materials.

Reorganization energy is the parameter that governs the dynamics of ET processes.^{31,32,36,38,39,41} This parameter is defined as the sum of the energy associated with changes in the structure of the molecules undergoing oxidation and reduction, and changes in the solvent environment around the species undergoing the ET process. In theory and in practice, donor-acceptor systems with smaller reorganization energy values give faster forward-electron transfer rates and slower back-electron transfer rates compared to those having larger values of the reorganization energy.

When exposed to sunlight, electron D-A artificial assemblies capture part of the radiation energy as excited electron-hole pairs (charge-separated states) that can be tapped off for immediate conversion to electrical power (photovoltaics)^{7,42} or transferred to other molecules in solution for conversion into fuels, including methane, ethanol and hydrogen (artificial photosynthesis). The ultimate goal is to design and assemble much simpler systems than the natural analog that can efficiently process and store light as potential energy, which can then be used for practical applications.^{17,18}

The electron donors and acceptors used in artificial photosynthetic systems often resemble the natural ones, including porphyrins, carotinic polyenes and quinones.^{18,38,43} However, new synthetic structures such as

transition-metal complexes,^{4,44,45} aromatic bisimides¹⁰ and fullerenes,^{36,37,41} have proven to be very efficient as donors and acceptors, respectively. Studies on the optimization of the free energy changes, distances, and orientations between the various donors and acceptors in artificial arrays have allowed organic chemists to develop novel molecular structures to tailor the charge separation and storage characteristics for specific applications.

These findings, together with the development of powerful methods of structural characterization on the molecular as well as the macroscopic level, ultrafast dynamic measurements using lasers, and computer simulation, have opened new rational solutions to the problem of creation and interconnection of the molecular components needed for efficient light-energy conversion. For example, the electron donors and acceptors used in bio-inspired artificial photosynthetic systems need not be covalently linked to one another. In fact, natural photosynthetic systems use the surrounding protein to position the electron donor and acceptor moieties close to one another. The assembly of complex supramolecular photoconversion systems with synergistic functionality depends on a variety of weak intermolecular interactions, rather than strong individual covalent chemical bonds.^{10,15,17,38}

3. Supramolecular Artificial Photosynthesis — Catenanes and Rotaxanes

A critical step towards fully functional photoconversion systems involves the ability to create increasingly larger arrays of interactive molecules.² Covalent synthesis of macromolecular arrays is by its very nature highly inefficient and costly. A better approach to achieve large ordered architectures involves self-assembly from properly functionalized building blocks.^{46–48} Central to this mission is the development of simple chemical systems capable of instructing their own organization into large molecular aggregates through their mutual recognition properties.⁴⁹ By utilizing interactions as diverse as π - π interactions, hydrogen bonding, electrostatic and metal coordination as the driving source for self-assembly, chemists have begun to use supramolecular concepts to construct photoactive nanoscale structures and superstructures which are able to undergo photoinduced electron transfer to generate long-lived charge-separated states.^{15,50–55}

Our laboratory has been interested for some time in constructing artificial photosynthetic arrays by self-assembly of suitable D-A components to generate well-defined supramolecular structures.^{56,57} More specifically, our research is directed at understanding the mechanisms and dynamics of



Figure 1. Schematic representation of rotaxane and catenane structures. In catenane nomenclature, the numbers in the square brackets preceding the word “catenane” represent how many rings are involved in the interlocked structure.

electron and energy transfer processes in photoactive interlocked molecules, specifically catenanes⁵⁸ and rotaxanes.^{59–63} Catenanes (named from the Latin *catena* meaning “chain”) are a class of molecules composed of two or more interlocked rings, which can not be separated without breaking a covalent bond in one of the macrocycles (Figure 1). Rotaxanes (named from the Latin *rota* for “wheel” and *axe* for “axis”) are systems in which a ring is threaded by a rod, to which are attached two terminal groups that are larger than the internal diameter of the ring in order to prevent dissociation (Figure 1).⁶⁴

The main attractive feature of catenane and rotaxane structures is the possibility of exploring the intrinsic submolecular movements of the components arising from external inputs.^{65,66} Circumrotation, shuttling, pirouetting and rocking motions are examples of dynamic processes that can occur in interlocked molecules. Such topological behavior has been explored as the principle for construction of molecular machines and motors.^{64–74} In artificial photosynthesis, the submolecular motions can be used to position electron donor and acceptor groups in configurations that will improve electronic interactions among the chromophores in the supramolecular array, facilitating ET reactions. As a consequence, the dynamics of charge-separated states can be finely tuned to afford longer lifetimes.^{75–78}

The key to preparing interlocked molecules is template-directed synthesis.^{46,49,64,79–80} In this strategy, *non-covalent* interactions are employed to gather and position molecular fragments in a specific orientation so that subsequent covalent bond formation will create a mechanical bond between the fragments. Templates based on well controllable π - π interactions, hydrogen bonding, solvophobic forces and coordinate bonding have been described, in which catenanes and rotaxanes are afforded under kinetic or thermodynamic control.^{64–66,80–87}

The first highly-controllable self-assembly protocol to prepare catenanes was based on metal-ligand coordination, and was reported by Sauvage and coworkers in Strasbourg in 1983 (Figure 2).^{81,88–90} This protocol consists of preparing functionalized-2,9-diaryl-1,10-phenanthroline (phen) ligands

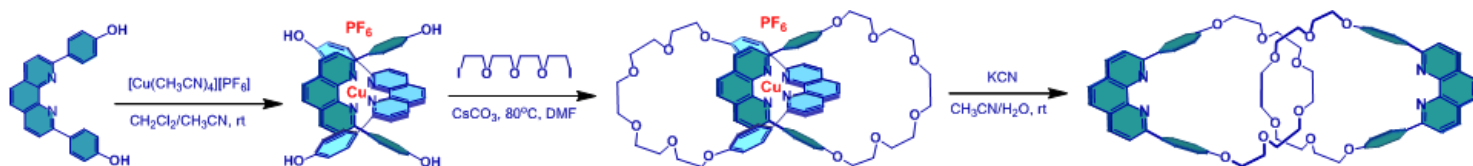


Figure 2. Original protocol for Cu(I) template synthesis of catenanes: (i) coordination of two phen-ligands to the Cu(I) ion template; (ii) double-Williamson-macrocyclization reactions of the pre-orientated phen moieties to give a [2]catenane; (iii) formation of the [2]catenane through a demetallation reaction. (a) $[\text{Cu}(\text{CH}_3\text{CN})_4][\text{PF}_6]$, $\text{CH}_2\text{Cl}_2/\text{CH}_3\text{CN}$, rt, 1 h, quantitative; (b) di-iodopentaethyleneglycol, CsCO_3 , DMF, high dilution conditions, 50°C , 48 h, 27% yield; (c) $\text{CH}_2\text{Cl}_2/\text{MeOH}$, KCN, rt, 3h, 92% yield.

designed to encapsulate a Cu(I) ion-template, which forms a relatively stable pseudotetrahedral $[\text{Cu}(\text{phen})_2]^+$ complex that orients the functional groups in an orthogonal fashion such that they can undergo macrocyclization reactions to afford metalated-[2]catenanes (also called [2]catenates). Subsequently, demetalation using an excess of potassium cyanide produces the metal-free [2]catenanes (also known as [2]catenands) in high yields.

In artificial photosynthetic systems, metal coordination is a particularly promising protocol because in many cases transition metal complexes not only serve as building blocks to assemble the supramolecular system, but can also act as electronic relays, facilitating long-range electron and energy transfer processes among the chromophores.^{4,44,45,91-93} In particular, the $[\text{Cu}(\text{phen})_2]^+$ complex is a useful component for incorporation into photoactive arrays due to its absorption with high extinction coefficients in the visible region of the solar spectrum, its long-lived excited states and photostability.^{44,45} Thus, the possibility of preparing interlocked molecules composed of D-A subunits in high-yields using a $[\text{Cu}(\text{phen})_2]^+$ complex to assemble the system is very attractive.

Because of their stability, synthetic accessibility, remarkable spectroscopic and electrochemical properties, as well as their structural relationship to chlorophyll, porphyrinic pigments are the most widely used electron donors in artificial photosynthetic model systems.^{18,38,43} Substituted porphyrins can be obtained from acid-catalyzed condensation reactions between suitable aldehydes and pyrrole, followed by oxidation of the crude mixture, according to well-established methods.⁹⁴⁻⁹⁶ Mild reaction conditions allow the preparation of porphyrins bearing various types of functional groups, which makes this family of tetrapyrrolic macrocycles excellent building blocks for supramolecular systems.⁹⁶ The electronic properties of porphyrins can be tuned by metal coordination to the four nitrogen atoms in the core of the structure. For example, zinc(II)porphyrins are known to be better electron donors in artificial photosynthetic systems than the corresponding free-base analogs. Coordination to a Zn^{2+} cation stabilizes the π -system of the porphyrinic structure, resulting in lower oxidation potentials.⁴³

On the other hand, fullerenes are a unique class of spherical molecules containing a conjugated π -system that have proven to be excellent electron acceptors both in solution and in the solid state. The redox and spectroscopic properties of [60]fullerene (C_{60}), the most abundant compound of the fullerene family, have been extensively investigated. It has been shown that C_{60} can reversibly accept up to six electrons in the ground state into three low-lying degenerate unoccupied orbitals, while its rigid 3D-structure offers enough room for these charges in the reduced state to minimize repulsive

forces.^{34–37} As a result, C_{60} is known to have an unusually small reorganization energy in ET processes, which accelerates forward-electron transfer (charge separation), while retarding back-electron transfer (charge recombination) reactions.^{38–41,97,98}

Building on these principles, we have developed new strategies at New York University for the synthesis of interlocked D-A molecules, both rotaxanes^{59–61,99,100} and catenanes.^{58,101,102} We have prepared new families of organic-inorganic hybrid systems, where the organic subunits are zinc(II)porphyrins (ZnP) and fullerenes (C_{60}), while the inorganic component is the $[Cu(phen)_2]^+$ complex. Figure 3 shows some of the structures we have prepared. Due to the complementary photophysical properties of porphyrins as electron donors and fullerenes as electron acceptors, photoinduced energy and electron transfer processes occur between the various organic and inorganic subunits. Addressing light excitation to a given molecular component by choice of excitation wavelength has enabled the assignment of specific roles to each entity in the hybrid structure, and the ET and EnT dynamics have been determined using ultrafast spectroscopic detection techniques.^{58–60,101,102}

The main challenge in the preparation of the catenanes and rotaxanes depicted in Figure 3 arises from the synthetic difficulties for introduction of the C_{60} group into interlocked molecules. Fullerenes are generally not chemically compatible with the classical procedures employed in the synthesis of rotaxanes and catenanes.^{64–66,69,80–87} For example, the entwined precursors available in the literature for preparation of catenanes and rotaxanes are not stable and easily dissociate under the conditions that might be used to attach the C_{60} on the interlocked system.⁹⁸ In the case of the $[Cu(phen)_2]^+$ complex template, the presence of competing ligands, strong base and high temperatures are known to cause dissociation.⁸⁰

In order to circumvent these problems and prepare catenanes and rotaxanes as shown in Figure 3, a straightforward strategy was conceived taking into consideration the reactivity/solubility issues of the C_{60} group and the inherent instability of the $[Cu(phen)_2]^+$ complex template. This strategy (see Figure 4) comprises three steps and allows the preparation of both catenanes and rotaxanes from the same basic building blocks and precursors. First, C_{60} is attached to a previously prepared phen-based macrocycle, which is then threaded by another phen string-like fragment, using a Cu(I) ion as template, affording a pseudorotaxane precursor. Finally, covalent-stoppering or macrocyclization reactions between the pseudorotaxane precursor and a mono- or difunctionalized electron donor afford catenanes and rotaxanes respectively.

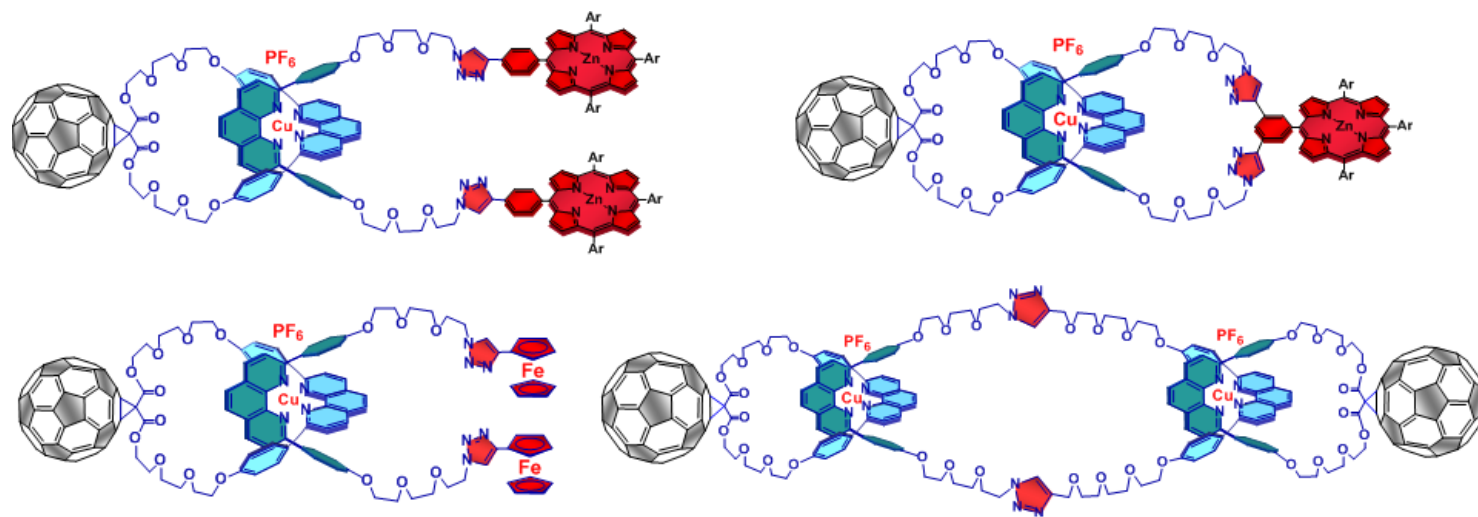


Figure 3. Some rotaxanes and catenanes composed of ferrocene, zinc(II)porphyrin and C₆₀ subunits prepared in our lab.

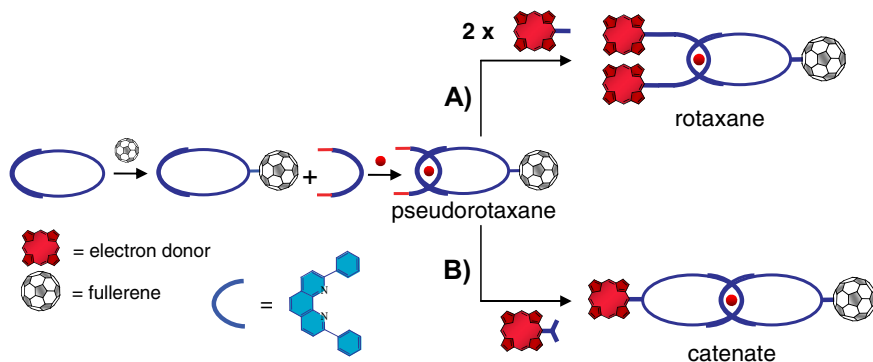


Figure 4. Schematic representation of the approach used to prepare electron donor- C_{60} mechanically-linked molecules using Cu(I) template synthesis. Adapted from Reference 107.

The key point in this approach is kinetic control⁸⁵ of the final stoppering (rotaxanes) and macrocyclization (catenanes) reactions. In the case of rotaxanes, introduction of the bulky end groups should occur as fast as possible in order to capture the final interlocked structure by covalent bond formation before an undesirable unthreading reaction takes place. For catenanes, the strategy is more complex because cyclization reactions necessarily involve low concentrations or a heterogeneous medium. Besides accelerating the kinetics of the covalent bond formation under high-dilution conditions, the macrocyclization reaction should occur, if possible, in a synchronous way so as to avoid dissociation of the $[Cu(phen)_2]^+$ complex or formation of other cyclic or oligomeric structures. A highly substrate-tolerant covalent bond forming reaction, along with molecular engineering that involves catalysis, solvent medium and concentration/temperature dependence studies, is required to address these problems.

4. Synthesis of Ferrocene- C_{60} -Rotaxane

The so-called Huisgen–Sharpless–Medal-Cu(I)-catalyzed-1,3-dipolar cycloaddition of organic azides and terminal-alkynes (CuAAC or “click” reaction)^{103–105} is a powerful, general, and robust synthetic tool for construction of complex materials such as dendrimers, macrocycles, polymers, as well as derivatization of biological materials for drug discovery and *in vivo* tagging.¹⁰⁶ The basis for the unique properties of this reaction is the dramatic improvement in both rate and regioselectivity caused by the presence of Cu(I), which accelerates the rate of reaction about 7 orders of magnitude.¹⁰⁶ Another interesting characteristic that makes this protocol ideal for our purposes is the unusually mild reaction conditions, involving reaction at room temperature.

Taking advantage of the mild conditions of the CuAAC reaction, coupled with its tolerance to potentially sensitive appended groups, including porphyrins and fullerenes, the straightforward strategy schematically described in Figure 5 was developed. Another interesting characteristic of this approach resides in the fact that Cu(I) ions acts as both template⁸¹ and catalyst,^{104,105} which allows the preparation of donor- C_{60} -based interlocked molecules in a convenient one-pot procedure.

The synthetic work began with oligo(ethyleneglycol)-2,9-diphenyl-1,10-phenanthroline derivative **1**, originally prepared by Sauvage and Dietrich-Buchecker.^{88,90} Macrocycle **3** was prepared from coupling of **1** and malonic acid **2** using bis(2-oxo-3-oxazolidinyl)phosphonic chloride (BOP-Cl) as the coupling agent.⁵⁸ C_{60} was attached to **3** using the standard Bingel–Hirsch protocol⁹⁸ to give macrocycle **4**. Diol **1** was converted into the ditosylate, which in turn was converted into diazide **6** by reaction with sodium azide.⁵⁸ The threading of **6** through macrocycle **4**, using Sauvage's Cu(I) template protocol,⁸⁸ quantitatively afforded the C_{60} -linked pseudorotaxane **7**, as revealed by ¹H NMR spectroscopy.⁵⁸

The robustness of the CuAAC reaction allows for manipulation of conditions for the final stoppering and macrocyclization reactions. While a wide variety of “click” protocols have been reported, there is no correlation between methods used and yield of reaction, resulting in case-to-case optimization.¹⁰⁶ Accordingly, exploration was undertaken of different CuAAC protocols in order to optimize parameters such as the copper source, solvent system, concentration, use of auxiliary ligands and reducing agents.¹⁰⁷ To test different CuAAC reaction conditions, preparation of ferrocene-stoppered-rotaxane **9**¹⁰⁰ (Figure 6) was chosen as the model reaction due to easy access to alkynylferrocene **8** as well as our interest in exploring the ability of ferrocene to act as an electron donor in interlocked photoactive systems.

The “click” conditions explored for the final “double-stoppering” reaction in the synthesis of **9** are provided in Table 1.¹⁰⁷ Except for entry 6, ethynylferrocene **8** was added as a solid to the dichloromethane/acetonitrile (DCM/ACN) solution containing the precursor **7**. The copper catalyst, sodium ascorbate (SA, Figure 7) and the “click” additive (see entries 3–5, Table 1), dissolved in the appropriate oxygen-free solvent, were added by syringe to the above solution. Finally, 1,8-diaza[5.4.0]-bicycloundec-7-ene (DBU, Figure 7) was added (entries 2, 3 and 5) and the reaction mixture was stirred under an inert atmosphere for 12 h. In the case of entry 6, CuI, SA and sulfonated bathophenanthroline (SBP, Figure 7) were dissolved in a degassed mixture of H₂O/EtOH (1:1, v/v), and the pink suspension was heated at reflux for 2 min under nitrogen in order to increase the solubility of the

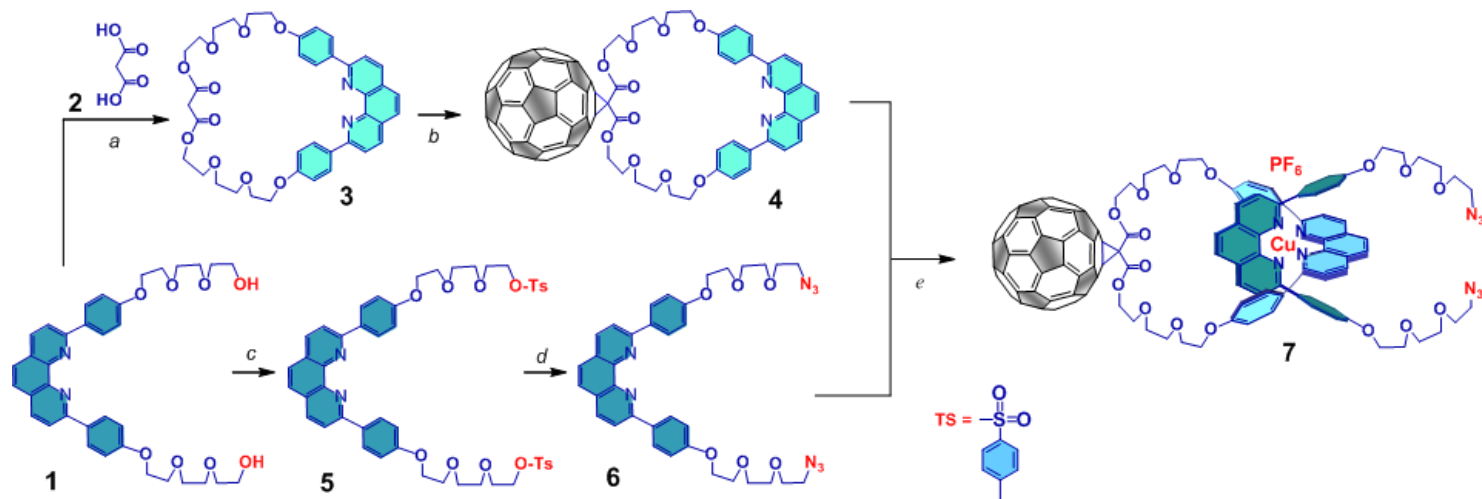


Figure 5. Building blocks and synthetic route for preparation of the C_{60} -pseudorotaxane precursor 7 needed for rotaxane and catenane preparation. a) BOP-Cl, Et_3N , CH_2Cl_2 , rt, 12 h, 45% yield; b) C_{60} , DBU, I_2 , toluene, rt, 24 h, 55% yield; c) TsCl, Et_3N , CH_2Cl_2 , $0^\circ C$ for 4 h and rt for 20 h, 75% yield; d) NaN_3 , DMF, $80^\circ C$, 24 h, 93% yield; e) $[Cu(CH_3CN)_4][PF_6]$, CH_2Cl_2/CH_3CN , rt, 3 h, quantitative.

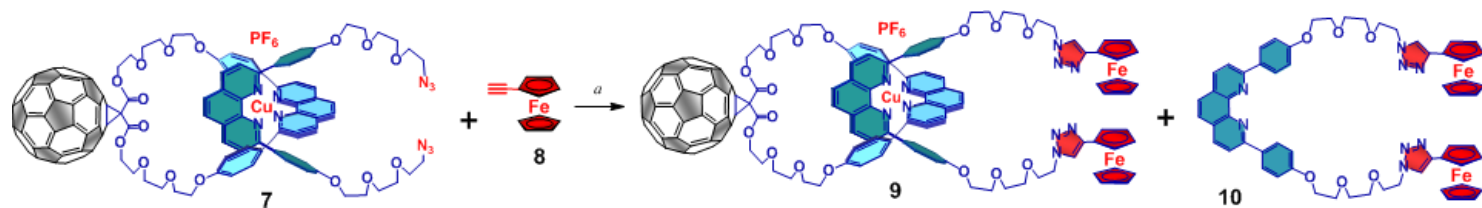


Figure 6. Synthetic route to (ferrocene)₂-stoppered fullerene rotaxanes. a) See Table 1 for conditions.

Table 1. “Click” reaction conditions studied for the ultimate stoppering reactions in the synthesis of rotaxane **9**. Adapted from Reference 107.

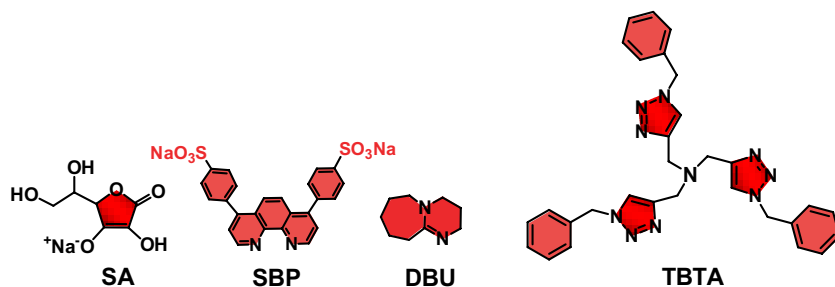
Entry	Cu source ^a	Solvent	Base ^b	Additive ^b	Rotaxane	Dumbbell
					9 (%) ^c	10 (%) ^c
1	CuSO ₄	EtOH/H ₂ O	—	—	12	56
2	[Cu(CH ₃ CN) ₄][PF ₆]	CH ₂ Cl ₂	DBU	—	38	58
3	[Cu(CH ₃ CN) ₄][PF ₆]	CH ₂ Cl ₂	DBU	2 eq. TBTA	82	16
4	CuI	CH ₂ Cl ₂ /EtOH/H ₂ O	—	4 eq. SBP	—	—
5	CuI	CH ₂ Cl ₂ /EtOH/H ₂ O	DBU	4 eq. SBP	83	—
6 ^d	CuI	CH ₂ Cl ₂ /EtOH/H ₂ O	DBU	4 eq. SBP	92	—

(a) In all cases, two equivalents of copper and four equivalents of sodium ascorbate per equivalents of pseudo-rotaxane **7** were used.

(b) For chemical structures, see Figure 7.

(c) Isolated yields, 12 h reaction time.

(d) Initial hot solubilization of the “click brew” as described in the text.

**Figure 7.** Chemical structures of the “click” additives used in the preparation of rotaxane **9**: SA = sodium ascorbate; SBP = sulfonated bathophenanthroline; DBU = 1,8-diaza[5.4.0]-bicycloundec-7-ene; TBTA = tris[(1-benzyl-1H-1,2,3-triazol-4-yl)methyl]amine.

catalyst brew. The deep red mixture was then cooled to room temperature before being added to the solution containing **7**, followed by addition of **8** (as a solid) and DBU. The same workup was done in all cases, which includes extraction of the crude product with DCM, followed by washing with a saturated methanol solution of KPF₆ to effectuate anion exchange. Final purification was achieved by column chromatography using DCM/methanol (from 0 to 3%, v:v) as eluent.

The most common “click” protocol reported in the literature employs CuSO₄ as the copper source and relies on *in situ* reduction of inactive Cu(II) ions with sodium ascorbate (SA) to form the catalytically active Cu(I) species in water/alcohol mixtures.¹⁰⁶ Although this CuSO₄/SA “click” protocol

(entry 1) has been successfully utilized in the synthesis of other interlocked structures,^{108–110} we found that this approach afforded only 12% of the target rotaxane **9**. The corresponding dumbbell compound **10** was isolated in relatively high yield, indicating that unthreading occurred before stoppering took place.^{81,88–90} Another isolated byproduct was the mono-stoppered ferrocene thread, indicating incomplete reaction.

We rationalize the low rotaxane yield obtained with the CuSO₄/SA “click” protocol in terms of the kinetics of the cycloaddition stoppering reactions. The formation of the rotaxane structure depends on the formation of connecting triazole rings, which in turn depends on the *in situ* generation of catalytic Cu(I) species through reduction of Cu(II) ions with SA. It has been reported in the literature that *in situ* reduction of Cu(II) to Cu(I) does not take place immediately, resulting in a latency period for the active catalytic species to form, which slows down the “click” reaction.¹⁰⁶ This induction period allows coordination of solvent molecules (H₂O and/or ethanol) to the [Cu(phen)₂]⁺ complex, leading to dissociation of pseudorotaxane precursor **7**.^{81,88–90}

The use of dichloromethane (DCM), a non-coordinating organic solvent (requiring a change in the copper source), in conjunction with the base DBU, resulted in a reasonable rotaxane yield (38%, Table 1, Entry 2). However, the addition of two equivalents of tris[(1-benzyl-1*H*-1,2,3-triazol-4-yl)methyl]amine (TBTA, Figure 7), a so-called “click” additive,^{111,112} dramatically improved the yield of target rotaxane **9** to 82%, although a small amount of **10** was still isolated. Such additives have been used to enhance the kinetics of “click” reactions in order to prevent damage to sensitive substrate molecules, such as peptides and proteins.^{112,113}

The use of the water-soluble “click” additive SBP^{112,113} in a heterogeneous medium with CuI as the copper source (see Table 1, Entry 4), surprisingly resulted in no reaction, as the starting materials **4** and **6** were recovered after reaction. When DBU was added to the reaction flask (Table 1, Entry 5), the target rotaxane **9** was isolated in very good yield (83%), while the undesired dumbbell **10** was not formed. The best results were obtained using the conditions described in (Table 1, Entry 6).^{58,100–102} Initial hot solubilization of the “click” brew proved to be very effective in accelerating the stoppering reactions, affording the target rotaxane **9** in excellent yield (92%) and preventing detrimental unthreading from taking place. A reasonable explanation for this high yield could be that the [Cu(phen)₂]⁺ complex in the pseudorotaxane structure **7** is less susceptible to unthreading in the DCM phase,^{81,88–90} while the potentially aggressive CuAAC reagents remain mainly in the aqueous phase; at the interface, the “click” reactions to connect the

pieces take place with enhanced kinetics due to the presence of the “click additives” SBP and DBU, affording the final rotaxane structure *via* triazole ring formation.

The interlocked structure of **9** was confirmed by ^1H NMR spectroscopy and MALDI-TOF analysis. The ^1H NMR spectrum showed the expected upfield shift for the phenyl protons (for assignments, see Figure 8) in the two phen fragments entwined around the Cu(I) core.^{81,88–90} This high-field shift is induced by the intense ring-current effect of the phenanthroline nuclei, which are located between the two pairs of phenyl rings in the $[\text{Cu}(\text{phen})_2]^+$ complex topography.

5. Synthesis of Zn(II)-Porphyrin-“Stoppered”-C₆₀-Rotaxane

For study of electron transfer mechanisms involved in mechanically interlocked D-A structures, electron donors other than ferrocene need to be introduced into the system. With these optimized conditions in hand, we next turned our attention to the corresponding (ZnP)₂-C₆₀-rotaxane. The same methodology used for **9** (Table 1, Entry 6) was applied to the synthesis of porphyrin-stoppered fullerene-rotaxane **14** (Figure 9). The ethynylphenyl zinc(II) porphyrin derivative **13** was prepared by condensation of 3,5-di-*tert*-butylbenzaldehyde **11**, 4-((trimethylsilyl)ethynyl)benzaldehyde **12** and pyrrole, following the Lindsey procedure,^{96,114} yielding the free base porphyrin **13a**, which was then metallated using zinc acetate (Zn(OAc)₂) to give **13b**. Deprotection of the alkyne group using tetrabutylammonium fluoride (TBAF) in THF gave the desired Zn(II) porphyrin **13**.

The final stoppering reaction was carried out following the optimum procedure developed for rotaxane **9** (Table 1, Entry 6). Workup and chromatographic purification resulted in four major products. The first eluted compound was unreacted **13** (which had been added in slight excess), while the second compound was identified as the unthreaded *bis*-porphyrin dumbbell **15** (MALDI-TOF *m/z* 2816, $[\text{M} + \text{Cu}]^+$). The target rotaxane **14** was then eluted as a purple solid in 70% yield. Fullerene-macrocycle **4** was also isolated.

We rationalize the lower yield obtained for **14** when compared to **9** in terms of the size difference between ethynylferrocene **8** and the much larger ethynyl-ZnP **13**. After the first “click” reaction take place, the higher constraints imposed on pseudorotaxane **7** by the bulky ZnP moiety might slow down the conversion to **14**. As a consequence, **7** may be more susceptible to dissociation *en route* to **14** as compared to **9**.^{81,88–90} Nonetheless, we consider

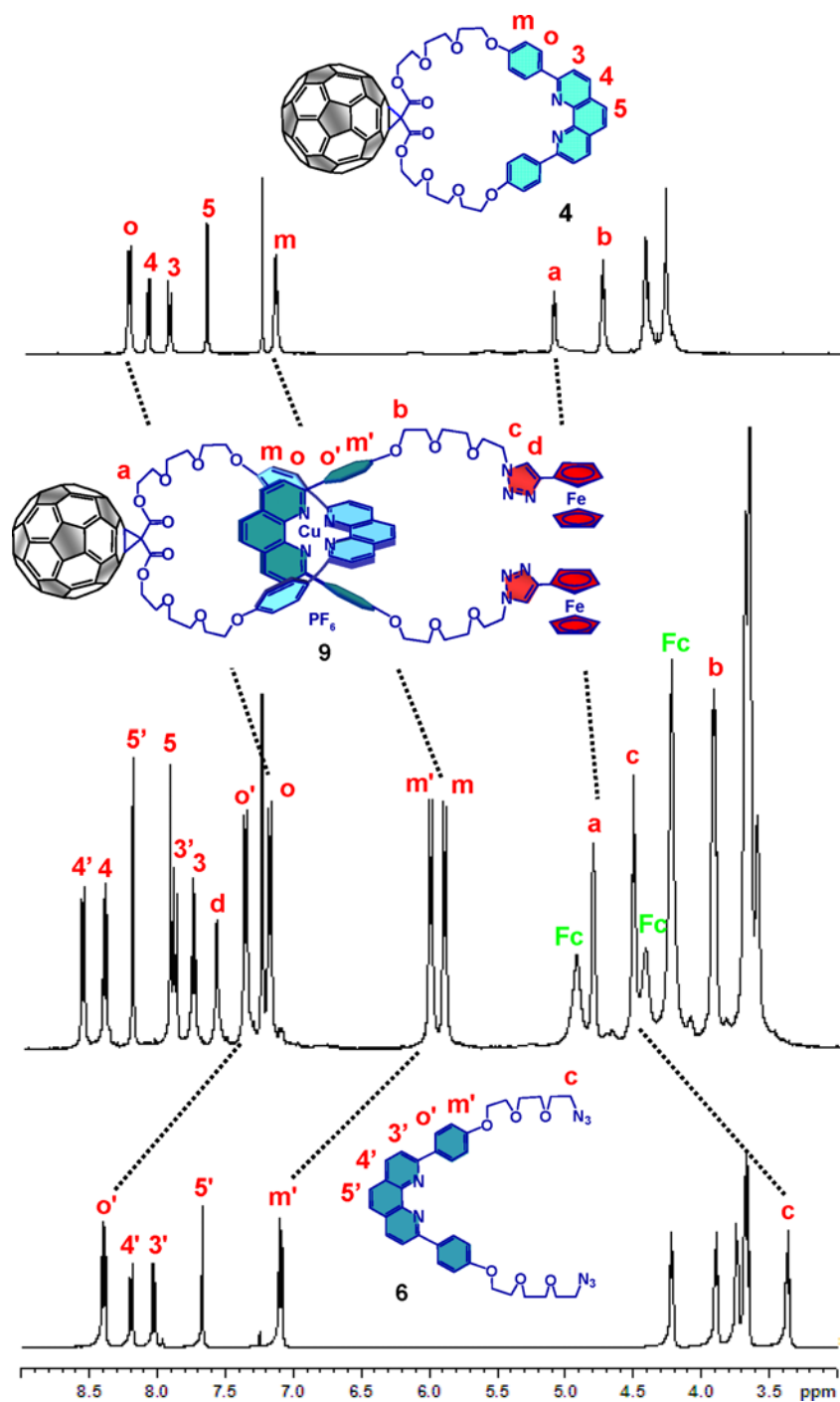


Figure 8. ^1H NMR spectra (400 MHz, CDCl_3 , 298 K) of macrocycle **4**, ferrocene- C_{60} -rotaxane **9** and diazidophen-“thread” **6**.

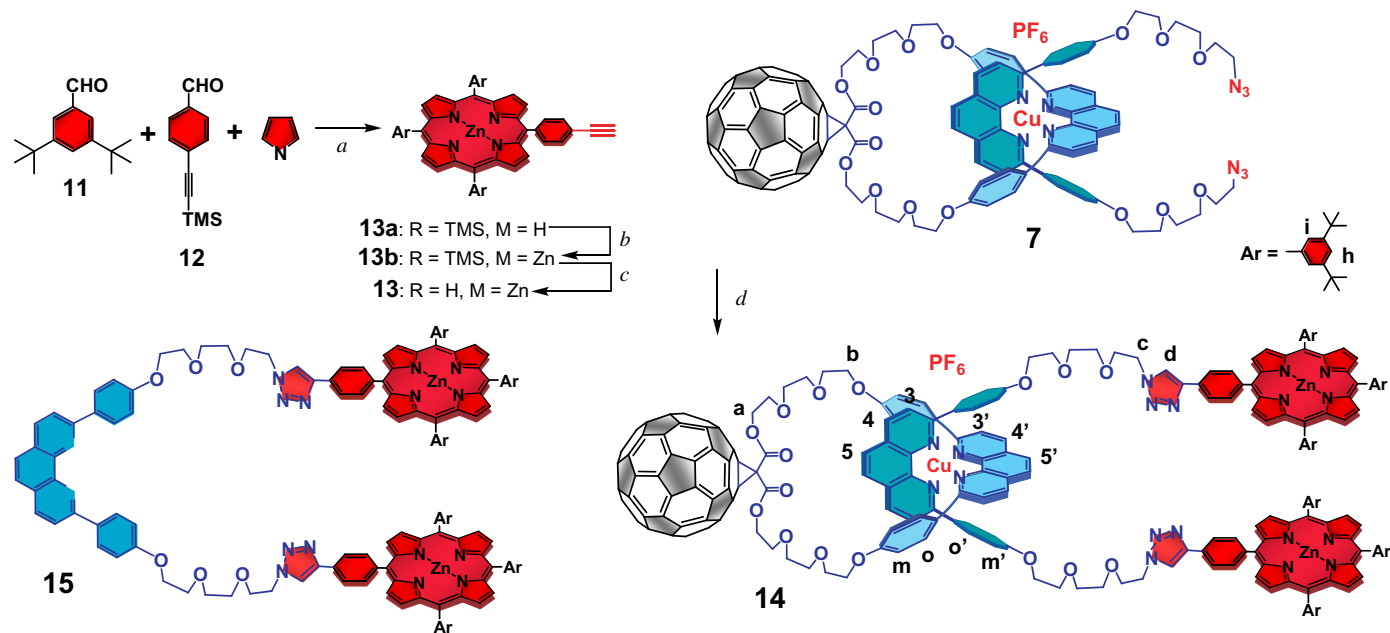


Figure 9. Precursors and synthetic route for preparation of $(\text{ZnP})_2\text{-C}_{60}$ rotaxane **14**. (a) BF_3OEt_2 , PPh_4Cl , CH_2Cl_2 , rt, 12 h and then 2,3-dichloro-5,6-dicyanobenzoquinone (DDQ), rt, 12 h, 9% yield; (b) $\text{Zn}(\text{OAc})_2$, $\text{CH}_2\text{Cl}_2/\text{CH}_3\text{OH}$, reflux, 6 h, quantitative; (c) TBAF, THF, rt, 30 min, quantitative; (d) CuI , SA, SBP, DBU, $\text{H}_2\text{O}/\text{EtOH}$, rt, 12 h, 70% yield.

a 70% yield to be remarkable for synthesis of a complex rotaxane such as **14** by a double-“click” cycloaddition reaction.¹¹⁵

Key evidence supporting the structure assignment to rotaxane **14** came from MALDI-TOF analysis. The mass spectrum of the isolated product shows a peak at m/z 4228 ($M - PF_6$)⁺, corresponding to structure **14**.^{116,117} The fragmentation pattern can be unambiguously assigned to the individual molecular components, strongly supporting the rotaxane structure for **14**, in which two porphyrins moieties act as stoppers on the rod and C₆₀ is attached to the macrocyclic ring.¹⁰⁷

6. Synthesis of Zn(II)-Porphyrin-C₆₀-[2]Catenates

To check if the kinetic control and the heterogeneous medium conditions utilized for rotaxane preparation are suitable for catenanes, we applied the same methodology to the synthesis of the [2]catenate **17** bearing ZnP and C₆₀ moieties (see Figure 10).^{58,107} This was again accomplished in a one-pot procedure by combination of pseudorotaxane precursor **7** with meta-diethynyl-ZnP **16**^{96,114} under the “click” conditions of entry 6 in Table 1. In this case, a dilute medium (10 times more dilute than that used for rotaxane preparation) was used, as is customary for macrocyclic reactions. The ZnP-C₆₀-[2]catenate was obtained in 57% yield.

Key evidence supporting the structure assignment to catenate **17** came from MALDI-TOF analysis. The general pattern of the mass spectrum is very characteristic of catenanes,¹¹⁸ featuring stepwise fragmentation of each ring from the interlocked system. Thus, one observes the molecular ion peak for **17** at m/z 3215 ($M - PF_6$)⁺ as well as peaks for the individual macrocycles at m/z 1805 (ZnP-macrocycle + Cu)⁺ and m/z 1477 (C₆₀-macrocycle + Cu)⁺. Detection of pristine C₆₀ at m/z 720 indicates that rupture and loss of the C₆₀-containing macrocycle component occurs through cleavage of the methanofullerene appended group, followed by release of C₆₀ from the structure **17** and consequential detection of the ZnP-macrocycle subunit at m/z 1805. On the other hand, loss of N₂ molecules observed in the MALDI-TOF spectrum suggests that fragmentation and loss of the ZnP-ring component occurs through cleavage of the triazole moieties,^{119,120} resulting in detection of the C₆₀-macrocycle at m/z 1477. The absence of fragments between the molecular ion peak and the peaks corresponding to the individual macrocycles provides strong evidence for attached structure **17** in which the ZnP and C₆₀ moieties are covalently attached at opposite ends of the [2]catenate framework.

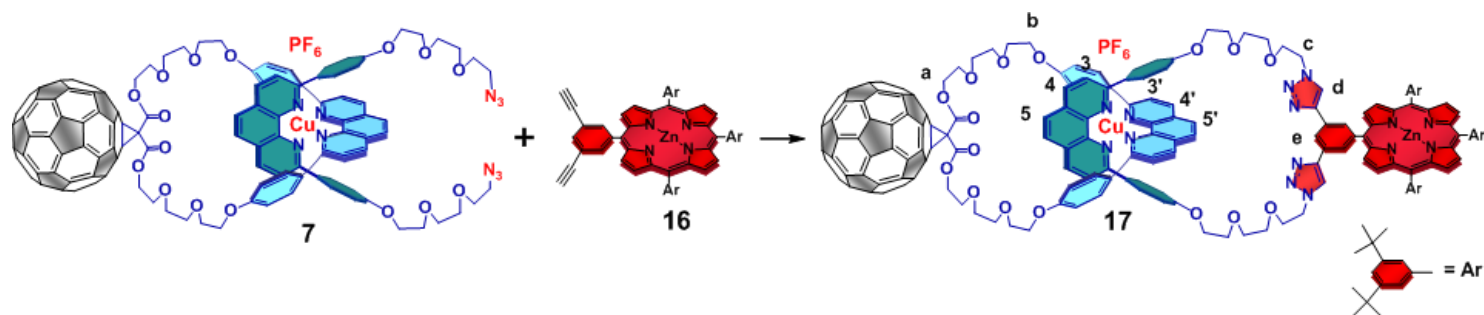


Figure 10. Precursors and synthetic route for preparation of ZnP-C₆₀-[2]catenate **17**.

7. Structural Characterization

ZnP- C_{60} rotaxane **14** and ZnP- C_{60} -[2]catenate **17** were also characterized by ^1H NMR spectroscopy (for spectra, see Figure 11, while for atom numbering, see Figures 9 and 10) and left no doubts about their interlocked nature.¹⁰⁷ In both cases, this was the general pattern expected for such structures. The pyrrolic protons of the ZnP moiety resonate at typical values, while the two ddp ligands intertwined around a Cu(I) ion give signals in a region similar to that observed for other Cu(I)-rotaxanes and -catenanes.^{81,88–90} The presence of triazole rings in the structures can be inferred by the appearance of a new signal in the aromatic region of the spectra and by the downfield shift observed for the CH_2 adjacent to the azido group on the phen-string like fragment **6** (*d* and *e* in Figure 11, respectively). Other features included resonances for the methylene group adjacent to the malonate moiety (*a* in Figure 11), and for the oxyethyl linkers, confirming successful formation of rotaxane **14** and [2]catenate **17**.^{58,99–102,121}

A comparison between the ^1H NMR spectra of rotaxane **14** and [2]catenate **17** (Figure 11) revealed that, although the two interlocked molecules are composed of similar components and are prepared from a common pseudorotaxane precursor, they adopt very different conformations in solution. In the case of rotaxane **14**, two sets of pyrrolic protons around 9 ppm indicate that the two ZnP moieties are not equivalent, suggesting a folded conformation for **14** in solution in which the two ZnP moieties are located in different environments. We propose that the well-documented^{50,51,122} attractive interactions among the ZnP, $[\text{Cu}(\text{phen})_2]^+$ and C_{60} moieties associated with the high flexibility of the glycol linkers drive these conformational changes in rotaxane **14**, resulting in formation of secondary structures stabilized by van der Waals attractive forces and π - π stacking. In contrast to rotaxane **14**, these attractive interactions between the chromophores are not strong enough to cause the same effect in the more rigid catenane structure. Accordingly, the ^1H NMR spectrum of catenate **17** shows just one set of signals for the ZnP pyrrolic protons at 8.5–8.8 ppm, suggesting an extended conformation in which the ZnP and C_{60} moieties are as far apart as possible.

Computational studies support this hypothesis (see Figure 12).^{58,100,107} Using Spartan'06 software (PM3 minimization), calculations point to a folded structure as the most stable one for rotaxane **14**, with one of the ZnP groups much closer to the C_{60} moiety, while the other is further away. Interestingly, computational simulation of the identical rotaxane lacking

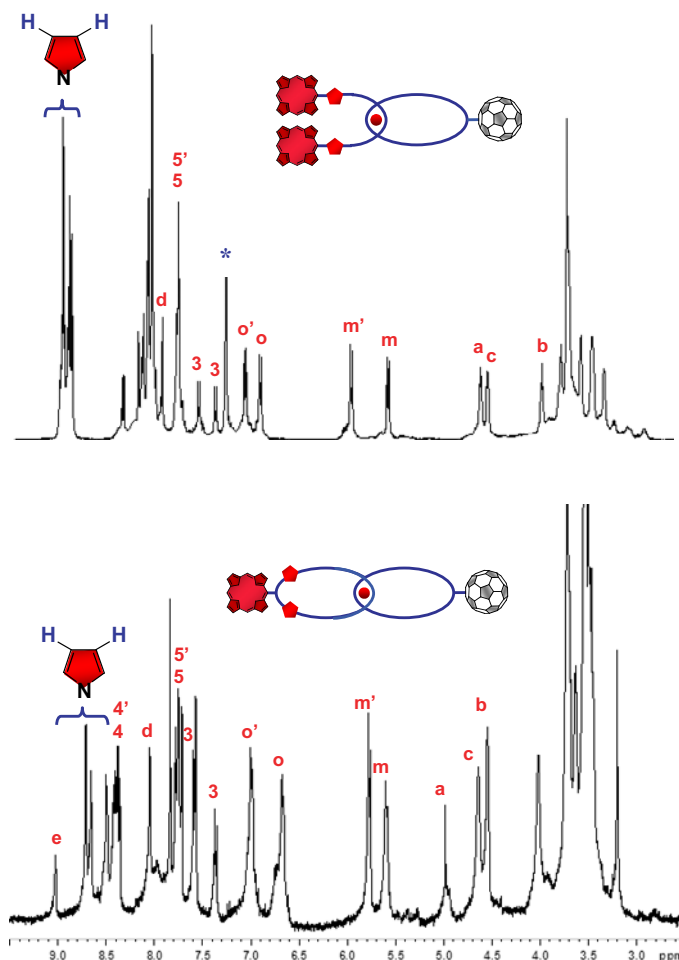


Figure 11. ^1H NMR spectrum (800 MHz, 298 K) $(\text{ZnP})_2\text{-C}_{60}$ -rotaxane **14** (CDCl_3), $\text{ZnP-C}_{60}\text{-[2]catenate} **17** (CD_3CN). Peak marked with an asterisk is due to residual solvent.$

C_{60} indicates that an extended conformation is the most stable, with the two ZnP subunits parallel to each other, suggesting that attractive interactions between ZnP and C_{60} components play an important role in determining the preferred conformation of the rotaxane **14** in solution. In the case of more rigid structure $\text{[2]catenate} **17**, computational simulations indicate the extended conformation is the most stable, with the two chromophores well-separated from each other. These results are in agreement with the ^1H NMR structural analysis.$

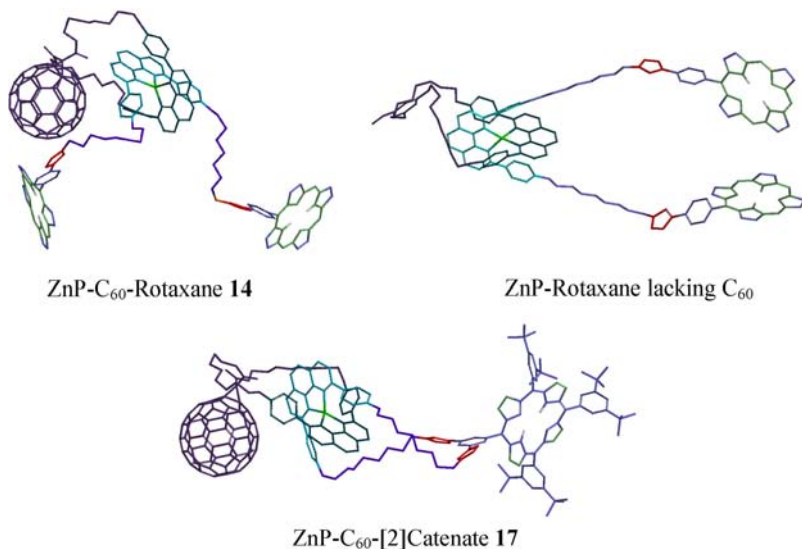


Figure 12. Molecular models of ZnP-C₆₀-rotaxane **14**, of ZnP-C₆₀-[2]catenate **17** and of a ZnP rotaxane lacking the C₆₀ group, as calculated *via* Spartan. Energy was minimized with 3,5-di-*tert*-butylphenyl groups in the meso positions of the porphyrins, which were later removed for clarity of presentation.

8. Synthesis of [3]Catenates

The synthesis of higher interlocked molecules, such as [3]catenanes has been a synthetic challenge for decades.^{64,123–129} Although some templated strategies have been conceived and have afforded [3]catenanes in reasonable-to-high yields, the introduction of functional groups into the interlocked structure for further elaboration or attachment of appended groups to produce [3]catenanes with new properties still stands as a barrier to be overcome. In particular, the synthesis of *nonsymmetrical* [3]catenanes composed of three different rings challenges the synthetic methodologies previously described in the literature.

Due to the mild conditions, and the high-tolerance of our “click” procedure toward a large variety of functional and sensitive groups, we have generalized our synthetic approach based on the templating effects of the Cu(I)-phenanthroline system and CuAAC reaction in order to prepare [3]catenanes.^{101,107} The strategy and building blocks to afford such *nonsymmetrical* systems is depicted in Figure 13.

In our first approach, two different phen-based macrocycles containing carboxylate and carbomethoxy groups were prepared according to literature procedures.¹⁰¹ Each functionalized ring was then threaded using a phen-filament

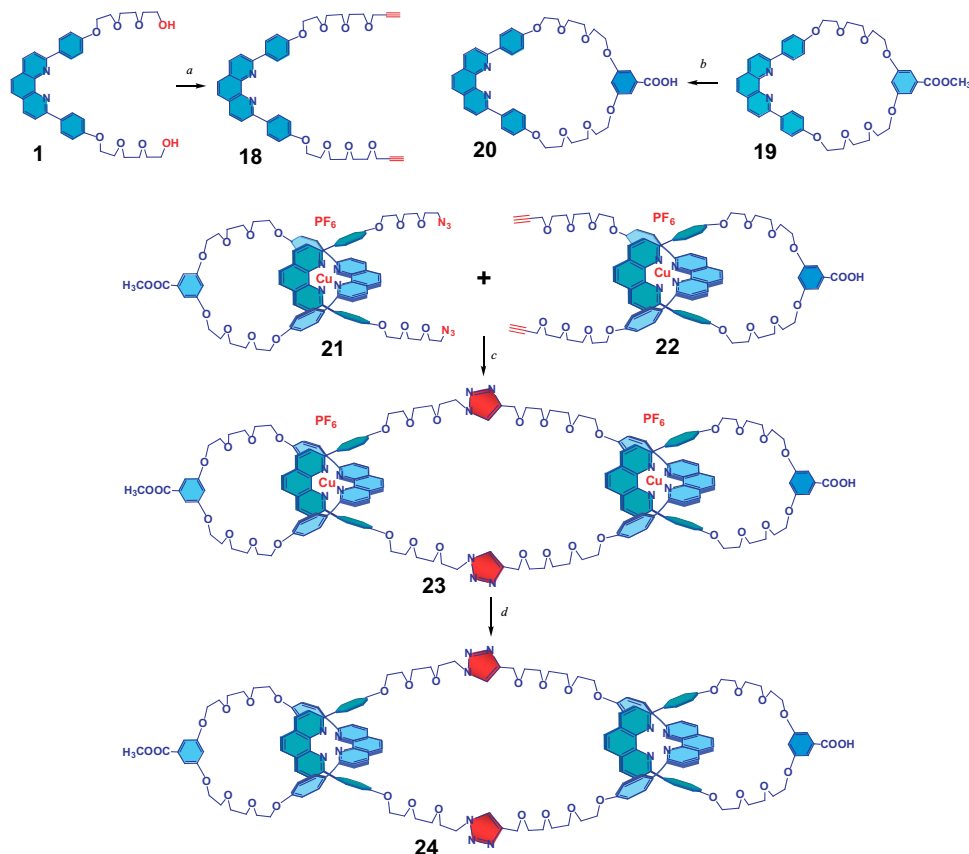


Figure 13. Building blocks and synthesis of *nonsymmetrical* functionalized-[3]catenates **23** and the metal-free catenand **24**. a) propargylbromide, NaH, DMF, 80°C, 12h, 85% yield; b) NaOH, dioxane/H₂O, 6h, reflux, quantitative; c) CuI, SA, SBP, DBU H₂O/EtOH, 12h, rt, 65–70% yield; d) CH₂Cl₂/MeOH, KCN, 3h, rt, quantitative.

bearing terminal azido and alkynyl groups, respectively, using Cu(I) ion as template, generating the pseudorotaxanes **21** and **22**. An intermolecular double “click” macrocyclization reaction between **21** and **22** using the optimized conditions for synthesis of rotaxane **9** (see Table 1, Entry 6), except at 20 times greater dilution, afforded **23**. This [3]catenane structure consists of two smaller rings bearing different functional groups interlocked with a 74-membered central ring containing the two triazole linkers.

Evidence supporting the structure assignment of the isolated product as a metallated [3]catenane **23** came from the comparison of the ¹H NMR data for the product and the macrocyclic precursor **19**. The ¹H NMR spectrum of the isolated product (Figure 14) has features indicative of two

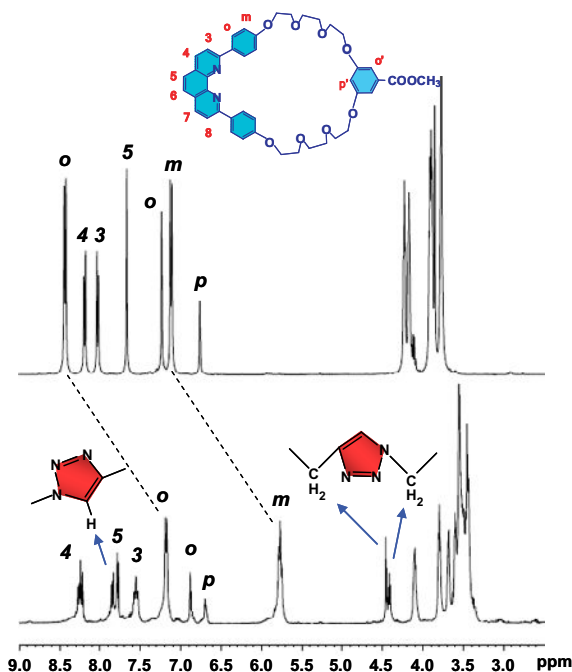


Figure 14. ^1H NMR spectra (400 MHz, 298 K, CD_3CN) of macrocycle **19** (top) and *non-symmetrical* [3]catenane **23** (bottom).

diphenylphenanthroline (dpp) moieties entwined around a Cu(I) center (in particular the phenyl protons identified as *o* and *m* in Figure 14 show fielding effects similar to those in other metalocatenanes and rotaxanes),^{58,81,88–90,100,124} the oxyethyl linkers, and the triazole ring proton resonance at 7.8 ppm.

MALDI-TOF analysis confirmed the postulated *nonsymmetric* metallated [3]catenane structure **23** with peripheral carboxyl and carboxymethyl substituents. The MALDI-TOF spectrum of the isolated product exhibits peaks at m/z 3160 ($M - \text{PF}_6$)⁺, 2205 ($M - 2\text{PF}_6 - 823$, corresponding to ring opening and loss of one of the peripheral esterified macrocycles and one Cu ion), 1507 ($M - 2\text{PF}_6$)²⁺, 823 (M for the esterified macrocycle + Cu)⁺ and 809 (carboxylate-containing macrocycle + Cu)⁺.¹⁰¹

This large interlocked structure could be demetalated using the standard KCN procedure,^{81,89,90} generating the Cu-free [3]catenane **24**, demonstrating that the introduction of peripheral functional groups and the triazole rings does not noticeably alter the physical properties of the [3]catenane in solution. However, the ^1H NMR spectrum of **24** is highly complex, suggesting the molecule adopts several conformations in solution. Variable temperature

^1H NMR studies (298 – 233 K) in the same solvent show increasing broadening of the peaks as the temperature is lowered, further indication that the molecule exists in interconverting conformations.

This lack of order is presumably due to the large size and shape of the macrocycle components of [3]catenand **24**. The three rings are apparently free to reorient around and through one another at a rate which is fast on the ^1H NMR time scale, even at temperatures as low as 213 K in CDCl_3 . These relatively facile conformational changes are desirable features, making the peripheral groups available for further reactions. This opens up the possibility of using functionalized [3]catenanes as synthetic building blocks, even after removing the metal-template ion needed to assemble the structure. The MALDI-TOF spectrum of **24** (Figure 15) clearly supports the assigned Cu-free structure: the peak at 2890 corresponds to [3]catenane **24** ($M + \text{H}$) $^+$; two peaks at 2144 ($M - 746 + \text{H}$) $^+$ and 2130 ($M - 760 + \text{H}$) $^+$, correspond to the [2]catenane fragments comprised of the large central macrocycle and the smaller attached macrocycles, while peaks at 761 and 747 correspond to the individual protonated macrocycles.

These results show that our methodology allows the preparation of *nonsymmetrical* [3]catenates, paving the way for the preparation of higher interlocked D-A systems. To demonstrate that peripheral functional groups on [3]catenates can be used for attachment of additional chromophores, the amine-ZnP derivative **25** (Figure 16) was coupled with the carboxylic acid group on metalated-[3]catenate **23**, using

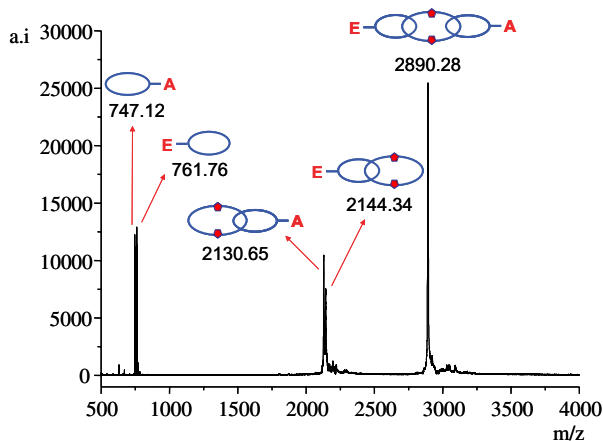


Figure 15. MALDI-TOF mass spectrum of triazole-linked Cu-free [3]catenand **24** (positive mode, α -cyano-4-hydroxycinnamic acid matrix). **A** = carboxyl group and **E** = carbomethoxy ester group.

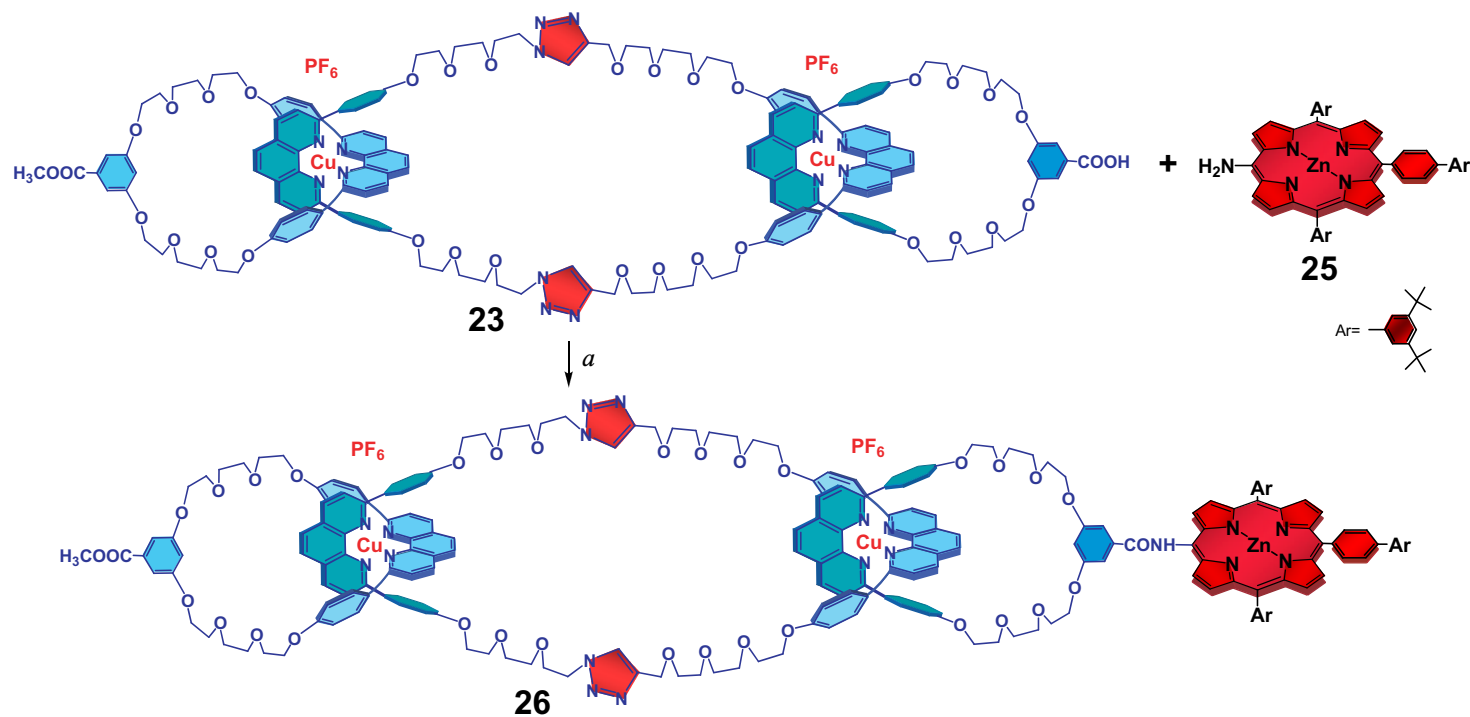


Figure 16. Introduction of a porphyrin moiety into a [3]catenane structure *via* amide coupling reaction with peripheral carboxylic acid group.
a) EDC, DMAP, CH_2Cl_2 , rt, 10h.

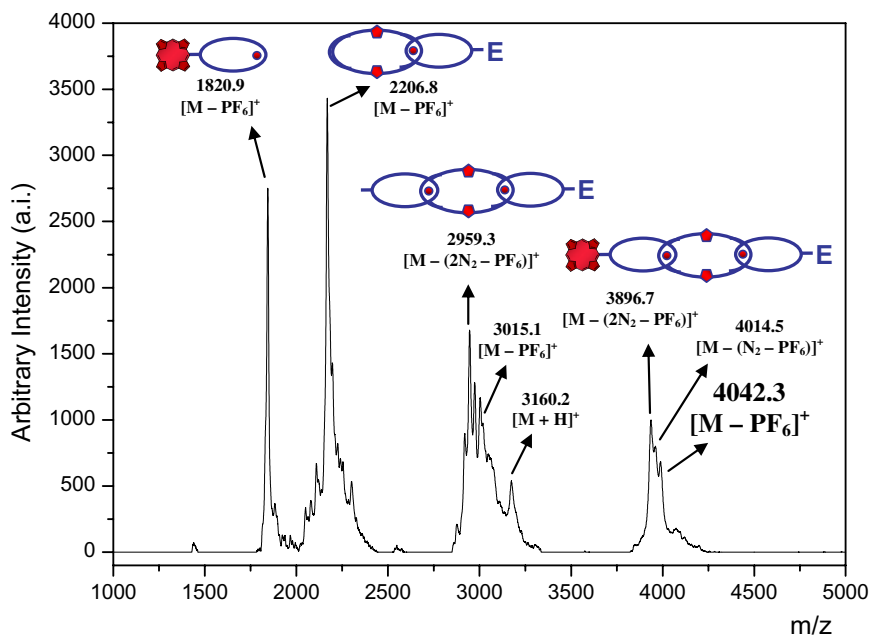


Figure 17. MALDI-TOF spectrum of ZnP-[3]catenane **26**. Positive mode, α -cyano-4-hydroxycinnamic acid matrix (CCA). E = carboxyl-methyl ester group.

1-ethyl-3-(3-dimethylaminopropyl)carbodiimide (EDC) as coupling agent and 4-dimethylaminopyridine (DMAP) as base in DCM at room temperature, to give the ZnP-[3]catenane **26** in 60% yield.

Compound **26** was characterized by MALDI-TOF spectrometry. The spectrum (Figure 17) shows a peak at m/z 4042.3, corresponding to the target structure **26** ($M - PF_6$)⁺, while the peak at m/z 1820.9 assigned to the ZnP-macrocycle ($M + Cu$)⁺ is strong evidence for the successful formation of the amide linkage. The characteristic fragmentation pattern of catenanes is also observed. Loss of N_2 molecules from the triazole rings suggest fragmentation of the larger central ring occurs through cleavage of the triazole rings.^{119,120}

These results prompted us to use the same methodology to introduce C_{60} moieties on [3]catenanes, in order to prepare new materials for long distance electron transfer studies. Two different strategies (Figure 18) were conceived starting from the same set of building blocks used to prepare [2] and [3]catenanes **17** and **23** (Figures 10 and 13, respectively). In the first approach (Strategy A), nearly symmetrical *bis*- C_{60} -[3]catenane **28** was prepared in 34% yield by intermolecular macrocyclization reactions between the C_{60} -pseudorotaxanes

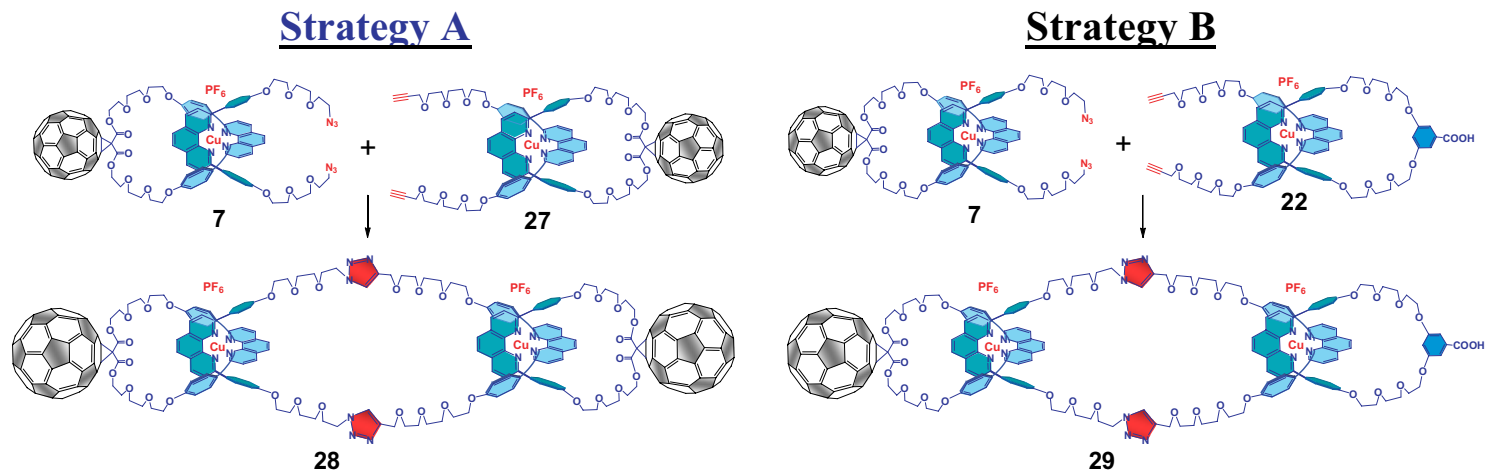


Figure 18. Synthesis of triazole-linked [3]catenates composed of C₆₀ subunits. Strategy A affords nearly symmetrical *bis*-C₆₀-[3]catenate, while Strategy B allows the preparation of a nonsymmetrical [3]catenate **29** bearing one C₆₀ appended group.

7 and 27.¹⁰⁷ Using Strategy B, the [3]catenate **29**, comprising three different rings, one of which contains an appended C₆₀ group and the other a peripheral carboxylate group, was obtained in 24% yield.

In the case of *bis*-C₆₀-[3]catenate **28**, the usual workup⁵⁸ followed by column chromatography, afforded three major components, which were identified by MALDI-TOF analysis, along with minor unidentified byproducts. The first brownish fraction eluted was a mixture of C₆₀-macrocycle **4** (see Figure 5) and the 74-membered macrocycle **30** (Figure 19), revealing that some unthreading^{81,89,90} took place under the reaction conditions. The second brown fraction was the C₆₀-based [2]catenate **31** (Figure 19). Finally the target *bis*-C₆₀-[3]catenate **28** was isolated as a brown solid.

Chromatographic purification of the nonsymmetrical C₆₀-[3]catenate **29** proved to be much more difficult. After a succession of chromatographic purification procedures, five major fractions were isolated, along with unidentified byproducts. MALDI-TOF analysis of these fractions showed that the first fraction corresponded to a mixture of C₆₀-macrocycle **4** (Figure 5) and the 74-membered macrocycle **30** (Figure 19), as found in the case of **28**. The second fraction consisted of carboxylic acid macrocycle **20** (see Figure 13). The third brown fraction was identified as the C₆₀-[2]catenate **31**, while the fourth deep red fraction corresponded to the analogous carboxylic acid functionalized-[2]catenate **32** (Figure 19). The target [3]catenate **29** was finally isolated as a brown solid.

Both C₆₀-based [3]catenanes could be characterized by ¹H NMR and MALDI-TOF analysis. Due to the higher symmetry of the *bis*-C₆₀-[3]catenate **28**, its ¹H NMR spectrum (Figure 20) is simpler than that of the corresponding *mono*-C₆₀-[3]catenate **29**. Although the peaks are broad, the protons in the ¹H NMR spectrum of **28** that are considered to be probes for a Cu(I) interlocked structure could be identified.^{81,89–90,101} The two ddp groups entwined around the Cu(I) core, the methylene groups adjacent to the malonate moiety on the C₆₀-macrocycle and the triazole rings on the polyoxoethyleneglycol linkers, the triazole ring protons and the protons belonging to the polyoxoethyleneglycol linkers were all observed (for assignments, see Figure 20). Due to the large number of heteroatoms and the cyclic nature of [3]catenate **28**, we speculate that peak broadening is most likely due to the presence of paramagnetic Cu(II) impurities, which might come from residual copper catalyst used for the CuAAC reaction.¹³⁰ For the *mono*-C₆₀-[3]catenate **29**, similar considerations apply.

MALDI-TOF spectra again show that these multi-ring interlocked systems possess [Cu(phen)₂][PF₆]₂ and C₆₀ subunits. For coordination compounds, the

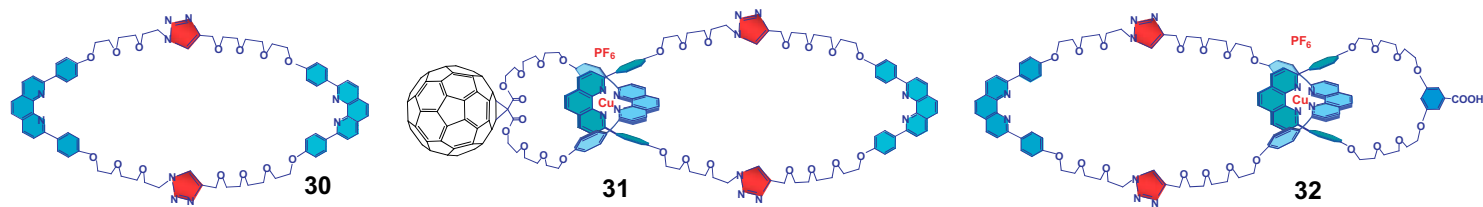


Figure 19. Cyclic and interlocked byproducts identified in the crude mixture resulting from the “click” macrocyclization reaction between pseudorotaxanes **7** and **22** or **7** and **27**.

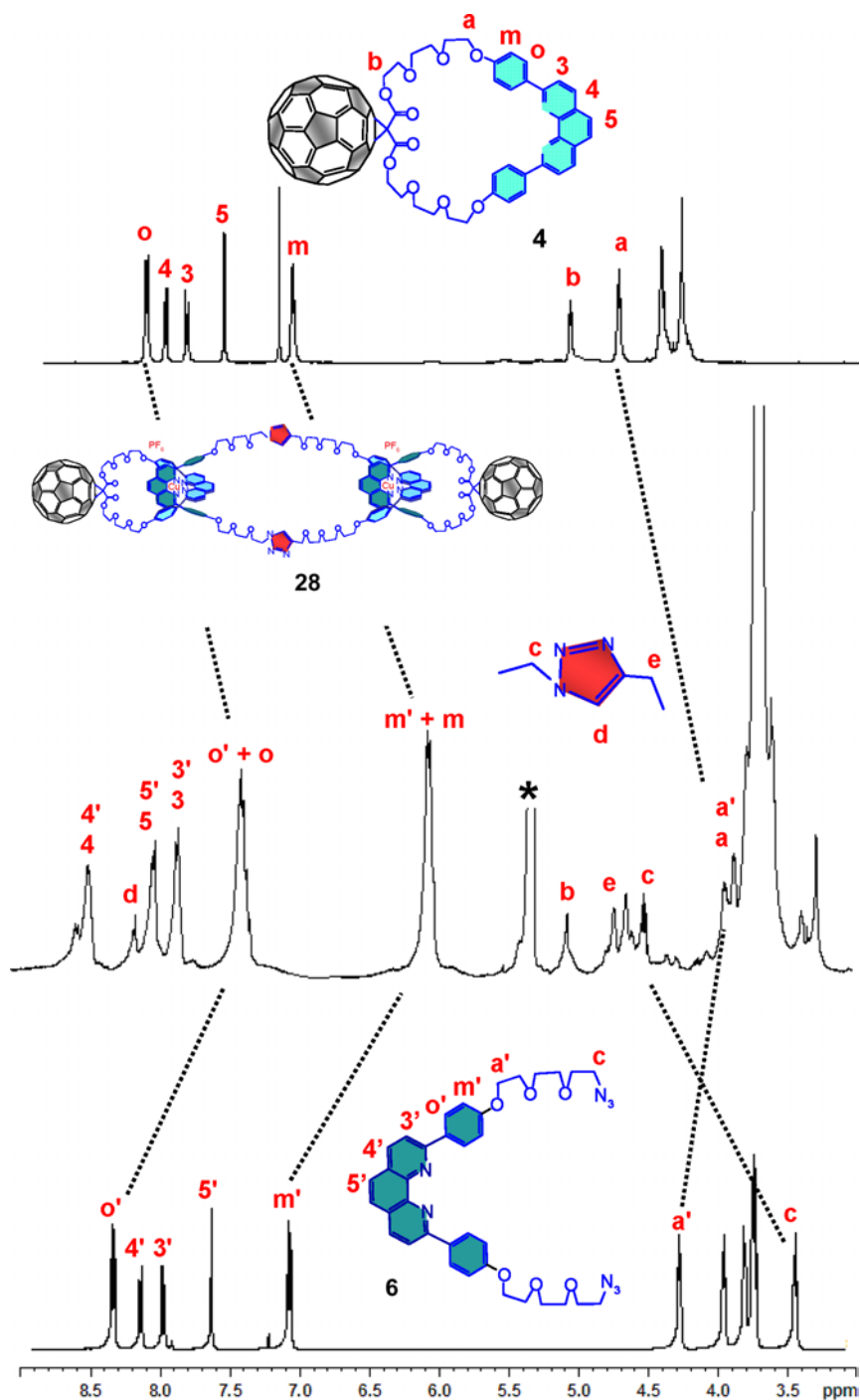


Figure 20. ^1H NMR spectrum of macrocycle **4**, [3]catenate **28** and thread **6** (800 MHz, CDCl_3 , 298 K).

ionization involves loss of the counterions (in this case, PF_6^- anions).¹¹⁷ Since the [3]catenates **28** and **29** each bear two positive charges, two values for the molecular ion are observed; one corresponds to the mono- positive ion (loss of one PF_6^- anion), resulting in a peak at m/z equal to the molecular mass; the other results from the loss of two PF_6^- anions, producing a double-charged species $[\text{M} + (2\text{Cu})]^{2+}$, corresponding to m/z equal to half the molecular mass.

In C_{60} -[3]catenates **28** and **29** similar MALDI-TOF results were obtained. In the case of **28**, the monopositive ion $(\text{M} - \text{PF}_6)^+$, was not detected, but a peak at m/z 1168.1, corresponding to $[\text{M} - (2\text{PF}_6)]^{2+}$ was observed. The fragmentation pattern features a peak at m/z 1477.3 attributed to the dissociated macrocycle **4** $(\text{M} + \text{Cu})^+$, suggesting fragmentation of the large central ring occurs under the conditions of analysis. Pristine C_{60} and the phen-based macrocycle are detected at m/z 721 and 697 $(\text{M} + \text{H})^+$, respectively, arising from cleavage of the methanofullerene group followed by release of C_{60} . The absence of peaks between the molecular ion peak and the peaks corresponding to the individual macrocycle fragments is characteristic of catenanes,¹¹⁸ and strongly supports the [3]catenane structure assignment to **28**, in which two smaller rings bearing peripheral C_{60} groups are interlocked with a large 74-atom central ring containing two triazole linkers.¹⁰⁷

9. Conclusion and Perspectives

In conclusion, a new powerful and versatile methodology for the preparation of nanoscale interlocked structures with [60]fullerene appendages has been developed, combining the virtues of both “click” chemistry and Sauvage’s Cu(I) template techniques. Under the conditions of this new protocol, the reactivity of C_{60} toward organic azides⁹⁸ was overcome and the stability problems of the Cu(I) pseudorotaxane precursors were minimized by accelerating the kinetics of the “click” cycloaddition reactions using a special catalyst mixture. The attractiveness of the method is exemplified by the preparation of the first ZnP-C_{60} -[2]catenane, bifunctional [3]catenates, a *bis*- C_{60} -substituted [3]catenane, as well as C_{60} -based rotaxanes.

The possibility of introducing different peripheral functional groups into the higher interlocked structures allows the preparation of structurally more elaborate materials, such as ZnP-C_{60} -[3]catenate **35** (see Figure 21). Two strategies are currently being explored in order to afford **35**. In Strategy A, the amine-ZnP derivative **25** is attached to the carboxylic group of the *nonsymmetrical* C_{60} [3]catenate **29** using classical coupling reagents. In Strategy B,

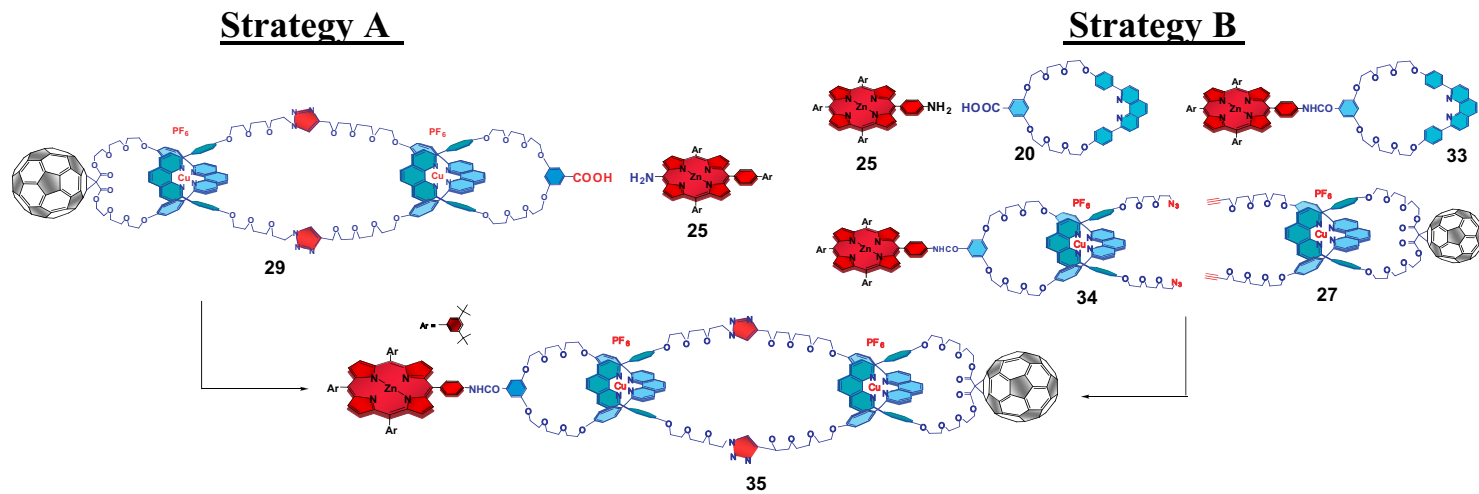


Figure 21. Two strategies for preparation of ZnP-C₆₀-[3]catenates.

the ZnP and C₆₀ appended groups are first introduced on the phen-macrocycles that are then used to generate pseudorotaxanes functionalized with terminal azido and alkynyl groups, **34** and **27**, respectively. CuAAC macrocyclization would then afford **35** in one step. The complete synthesis of ZnP-C₆₀-[3]catenates, as well as their photochemical and electrochemical properties will be reported in due course.

References

1. Hide, F.; DiazGarcia, M. A.; Schwartz, B. J.; Heeger, A. J. *Acc. Chem. Res.* **1997**, *30*, 430–436.
2. Armaroli, N.; Balzani, V. *Angew. Chem. Int. Ed.* **2007**, *46*, 52–66.
3. Whitesides, G. M.; Crabtree, G. W. *Science* **2007**, *315*, 796–798.
4. Flamigni, L.; Collin, J. P.; Sauvage, J.-P. *Acc. Chem. Res.* **2008**, *41*, 857–871.
5. Bredds, J. L.; Durrant, J. R. *Acc. Chem. Res.* **2009**, *42*, 1689–1690.
6. Dempsey, J. L.; Brunschwig, B. S.; Winkler, J. R.; Gray, H. B. *Acc. Chem. Res.* **2009**, *42*, 1995–2004.
7. Grätzel, M. *Acc. Chem. Res.* **2009**, *42*, 1788–1798.
8. Gust, D.; Moore, T. A.; Moore, A. L. *Acc. Chem. Res.* **2009**, *42*, 1890–1898.
9. Lewis, N. S. *Science* **2007**, *315*, 798–801.
10. Wasielewski, M. R. *Acc. Chem. Res.* **2009**, *42*, 1910–1921.
11. Hader, D. P.; Tevini, M. *General Photobiology*. NY: Pergamon: Elmsford, **1987**.
12. Fleming, G. R.; Martin, J. L.; Breton, J. *Nature* **1988**, *333*, 190–192.
13. Deisenhofer, J.; Michel, H. *Angew. Chem. Int. Ed.* **1989**, *28*, 829–847.
14. Feher, G.; Allen, J. P.; Okamura, M. Y.; Rees, D. C. *Nature* **1989**, *339*, 111–116.
15. Balzani, V.; Scandola, F., Eds.; *Supramolecular Photochemistry*. Horwood: Chichester, U.K., **1991**.
16. Moser, C. C.; Keske, J. M.; Warncke, K.; Farid, R. S.; Dutton, P. L. *Nature* **1992**, *355*, 796–802.
17. Wasielewski, M. R. *Chem. Rev.* **1992**, *92*, 435–461.
18. Gust, D.; Moore, T. A.; Moore, A. L. *Acc. Chem. Res.* **2001**, *34*, 40–48.
19. Sauvage, J.-P.; Collin, J.-P.; Chambron, J. C.; Guillerez, S.; Coudret, C.; Balzani, V.; Barigelletti, F.; Cola, L. D.; Flamigni, L. *Chem. Rev.* **1994**, *94*, 993–1019.
20. Collin, J.-P.; Harriman, A.; Heitz, V.; Odobel, F.; Sauvage, J.-P. *J. Am. Chem. Soc.* **1994**, *116*, 5679–5690.
21. Schuster, D. I.; Cheng, P.; Wilson, S. R.; Prokhorenko, V.; Katterle, M.; Holzwarth, A. R.; Braslavsky, S. E.; Klihm, G.; Williams, R. M.; Luo, C. P. *J. Am. Chem. Soc.* **1999**, *121*, 11599–11600.
22. Tsue, H.; Imahori, H.; Kaneda, T.; Tanaka, Y.; Okada, T.; Tamaki, K.; Sakata, Y. *J. Am. Chem. Soc.* **2000**, *122*, 2279–2288.
23. Luo, C.; Guldi, D. M.; Imahori, H.; Tamaki, K.; Sakata, Y. *J. Am. Chem. Soc.* **2000**, *122*, 6535–6551.
24. Schuster, D. I.; Cheng, P.; Jarowski, P. D.; Guldi, D. M.; Luo, C.; Echegoyen, L.; Pyo, S.; Holzwarth, A. R.; Braslavsky, S. E.; Williams, R. M.; Klihm, G. *J. Am. Chem. Soc.* **2004**, *126*, 7257–7270.

25. Hagemann, M.; Jørgensen, O. M.; Krebs, F. C. *J. Org. Chem.* **2006**, *71*, 5546–5559.
26. Schuster, D. I.; Li, K.; Guldi, D. M.; Palkar, A.; Echegoyen, L.; Stanisky, C.; Cross, R. J.; Niemi, M.; Tkachenko, N. V.; Lemmetyinen, H. *J. Am. Chem. Soc.* **2006**, *129*, 15973–15982.
27. Vail, S. A.; Schuster, D. I.; Guldi, D. M.; Isosomppi, M.; Tkachenko, N.; Lemmetyinen, H.; Palkar, A.; Echegoyen, L.; Chen, X.; Zhang, J. Z. H. *J. Phys. Chem. B* **2006**, *110*, 14155–14166.
28. Sgobba, V.; Giancane, G.; Conoci, S.; Casilli, S.; Ricciardi, G.; Guldi, D. M.; Prato, M.; Valli, L. *J. Am. Chem. Soc.* **2007**, *129*, 3148–3146.
29. Fazio, M. A.; Lee, O. P.; Schuster, D. I. *Org. Lett.* **2009**, *11*, 1041–1041.
30. Subbaiyan, N. K.; Wijesinghe, C. A.; D'Souza, F. *J. Am. Chem. Soc.* **2009**, *131*, 14646–14647.
31. (a) Marcus R. A. *J. Chem. Phys.* **1956**, *24*, 966–978; (b) Marcus, R. A. *Angew. Chem. Int. Ed.* **1993**, *32*, 1111–1121.
32. Astruc, D. *Electron Transfer and Radical Processes in Transition-Metal Chemistry*, New York: Wiley VCH, **1995**.
33. Hagfeldt, A.; Grätzel, M. *Chem. Rev.* **1995**, *95*, 49–68.
34. Imahori, H.; Sakata, Y. *Adv. Mater.* **1997**, *9*, 537–546.
35. Echegoyen, L.; Echegoyen, L. E. *Acc. Chem. Res.* **1998**, *31*, 593–601.
36. Guldi, D. M. *Chem. Commun.* **2000**, *5*, 321–327.
37. Guldi, D. M.; Prato, M. *Acc. Chem. Res.* **2000**, *33*, 695–703.
38. Guldi, D. M. *Chem. Soc. Rev.* **2002**, *31*, 22–36.
39. Balzani, V. *Electron Transfer in Chemistry*, Vol. 1–5., Weinheim, Germany: Wiley-VCH, **2003**.
40. Fukuzumi, S.; Ohkubo, K.; Imahori, H.; Guldi, D. M. *Chem. –Eur. J.* **2003**, *9*, 1585–1593.
41. Imahori, H.; Hagiwara, K.; Akiyama, T.; Aoki, M.; Taniguchi, S.; Okada, T.; Shirakawa, M.; Sakata, Y. *Chem. Phys. Lett.* **1996**, *263*, 545–550.
42. Hagfeldt, A.; Grätzel, M. *Acc. Chem. Res.* **2000**, *33*, 269–277.
43. Beletskaya, I.; Tyurin, V. S.; Tsivadze, A. Y.; Guillard, R.; Stern, A. C. *Chem. Rev.* **2009**, *109*, 1659–1731.
44. McMillin, D. R.; McNett, K. M. *Chem. Rev.* **1998**, *98*, 1201–1220.
45. Armaroli, N. *Chem. Soc. Rev.* **2001**, *30*, 113–124.
46. Lehn, J.-M. *Supramolecular Chemistry*, Weinheim, Germany: Wiley-VCH, **1995**.
47. Fyfe, M. C. T.; Stoddart, J. F. *Acc. Chem. Res.* **1997**, *30*, 393–401.
48. Badjic, J. D.; Nelson, A.; Cantrill, S. J.; Turnbull, W. B.; Stoddart, J. F. *Acc. Chem. Res.* **2005**, *38*, 723–732.
49. Philp, D.; Stoddart, J. F. *Angew. Chem. Int. Ed.* **1996**, *35*, 1154–1196.
50. Olmstead, M. M.; Costa, D. A.; Maitra, K.; Noll, B. C.; Phillips, S. L.; Van Calcar, P. M.; Balch, A. L. *J. Am. Chem. Soc.* **1999**, *121*, 7090–7097.
51. Boyd, P. D. W.; Hodgson, M. C.; Rickard, C. E. F.; Oliver, A. G.; Chaker, L.; Brothers, P. J.; Bolskar, R. D.; Tham, F. S.; Reed, C. A. *J. Am. Chem. Soc.* **1999**, *121*, 10487–10495.
52. Guldi, D. M.; Zerbetto, F.; Georgakilas, V.; Prato, M. *Acc. Chem. Res.* **2005**, *38*, 38–43.
53. Sanchez, L.; Otero, R.; Gallego, J. M.; Miranda, R.; Martin, N. *Chem. Rev.* **2009**, *109*, 2081–2091.
54. D'Souza, F.; Subbaiyan, N. K.; Xie, Y. S.; Hill, J. P.; Ariga, K.; Ohkubo, K.; Fukuzumi, S. *J. Am. Chem. Soc.* **2009**, *131*, 16138–16146.

55. Kira, A.; Umeyama, T.; Matano, Y.; Yoshida, K.; Isoda, S.; Park, J. K.; Kim, D.; Imahori, H. *J. Am. Chem. Soc.* **2009**, *131*, 3198–3199.
56. Wilson, S. R.; MacMahon, S.; Tat, F. T.; Jarowski, P. D.; Schuster, D. I. *Chem. Commun.* **2003**, *2*, 226–227.
57. Regev, A.; Galili, T.; Levanon, H.; Schuster, D. I. *J. Phys. Chem. A* **2006**, *110*, 8593–8598.
58. Megiatto, Jr., J. D.; Schuster, D. I.; Abwandner, S.; Miguel, G. de; Guldi, D. M. *J. Am. Chem. Soc.* **2010**, *132*, 3847–3861.
59. Li, K.; Bracher, P. J.; Guldi, D. M.; Herranz, M. A.; Echegoyen, L.; Schuster, D. I. *J. Am. Chem. Soc.* **2004**, *126*, 9156–9157.
60. Li, K.; Schuster, D. I.; Guldi, D. M.; Herranz, M. A.; Echegoyen, L. *J. Am. Chem. Soc.* **2004**, *126*, 3388–3389.
61. Schuster, D. I.; Li, K.; Guldi, D. M. *Org. Lett.* **2004**, *6*, 1919–1922.
62. Schuster, D. I.; Li, K.; Guldi, D. M. *C. R. Chim.* **2006**, *9*, 892–908.
63. Jakob, M.; Berg, A.; Rubin, R.; Levanon, H.; Li, K.; Schuster, D. I. *J. Phys. Chem. A* **2009**, *113*, 5846–5854.
64. Amabilino, D. B.; Stoddart, J. F. *Chem. Rev.* **1995**, *95*, 2725–2828.
65. Stoddart, J. F. *Chem. Soc. Rev.* **2009**, *38*, 1802–1820.
66. Fang, L.; Olson, M. A.; Benitez, D.; Tkatchouk, E.; Goddard, W. A., III; Stoddart, J. F. *Chem. Soc. Rev.* **2010**, *39*, 17–29.
67. Balzani, V.; Gomez-Lopez, M.; Stoddart, J. F. *Acc. Chem. Res.* **1998**, *31*, 405–414.
68. Collin, J. P.; Dietrich-Buchecker, C.; Gavina, P.; Jimenez-Molero, M. C.; Sauvage, J.-P. *Acc. Chem. Res.* **2001**, *34*, 477–487.
69. Balzani, V.; Credi, A.; Venturi, M. *Molecular Devices and Machines-A Journey into the Nano World*, Weinheim, Germany: Wiley-VCH, **2003**.
70. Leigh, D. A.; Wong, J. K. Y.; Dehez, F.; Zerbetto, F. *Nature* **2003**, *424*, 174–179.
71. Thordarson, P.; Bijsterveld, E. J. A.; Rowan, A. E.; Nolte, R. J. M. *Nature* **2003**, *424*, 915–918.
72. Badijic, J. D.; Credi, V.; Silvi, S.; Stoddart, J. F. *Science* **2004**, *303*, 1845–1849.
73. Champin, B.; Mobian, P.; Sauvage, J.-P. *Chem. Soc. Rev.* **2007**, *36*, 358–366.
74. Serreli, V.; Lee, C. F.; Kay, E. R.; Leigh, D. A. *Nature* **2007**, *445*, 523–527.
75. Mateo-Alonso, A.; Fioravanti, G.; Marcaccio, M.; Paolucci, F.; Jagesar, D. C.; Brouwer, A. M.; Prato, M. *Org. Lett.* **2006**, *8*, 5173–5176.
76. Mateo-Alonso, A.; Ehli, C.; Rahman, G. M. A.; Guldi, D. M.; Fioravanti, G.; Marcaccio, M.; Paolucci, F.; Prato, M. *Angew. Chem. Int. Ed.* **2007**, *46*, 3521–3525.
77. Mateo-Alonso, A.; Guldi, D. M.; Paolucci, F.; Prato, M. *Angew. Chem. Int. Ed.* **2007**, *46*, 8120–8126.
78. Mateo-Alonso, A.; Fioravanti, G.; Marcaccio, M.; Paolucci, F.; Rahman, G. M. A.; Ehli, C.; Guldi, D. M.; Prato, M. *Chem. Commun.* **2007**, *19*, 1945–1947.
79. Anderson, S.; Anderson, H. L.; Sanders, J. K. M. *Acc. Chem. Res.* **1993**, *26*, 469–475.
80. Sauvage, J.-P.; Dietrich-Buchecker, C. O. *Molecular Catenanes, Rotaxanes and Knots*, Weinheim, Germany: Wiley-VCH, **1999**.
81. Dietrich-Buchecker, C. O.; Sauvage, J.-P. *Chem. Rev.* **1987**, *87*, 795–810.
82. Amabilino, D. B.; Ashton, P. R.; Boyd, S. E.; Lee, J. Y.; Menzer, S.; Stoddart, J. F.; Williams, D. J. *Angew. Chem. Int. Ed.* **1997**, *36*, 2070–2072.
83. Raymo, F. M.; Stoddart, J. F. *Chem. Rev.* **1999**, *99*, 1643–1663.

84. Feringa, B. L. *Acc. Chem. Res.* **2001**, *34*, 504–513.
85. Rowan, S. J.; Cantrill, S. J.; Cousins, G. R. L.; Sanders, J. K. M.; Stoddart, J. F. *Angew. Chem. Int. Ed.* **2002**, *41*, 898–952.
86. Lankshear, M. D.; Beer, P. D. *Acc. Chem. Res.* **2007**, *40*, 657–668.
87. Crowley, J. D.; Goldup, S. M.; Lee, A. L.; Leigh, D. A.; McBurney, R. T. *Chem. Soc. Rev.* **2009**, *38*, 1530–1541.
88. Dietrich-Buchecker, C. O.; Sauvage, J.-P.; Kintzinger, J.-P. *Tetrahedron Lett.* **1983**, *24*, 5095–5098.
89. Dietrich-Buchecker, C.O.; Sauvage, J.-P.; Kern, J. M. *J. Am. Chem. Soc.* **1984**, *106*, 3043–3045.
90. Dietrich-Buchecker, C.O.; Sauvage, J.-P. *Tetrahedron* **1990**, *46*, 503–512.
91. Balzani, V.; Juris, A.; Venturi, M.; Campagna, S.; Serroni, S. *Chem. Rev.* **1996**, *96*, 759–833.
92. Serroni, S.; Campagna, S.; Puntoriero, F.; Di Pietro, C.; McClenaghan, N. D.; Loiseau, F. *Chem. Soc. Rev.* **2001**, *30*, 367–375.
93. Armaroli, N. *Photochem. Photobiol. Sci.* **2003**, *2*, 73–87.
94. Rothmund, P. *J. Am. Chem. Soc.* **1936**, *58*, 625–627.
95. Adler, A. D.; Longo, F. R.; Finarelli, J. D.; Goldmacher, J.; Assour, J. *J. Org. Chem.* **1967**, *32*, 476–476.
96. Lindsey, J. S. *Acc. Chem. Res.*, **2010**, *43*, 300–311.
97. Guldi, D. M.; Martin, N. *Fullerenes: From Synthesis to Optoelectronic Properties*, Dordrecht, The Netherlands: Kluwer Academic Publishers, **2002**.
98. Hirsch, A.; Brettreich, M. *Fullerenes*, Weinheim, Germany: Wiley-VCH, **2005**.
99. Megiatto, Jr., J. D.; Schuster, D. I. *J. Am. Chem. Soc.* **2008**, *130*, 12872–12873.
100. Megiatto, Jr., J. D.; Spencer, R.; Schuster, D. I. *Org. Lett.* **2009**, *11*, 4152–4155.
101. Megiatto, Jr., J. D.; Schuster, D. I. *Chem. –Eur. J.* **2009**, *15*, 5444–5448.
102. Megiatto, Jr., J. D.; Schuster, D. I. *New J. Chem.* **2010**, *34*, 276–286.
103. Huisgen, R. *Angew. Chem. Int. Ed.* **1968**, *7*, 321–328.
104. Kolb, H. C.; Finn, M. G.; Sharpless, K. B. *Angew. Chem. Int. Ed.* **2001**, *40*, 2004–2021.
105. Tornøe, C. W.; Christensen, C.; Meldal, M. *J. Org. Chem.* **2002**, *67*, 3057–3064.
106. Meldal, M.; Tornøe, C. W. *Chem. Rev.* **2008**, *108*, 2952–3015.
107. Megiatto, Jr., J. D.; Spencer, R.; Schuster, D. I. *J. Mater. Chem.* **2010**, in press.
108. Durot, S.; Mobian, P.; Collin, J. P.; Sauvage, J.-P. *Tetrahedron* **2008**, *64*, 8496–8503.
109. Collin, J. P.; Frey, J.; Heitz, V.; Sauvage, J.-P.; Tock, C.; Allouche, L. *J. Am. Chem. Soc.* **2009**, *131*, 5609–5620.
110. Prikhod'ko, A. I.; Sauvage, J.-P. *J. Am. Chem. Soc.* **2009**, *131*, 6794–6807.
111. Chan, T. R.; Hilgraf, R.; Sharpless, K. B.; Fokin, V. V. *Org. Lett.* **2004**, *6*, 2853–2855.
112. Wu, P.; Fokin, V.V. *Aldrichim. Acta* **2007**, *40*, 7–17.
113. Lewis, W. G.; Magallon, F. G.; Fokin, V. V.; Finn, M. G. *J. Am. Chem. Soc.* **2004**, *126*, 9152–9153.
114. Lindsey, J. S.; Prathapan, S.; Johnson, T. E.; Wagner, R. W. *Tetrahedron* **1994**, *50*, 8941–8968.
115. Hanni, K. D.; Leigh, D. A. *Chem. Soc. Rev.* **2010**, *39*, 1240–1251.
116. Vetter, W.; Schill, G. *Tetrahedron* **1967**, *23*, 3079–3093.
117. Bitsch, F.; Dietrich-Buchecker, C. O.; Khemiss, A. K.; Sauvage, J.-P.; Vandorsselaer, A. *J. Am. Chem. Soc.* **1991**, *113*, 4023–4025.
118. Weck, M.; Mohr, B.; Sauvage, J.-P.; Grubbs, R. H. *J. Org. Chem.* **1999**, *64*, 5463–5471.

119. Yoo, E. J.; Ahlquist, M.; Kim, S. H.; Bae, I.; Fokin, V. V.; Sharpless, K. B.; Chang, S. *Angew. Chem. Int. Ed.* **2007**, *46*, 1730–1733.
120. Ornelas, C.; Aranzaes, J. R.; Cloutet, E.; Alves, S.; Astruc, D. *Angew. Chem. Int. Ed.* **2007**, *46*, 872–877.
121. Chambron, J. C.; Heitz, V.; Sauvage, J.-P. *J. Am. Chem. Soc.* **1993**, *115*, 12378–12384.
122. Schill, G.; Zurcher, C. *Angew. Chem. Int. Ed.* **1969**, *8*, 988–992.
123. Sauvage, J.P.; Weiss, J. *J. Am. Chem. Soc.* **1985**, *107*, 6108–6110.
124. Dietrich-Buchecker, C. O.; Hemmert, C.; Khemiss, A. K.; Sauvage, J.-P. *J. Am. Chem. Soc.* **1990**, *112*, 8002–8008.
125. Seel, C.; Parham, A. H.; Safarowsky, O.; Hübner, G. M.; Vögtle, F. *J. Org. Chem.* **1999**, *64*, 7236–7242.
126. Yamamoto, H.; Itoh, K.; Nagamiya, H.; Fukuzawa, Y. *Tetrahedron Lett.* **2003**, *44*, 5773–5776.
127. Blanco, V.; Chas, M.; Abella, D.; Peinador, C.; Quintela, J. M. *J. Am. Chem. Soc.* **2007**, *129*, 13978–13986.
128. Gupta, M.; Kang, S.; Mayer, M.F. *Tetrahedron Lett.* **2008**, *49*, 2946–2950.
129. Ornelas, C.; Broichhagen, J.; Weck, M. *J. Am. Chem. Soc.* **2010**, *132*, 3923–3931.

Chapter 8

Solubilized Carbon Nanotubes and Their Redox Chemistry

Naotoshi Nakashima, Yasuhiko Tanaka and Tsuyohiko Fujigaya*

*Department of Applied Chemistry, Kyushu University
Motooka, Fukuoka 819-0395, Japan*

1. Introduction	245
2. Characterizations of Individually Solubilized Carbon Nanotubes	247
3. Individual Solubilization of SWNTs Using Surfactant Micelles	247
4. DNA/Carbon Nanotube Hybrids	249
5. Individual Solubilization of SWNTs Using Functional Aromatic Molecules	251
6. Nanotube/Polymer Composites	254
7. Redox Reaction and Determination of Electronic States of Carbon Nanotubes	254
8. Electrocatalyst for Fuel Cell using Soluble CNTs	258
9. Concluding Remarks	262
References	263

1. Introduction

CNTs are made of rolled-up graphene sheets with one-dimensional extended π -conjugated structures, discovered in 1991 by Iijima.¹ The materials are classified into mainly three types of CNTs in terms of the number of graphene

*Corresponding author. Email: nakashima-tcm@mail.cstm.kyushu-u.ac.jp

layers within CNTs, that is, single-walled carbon nanotubes (SWNTs), double-walled carbon nanotubes (DWNTs) and multi-walled carbon nanotubes (MWNTs), which have one, two and more than three walls, respectively. The electrical properties of SWNTs, which range from semiconducting to metallic depending on their chirality, should cause them to be excellent materials for nanowires, rectifying heterojunctions, field-effect transistors, and electronic devices. High Young's modulus and aspect ratios of CNTs make it possible to use them for the reinforcement of fibers. The use of SWNTs in biological applications such as gene delivery, cancer therapy and biosensors is also being exploited.

One of the key issues in the utilization of such novel nanomaterials for basic research as well as applications is to develop a methodology to solubilize/disperse them in solvents (Figure 1)²⁻⁴ since CNTs that have just been synthesized form tight bundled structures⁵ due to their strong van der Waals interaction (0.9 eV/nm).⁶ Solubilization/dispersion techniques of the nanotubes toward their functionalization can be categorized mainly into two methods, namely 'chemical (covalent) functionalization' and 'physical (non-covalent) functionalization'. Solubilization/dispersion of CNTs based on physical adsorption of dispersant molecules has advantages such as ease of preparation and remaining intrinsic CNT properties, which show sharp contrast with covalent modification.⁷⁻⁹

In this review article, we first describe general strategies for CNT solubilization and then our recent studies on electrochemical applications using solubilized CNTs, namely, experimental determination of precise redox states of individual SWNTs and fabrication of a novel electrocatalyst for fuel cells using polybenzimidazole-wrapped soluble carbon nanotubes as materials. Carbon nanotubes are interesting materials in electrochemistry and other related areas. Several review articles covering this topic having been published.¹⁰⁻¹⁵

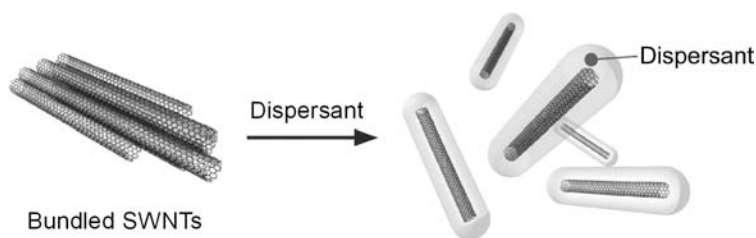


Figure 1. Schematic illustration showing individual solubilization of SWNTs using a dispersant.

2. Characterizations of Individually Solubilized Carbon Nanotubes

Typical procedures for the preparation of individual solutions of CNTs are ultrasonication of the CNTs in a dispersant solution, followed by centrifugation to give grey- or colorless transparent supernatant solutions. Individually solubilized/dispersed CNTs are visualized by atomic force microscopy (AFM)^{16,17} and transmission electron microscopy (TEM).^{18,19} Near-IR (NIR) absorption and photoluminescence (PL) spectroscopy are strong tools to evaluate the dispersion states of SWNTs in both solution and films. Bachilo *et al.*²⁰ and O'Connell *et al.*²¹ revealed that PL in the NIR region is detected from surfactant-dissolved SWNTs and then succeeded in the determination of the SWNT chirality indices (n,m). Only individually dissolved semiconducting-SWNTs and small bundled SWNTs in some case²² exhibit PL since bundled SWNTs cause PL quenching by the metallic-SWNTs in the bundles. The PL observation serves as an excellent indicator of the individual solubilization of SWNTs in solution as well as in films.^{23,24} Nowadays, it is possible to detect the PL from a single SWNT molecule dissolved in solution and immobilized in a gel by combining an inversed microscope technique.^{25–27} Even in the absence of PL signals due to the bundling, UV-visible NIR absorption spectroscopy is quite helpful for roughly evaluating the degree of bundling of SWNTs both in solution and film states.²⁸

3. Individual Solubilization of SWNTs Using Surfactant Micelles

SWNTs are individually solubilized by the aid of a variety of dispersants (Figure 2). The most convenient and frequently-used solubilizer for SWNTs in water include surfactants such as sodium dodecyl sulfate (SDS),^{29–31} sodium

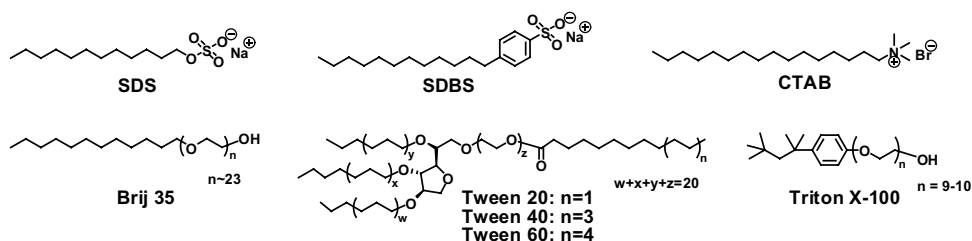


Figure 2. Chemical structures of surfactants for CNTs solubilization.

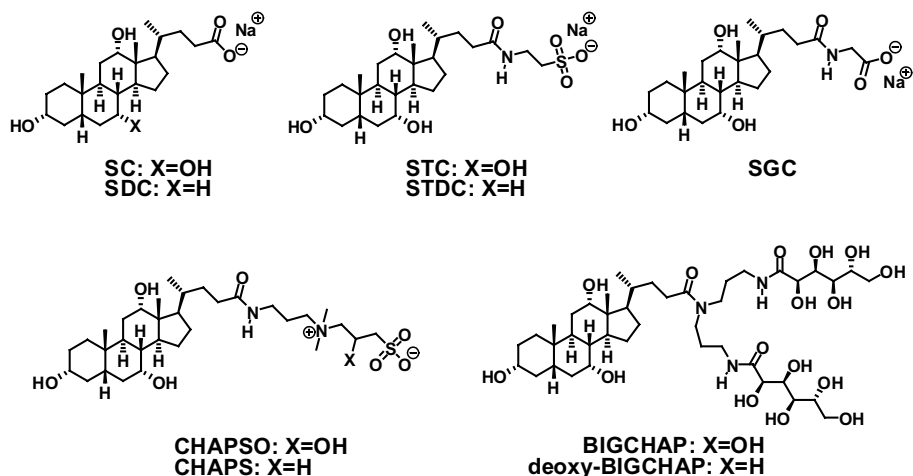
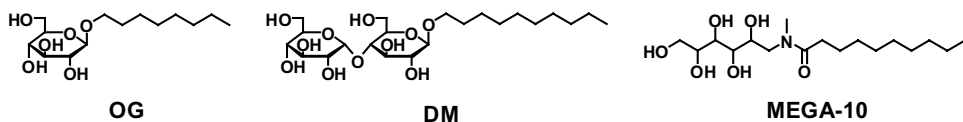
Bile saltsNonionic biosurfactants

Figure 3. Chemical structures of biological surfactants for CNTs solubilization.

dodecylbenzene sulfonate (SDBS),^{18,32–35} octadecyltrimethylammonium bromide,^{18,36} Brij,^{18,37} Tween,^{18,37} and Triton X.^{18,32,37,38} Among them, SDBS is one of the most efficient SWNT solubilizers. Biological surfactants such as bile salts also act as SWNT solubilizers in water (Figure 3).^{37,39,40} We reported solubilization/dispersion of SWNTs using aqueous micelles of anionic-, zwitter ionic- and nonionic steroid biosurfactants as well as sugar biosurfactants including sodium cholate (SC), sodium deoxycholate, sodium taurocholate, sodium taurodeoxycholate, sodium glycocholate, *N,N*-bis(3-D-gluconamidopropyl)cholamide and *N,N*-bis(3-D-gluconamidopropyl)deoxycholamide, *n*-octyl-β-D-glucoside, *n*-decyl-β-D-maltoside, *n*-decanoyl-*N*-methylglucamide, 3-[(3-cholamidopropyl)dimethylammonio]propanesulfonic acid and 3-[(3-cholamidopropyl)dimethylammonio]-2-hydroxypropanesulfonic acid. The chemical structures, especially, the substituent groups of the bile salts play an important role in the solubilization of SWNTs.^{2,3,39,40}

4. DNA/Carbon Nanotube Hybrids

The combination of CNTs and DNA (or RNA) is of fundamental and applied interest in many chemical and biochemical areas. We have reported the finding that double-stranded DNA (dsDNA) molecules dissolve single-walled carbon nanotubes (SWNTs) in aqueous solutions.⁴¹ Figure 4 shows a schematic drawing of a dsDNA-wrapped SWNT. Electrochemical deposition of SWNTs/dsDNA complexes by poly(ethylenedioxythiophene) (poly(EDOT)) on an ITO electrode is possible.⁴² A number of groups have now used this scheme in their studies of various dsDNA and CNTs structures. Barisci *et al.*⁴³ fabricated SWNTs/dsDNA fibers that were mechanically strong and conductive, and exhibited useful capacitance values up to 7.2 Fg^{-1} . Iijima *et al.*⁴⁴ showed high-resolution TEM and STM images of dsDNA/multi-walled CNTs. Gladchenko *et al.*⁴⁵ characterized fragmented dsDNA-wrapped SWNTs in aqueous solutions. He *et al.*⁴⁶ described the layer-by-layer fabrication and characterization of ds-wrapped SWNTs particles. Pantarotto *et al.*⁴⁷ described binding of plasmid DNA onto functionalized CNTs in the construction of CNT-based gene transfer vector systems. Rege *et al.*⁴⁸ reported *in vitro* transcription and protein translation from CNTs/DNA assemblies. Cathcart *et al.*⁴⁹ reported spontaneous dispersion of SWNTs by dsDNA.

At the same time as our report that dsDNA solubilizes SWNTs, Zheng *et al.*^{50,51} showed that single-stranded DNA (ssDNA) solubilizes SWNTs. After this report, many papers describing the properties of the SWNTs/ssDNA were published. An interesting finding is the ability to separate metallic- and semiconducting SWNTs using size-exclusion chromatography.⁵² Molecular modeling for the SWNTs/ssDNA composites suggests that ssDNA can bind to SWNTs through π -stacking, resulting in the helical wrapping of SWNTs.⁵⁰ Molecular dynamics simulation of DNA adsorption on a SWNT in aqueous environment is reported by Zhao and Johnson.⁵³ A binding model of a (10,0) SWNTs wrapped by a poly(T) was reported and the binding of ssDNA to SWNTs was probed by flow linear dichroism.^{54,55}

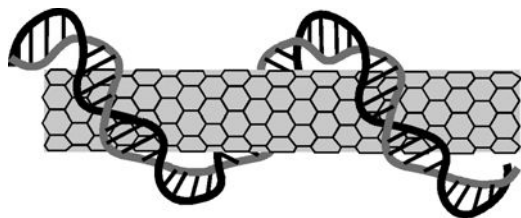


Figure 4. Possible structure of a dsDNA/SWNT hybrid. Adapted from Reference 77.

Detailed optical properties including near-IR absorption and photoluminescence (PL) and Raman study for CoMoCAT-SWNTs/ssDNA hybrids have been characterized.^{56, 57} Fagan *et al.*⁵⁸ described length-dependent optical effects in SWNTs dissolved in ssDNA (30 mer). SWNTs/ssDNA solutions were used to discuss about solution redox chemistry of CNTs⁵⁹, photoinduced charge transfer on an $\text{Ag}^+/\text{DNA}/\text{CNTs}$ complex⁶⁰, and electrocatalytic oxidation.⁶¹ Phonon-assisted excitation dynamics for (6,5)-enriched ssDNA-wrapped SWNTs has been discussed theoretically.^{62, 63} Adsorption behavior of ssDNA-wrapped SWNTs on substrates was examined using reflection absorption FTIR, XPS and Raman spectroscopy.^{64, 65} Optical detection of DNA conformational polymorphism on SWNTs was described by Strano *et al.*⁶⁵ Li *et al.* described the CNT-destabilized duplex and triplex DNAs inducing B-A transition in solution.⁶⁶ The DNA-immobilized aligned carbon nanotubes are useful for sensing complementary DNA and/or target DNA chains of specific sequences with a high sensitive and selectivity.⁶⁷ Fantini *et al.*⁶⁸ characterized GT-DNA oligomer-wrapped SWNTs by Raman and optical spectroscopies and revealed different interactions for semiconducting- and metallic SWNTs. Chou *et al.*⁶⁹ described length characterization of ssDNA-wrapped SWNTs using Raman spectroscopy. Racemic SWNTs exhibit circular dichroism when wrapped with ssDNA oligomer d(GT)₂₀.⁷⁰

Optical absorbance spectra of SWNTs dispersed by ssDNA homopolymers show anisotropic absorbance of SWNTs.⁷¹ Ishibashi *et al.* have constructed multilayer assemblies with alternating monolayers of poly(G)-wrapped SWNTs and of poly(C)-wrapped SWNTs on quartz based on the complementary base pairing between nucleic bases G and C, which would be applicable in wide fields of nanoscience and technology.⁷² SWNTs/ssDNA (RNA) solutions can be used as materials for gene and protein delivery and nanotherapy.⁷³ DNA (RNA)-CNT hybrids play important roles in the rapid development of nanotechnologies.⁷⁴ SWNTs/ssDNA induce the alignment of membrane proteins⁷⁵ and can serve as rigid templates for the self-assembly of gold nanoparticles.⁷⁶ Noguchi *et al.* described the modulation of near-IR optical properties of individually dissolved SWNTs in aqueous solutions of dsDNA.⁷⁷ Near-IR PL mapping of the individually solubilized SWNTs in pure water gave only one spot from the (6,5) SWNTs, and the PL behaviors dramatically changed with pH. A possible mechanism for the tunable near-IR optical behaviors is also reported.

5. Individual Solubilization of SWNTs Using Functional Aromatic Molecules

The surfaces of CNTs can be readily functionalized through π - π interactions with compounds having π -electron-rich structures due to the highly delocalized π -electrons of CNTs. The π - π interaction between polycyclic aromatic compounds and CNT sidewalls has been discussed based on both theoretical⁷⁸ and experimental⁷⁹ approaches. We reported that a pyrene-based ammonium salt (compound **1**, Figure 5) can solubilize SWNTs⁸⁰ and fullerene-filled CNTs (so-called peapods)⁸¹ in water. The pyrene-carrying compound acts as an efficient CNT solubilizer compared to naphthyl- and phenyl-based ammonium salts.⁸² This is due to the strong binding affinity between the pyrene group and the CNT sidewalls. Now pyrene derivatives have been widely recognized as excellent solubilizers for CNTs (see Figure 5, in which chemical structures of pyrene-carrying compounds that dissolve/disperse CNTs are shown).⁸⁰⁻⁸⁸ By taking advantage of the efficient adsorbing capability on the CNT surfaces, pyrene derivatives have been used as decent interlinkers to anchor functional materials that can communicate with CNTs.⁸⁹⁻¹⁰⁸ Other polycyclic aromatic moieties such as anthracene,^{109,110} terphenyl,^{110,111} perylene,¹¹² triphenylene,¹¹³ phenanthrene,¹¹⁴ and pentacene¹¹⁵ also have affinity for the sidewalls of CNTs and various solubilizers bearing these molecules have been developed. We have reported that green tea solution also acts as excellent SWNT dispersant.¹¹⁶ Our dissolution scenario is that catechin, a polycyclic aromatic compound, mainly contributes to the dispersion because epigallocatechin gallate also disperses the SWNTs in water.

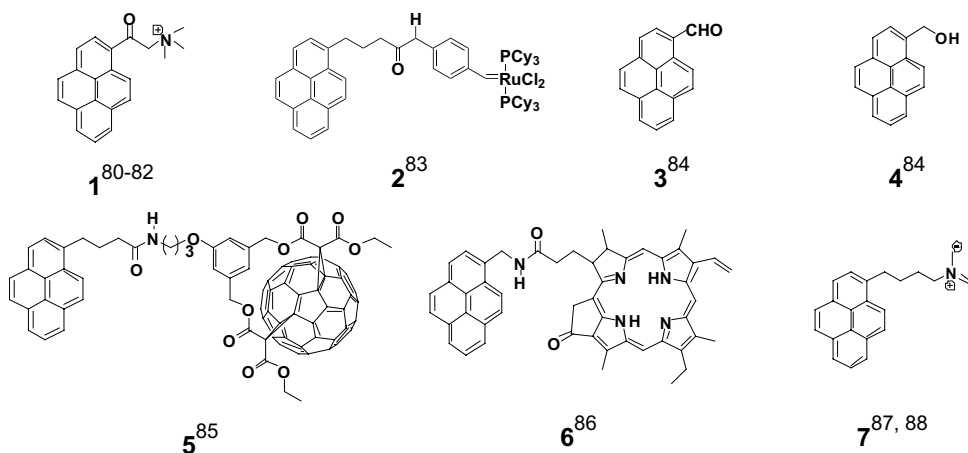
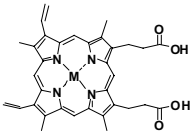
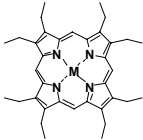
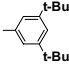


Figure 5. Pyrene-based dispersants for CNTs.

Porphyrin compounds are excellent SWNT solubilizers.¹¹⁷ We used zinc protoporphyrin IX (compound **8**, Table 1) and discovered that the compound can dissolve SWNTs individually. Fluorescence quenching of the porphyrin in the **8**/SWNT evidenced the adsorption of the porphyrin onto the surfaces of the SWNTs. A wide range of porphyrin derivatives including **9** and **10** (Table 1) also act as effective solubilizers for SWNTs.¹¹⁸ The finding lead to theoretical as well as experimental attempts to understand the interactions between porphyrins and CNTs.^{119–122} Importantly, π – π and charge-transfer interactions have been highlighted to serve the adsorption of porphyrin derivatives on the surfaces of CNTs.¹²² The center metals in the porphyrin also affect solubilization of CNTs.^{122,123}

The combination of porphyrin and CNTs has attracted intense interest due to the unique photophysical,^{92,124,125} electrochemical,^{126–128} electronic,^{124,129–131} and optical^{132,133} properties of the composites. Extensive efforts have been carried out on the photoinduced electron transfer from porphyrins to CNTs including not only for physically connected but covalently bonded porphyrin/CNT hybrids.¹²⁴ A porphyrin compound was used for the separation of CNT chirality based on molecular recognition,¹²³ by Peng *et al.*¹³⁴ who found that optically active porphyrin dimers compound **25**. recognize right- or left-handed helicity of racemic SWNT mixtures depending on the chirality of compound **25**. The chemical structures of porphyrins that dissolve/disperse CNTs are summarized in Table 1.

Table 1. Porphyrin-based CNT solubilizers.

Compound	Chemical structure	M	R	Ref.
8		Zn		117
9		2H		118
10		FeCl		118
11		Co		119
12		2H		124

(Continued)

Table 1. (Continued)

Compound	Chemical structure	M	R	Ref.
13		2H		135
14		Zn		129
15		2H		124
16		2H, Zn		133
17		2H, Zn		122
18		2H		124
19		4H		136
20		2H, Zn		123
21		2H, Zn		137
22		Zn		138
23		Zn		139
24				140
25		(R) : R ₁ =CH ₂ Ph, R ₂ =H, R ₃ =NHCO ₂ t-Bu (S) : R ₁ =H, R ₂ =CH ₂ Ph, R ₃ =NHCO ₂ t-Bu		134
26		2H		141

6. Nanotube/Polymer Composites

Many papers describing the nanocomposite formation of CNTs with condensation polymers such as polyesters and polyamides have been published.^{142–146} Most of them were prepared by melt mixing, polymer grafting and *in situ* polymerization methods. We have reported an extremely efficient individual dissolution of SWNTs by a totally aromatic polyimide (**PI-1** in Figure 6).¹⁴⁷ As much as 2.0 mg/mL of the SWNTs is individually dissolved in the 1.0 mg/mL DMSO solution of **PI-1**. The major driving force for the solubilization of SWNTs is attributed to a π - π interaction between the condensed aromatic moieties on the polyimide and the surfaces of SWNTs. Generally speaking, the composite films arising from the individual dispersion of CNTs would maximize the performances of the materials such as mechanical properties with minimum addition of the CNTs. For this reason, the precise analysis of the degree of dispersion will become a strong focus of interest also for other polyimide/CNT^{148–158} since polyimides are widely known to possess excellent mechanical strength and heat resistance.¹⁵⁹

Polybenzimidazole (**PBI** in Figure 6) is also recognized as a highly thermal stable polymer.¹⁶⁰ Different from the typical aromatic polyimides, **PBI** is soluble in common organic solvents such as DMAc, DMSO and DMF. We have reported that the **PBI** acts as a good dispersant for SWNTs due to the π - π interaction between the polymer and SWNT sidewalls.¹⁶¹ The vis-NIR absorption and PL spectra of a **PBI**/SWNT solution in DMAc clearly show the characteristic absorption peaks and strong PL spots, respectively, derived from the individual SWNTs. Effective dispersion of the SWNTs in the matrix **PBI** results in the dramatic reinforcement in the composite film. We have found that the addition of very small amounts of SWNTs (0.06 wt%) reinforces the mechanical properties of the original polymer by *ca.* 150% without reducing their thermal stabilities.

7. Redox Reaction and Determination of Electronic States of Carbon Nanotubes

The electronic states of CNTs, one of the most fundamental features of nanotubes, strongly depend on the chirality of the carbon nanotubes.¹⁶²

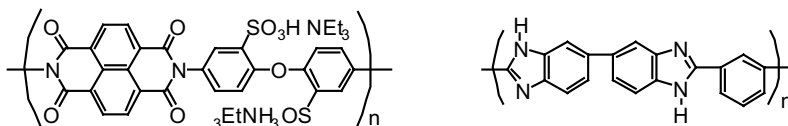


Figure 6. Chemical structure of **PI-1** (left) and **PBI** (right).

The electric properties of SWNTs are closely related to the structures of SWNTs that identified a specified diameter and chiral angle uniquely relating to a pair of integers (n,m): the so-called chirality indices. The first principle calculation explains well the electronic properties of SWNTs that are characterized by van Hove singularities.^{163–165} Several papers describing solution redox chemistry of SWNTs have been published.^{59,166–168} Kazaoui and coauthors¹⁶⁶ reported the absorption spectral changes of SWNTs induced by chemical oxidation. Zheng and coauthor⁵⁹ reported oxidation potentials of the (6,5)-enriched SWNT using chemical oxidation with an oxidant (K_2IrCl_6). They estimated an oxidation potential of (6,5)-SWNTs to be approximately 0.8 V *vs.* SHE (SHE = standard hydrogen electrode potential).

In situ spectroelectrochemistry of SWNTs is a powerful technique for investigating the potential-controlled electronic structures of the nanotubes and many spectroelectrochemical studies have been carried out using bundled CNTs as materials.^{168–172} For examples, Kavan and coauthors^{169,171} reported electrochemical-potential dependent Raman spectra of SWNT films on electrodes, and Murakoshi and coauthors¹⁷² reported chirality-dependent redox potentials and Fermi levels of semiconducting SWNTs on an electrode using electrochemical-Raman spectroscopy.

Although many groups have endeavored to understand the fundamental properties of CNTs and many attempts have been made to determine the electronic properties of SWNTs, it has not been easy to determine the redox potentials of isolated (n,m) SWNTs. In order to determine the electronic states of isolated (n,m) SWNTs, we fabricated a transparent indium tin oxide (ITO) electrode modified with a film of SWNT/carboxymethylcellulose sodium salt (CMC)/poly(diallyldimethylammonium chloride). From the near-IR PL spectrum of the film (Figure 7), it was found that the film contains isolated SWNTs whose chiralities are: (6,5), (8,3), (7,5), (8,4), (10,2), (7,6), (9,4), (10,3), (8,6), (9,5), (12,1), (11,3), (8,7), (10,5), and (9,7).¹⁷³

We carried out *in situ* near-IR absorption spectroelectrochemistry using the modified electrode.¹⁷³ The near-IR absorption spectra of the individually solubilized SWNTs were found to bleach when the external potential was applied to the electrode by arbitrary step from 0.0 V to -1.0 V and from 0.0 V to $+1.1$ V. Unfortunately, the determination of the redox potentials of the individual SWNTs having their own chirality indices was difficult because the near-IR absorption peaks from the nanotubes with several different chirality indices have bandgaps that overlap one another.

The PL of SWNTs is consistent with isolated SWNTs and therefore characterization of isolated SWNTs is possible. We carried out *in situ* near-IR PL

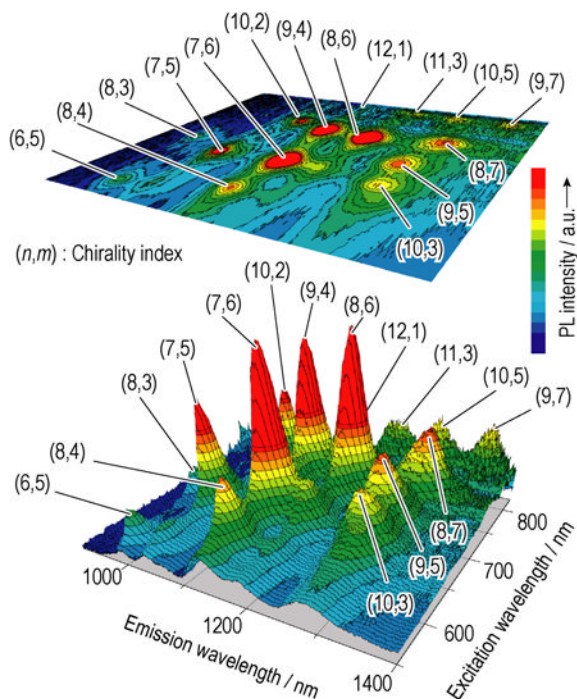


Figure 7. 2D contour (top) and 3D surface (bottom) plots of PL intensity as a function of emission and excitation wavelengths. The data were obtained for a film containing isolated SWNTs coated on an ITO electrode. Adapted from Reference 173.

spectroelectrochemistry in a way similar to the *in situ* near-IR absorbance spectroelectrochemistry. As a typical example, in Figure 8, we show the PL spectra of (7,5), (7,6), and (10,3)SWNTs at given applied potentials from 0.0 to -1.0 V and then from 0.0 to $+1.1$ V. It is evident that the PL spectra show a strong applied potential dependence. Figure 9 shows normalized PL intensity of (7,5), (7,6), and (10,3)SWNTs as a function of external applied potential and the Nernst analysis curves (solid line) of the experimental results. From the observed inflection point, we can determine oxidation and reduction potentials of (7,5), (7,6), and (10,3)SWNTs. By a similar way, the redox potentials of the above mentioned 15 isolated (n,m)SWNTs were determined and the values together with Fermi levels and bandgaps of these nanotubes are summarized in Table 2, where E_{ox}^0 , E_{red}^0 , E_{f} , and E_{electr} are the oxidation potential, reduction potential, Fermi level, and electrochemical band gap, respectively. The finding advances the basic science and understanding of carbon nanotubes and opens the way to a new breed of nanoscience.

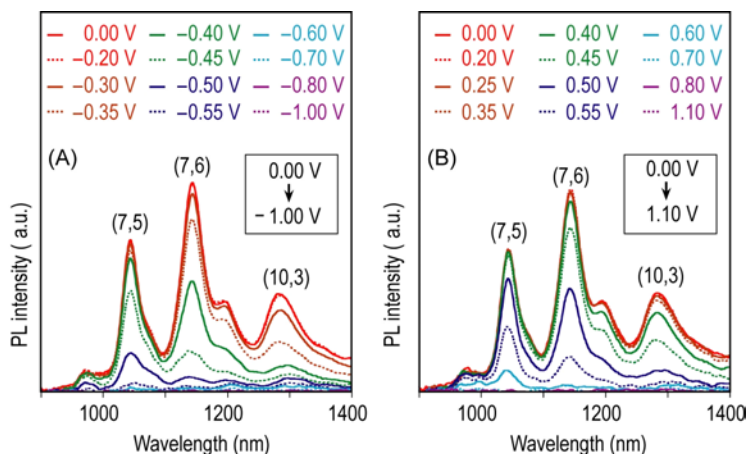


Figure 8. Dependence of external applied potential on the PL spectra of the film containing isolated SWNTs on an ITO electrode. (A) and (B): PL spectra excited at 650 nm, in which (7,5), (7,6), and (10,3) SWNTs appeared. In this experiment, the potential was applied to the electrode from 0.0 V to -1.0 V (A) and from 0.0 V to +1.1 V (B). Adapted from Reference 173.

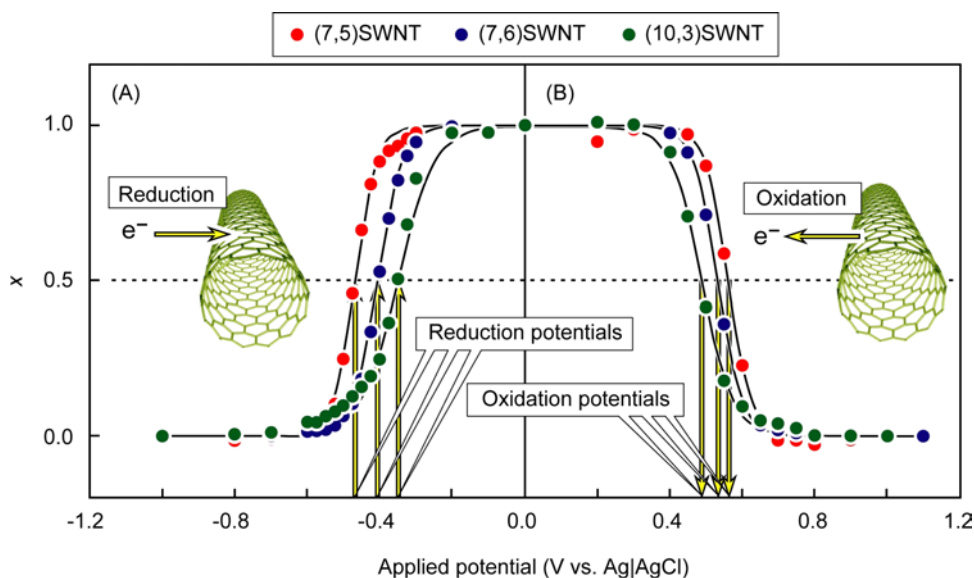


Figure 9. Normalized PL intensity of the film containing isolated SWNTs on an ITO electrode as a function of external applied potential and the Nernst analysis curves (each solid line) of the experimental results. In the experiment, a potential was applied to the electrode by arbitrary step from 0.0 V to -1.0 V (A) and from 0.0 V to +1.1 V (B). Adapted from Reference 173.

Table 2. Experimentally determined redox properties of fifteen isolated SWNTs. Adapted from Reference 173.

Chirality index (<i>n,m</i>)	Nanotube diameter (nm)	E°_{ox} (V <i>vs.</i> vacuum)	E°_{red} (V <i>vs.</i> vacuum)	E_{f} (V <i>vs.</i> vacuum)	ΔE_{electr} (eV)
(6,5)	0.757	5.08	4.01	4.55	1.07
(8,3)	0.782	5.03	3.95	4.49	1.08
(7,5)	0.829	4.98	3.97	4.48	1.01
(8,4)	0.840	4.96	4.05	4.50	0.91
(10,2)	0.884	4.93	3.95	4.44	0.98
(7,6)	0.895	4.94	4.03	4.49	0.91
(9,4)	0.916	4.92	4.01	4.47	0.91
(10,3)	0.936	4.89	4.09	4.49	0.81
(8,6)	0.966	4.90	4.05	4.47	0.85
(9,5)	0.976	4.89	4.09	4.49	0.79
(12,1)	0.995	4.93	4.03	4.48	0.90
(11,3)	1.014	4.87	4.05	4.46	0.82
(8,7)	1.032	4.88	4.09	4.49	0.79
(10,5)	1.050	4.86	4.08	4.47	0.78
(9,7)	1.103	4.85	4.10	4.47	0.75

8. Electrocatalyst for Fuel Cell Using Soluble CNTs

We described in Section 6 that PBI molecules individually dissolve SWNTs based on the π - π interaction between SWNTs and PBI.¹⁶¹ PBI is a proton conducting material for polymer electrolyte fuel cells (PEFCs) that can operate even under dry conditions above 100°C,^{174,175} and is a promising candidate as a substitution of a Nafion, widely used in the low-temperature PEFC systems.¹⁷⁶⁻¹⁷⁸ The PEFC operations at higher temperatures afford many benefits such as a decreased carbon monoxide poisoning on the catalyst metal particles, an increase in the catalytic reaction rate, easy removal of generated water, etc.¹⁷⁹

We designed from scratch and developed a novel PBI nanocomposite, in which CNTs and platinum (Pt) nanoparticles are employed as a carbon support and redox catalyst, respectively. Especially, in our system, PBI is expected to act as: i) a Pt adsorbing material *via* the coordination of the Pt ion with the aromatic nitrogen on PBI, ii) a MWNT solubilizing material and iii) a proton conductor. Here we focus on the design and fabrication of an interfacial nanostructure formed from a Pt/MWNT/PBI nanocomposite. Such a study is highly important since the catalyst efficiency largely depends on the catalyst morphology at their interfaces.¹⁸⁰

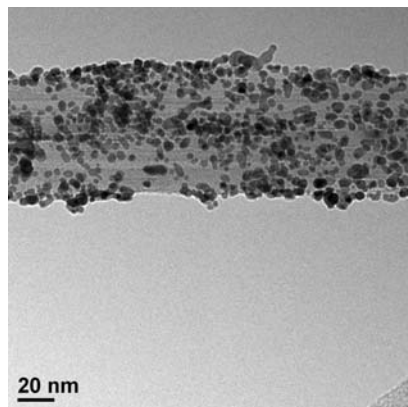


Figure 10. Typical TEM images of a MWNT/**PBI**/Pt composite. Adapted from Reference 181.

Transmission electron microscope (TEM) image (Figure 10) of the composite shows that the Pt nanoparticles are rather uniformly deposited on the MWNT/**PBI**. From the TEM image, the mean-diameter (d_{TEM}) of the Pt nanoparticles is 4.0 ± 1.8 nm.¹⁸¹

The capability of the composites as an electrocatalyst, can be evaluated by their electrochemical activities. Figure 11a (solid line) shows the cyclic voltammogram (CV) of the MWNT/**PBI**/Pt composite. Characteristic peaks in the negative region (from -0.2 to 0.1 V *vs.* Ag/AgCl) attributable to atomic hydrogen adsorption and desorption on the Pt nanoparticle surfaces are apparently detected. The electrochemically active surface area (ECSA) was calculated using the following formula (Eq. 1):¹⁸¹

$$\text{ECSA} = Q_{\text{H}} / (210 \times \text{Pt loading on electrode}) \quad (1)$$

where Q_{H} is the charge exchanged during the electroadsorption of H on Pt (from -0.13 to 0.2 V *vs.* Ag/AgCl). The amounts of Pt loaded on the electrode were determined by the amounts of composite solutions casted on the electrodes. ECSA of the MWNT/**PBI**/Pt composite was calculated to be 44.0 m²/g of Pt, which is much greater than that of the MWNT/Pt (22.5 m²/g of Pt, Figure 11a: dotted line). This higher ECSA value for the MWNT/**PBI**/Pt composite might be due to the homogeneous loading of the Pt particles on the MWNTs than MWNT/Pt. The obtained CV result strongly suggests that the Pt nanoparticles immobilized on the PBI are close enough to the MWNTs to undergo a facile electronic communication with the MWNTs and that the Pt particles are exposed to the electrolyte phase

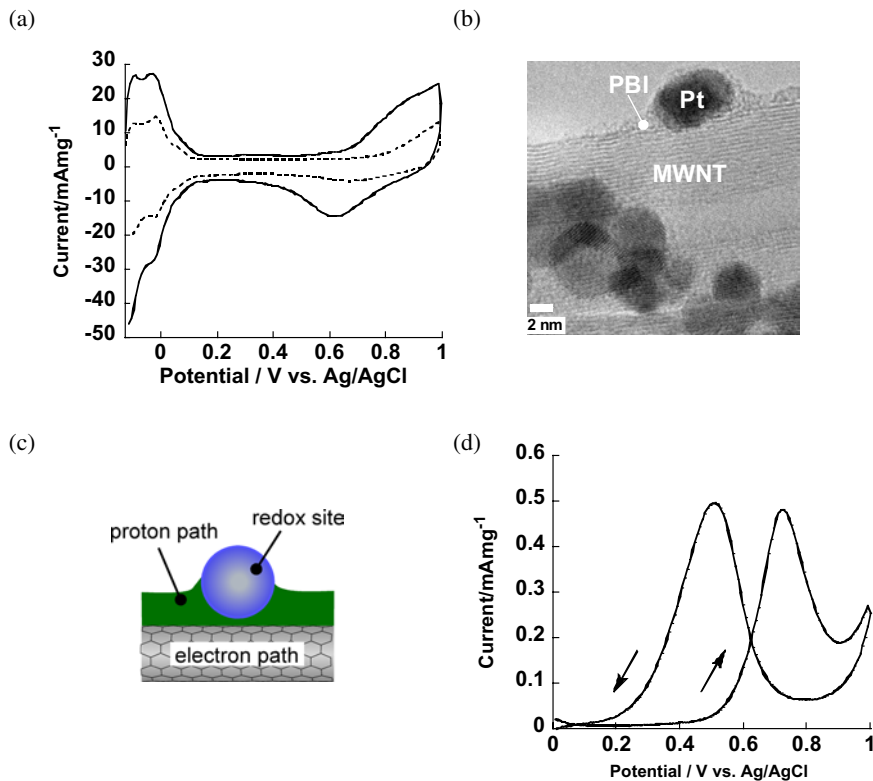


Figure 11. (a) CV of the MWNT/PBI/Pt (0.024 mg of Pt cm⁻²: solid line) and MWNT/Pt (0.011 mg of Pt cm⁻²: dotted line). (b) High-resolution TEM (HRTEM) image of the MWNT/PBI/Pt. (c) Illustration of an ‘ideal’ triple-phase boundary structure, in which all phases (electron path-, proton path-, gas phases) are attached to the redox site. (d) CV of methanol oxidation on MWNT/PBI/Pt (0.021 mg of Pt cm⁻²). Adapted from Reference 181.

(Figure 11b). This interface structure is most likely the structure that has been widely recognized as the ‘ideal’ triple-phase boundary structure (Figure 11c) that enables an excellent catalyst efficiency.¹⁸³ The formation mechanism of the above mentioned structure is the growth of the Pt nanoparticles on the PBI layer, followed by penetration into the PBI layer to form a close contact structure with the MWNT surfaces.

Pt utilization efficiency (η_{Pt}) is the essential parameter to describe the catalyst performance and is calculated by dividing ESCA by the chemical surface area (CSA). CSA of the MWNT/PBI/Pt and MWNT/Pt were determined to be 71.1 and 58.1 m²/g, respectively, when we used Eq. 3,

$$\text{CSA} = 6/\rho d \quad (3)$$

where ρ is the density of Pt (21.09 g cm^{-3}) and d is the mean diameter of the Pt nanoparticles obtained from the XRD (d_{XRD} and d'_{XRD}). Thus the Pt utilization efficiency η_{Pt} ($=\text{ECSA}/\text{CSA}$) of the MWNT/**PBI**/Pt was determined to be as high as 74%, while that of the MWNT/Pt was 39%. The Pt utilization of the commercial catalyst (CB/Pt) is reported to be 54.8%.¹⁸⁴ The observed higher utilization efficiency of the MWNT/**PBI**/Pt is explained by the formation of the ‘ideal’ triple-phase boundary structure of the MWNT/**PBI**/Pt realized by the PBI adsorption onto MWNT and adsorption of Pt.

Figure 11d shows the typical CV of MWNT/**PBI**/Pt in 2 M methanol+1 M H_2SO_4 aqueous solution. In the forward scan, methanol oxidation produces an anodic peak at around 0.75 V *vs.* Ag/AgCl, where the peak current of methanol oxidation on MWNT/**PBI**/Pt is 480 mA mg^{-1} of Pt. The anodic peak at around 0.5 V *vs.* Ag/AgCl in the reverse scan can be attributed to the removal of the incompletely oxidized carbonaceous species formed in the forward scan. The catalytic activity of the composite strongly suggests that the materials work in a membrane-electrode assembly system.

We have also used pyridine-containing polybenzimidazole (**PyPBI**, Figure 12) in place of **PBI**.¹⁸⁵ **PyPBI** acts as an efficient dispersant for CNT wrapping and produces a stable complex after removal of the unbound **PyPBI**. The wrapped **PyPBI** serves as a glue for immobilizing Pt nanoparticles onto the surface of MWNTs without any strong oxidation process for the MWNTs. A highly homogeneous and remarkably efficient Pt loading onto the surface of MWNTs through a coordination reaction between Pt and **PyPBI** is achieved. CV measurements have revealed that the Pt nanoparticles deposited on the **PyPBI**-wrapped MWNTs have a high electrochemically active surface area (Figure 13). The characteristic peaks in the negative region (from -0.13 to $0.2 \text{ V vs. Ag/AgCl}$) attributable to atomic hydrogen adsorption and desorption on the Pt nanoparticle surfaces together with the Pt oxidation and Pt oxide reduction in the positive region (from 0.6 to $1.0 \text{ V vs. Ag/AgCl}$) are apparently detected, which are similar to the reported profiles.^{186,187} ECSA of the MWNT/**PyPBI**/Pt hybrid is calculated to be

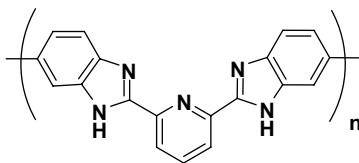


Figure 12. Chemical structure of **PyPBI**.

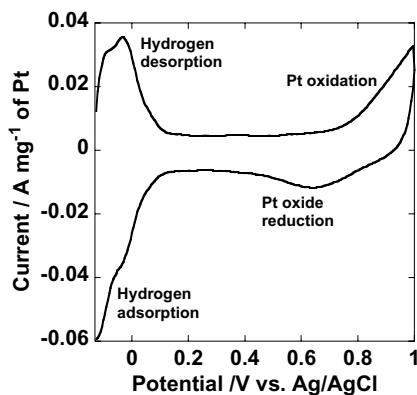


Figure 13. CV of the MWCNT/PyPBI/Pt measured in 1.0 M H_2SO_4 aqueous solution. The ECSA value is determined from the characteristic peak in the negative region (from -0.13 to 0.2 V *vs.* Ag/AgCl) attributable to atomic hydrogen adsorption on the Pt nanoparticle surfaces. Adapted from Reference 185.

$51.6 \text{ m}^2/\text{g}$ of Pt. The obtained ECSA value is higher than our previously reported value ($44.0 \text{ m}^2/\text{g}$ of Pt) for the MWNT/**PBI**/Pt¹⁸¹ and as high as the conventional CB/Pt system ($55.8 \text{ m}^2/\text{g}$ of Pt). Such a high ECSA value is explained by the excellent accessibility of the reactant on the surfaces of the homogeneously dispersed Pt and efficient electron conduction of the MWNTs lying beneath the Pt nanoparticles.

9. Concluding Remarks

In this review article, we summarized recent progress on soluble CNTs based on non-covalent modification using surfactants, DNA, polycyclic aromatic compounds and polycondensed polymers as well as their applications. Individual solubilization of CNTs is necessary for a wide range of science and technology of carbon nanotubes, and the preparation of individually dissolved SWNTs is the first step to afford them to several practical uses as well as fundamental studies. The individual solubilization based on non-covalent modification maintains intrinsic properties of SWNTs. A tremendous number of papers describing the applications of soluble CNTs have been reported and some of them are unique for the CNT properties. We like to emphasize that combination of soluble nanotubes and spectro-electrochemistry makes direct determination of the precise electronic properties of SWNTs possible. We also highlighted the fabrication of a novel CNT-based novel electrocatalyst for fuel cell that can operate in non-humid atmosphere. CNT composites using

soluble carbon nanotubes have high potential for their applications in the vast fields of nanomaterials science and technology.

References

1. Iijima, S. *Nature* **1991**, *354*, 56–58.
2. Nakashima, N. *Int. J. Nanosci.* **2005**, *4*, 119–137.
3. Murakami, H.; Nakashima, N. *J. Nanosci. Nanotechnol.* **2006**, *6*, 16–27.
4. Nakashima, N.; Fujigaya, T. *Chem. Lett.* **2007**, *36*, 692–697.
5. Dyke, C. A.; Tour, J. M. *J. Phys. Chem. A* **2004**, *108*, 11151–11159.
6. Girifalco, L. A.; Hodak, M.; Lee, R. S. *Phys. Rev. B* **2000**, *62*, 13104.
7. Tasis, D.; Tagmatarchis, N.; Bianco, A.; Prato, M. *Chem. Rev.* **2006**, *106*, 1105–1136.
8. Balasubramanian, K.; Burghard, M. *Small* **2005**, *1*, 180–192.
9. Tasis, D.; Tagmatarchis, N.; Georgakilas, V.; Prato, M. *Chem. –Eur. J.* **2003**, *9*, 4000–4008.
10. Gooding, J. J. *Electrochim. Acta* **2005**, *50*, 3049–3060.
11. Kavan, L.; Dunsch, L.; *ChemPhysChem* **2007**, *8*, 974–998.
12. Kauffman, D. R.; Star, A. *Angew. Chem. Int. Ed.* **2008**, *47*, 6550–6570.
13. Claussen, J. C.; Franklin, A. D.; ul Haque, A.; Porterfield, D. M.; Fisher, T. S. *ACS Nano* **2009**, *3*, 37.
14. Martin, P. *Chem. –Eur. J.* **2009**, *15*, 4970–4978.
15. Lurlo, M.; Marcaccio, M.; Paolucci, F. In *Carbon Nanotubes and Related Structures*. Ed. Guldi, D. M.; Martín, N.; Wiley-VCH, Weinheim, **2010**, 53–75.
16. Boul, P. J.; Liu, J.; Mickelson, E. T.; Huffman, C. B.; Ericson, L. M.; Chiang, I. W.; Smith, K. A.; Colbert, D. T.; Hauge, R. H. Margrave, J. L.; Smalley, R. E. *Chem. Phys. Lett.* **1999**, *310*, 367–372.
17. Furtado, C. A.; Kim, U. J.; Gutierrez, H. R.; Pan, L.; Dickey, E. C.; Eklund, P. C. *J. Am. Chem. Soc.* **2004**, *126*, 6095–6105.
18. Moore, V. C.; Strano, M. S.; Haroz, E. H.; Hauge, R. H.; Smalley, R. E. *Nano Lett.* **2003**, *3*, 1379–1382.
19. Dror, Y.; Pyckhout-Hintzen, W.; Cohen, Y.; *Macromolecules* **2005**, *38*, 7828–7836.
20. Bachilo, S. M.; Strano, M. S.; Kittrell, C.; Hauge, R. H.; Smalley, R. E.; Weisman, R. B. *Science* **2002**, *298*, 2361–2366.
21. O’Connell, M. J.; Bachilo, S. M.; Huffman, C. B.; Moore, V. C.; Strano, M. S.; Haroz, E. H.; Rialon, K. L.; Boul, P. J.; Noon, W. H.; Kittrell, C.; Ma, J.; Hauge, R. H.; Weisman, R. B.; Smalley, R. E. *Science* **2002**, *297*, 593–596.
22. Torrens, O. N.; Milkie, D. E.; Zheng, M.; Kikkawa, J. M. *Nano Lett.* **2006**, *6*, 2864–2867.
23. Kim, Y.; Minami, N.; Kazaoui, S. *Appl. Phys. Lett.* **2005**, *86*, 073103/073101–073103/073103.
24. Kazaoui, S.; Minami, N.; Nalini, B.; Kim, Y.; Hara, K. *J. Appl. Phys.* **2005**, *98*, 084314/084311–084314/084316.
25. Cognet, L.; Tsybolski, D. A.; Weisman, R. B. *Nano Lett.* **2008**, *8*, 749–753.
26. Tsybolski, D. A.; Rocha, J-DR.; Bachilo, S. M.; Cognet, L.; Weisman, R. B. *Nano Lett.* **2007**, *7*, 3080–3085.

27. Cognet, L.; Tsyboulski, D. A.; Rocha, J.-D. R.; Doyle, C. D.; Tour, J. M.; Weisman, R. B. *Science* **2007**, *316*, 1465–1468.
28. Tan, Y.; Resasco, D. E. *J. Phys. Chem. B* **2005**, *109*, 14454–14460.
29. Richard, C.; Balavoine, F.; Schultz, P.; Ebbesen, T. W.; Mioskowski, C. *Science* **2003**, *300*, 775–778.
30. Duesberg, G. S.; Burghard, M.; Muster, J.; Philipp, G.; Roth, S. *Chem. Commun.* **1998**, 435–436.
31. Burghard, M.; Duesberg, G.; Philipp, G.; Muster, J.; Roth, S. *Adv. Mater.* **1998**, *10*, 584–588.
32. Islam, M. F.; Rojas, E.; Bergey, D. M.; Johnson, A. T.; Yodh, A. G. *Nano Lett.* **2003**, *3*, 269–273.
33. Paredes, J. I.; Burghard, M. *Langmuir* **2004**, 5149–5152.
34. Hough, L. A.; Islam, M. F.; Hammouda, B.; Yodh, A. G.; Heiney, P. A. *Nano Lett.* **2006**, *6*, 313–317.
35. Islam, M. F.; Nobili, M.; Ye, F.; Lubensky, T. C.; Yodh, A. G. *Phys. Rev. Lett.* **2005**, *95*, 148301/148301–148301/148304.
36. Kim, Y.; Hong, S.; Jung, S.; Strano, M. S.; Choi, J.; Baik, S. *J. Phys. Chem. B* **2006**, *110*, 1541–1545.
37. Wenseleers, W.; Vlasov, I. I.; Goovaerts, E.; Obratzsova, E. D.; Lobach, A. S.; Bouwen, A. *Adv. Funct. Mater.* **2004**, *14*, 1105–1112.
38. Lisunova, M. O.; Lebovka, N. I.; Melezhyk, O. V.; Boiko, Y. P. *J. Colloid Interf. Sci.* **2006**, *299*, 740–746.
39. Ishibashi, A.; Nakashima, N. *Chem.-Eur. J.* **2006**, *12*, 7595–7602.
40. Ishibashi, A.; Nakashima, N. *Bull. Chem. Soc. J.* **2006**, *79*, 357–359.
41. Nakashima, N.; Okuzono, S.; Murakami, H.; Nakai, T.; Yoshikawa, K. *Chem. Lett.* **2003**, *32*, 456–457.
42. Bae, A.-H.; Hatano, T.; Nakashima, N.; Murakami, H.; Shinkai, S. *Org. Biomol. Chem.* **2004**, *2*, 1139–1144.
43. Barisci, J. N.; Tahhan, M.; Wallace, G. G.; Badaire, S.; Vaugien, T.; Maugey, M.; Poulin, P. *Adv. Funct. Mater.* **2004**, *14*, 133–138.
44. Iijima, M.; Watabe, T.; Ishii, S.; Koshio, A.; Yamaguchi, T.; Bandow, S.; Iijima, S.; Suzuki, K.; Maruyama, Y. *Chem. Phys. Lett.* **2005**, *414*, 520–524.
45. Gladchenko, G. O.; Karachevtsev, M. V.; Leontiev, V. S.; Valeev, V. A.; Glamazda, A. Y.; Plokhotnichenko, A. M.; Stepanian, S. G. *Mol. Phys.* **2006**, *104*, 3193–3201.
46. He, P.; Bayachou, M. *Langmuir* **2005**, *21*, 6086–6092.
47. Pantarotto, D.; Singh, R.; McCarthy, D.; Erhardt, M.; Briand, J. P.; Prato, M.; Kostarelos, K.; Bianco, A. *Angew. Chem. Int. Ed.* **2004**, *43*, 5242–5246.
48. Rege, K.; Viswanathan, G.; Zhu, G.; Vijayaraghavan, A.; Ajayan, P. M.; Dordick, J. S. *Small* **2006**, *2*, 718–722.
49. Cathcart, H.; Quinn, S.; Nicolosi, V.; Kelly, J. M.; Blau, W. J.; Coleman, J. N. *J. Phys. Chem. C* **2007**, *111*, 66–74.
50. Zheng, M.; Jagota, A.; Semke, E. D.; Diner, B. A.; Mclean, R. S.; Lustig, S. R.; Richardson, R. E.; Tassi, N. G. *Nat. Mater.* **2003**, *2*, 338–342.
51. Zheng, M.; Jagota, A.; Strano, M. S.; Santos, A. P.; Barone, P.; Chou, S. G.; Diner, B. A.; Dresselhaus, M. S.; Mclean, R. S.; Onoa, G. B.; Samsonidze, G. G.; Semke, E. D.; Usrey, M.; Walls, D. J. *Science* **2003**, *302*, 1545–1548.

52. Huang, X.; McLean, R. S.; Zheng, M. *Anal. Chem.* **2005**, *77*, 6225–6228.
53. Zhao, X.; Johnson, J. K. *J. Am. Chem. Soc.* **2007**, *129*, 10438–10445.
54. Rajendra, J.; Baxendale, M.; Rap, L. G. D.; Rodger, A. *J. Am. Chem. Soc.* **2004**, *126*, 11182–11188.
55. Rajendra, J.; Rodger, A. *Chem. –Eur. J.*, **2005**, *11*, 4841–4847.
56. Chou, S. G.; Ribeiro, H. B.; Barros, E. B.; Santos, A. P.; Nezich, D.; Samsonidze, Ge. G.; Fantini, C.; Pimenta, M. A.; Jorio, A.; Plentz Filho, F.; Dresselhaus, M. S.; Dresselhaus, G.; Saito, R.; Zheng, M.; Onoa, G. B.; Semke, E. D.; Swan, A. K.; Ünlü, M. S.; Goldberg, B. B. *Chem. Phys. Lett.* **2004**, *397*, 296–301.
57. Kawamoto, H.; Uchida, T.; Kojima, K.; Tachibana, M. *J. Appl. Phys.* **2006**, *99*, 094309/094301–094309/094304.
58. Fagan, J. A.; Simpson, J. R.; Bauer, B. J.; Lacerda, S. H. De. P.; Becker, M. L.; Chun, J.; Migler, K. B.; Walker, A. R. H.; Hobbie, E. K. *J. Am. Chem. Soc.* **2007**, *129*, 10607.
59. Zheng, M.; Diner, B. A. *J. Am. Chem. Soc.* **2004**, *126*, 15490–15494.
60. Zheng, M.; Rostovtsev, V. V. *J. Am. Chem. Soc.* **2006**, *128*, 7702–7703.
61. Napier, M. E.; Hull, D. O.; Thorp, H. H. *J. Am. Chem. Soc.* **2005**, *127*, 11952–11953.
62. Chou, S. G.; DeCamp, M. F.; Jiang, J.; Samsonidze, Ge. G.; Barros, E. B.; Plentz, F.; Jorio, A.; Zheng, M.; Onoa, G. B.; Semke, E. D.; Tokmakoff, A.; Saito, R.; Dresselhaus, G.; Dresselhaus, M. S. *Phys. Rev. B: Condens. Matter Mater. Phys.* **2005**, *72*, 195415/195411–195415/195418.
63. Chou, S. G.; Plentz, F.; Jiang, J.; Saito, R.; Nezich, D.; Ribeiro, H. B.; Jorio, A.; Pimenta, M. A.; Samsonidze, Ge. G.; Santos, A. P.; Zheng, M.; Onoa, G. B.; Semke, E. D.; Dresselhaus, G.; Dresselhaus, M. S. *Phys. Rev. Lett.* **2005**, *94*, 127402/127401–127402/127404.
64. Zangmeister, R. A.; Maslar, J. E.; Opdahl, A.; Tarlov, M. J. *Langmuir* **2007**, *23*, 6252–6256.
65. Heller, D. A.; Jeng, E. S.; Yeung, T.-K.; Martinez, B. M.; Moll, A. E.; Gastala, J. B.; Strano, M. S. *Science* **2006**, *311*, 508–511.
66. Li, X.; Peng, Y.; Qu, X. *Nucleic Acids Res.* **2006**, *34*, 3670–3676.
67. He, P.; Li, S.; Dai, L. *Synth. Met.* **2005**, *154*, 17–20.
68. Fantini, C.; Jorio, A.; Santos, A. P.; Peressinotto, V. S. T.; Pimenta, M. A. *Chem. Phys. Lett.* **2007**, *439*, 138–142.
69. Chou, S. G.; Son, H.; Kong, J.; Jorio, A.; Saito, R.; Zheng, M.; Dresselhaus, G.; Dresselhaus, M. S. *Appl. Phys. Lett.* **2007**, *90*, 131109/131101–131109/131103.
70. Dukovic, G.; Balaz, M.; Doak, P.; Berova, N. D.; Zheng, M.; Mclean, R. S.; Brus, L. E. *J. Am. Chem. Soc.* **2006**, *128*, 9004–9005.
71. Hughes, M. E.; Brandin, E.; Golovchenko, J. A. *Nano. Lett.* **2007**, *7*, 1191–1194.
72. Ishibashi, A.; Yamaguchi, Y.; Murakami, H.; Nakashima, N. *Chem. Phys. Lett.* **2006**, *419*, 574–577.
73. Kam, N.; Wong, S.; O’Connell, M.; Wisdom, J. A.; Dai, H. *Proc. Natl. Acad. Sci. USA* **2005**, *102*, 11600–11605.
74. Onoa, B.; Zheng, M.; Dresselhaus, M. S.; Diner, B. A. *Phys. Status Solidi. A* **2006**, *203*, 1124–1131.
75. Douglas, S. M.; Chou, J. J.; Shih, W. M. *Proc. Natl. Acad. Sci. USA* **2007**, *104*, 6644–6648.
76. Han, X.; Li, Y.; Deng, Z. *Adv. Mater. (Weinheim, Ger.)* **2007**, *19*, 1518–1522.
77. Noguchi, Y.; Fujigaya, T.; Niidome, Y.; Nakashima, N. *Chem. –Eur. J.* **2008**, *14*, 5966–5973.

78. Park, K. A.; Lee, S. M.; Lee, S. H.; Lee, Y. H. *J. Phys. Chem. C* **2007**, *111*, 1620–1624.
79. Leyton, P.; Gomez-Jeria, J. S.; Sanchez-Cortes, S.; Domingo, C.; Campos-Vallette, M. *J. Phys. Chem. B* **2006**, *110*, 6470–6474.
80. Nakashima, N.; Tomonari, Y.; Murakami, H. *Chem. Lett.* **2002**, 638–639.
81. Nakashima, N.; Tanaka, Y.; Tomonari, Y.; Murakami, H.; Kataura, H.; Sakaue, T.; Yoshikawa, K. *J. Phys. Chem. B* **2005**, *109*, 13076–13082.
82. Tomonari, Y.; Murakami, H.; Nakashima, N. *Chem. –Eur. J.* **2006**, *12*, 4027–4034.
83. Gomez, F. J.; Chen, R. J.; Wang, D.; Waymouth, R. M.; Dai, H. *Chem. Commun. (Cambridge, U.K.)* **2003**, 190–191.
84. Fifield, L. S.; Dalton, L. R.; Addleman, R. S.; Galhotra, R. A.; Engelhard, M. H.; Fryxell, G. E.; Aardahl, C. L. *J. Phys. Chem. B* **2004**, *108*, 8737–8741.
85. Guldi, D. M.; Menna, E.; Maggini, M.; Marcaccio, M.; Paolucci, D.; Paolucci, F.; Campidelli, S.; Prato, M.; Rahman, G. M.; Schergna, S. *Chem. –Eur. J.* **2006**, *12*, 3975–3983.
86. Kavakka, J. S.; Heikkinen, S.; Kilpeläinen, I.; Mattila, M.; Lipsanen, H.; Helaja, J. *Chem. Commun. (Cambridge, U.K.)* **2007**, 519–521.
87. Menard-Moyon, C.; Izard, N.; Doris, E.; Mioskowski, C. *J. Am. Chem. Soc.* **2006**, *128*, 6552–6553.
88. Campidelli, S.; Meneghetti, M.; Prato, M. *Small* **2007**, *3*, 1672–1676.
89. Chen, R. J.; Zhang, Y.; Wang, D.; Dai, H. *J. Am. Chem. Soc.* **2001**, *123*, 3838–3839.
90. Liu, L.; Wang, T.; Li, J.; Guo, Z.-X.; Dai, L.; Zhang, D.; Zhu, D. *Chem. Phys. Lett.* **2002**, *367*, 747–752.
91. Artyukhin, A. B.; Bakajin, O.; Stroeve, P.; Noy, A. *Langmuir* **2004**, *20*, 1442–1448.
92. Sgobba, V.; Rahman, G. M. A.; Guldi, D. M.; Jux, N.; Campidelli, S.; Prato, M. *Adv. Mater. (Weinheim, Ger.)* **2006**, *18*, 2264–2269.
93. Ehli, C.; Rahman, G. M. A.; Jux, N.; Balbinot, D.; Guldi, D. M.; Paolucci, F.; Marcaccio, M.; Paolucci, D.; Melle-Franco, M.; Zerbetto, F.; Campidelli, S.; Prato, M. *J. Am. Chem. Soc.* **2006**, *128*, 11222–11231.
94. Guldi, D. M.; Rahman, G. M. A.; Prato, M.; Jux, N.; Qin, S.; Ford, W. *Angew. Chem. Int. Ed.* **2005**, *44*, 2015–2018.
95. Guldi, D. M.; Rahman, G. M. A.; Jux, N.; Balbinot, D.; Tagmatarchis, N.; Prato, M. *Chem. Commun. (Cambridge, U.K.)* **2005**, 2038–2040.
96. Guldi, D. M.; Rahman, G. M. A.; Sgobba, V.; Kotov, N. A.; Bonifazi, D.; Prato, M. *J. Am. Chem. Soc.* **2006**, *128*, 2315–2323.
97. Rahman, G. M. A.; Guldi, D. M.; Cagnoli, R.; Mucci, A.; Schenetti, L.; Vaccari, L.; Prato, M. *J. Am. Chem. Soc.* **2005**, *127*, 10051–10057.
98. Guldi, D. M.; Rahman, G. M. A.; Jux, N.; Balbinot, D.; Hartnagel, U.; Tagmatarchis, N.; Prato, M. *J. Am. Chem. Soc.* **2005**, *127*, 9830–9838.
99. Georgakilas, V.; Tzitzios, V.; Gournis, D.; Petridis, D. *Chem. Mater.* **2005**, *17*, 1613–1617.
100. Li, X. L.; Liu, Y. Q.; Fu, L.; Cao, L. C.; Wei, D. C.; Wang, Y. *Adv. Funct. Mater.* **2006**, *16*, 2431–2437.
101. Granot, E.; Basnar, B.; Cheglakov, Z.; Katz, E.; Willner, I. *Electroanalysis* **2006**, *18*, 26–34.
102. Ou, Y.-Y.; Huang, M. H. *J. Phys. Chem. B* **2006**, *110*, 2031–2036.
103. Paloniemi, H.; Lukkari, M.; Aäritalo, T.; Areva, S.; Leiro, J.; Heinonen, M.; Haapakka, K.; Lukkari, J. *Langmuir* **2006**, *22*, 74–83.
104. Holder, P. G.; Francis, M. B. *Angew. Chem. Int. Ed.* **2007**, *46*, 4370–4373.

105. Chitta, R.; Sandanayaka, A. S. D.; Schumacher, A. L.; D'Souza, L.; Araki, Y.; Ito, O.; D'Souza, F. *J. Phys. Chem. C* **2007**, *111*, 6947–6955.
106. Ogoshi, T.; Takashima, Y.; Yamaguchi, H.; Harada, A. *J. Am. Chem. Soc.* **2007**, *129*, 4878–4879.
107. Hu, L.; Zhao, Y.-L.; Ryu, K.; Zhou, C.; Stoddart, J. F.; Grüner, G. *Adv. Mater. (Weinheim, Ger.)* **2008**, *20*, 939–946.
108. Wu, P.; Chen, X.; Hu, N.; Tam, U. C.; Blixt, O.; Zettl, A.; Bertozzi, C. R. *Angew. Chem., Int. Ed.* **2008**, *47*, 5022–5025.
109. Zhang, J.; Lee, J. K.; Wu, Y.; Murray, R. W. *Nano Lett.* **2003**, *3*, 403–407.
110. Gregan, E.; Keogh, S. M.; Maguire, A.; Hedderman, T. G.; Neill, L. O.; Chambers, G.; Byrne, H. J. *Carbon* **2004**, *42*, 1031–1035.
111. Hedderman, T. G.; Keogh, S. M.; Chambers, G.; Byrne, H. J. *J. Phys. Chem. B* **2004**, *108*, 18860–18865.
112. Feng, W.; Fujii, A.; Ozaki, M.; Yoshino, K. *Carbon* **2005**, *43*, 2501–2507.
113. Yamamoto, T.; Miyauchi, Y.; Motoyanagi, J.; Fukushima, T.; Aida, T.; Kato, M.; Maruyama, S. *Jpn. J. Appl. Phys.* **2008**, *47*, 2000–2004.
114. Gotovac, S.; Hattori, Y.; Noguchi, D.; Miyamoto, J.; Kanamaru, M.; Utsumi, S.; Kanoh, H.; Kaneko, K. *J. Phys. Chem. B* **2006**, *110*, 16219–16224.
115. Gotovac, S.; Honda, H.; Hattori, Y.; Takahashi, K.; Kanoh, H.; Kaneko, K. *Nano Lett.* **2007**, *7*, 583–587.
116. Nakamura, G.; Narimatsu, K.; Niidome, Y.; Nakashima, N. *Chem. Lett.* **2007**, *36*, 1140–1141.
117. Murakami, H.; Nomura, T.; Nakashima, N. *Chem. Phys. Lett.* **2003**, *378*, 481–485.
118. Murakami, H.; Nakamura, G.; Nomura, T.; Miyamoto, T.; Nakashima, N. *J. Porphyrins Phthalocyanines* **2007**, *11*, 418–427.
119. Cambré, S.; Wenseleers, W.; Culin, J.; Van Doorslaer, S.; Fonseca, A.; Nagy, J. B.; Goovaerts, E. *Chem. Phys. Chem.* **2008**, *9*, 1930–1941.
120. Basiuk, V. A. *J. Comput. Theor. Nanosci.* **2006**, *3*, 767–774.
121. Yamaguchi, Y. *J. Chem. Phys.* **2004**, *120*, 7963–7970.
122. Rahman, G. M. A.; Guldi, D. M.; Campidelli, S.; Prato, M. *J. Mater. Chem.* **2006**, *16*, 62–65.
123. Li, H.; Zhou, B.; Lin, Y.; Gu, L.; Wang, W.; Fernando, K. A.; Kumar, S.; Allard, L. F.; Sun, Y. P. *J. Am. Chem. Soc.* **2004**, *126*, 1014–1015.
124. Hasobe, T.; Fukuzumi, S.; and Kamat, P. V. *J. Phys. Chem. B* **2006**, *110*, 25477–25484.
125. Saito, K.; Troiani, V.; Qiu, H.; Solladié, N.; Sakata, T.; Mori, H.; Ohama, M.; Fukuzumi, S. *J. Phys. Chem. C* **2007**, *111*, 1194–1199.
126. Alvaro, M.; Atienzar, P.; de la Cruz, P.; Delgado, J. L.; Troiani, V.; Garcia, H.; Langa, F.; Palkar, A.; Echegoyen, L. *J. Am. Chem. Soc.* **2006**, *128*, 6626–6635.
127. Zhao, Q.; Gu, Z.-N.; Zhuang, Q.-K. *Electrochem. Commun.* **2004**, *6*, 83–86.
128. Qu, J.; Shen, Y.; Qu, X.; Dong, S. *Electroanalysis* **2004**, *16*, 1444–1450.
129. Tanaka, H.; Yajima, T.; Matsumoto, T.; Otsuka, Y.; Ogawa, T. *Adv. Mater. (Weinheim, Ger.)* **2006**, *18*, 1411–1415.
130. Hecht, D. S.; Ramirez, R. J.; Briman, M.; Artukovic, E.; Chichak, K. S.; Stoddart, J. F.; Grüner, G. *Nano Lett.* **2006**, *6*, 2031–2036.
131. Tanaka, H.; Yajima, T.; Kawao, M.; Ogawa, T. *J. Nanosci. Nanotechnol.* **2006**, *6*, 1644–1648.

132. Guo, Z.; Du, F.; Ren, D.; Chen, Y.; Zheng J.; Liu, Z.; Tian, J. *J. Mater. Chem.* **2006**, *16*, 3021–3030.
133. Mhuirheartaigh, E. M. N.; Giordani, S.; Blau, W. J. *J. Phys. Chem. B* **2006**, *110*, 23136–23141.
134. Peng, X.; Komatsu, N.; Bhattacharya, S.; Shimawaki, T.; Aonuma, S.; Kimura, T.; Osuka, A. *Nat. Nanotechnol.* **2007**, *2*, 361–365.
135. Hasobe, T.; Fukuzumi, S.; Kamat, P. V. *J. Am. Chem. Soc.* **2005**, *127*, 11884–11885.
136. Chen, J.; Collier, C. P. *J. Phys. Chem. B* **2005**, *109*, 7605–7609.
137. Geng, J.; Ko, Y. K.; Youn, S. C.; Kim, Y.-H.; Kim, S. A.; Jung, D.-H.; Jung, H.-T. *J. Phys. Chem. C* **2008**, *112*, 12264–12271.
138. Cheng, F.; Adronov, A. *Chem. –Eur. J.* **2006**, *12*, 5053–5059.
139. Chichak, K. S.; Star, A.; Altoe, M. V. P.; Stoddart, J. F. *Small* **2005**, *1*, 452–461.
140. Cheng, F.; Zhang, S.; Adronov, A.; Echegoyen, L.; Diederich, F. *Chem. –Eur. J.* **2006**, *12*, 6062–6070.
141. Guldi, D. M.; Taieb, H.; Rahman, G. M. A.; Tagmatarchis, N.; Prato, M. *Adv. Mater. (Weinheim, Ger.)* **2005**, *17*, 871–875.
142. Lin, Y.; Meziani, M. J.; Sun, Y.-P. *J. Mater. Chem.* **2007**, *17*, 1143–1148.
143. Coleman, J. N.; Khan, U.; Gun'ko, Y. K. *Adv. Mater. (Weinheim, Ger.)* **2006**, *18*, 689–706.
144. Coleman, J. N.; Khan, U.; Blau, W. J.; Gun'ko, Y. K. *Carbon* **2006**, *44*, 1624–1652.
145. Yerushalmi-Rozen, R.; Szleifer, I. *Soft Matter* **2006**, *2*, 24–28.
146. Moniruzzaman, M.; Winey, K. I. *Macromolecules* **2006**, *39*, 5194–5205.
147. Shigeta, M.; Komatsu, M.; Nakashima, N. *Chem. Phys. Lett.* **2006**, *418*, 115–118.
148. Lillehei, P. T.; Park, C.; Rouse, J. H.; Siochi, E. J. *Nano Lett.* **2002**, *2*, 827–829.
149. Park, C.; Crooks, R. E.; Siochi, E. J.; Harrison, J. S.; Evans, N.; Kenik, E. *Nanotechnology* **2003**, *14*, L11–L14.
150. Park, C.; Ounaies, Z.; Watson, K. A.; Crooks, R. E.; Smith, J.; Lowther, S. E.; Connell, J. W.; Siochi, E. J.; Harrison, J. S.; Clair, T. L. S. *Chem. Phys. Lett.* **2002**, *364*, 303–308.
151. Ounaies, Z.; Park, C.; Wise, K. E.; Siochi, E. J.; Harrison, J. S. *Compos. Sci. Technol.* **2003**, *63*, 1637–1646.
152. Qu, L.; Lin, Y.; Hill, D. E.; Zhou, B.; Wang, W.; Sun, X.; Kitaygorodskiy, A.; Suarez, M.; Connell, J. W.; Allard, L. F.; Sun, Y.-P. *Macromolecules* **2004**, *37*, 6055–6060.
153. Jiang, X.; Bin, Y.; Matsuo, M. *Polymer* **2005**, *46*, 7418–7424.
154. Lin, Y.; Zhou, B.; Martin, R. B.; Henbest, K. B.; Harruff, B. A.; Riggs, J. E.; Guo, Z. X.; Allard, L. F.; Sun, Y.-P. *J. Phys. Chem. B* **2005**, *109*, 14779–14782.
155. Park, C.; Kang, J. H.; Harrison, J. S.; Costen, R. C.; Lowther, S. E. *Adv. Mater. (Weinheim, Ger.)* **2008**, *20*, 2074–2079.
156. Yuen, S.-M.; Ma, C.-C. M.; Chiang, C.-L.; *Compos. Sci. Technol.* **2008**, *68*, 2842–2848.
157. Chou, W.-J.; Wang, C.-C.; Chen, C.-Y. *Compos. Sci. Technol.* **2008**, *68*, 2208–2213.
158. Sun, K. J.; Wincheski, R. A.; Park, C. *J. Appl. Phys.* **2008**, *103*, 023908/023901–023908/023906.
159. Mittal, K. L.; *Polyimides and other high temperature polymers: synthesis, characterization and application*. 2, Brill Academic Pub. 2003.
160. Chung, T.-S. *Plastics Engineering* **1997**, *41*, 701–731.
161. Okamoto, M.; Fujigaya, T.; Nakashima, N. *Adv. Funct. Mater.* **2008**, *18*, 1776–1782.

162. Saito, R.; Dresselhaus, G.; Dresselhaus, M. S. *Physical properties of carbon nanotubes*. Imperial College Press, London, **1998**.
163. Kataura, H.; Kumazawa, Y.; Maniwa, Y.; Umez, I.; Suzuki, S.; Ohtsuka, Y.; Achiba, Y. *Synth. Met.* **1999**, *103*, 2555–2558.
164. Saito, R.; Dresselhaus, G.; Dresselhaus, M. S. *Phys. Rev. B: Condens. Matter Mater. Phys.* **2000**, *61*, 2981–2990.
165. Hamada, N.; Sawada, S. I.; Oshiyama, A. *Phys. Rev. Lett.* **1992**, *68*, 1579–1581.
166. Kazaoui, S.; Minami, N.; Kataura, H.; Achiba, Y. *Synth. Met.* **2001**, *121*, 1201–1202.
167. O’Connell, M. J.; Eibergen, E. E.; Doorn, S. K. *Nat. Mater.* **2005**, *4*, 412–418.
168. Paolucci, D.; Franco, M. M.; Iurlo, M.; Marcaccio, M.; Prato, M.; Zerbetto, F.; Pénicaud, A.; Paolucci, F. *J. Am. Chem. Soc.* **2008**, *130*, 7393–7399.
169. Kavan, L.; Rapt, P.; Dunsch, L. *Chem. Phys. Lett.* **2000**, *328*, 363–368.
170. Kazaoui, S.; Minami, N.; Matsuda, N.; Kataura, H.; Achiba, Y. *Appl. Phys. Lett.* **2001**, *78*, 3433–3435.
171. Kavan, L.; Rapt, P.; Dunsch, L.; Bronikowski, M. J.; Willis, P.; Smalley, R. E. *J. Phys. Chem. B* **2001**, *105*, 10764–10771.
172. Okazaki, K.-i.; Nakato, Y.; Murakoshi, K. *Phys. Rev. B: Condens. Matter Mater. Phys.* **2003**, *68*, 354341–354345.
173. Tanaka, Y.; Hirana, Y.; Niidome, Y.; Kato, K.; Saito, S.; Nakashima, N. *Angew. Chem. Int. Ed.* **2009**, *48*, 7655–7659.
174. Wang, J. T.; Savinell, R. F.; Wainright, J.; Litt, M.; Yu, H. *Electrochim. Acta* **1996**, *41*, 193–197.
175. Li, Q.; He, R.; Jensen, J. O.; Bjerrum, N. J. *Fuel Cells (Weinheim, Ger.)* **2004**, *4*, 147–159.
176. Heitner-Wirguin, C. *J. Membr. Sci.* **1996**, *120*, 1–33.
177. Kerres, J. A. *J. Membr. Sci.* **2001**, *185*, 3–27.
178. Deluca, N. W.; Elabd, Y. A. *J. Polym. Sci. Part B: Polym. Phys.* **2006**, *44*, 2201.
179. Li, Q.; He, R.; Gao, J.-A.; Jensen, J. O.; Bjerrum, N. J. *J. Electrochem. Soc.* **2003**, *150*, A1599–A1605.
180. Lee, S. J.; Mukerjee, S.; McBreen, J.; Rho, Y. W.; Kho, Y. T.; Lee, T. H. *Electrochim. Acta* **1998**, *43*, 3693–3701.
181. Okamoto, M.; Fujigaya, T.; Nakashima, N. *Small* **2009**, *5*, 735–740.
182. Reddy, A. L. M.; Ramaprabhu, S. *J. Phys. Chem. C* **2007**, *111*, 16138–16146.
183. Munakata, H.; Ishida, T.; Kanamura, K. *J. Electrochem. Soc.* **2007**, *154*, B1368–B1372.
184. Wang, J. J.; Yin, G. P.; Zhang, J.; Wang, Z. B.; Gao, Y. Z. *Electrochim. Acta* **2007**, *52*, 7042–7050.
185. Fujigaya, T.; Okamoto, M.; Nakashima, N. *Carbon* **2009**, *47*, 3227–3232.
186. Solla-Gullon, J.; Lafuente, E.; Aldaz, A.; Martinez, M. T.; Feliu, J. M. *Electrochim. Acta* **2007**, *52*, 5582.
187. Colon-Mercado, H. R.; Popov, B. N. *J. Power Sources* **2006**, *155*, 253–263.

This page intentionally left blank

Chapter 9

Recent Advances in Covalent Functionalization and Characterization of Carbon Nanotubes

Maria Antonia Herrero[†], Ester Vazquez* and Maurizio Prato^{†,‡}*

**Departamento de Química Orgánica-IRICA, Facultad de Química, Universidad de Castilla-La Mancha, 13071 Ciudad Real, Spain*

[†]Dipartimento di Scienze Farmaceutiche, Università di Trieste, Piazzale Europa 1, 34127 Trieste, Italy.

1. Introduction	272
2. Carbon Nanotubes: Type, Structure and Properties	273
3. Synthesis of Carbon Nanotubes	274
4. Characterization of CNTs	276
4.1. Thermogravimetric analysis	276
4.2. Spectroscopic characterization	278
4.2.1. Electron energy loss spectroscopy (EELS)	278
4.2.2. Resonance Raman spectroscopy	278
4.2.3. UV-vis–NIR absorption spectroscopy	280
4.2.4. Infrared spectroscopy	282
4.2.5. Emission spectroscopy	283
4.2.6. Nuclear magnetic resonance spectrometry	284
4.2.7. X-ray photoelectron spectroscopy	285
4.3. Scanning probe microscopy	285
4.3.1. Atomic force microscopy	286
4.3.2. Scanning tunneling microscopy	287

[†]Corresponding author. Email: prato@units.it

4.4.	Electron microscopy	289
4.4.1.	Transmission electron microscopy	289
4.4.2.	Scanning electron microscopy	289
5.	Organic Functionalization of CNTs	291
5.1.	Covalent surface chemistry of CNTs	291
5.1.1.	Amidation and esterification of oxidized CNTs	292
5.1.1.1.	Esterification reactions	292
5.1.1.2.	Amidation reactions	293
5.1.2.	Covalent sidewall (and tip) functionalization	295
5.1.2.1.	Halogenation	296
5.1.2.2.	Addition of carbenes and nitrenes	297
5.1.2.3.	1,3-dipolar cycloaddition	298
5.1.2.4.	Diels–Alder cycloadditions	301
5.1.2.5.	Nucleophilic and electrophilic additions	303
5.1.2.6.	Free-radical additions	304
5.1.2.7.	Reduction and reductive alkylations	305
5.1.2.8.	Direct arylations	306
5.1.2.8.1.	Diazonium coupling	306
5.1.2.8.2.	C–C coupling chemistry catalyzed by palladium	308
5.1.2.9.	Ozonolysis	308
5.1.2.10.	Grafting of polymers	309
5.1.2.11.	Mechanochemical functionalizations	310
5.2.	Non-covalent adsorption or wrapping of functional molecules	310
5.3.	The endohedral filling of the CNTs inner empty cavity	311
6.	Double functionalization reactions	312
7.	Applications: Supramolecular Chemistry	312
	Conclusions and Perspectives	315
	References	316

1. Introduction

Scaling the particle size down to nanometer dimensions provides exciting challenges and opportunities for chemists, physicists, biologists, and materials scientists.¹ One of the major challenges in nanoscale science begins with the synthesis of new nanomaterials with monodispersed sizes, uniform morphologies, and comprehensive and functionalized surfaces.

Several carbon nanoforms have recently been generated by new synthetic processes. These novel forms of carbon include fullerenes, nanotubes (CNTs), nanoonions (CNOs) and nanohorns (CNHs). All these forms exhibit very

interesting properties and offer new opportunities for applications in materials science and medicinal chemistry. The main problem when dealing with these materials is their difficult manipulation. In their pristine forms (as-produced by many companies) most of them are completely intractable and very difficult to handle.

In this chapter, we describe some of the main analytical techniques necessary to characterize the functionalized CNTs, and report the most common methods currently available for the functionalization of carbon nanotubes (CNTs). We present various schemes for a better explanation of the different modifications of these carbon nanostructures. Especially, we will focus on the covalent approach, allowing for the introduction of many functional groups onto the surface of carbon nanotubes, and therefore for the modulation of CNT properties in different applications.

2. Carbon Nanotubes: Type, Structure and Properties

Carbon nanotubes are a new carbon allotropic form, composed of sp^2 carbon atoms, similar to graphite but arranged in a cylindrical fashion. The curvature that these graphene sheets possess gives rise to (i) an appreciable change in the pyramidalization angle and (ii) a misalignment of p -orbitals. Consequently, CNTs show an increased reactivity² towards addition reactions.³ Due to these facts, the CNT sidewalls are supposed to be more reactive than the planar sheets of graphene. However, at the same time, they are found to be less reactive than fullerenes, which have larger curvatures and therefore higher strains.

CNTs are categorized depending on the number of concentrically arranged graphene layers. Single-walled CNTs (SWCNTs) are composed of a unique graphene layer, usually produced with a random distribution of diameters (0.7–2 nm) in hexagonally close-packed bundles. The origin of these bundles are based on van der Waals forces among SWCNTs. The smallest SWCNTs reported so far have a diameter of 0.4 nm,⁴ which corresponds to a hemispherical fragment of the C_{20} dodecahedron. Double-walled CNTs (DWCNTs) are composed of two concentric graphene layers, and represent an intermediate structure between Multi-Walled CNTs (MWCNTs) and SWCNTs. MWCNTs consist of several concentric graphene layers with their ends individually capped with fullerene-like hemispheres. Typically, their outer diameter ranges from 2 to 100 nm, while their inner diameter is about 1–3 nm. MWCNT lengths may reach several μm .

SWCNTs are classified as armchair, zigzag and chiral, based on their hexagonal lattice structure. The electronic properties of SWCNTs are due to

the wrapping angle of the graphene sheet.⁵ The zigzag and chiral nanotubes can be either metallic or semiconducting while armchair nanotubes are always conducting (metallic). Most currently available synthetic methods produce SWCNTs with a random distribution of metallic and semiconducting nanotubes, in a ratio of 1:2. These fascinating properties make CNTs unique materials with a high potential for molecular electronics. In fact, it has been reported that SWCNTs can act as ballistic conductors, with high effective electron mobilities and can sustain very high current densities. A rope of SWCNTs has conductivity in the range 10000–30000 S cm⁻¹ at room temperature.⁶ These properties, combined with the materials nanosize, offer unique opportunities to develop miniature advanced sensors⁷ for rapid, label-free electronic detection of different biological materials. The fabrication of these sensors is supported by the exceptional mechanical strength — an useful feature for tissue scaffolds and engineering that is demonstrated by a Young modulus of ~1 TPa.⁸

3. Synthesis of Carbon Nanotubes

Different methods to generate CNTs can be categorized as (a) arc-discharge,⁹ (b) laser ablation,¹⁰ (c) chemical vapor deposition (CVD),¹¹ (d) catalytic gas-phase growth starting with carbon monoxide or other carbon sources (*e.g.*, HiPco methods).¹²

The first two methods involve the vaporization of carbon in an inert atmosphere, whereas CVD and HiPco are based on catalytic decomposition of hydrocarbons. The synthesis of CNTs has advanced to the point that patterns of aligned MWCNTs or SWCNTs can be engineered. Such patterned growth is of interest in tissue engineering.¹³ CNT-based scaffolds have some advantages over bio-degradable synthetic polymers currently used in tissue engineering. As they possess the structural integrity and high mechanical stability to support developing tissues and withstand *in vivo* forces.

According to the procedure used to synthesize CNTs, different types of materials can be obtained with different degrees of contamination of metals, other impurities, and in a range of diameters and chiral angles. Consequently, mixtures of metallic and semiconducting CNTs coexist with their correspondingly different electronic structures. For instance, the electrical conductivity of the nanotube mixture is up to 1000 times higher than copper. Moreover, the conductivity largely depends on the chiral angle of tubes and their diameter, the presence of these mixtures limits the applications of CNTs as versatile building blocks for molecular electronics. Because semiconducting¹⁴ and metallic tubes have different functions in electronic devices,

semiconducting SWCNTs, for example, exhibit a significant electronic response to field gating effects and chemical doping effects. These characteristics are essential for FET (field effects transistors) and chemical sensors. Metallic SWCNTs, on the other hand, are needed as nanometer-sized conductors. While targeting their versatile applications in nanotechnology, many researchers have focused on the selective purification of metallic and semiconductive SWCNTs. Therefore, and not surprisingly, the chemistry of CNTs has emerged as a powerful tool for separating metallic from semiconducting species.¹⁵

CNTs are usually obtained as ropes or bundles, of up to tens of nanometers in diameter (10–30 nm) for SWCNTs. This issue affects the characterization and applications of CNTs. Because of their lack of solubility, increasing the solubility by the addition of other chemicals or the introduction of different functional groups, promotes the formation of CNT solutions, making possible their characterization, purification, and the optimization of their intrinsic properties in the search of new applications. Depending on the origin of CNTs, the amount of impurities and the procedure used to purify them, different dispersability degrees can be obtained. As far as purification is concerned, treatment with a strong acid such as hot nitric acid is one of the most common methods used to oxidize the metallic impurities.¹⁶ Unfortunately, this technique implies harsh conditions that lead to a shortening in the CNT length (average value smaller than 500 nm). A softer method consists of treating the raw material in a multimode microwave in the absence of solvent and under air.¹⁷ The irradiation will induce oxidation, while the subsequent treatment with concentrated hydrochloric acid will wash away the metal oxides. Other methodologies, like flocculation and selective sedimentation,¹⁸ filtration,¹⁹ size-exclusion chromatography²⁰ or interaction with organic polymers,²¹ have been used. In any case, the slight difference in the resistance to oxidation between CNTs and most impurities makes the purification a very difficult task. The quality of CNTs can be improved by progress in the synthesis or purification techniques, and significant achievements in both areas have been reported. Recently, very high purity, metal-free SWCNTs (carbonaceous purity of 99.98%) have been synthesized.²² The purification processes are based on a combination of several steps, which usually include gas or vapor oxidation, wet chemical oxidation, centrifugation, filtration or chromatography.^{16,23}

As commented above, the procedure used to synthesize CNTs causes the presence of impurities and affects their solubility. For example, solvents that present high polarity such as *N,N*-dimethylformamide (DMF), *N*-methylpyrrolidine (NMP) and hexamethylphosphoramide (HMPA) have

been chosen for enhancing the dispersability of laser-oven-produced SWCNTs.²⁴ By the use of sonication, it has also been possible to obtain stable suspensions.²⁵ Aromatic amines have proven to be a suitable solvent for SWCNTs purified by oxidation.¹⁶ Some authors have justified this fact because of the formation of charge-transfer complexes between molecules of solvent and CNT moieties. Small diameter HiPco SWCNTs can be dissolved in different organic solvents according to a UV-vis spectroscopic study, where 1,2-dichlorobenzene was the solvent that gave the best results.²⁶ Enhancement of solubility will facilitate purification, dispersion, and will improve the properties of CNTs.^{27,31} Different approaches have been envisaged such as non-covalent ones, where van der Waals and π - π stacking interactions govern the solubilization mechanism, while procedures that involve a chemical modification in the structure of CNTs are categorized within the covalent approach methodology.

4. Characterization of CNTs

The emerging applications of functionalized carbon nanotubes (*f*-CNTs) in various research domains necessitate the use of many different analytical techniques to confirm their structural modifications in a fast and reliable manner. One of the most challenging problems in this field consists of proving unequivocally that a new covalent bond has been created on the CNTs and, therefore, that the nanotube structure has been modified. In general, to solve this issue, there is not a universal and simple technique but rather a combination of techniques.

4.1. Thermogravimetric analysis

Thermogravimetric analysis (TGA) and the related differential thermal analyses (DTA) are widely used for the characterization of both pristine and functionalized carbon nanotubes (*f*-CNTs).²⁸ The following properties of CNTs can be determined by the TGA method:

1. The mass of metal catalyst impurity in “as synthesized” CNTs: In order to calculate the mass of catalyst residue, CNTs are pyrolyzed under air or O₂, and the residue is assumed to be the oxide derivative of the metal catalyst.
2. The number of functional groups per CNT carbon (C_{CNT}). This method implies the use of inert atmosphere. Under these conditions, functional groups are labile or decompose upon heating. As CNTs are stable up to

1200 °C, any weight loss before 800 °C is used to determine the functionalization ratio of *f*-CNTs.

3. The mass of reactive species adsorbed by a functional group on a CNT. It should be performed under inert atmosphere.

Quantitative determination of these parameters is used to define the purity of CNTs, and the extent of their functionalization. The main function of TGA is monitoring the thermal stability of a material by recording the mass change of the sample with respect to temperature. Interestingly, this methodology has been used to remove functional groups and recover non-functionalized, cleaner CNTs from a useful procedure.^{28c}

In Figure 1, the amount of functional groups in the *f*-MWCNTs was quantified by TGA.²⁹ The weight loss for the highly functionalized conjugates, as calculated from the thermogravimetric curves at 450 °C, was directly correlated to the mass increase around the CNTs introduced. The mass attributed to functionalities increased from 12.5%, in the first-generation dendron-MWCNT **1**, to 18% in the second-generation dendron-MWCNT **2**. It is clearly shown that the weight loss increases with increasing functionalization degree.

A single curve is usually observed when the TGA measurement of *f*-CNT-based materials are analyzed under inert atmosphere, as it is mainly due to the

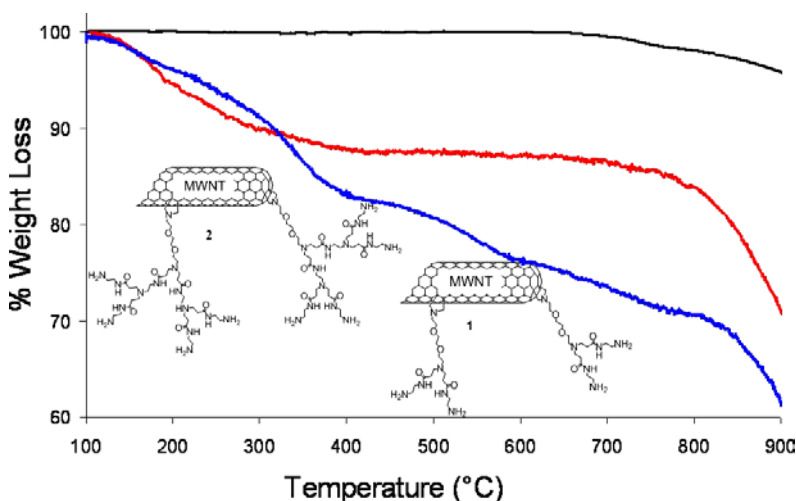


Figure 1. TGA curves for pristine MWCNTs (black line), G₁ dendron-MWCNTs **1** (red line) and G₂ dendron-MWCNTs **2** (blue line). All the experiments were performed under a N₂ atmosphere. Adapted from Reference 29.

organic functionalization that decomposes rapidly. The difference in thermal stability of parts of the appended fragments may produce more than one curve. There are some examples in the literature that show different stabilities of protected groups with respect to the rest of the organic chain (*e.g.* thermally labile Boc groups). Therefore, in these cases, two peaks are usually observed in the thermograms.

4.2. Spectroscopic characterization

4.2.1. Electron energy loss spectroscopy (EELS)

EELS can measure the elemental composition of CNTs by measuring the energy loss produced by incident electrons as they interact with CNT atoms. This creates an absorption edge at element-specific energies because of core-shell ionization events. The composition of the CNT can be determined by the analysis of the energy and relative intensities of different adsorption edges. Used in conjunction with TEM, EELS can generate elemental maps of CNTs; for example Cech *et al.* were able to show the location of sulphur atoms in a MWCNT after thiolation.³⁰ Routine use of EELS is limited, however, because it requires a specialized equipment.

4.2.2. Resonance Raman spectroscopy

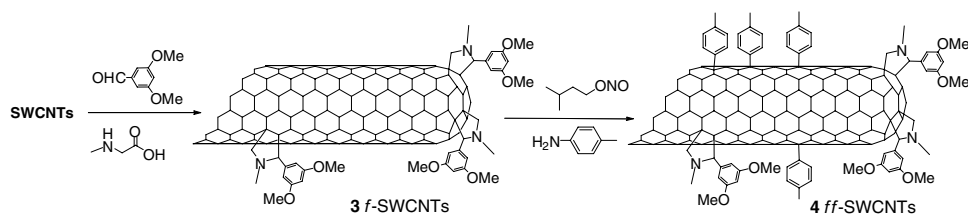
Raman spectroscopy has proven to be an excellent technique for a comprehensive study of CNTs,³¹ being useful in the understanding of the vibrational properties and electronic structures of CNTs.³² These data are invaluable for the characterization of CNTs with respect to their diameters, and quality of the sample properties.³³ By Raman spectroscopy different carbon materials can be analyzed, including SWCNTs, DWCNTs and MWCNTs, but unfortunately a quantitative determination for each type is presently not possible.³⁴

Raman spectra present different features which are all sensitive to (n,m) indexes, such as the radial breathing mode (RBM, between 100–300 cm⁻¹), where all the carbon atoms are moving in-phase in the radial direction, the G-band (between 1500–1600 cm⁻¹), where neighbouring atoms are moving in opposite directions along the tube surface (as in 2D graphite), the dispersive disorder-induced D-band and its second-order related harmonic G'-band. By measurement of RBM exciting at different laser energies, the diameter distribution of the nanotubes in a particular SWCNT bundle can be found.³⁵ The D band (diamond band, or disorder band) is typically located in the 1200–1400 cm⁻¹ region.

By determining the ratio between the intensities of these two bands (I_D/I_G), a qualitative indication of the defect density in the CNT sidewall can be determined. Consequently, I_D/I_G band analysis are extracted to obtain information regarding structural changes as a result of functionalization. Unfortunately, many CNTs can have amorphous carbon adsorbed on the sidewalls, which also contributes to the D-band. The relation between both of them can be very useful to determine the covalent attachment to the structure in the absence of amorphous carbon.

Scheme 1 shows the synthetic route to achieve doubly-functionalized SWCNTs. In this example, we can notice the critical information that is extracted from Raman analysis. On a SWCNT, a 1,3-dipolar cycloaddition is first performed (**3**), followed by a direct arylation reaction (**4**).³⁶

The combination of these two reactions in sequence, using microwave activation as the energy source, gives rise to a rich multiple functionalization, which can be efficiently followed by Raman spectroscopy. Figure 2 reports



Scheme 1. Double functionalization of SWCNT: 1,3-dipolar cycloaddition (**3**) followed by direct arylation (**4**) under microwave irradiation.

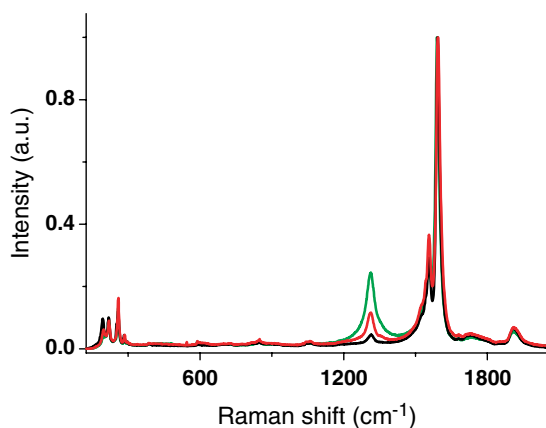


Figure 2. Raman spectra ($\lambda_{\text{exc}} = 632.8$ nm) of pristine SWCNTs (black line), cycloadduct **3** (red line) and adduct **4** (green line). Reproduced from Reference 36a with permission of ACS (2009).

the Raman spectra of the pristine starting material, cycloadduct (**3**) and the product of arylation (**4**).

The intensity of the D band reveals that the arylation reaction further increases the functionalization degree of the SWCNT after the cycloaddition has occurred.

Most of the characteristic differences that distinguish Raman spectra in SWCNTs from graphite spectra are not so obvious in MWCNTs. For example, the RBM Raman feature associated with a small diameter inner tube (less than 2 nm) can sometimes be observed when a good resonance condition is established.³⁷ Nevertheless, this is not the usual result, since the RBM signal from large diameter tubes is normally too weak to be detected, and the average of the inner tube diameter broadens the signal. However, when hydrogen gas is employed in the arc discharge method, it is possible to obtain very thin nanotubes within a MWCNT, even less than 1 nm in diameter,³⁸ and in this case a strong RBM peak at the isolated MWNT level is clearly noticed in the Raman spectra. An example of MWCNT Raman spectrum is shown in Figure 3. The micro-Raman spectra³⁹ of the purified MWCNTs excited by an Ar-laser (514.5 nm) were taken in the frequency range 12–4800 cm. Raman spectra of four carbon allotropes, *i.e.* graphene sheets, an outer shell, purified MWCNTs and a raw graphite rod, are shown in Figure 3 in the frequency region 12–2000 cm⁻¹. As a conclusion of this study, it is shown that a strong new peak is observable on purified MWCNTs at 1837 cm⁻¹, and several weak peaks in the frequency range 180–500 cm⁻¹ were noticed. It is likely that the latter could come from the breathing modes.

4.2.3. UV-vis–NIR absorption spectroscopy

In the UV-vis–NIR region, SWCNTs exhibit characteristic peaks of additional adsorption due to 1D van Hove singularities.⁴⁰ Each (n,m) CNT shows a different set of van Hove singularities in its valence and conduction bands; therefore, optical absorption can be used to determine the nanotube chirality.

In Figure 4, the change in the van Hove singularities by the covalent modification of pristine SWCNTs is reported,^{36a} due to the changes in the electronic structure. With increasing functionalization degree, the π -conjugation is correspondingly deteriorated. Such a behavior, for instance, has been reported for oxidized SWCNTs,⁴¹ or for SWCNTs modified by the addition of nitrenes.^{2b} At higher functionalization degrees, a complete loss of S_{11} , S_{22} (typical from semiconducting CNTs) and M_{11} (corresponding to metallic CNTs) features is observed, as it was documented for the addition of various types of organic residues to CNTs.^{28a}

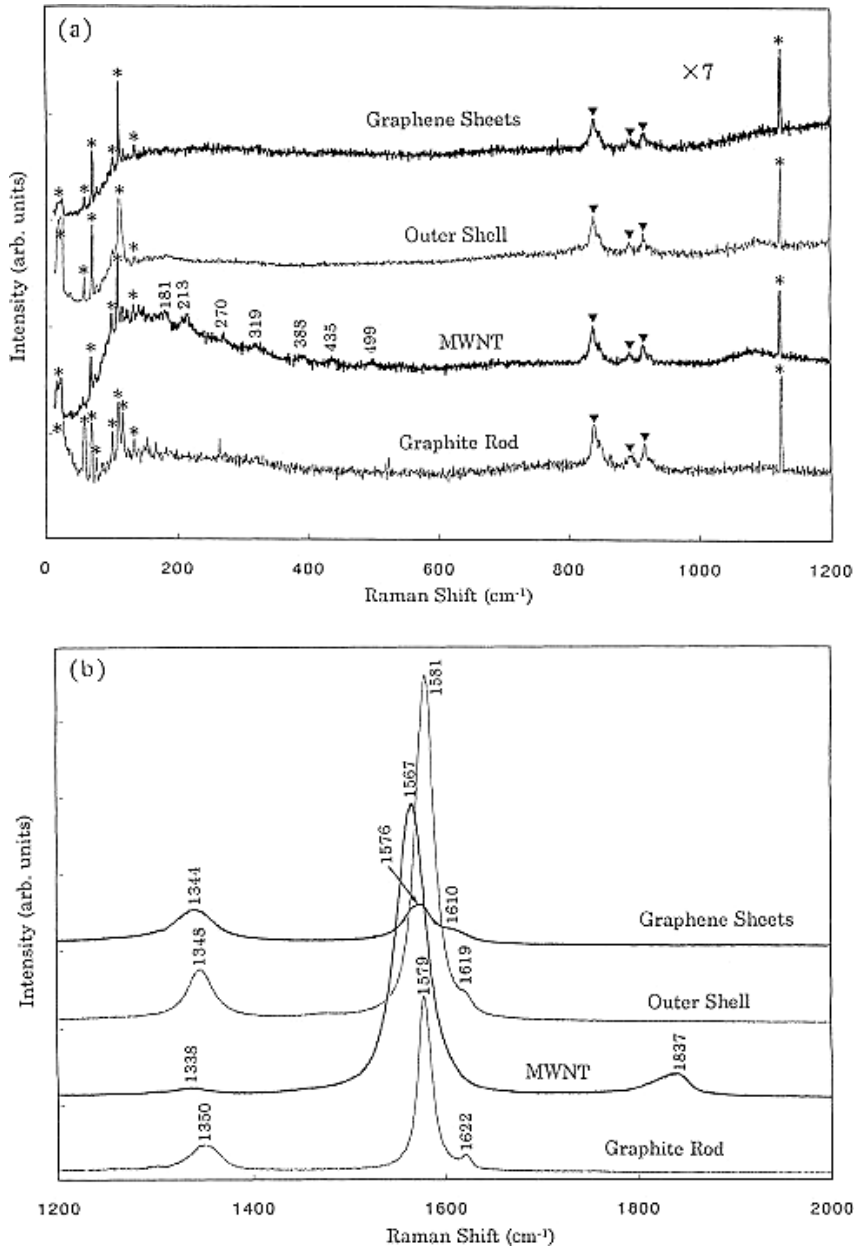


Figure 3. Raman spectra in the frequency range 12–2000 cm of graphene sheets, outer shell, purified MWCNTs (indicated as MWNT) and graphite (a) Raman spectra in the range 12–1200 cm⁻¹; and (b) 1200–2000 cm⁻¹. Reproduced from Reference 39 with permission of Elsevier (1999).

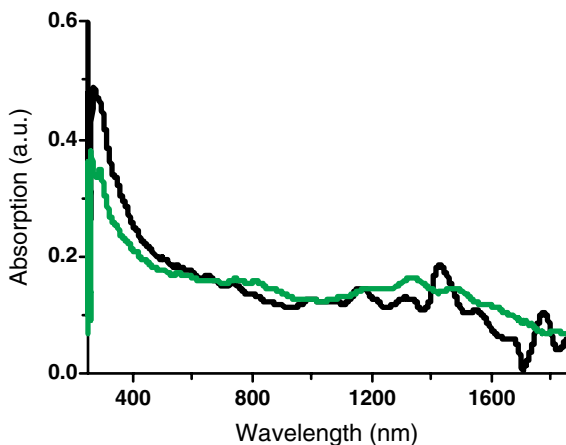


Figure 4. UV-vis-NIR absorption spectrum in DMF of Pristine SWCNTs (black line) and functionalized-SWCNTs (green line). Reproduced from Reference 36a with permission of ACS (2008).

4.2.4. Infrared spectroscopy

SWCNTs show a strong absorption in the IR range,⁴² which can interfere with those of the functional groups covalently attached. Some CNT purification processes attach functional groups to the nanotubes surfaces⁴² that can be characterized by IR. In fact, oxidation introduces carbonyl and carboxyl groups, that are easily detected on the basis of their, strong C=O stretching band, which is around 1700 cm^{-1} .⁴³ The coupling between the amines and acid groups on the CNTs shifts the C=O band towards smaller wavenumbers (below 1700 cm^{-1}).^{2a,44} Therefore, a careful examination of the band positions can give relevant indications on the reaction extent.

The FT-IR spectra of MWCNT treated with alkali and mixed acids (Figure 5) have been reported.⁴⁵ All spectra share a peak at about 3131 cm^{-1} , which is attributed to C-H stretching vibration in the MWCNT, and a peak at about 1401 cm^{-1} , assigned to the O-H deformation vibration in C-OH groups.⁴⁶ The absorbance peak at 3410 cm^{-1} for spectrum (b) in Figure 5 is assigned to the O-H stretching vibration.⁴⁷ Note that the peak intensity of MWCNT-OH increases, as compared to untreated MWCNT (see Figure 5a). This result indicates that there is a large number of hydroxyl groups on the surface of MWCNT treated by alkali. The spectra (c) and (d) in Figure 5 relate to MWCNT-COOH and MWCNT-OH-COOH. These spectra present a sharp peak at about 1745 cm^{-1} , which is attributed to the carbonyl stretching vibration of the carboxyl groups.⁴⁸ The broad absorbance band around 1300 cm^{-1} is due to O-H bending deformation in -COOH, while the

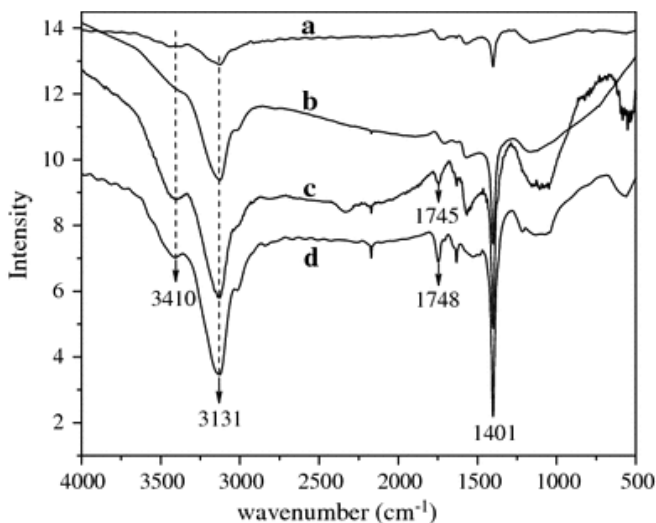


Figure 5. FTIR spectra of MWCNT (a), MWCNT-OH (b), MWCNT-COOH (c) and MWCNT-OH-COOH (d). Reproduced from Reference 45 with permission of Springer (2010).

enhanced and broadened peak at 3131 cm^{-1} is assigned to O–H stretching vibration in the carboxyl groups.

4.2.5. Emission spectroscopy

Distinct properties are expected for metallic and semiconducting CNTs. Hence, individual semiconducting SWCNTs emit band-gap photoluminescence (PL) in the near-infrared.⁴¹ Idiosyncratic electronic absorption and emission transitions for more than 30 semiconducting nanotubes were reported. The emission peaks are shifted to higher wavelengths by $\sim 40\text{ cm}^{-1}$ with respect to the corresponding absorption bands. This red-shift involves minor geometrical changes upon optical excitation. Quantum yields of SWCNTs have been reported as high as 10^{-3} and their lifetimes are in the low picosecond range.^{41,49} The E_{11} and E_{22} optical transitions have been assigned to specific tube chiralities (n,m) indexes.^{49,50} These assignments exemplify the importance of fluorescence techniques in the search of a better understanding and identification of the structures of individual SWCNTs. Figure 6 shows⁵¹ the fluorescence map of HiPco SWCNTs dispersed in a non-protic polar solvent such as *N*-methyl-2-pyrrolidone (NMP) and deuterated water. Each peak corresponds to a specific and unique (n,m) SWCNT. The red circles on the map indicate PL maxima of individualized semiconducting

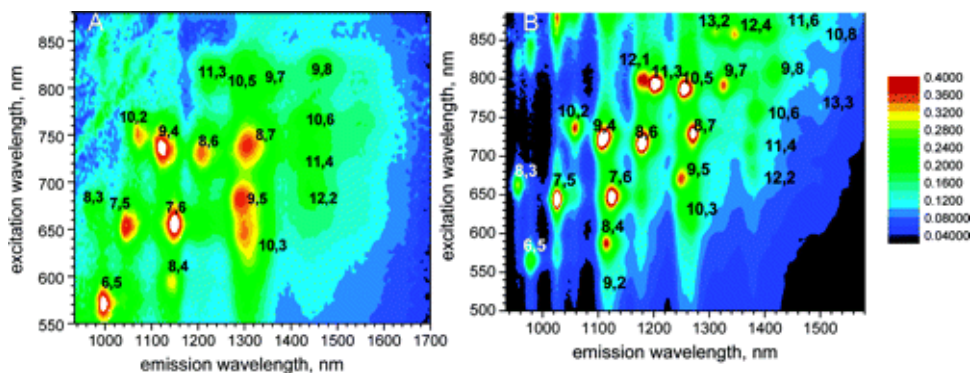


Figure 6. (A) Photoluminescence map (emission intensity vs excitation and emission wavelengths) of HiPCO nanotubes dispersed in NMP at a concentration of 0.006 mg/mL. (B) PL map of HiPCO SWCNTs in NaDDBS/D₂O dispersion. Reproduced from Reference 51 with permission of ACS (2006).

nanotubes dispersed in (i) NMP as solvent or by (ii) using a surfactant that helps in the solubilization and debundling of SWCNTs. In this case, sodium dodecylbenzene sulfonate (DDBS) was chosen as the surfactant.⁵⁰

Metallic tubes present in the bundles strongly quench the emission of the semiconducting tubes,⁵² therefore big bundles of nanotubes do not present emission. However, Tan *et al.*⁵³ have recently showed that it is possible to perceive and interpret the PL of carbon nanotubes in bundles by considering the exciton energy transfer between tubes. Other processes that can severely suppress PL emission consist of chemical functionalization of SWCNTs. Cognet *et al.*⁵² reported reversible stepwise quenching of individual SWCNTs by acid and irreversible quenching of individual SWCNT exposed to diazonium salts.

4.2.6. Nuclear magnetic resonance spectrometry

Nuclear magnetic resonance (NMR) has not been among the main tools for characterization of organically modified carbon nanostructures. ¹H-NMR analysis is limited, since the signals in these derivatives are typically weak and broad, and because of the strong interference of residual solvent signals. To overcome these limitations, the applicability of proton NMR spectroscopy based on gradient-edited diffusion pulse sequences 1D diffusion-ordered spectroscopy, (1D DOSY) has been investigated⁵⁴ in the characterization of CNT derivatives. In general, diffusion NMR experiments allow the separation of NMR signals of different species present in a mixture, according to their own diffusion coefficients, merging spectroscopy information with size analysis.

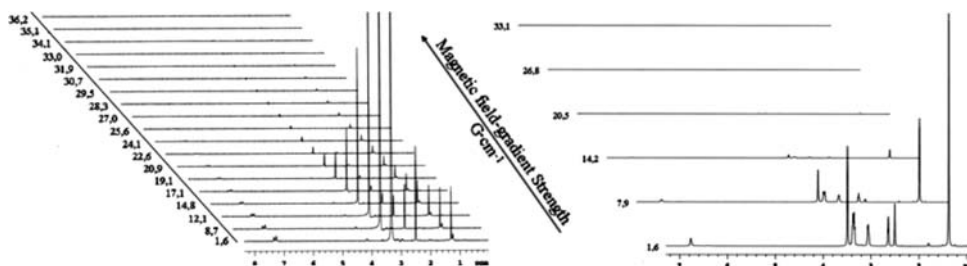


Figure 7. 1D DOSY-arrayed spectra of *d*₆-DMSO solutions of HCl · H-Phe-O-*t*Bu (with 19 increments of magnetic field gradient from 1.6 to 36.2 G cm⁻¹, left) and Boc-NH-TEG-NH₂ (with six increments from 1.6 to 33.1 G cm⁻¹, right). Reproduced from Reference 54 with permission of ACS (2009).

This study reports (Figure 7) for the first time the application of a diffusion-based NMR experiment (1D DOSY) for the characterization of covalently modified CNT derivatives. DOSY results combined with other characterization techniques support the formation of covalent derivatives of ox-SWCNTs. This analytical approach can in principle be applied to other CNT derivatives, including functionalized multiwalled CNTs or non-oxidized SWCNTs. The only limitation consists of the poor solubility of the final derivative. In addition, the amount of organic moieties able to generate adequately intense ¹H NMR signals is low in relation to the overall molecular weight. However, this technique can become very useful for determining the molecular structure and the covalent attachment in functionalized CNTs.

4.2.7. X-ray photoelectron spectroscopy

X-ray photoelectron spectroscopy (XPS) measures CNT surface composition by determining the binding energy of photoelectrons ejected when CNTs are irradiated with X-rays. The elemental composition (except for hydrogen) of the near surface region could be quantified. One main limitation of this technique is that it requires a relatively large sample amount (about 5 mg), as required by a comparatively large analysis area (about 10 μm in diameter), even for state-of-the art XP spectrometers.

4.3. Scanning probe microscopy

The techniques described in this part share some common features that consist of the application of an extremely sharp tip (3–50 nm radius of curvature) across the surface of an object and provides with valuable nanoscale information

(atomic resolution).⁵⁵ The instruments are based on a tip that is mounted on a flexible cantilever, allowing the tip to follow the surface profile. When the tip moves in proximity of the target, the interactions between the tip and the surface influence the movement of the cantilever. These changes in the amplitude of the tip movements are detected by selective sensors. Various interactions can be studied depending on the mechanics and working principle of the probe. Atomic force microscopy (AFM) and scanning tunneling microscopy (STM) are the two most common scanning techniques for characterizing *f*-CNTs. There is no gold standard technique for CNT characterization; a combination of the techniques exposed in this book chapter being more advisable.

4.3.1. Atomic force microscopy

AFM measures the interaction forces between the tip and the surface, while the tip is dragged across the surface or it vibrates as it moves. Diameter and length distributions can be determined by this technique. AFM measurements on deposited films, usually obtained from spin-coated dispersions of SWCNTs in polar solvents such as NMP at different concentrations, reveal that the bundle diameter distribution diminishes dramatically with decreasing concentration.⁵¹ The use of polar solvents is not a requirement, but it helps in the solubilization and debundling of SWCNTs. The combination of techniques acts cooperatively. SWCNT diameter distributions *in situ* measured by AFM have been backed up by photoluminescence studies over the same concentration range.⁵¹ Two representative images of singly (*f*-SWCNTs **3**) and doubly-functionalized (*ff'*-SWCNTs **4**) are shown in Figure 8. The mean length of both types of functionalized nanotubes is typically of the order of magnitude of several micrometers, while their diameters are quite different. *f*-SWCNTs (**3**) show heights between 3 and 18 nm, diameter values that are consistent with small aggregates, whereas *ff'*-SWCNTs (**4**) present diameters between 1 and 3 nm, which corresponds to individual SWCNTs and thin bundles.^{36a}

AFM can also be used to differentiate SWCNTs from other types of tubes like DWCNTs as distinct mechanical and physical features can be measured, such as the height.⁵⁶ AFM was also used to indirectly monitor the functionalization of the CNT surface. The strategy consists of using metallic particles that are selectively anchored to the organic fragments decorating the CNTs. As examples, selenium nanoparticles adsorbed on polar functional groups, introduced by an oxidative process,⁵⁷ or gold nanoparticles adsorbed on sulphur-containing substituents,⁵⁸ have been detected. However, the use of

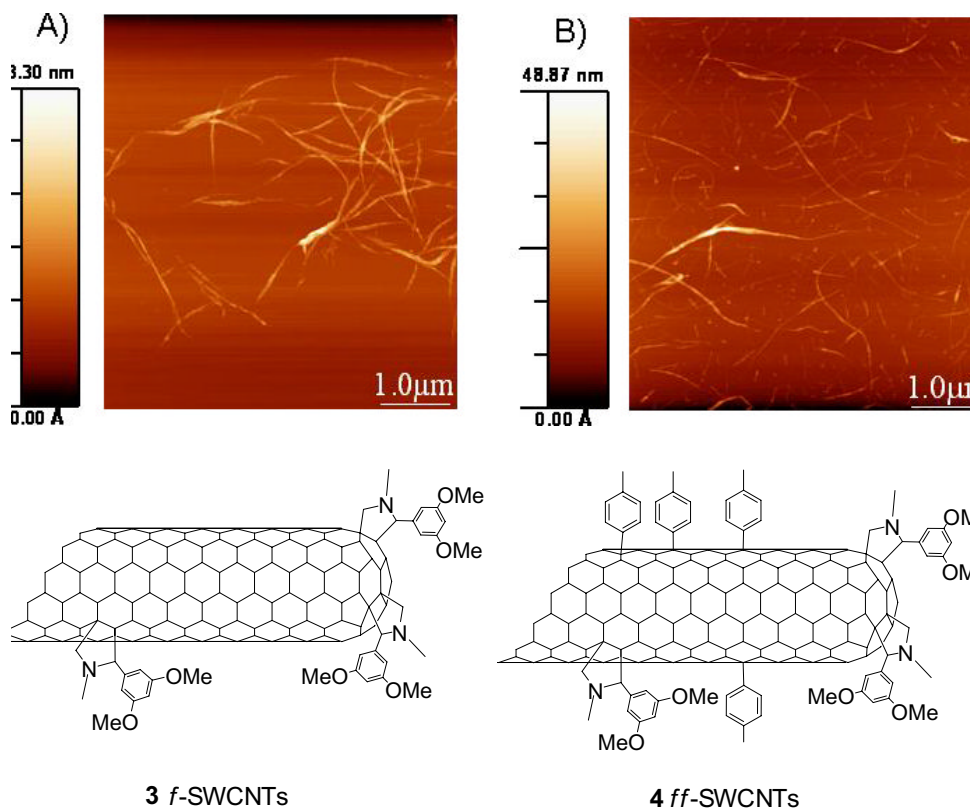


Figure 8. AFM images prepared by spin-coating on silicon wafer from DMF solution. Two representative images of (A) *f*-SWCNTs (3) and (B) *ff*-SWCNTs (4). TEM images agree with the AFM observations. Compound (3) shows small bundles of *f*-SWCNTs, whereas *ff*-SWCNT (4) presents as individuals and well-dispersed thin bundles. Reproduced from Reference 36a with permission of ACS (2008).

nanoparticles as chemical markers for AFM could lead to ambiguous results for substituent distribution, as proven with STM studies.⁵⁹

4.3.2. Scanning tunneling microscopy

STM measures the tunneling current flowing between the tip and the sample at a fixed distance. Chirality in CNTs is a significant characteristic that can also be detected by STM. Various chiralities in SWCNTs have been checked by the measurement of real-space atomic structures, according to some works reported by Lieber and Dekker groups (Figure 9).⁶⁰ They obtained hexagonal lattice images of SWCNTs and (n,m) indexes from the experimentally

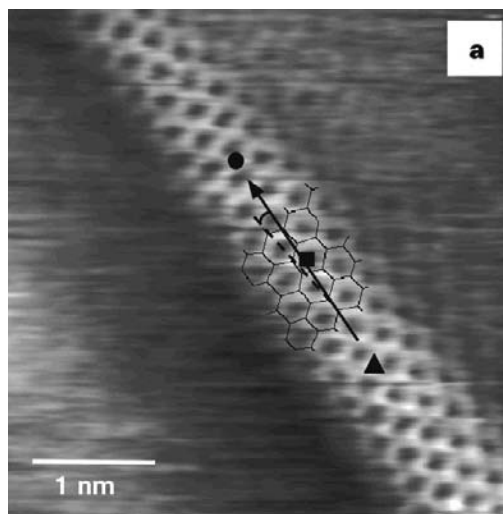


Figure 9. Atomic structure and spectroscopy of metallic SWCNTs. STM image of a SWNT exposed at the surface of a rope. The image was recorded in the constant-current mode with bias voltages of 50 and 150 mV, respectively, and tunneling current of 150 pA. The image was low-pass filtered. The tube axis in the image is indicated with solid, black arrow, and the zigzag direction is highlighted by a dashed line. A portion of a two-dimensional graphene layer is overlaid in this image to highlight the atomic structure. The symbols correspond to the locations where I–V were measured. Reproduced from Reference 60 with permission of Nature Publishing Group (1998).

measured values of the chiral angle and diameter. The usefulness of these techniques is based on the fact that a simultaneous correlation of the atomic structures with the electronic properties of nanotubes can be found by the use of Scanning tunneling microscopy and spectroscopy (STS).

One of the most relevant STM applications resides in the possibility of imaging organic functional groups covalently attached to the nanotubes. Examples are numerous in the literature, as images for fluorinated SWCNTs, SWCNTs functionalized *via* a Bingel reaction, and for thiol- and thiophene-functionalized SWCNTs were reported.⁶¹ Our STM studies on short SWCNTs, functionalized with alkylamino chains such as octylamine and octadecylamine, have unambiguously shown the presence of aliphatic moieties attached predominantly to the tips of the oxidized nanotubes.⁶² This finding agrees with the higher reactivity of the tips produced by the higher strain at these locations which are due to the high presence of carbon pentagons. This concurs with Sano *et al.* that synthesized star-shaped adducts from SWCNTs shortened with acids, obtaining a bigger functionalization at the tips and treating them with tenth-generation amine-terminated PAMAM dendrimers.⁶³

4.4. Electron microscopy

4.4.1. Transmission electron microscopy

Transmission electron microscopy (TEM) is very likely the main tool for the morphological visualization of CNTs. At low magnification, it is useful to visualize the bulk sample and measure CNT lengths and diameters. The purity of the sample can also be studied. However, one of the main drawbacks is the lack of representativity of TEM studies. In fact, due to several limitations of this technique, only a tiny fraction of the whole sample is studied. On the contrary, high resolution TEM (HRTEM) can provide images with atomic resolution. With the development of HRTEM techniques, applications such as direct imaging of chiral structures of nanotubes have been achieved in addition to diffraction studies.⁶⁴ To avoid damages caused by the beam, the energy should be kept to 100 keV.⁶⁵ Recently, Qin has shown that electron diffraction patterns could provide an accurate and unambiguous assignment of the chiral indexes of SWCNTs.⁶⁶ The chiral indexes can be read with a high accuracy from the intensity distribution on the principal layer lines in an electron diffraction pattern.⁶⁷ Hirahara *et al.* recently reported the first 3D-like aberration-corrected HRTEM imaging of SWCNTs.⁶⁸ Luzzi and collaborators published⁶⁵ images of “nanoscopic peapods” nanotubes containing tightly packed chains of spherical-cage-like “buckyball” carbon molecules. This work demonstrated a new way to exploit the open space in the tubes and possibly gain more control over their properties, but ordinary C₆₀ buckyballs were not expected to have much of an effect.

HRTEM can be used to count the number of walls in MWCNTs and measure inner and outer diameters. Figure 10, taken by Ijima,⁶⁹ shows the different walls on MWCNTs.

4.4.2. Scanning electron microscopy

Scanning electron microscope (SEM) is a type of electron microscope that images the sample surface by scanning it with a high-energy beam of electrons in a raster scan pattern. Electrons interact with the atoms that make up the sample producing signals that contain information about the sample's surface topography, composition and other properties such as electrical conductivity. One of the main disadvantages of this technique is the low magnification, that is, it is not possible to provide atomic resolution. Another interesting technique is Z-contrast scanning transmission electron microscopic (STEM), which allows the detection of a mass thickness contrast, resulting in higher intensities in correspondence to thicker regions and/or heavier elements.

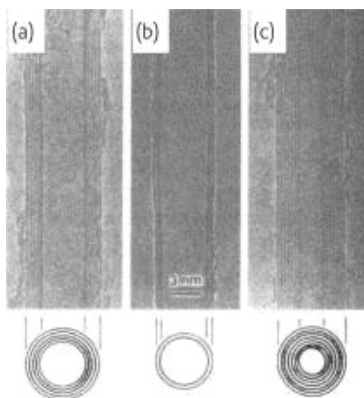


Figure 10. HRTEM images of MWCNTs, with 3, 5 and 7 concentric walls respectively (Images from Ijima.). Reproduced from Reference 69 with permission of Nature Publishing Group (1991).

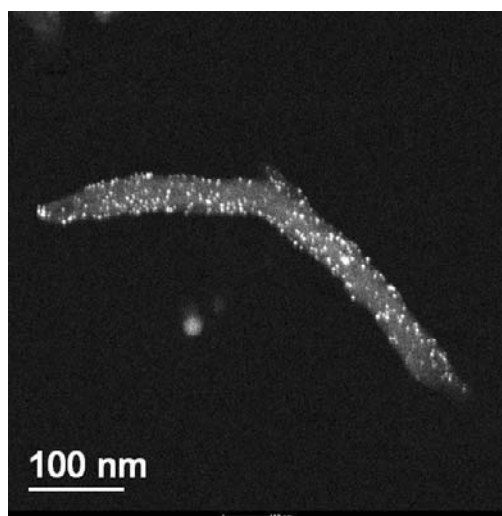


Figure 11. STEM-HAADF (scanning transmission electron microscopy-high angular annular dark-field) image of the gold nanoparticles encapsulated in dendrimers attached to cut-MWCNTs. Reproduced from Reference 92 with permission of ACS (2010).

Figure 11 shows a STEM-HAADF (scanning transmission electron microscopy-high angular annular dark-field) image of the gold nanoparticles encapsulated in dendrimers attached to cut-MWCNTs. The high nuclear density of Au particles provides with a good contrast of the metal along the MWNT surface.⁷⁰ In future studies, this will facilitate the recognition of the MWCNTs in the cellular media, because cellular organelles have dimensions

and an electron contrast that are similar to MWCNTs. Au DENs are suitable as biological markers, as Baker and coworkers have recently shown.⁷¹

5. Organic Functionalization of CNTs

Owing to the extraordinary structural, mechanical and electronic properties, CNTs show a strong potential for applications in electronics, scanning probe microscopy, chemical and biological sensing, medicinal chemistry, reinforced composite materials, and many other areas.⁷²

The manipulation of CNTs is a tough matter, and the main reasons are the following:

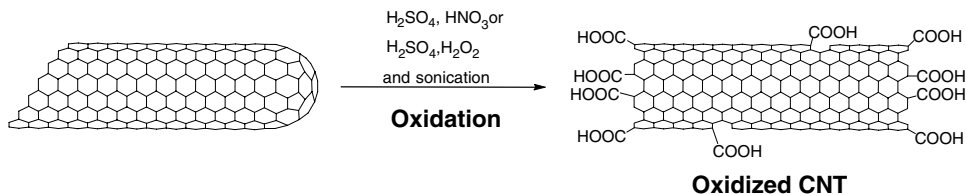
- (a) Pristine CNTs form bundles, very difficult to separate, arising from strong van der Waals forces. The bundles can be dispersed in some solvents by sonication, but precipitation occurs immediately as soon as the process is interrupted.
- (b) Pristine CNTs have very low solubility in all organic solvents and aqueous solutions.
- (c) Pristine CNTs were found to be inert under many chemical reaction conditions.

Significant advances have been achieved towards solubilizing and functionalizing CNTs since their discovery.^{3j,73} The main approaches for the modification of CNTs can be categorized as: (i) the covalent^{27b,74} attachment of chemical groups onto the surface of CNTs; (ii) the non-covalent⁷⁵ adsorption or wrapping of functional molecules; and (iii) the endohedral filling of the inner empty cavity of CNTs. In this chapter, we will mainly focus on the covalent attachment of chemical groups onto the surface of CNTs.

5.1. Covalent surface chemistry of CNTs

Two approaches have been developed for the covalent functionalization of carbon nanotubes:

- (a) Defect-site functionalization (amidation and esterification of oxidized CNTs). The treatment of pristine CNTs with strong acidic and oxidative conditions produces short opened CNTs with functionalities such as carbonyl, carboxyl, hydroxyl, etc.¹⁶ The acidic functions can give ester or amide derivatives by reaction with alcohols or amines, respectively.



Scheme 2. Oxidation scheme with different oxidizing agents.

- (b) Addition chemistry to CNTs (covalent sidewall and tip functionalization). Several methods have been developed to attach organic moieties directly onto the nanotube sidewalls. Some of the most representative reactions are: cycloadditions, electrophilic and nucleophilic or radical additions, etc.^{3j,76}

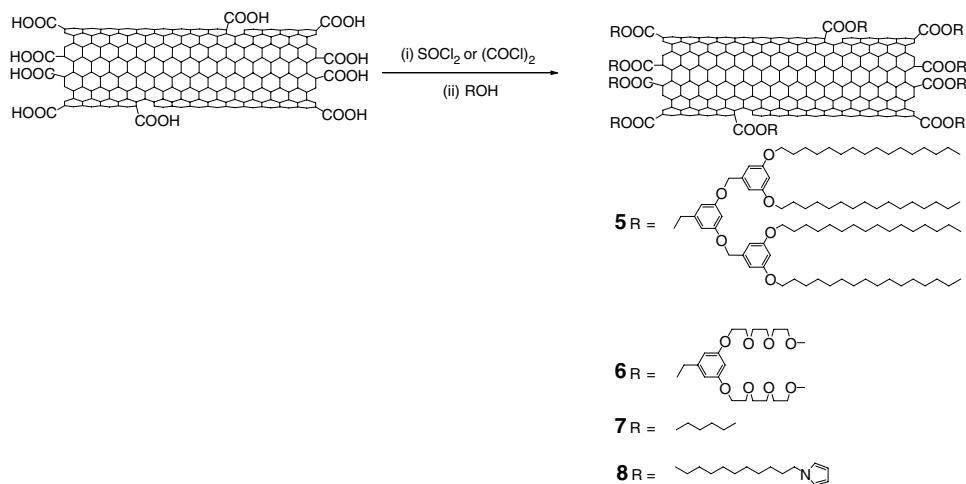
5.1.1. Amidation and esterification of oxidized CNTs

The terminal carbons and the carbons at the defect sites were converted into carboxylic acids by the treatment of pristine CNTs with nitric acid or a mixture of concentrated sulfuric acid and nitric acid. This treatment have been found to be effective to decap⁷⁷ or shorten CNTs.¹⁶ The coupling in the amidation and esterification reactions could be performed by two basic ways: (i) *via* an acyl chloride intermediate obtained by reaction of oxidized SWCNTs with oxalyl chloride/thionyl chloride or (ii) by the formation of zwitterions through an acid base reaction using coupling agents as EDC/HOBt.

5.1.1.1. Esterification reactions

Dendritic molecules (**5–6**) (Scheme 3) which are terminated with long alkyl chains and oligomeric polyethylene glycol (PEG) moieties have been attached to SWCNTs by Sun *et al.*⁷⁸ The derivative containing oligomeric PEG moieties (**6**) shows good solubility in organic solvents and water. Following a similar procedure, the esterification of acid SWCNTs with *n*-pentanol was reported by Alvaro *et al.*⁷⁹ The final derivative (**7**) is soluble in organic solvents, exhibiting high quantum yield, and short-lived vibrationally-structured photoluminescence.

The esterification reaction between the acidic groups of CNTs⁸⁰ and porphyrin units with different moieties has been executed. The different chains attached to the porphyrin are responsible of the behaviour of the final derivatives. Recently, the esterification reaction of long alkyl pyrrole moieties



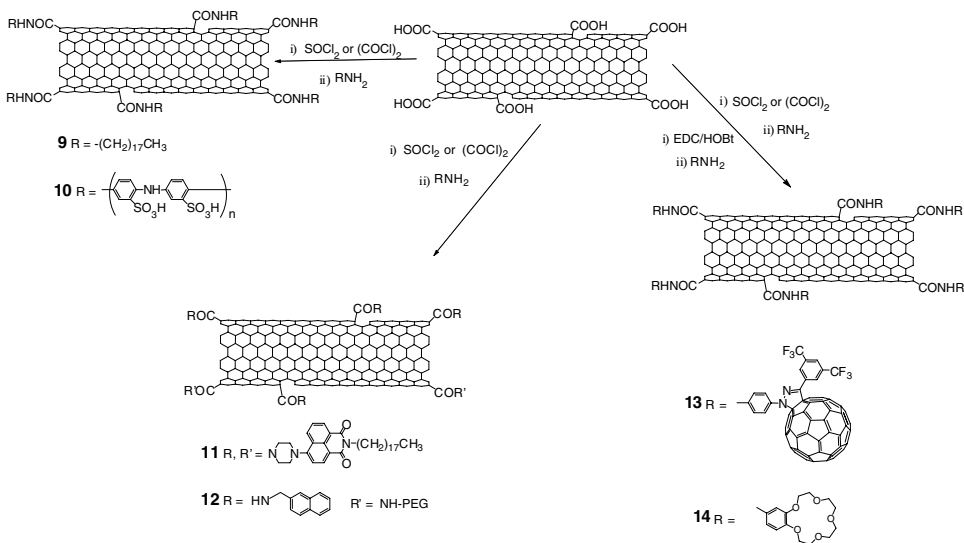
Scheme 3. Functionalization of SWCNTs *via* ester linkages.

to oxidized SWCNTs has been reported by Cosnier and Holzinger.⁸¹ The pyrrole-ester-SWCNTs (**8**) were solubilized in THF and electropolymerized by controlled potential electrolysis at 0.95V.

5.1.1.2. Amidation reactions

The covalent functionalization with octadecylamine (**9**) and 4-tetradecylaniline groups *via* an amide link was the first approach reported,⁸² and the final derivatives are soluble in most of the organic solvents (Scheme 4). In order to improve the solubility in water, the poly(*m*-aminobenzene sulphonic acid) (PABS)⁸³ group was linked (**10**) to the CNTs. Using a similar strategy, various fluorescent probes were attached at the ends of SWCNTs for photophysical studies (Scheme 4). The synthesis of chromophore functionalized SWCNTs was reported by amidation reaction between a fluorescent moiety and oxidized SWCNTs (**11**) by Zhu *et al.*⁸⁴ Simultaneously, it was successfully performed a double-functionalization through amidation reaction of poly(ethylene glycol) amine (PEG-NH₂) and amine derivatives of aromatic fluorophores like naphthalene (**12**), fluorene and anthracene onto SWCNTs bearing carboxylic end groups by Menna and collaborators.⁸⁵ The strong intramolecular interactions between tubes and the attached aromatic fluorophores suggested quenching of fluorescence.

Novel photovoltaic devices and nanohybrid materials can be constructed by the attachment of modified supramolecular moieties to oxidized nanotubes

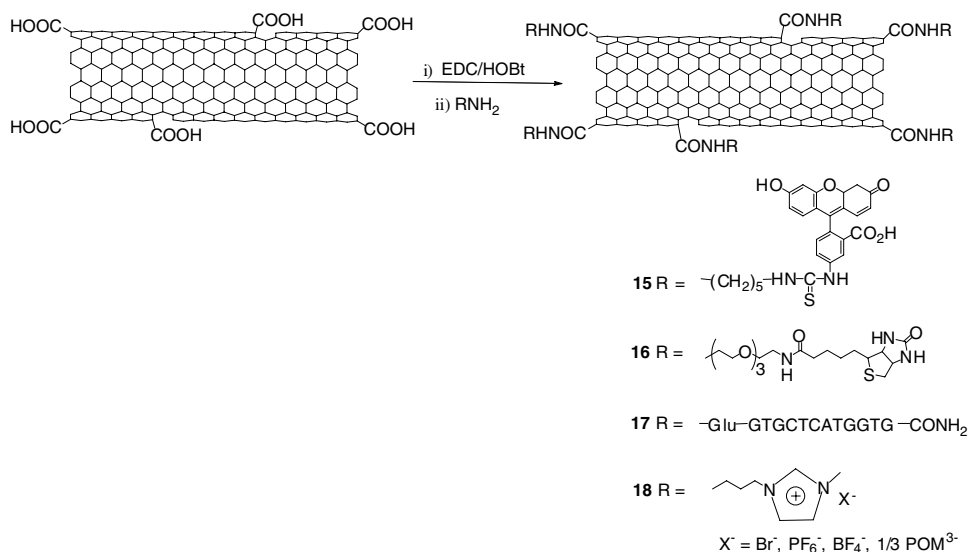


Scheme 4. Covalent functionalization of SWCNTs following amidation reaction of carboxylic groups.

(Scheme 4). SWCNT-fullerene derivatives had been prepared by similar strategies; the first conjugated nanohybrid material (**13**) was performed between a carboxylic-SWCNT and an aniline-fullerene derivative.⁸⁶ The decoration of SWCNTs with crown-ether chain (**14**) was performed by a direct heating method that formed a stable monolayer at the air-water interface by Feng *et al.*^{87a} The corresponding Langmuir–Blodgett films were stable and could be integrated into hydrophilic silicon substrates.

Multifunctional architecture obtained after the amidation reaction has been applied to biological applications and materials science.

Potential carriers that transport and deliver various bioactive components into cells have been studied with SWCNTs. New bioelectronics systems (*e.g.*, biosensors) are able to be designed by the combination of conducting properties of SWCNTs and the recognition properties of biomaterials. Nanotubes were functionalized either by fluorescein or biotin moieties (**15** and **16**, respectively) (Scheme 5) by Dai and collaborators.⁸⁸ Small nanotubes were also functionalized with a peptide nucleic acid (PNA).⁸⁹ The sequence of complementary DNA specifically interacted with the PNA-SWCNT conjugate (**17**). This recognition property can be exploited in biology as a new type of biosensor. Multifunctional architectures for charge transfer devices have been prepared by binding the carboxylic functions of SWCNTs to ionic liquids (ILs) and polyoxometalates (POMs) (**18**).⁹⁰



Scheme 5. Covalent functionalization of SWCNTs following amidation reaction of carboxylic groups.

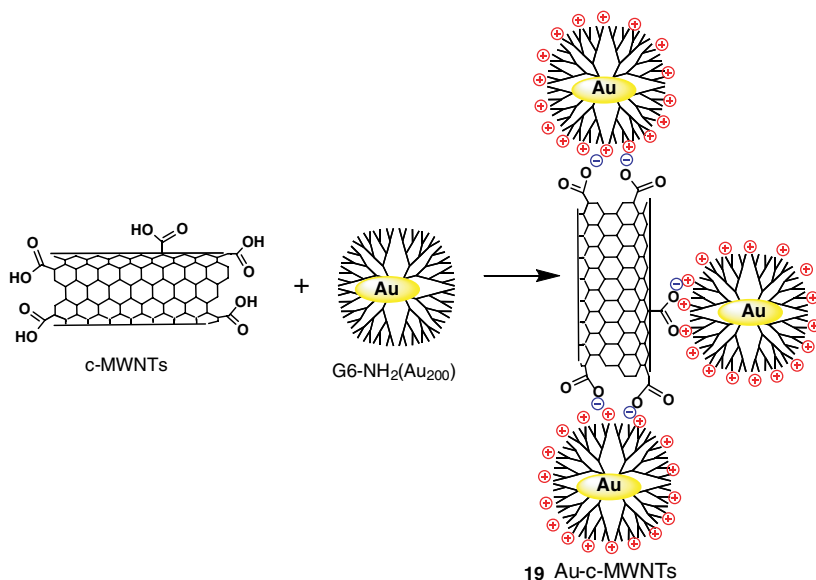
Under similar conditions, the coupling reaction between short MWCNTs and free amino groups was reported.

Zhu and collaborators⁹¹ studied the modification of MWCNTs by the reaction of a secondary alkylamine with the chlorinated acidic moieties of the tubes, following Haddon's approach.^{2a,82,83} The adduct exhibited good optical limiting properties.

Mild reaction conditions⁹² during Gold Dendrimer-Encapsulated Nanoparticles (Au DENs) attachment and high MWCNT solubility have been proven to be key factors for obtaining monodisperse Au nanoparticles which are fully distributed along the MWNT surface (**19**). The particle coverages obtained for MWNT/DEN composites at the lower temperatures used in that work are sufficient for potential applications such as the study of MWCNTs as carriers for drug delivery, gene transfer, and image contrast agents (Scheme 6).

5.1.2. Covalent sidewall (and tip) functionalization

Alternative to the functionalization on the carboxylic groups that are generated as focal points, addition reactions could be performed directly on pristine CNTs without further modifications. Chemical changes of CNTs are easier due to the presence of defects which form in their synthesis. Covalent



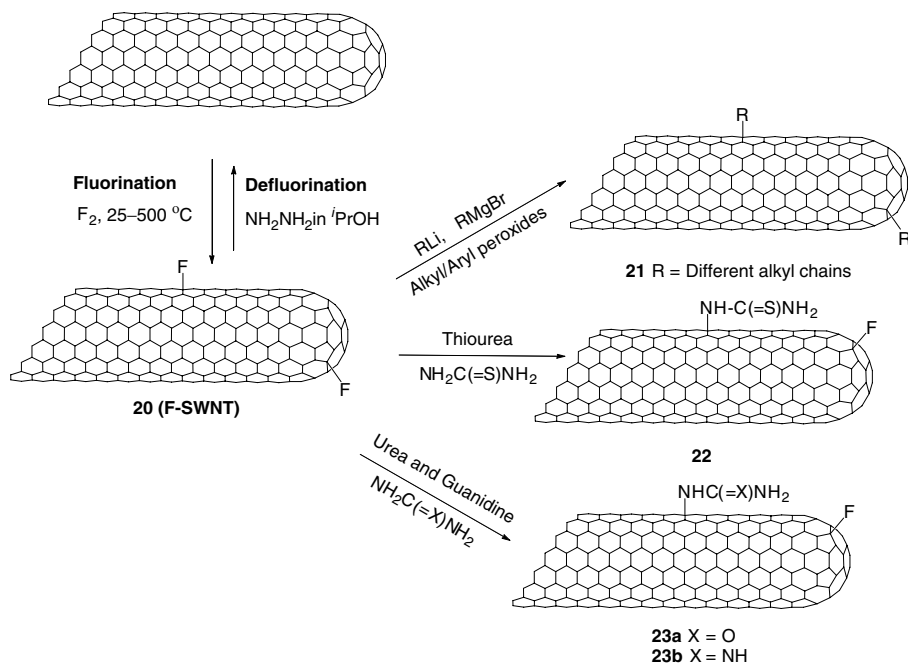
Scheme 6. Gold DENs attachment on the MWNT surface under mild conditions.

reactions are most likely to happen on the most reactive parts (near to defects, tips...).⁹³ The covalent bond on the surface causes the transformation of sp^2 - into sp^3 -hybridized carbon atoms. Sidewall functionalization has been achieved either on pristine or oxidized and/or modified CNTs.^{3j,94}

5.1.2.1. Halogenation

CNT fluorination introduces highly polar C-F bonds into the CNT side-walls, which alter the nanomaterial electronic properties. Fluorine atoms are often grafted into the CNT surface by exposing CNTs to F₂ at high temperatures. In several studies, XPS has been used to correlate the effect of the exposure time to F₂.⁹⁵ Shulga *et al.*^{95c} were able to determine that, after exposing MWCNTs to F₂ gas at 420 °C, most of the present species were C-F groups.

C-F groups are very useful as starting materials because further substitutions of F atoms make possible incorporating other functional groups.⁹⁶ The fluorine atom can be replaced with alkyl groups by using Grignard's^{25a} or organolithium reagents.⁹⁷ Alkylated CNTs are well dispersed in organic solvents and can be completely dealkylated upon heating at 500 °C in inert atmosphere or with anhydrous hydrazine, thus recovering pristine CNTs and demonstrating the process reversibility. The disappearance of fluorine

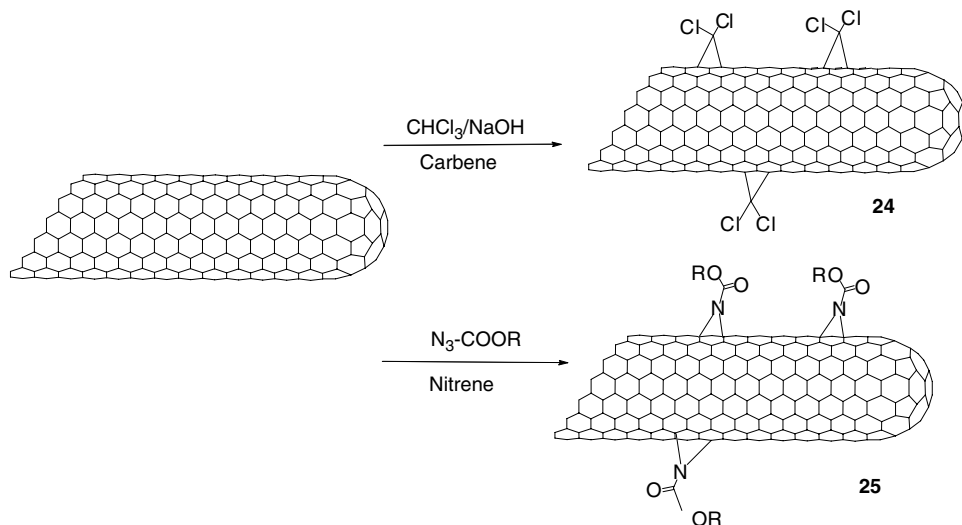


Scheme 7. Fluorination as a useful strategy to covalently modify the SWCNT skeleton.

atoms could be confirmed even by IR or XPS. Several diamines⁹⁸ and diols⁹⁹ were reported to substitute fluorine atoms on fluorinated CNTs. Some samples are shown in Scheme 7: the reaction of F-SWCNTs (**20**) with urea, guanidine and thiourea moieties (**22**, **23a–b**) was reported by Pulikkathara *et al.*¹⁰¹ (Scheme 7), leading to partial nucleophilic substitution of fluorine.¹⁰¹ Urea functionalized F-SWCNTs (**23b**) form stable dispersions in DMF and water. The introduction of more sophisticated functionalities could allow the synthesis of more complex molecules for many applications.

5.1.2.2. Addition of carbenes and nitrenes

The addition reactions of carbenes and nitrenes to CNTs are summarized in Scheme 8. Haddon group¹⁰² was the first to employ dichlorocarbene generated *in situ* by using a chloroform/sodium hydroxide or a phenyl(bromodichloromethyl)mercury reagent on oxidized CNTs. The attachment of the very reactive CCl_2 moiety to CNTs was confirmed by a combination of several characterization techniques (XPS, far-infrared spectra and chemical analysis). Some other cyclopropanation reactions have been described with



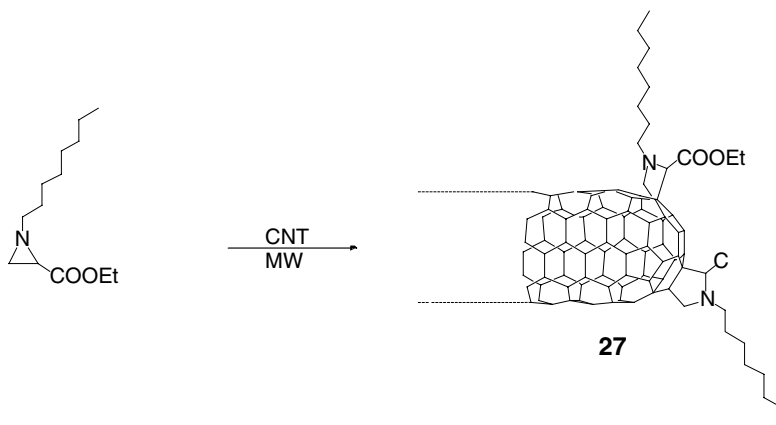
Scheme 8. Functionalization of carbon nanotubes by addition of carbenes and nitrenes.

different precursors of carbene.¹⁰³ The attachment of carbene groups with reactive moieties at the end of the alkyl chain could open the possibilities to modulate the CNTs for different applications.

Thermal decomposition of an organic azide renders to alkoxy carbonylnitrene, and the attachment of this intermediate resulted in the formation of alkoxy carbonylaziridino-CNT.^{2b,104} A variety of different functional groups have been attached onto CNTs by using different azides.^{3h,105} Some water soluble derivatives, prepared by this methodology, have been administrated to tumor-bearing mice and were found to specifically target to the tumor.¹⁰⁶ The irradiation of the photoactive azidothymidine in the presence of nanotubes was found to cause the formation of very active nitrene groups in the proximity of the carbon lattice. In a cycloaddition reaction, these nitrene groups couple to nanotubes and form aziridine adducts.¹⁰⁷

5.1.2.3. 1,3-dipolar cycloaddition

In a similar way to the known 1,3-dipolar cycloaddition of azomethine ylides to fullerenes,¹⁰⁸ our group has developed a strategy for functionalizing and solubilizing CNTs.¹⁰⁹ The azomethine ylides are generated *in situ* by the condensation of α -amino-acids and aldehydes (Scheme 9a). In our first application reported, the triethylene glycol group was used as one of the first *N*-substituent group of the α -amino acid (Scheme 9b).



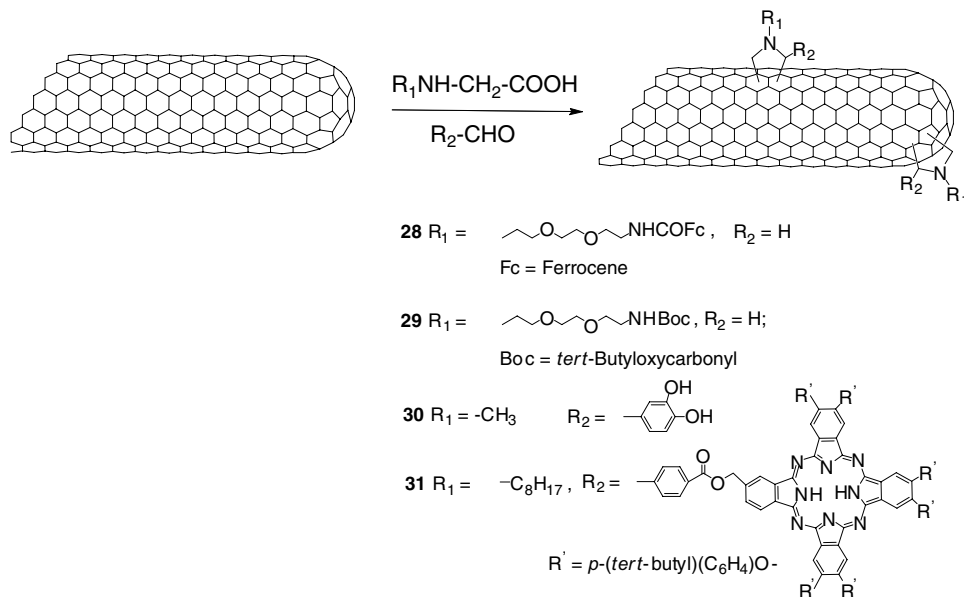
Scheme 10. Microwave irradiation applied to aziridine addition onto CNT surface.

different approach when considering the chemistry of CNTs, because in the absence of solvents, CNTs absorb directly the radiation and it is possible to take full advantage of the strong microwave absorption which is typical of pristine nanotubes. Moreover, the solvent-free conditions pave the way to green protocols and large-scale functionalization.

Considering the advantages of the microwave technique, CNTs have been functionalized by employing aziridines as starting materials under solvent-free conditions (Scheme 10). SWCNTs functionalized under microwaves in 1 hour, display a TGA loss of about 20%, which corresponds to the presence of one functional group for about 76 carbon atoms, while the same reaction performed in DMF under classical heating proceeds in 5 days and introduces only one functional group per about 138 carbon atoms of the CNT skeleton. Moreover, under microwaves the overall sequence can be repeated twice in order to further increase the number of pyrrolidine rings attached to the side-wall of the tubes. As an indirect proof of functionalization, retrocycloaddition of CNTs has been verified in the presence of C_{60} to trap the corresponding ylide.

The introduction of donor groups CNTs such as ferrocene¹¹³ (**28**) develops new model derivatives for application in photovoltaics (Scheme 11). In addition, these ferrocene-nanotube hybrid materials can be used as electrochemical sensors and biosensors for the selective recognition of anions.¹¹⁴

Due to its versatile characteristics, the 1,3-dipolar cycloaddition can be performed with protected amino end groups (**29**). After a deprotection step, an ideal anchor point is created for further reactions (Scheme 11).¹¹⁵ Stable



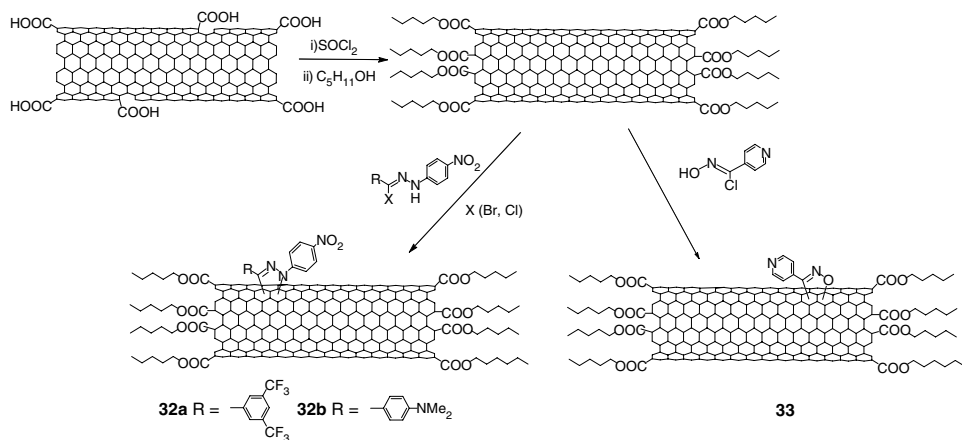
Scheme 11.

dispersions of CNTs in organic and aqueous solvents have been obtained by the attachment of phenol groups (**30**) to the sidewall of CNTs by 1,3-dipolar cycloaddition.¹¹⁶ The dispersion stability, in different solvents and water, allows the preparation of composites. The synthesis and photochemical properties of phthalocyanyl-SWNT ensembles (**31**) were described by Torres and co-workers.¹¹⁷

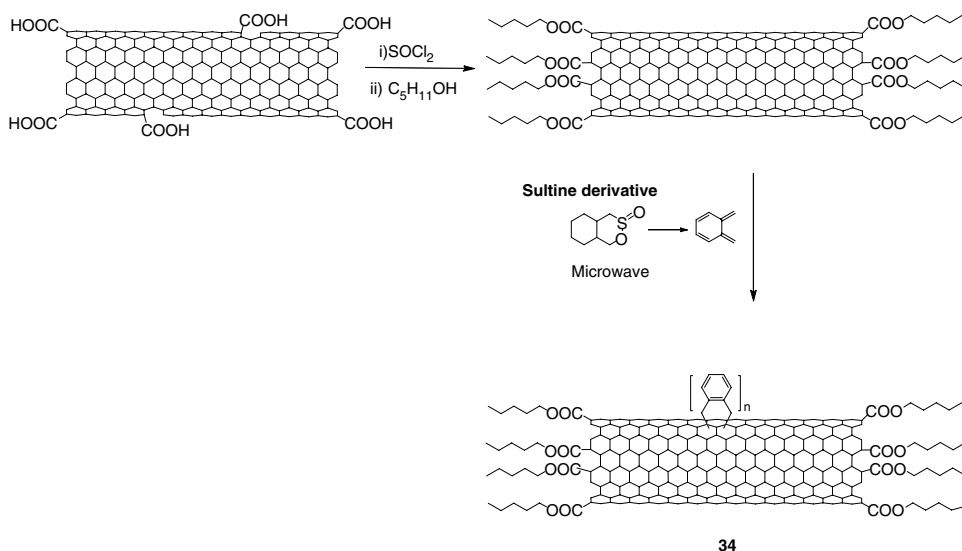
1,3-Dipolar cycloaddition of nitrile imines and nitrile oxide to the sidewalls of modified SWCNTs¹¹⁸ has been described by Langa and co-workers. Modified cut-CNTs with pentanol, were functionalized with 5-diarylpyrazoline or pyridyl-isoxazoline rings to produce (**32**) and (**33**) respectively.

5.1.2.4. Diels–Alder cycloadditions

Diels–Alder cycloaddition is one of the most general reactions in basic organic chemistry. However, due to its easy reversibility, this reaction is not very useful for the functionalization of CNTs. There are a few examples in the literature that use this reaction to modify the CNT backbone, sometimes taking advantage of the use of microwave irradiation. Short nanotubes, esterified with pentanol, were modified in the presence of *o*-quinodimethane generated



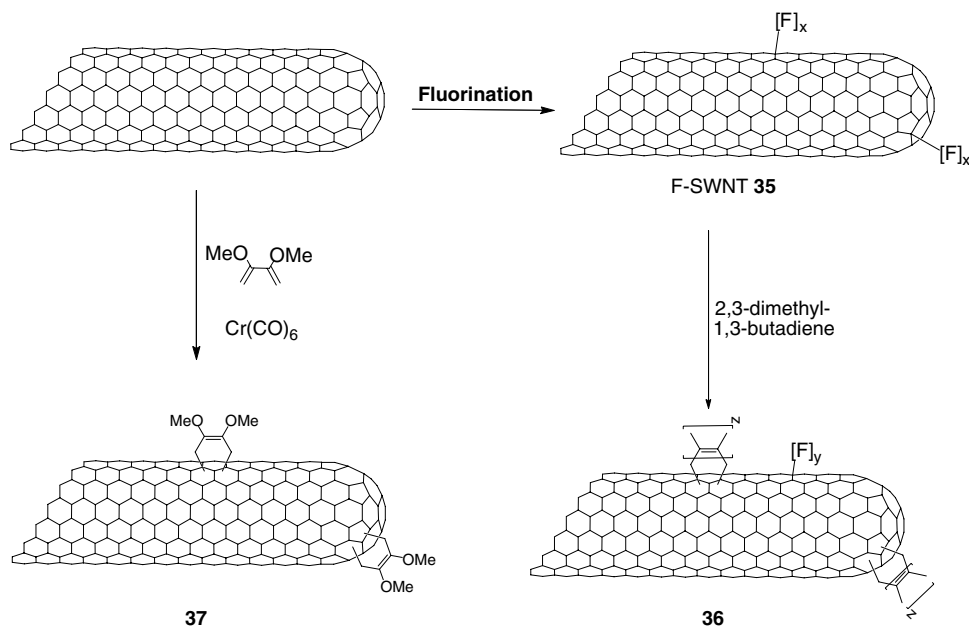
Scheme 12.



Scheme 13.

in situ from the corresponding 4,5-benzo-1,2-oxathiin-2-oxide (sultine) derivative (**34**) (Scheme 13) under microwave irradiation.¹¹⁹

Zhang *et al.*¹²⁰ performed facile Diels–Alder cycloaddition onto F-SWCNTs (**35**) with a large range of dienes (**36**). Another option, in order to avoid prior covalent modification, is the employment of chromium derivatives for the complexation with CNTs, and therefore the activation of the cycloaddition reaction with an electron-donating diene (**37**).^{2c}

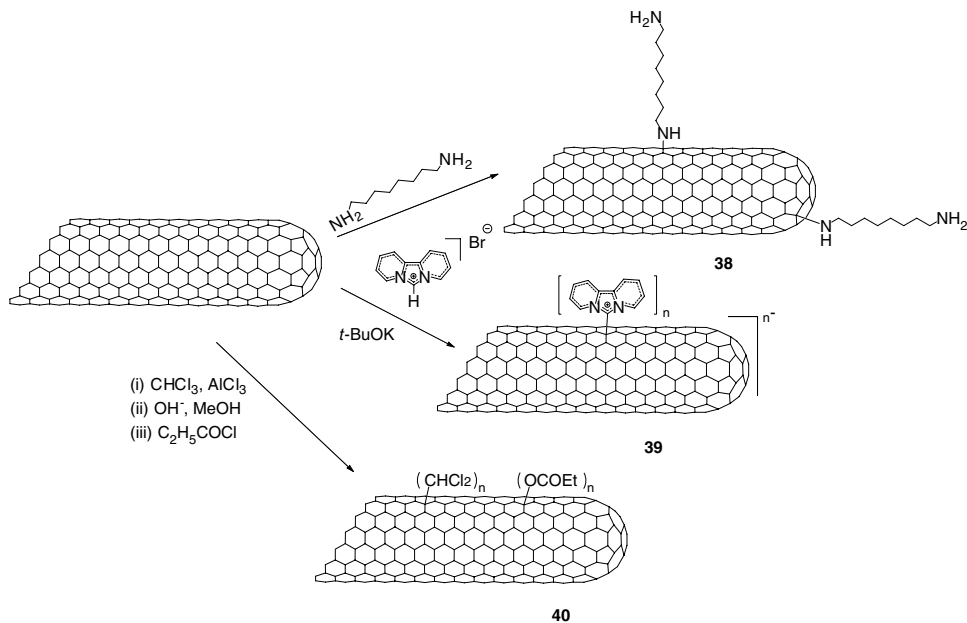


Scheme 14.

5.1.2.5. Nucleophilic and electrophilic additions

The nucleophilic addition of carbenes to CNTs¹⁰⁴ was reported by Hirsch and co-workers. The final compound (**39**), observed after the reaction, was the zwitterion as it is shown in Scheme 15. Several studies have been focused on the nucleophilic addition of amine derivative to the surface of the CNTs. Basiuk *et al.*¹²¹ reported the addition of octadecylamine to CNTs (**38**) in a solvent-free procedure. It was suggested that, due to the higher concentration of the five member rings, the addition takes place only on closed caps of MWCNTs. Nevertheless it should be taken into account that the real nanotube sidewalls must contain numerous reactive five-membered rings, like defects, and while reactions on the walls should not be overlooked. Treating pristine CNTs with *sec*-BuLi, and subsequently with carbon dioxide, was reported to be another example of nucleophilic addition.¹²²

Tagmatarchis *et al.*¹²³ reported an electrophilic addition. Upon mechanochemical reaction in the presence of a Lewis acid, such as aluminum trichloride, a molecule of $CHCl_3$ was found to add to the sidewalls of nanotubes in the form of $CHCl_2$ and Cl groups. The chlorine atoms were directly exchanged with hydroxyl groups that were esterified to yield the corresponding ester hybrid (**40**), providing with an enhanced solubility in organic solvents.

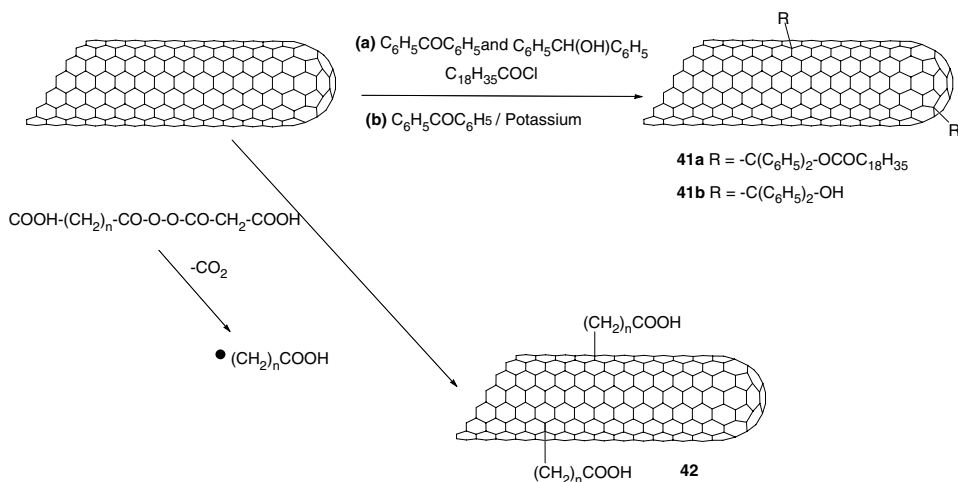


Scheme 15. Nucleophilic and electrophilic additions to CNTs.

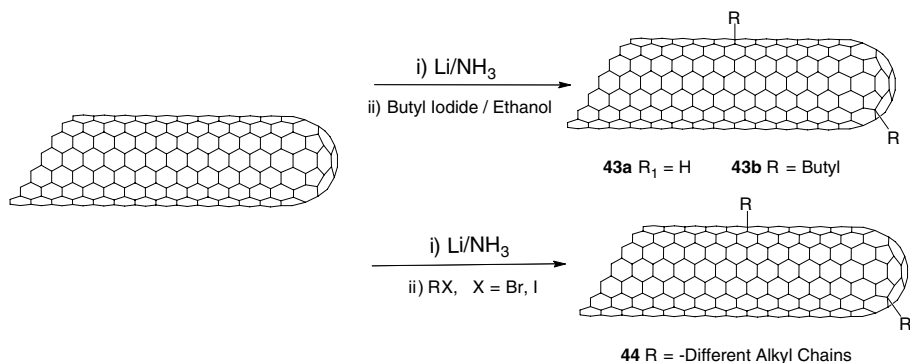
5.1.2.6. Free-radical additions

It has been reported that free radicals can react with CNTs. In general, radicals may be formed photochemically and/or thermally in oxidation/reduction reactions by inorganic ions, resulting into a single electron transfer, and by electrolysis. Covalent sidewall functionalization was reported by photoreduction of aromatic ketones.¹²⁴ In this methodology, benzophenone in the excited state removes a hydrogen atom from benzhydrol, leading to the generation of benzhydrol radical, which readily adds to the nanotubes. Since the excited benzophenone triplet is reactive to many types of other C-H bonds like amines, ether, hydrocarbons, or aliphatic sulphides, a wide variety of radicals could be generated by using this photochemical approach. Consequently, an esterification reaction was performed onto OH functional groups (**41a**). The functionalization of SWCNTs with diphenylcarbinol groups (**41b**) was also reported by the reaction of benzophenone in the presence of potassium.¹²⁵

The addition of carboxyalkyl radicals onto sidewalls **42** was performed by the reaction of CNT with succinic or glutaric acid acyl peroxides (Scheme 16).¹²⁶ These derivatives were converted to acid chlorides and then to amides with different amines.



Scheme 16. Functionalization of SWCNTs using radical additions.



Scheme 17. Functionalization of SWCNTs using Birch reduction and reductive alkylation, arylation and polymerization reactions.

5.1.2.7. Reduction and reductive alkylations

Carbanionic CNTs are very reactive intermediate that can be generated quite easily. The first example reported about the chemical hydrogenation of SWCNTs *via* a Birch reduction was performed with lithium and sodium in ethylene diamine or liquid ammonia and methanol by Pekker *et al.*¹²⁷ Similarly, different strategies have been applied to endow CNTs with alkyl chains (**44**). Wunderlich *et al.*¹²⁸ performed reductive hydrogenation (**43a**) and alkylation (**43b**) of SWCNTs in liquid ammonia by sodium metal in the presence of ethanol/butyl iodide, to investigate the SWCNT

reaction selectivity. It was found that SWCNTs with smaller diameters were considerably more reactive than tubes with larger diameters. Moreover, this reaction sequence favors the preferred functionalization of metallic over semiconducting SWCNTs. Catalytic amounts of 4,4'-di-*tert*-butylbiphenyl (DTBP), used as the electron carrier, efficiently promotes the formation of carbanionic SWCNTs in THF and in the presence of lithium metal.¹²⁹

5.1.2.8. Direct arylations

5.1.2.8.1. Diazonium coupling

One of the most useful reactions in the functionalization of CNTs is the diazonium coupling reaction on the surface of CNTs, as described by Dyke and Tour¹³⁰ (Scheme 18). Among the main features of it, we can highlight the high degree of functionalization on the CNTs surface; this results into a relevant decrease of the electronic properties and, therefore, a reduction on the van Hove singularities.

Different reaction conditions have been tested to implement such a reaction, that can be basically divided in two stages:

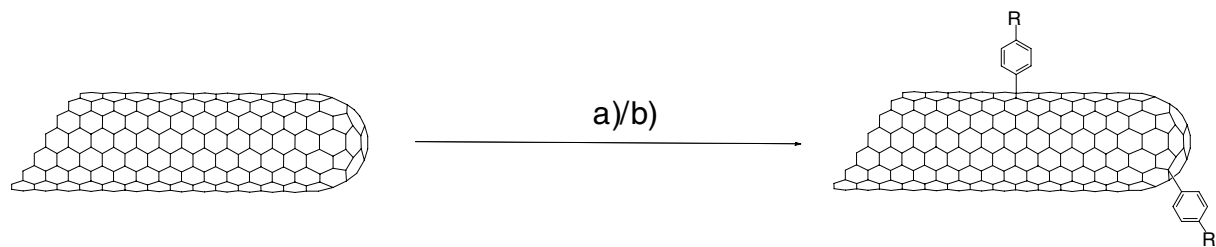
(a) diazonium salt addition to the medium hosting the reaction:

- Electrochemical reduction.
- In the presence of surfactant.
- In the presence of ionic liquids.

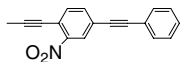
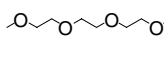
(b) diazonium salt generation *in situ*:

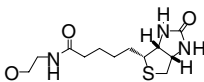
- Isoamyl nitrite, without solvent.
- NaNO_2 in Oleum, AIBN or $(t\text{-BuO})_2$.
- Isoamyl nitrite, in water.
- Triazines at different pH.

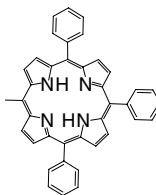
The first synthetic approach was (45) *via* electrochemical reduction of a variety of preformed aryl diazonium salts, followed by their addition onto the nanotube sidewalls.¹³⁰ Later, the SWCNT functionalization with aryl diazonium salt could be achieved, either by direct treatment with aryl diazonium tetrafluoroborate salts in solution or with the corresponding amine which was transformed *in situ* into the diazonium species by an alkyl nitrite. Aryldiazonium salts could efficiently react with SWCNTs, coated with sodium dodecyl sulphate (SDS), in water and at room temperature.

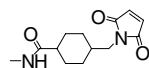


45a R = Br, Cl, F, I, NO₂, *tert*-butyl, CO₂CH₃, COOH, C₁₃H₂₉, *n*-Butyl, SO₃H, CH₂CH₂COOH

45b R = C≡C-C₆H₅, , , C≡CH,

45c R = 

45d R = 

45e R = 

Scheme 18. Functionalization of SWCNTs using diazonium coupling reactions under different conditions. For a)/b) conditions see text.

Under green chemical conditions, different approaches to arylation have been reported. Among those we can find: water as a solvent for the interaction between the aryldiazonium salt and SWCNTs coated with dodecyl sulphate (SDS) at room temperature, in the presence of ionic liquids (imidazolium-based ionic liquids with various alkyl branched chains) and K_2CO_3 by grinding them in pestle and mortar at room temperature for few minutes.¹³⁰ In aqueous media, a group from Tour also used organic triazenes as stable precursors to diazonium salts for functionalizing SWCNTs (**45d**).¹³¹

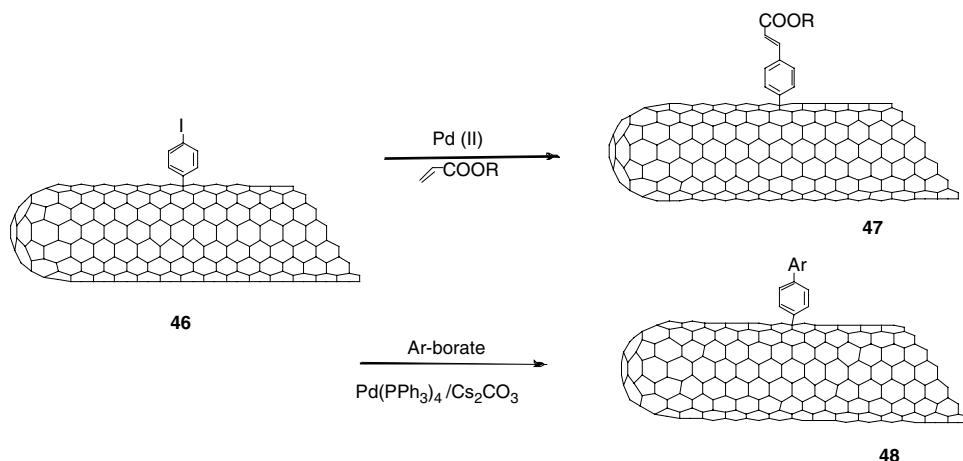
Recently, Ellison and Gasda¹³² reported the attachment of phenyl amine groups onto SWCNTs using diazonium chemistry. The free- NH_2 groups on the aryl moieties were able to undergo additional reactions, *e.g.* with the heterofunctional cross-linker succinimidyl-4-(*N*-maleimidomethyl)cyclohexane-1-carboxylate (**45e**). This facilitates the way for the coupling of additional functionalities onto SWCNTs. A similar approach, based on “click chemistry”, was recently explored to link zinc-phthalocyanine derivatives on SWCNTs that were pre-functionalized with phenylacetylene moieties.¹³³ Porphyrin diazonium compounds have also been generated *in situ* for interaction with CNTs¹³⁴ This methodology paves the way for introducing different functionalities. Hence, multifunctional SWCNTs have been synthesized by repetitive functionalization protocols, based on aryl diazonium salts, by Stephenson *et al.*¹³⁵

5.1.2.8.2. C-C coupling chemistry catalyzed by Palladium

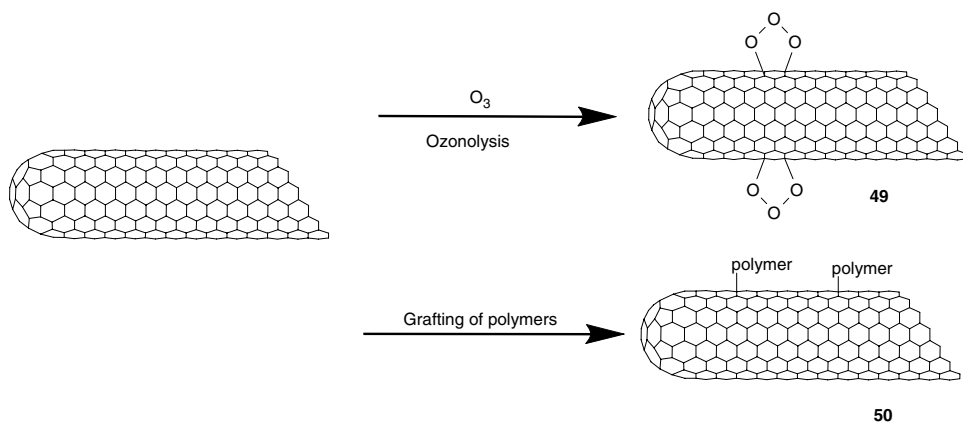
Heck¹³⁶ and Suzuki¹³⁷ couplings have been reported on iodophenyl prefunctionalized SWCNTs (**46**) in the presence of different palladium derivatives as the catalyst species. Final derivatives are potential chemicals in materials, science applications. The functionality of the organic addends attached to the CNT surface will depend, respectively, on the employed acrylates (**47**) or boronic acid (**48**) derivatives.

5.1.2.9. Ozonolysis

Owing to the different diameter of the nanotubes, a different behaviour of SWCNTs has been observed in the ozonolysis reaction.¹³⁸ Smaller diameter shows a higher reactivity. At very low temperature ($-78\text{ }^{\circ}C$)^{119,139} and room temperature,¹⁴⁰ ozonolysis has been induced at the surface of pristine SWCNTs, followed by controlled modification. Once the SWCNTs-ozonides have been treated with different agents, various groups such as carboxylic acid/ester, ketone/aldehyde, and alcohol groups surface were attached on the tube surface.



Scheme 19. Functionalization of SWCNTs using Heck and Suzuki-coupling reactions.



Scheme 20.

5.1.2.10. Grafting of polymers

One of the main advantages of the attachment of polymers to CNTs is the solubility increment of the final derivatives due to the long polymer chains. Two are the main methods for covalently attaching polymers to the graphitic surface of CNTs, which are defined as “grafting to” and “grafting from” methods (Scheme 20).

The “grafting to” method relies on the synthesis of a polymer with reactive functional groups and subsequent covalent attachment of this polymer chain to the surface of CNTs *via* coupling reactions.

The “grafting from” method is based on the covalent immobilization of the polymer precursors on the CNT surface and subsequent polymer chain elongation in the presence of monomeric species.

5.1.2.11. Mechanochemical functionalizations

The milling technique has been applied on pristine CNTs. Ball-milling of MWCNTs in the presence of reactive atmospheres generated final decorated CNTs.¹⁴¹ The attachment of the different groups such as amines, amide, thiols and mercaptans were confirmed by IR and XPS. Following a similar approach, due to the presence of potassium hydroxide on the media, SWCNTs were covered by hydroxyl groups.¹⁴²

It was mentioned before (5.1.2.5.) another example of a mechanochemical reaction by Tagmatarchis *et al.*¹²³

5.2. Non-covalent adsorption or wrapping of functional molecules

Van der Waals interactions and hydrogen bonding are two main interactions that are involved in non-covalent functionalization. CNTs solubility in hydrophilic solvents is commonly increased surfactants and polymers, this approach is being also used to improve their dispersion in polymer or ceramic matrices.¹⁴³ Currently, there is much interest in functionalizing CNTs with biomolecules such as peptides or DNA.^{115,144} Another approach uses the well-known π - π interactions between aromatic compounds (*e.g.*, porphyrins, pyrens) and the delocalized electron system in CNTs.^{51,145} As it has been mentioned before, the reactivity on the tips seems to be higher than on the walls.^{3j}

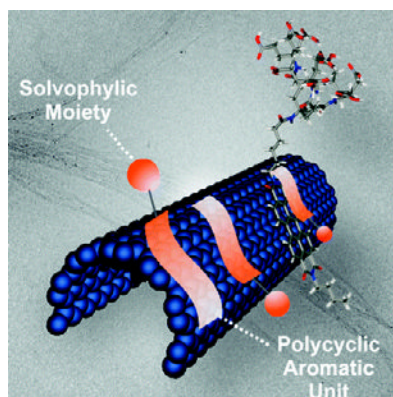


Figure 12. Reproduced from Reference 146 with permission of ACS (2009).

In contrast, by using non-covalent interactions, surfactants, aromatic compounds, and biomolecules, the different molecules can be attached equally on both tips and sidewalls for further applications. Depending on the final application of the different derivatives, the methodology should be chosen in the search of an optimal decoration. The aqueous dispersion of SWCNTs with amounts of water-soluble perylene derivatives is reported by Hirsch and collaborators.¹⁴⁶ The individualization of SWCNTs in water after ultrasonication in the presence of water-soluble aromatic perylenes was investigated in detail. The π - π -stacking interaction and the electronic interaction between the perylene unit and the nanotube surface are reflected.

5.3. The endohedral filling of the CNTs inner empty cavity

One of the main motivations for this strategy is to protect the encapsulated material from reduction/oxidation in contact with the atmosphere, and even as nanoreactors, whose confined reaction volume was expected to yield nanomaterials with new crystal structures, chemical compositions and novel properties. There have been various methods of filling, mainly depending on the cavity diameter to be filled and on the physical properties of the material being inserted (*e.g.*, viscosity, surface tension). According to them, the inserted material can be solid, liquid, or vapor.¹⁴⁷ Furthermore, the inner CNT diameter will determine the maximum size of the inserted molecules or compounds and, hence, the filling efficiency.¹⁴⁸ CNTs can be filled *in situ* during the synthetic process with materials that are used for the CNT growth (Fe, Co, Ni, etc).¹⁴⁹ In contrast to *via* washing, or vacuum annealing,¹⁵⁰ the

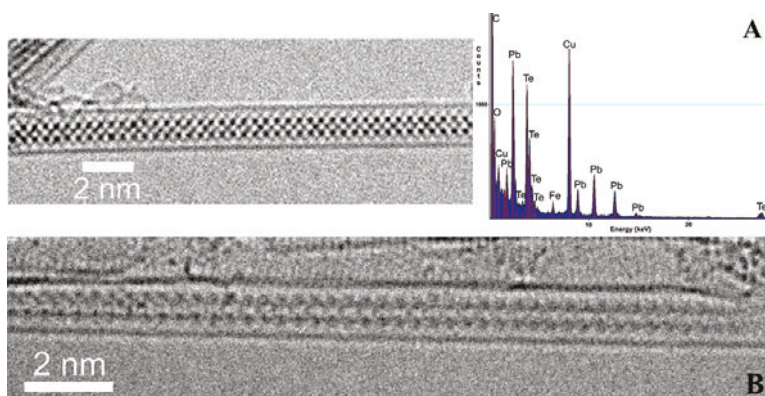


Figure 13. HRTEM imaging and EDX spectra of PbTe@SWNT (A) and ZnTe@SWNT (B) nanocomposites. Reproduced from Reference 149c with permission of ACS (2009).

filling is either carried out from the gas phase (sublimation or capillary condensation)¹⁵¹ or from the liquid phase (capillary wetting from suspension, solution, or melt).¹⁵² Monthioux *et al.*¹⁴⁷ summarized the filling strategies with their various advantages and problems. Although both MWCNTs and SWCNTs have been filled with a vast number of compounds, little is known about their properties and potential in applications.

MWCNTs were filled with metal oxides (PbO^{153} and $\text{Bi}_2\text{O}_5^{154}$), carbides (Y_3C and TiC^{155}), and metals (Ni^{156}) in 1993. Filling SWCNTs was a hard task due to their smaller diameter (1–1.5 nm). The first example with SWCNTs was performed with RuCl_3 by Sloan *et al.*¹⁵⁷ Since then, many atoms, molecules, and compounds have been incorporated into both MWCNTs and SWCNTs,¹⁴⁷ including such fascinating molecules as fullerenes ($\text{C}_{60}@\text{CNT}$, “peapods”¹⁵⁸).

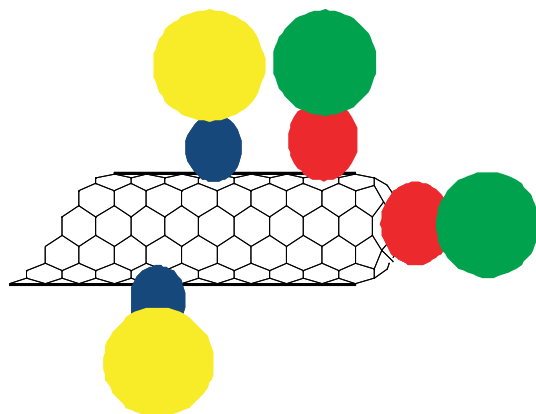
6. Double functionalization reactions

An alternative strategy¹⁵⁹ for introducing two different and orthogonal functionalizations to CNTs is to perform the 1,3-dipolar cycloaddition on the oxidized tubes. In this way, two distinctive functionalities coexist on the CNT surface. This approach enabled us to simultaneously link fluorescent probes to CNTs for tracking the uptake of material as well as an antibiotic moiety as the active molecule. For this purpose our group chose fluorescein and amphotericin B (AmB), respectively. AmB is considered to be the most effective antibiotic in the treatment of chronic fungal infections.^{36,112} The results were very promising as it was observed that appropriate conjugation can increase the effectiveness of AmB, while decreasing its toxicity on human cells.

The combination of the two most common reactions on the covalent functionalization approach of CNTs renders doubly functionalized materials very effective in this respect. By using a combination of two different addition reactions the 1,3-dipolar cycloaddition of azomethine ylides, and the addition of diazonium salts both *via* a simple, fast and environmentally friendly method.^{36a} This methodology was also applied to produce multifunctionalized CNTs. These molecules are very attractive for drug delivery applications,¹⁶⁰ sensors¹⁶¹ or in the preparation of composites.¹⁶²

7. Applications: Supramolecular Chemistry

In supramolecular chemistry, dendrimers are very interesting macromolecules which possess a globular structure with a high density of functional groups on

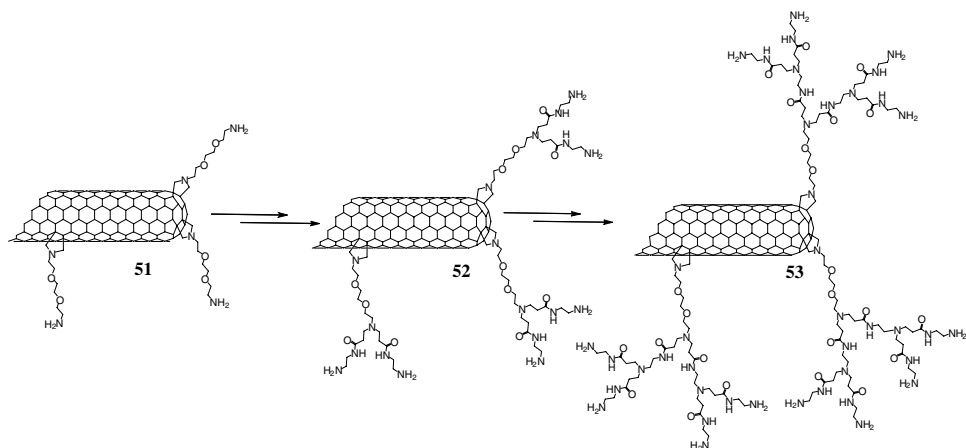


Scheme 21.

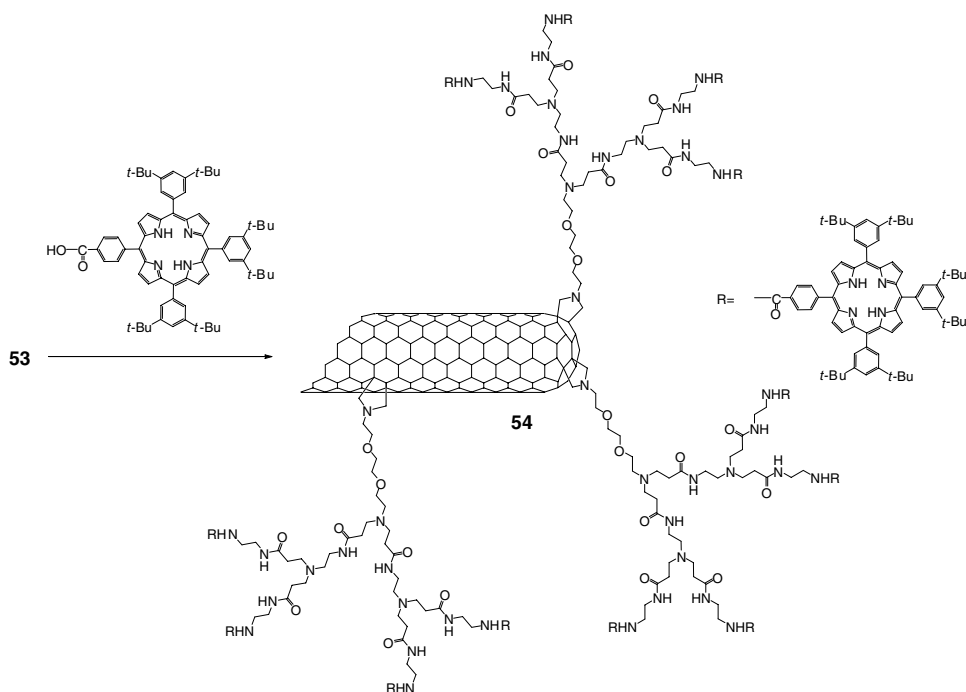
the periphery.^{78,163} Accordingly, we decided to build polyamidoamine (PAMAM) dendrimer following a divergent methodology onto CNT supports. In the divergent route, growth starts from the core building layers around it.¹⁶⁴ PAMAM dendrimer, first synthesized by Tomalia and coworkers,¹⁶⁵ is made by an iterative synthesis, starting with ethylenediamine as a core reacting with methyl acrylate in a Michael addition reaction, followed by subsequent amidation reactions with ethylene diamine.

In our case, a sample of pristine HiPco SWCNT was previously functionalized with an *N*-protected amino acid and paraformaldehyde in DMF giving rise to functionalized SWCNTs. Deprotection of amino groups anchored to CNTs supplied the focal points (**51**) from which the synthesis took place. Successive reactions with methyl acrylate and repetition of this route rendered the 2nd generation dendrimer-CNT adduct (**53**) (Scheme 22). Because of the solubility and high dispersability of these compounds, a full characterization with Raman spectroscopy, UV/vis-NIR spectroscopy, thermogravimetric analysis (TGA) and microscopy techniques, such as TEM (transmission electron microscopy) and AFM (atomic force microscopy), was successfully performed. Importantly, the Kaiser test allowed us to discern the amount of free primary amines in the dendrimer periphery. These amino groups played a crucial role because they were the anchor points for linking porphyrin derivatives. The condensation reaction between the amino groups and the porphyrin derivative was performed in the presence of EDC (*N*-[3-(dimethylamino)propyl]-*N'*-ethylcarbodiimide) and HOBt (1-hydroxybenzotriazole).

Photophysical^{2a} studies were performed on conjugate (**54**). Fluorescence kinetics showed transient decays similar to the free porphyrin derivative. For

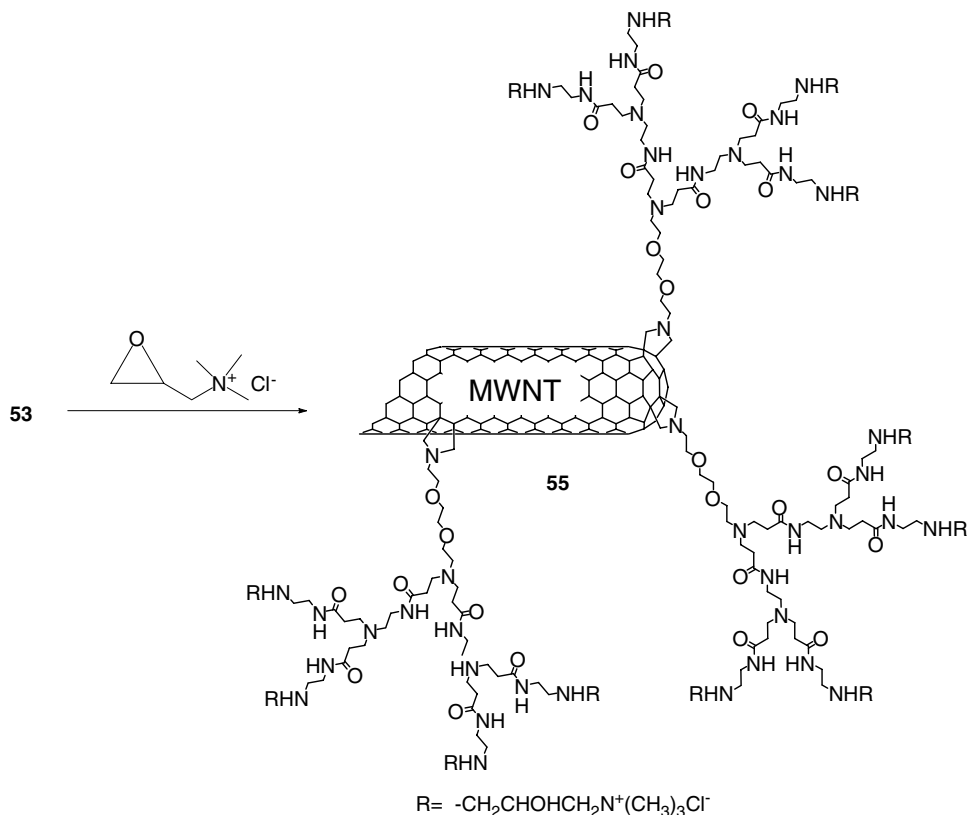


Scheme 22.



Scheme 23.

this reason, no interaction between CNTs and porphyrin rings could be detected. Photoinduced electron transfer was observed from the porphyrin unit to CNTs. The lifetime of the charge-separated species was in the range of microseconds (Scheme 23). Alternatively, dendron (**53**) was allowed to react



Scheme 24.

with epoxide (55), affording the polycationic species 5, which was employed in promising experiments of gene silencing experiments (Scheme 24).²⁹

Conclusions and Perspectives

The proper structural modulation of CNT functionalization is a critical issue for the successful applications of these nanomaterials in the emerging technologies. New methodologies are continuously adopted in order to control the properties of the final derivatives, which will define the eventual application. Hence, an application based on the electronic properties of nanotubes will require an unaltered CNT structure and, therefore, a non-covalent coating or a mild covalent modification will be preferred. On the other hand, when CNTs act as a mere support in fields like catalysis, or as drug carriers, then a covalent functionalization will provide a stronger interaction among the organic addends and the carbon nanostructure. A proper functionalization

of CNTs not only increases the stability of the final hybrids but also allows for an optimum decoration of the nanomaterials based on the final applications. It will also enhance the materials solubility, facilitating their handling. In terms of characterization of the new derivatives, a combination of techniques is necessary to confirm the successful modification of the CNT surface.

From materials science to biological applications, the integration of carbon nanostructures may yield interesting and innovative structural variations, making CNT functionalization an incredibly rich and modern research field.

References

1. Roco, M. C.; Williams, R. S.; Alivisatos, A. P. *Nanotechnology Research Directions*; Kluwer Academic Publishers: Boston, **2000**.
2. (a) Hu, H.; Zhao, B.; Hamon, M. A.; Kamaras, K.; Itkis, M. E.; Haddon, R. C. *J. Am. Chem. Soc.* **2003**, *125*, 14893. (b) Holzingner, M.; Abraham, J.; Whelan, P.; Graupner, R.; Ley, L.; Hennrich, F.; Kappes, M.; Hirsch, A. *J. Am. Chem. Soc.* **2003**, *125*, 8566. (c) Ménard-Moyon, C.; Izard, N.; Doris, E.; Miokowski, C. *J. Am. Chem. Soc.* **2006**, *128*, 14764.
3. (a) Balasubramanian, K.; Burghard, M. *Small*, **2005**, *1*, 180. (b) Banerjee, S.; Hemraj-Benny, T.; Wong, S. S. *Adv. Mater.* (Weinheim, Ger.) **2005**, *17*, 17. (c) Hirsch, A. *Angew. Chem. Int.* **2002**, *41*, 1853. (d) Banerjee, S.; Kahn, M. G. C.; Wong, S. S. *Chem.-Eur. J.* **2003**, *9*, 1898. (e) Lu, X.; Chen, Z. *Chem. Rev.* **2005**, *105*, 3643. (f) Bahr, J. L.; Tour, J. M. *Mater. Chem.* **2002**, *12*, 1952. (g) Nalwa, H. S. *ACS, Stevenson Ranch CA*, **2004**, *1*, 761. (h) Hirsch, A.; Vostrowsky, O. *Top. Curr. Chem.* **2005**, *245*, 193. (i) Kuzmany, H.; Kukovecz, A.; Simona, F.; Holzweber, M.; Kramberger, C.; Pichler, T. *Synth. Met.* **2004**, *141*, 113. (j) Tasis, D.; Tagmatarchis, N.; Bianco, A.; Prato, M. *Chem. Rev.* **2006**, *106*, 1105. (k) Ciraci, S.; Dag, S.; Yildirim, T.; Gülseren, O.; Senger, R. T. *J. Phys.: Condens. Matter* **2004**, *16*, R901.
4. (a) Quin, L. C.; Zhao, X.; Hirahara, K.; Miyamoto, Y.; Ando, Y.; Iijima, S. *Nature*, **2000**, *408*, 50. (b) Wang, N.; Tang, Z. K.; Li, G. D.; Chen, J. S. *Nature* **2000**, *408*, 50.
5. (a) Mintmire, J. W.; Dunlap, B. I.; White, C. T. *Phys. Rev. Lett.* **1992**, *68*, 631. (b) Hamada, N.; Sawada, S. I.; Oshiyama, A. *Phys. Rev. Lett.* **1992**, *68*, 1579. (c) Saito, R.; Fujita, M.; Dresselhaus, G.; Dresselhaus, M. S. *Appl. Phys. Lett.* **1992**, *60*, 2204.
6. Fisher, J. E.; Dai, H.; Thess, A.; Lee, R.; Hanjani, N. M.; Dehaas, D. L.; Smalley, R. E. *Phys. Rev. B* **1997**, *55*, R4921.
7. Bekyarova, E.; Davis, M.; Burch, T.; Itkis, M. E.; Zhao, B.; Sunshine, S.; Haddon, R. C. *J. Phys. Chem. B* **2004**, *108*, 19717.
8. (a) Salvetat, J. P.; Briggs, G. A. D.; Bonard, J. M.; Basca, R. R.; Kulik, A. J.; Stockli, T.; Brunnham, N. A.; Forro, L. *Phys. Rev. Lett.* **1999**, *82*, 944. (b) Yu, M. F.; Files, B. S.; Arepalli, S.; Ruoff, R. S. *Phys. Rev. Lett.* **2000**, *84*, 5552.
9. Journet, C.; Maser, W. K.; Bernier, P.; Lamy de la Chapelle Loiseau, A.; Lefrant, A.; Denart, P.; Lee, R.; Fischer, J. E. *Nature* **1997**, *388*, 756.
10. Rinzler, A. G.; Liu, J.; Dai, H.; Nikolaev, P.; Huffman, C. B.; Rodriguez-Macias, F. J.; Boul, P. J.; Lu, A. H.; Heymann, D.; Colbert, D. T.; Lee, R. S.; Fischer, J. E.; Rao, A. M.; Eklund, P. C.; Smalley, R. E. *Appl. Phys. A* **1998**, *67*, 29.

11. Endo, M.; Takeuchi, K.; Kobori, K.; Takahashi, K.; Kroto, H. W.; Sarkar, A. *Carbon* **1995**, *33*, 873.
12. Nikolaev, P.; Broniko, M.; Bradley, R.; Rohmund, F.; Colbert, D. T.; Smith, K.; Smalley, R. E. *Chem. Phys. Lett.* **1999**, *313*, 91.
13. Correa-Duarte, M. A.; Wagner, N.; Rojas-Chapana, J.; Morscizek, C.; Thie, M.; Giersig, M. *Nano Lett.* **2004**, *4*, 2233.
14. (a) Javey, A.; Guo, J.; Wang, Q.; Lundstrom, M.; Dai, H. *Nature* **2003**, *424*, 654. (b) Latil, S.; Roche, S.; Charlier, J.-C. *Nano Lett.* **2005**, *5*, 2216.
15. *Fullerenes: Principles and Applications*, Ed. F. Langa, J.-F. Nierengarten, Springer Verlag, **2007**.
16. Liu, J.; Rinzler, A. G.; Dai, H.; Hafner, J. H.; Bradley, R. K.; Boul, P. J.; Lu, A.; Iverson, T.; Shelimov, K.; Huffman, C. B.; Rodriguez-Macias, F. J.; Shon, Y. -S.; Lee, T. R.; Colbert, D. T.; Smalley, R. E. *Science*, **1998**, *280*, 1253.
17. (a) Martinez, M.; Callejas, M.; Benito, A. M.; Maser, W. K.; Cochet, M.; Andres, J. M.; Shreiber, J.; Chauvet, O.; Fierro, J. L. G. *Chem. Commun.* **2002**, 1000. (b) Vazquez, E.; Georgakilas, V.; Prato, M. *Chem. Commun.* **2002**, 2308. (c) Harutyunyan, A. R.; Pradhan, B. K.; Chang, J.; Chen, G.; Eklund, P. C. *J. Phys. Chem. B* **2002**, *106*, 8671.
18. Bonard, J. M.; Stora, T.; Salvatat, J.-P.; Maier, F.; Stockli, T.; Duschl, C.; Forro, L.; de Heer, W. A.; Chatelain, A. *Adv. Mater* **1997**, *9*, 827.
19. Bandow, S.; Rao, A. M.; Williams, K. A.; Thess, A.; Smalley, R. E.; Eklund, P. C. *J. Phys. Chem. B* **1997**, *101*, 8839.
20. Duesberg, G. S.; Burghard, M.; Muster, J.; Philipp, G.; Roth, S. *Chem. Commun.* **1998**, 435.
21. (a) Curran, S. A.; Ajayan, P. M.; Blau, W. J.; Carroll, D. L.; Coleman, J. N.; Dalton, A. B.; Davey, A. P.; Drury, A.; McCarthy, B.; Maier, S.; Strevens, A. *Adv. Mater.* **1998**, *10*, 1091. (b) Star, A.; Stoddart, J. F.; Steuerman, D.; Diehl, M.; Boukai, A.; Wong, E. W.; Yang, X.; Chung, S.-W.; Choi, H.; Hearth, J. R. *Angew. Chem.* **2001**, *113*, 1771; *Angew. Chem. Int. Ed.* **2001**, *40*, 1721. (c) Coleman, J. N.; Dalton, A. B.; Curran, S.; Rubio, A.; Davey, A. P.; Drury, A.; McCarthy, B.; Lahr, B.; Ajayan, P. M.; Roth, S.; Blau, R.; Barklie C. *Adv. Mater.* (Weinheim, Ger.) **2000**, *12*, 313. (d) Bandyopadhyaya, R. E.; Nativ-Roth, O.; Regev, R.; Yerushalmi-Rozen. *Nano Lett.* **2002**, *2*, 25.
22. Hata, K.; Fubata, D. N.; Mizuno, K.; Namai, T.; Yumura, M.; Iijima, S. *Science* **2004**, *306*, 1362.
23. (a) Chiang, I. W.; Brinson, B. E.; Smalley, R. E. *J. Phys. Chem. B*, **2001**, *105*, 1157. (b) Niyogi, S.; Hu, H.; Hamon, M. A.; Bhowmik, P.; Zhao, B.; Rozenzhak, S. M.; Chen, J.; Itkis, M. E.; Meier, M. S.; Haddon, R. C. *J. Am. Chem. Soc.* **2001**, *123*, 733. (c) Hu, H.; Zhao, B.; Itkis, M. E.; Haddon, R.C. *J. Phys. Chem. B* **2003**, *107*, 13838. (d) Haddon, R. C.; Sippel, J.; Rinzler, A. G.; Papadimitrakopoulos, F. *MRS Bull.* **2004**, *29*, 252.
24. Ausman, K.; Piner, R.; Lourie, O.; Ruoff, R. S.; Korobov, M. *J. Phys. Chem. B* **2000**, *104*, 8911.
25. (a) Boul, P. J.; Liu, J.; Mickelson, E. T.; Huffman, C. B.; Ericson, L. M.; Chiang, I. W.; Smith, K. A.; Colbert, D. T.; Hauge, R. H.; Margrave, J. L.; Smalley, R. E. *Chem. Phys. Lett.* **1999**, *310*, 367. (b) Liu, J.; Casavant, M. J.; Cox, M.; Walters, D. A.; Boul, P.; Lu, W.; Rimberg, A. J.; Smith, K. A.; Colbert, D. T.; Smalley, R. E. *Chem. Phys. Lett.* **1999**, *303*, 125.

26. Bahr, J.; Mickelson, E.; Bronikowski, M.; Smalley, R. E.; Tour, J. M. *Chem. Commun.* **2001**, 193.
27. (a) Tasis, D.; Tagmatarchis, N.; Georgakilas, V.; Prato, M. *Chem.-Eur. J.* **2003**, 9, 2. (b) Hirsch, A. *Angew. Chem. Int. Ed.* **2002**, 41, 11.
28. (a) Peng, H.; Alemany, L. B.; Margrave, J. L.; Khabashesky, V. N. *J. Am. Chem. Soc.* **2003**, 125, 15174. (b) Campidelli, S.; Sooambar, C.; Lozano-Diz, E.; Ehli, C.; Guldi, D. M.; Prato, M. *J. Am. Chem. Soc.* **2006**, 128, 12544. (c) Georgakilas, V.; Kordatos, K.; Prato, M.; Guldi, D.M.; Holzinger, M.; Hirsch, A. *J. Am. Chem. Soc.* **2002**, 124, 760.
29. Herrero, M. A.; Toma, F. M.; Al-Jamal, K. T.; Kostarelos, K.; Bianco, A.; Da Ros, T.; Bano, F.; Casalis, L.; Scoles, G.; Prato, M. *J. Am. Chem. Soc.* **2009**, 131, 9843.
30. Cech, J.; Kalbák, M.; Curran, S. A.; Zhang, D.; Dettlaff-Weglikowska, U.; Dunsch, L.; Yang, S.; Roth, S. *Physica E.* **2007**, 37, 109.
31. (a) Dresselhaus, M. S.; Dresselhaus, G.; Saito, R.; Jorio, A. *Phys. Rep.* **2005**, 409, 47. (b) Jorio, A.; Pimenta, M. A.; Fantini, C.; Souza, M.; Souza Filho, A. G.; Samsonidze, G. E. G.; Dresselhaus, G.; Dresselhaus, M. S.; Saito, R. *Carbon* **2004**, 42, 1067.
32. (a) Kavan, L.; Raptá, P.; Dunsch, L.; Bronikowski, M. J.; Wills, P.; Smalley, R. E. *J. Phys. Chem. B* **2001**, 105, 10764. (b) Alvarez, L.; Righi, A.; Guillard, T.; Rols, S.; Anglaret, E.; Laplace, D.; Sauvajol, J.-L. *Chem. Phys. Lett.* **2000**, 316, 186.
33. (a) Astakhova, T.; Vinogradov, G. A.; Menon, M. *Russ. Chem. Bull.* 52, **2003**, 4, 823. (b) Dresselhaus, M. S.; Dresselhaus, G.; Jorio, A.; Souza Filho, A. G.; Pimenta, M. A.; Saito, D. R. *Acc. Chem. Res.* **2002**, 35, 1070.
34. Qian, W.; Liu, T.; Wei, F.; Yuan, H. *Carbon* **2003**, 41, 1851.
35. Dresselhaus, M. S.; Dreselhaus, G.; Jorio, A.; Souza Filho, A. G.; Saito, R. *Carbon* **2002**, 40, 2043.
36. (a) Brunetti, F. G.; Herrero, M. A.; Muñoz, J. De M.; Diaz-Ortiz, A.; Alfonsi, J.; Meneghetti, M.; Prato, M.; Vazquez, E. *J. Am. Chem. Soc.* **2008**, 130, 8094. (b) Brunetti, F. G.; Herrero, M. A.; Muñoz, J. De M.; Giordani, S.; Diaz-Ortiz, A.; Fillippone, S.; Ruaro, G.; Meneghetti, M.; Prato, M.; Vazquez, E. *J. Am. Chem. Soc.* **2007**, 129, 14580.
37. (a) Benoit, J. M.; Buisson, J. P.; Chauvet, O.; Godon C.; Lefrant, S. *Phys. Rev. B*, **2002**, 66, 073417. (b) Zhao, Y.; Yakobson B. I.; Smalley, R. E. *Phys. Rev. Lett.* **2002**, 88, 185501.
38. Zhao, X.; Ando, Y.; Qin, L.-C.; Kataura, H.; Maniwa Y.; Saito, R. *Chem. Phys. Lett.* **2002**, 361, 169.
39. Ando, Y.; Zhao, X.; Shimoyama, H.; Sakai, G.; Kaneto, K. *Int. J. Inorg. Mater.* **1999**, 1, 77.
40. Kataura, H.; Kumazawa, Y.; Maniwa, Y.; Umezu, I.; Suzuki, S.; Ohtsuka Y.; Achiba, Y. *Synth. Met.* **1999**, 103, 2555.
41. O'Connell, M. J.; Bachilo, S. M.; Huffman, C. B.; Moore, V. C.; Strano, M. S.; Haroz, E. H.; Rialon, K. L.; Boul, P. J.; Noon, W. H.; Kittrell, C.; Ma, J. P.; Hauge, R. H.; Weisman R. B.; Smalley, R. E. *Science* **2002**, 297, 593.
42. Burghard, M. *Sur. Sci. Rep.* **2005**, 58, 1.
43. Kim, U. J.; Furtado, C. A.; Liu, X.; Chen, G.; Eklund, P. C. *J. Am. Chem. Soc.* **2005**, 127, 15437.
44. Pompeo, F.; Resasco, D. E. *Nano Lett.* **2002**, 2, 369.
45. Kan, K.; Xia, T.; Yang, Y.; Bi, H.; Fu, H.; Shi, K. *J. Appl. Electrochem.* **2010**, 40, 593.

46. Kovtyukhova, N. I.; Malouk, T. E.; Pan, L.; Dickey, E. C. *J. Am. Chem. Soc.* **2003**, *125*, 9761.
47. Colthup, N. B.; Daly, L. H.; Wiberlay, S. E. *Introduction to infrared and Raman spectroscopy*. Academic Press, Boston, **1990**, 547.
48. Kuznetsova, A.; Mawhinney, D. B.; Naumenko, V.; Yates, J. T.; Liu, J.; Smalley, R. E. *Chem. Phys. Lett.* **2000**, *321*, 292.
49. Lebedkin, S.; Arnold, K.; Hennrich, F.; Krupke, R.; Renker, B.; Kappes, M. M. *New J. Phys.* **2003**, *5*.
50. Bachilo, S. M.; Strano, M. S.; Kittrell, C.; Hauge, R. H.; Smalley, R. E.; Weisman, R. B. *Science* **2002**, *298*, 2361.
51. Giordani, S.; Bergin, S. D.; Nicolosi, V.; Lebedkin, S.; Kappes, M. M.; Blau, W. J.; Coleman, J. N. *J. Phys. Chem B* **2006**, *110*, 15708.
52. Cognet, L.; Tsyboulski, D. A.; Rocha, J. D. R.; Doyle, C. D.; Tour, J. M.; Weisman, R. B. *Science* **2007**, *316*, 1465.
53. Tan, P. H.; Rozhin, A. G.; Hasan, T.; Hu, P.; Scardaci, V.; Milne, W. I.; Ferrari, A. C. *Phys. Rev. Lett.* **2007**, *99*, 137402.
54. Marega, R.; Aroulmoji, V.; Dinon, F.; Vaccari, L.; Giordani, S.; Bianco, A.; Murano, E.; Prato, M. *J. Am. Chem. Soc.* **2009**, *131*, 9086.
55. Billinge, S. J. L.; Levin, I. *Science* **2007**, *316*, 561.
56. DeBorde, T.; Joiner, J. C.; Leyden, M. R.; Monit, E. D. *Nano Lett.* **2008**, *8*, 3568.
57. Fan, Y. W.; Burghard M.; Kern, K. *Adv. Mater.* (Weinheim, Ger.) **2002**, *14*, 130.
58. Azamian, B. R.; Coleman, K. S.; Davis, J. J.; Hanson N.; Green, M. L. H. *Chem. Commun.* **2002**, 366.
59. Zhang, L.; Zhang, J.; Schmandt, N.; Cratty, J.; Khabashesku, V. N.; Kelly, K. F.; Barron, A. R. *Chem. Commun.* **2005**, 5429.
60. (a) Odom, T. W.; Huang, J. L.; Kim, P.; Lieber, C. M. *Nature* **1998**, *391*, 62. (b) Wildoer, J. W. G.; Venema, L. C.; Rinzler, A. G.; Smalley, R. E.; Dekker, C. *Nature* **1998**, *391*, 59.
61. Zhang, L.; Yang, J.; Edwards, C. L.; Alemany, L. B.; Khabashesku, V. N.; Barron, A. R. *Chem. Commun.* **2005**, 3265.
62. Bonifazi, D.; Nacci, C.; Marega, R.; Campidelli, S.; Ceballos, G.; Modesti, S.; Meneghetti, M.; Prato, M. *Nano Lett.* **2006**, *6*, 1408.
63. Sano, M.; Kamino, A.; Shinkai, S. *Angew. Chem. Int. Ed.* **2001**, *40*, 4661.
64. (a) Hashimoto, A.; Suenaga, K.; Gloter, A.; Urita, K.; Iijima, S. *Nature* **2004**, *430*, 870. (b) Zuo, J. M.; Vartanyants, I.; Gao, M.; Zhang R.; Nagahara, L. A. *Science* **2003**, *300*, 1419.
65. Smith, B. W.; Luzzi, D. E. *J. Appl. Phys.* **2001**, *90*, 3509.
66. Qin, L. C. *Rep. Prog. Phys.* **2006**, *69*, 2761.
67. Meyer, R. R.; Friedrichs, S.; Kirkland, A. I.; Sloan, J.; Hutchison, J. L.; Green, M. L. H. *J. Microsc.* **2003**, *212*, 152.
68. Hirahara, K.; Saitoh, K.; Yamasaki, J.; Tanaka, N. *Nano Lett.* **2006**, *6*, 1778.
69. Iijima, S. *Nature* **1991**, *354*, 56.
70. Garcia-Gutierrez, D.; Gutierrez-Wing, C.; Miki-Yoshida, M.; Jose-Yacamán, M. *Appl. Phys. A* **2004**, *79*, 481.
71. Shukla, R.; Hill, E.; Shi, X.; Kim, J.; Muniz, M. C.; Sun, K.; Baker, J. R. *Jr. Soft. Matter.* **2008**, *4*, 2160.
72. (a) Ajayan, P. M. *Chem. Rev.* **1999**, *99*, 1787. (b) Dresselhaus, M. S.; Dresselhaus, G.; Avouris, P. *Carbon Nanotubes: Synthesis, Structure, Properties, and Applications*, Springer,

2001. (c) Baughman, R. H.; Zakhidov, A. A.; de Heer, W. A. *Science* **2002**, 297, 787.
- (d) Robertson, N.; McGowan, C. A. *Chem. Soc. Rev.* **2003**, 32, 96.
73. Peng, X. H.; Wong, S. S. *Adv. Mater.* (Weinheim, Ger.) **2009**, 21, 625.
74. (a) Tasis, D.; Tagmatarchis, N.; Georgakilas, V.; Prato, M. *Chem.-Eur. J.* **2003**, 9, 4000. (b) Dyke, C. A.; Tour, J. M. *Chem.-Eur. J.* **2004**, 10, 812. (c) Banerjee, S.; Hemraj-Benny, T.; Wong, S. S. *Adv. Mater.* (Weinheim, Ger.) **2005**, 17, 17.
75. (a) Nakashima, N.; Tomonari, Y.; Murakami, H. *Chem. Lett.* **2002**, 638. (b) Lin, Y.; Tailor, S.; Li, H.; Shiral Fernando, K. A.; Wang, W.; Gu, L.; Zhou, B.; Sun Y.-P. *J. Mater. Chem.* **2004**, 14, 527.
76. Dyke, C. A.; Tour, J. M. *J. Phys. Chem. B* **2004**, 108, 11151.
77. Tsang, S. C.; Chen, Y. K.; Harris, P. J. F.; Green, M. L. H. *Nature* **1994**, 372, 159.
78. Sun, Y.-P.; Huang, W.; Lin, Y.; Fu, K.; Kitaygorodskiy, A.; Riddle, L. A.; Yu, Y. J.; Carroll, D. L. *Chem. Mater.* **2001**, 13, 2864.
79. Alvaro, M.; Atienzar, P.; Cruz, P. de la; Delgado, J. L.; Garcia H.; Langa, F. *Chem. Phys. Lett.* **2004**, 386, 342.
80. (a) Li, H.; Martin, R. B.; Harruff, B. A.; Carino, R. A.; Allard, L. F.; Sun, Y.-P. *Adv. Mater.* (Weinheim, Ger.) **2004**, 16, 896. (b) Baskaran, D.; Mays, J. W.; Zhang, X. P.; Bratcher, M. S. *J. Am. Chem. Soc.* **2005**, 127, 6916.
81. Cosnier, S.; Holzinger, M. *Electrochim. Acta* **2008**, 53, 3948.
82. Hamon, M. A.; Chen, J.; Hu, H.; Chen, Y.; Itkis, M. E.; Rao, A. M.; Eklund, P. C.; Haddon, R. C. *Adv. Mater.* (Weinheim, Ger.) **1999**, 11, 834 and references therein.
83. Zhao, B.; Hu, H.; Haddon, R. C. *Adv. Funct. Mater.* **2004**, 14, 71.
84. Zhu, W.; Minami, N.; Kazaoui, S.; Kim, Y. *J. Mater. Chem.* **2003**, 13, 2196.
85. Déste, M.; Nardi, M. D.; Menna, E. *Eur. J. Org. Chem.* **2006**, 2517.
86. Delgado, J. L.; de la Cruz, P.; Urbina, A.; Navarrete, J. T. L.; Casado J.; Langa, F. *Carbon* **2007**, 45, 2250.
87. (a) Feng, L.; Li, H.; Li, F.; Shi Z.; Gu, Z. *Carbon* **2003**, 41, 2385. (b) Khan, M. G.; Banerjee, S.; Wong, S. S. *Nano Lett.* **2002**, 2, 1215.
88. Kam, N. W. S.; Jessop, T. C.; Wender, P. A.; Dai, H. *J. Am. Chem. Soc.* **2004**, 126, 6850.
89. Williams, K. A.; Veenhuizen, P. T. M.; de la Torre, B. G.; Eritja R.; Dekker, C. *Nature* **2002**, 420, 761.
90. Zhang, Y.; Shen, Y.; Yuan, J.; Han, D.; Wang, Z.; Zhang, Q.; Niu, L. *Angew. Chem. Int. Ed.* **2006**, 45, 5867.
91. (a) Liu, L. Q.; Zhang, S. A.; Hu, T. J.; Guo, Z. X.; Ye, C.; Dai, L. M.; Zhu, D. B. *Chem. Phys. Lett.* **2002**, 359, 191. (b) Liu, L.; Qin, Y.; Guo, Z.-X.; Zhu, D. *Carbon* **2003**, 41, 331. (c) Qin, Y.; Liu, L.; Shi, J.; Wu, W.; Zhang, J.; Guo, Z. X.; Li, Y.; Zhu, D. *Chem. Mater.* **2003**, 15, 3256. (d) Liu, L.; Wang, T.; Li, J.; Guo, Z.-X.; Dai, L.; Zhang, D.; Zhu, D. *Chem. Phys. Lett.* **2003**, 367, 747.
92. Herrero, M. A.; Guerra, J.; Myers, V. S.; Gómez, M. V.; Crooks, R. M.; Prato, M. *ACS Nano* **2010**, 4, 905.
93. Srivastava, D.; Brenner, D. W.; Schall, J. D.; Ausman, K. D.; Yu, M.; Ruoff, R. S. *J. Phys. Chem. B* **1999**, 103, 4330.
94. (a) Singh, P.; Campidelli, S.; Giordani, S.; Bonifazi, D.; Bianco, A.; Prato, M. *Chem. Soc. Rev.* **2009**, 38, 2214 and references therein. (b) Wu, H.-C.; Chang, X.; Liu, L.; Zhao, F.; Zhao, Y. *J. Mater. Chem.* **2010**, 20, 1036.

95. (a) Maroux, P. R.; Schreiber, J.; Batail, P.; Lefrant, S.; Renouard, J.; Jacob, G.; Albertini, D.; Mevellec, J.-Y. *Phys. Chem. Chem. Phys.* **2002**, *4*, 2278. (b) An, K. H.; Heo, J. G.; Bae, D. J.; Jo, C.; Yang, C. W.; Park, C.-Y.; Lee, Y. H. *Appl. Phys. Lett.* **2002**, *80*, 4235. (c) Shulga, Y. M.; Tien, T.-C.; Huang, C.-C.; Lo, S.-C.; Muradyan, V. E.; Polyakova, N. V.; Ling, Y.-C.; Loutfy, R. O.; Moravsky, A. P. *J. Electron Spectrosc. Relat. Phenom.* **2007**, *160*, 22.
96. Khabashesku, V. N.; Billups, W. E.; Margrave, J. L. *Acc. Chem. Res.* **2002**, *35*, 1087.
97. Saini, R. K.; Chiang, I. W.; Peng, H.; Smalley, R. E.; Billups, W. E.; Hauge, R. H.; Margrave, J. L. *J. Am. Chem. Soc.* **2003**, *125*, 3617.
98. Stevens, J. L.; Huang, A. Y.; Peng, H.; Chiang, I. W.; Khabashesku, V. N.; Margrave, J. L. *Nano Lett.* **2003**, *3*, 331.
99. Zhang, L.; Kiny, V. U.; Peng, H.; Zhu, J.; Lobo, R. F. M.; Margrave, J. L.; Khabashesku, V. N. *Chem. Mater.* **2004**, *16*, 2055.
100. See articles in *Acc. Chem. Res.* **2002**, *35*, 997–1113, special issue on “Carbon Nanotubes”, Ed R. C. Haddon.
101. Pulikkathara, M. X.; Kuznetsov, D. V.; Khabashesku, V. N. *Chem. Mater.* **2008**, *20*, 2685, and references therein.
102. (a) Chen, J.; Hamon, M. A.; Hu, H.; Chen, Y. S.; Rao, A. M.; Eklund, P. C.; Haddon, R. C. *Science* **1998**, *282*, 95 (b) Chen, Y.; Haddon, R. C.; Fang, S.; Rao, A. M.; Lee, W. H.; Dickey, E. C.; Grulke, E. A.; Pendergrass, J. C.; Chavan, A.; Haley, B. E.; Smalley, R. E. *J. Mater. Res.* **1998**, *13*, 2423.
103. Coleman, K. S.; Bailey, S. R.; Fogden, S.; Green, M. L. H. *J. Am. Chem. Soc.* **2003**, *125*, 8722.
104. Holzinger, M.; Vostrowsky, O.; Hirsch, A.; Hennrich, F.; Kappes, M.; Weiss, R.; Jellen, F. *Angew. Chem., Int. Ed.* **2001**, *40*, 4002.
105. Holzinger, M.; Steinmetz, J.; Samaille, D.; Glerup, M.; Paillet, M.; Bernier, P.; Ley L.; Graupner, R. *Carbon* **2004**, *42*, 941.
106. Yinghuai, Z.; Peng, A. T.; Carpenter, K.; Maguire, J. A.; Hosmane, N. S.; Takagaki, M. *J. Am. Chem. Soc.* **2005**, *127*, 9875.
107. (a) Moghaddam, M. J.; Taylor, S.; Gao, M.; Huang, S.; Daí, L.; McCall, M. J. *Nano Lett.* **2004**, *4*, 89. (b) Min Lee, K.; Li, L.; Dai, L. *J. Am. Chem. Soc.* **2005**, *127*, 4122.
108. (a) Maggini, M.; Scorrano, G.; Prato, M. *J. Am. Chem. Soc.* **1993**, *115*, 9798. (b) Prato, M.; Maggini, M. *Acc. Chem. Res.* **1998**, *31*, 519. (c) Tagmatarchis, N.; Prato, M. *Synlett*, **2003**, *6*, 768.
109. Georgakilas, V.; Tagmatarchis, N.; Pantarotto, D.; Bianco, A.; Briand, J.-P.; Prato, M. *Chem. Commun.* **2002**, 3050.
110. (a) De la Hoz, A.; Díaz-Ortiz, A.; Moreno, A. *Chem. Soc. Rev.* **2005**, *34*, 164. (b) Dallinger, D.; Kappe, C. O. *Chem. Rev.* **2007**, *107*, 2663. (c) Polshettiwar, V.; Varma, R. S. *Acc. Chem. Res.* **2008**, *41*, 629.
111. Imholt, T. J.; Dyke, C. A.; Hasslacher, B.; Perez, J. M.; Price, D. W.; Roberts, J. A.; Scott, J. B.; Wadhawan, A.; Ye, Z.; Tour, J. M. *Chem. Mater.* **2003**, *15*, 21.
112. Langa, F.; de la Cruz, P. *Comb. Chem. High Throughput Screening* **2007**, *10*, 766.
113. Guldi, D. M.; Marcaccio, M.; Paolucci, D.; Paolucci, F.; Tagmatarchis, N.; Tasis, D.; Vázquez, E.; Prato, M. *Angew. Chem. Int. Ed.* **2003**, *42*, 4206.
114. Callegari, A.; Marcaccio, M.; Paolucci, D.; Paolucci, F.; Tagmatarchis, N.; Tasis, D.; Vázquez, E.; Prato, M. *Chem. Commun.* **2003**, 2576.

115. Prato, M.; Kostarelos, K.; Bianco, A. *Acc. Chem. Res.* **2008**, *41*, 60.
116. Georgakilas, V.; Bourlinos, A.; Gournis, D.; Tsoufis, T.; Trapalis, C.; Mateo-Alonso A.; Prato, M. *J. Am. Chem. Soc.* **2008**, *130*, 8733 and references therein.
117. Ballesteros, B.; da la Torre, G.; Ehli, C.; Rahman, G. M. A.; Agullo-Rueda, F.; Guldi, D. M.; Torres, T. *J. Am. Chem. Soc.* **2007**, *129*, 5061.
118. Alvaro, M.; Atienzar, P.; de la Cruz, P.; Delgado, J. L.; Troiani, V.; Garcia, H.; Langa, F.; Palkar, A.; Echegoyen, L. *J. Am. Chem. Soc.* **2006**, *128*, 6626 and references therein.
119. Delgado, J. L.; de la Cruz, P.; Langa, F.; Urbina, A.; Casado, J.; Navarrete, J. T. L. *Chem. Commun.* **2004**, 1734.
120. Zhang, L.; Yang, J.; Edwards, C. L.; Alemany, L. B.; Khabashesku, V. N.; Barron, A. R. *Chem. Commun.* **2005**, 3265.
121. Basiuk, E. V.; Monroy-Pelaez, M.; Puente-Lee, I.; Basiuk, V. A. *Nano Lett.* **2004**, *4*, 863.
122. Chen, S. M.; Shen, W. M.; Wu, G. Z.; Chen, D. Y.; Jiang, M. *Chem. Phys. Lett.* **2005**, *402*, 312.
123. Tagmatarchis, N.; Georgakilas, V.; Prato, M.; Shinohara, H. *Chem. Commun.* **2002**, 2010.
124. Wei, L.; Zhang, Y. *Nanotechnology*, **2007**, *18*, 495703.
125. Wei, L.; Zhang, Y. *Chem. Phys. Lett.* **2007**, *446*, 142.
126. Peng, H.; Alemany, L. B.; Margrave, J. L.; Khabashesku, V. N. *J. Am. Chem. Soc.* **2003**, *125*, 15174.
127. Pekker, S.; Salvétat, J.-P.; Jakab, E.; Bonard, J.-M.; Forro, L. *J. Phys. Chem. B*, **2001**, *105*, 7938.
128. Wunderlich, D.; Hauke, F.; Hirsch, A. *Mater. Chem.* **2008**, *18*, 1493.
129. Garcia-Gallastegui, A.; Obieta, I.; Bustero, I.; Imbuluzqueta, G.; Arbiol, J.; Miranda, J. I.; Aizpurua, J. M. *Chem. Mater.* **2008**, *20*, 4433 and references therein.
130. Dyke, C. A.; Tour, J. M. *Chem.-Eur. J.* **2004**, *10*, 812
131. Hudson, J. L.; Jian, H.; Leonard, A. D.; Stephenson, J. J.; Tour, J. M. *Chem. Mater.* **2006**, *18*, 2766.
132. Ellison, M. D.; Gasda, P. J. *J. Phys. Chem. C* **2008**, *112*, 738.
133. Campidelli, S.; Ballesteros, B.; Filoramo, A.; Díaz Díaz, D.; de la Torre, G.; Torres, T.; Rahman, G. M. A.; Ehli, C.; Kiessling, D.; Werner, F.; Sgobba, V.; Guldi, D. M.; Cioffi, C.; Prato, M.; Bourgoign, J.-P. *J. Am. Chem. Soc.* **2008**, *130*, 11503.
134. Gho, Z.; Du, F.; Ren, D.; Chen, Y.; Zheng, J.; Liu, Z.; Tian, J. *J. Mater. Chem.* **2006**, *16*, 3021.
135. Stephenson, J. L.; Hudson, J. L.; Leonard, A. D.; Price, B. K.; Tour, J. M. *Chem. Mater.* **2007**, *19*, 3491.
136. Gomez-Escalonilla, M. J.; Atienzar, P.; Fierro, J. L. G.; Garcia, H.; Langa, F. *J. Mater. Chem.* **2008**, *18*, 1592.
137. Cheng, F.; Adronov, A. *Chem. Mater.* **2006**, *18*, 5389.
138. Banerjee, S.; Wong, S. S. *Nano Lett.* **2004**, *4*, 1445.
139. Banerjee, S.; Wong, S. S. *J. Phys. Chem. B*, **2002**, *106*, 12144.
140. Mawhinney, D. B.; Naumenko, V.; Kuznetsova, A.; Yates, J. T.; Liu, J.; Smalley, R. E. *J. Am. Chem. Soc.* **2000**, *122*, 2383.
141. (a) Kónya, Z.; Vesselenyi, I.; Niesz, K.; Kukovecz, A.; Demortier, A.; Fonseca, A.; Delhalle, J.; Mekhalif, Z.; Nagy, J. B.; Koós, A. A.; Osváth, Z.; Kocsonya, A.; Biro', L. P.; Kiricsi, I. *Chem. Phys. Lett.* **2002**, *360*, 429. (b) Barthos, R.; Mèhn, D.; Demortier, A.; Pierard, N.; Morciaux, Y.; Demortier, G.; Fonseca, A.; Nagy, J. B. *Carbon* **2005**, *43*, 321.

142. Pan, H. L.; Liu, L. Q.; Guo, Z. X.; Dai, L. M.; Zhang, F. S.; Zhu, D. B.; Czerw, R.; Carroll, D. L. *Nano Lett.* **2003**, 3, 29.
143. Xie, X. L.; Mai, Y. W.; Zhou, X. P. *Mater. Sci. Eng. R.* **2005**, 49, 89.
144. (a) Cui, D. X. *J. Nanosci. Nanotechnol.* **2007**, 7, 1298. (b) Katz, E.; Willner, I. *Chem. Phys. Chem.* **2004**, 5, 1085.
145. Cambre, S.; Wenseleers, W.; Culin, J.; Doorslaer, S. V.; Fonseca, A.; Nagy, J.; Goovaerts, E. *ChemPhysChem.* **2008**, 9, 1930.
146. Backes, C.; Schmidt, C. D.; Hauke, F.; Böttcher, C.; Hirsch, A. *J. Am. Chem. Soc.* **2009**, 131, 2172.
147. Monthieux, M.; Flahaut, E.; Cleuziou, J. P. *J. Mater. Res.* **2006**, 21, 2774.
148. Ugarte, D.; Chatelain, A.; Heer, W. A. d. *Science* **1996**, 274, 1897.
149. (a) Thamavaranukup, N.; Höppe, H. A.; Ruiz-Gonzalez, L.; Costa, P. M. F. J.; Sloan, J.; Kirkland, A.; Green, M. L. H. *Chem. Commun.* **2004**, 15, 1686. (b) Watts, P. C. P.; Hsu, W. K.; Kotzeva, V.; Chen, G. Z. *Chem. Phys. Lett.* **2002**, 366, 42. (c) Eliseev, A. A.; Chernysheva, M. V.; Verbitskii, N. I.; Kiseleva, E. A.; Lukashin, A. V.; Tretyakov, Yury D.; Kiselev, N. A.; Zhigalina, O. M.; Zakalyukin, R. M.; Vasiliev, A. L.; Krestinin, A. V.; Hutchison, J. L.; Freitag, B. *Chem. Mater.* **2009**, 21, 5001.
150. Ugarte, D.; Stöckli, T.; Bonard, J. M.; Châtelain, A.; Heer, W. A. D. *Appl. Phys. A: Mater. Sci. Process.* **1998**, 67, 101.
151. (a) Chancolon, J.; Archaimbault, F.; Pineau, A.; Bonnamy, S. *J. Nanosci. Nanotechnol.* **2006**, 6, 1. (b) Brown, G.; Bailey, S.; Sloan, J.; Xu, C.; Friedrichs, S.; Flahaut, E.; Coleman, K. S.; Hutchison, J. L.; Dunin-Borkowski, R. E.; Green, M. L. H. *Chem. Commun.* **2001**, 845.
152. Dujardin, E.; Ebbesen, T. W.; Hiura, H.; Taginaki, K. *Science* **1994**, 265, 1850. (b) Kim, B. M.; Qian, S.; Bau, H. H. *Nano Lett.* **2005**, 5, 873.
153. Ajayan, P. M.; Iijima, S. *Nature* **1993**, 361, 333.
154. Ajayan, P. M.; Ebbesen, T. W.; Ichihashi, T.; Iijima, S.; Tanigaki, K.; Hiura, H. *Nature* **1993**, 362, 522.
155. Seraphin, S.; Zhou, D.; Jiao, J.; Withers, J. C.; Loufty, R. *Nature* **1993**, 362, 503.
156. Saito, Y.; Yoshikawa, T. *J. Cryst. Growth* **1993**, 134, 154.
157. Sloan, J.; Hammer, J.; Zwiefka-Sibley, M.; Green, M. L. H. *Chem. Commun.* **1998**, 3, 347.
158. Smith, B. W.; Monthieux, M.; Luzzi, D. E. *Nature* **1998**, 296, 323.
159. Wu, W.; Wieckowski, S.; Pastorin, G.; Benincasa, M.; Klumpp, C.; Briand, J.-P.; Gennaro, R.; Prato, M.; Bianco, A. *Angew. Chem. Int. Ed.* **2005**, 44, 6358.
160. Pastorin, G.; Wu, W.; Wieckowski, S.; Briand, J.-P.; Kostarelos, K.; Prato, M.; Bianco, A. *Chem. Commun.* **2006**, 1182.
161. Yan, Y.-M.; Yehezkeli, O.; Willner, I. *Chem. -Eur. J.* **2007**, 13, 10168.
162. Ajayan, P. M.; Tour, J. M. *Nature* **2007**, 447, 1066.
163. (a) Holizinger, M.; Abraham, J.; Whelan, P.; Graupner, R.; Ley, L.; Hennrich, F.; Kappes, M.; Hirsch, A. *J. Am. Chem. Soc.* **2003**, 125, 8566. (b) Cao, L.; Yang, W.; Yang, J. W.; Wang, C. C.; Fu, S. K. *Chem. Lett.* **2004**, 33, 490.
164. (a) Vögtle, F., *Dendrimers II Architecture, Nanostructure and Supramolecular Chemistry*; Springer: Berlin, Germany, 2000 (b) Majoral, J.-P.; Caminade, A.-M. *Chem. Rev.* **1999**, 99, 845. (c) Bosman, A. W.; Janssen, H. M.; Meijer, E. W. *Chem. Rev.* **1999**, 99, 1665. (d) Newkome, G. R.; He, E.; Moorefield, C. N. *Chem. Rev.* **1999**, 99, 1689. (e) Grayson, S. M.; Fréchet, J. M. J. *Chem. Rev.* **2001**, 101, 3819.
165. Tomalia, D. A.; Baker, H.; Dewald, J. R.; May, M.; Kallos, G.; Martin, S.; Roeck, J.; Ryder, J.; Smith, P. P. *Polym. J.* **1985**, 17, 117.

This page intentionally left blank

Chapter 10

Reactions and Retro-reactions of Fullerenes

Angy L. Ortiz^{}, Luis Echegoyen^{†,¶}, Juan Luis Delgado^{‡,§}
and Nazario Martín^{‡,§,¶}*

^{}Department of Chemistry, Clemson University, Clemson, SC, 29634, USA*

*[†]Department of Chemistry, University of Texas at El Paso,
El Paso, TX 79968, USA*

*[‡]Departamento de Química Orgánica, Facultad de Ciencias Químicas,
Universidad Complutense de Madrid, E-28040, Madrid, Spain*

*[§]IMDEA-Nanociencia, Facultad de Ciencias, Módulo C-IX, 3^a planta,
Ciudad Universitaria de Cantoblanco, E-28049 Madrid, Spain*

1. Introduction	326
2. Retro-Diels Alder Reaction	327
2.1. Thermal <i>vs.</i> electrochemical stability of Diels-Alder adducts	327
2.2. Tether-directed remote functionalization	333
2.3. Orthogonal transposition approach	335
2.4. Diels-Alder adducts of substituted isobenzofurans and C ₆₀	337
3. Retro-cyclopropanation Reaction	339
3.1. Electrochemically induced retro-cyclopropanation reactions	340
3.1.1. C ₆₀ Fullerene Derivatives	340
3.1.1.1. Walk-on-the-sphere rearrangements	350
3.1.2. C ₇₀ Fullerene derivatives and higher fullerenes	352
3.2. Chemical retro-cyclopropanation reaction	355
3.2.1. Tandem reductive ring opening-retro-Bingel reaction	357

[¶]Corresponding authors. E-mail: echegoyen@utep.edu (Prof. Dr. Luis Echegoyen);
nazmar@quim.ucm.es (Prof. Dr. Nazario Martin)

4. Retro-1,3-dipolar Cycloaddition Reactions	357
4.1. Chemical retro-cycloaddition of pyrrolo[3,4:1,2] [60]fullerenes	359
4.1.1. Electrochemical retro-cycloaddition of pyrrolo [3,4:1,2] [60]fullerenes	362
4.1.2. Endohedral derivatives and their stability	363
4.2. Retro-cycloaddition reaction of isoxazolo[3,4:1,2] [60]fullerenes	364
4.2.1. Chemical retro-cycloaddition	365
4.2.2. Electrochemical retro-cycloaddition	365
4.3. Retro-cycloaddition reaction of pyrazolino[3,4:1,2] [60]fullerenes	366
4.3.1. Chemical retro-cycloaddition	366
4.3.2. Competitive retro-cycloaddition of fullerene dimers	367
5. Conclusions and Outlook	368
Acknowledgments	369
References	369

1. Introduction

Fullerenes are spherically shaped allotropes of carbon with pyramidalized sp^2 C-atoms that can exist as empty cages or endohedral structures, where the cage can act as a host for isolated atoms or clusters. The first characterized endohedral fullerene was a La containing I_b -C₆₀ and this discovery was followed by encapsulation of other metals from groups II, III and the lanthanides, metallic nitride clusters, metallic carbides, noble gases, phosphorus, nitrogen and even metal oxides have been hosted by different carbon cages.¹

The principal characteristics of the fullerenes are; (i) The number of carbons of the cage must be equal to $2(10+N)$ where N = number of hexagons, following the Euler's theorem;^{2,3} (ii) each cage is formed by N hexagons and 12 pentagons (pentagons provides the curvature or spherical shape of the fullerene); (iii) The cage can be classified as IPR or non-IPR (Isolated Pentagon Rule, in which pentagons can only be surrounded by six membered rings);^{4,5} (iv) The double bonds on the cage can be between two six membered rings ([6,6]-junction) and/or between a six membered and a five membered ring ([6,5]-junction); (v) The electron deficient nature of such alkenes along with high strain makes them susceptible for efficient addition reactions. For example, 1,2-cycloaddition on I_b -C₆₀ and D_{5h} -C₇₀ are observed only on [6,6]-junctions with some exceptions of [6,5]-junction opened addition, where the latter reaction is due to insertion of a methylene group or a metal atom.⁶ In the case of IPR- I_b -C₈₀ endohedral fullerene; 1,2-cycloadditions

on [6,6]-junction and [6,5]-junction are reported.¹ The most commonly reported reactions on fullerenes are: [2+2]-cycloaddition, [3+2]-cycloaddition, [4+2]-cycloaddition and nucleophilic additions.⁶⁻⁸

This chapter will describe the retro-cycloaddition reactions (retro-Diels–Alder, retro-Bingel and retro-1,3-Dipolar cycloaddition reactions) of fullerene derivatives and their potential applications in the regio-synthesis of new fullerene derivatives.

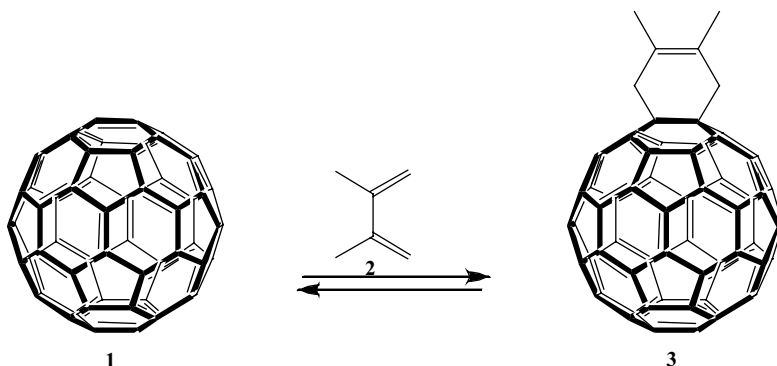
2. Retro–Diels–Alder Reaction

Fullerenes, are excellent dienophiles that can undergo [4+2] cycloaddition reactions (Scheme 1), with different dienes such as anthracene, furan and cyclopentadiene. This reaction is controlled by the properties of the dienes and can proceed at room temperature, at reflux or under microwave conditions, where the rate of Diels–Alder reaction is affected by the overall gain or loss of aromaticity of the dienophile (fullerene core) and/or the diene.⁹

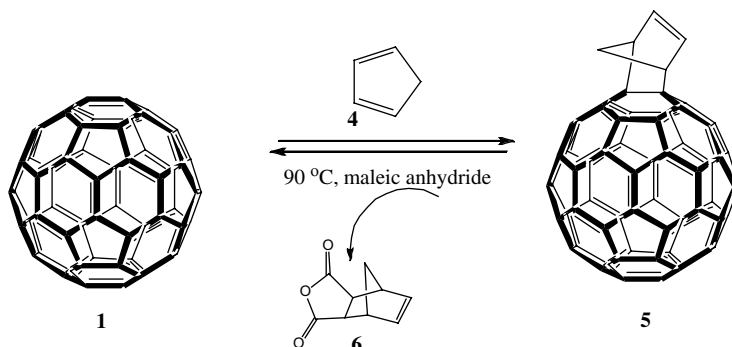
Most of these Diels–Alder adducts are thermally unstable and can undergo rapid retro-Diels–Alder upon mild heating.¹⁰ Even though the regiochemistry of Diels–Alder additions is low, a few exceptions have been reported such as the reaction of C₆₀ with an excess of 2,3-dimethyl-1,3-butadiene at elevated temperatures for several days, which yields an hexakis-adduct with *T_h* symmetry with an average effective selectivity >80% for each addition step.¹¹

2.1. Thermal *vs.* electrochemical stability of Diels–Alder adducts

The kinetic, thermal and electrochemical stability of Diels–Alder and retro–Diels Alder reactions have been studied for various fullerene adducts



Scheme 1. [4+2] cycloaddition reaction of C₆₀ (1).



Scheme 2. Diels–Alder reaction of C_{60} (1) with cyclopentadiene (4) and retro-cycloreaction in presence of maleic anhydride.

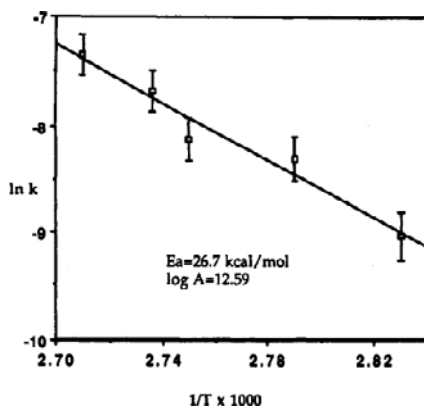
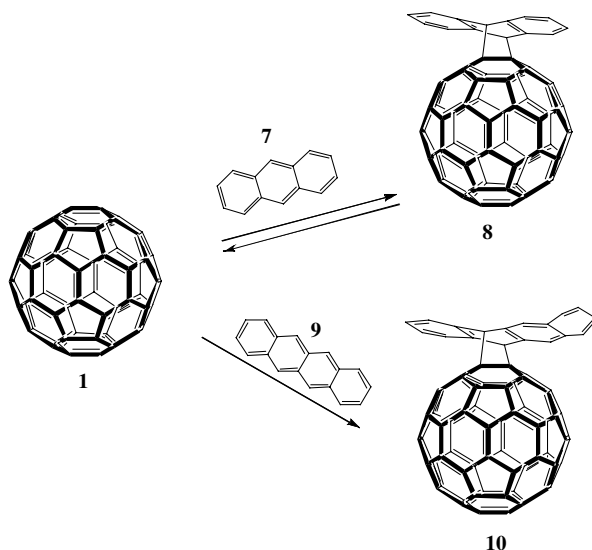


Figure 1. Plot of $\ln k$ vs. $1/T$ (K) for the retro-cycloaddition of 5. Error bars represent the standard error of the data points. Reprinted from Reference 12 with permission. Copyright 2010 American Chemical Society.

such as mono-cyclopentadiene- C_{60} , mono-anthracene- C_{60} , and mono-tetracene- C_{60} . The mono-cyclopentadiene- C_{60} 5 (Scheme 2) was formed at room temperature and decomposed to its starting material at 95 °C (Scheme 2), and maleic anhydride was used as a scavenger to trap the cyclopentadiene. Kinetic studies of retro-Diels–Alder reactions established a first order process within the temperature range of 80.0–95.0 °C (Figure 1)¹² and an activation energy (E_a) of 26.7 ± 2.2 kcal/mol, which is 5–15 kcal/mol lower than most retro-Diels–Alder reactions. This low value was attributed to the aromaticity loss of the fullerene core upon the [6,6]-addition.¹²

The mono-anthracene- C_{60} 8 (Scheme 3) derivative was isolated and characterized by means of ^1H -NMR, UV-vis, IR, mass spectrometry and thermal gravimetric analysis (TGA) in 1993.¹³ As shown in the TG trace (Figure 2)



Scheme 3. Diels–Alder reaction of C₆₀ (1) with anthracene (7) and tetracene (9). Reprinted from Reference 14 with permission. Copyright 2010 Elsevier.

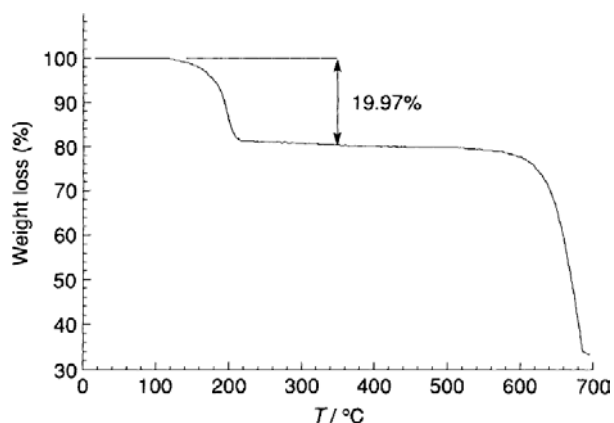


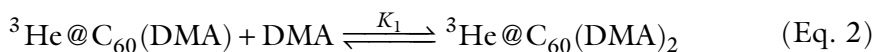
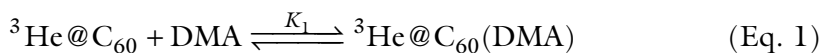
Figure 2. Thermal gravimetric analysis (TGA) of mono-anthracene-C₆₀ derivative. Reproduced from Reference 13 with permission of The Royal Society of Chemistry.

the weight lost from the anthracene moiety occurred in the temperature range between 120–194 °C.¹³ It took almost a decade to study the kinetics of this reaction.¹⁴ This study was conducted by the reaction of C₆₀ with anthracene 7 (Scheme 3) in toluene within a temperature range of 22–63 °C at a constant concentration of fullerene 1. The absorbance of the reaction reversibly decreases as the temperature increases which proves that the reaction is reversible at high temperatures.¹⁴

Another studied derivative was the mono-tetracene C_{60} adduct **10** (Scheme 3). The kinetic study was carried out in toluene with a molar ratio 10:13 of C_{60} :**9** within a temperature range of 25–59 °C (Scheme 3). In this case the absorbance was temperature independent so this reaction is irreversible at all temperatures studied.¹⁴ The difference between **8** and **10** was attributed to the fact that the activation energy of these cycloadditions reactions differs by 10 kJ/mol, the anthracene reaction exhibiting the higher one.¹⁴

In addition, thermodynamic studies with 9-substituted anthracene were also reported. The Diels-Alder reaction of 9,10-dimethylantracene (DMA) with C_{60} and C_{70} was reversible at room temperature, yielding mixtures of isomers of $C_{60}(\text{DMA})_n$ and $C_{70}(\text{DMA})_n$ respectively (Eq. 1).¹⁵

The thermodynamic parameters ΔG , ΔH and ΔS of these reactions were calculated by ^3He -NMR using endohedral $^3\text{He}@C_{60}$ fullerenes (Table 1). It was claimed that the ^3He inside the fullerenes exerts a negligible effect on the rates and equilibrium constants for these reactions. Cycloaddition of the first addend for both C_{60} and C_{70} was determined to be first order rate. Their ΔS values were large and negative which further confirmed their reversibility (Table 1).¹⁶



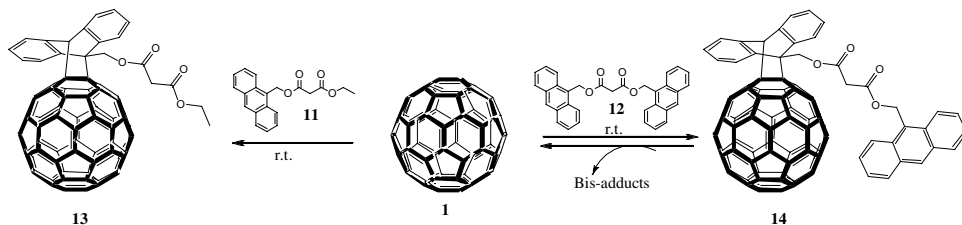
The thermodynamic parameters and activation energies of the Diels-Alder reactions depend on the overall gain or loss of aromaticity of the diene as shown in Table 1. The activation enthalpy for the cyclopentadiene additions was the lowest because no reduction of aromaticity occurs on the cyclopentadiene ring.

The anthracene moiety had the highest aromaticity reduction, and hence the highest activation enthalpy as well as activation energy. The activation and reaction entropies were always large and negative, as expected for a Diels-Alder reaction.¹⁴ In the retro-Diels-Alder reaction, the activation enthalpies were high and the activation entropies of the anthracene and cyclopentadiene were opposite, with the anthracene having a positive activation entropy. The reaction entropy observed for the 9,10-dimethylantracene was the largest one, possibly related to the particularly facile retro-Diels-Alder reaction.¹⁴

Electrochemistry can be an useful tool to study Diels-Alder adduct stability. The anthracene malonates **11** and **12** react with C_{60} to form monoadducts **13** and **14**. Monoadduct **13** is stable for months when stored

Table 1. Activation energy and thermodynamic parameters (1M, 298 K) for the Diels–Alder reaction of C₆₀ with several dienes. Adapted from Reference 17 with permission. Copyright 2010 American Chemical Society. Reprinted from Reference 18 with permission. Copyright 2010 Elsevier.

Diene	Diels–Alder		Retro-Diels–Alder			Reaction		Reference
	$\Delta^\ddagger H$ (kJ/mol)	$\Delta^\ddagger S$ (J/K.mol)	$\Delta^\ddagger H$ (kJ/mol)	$\Delta^\ddagger S$ (J/K.mol)	Ea (kJ/mol)	$\Delta^\ddagger H$ (kJ/mol)	$\Delta^\ddagger S$ (J/K.mol)	
Cyclopentadiene	27	−161	109	−12	111.8	−82	−149	12, 17
9, 10-Dimethylantracene	—	—	—	—	—	−96	−256	16
9-Hydroxymethylantracene	—	—	—	—	108	—	—	18
Anthracene	57	−123	−138	71	140	−81	−195	14
Tetracene	47	−111	—	—	—	−82	—	14



Scheme 4. Diels–Alder reaction of anthracene malonates **11** and **12** with C_{60} **1**. Reproduced from Reference 19 by permission of The Royal Society of Chemistry (RSC) for the Centre National de la Recherche Scientifique (CNRS) and the RSC.

Table 2. Redox potentials of adducts **13** and **14** *vs.* ferrocene in *o*-DCB (in mV) at a scan rate of 200 mV s^{−1}. a. Values quoted: $(E_{pa} + E_{pc})/2$. Reproduced from Reference 19 by permission of The Royal Society of Chemistry (RSC) for the Centre National de la Recherche Scientifique (CNRS) and the RSC.

Compound	Reduction ^a					
	E_1	$E_{1'}$	E_2	$E_{2'}$	E_3	$E_{3'}$
C_{60} , 1	−1083	—	−1470	—	−1937	—
13	−1153	—	−1533	—	−2082	—
14	−1162	−1275	−1536	−1666	−1936	−2099

in a freezer (−10 °C); however, cycloadduct **14** forms bis-adducts and C_{60} in less than a week (Scheme 4).¹⁹

The redox potential of anthracene malonates **11** and **12** and monoadducts **13** and **14** are reported in Table 2. For monoadduct **13**, three reversible reduction processes were observed that, as expected, were cathodically shifted compared with the values of pristine C_{60} . On the other hand monoadduct **14** exhibited two sets of three reduction processes approximately 100 mV apart from each other, which indicated the presence of two different compounds (see Table 2). The first set was attributed to monoadduct **14** and the second to regioisomeric bis-adducts resulting from a second Diels–Alder reaction on **14**.¹⁹

The electrochemical stability of monoadduct **13** was investigated by cyclic voltammetry (CV) at different temperatures and controlled potential electrolysis (CPE) experiments. The CV was done between 5 and 90 °C (Figure 3a) and the waves became broader as the temperature increased because of the presence of additional species (dotted line, Figure 3a). Also, a complete retro-Diels–Alder reaction was obtained at 90 °C (dashed line, Figure 3a), at which point the voltammogram corresponded to that of

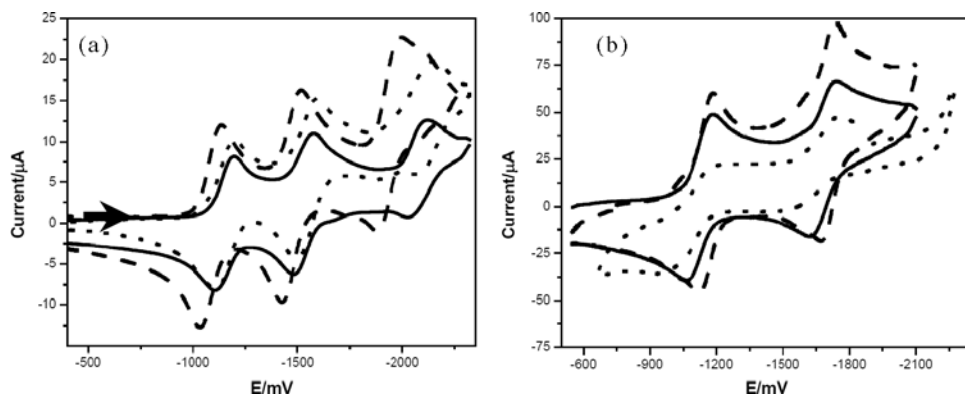


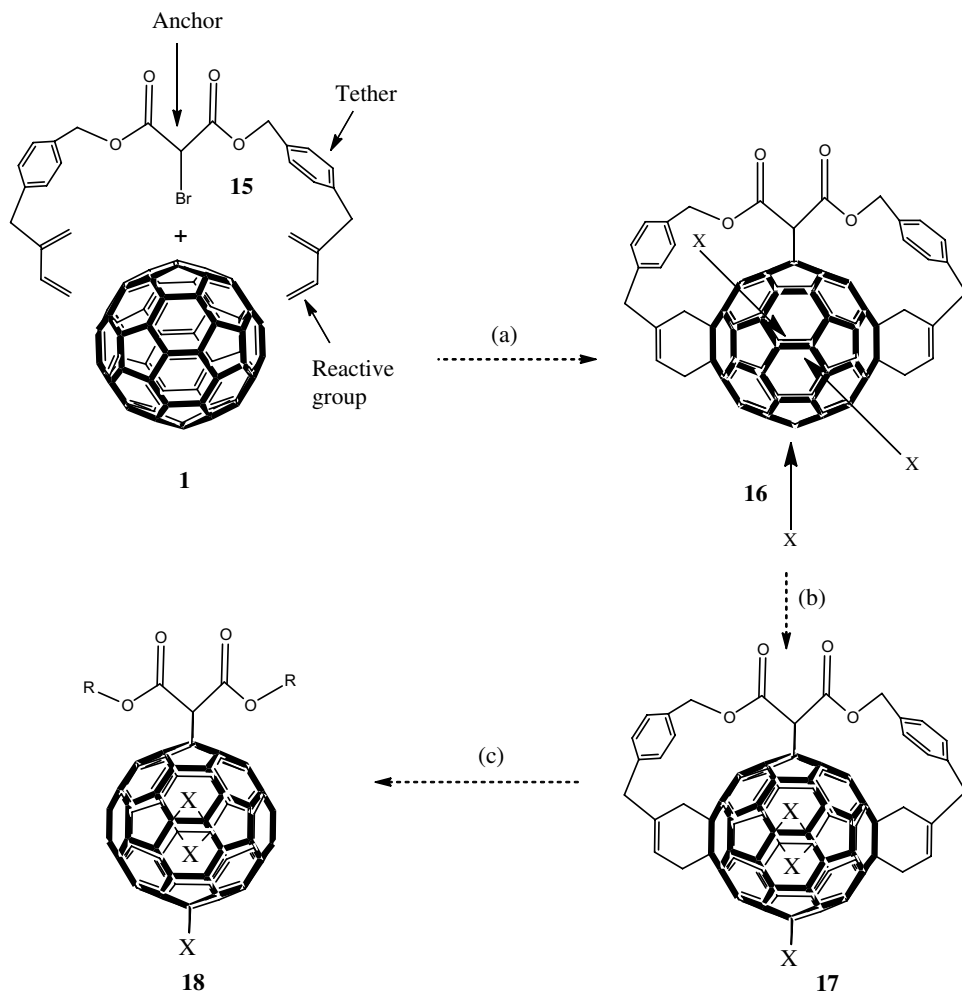
Figure 3. Thermal and electrochemical behavior of **13**. (a) CV at room temperature (solid line), CV at 50 °C (dotted line), CV at 90 °C (dashed line); (b) initial CV (solid line), CV after $2e^-$ reduction (dotted line), CV after $2e^-$ reduction and re-oxidation (dashed line). Reproduced from Reference 19 by permission of The Royal Society of Chemistry (RSC) for the Centre National de la Recherche Scientifique (CNRS) and the RSC.

pristine C_{60} . Two electrons were added to **13** at the second electron reduction potential (Figure 3b) by CPE. The process was fully reversible and no changes in the cyclic or OSWV voltammograms were observed. After re-oxidation and purification, monoadduct **13** was recovered in 98% yield indicating that the C_{60} -anthracene Diels–Alder derivatives are stable upon electrochemical reduction.¹⁹

2.2. Tether-directed remote functionalization

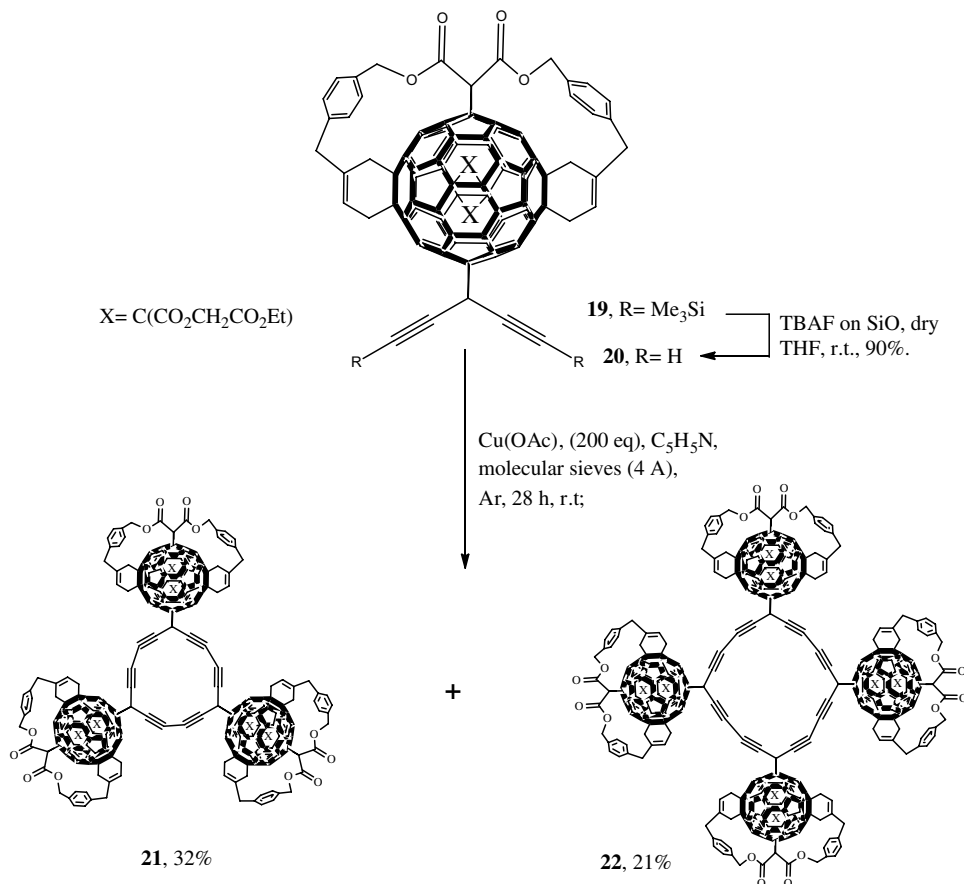
Diels–Alder and Retro-Diels–Alder reactions have been used as protection-deprotection steps for further functionalization of the fullerene in order to have regiocontrol of multiple cycloadditions. One of the approaches introduced by Isaacs *et al.* is the versatile “Tether-Directed Remote Functionalization” approach (Scheme 5),²⁰ where C_{60} was protected by a reactive group anchored on a tether **15** (Scheme 5). Sequential cyclopropanation followed by intramolecular Diels–Alder reactions led to **16** (Scheme 5), and this was followed by the addition of new additional groups to produce **17** (Scheme 5). A final retro-Diels–Alder reaction leads to a fullerene that is functionalized selectively on an equatorial belt, **18** (Scheme 5).^{20–25} Selective e_{face} bond attack can be achieved over e_{edge} , *cis*-3 and *trans*-4 bonds by careful selection of the reactive group and length of the tether.²⁰

In order to remove the cyclohexene rings from the hexakis-adduct **17** (Scheme 5), Rubin and co-workers²⁶ successfully used a retro-Diels–Alder



Scheme 5. Reversible tether-directed remote functionalization. (a) The anchor-tether-reactive-group conjugate is introduced. (b) The anchor-tether-reactive group directs newly incoming addends into equatorial positions. (c) Subsequently, the tether-reactive-group conjugate is removed. Reproduced from Reference 25 with permission. Copyright Wiley-VCH Verlag GmbH & Co. KGaA.

reaction after the transformation of the cyclohexene rings to cyclohexadieno rings. This approach allowed the isolation of the compound in quantitative yield without the need for separation HPLC method.^{25–26} This approach was also used for the synthesis of novel fullerene-acetylene hybrid carbon allotropes C₁₉₅ **21** (Scheme 6) and C₂₆₀ **22** (Scheme 6) by oxidative cyclization of diethynylmethanofullerene **20** (Scheme 6) under *Eglinton–Glaser* conditions.^{21,24}

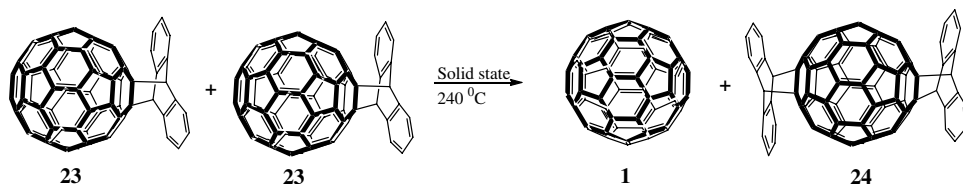


Scheme 6. Synthesis of Soluble Derivatives C_{195} **21** and C_{260} **22**. Reproduced from Reference 24 with permission. Copyright Wiley-VCH Verlag GmbH & Co. KGaA.

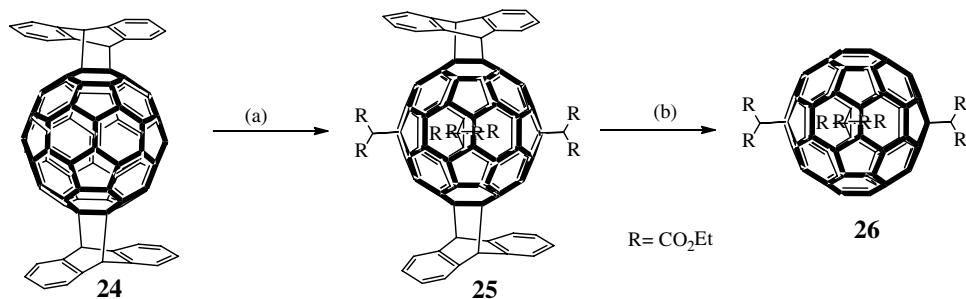
2.3. Orthogonal transposition approach

In 1995, the use of DMA as a reversible template was reported to activate equatorial double bonds for the addition of bromoethyl malonates on the C_{60} fullerene framework.²⁷ The addition of bromoethyl malonate on all of the e -positions was favored due to the presence of DMA. This octahedral addition pattern was explained in terms of thermodynamic arguments and the enhanced orbital coefficient frontier orbital on the e positions. The hexakis-adduct with T_h symmetry was isolated with 23% yield, which was not formed in absence of DMA.²⁷

Later in 1996, an elegant topochemical and highly regiospecific functionalization of C_{60} fullerene was reported (Scheme 7). A thermal



Scheme 7. Synthesis of antipodal fullerene derivative **24**. Reproduced from Reference 28 with permission. Copyright Wiley-VCH Verlag GmbH & Co. KGaA.



Scheme 8. Synthesis of the tetra-adduct **26** by the orthogonal transposition approach. (a) $\text{BrHC}(\text{CO}_2\text{Et})_2/\text{DBU}$ in $\text{CH}_2\text{Cl}_2/\text{r.t.}$, 2 d; (b) $195\text{ }^{\circ}\text{C}$, 5 min.; Reprinted from Reference 29 with permission. Copyright 2010 American Chemical Society.

transformation of mono-anthracene C_{60} **23** in the solid state led to C_{60} and the antipodal bis-adduct **24** resulting from an intermolecular anthracene transfer. Compound **23** packs in the crystalline state so that the [6,6]-junction of the neighboring fullerene is close enough to let the anthracene moiety of the neighboring molecule to transfer the addend selectively. The yield obtained was 48% for C_{60} and also for the bis-adduct **24**, with 96% overall conversion (Scheme 7).²⁸

The antipodal bis-adduct **24** can be used as a template in a synthetic transformation sequence called “Orthogonal transposition” for addition over the equator belt (Scheme 8). Compound **24** was suspended in dichloromethane and treated with an excess of diethyl bromomalonate and amidine base diazabicycloundecene (DBU) at room temperature for 2 days (Scheme 8), and after purification the hexaadduct **25** was isolated in 95% yield. Then **25** was heated up to $195\text{ }^{\circ}\text{C}$ to remove the anthracene groups to obtain the tetra-adduct **26** with D_{2h} symmetry (Scheme 8).²⁹

An extension of this approach was reported by Echegoyen and co-workers,³⁰ where pyrrolidine groups were introduced in a step-by-step fashion by 1,3-dipolar reactions starting with the tetra-adduct **26** as a template. Synthesis of the pentakis-adducts **27** (Figure 4), hexakis-adducts

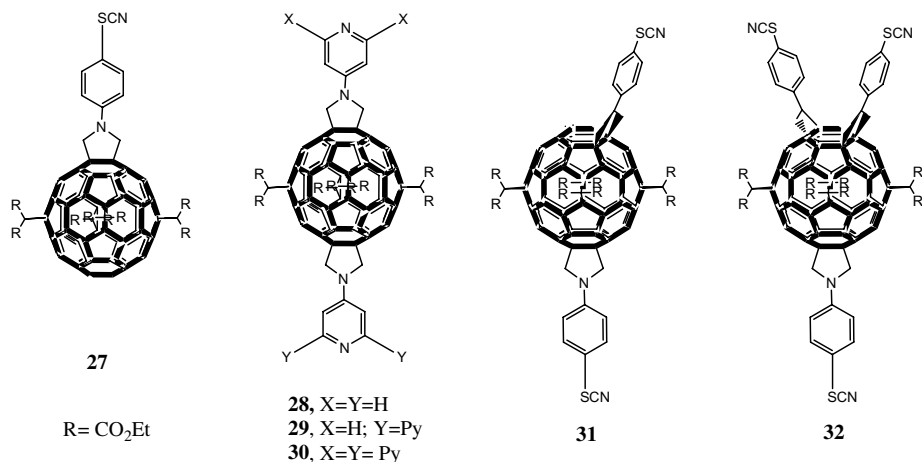


Figure 4. Pentakis-adduct **27**, hexakis-adducts **28–31** and heptakis-adducts **32** of C₆₀ fullerene. Reproduced from Reference 30 with permission. Copyright Wiley-VCH Verlag GmbH & Co. KGaA.

28–31 (Figure 4) and heptakis-adduct **32** (Figure 4) with better regiocontrol than direct [3+2]-cycloaddition reaction were reported.³⁰

2.4. Diels–Alder adducts of substituted isobenzofurans and C₆₀

Another approach was the use of substituted isobenzofurans on C₆₀ to open the cage (“molecular surgery”), in order to encapsulate the atoms and then close it back to form unusual and new endohedral fullerenes. The first isobenzofuran-C₆₀ derivative was reported in 1993, where the isobenzofuran was formed *in situ* from 1,4-dihydro-1,4-epoxy-3-phenylisoquinoline in refluxing C₆₀ benzene solution and it was stable in solution and in the solid state.³¹ It was in 2006 when the reported use of this type of derivatives for molecular surgery of the C₆₀ cage was successfully realized.³² The concept behind this is the saturation of the three (Strategy 1, Figure 5), two (Strategy 2, Figure 5) or one (Strategy 3, Figure 5) double bonds within one of the six membered rings using dienes such as isobenzofurans. Isobenzofurans resulted in the large scale synthesis and the Diels–Alder products are not too labile but can be easily removed through retro-Diels–Alder reactions.^{33a}

Strategy 2 (Figure 5)³³ was achieved using a tandem addition of two tethered isobenzofuran units with different linkages [such as sulfide, methylene, C(CH₃)₂, 2,3-quinoxaline-diyl, or CH₂OCH₂ units] to adjacent double bonds of C₆₀ with a possible *cis-1* addition pattern (Scheme 9).^{33b} The retro-Diels–Alder reactions of these bis-adducts were highly kinetically stable, but

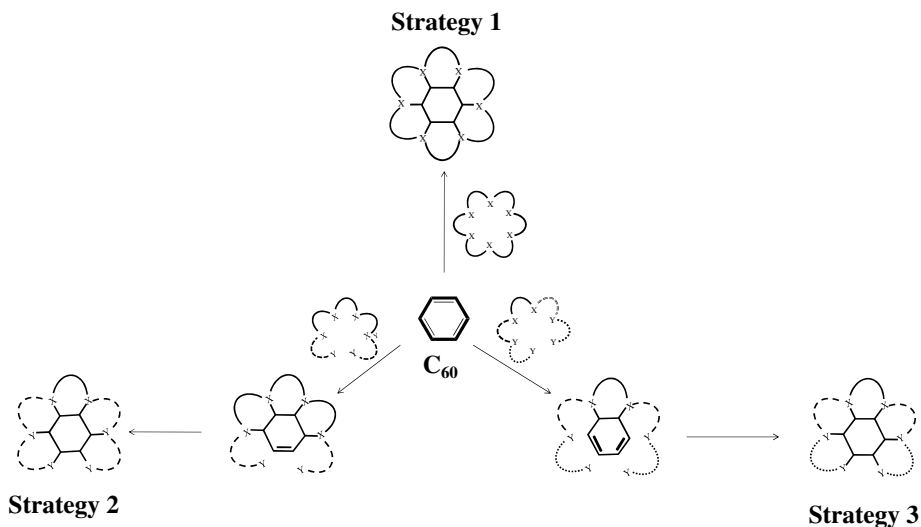
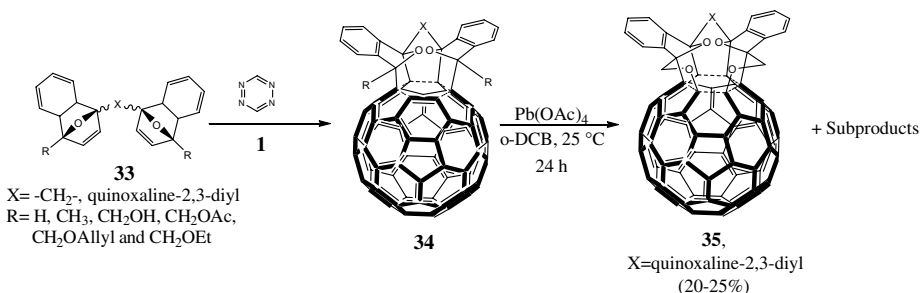


Figure 5. Three conceptual strategies for the stepwise addition of tethered reactive units to three adjacent C=C bonds of a single six-membered ring of C_{60} . Reprinted from Reference 32a with permission. Copyright 2010 American Chemical Society.



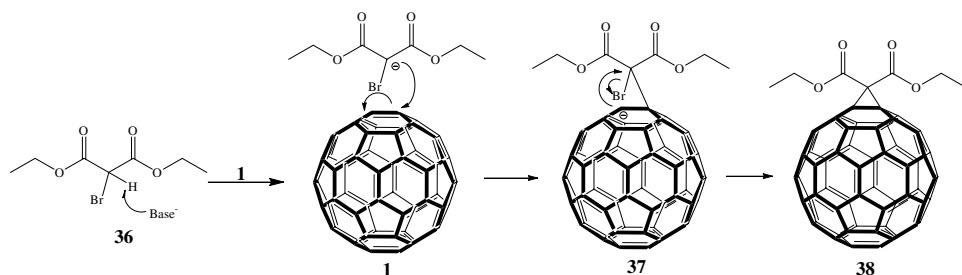
Scheme 9. Double Diels-Alder cycloadditions of bis(isobenzofuran)s to fullerene C_{60} . Reprinted from Reference 32b with permission. Copyright 2010 American Chemical Society.

of different linkers only the one carbon methylene and the two-carbon 2,3-quinoxaline linkers were in close proximity to the *cis-1* C=C bond for a favorable transition state geometry. On the other hand, other linkers like S, $C(CH_3)_2$, and CH_2-OCH_2 did not favor the *cis-1* addition pattern, which was either due to unfavorable electronics, excessive steric hindrance or because of a poor angle of approach for the second addition.^{33b} The next step in order to open the cage was to saturate the remaining double bond *via* the side chains of the isobenzofurans. For example, two sequential 5-exo-trig additions of alkoxy radicals generated from diol **34** with lead tetraacetate (Scheme 9) generated the 1,2,3,4,5,6-hexaki- C_{60} adduct **35**.³²

Diels–Alder and retro-Diels–Alder reactions have also been used in other applications such as to improve fullerene solubility^{26,34} and fullerene separation.³⁵ Fullerene solubility has been one of the major challenges for their modification and characterization. Rubin and co-workers reported that the solubility of fullerenes could be increased by the introduction of a protecting group *via* Diels–Alder reaction, and then they could be modified with new additions and followed by deprotection *via* the retro-Diels–Alder reaction.²⁶ In addition, Heeger and co-workers³⁴ reported an enhanced performance and better morphology of P3HT/C₆₀ bulk-heterojunction (BHJ) solar cells in which the fullerene solubility was increased by the addition of a polymer using a Diels–Alder reaction, which created a better BHj homogenous layer during the deposition thanks to the retro-Diels–Alder reaction.³⁴ Another challenge that has been overcome by a Diels–Alder reaction was trimetallic nitride endohedral fullerene purification, which was accomplished using a modified resin with pendant cyclopentadiene groups. When the mixture of fullerenes was passed through the resin only empty cages and classical endohedrals reacted *via* Diels–Alder reactions, and the metallic nitride remained endohedrals unreacted and eluted quickly from the column.^{35c–f} The empty cages and classical endohedrals eluted later and were recovered since the Diels–Alder reaction is reversible.^{35a–b}

3. Retro-cyclopropanation Reaction

Nucleophilic attacks on fullerenes have been extensively studied. A very common example of this is the addition-elimination Bingel–Hirsch reaction. In this reaction, the deprotonation of an α -halomalonate **36** (Scheme 10) leads to a nucleophilic anion which attacks the fullerene core (Scheme 10), followed by an intramolecular displacement of the halide by cyclization with the anionic center formed in the core **37** (Scheme 10).³⁶ This versatile reaction



Scheme 10. Addition-elimination mechanism of Bingel–Hirsch reaction. Reproduced from Reference 36 with permission. Copyright Wiley-VCH Verlag GmbH & Co. KGaA.

has been used to synthesize a wide range of fullerene derivatives such as donor-acceptor systems,³⁷ dendrimers,³⁸ catenanes and rotaxanes,³⁹ among others. Even though these di(alkoxycarbonyl)methano-fullerene derivatives **38** (Scheme 10) are stable in air, and under high thermal and oxidative conditions, they can be removed efficiently under reduction conditions (chemically and electrochemically). This section intends to give a comprehensive review of the work done with retro-cyclopropanation reactions and its applications.

3.1. Electrochemically induced retro-cyclopropanation reactions

3.1.1. C₆₀ Fullerene derivatives

The first indication of methanofullerene decomposition to C₆₀ upon coulometric reduction with two electrons was reported by Arias *et al.* in 1995.^{40a} Later in 1996, Wudl and co-workers reported the detection of C₆₀ by cyclic voltammetry (CV) upon addition of one electron to **39–41** (Figure 6).^{40b} Later during the study of the “Tether-Directed Remote Functionalization” approach the instability of some di(alkoxycarbonyl)methanofullerene dianions under CV and steady-state voltammetry (SSV) was reported.²⁵ In 1998, Echegoyen, Diederich and co-workers⁴¹ reported the retro-Bingel reaction of the (alkoxycarbonyl)methanofullerenes of C₆₀, C₇₀, C₇₆ and *ent*-C₇₆ at the second reduction potential by controlled potential electrolysis (CPE), after the addition of four electrons per molecule. The parent fullerenes were recovered in 75–82%, 70% and 5–9% yield, respectively.⁴¹

The retro-cyclopropanation by CPE was selective for the methano addend, which must have at least one strong electron-withdrawing group (Scheme 11).⁴² For example, derivatives **39–41**⁴⁰ and mono(ethoxycarbonyl)methano-C₆₀ fullerene **42** (Scheme 11)⁴² can undergo retro-cycloaddition thanks to the nitrile and ester groups that are present. The presence of others groups such as

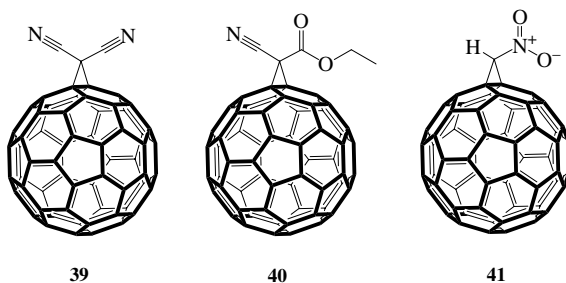
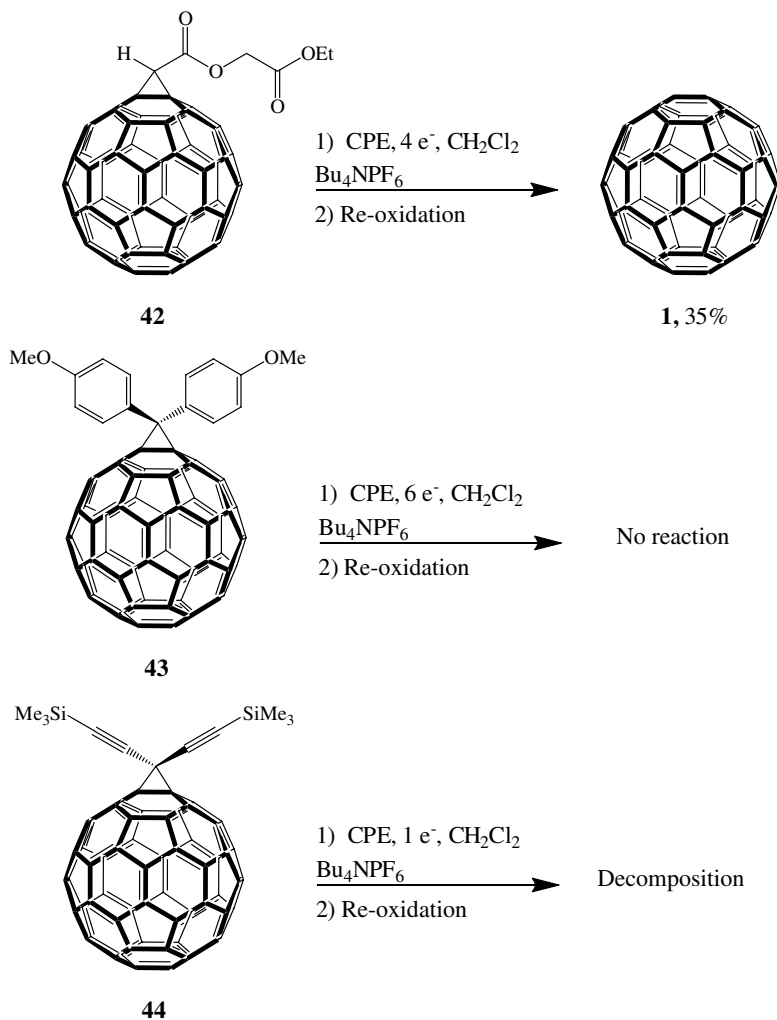


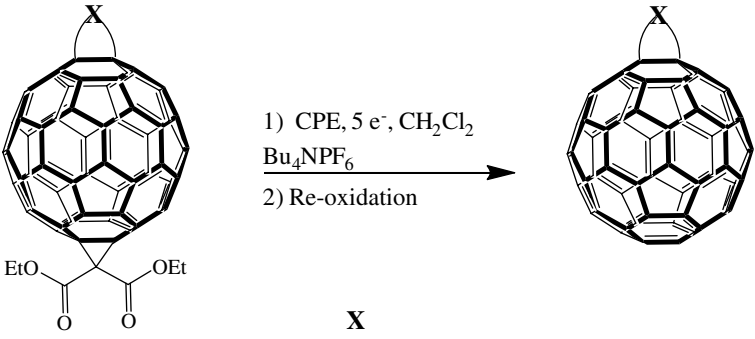
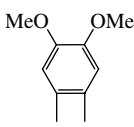
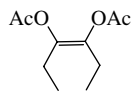
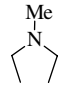
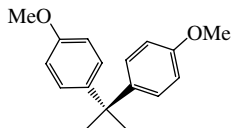
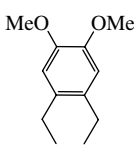
Figure 6. Methano-C₆₀ fullerene derivatives.



Scheme 11. Controlled potential electrolysis of **42–44** fullerene derivatives. Reproduced from Reference 42 with permission. Copyright Wiley-VCH Verlag GmbH & Co. KGaA.

cyclohexene, pyrrolidine and benzocyclobutene rings fused to the [6,6]-bond were not affected by CPE (Table 3).⁴² This singularity offered a new and versatile protecting/deprotecting group strategy. For example, the CPE (Figure 7a) of the hexakis-adducts **29** and **30** (Figure 4) were conducted in order to remove the four malonate groups and obtain the *trans*-1 bis-adducts **55** and **56** (Figure 7), respectively.^{30a} The formation of the *trans*-1 bis-adduct by the direct 1,3-dipolar reaction produces a very low yield (1–6% relative yield) and the isolation involves tedious HPLC work.⁴³

Table 3. Selective removal of bis(ethoxycarbonyl)methano addends in mixed C₆₀ bis-adducts. Reproduced from Reference 42 with permission. Copyright Wiley-VCH Verlag GmbH & Co. KGaA.

<div style="display: flex; align-items: center; justify-content: center;">  </div>		
45		50, 67%
46		51, 43%
47		52, 63%
48		53, 60%
49		54, 61%

The retro-cyclopropanation reaction had been reported not only for Bingel type addends, but also for some methanofullerenes with quinone type addends containing electron-withdrawing groups (Figure 8).⁴⁴ These spiromethanofullerenes exhibited irreversible reduction electrochemistry on the CV timescale. The electrolysis of **57** (Figure 8) consumed 3.9 electrons per molecule and yielded 60% of fullerenes product and not C₆₀. The electrolysis of **58** and **59** (Figure 8) consumed 3.7 and 2.3 electrons per molecule and yielded 65% and 58% of C₆₀, respectively.

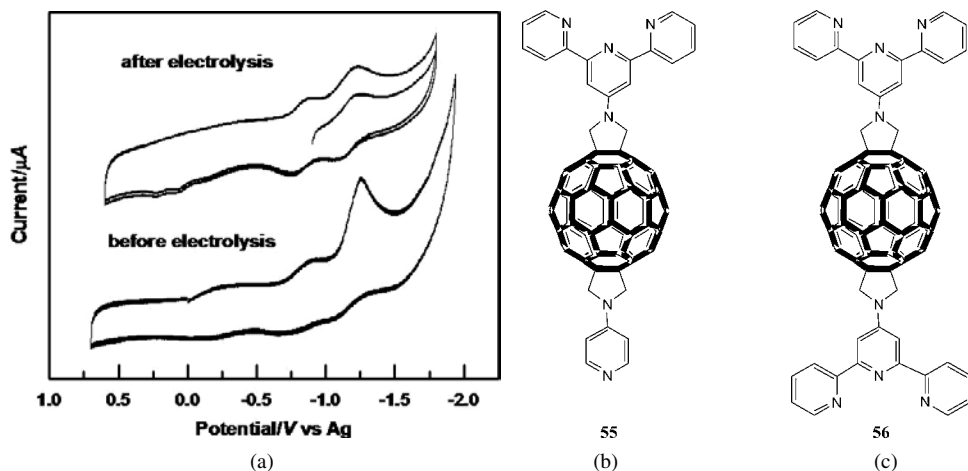


Figure 7. (a) Cyclic voltammograms of **30** before and after CPE. Supporting electrolyte: 0.1 M Bu₄NPF₆, scan rate 0.1 V.s⁻¹; (b) product from CPE of **29**, c) product from CPE of **30**. Reproduced from Reference 32a with permission. Copyright Wiley-VCH Verlag GmbH & Co. KGaA.

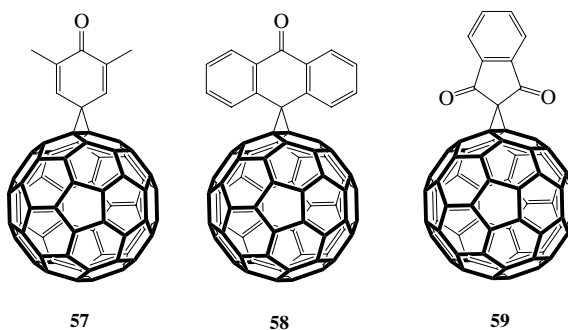


Figure 8. Spiromethanofullerenes, Bingel-like addends. Reproduced from Reference 44 by permission of The Royal Society of Chemistry.

Nuretdinov and co-workers⁴⁵ reported a mechanistic study for the retro-cyclopropanation reaction based on CV measurements using Nicholson's treatment.⁴⁶ However, the proposed mechanism was not supported by simulations or product characterizations. Compounds **38** (Scheme 10), **59** (Figure 8), **60–67** (Figure 9) were used to study the mechanisms and characterize the electro-reduced intermediates of the retro-cyclopropanation reaction. Compounds **60** and **61** were chosen because the nitrophenyl group had a strong and easily recognizable ESR signal upon reduction.⁴⁷ The electrochemistry was conducted in THF and at least three reduction processes

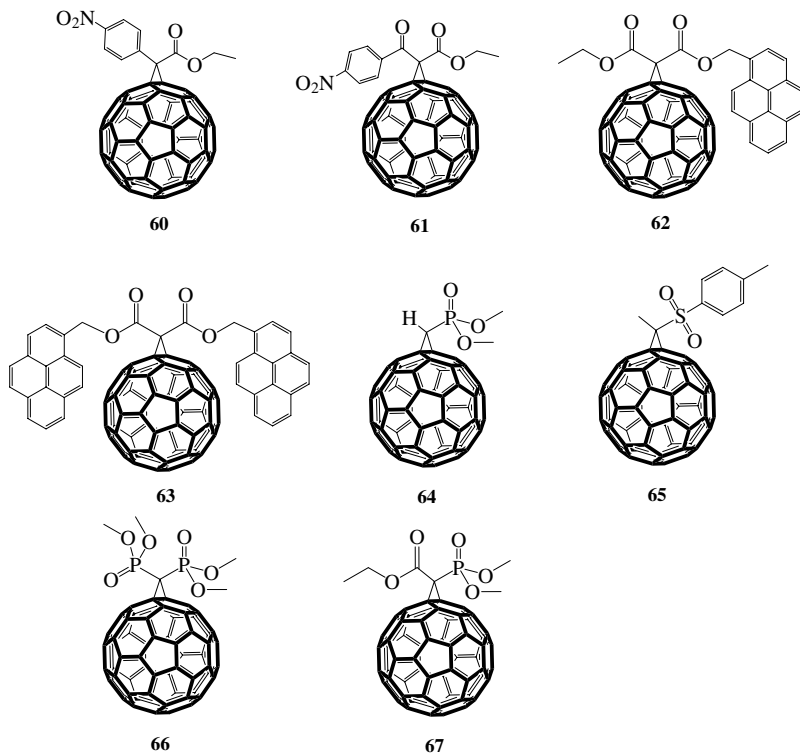


Figure 9. Fullerene derivatives studied under retro-cyclopropanation conditions.

were detected. The CPE of **60** and the ESR measurements (a–e, Figure 10) were performed after the first, second and third reduction waves.⁴⁷

Only after the electrolysis at the third reduction and reoxidation at 0 V was it possible to obtain 23% C₆₀, 40% of **60**, and 18% bis-adducts. The ESR spectra after one-electron and two-electron coulometric reductions were typically fullerene-based radicals⁴⁸ with *g* factors of 2.00191 and 2.00139 respectively (a and b, Figure 10). At the third reduction the fullerene and nitrophenyl-based radical anions were observed with a *g* value of 2.00265 and 2.00522, respectively.⁴⁷ The coupling constants corresponding to one N and two sets of two equivalent protons were $a_N = 9.55$ G, $a_O = 3.25$ G and $a_m = 0.91$ G.⁴⁹

In the case of methanofullerene **61**, the retro-cyclopropanation reaction was obtained after the fourth reduction, and it yielded 52% of C₆₀, 11% of bis-adducts and 37% of uncharacterized materials. The ESR analysis was similar to that of compound **60**, where the presence of both nitrophenyl and fullerenyl radicals were detected after the 3rd reduction, with *g* factors of 2.00471 and 2.00105, respectively. The coupling constants for the *p*-nitrophenyl-based radical were $a_N = 7.35$ G, $a_O = 2.96$ G and $a_m = 0.81$ G. These

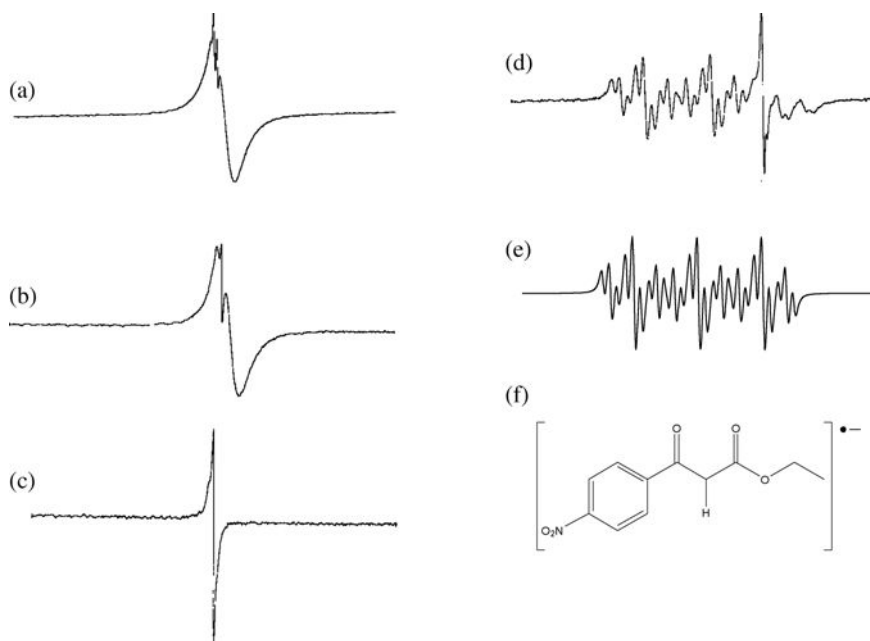
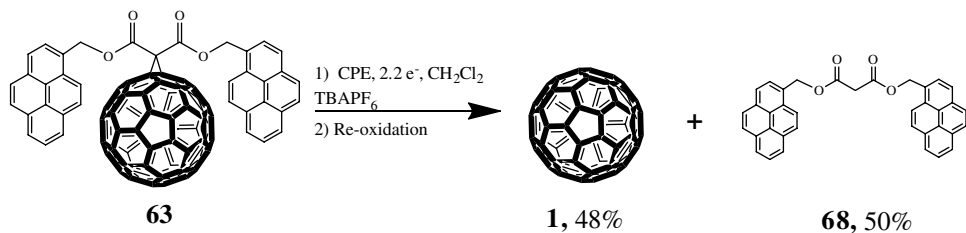


Figure 10. ESR spectra for the reduction of **60** in THF. (a) after one-electron coulometric reduction, (b) after two electrons, (c) four electrons, (d) three electrons, (e) computer simulation for three-electron reduction spectrum, the parameters used for this simulation are: $a_N = 9.15$ G, $a_o = 3.35$ G and $a_m = 1.02$ G, linewidth = 0.50 G, and f) Possible intermediate during electrolysis of **61**. Reproduced from Reference 47 by permission of The Royal Society of Chemistry. Reproduced from Reference 52 with permission. Copyright Wiley-VCH Verlag GmbH & Co. KGaA

coupling constants changed after the 4th reduction to $a_N = 9.18$ G, $a_O = 3.26$ G, $a_m = 1.02$ G and an additional doublet splitting of 0.40 G was observed. Even though the change of a_N value from 7.35 G to 9.18 G was not explained, this hyperfine coupling constant is very sensitive to solvent and counterion effects.⁵⁰ From the simulated ESR spectra it was determined that the generated radical contains a single spin $1/2$ nucleus, most probably a proton, suggesting a possible radical intermediate f (Figure 10).⁴⁷

The analysis of the products after electrolysis of compounds **62** and **63** (Figure 9) was reported later.⁵¹ The CPE of **63** at the second reduction potential and after addition of 2.2 electrons per molecule yielded 48% of **C₆₀** and 50% of the malonate **68** (Scheme 12).⁵² The electrochemical properties were analyzed using digital simulations (BAS digital simulation program Digisim) for compounds **38** (Scheme 10) and **59** (Figure 8).⁵³ The CV in THF was studied for the first three reduction processes at different scan rates, because the electrochemically induced retro-cyclopropanation reaction



Scheme 12. Retro-cyclopropanation of compound **63**.

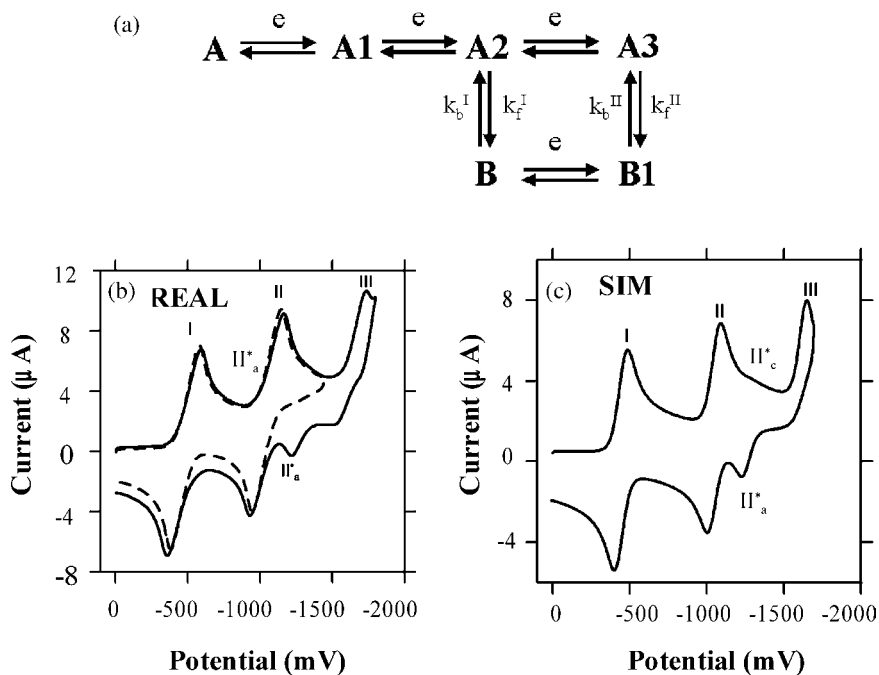


Figure 11. (a) Mechanism at 0.5 V·s⁻¹; (b) Cyclic voltammetric (CV) curves for a 0.1 mM THF solution of **38** at 1 V·s⁻¹, Pt as working electrode, Pt-mesh counter electrode and Ag wire as a quasi-reference electrode; and c) best simulated curve for **38**. Reprinted from Reference 52 with permission. Copyright 2010 American Chemical Society.

generally occurs after the second reduction process.⁵³ The CV of compound **38** showed two reversible (I and II, Figure 11b) and one chemically irreversible (III, Figure 11b) processes. Additionally, a small peak between the second and third C₆₀-based reductions was designated II* (Figure 11b). The cathodic peak II_c*, indicated an unstable species from a chemical reaction because it completely disappeared upon increasing the scan rate. On the contrary, its anodic counterpart II_a* increased when the scan rate increased. Figure 11c shows the simulated CV and Figure 11a shows the mechanism

proposed based on the data. The proposed mechanism consists of three main reduction (A) processes with the two last (A2 and A3) being related to a new electro-active species (B), which results in a square Scheme (Figure 11a). The decrease of peak (II^*) was attributed to a slow initial chemical reaction in the forward scan (Figure 11c) and another fast reaction accounted for the irreversibility of the third reduction. Peaks I and II were reversible for all the scan rates recorded. This was in agreement with a reversible chemical reaction, such as the opening of the cyclopropane ring.⁵³

A rather complex CV was obtained for compound **59** (Figure 12b), with an initial two electron reduction process (solid line, Figure 12b), and an intermediate irreversible peak (II) whose intensity increases relative to the other two peaks with the scan rate (3 V.s^{-1}). The current-function ratios between peaks I, II, and III were evidently different (dotted line, Figure 12b) when compared at 0.5 V.s^{-1} (solid line, Figure 12b).⁵³ This feature, and the general shape of the curve was reminiscent of a bi-electronic slow electron-transfer process.⁵¹ Figure 12c shows the simulated curve and Figure 12a the proposed mechanism according to the experimental data.^{53,54} This mechanism also involved the cleavage of the cyclopropane ring after the first electron reduction but not at the second as for **38**. At slower rates, a second electron was transferred at the same potential as the first one and increasing the scan rate

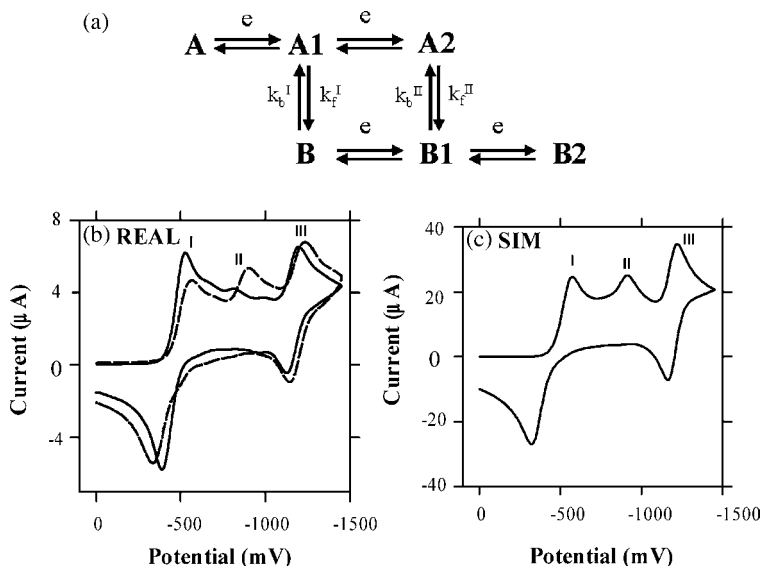


Figure 12. (a) Mechanism at 3 V.s^{-1} ; (b) Cyclic voltammetric (CV) curves for a 0.5 mM THF solution of **59** at 0.5 V.s^{-1} (—) and 3 V.s^{-1} (---), Pt as working electrode, Pt-mesh counter electrode and Ag wire as a quasi-reference electrode; and (c) best simulated curve for **59**. Reprinted from Reference 52 with permission. Copyright 2010 American Chemical Society.

allowed the increase of the height of the intermediate peak (II), which was due to the original species.^{51,53}

The last set of C_{60} fullerene derivatives **64–67** (Figure 9) and C_{70} derivative **69** (Scheme 13) were also analyzed to further probe the mechanism of the retro-cyclopropanation reaction.⁵⁵ Approximately $3 e^-$ per molecule were required for cyclopropane ring removal and $2.3 e^-$ to generate a novel intermediate of derivatives **64–67** and **69**. This intermediate was stable and exhibits reversible electrochemical behavior (Circles, Figure 13a–c), which was assumed to be a singly bonded dimeric structure between the fullerene cores. The properties of the C_{70} derivative **69** (Scheme 13) intermediate

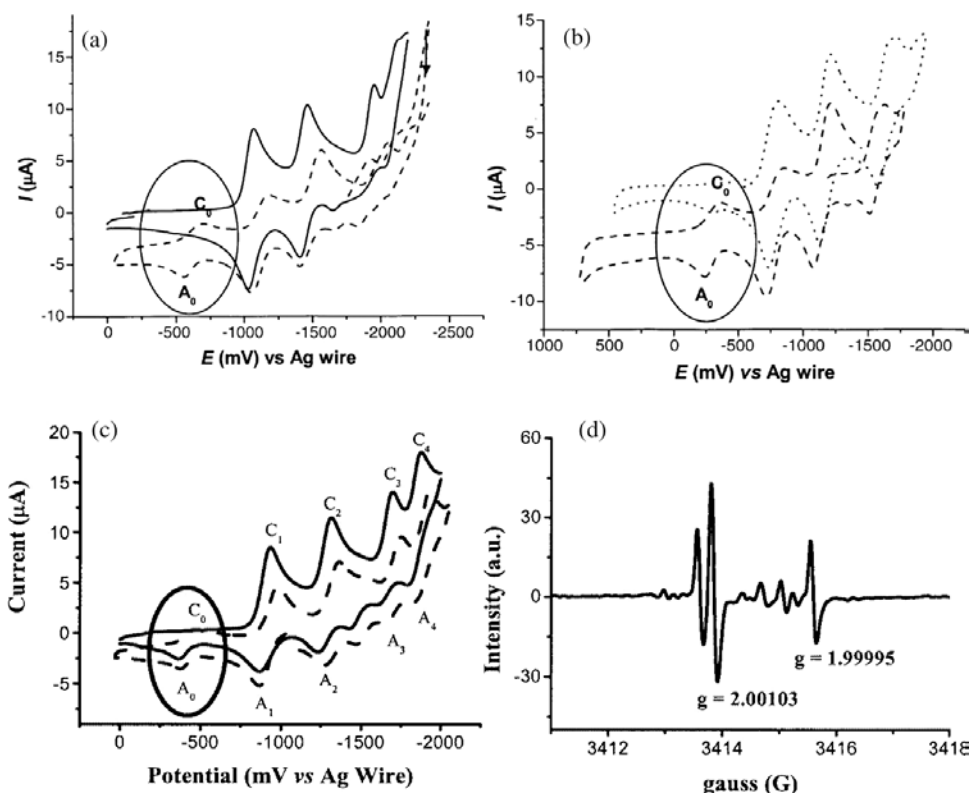
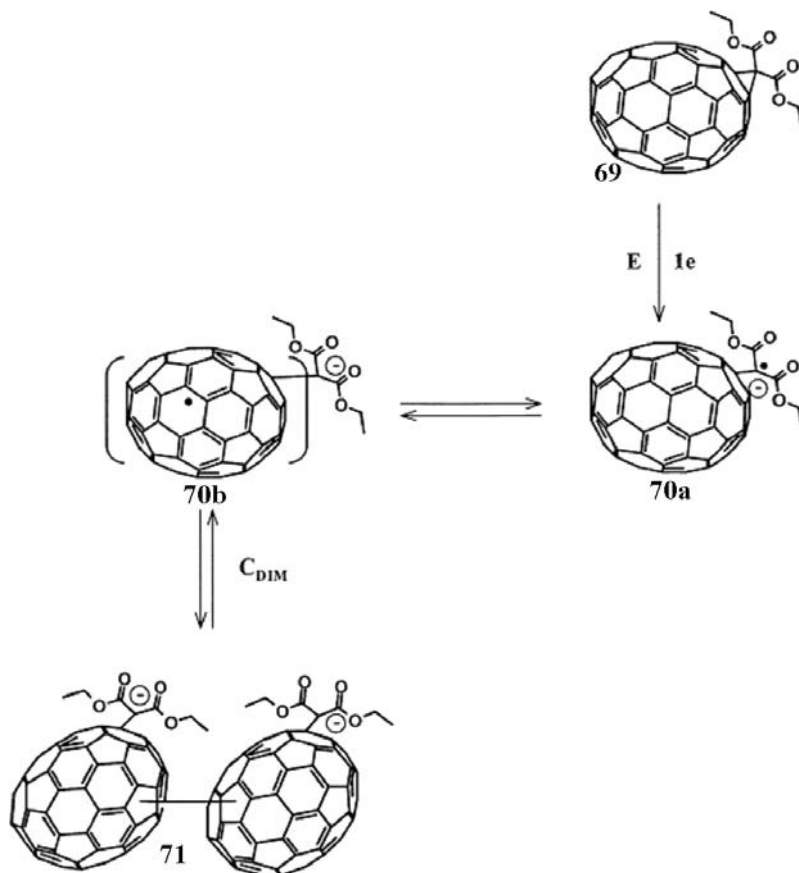


Figure 13. (a) CPE of **67**. Solid line: cyclic voltammogram (CV) before reduction; dashed line: CV after $2.3 e^-$ reduction. (b) CPE of **67**. Dashed line: CV after $2.75 e^-$ reduction; dotted line: CV after re-oxidation. (c) CPE of **69**. Solid line: CV before reduction; dashed line: CV after $1 e^-$ reduction. (d) ESR spectrum obtained after $1 e^-$ reduction of **69**. Reprinted from Reference 51 with permission. Copyright 2010 American Chemical Society. Reproduced from Reference 55 with permission. Copyright Wiley-VCH Verlag GmbH & Co. KGaA.



Scheme 13. Proposed mechanism for the formation of dimeric C₇₀ **71** fullerene derivatives from electrolysis of **69** (radical position and connecting bond between the C₇₀ units are chosen arbitrarily with respect to possible regioisomers). Reproduced from Reference 55 with permission. Copyright Wiley-VCH Verlag GmbH & Co. KGaA.

during CPE was studied by EPR spectroscopy (d, Figure 13) and MALDI mass spectrometry. The negative charge in the adduct was stabilized by the malonate group and by the possible formation of an intercage bond between two fullerene core radicals (Scheme 13).⁵⁵ This type of dimers had been reported previously by Konarev *et al.*⁵⁶ and Cheng *et al.*⁵⁷ Konarev and co-workers isolated a singly bonded (C₇₀⁻)₂ dimer from the complexation of hexamethoxycyclotrimeratrylene and C₇₀ fulleride.⁵⁶ Also, Komatsu and co-workers synthesized a singly bonded C₆₀ dimer by the reaction of C₆₀²⁻ with diethyl iodomethylphosphonate, and iodine.⁵⁷

3.1.1.1. Walk-on-the-sphere rearrangements

During the course of analyzing retro-cyclopropanation reaction mechanism an unexpected electrochemically induced isomerization of the addends by migration on the fullerene surface, known as “*walk on the sphere*” was discovered.⁵⁸ Kessinger *et al.* demonstrated that the *cis*-2-bis-adduct **72** was transformed to the *e* (57%), *trans*-3 (31%), *trans*-4 (8%) and *cis*-3 (4%) isomers after it was subjected to CPE with a charge transfer of one electron per molecule.⁵⁸ Other bis-adducts (**73**–**77**) were also isomerized upon CPE at the second reduction potential and monoadduct **38** and mixtures of isomeric bis-adducts were isolated after re-oxidation (Table 4). Interestingly, the bis-adducts *cis*-2 **72** and *cis*-3 were not formed.⁵⁸ These isomers had been calculated to be the most strained molecules because of the proximity of the two cyclopropane rings in one hemisphere.⁵⁹ The major isomers formed were always the *trans*-2–**77** derivative (40–50%), followed by *e*-**74** (25%) isomer (Table 4). Their predominance was explained in terms of their inherently higher stability.⁵⁸ Another surprising result was the formation of the *trans*-1-bis-adduct with 10% yield (Table 4),⁵⁸ which had been isolated only in 0.8–2% yield from the chemical reaction of **38** with 1 equiv of diethyl 2-bromomalonate.^{59b,60} The product distribution was fairly similar for all of the bis-adducts (Table 4), which suggests that the isomerization occurred under thermodynamic control. The fact that the isomerization takes place intra- and not intermolecularly was shown by the CPE of a 1:1 mixture of seven bis[(diethoxycarbonyl)methano] adducts {[*(EtOOC)*₂C]₂C₆₀} and the corresponding seven bis[(dipropoxycarbonyl)methano] adducts {[*(PrOOC)*₂C]₂C₆₀} and mixed adducts or tris-adducts were not detected.⁵⁸

Table 4. Relative distribution^a of C₆₀ bis-adducts after addition of two \bar{e} by CPE. Reprinted from Reference 58 with permission. Copyright 2010 American Chemical Society.

Starting material	<i>cis</i> -(1-3)	<i>e</i> (74)	<i>trans</i> -4 (75)	<i>trans</i> -3 (76)	<i>trans</i> -2 (77)	<i>trans</i> -1	mono ^b	Yield ^c
<i>cis</i> -2 (72)		23%	5%	8%	52%	12%	29%	49%
<i>cis</i> -3 (73)		22%	6%	10%	51%	11%	28%	53%
<i>e</i> (74)		26%	9%	12%	44%	9%	10%	44%
<i>trans</i> -4 (75)		23%	10%	12%	47%	8%	14%	61%
<i>trans</i> -3 (76)		23%	9%	12%	46%	10%	23%	43%
<i>trans</i> -2 (77)		22%	6%	9%	53%	10%	19%	39%
[<i>(PrOOC)</i> ₂ C] ₂ C ₆₀		25%	8%	12%	46%	9%	24%	55%

^aThe relative percentages of bis-adducts were determined from the integrated HPLC peak areas. ^bAbsolute isolated yield of **38**. ^cAbsolute recovered yield of bis-adducts.

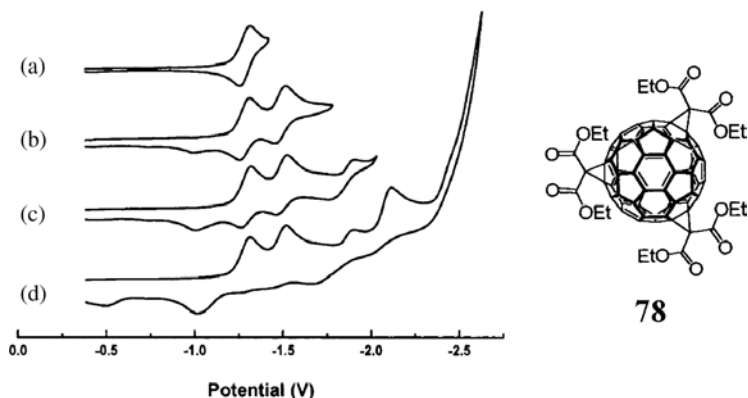


Figure 14. Cyclic voltammograms of trisadduct **78** in 0.1 M Bu₄NPF₆ in CH₂Cl₂, scan rate 200 mV.s⁻¹ reversing the scan after the (a) first, (b) second, (c) third, and (d) fourth reduction waves. Reprinted from Reference 61 with permission. Copyright 2010 American Chemical Society.

Seven out of the 46 possible tris-adducts (constitutional isomers) of $\{[(\text{EtOOC})_2\text{C}]_3\text{C}_{60}\}$ were isolated and their electrochemistry was studied.⁶¹ Different from the bis-adduct results mentioned earlier,⁵⁸ the addition of two electrons per molecule by CPE in CH₂Cl₂ generated the parent C₆₀ and exhibited loss of one or two addends. The retro-cyclopropanation reaction of the tris-adduct **78** was evident from the observation of (b, Figure 14) a small irreversible oxidation peak at -1.02 V on the reverse scan after the second reduction peak. The reversibility is enhanced as the temperature is decreased, and the degree of isomerization increases during electrolysis.⁶¹

The synthesis of regioselective tris-adducts by stepwise additions requires tedious separation and purification methods, hence retro-cyclopropanation reactions were performed in attempts to obtain these tris-adducts from tetrakis-, pentakis- and hexakis-malonate adducts of C₆₀, which are sometimes relatively easy to obtain.⁶² The removal of malonate addends by the electrolysis of the tetrakis- **79**, pentakis- **80** and hexakis-C₆₀ **81** adducts was effected by the addition of 1, 4, 5, 6, 8 or 11 e⁻ (Table 5). The best conditions to obtain tris-adducts (30%) from **79**, **80** and **81** was the addition of 4, 6 or 8 e⁻ by CPE, respectively.⁶² At least 8 peaks were observed in the HPLC spectrum out of the 46 possible tris-adducts, and 5 were identified (Table 7) based on their retention times, by co-elution with 7 known tris-adducts.⁶² The major isomers formed were the unsymmetrical (*trans*-4, *trans*-2, *e*) and (*trans*-3, *trans*-4, *e*) even though it was expected that the (*e*, *e*, *e*) isomer would be the main product since it is easily obtained by addend removal from the multiple adducts with octahedral symmetry without subsequent

Table 5. Distribution^a of products after CPE by HPLC analysis. Reproduced from Reference 62 by permission of The Royal Society of Chemistry.

Starting material + No electrons	C ₆₀	Mono	Bis	Tris (%)	Tetrakis (%)	Pentakis (%)	Hexakis	Other products (%)
79 + 4 e ⁻	0	0	5%	41	39	—	—	15
79 + 5 e ⁻	0	1%	15%	48	29	—	—	7
80 + 1 e ⁻	0	0	0	1	35	51	—	13
80 + 4 e ⁻	0	0	4%	25	49	21	—	1
80 + 6 e ⁻	1%	7%	12%	30	35	6	—	9
80 + 6 e ⁻ at 4 °C	0	0	7%	31	27	19	—	16
80 + 11.5 e ⁻	48%	5%	8%	11	7	6	—	15
81 + 8 e ⁻	0	0	6%	24	15	5	7%	43
81 + 11 e ⁻	0	4%	10%	29	21	1	0	35

^aThe relative percentages of bis-adducts were determined from the integrated HPLC peak areas.**Table 6.** Distribution of tris-adduct products after CPE by HPLC analysis. Reproduced from Reference 62 by permission of The Royal Society of Chemistry.

Starting material + No electrons	<i>t3t3t3</i>	<i>t2t3e/</i> <i>T4t4t2</i> ^a (%)	<i>t3t3t4</i> (%)	<i>t4t2e</i> (%)	<i>t3t4e</i> (%)	<i>eee</i> (%)	Other Isomers (%)
79 + 4 e ⁻	0 ^b	5	6	46	15%	6%	22
80 + 6 e ⁻	5%	5	4	36	31%	1% ^b	18
81 + 8 e ⁻	18% ^c	5	1	31	3%	16%	26

^aIsomers indistinguishable by co-injection. ^bLow quantity possibly due to initiating collection late or ending collection too early. ^cPossible mixture of 2 isomers.

rearrangement.⁶² This preference was supported by PM3 and AM1 calculations of the heats of formation of the tris-adduct dianions of C₆₀.⁶¹

3.1.2. C₇₀ Fullerene derivatives and higher fullerenes

The retro-cyclopropanation reaction of a series of methano derivatives of C₇₀ were studied (Scheme 13 and Figure 15)^{41–42} and the bis{[(ethoxy)carbonyl]methyl}- 1,2-methano[70]fullerene-71,71-dicarboxylate derivative **82** underwent retro-cyclopropanation reaction by CPE at the second reduction potential and resulted in 100% conversion to C₇₀ after a net charge of 4 e⁻ per molecule were discharged (Figure 16).⁴¹ On the contrary, the retro-cyclopropanation reaction of the derivative **69** (Scheme 13) goes only partially (C₇₀, 64% and **69**, 21%) at the reversible second reduction potential and after

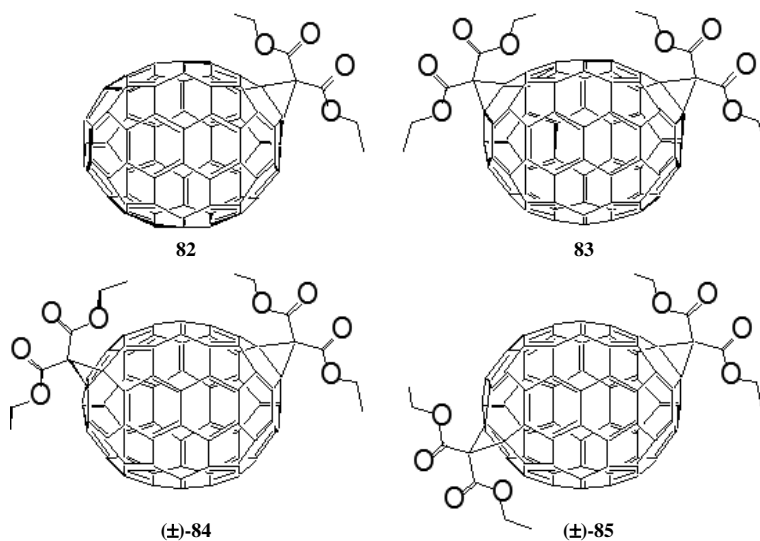


Figure 15. Methano C_{70} fullerene derivatives. Reproduced from Reference 42 with permission. Copyright Wiley-VCH Verlag GmbH & Co. KGaA.

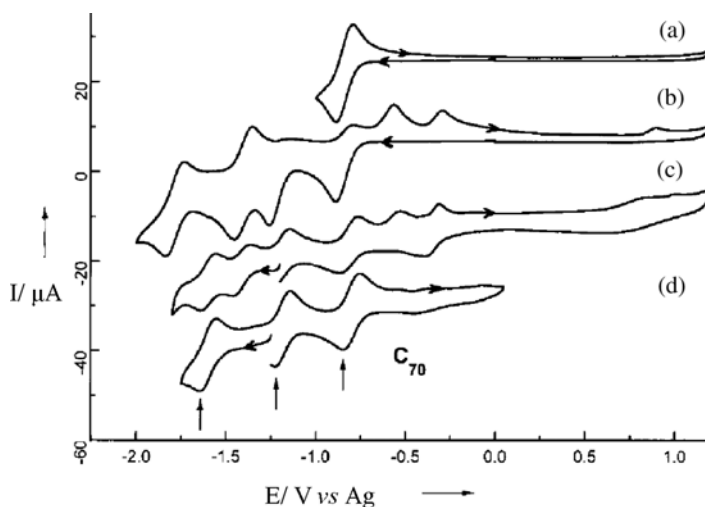


Figure 16. CV data for **82** in CH_2Cl_2 containing 0.1 M Bu_4NPF_6 , scan rate of $100\text{ mV}\cdot\text{s}^{-1}$ (a) first reduction; (b) Scan with a switching potential of -2 V (versus Ag), clearly showing the irreversibility of subsequent reductions, even the second one; (c) CV after CPE with a net charge corresponding to a four electron transfer per molecule; and (d) CV after 30 min of the CPE. Reproduced from Reference 41 with permission. Copyright Wiley-VCH Verlag GmbH & Co. KGaA.

a total charge of $2 e^-$ per molecule were transferred. This was expected based on the higher electron-withdrawing character of the addend in **82** compared to that in **69**.⁴² The bis-adducts **83**, (\pm)-**84**, (\pm)-**85** were subjected to CPE as well at the second reduction potential in two different experiments, with a total charge transfer of $2 e^-$ and $1.5 e^-$ per molecule. From the $2 e^-$ addition: bis-adduct **83** (93% recovered) underwent a minimal conversion (3% of **69**) and less than 1% of isomerization; the bis-adduct (\pm)-**84** (31% recovered) underwent partial conversion (27% of **69**) and a 10 % degree of isomerization (4% of **83** and 6% of (\pm)-**85**). The bis-adduct (\pm)-**85** (28% recovered) underwent partial conversion (27% of **69**) and 1% isomerization to (\pm)-**84**.⁴² From the $1.5 e^-$ addition: the bis-adduct **83** was not affected (94% recovered), the bis-adduct (\pm)-**84** (71% recovered) showed minimal changes and the bis-adduct (\pm)-**85** (32% recovered) underwent minimal conversion (5% of **69**), but a much higher degree of isomerization (4% of **83** and 20 % of (\pm)-**84**).⁴² It was concluded that isomerization plays only minor role in the electrochemically induced reactions of the dianions of C_{70} bis-adducts.⁴²

The retro-cyclopropanation reaction has also been applied successfully to higher fullerenes. The first example was the isolation of enantiomerically pure chiral C_{76} and *ent*- C_{76} using an optically active malonate as a chiral auxiliary to allow the chromatographic separation of the diastereoisomers **86** and **87**. This separation was followed by the removal of the addend *via* CPE to yield the pure enantiomers of C_{76} (a, Figure 17).⁴¹ The two isomers were purified

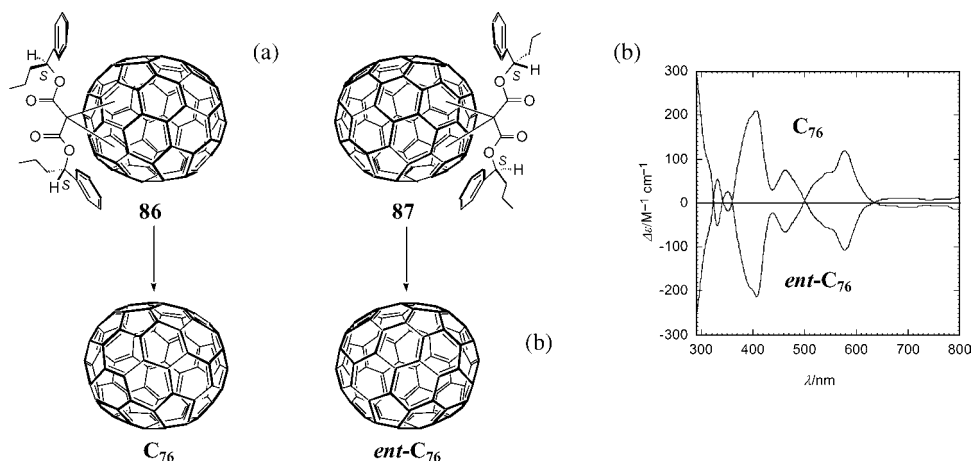


Figure 17. (a) Retro-Bingel reaction of the diastereoisomerically pure, optically active C_{76} monoadducts **86** and **87**. The location of the malonate addend is not exactly known; and (b) CD Spectra of C_{76} and *ent*- C_{76} in toluene. Reproduced from Reference 41 with permission. Copyright Wiley-VCH Verlag GmbH & Co. KGaA.

by HPLC in low yields (between 5–10%) and the CD spectra (b, Figure 17) exhibited the expected mirror-image relationship with band positions which are consistent with data reported⁶³ by Hawkins and Meyer. Nevertheless, the Cotton effect observed was almost a full order of magnitude larger than those previously reported, indicating the higher purity of the isolated C_{76} enantiomers.

Another example of the isolation of new fullerene derivatives using retro-cyclopropanation processes was a C_{2v} - C_{78} bisadduct that was not present after the regular Bingel reaction.⁶⁴ This bis-adduct was obtained after CPE was applied to a C_{2v} - C_{78} trisadduct with a yield of 55%. Moreover, this bisadduct seems to be the same intermediate that was formed during retro-Bingel reactions of other tris- and bis-adducts such as D_3 - C_{78} and C_{78} as a result of the “walk-on-the-sphere”⁵⁸ isomerization process.

A final example of the use of the retro-cyclopropanation reaction with higher fullerenes was the isolation of three constitutional isomers of D_2 - C_{84} .⁶⁵ Although C_{84} is the third most abundant fullerene obtained in a reactor, the chromatographic separation of the multiple isomers is extremely difficult. In the retro-cyclopropanation approach to isomer purification,⁶⁵ a C_{84} enriched fraction was treated in *o*-dichlorobenzene at 20 °C with bis[(*S*)-1-phenylbutyl]-2-bromomalonate in the presence of DBU. After purification by column chromatography and HPLC, two mono-adducts and four bis-adducts were isolated. One mono-adduct and one bis-adduct with symmetry C_1 and D_2 , respectively, displayed a weak Cotton effect in the CD spectra, thus they were assigned to the parent D_{2d} - C_{84} , which was isolated and characterized from these two derivatives after CPE.⁶⁵ The other two bis-adducts **88** and **89** (a, Figure 18) had C_2 symmetry, large Cotton effects and UV-vis spectra different from those of the isolated achiral D_{2d} - C_{84} bis-adduct, which suggested they were the parent chiral D_2 - C_{84} fullerene (a, Figure 18). The CPE of these two diastereoisomers afforded the pure enantiomers of D_2 - C_{84} as reflected by the mirror image CD spectra (c, Figure 18) in agreement with the spectra reported by Hawkins and Meyer.⁶³

It can thus be concluded that the retro-cyclopropanation reaction is able to afford methanofullerene derivatives that are otherwise not accessible, as well as enantiomerically pure higher fullerenes with intrinsic chiralities.

3.2. Chemical retro-cyclopropanation reaction

After the success of the retro-cyclopropanation reaction by CPE (electrochemical conditions) and its multiple applications, the retro-cyclopropanation reaction using chemical reducing conditions was reported.⁶⁶ The advantage of

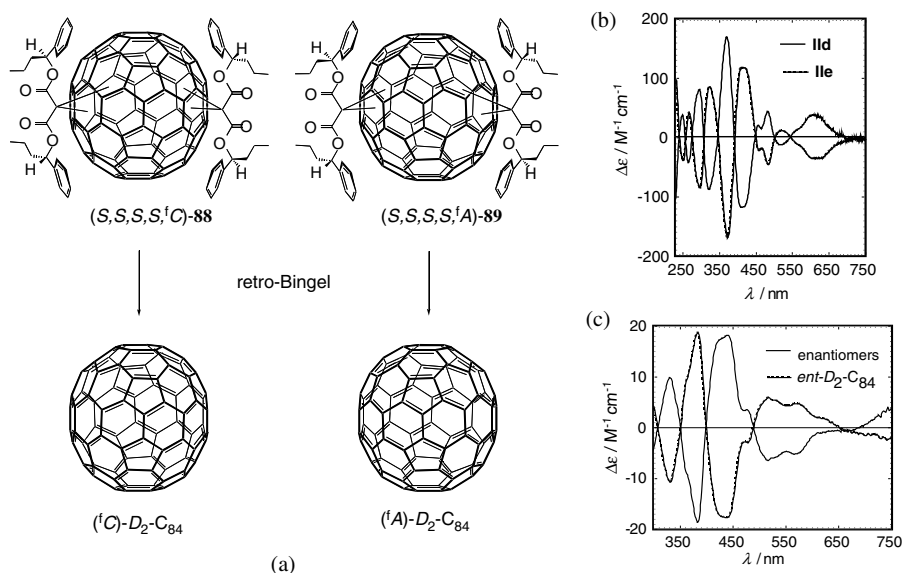
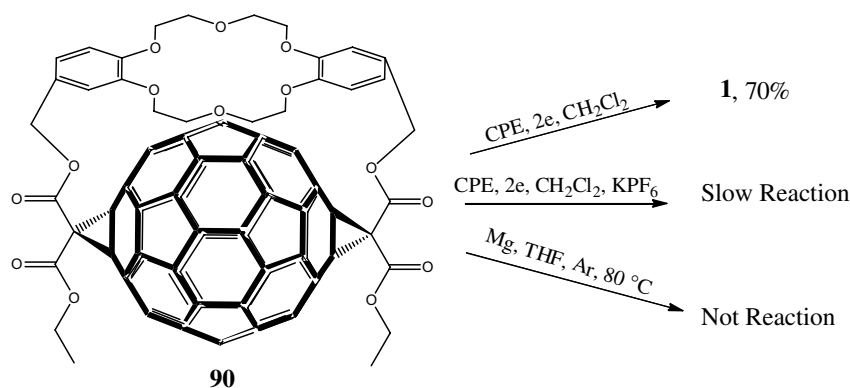


Figure 18. (a) Retro-Bingel reaction of the diastereoisomerically pure, optically active C_{84} bis-adducts **88** and **89**. The absolute configurations of the fullerene spheroids ($1C$ and $1A$; f: fullerene, C: clockwise, A: anticlockwise) reflect the structural drawings, but have not been assigned experimentally. (b) CD spectra of the diastereoisomeric bis-adducts **88** and **89**; and (c) CD spectra of the fullerene enantiomers in CH_2Cl_2 . Reproduced from Reference 65 with permission. Copyright Wiley-VCH Verlag GmbH & Co. KGaA.

this method is the accessibility of larger scale conversion without the use of supporting electrolyte or specialized electrochemical equipment. The methano-addend was removed from C_{60} and C_{70} mono-adducts after solutions of each were heated to reflux with amalgamated magnesium powder (10% $HgBr_2$) for 3 days, yielding 73% of C_{60} and 63% of C_{70} , respectively.⁶⁶ In the case of bis-adducts of C_{60} , the yield of recovered C_{60} varied between 13% and 48% and no isomerization reactions were detected. These chemical conditions can selectively remove only the methano addends in the presence of other functional groups such as pyrrolidines, see for example the chemical reduction of **47** to **52** in Table 3.⁶⁶

Another approach to effect the chemical retro-cyclopropanation reaction was to use crown ethers (18-crown-6) as Mg^{2+} binders to improve the efficiency and avoid the use of the highly toxic $HgBr_2$.⁶⁷ Using a mixture of $Mg/HgBr_2/18\text{-crown-6}$ as the reducing agent with derivatives **38**, **58** and **59** yielded between 86–89% of C_{60} with high reproducibility. In the absence of $HgBr_2$, the recovery of C_{60} was between 27–52% for derivative **38**, **58** and **59**.⁶⁷ Interestingly, the chemical reduction procedure completely failed with



Scheme 14. Retro-cyclopropanation reaction of *trans*-1 dianion **90** derivative. Reprinted from Reference 67 with permission. Copyright 2010 Elsevier.

compound **90** (Scheme 14). This probably resulted from the complexation of the 18-crown-6 moiety in **90** with a metal ion, which likely stabilizes the reduced compound and inhibits the retro-cyclopropanation reaction.⁶⁷

3.2.1. Tandem reductive ring opening-retro-Bingel reaction

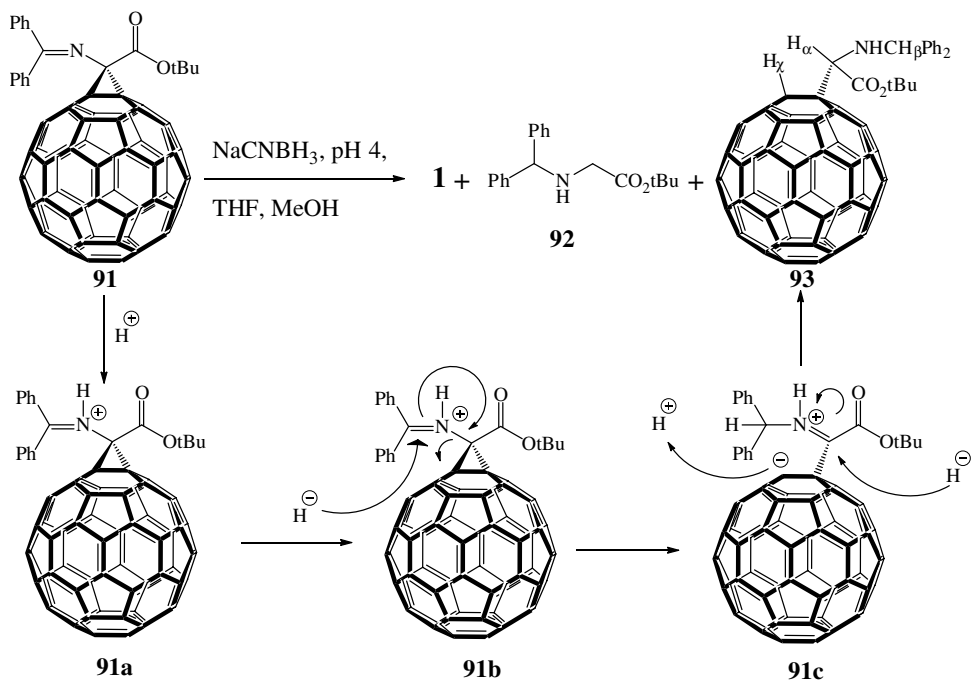
Another reductive chemical retro-cyclopropanation process was reported by Burley *et al.*⁶⁸ A new class of 1,2-dihydro[60]fullerenylglycine derivative was synthesized by the reductive ring-opening of a tethered bis-imino ester of C_{60} upon treatment with sodium cyanoborohydride, in the presence of protic or Lewis acid.

The proposed mechanism of this novel ring opening reaction under protic acidic conditions is shown in Scheme 15. The diphenyl imine can be activated by the formation of an iminium cation **91a**, followed by the attack by a hydride on the iminium carbon with subsequent cyclopropyl ring opening (Scheme 15), giving rise to the fullerenyl anion intermediate **17** and finally to the product **93**.^{68d}

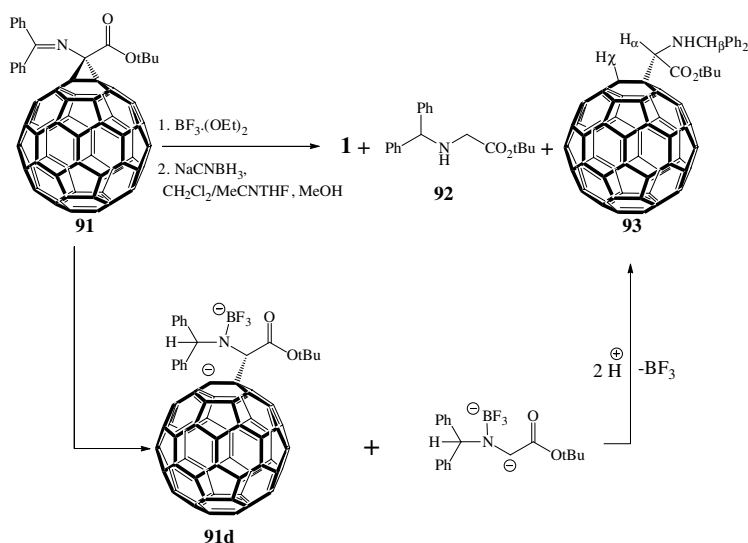
A fullerenyl carbanion intermediate was expected in the proposed mechanism for the corresponding Lewis acid which could be protonated to give **11–13** or undergo elimination of the addend to form C_{60} and eventually **14**.^{68c-d}

4. Retro-1,3-dipolar Cycloaddition Reactions

Among the many well-known exohedral reactions that occur on fullerene surfaces such as the addition-elimination described in detail earlier, 1,3-dipolar



Scheme 15. Proposed mechanism of reductive ring opening under protic acid conditions. Reprinted from Reference 68d with permission. Copyright 2010 American Chemical Society.



Scheme 16. Proposed mechanism of reductive ring opening under Lewis acid conditions. Reprinted from Reference 68d with permission. Copyright 2010 American Chemical Society.

cycloaddition reactions have played a prominent role as well, with applications in various fields such as medicinal chemistry⁶⁹ and materials science.⁷⁰ The 1,3 dipolar cycloaddition of azomethine ylides is considered as one of the simplest and most efficient procedures for the functionalization of fullerenes.⁷¹ Azomethine ylides are reactive intermediates that can be generated in several ways, although the decarboxylation of imminium salts, derived from condensation of α -amino acids with aldehydes or ketones, is the easiest and most general procedure commonly followed. The use of this methodology to obtain monoadducts of [60]fullerene, allows the concomitant introduction of two functional groups in one step, affording a single regioisomer usually in good yields. Among the many fullerene-based compounds described in the literature, pyrrolidino fullerenes are stable compounds, although in the last couple of years a number of methodologies have been described to promote the retro-cycloaddition reaction of these derivatives to afford pristine C₆₀ fullerene efficiently. Other fullerene-based derivatives like isoxazolinofullerenes or 2-pyrazolinofullerenes also undergo efficient retro-cycloaddition reactions. The conditions, mechanism and results of these retro-cycloaddition experiments will be discussed in this section.

4.1. Chemical retro-cycloaddition of pyrrolo[3,4:1,2] [60]fullerenes

Martín *et al.*,⁷² described recently the thermally induced retro-cycloaddition of pyrrolidino[3,4:1,2]fullerenes. The authors studied the retro-cycloaddition process on a series of pyrrolidinofullerenes under a variety of experimental conditions. Compounds **94a–c** were heated to reflux in *o*-dichlorobenzene (*o*-DCB) in the presence of a strong dipolarophile, maleic anhydride, in order to capture the thermally generated ylide. Under these conditions retro-cycloaddition was detected in low to moderate yields, but for compound **94e**, C₆₀ was recovered quantitatively. The authors also performed the reaction under the same conditions, in the presence of a metal Lewis acid (copper triflate), in order to see if coordination with the nitrogen atom could activate the retro-cycloaddition process (Figure 19).⁷²

Under these conditions, the reaction led to the quantitative formation of the parent unsubstituted C₆₀ in all cases. This methodology was also effective to induce the retrocycloaddition for the mono-adduct mixture of three isomers of [70]fulleropyrrolidine **95** which afforded pristine C₇₀ in 95% yield. Another important finding reported in this communication was the use of C₆₀ as a dipolarophile. A mixture of bis-adducts **96** was heated

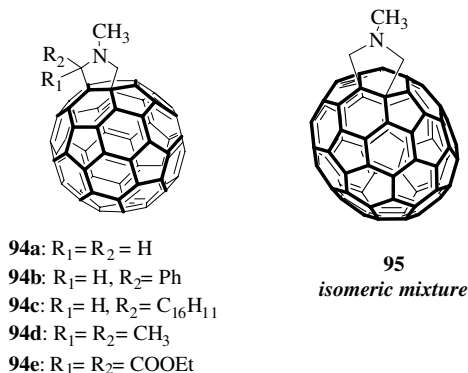
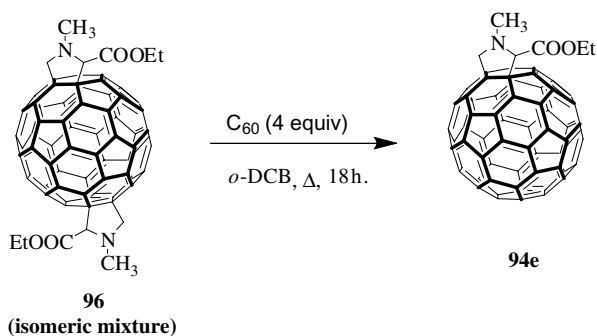
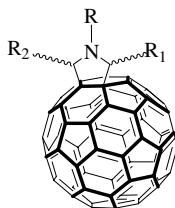


Figure 19. Retro-cycloaddition reaction of pyrrolidinofullerenes **94a–c** and isomeric mixture of C_{70} derivative **95**.



Scheme 17. Reaction of a mixture of bis-adducts **96** in the presence of C_{60} as dipolarophile.

to reflux in *o*-DCB in the presence of C_{60} and HPLC analysis of the reaction confirmed the quantitative formation of monoadduct **94e** (Scheme 17).⁷² This interesting result opened new avenues for improving the yields of mono-adduct formation from the usually undesired bis-cycloadducts obtained as byproducts in 1,3 dipolar cycloaddition reactions of azomethine ylides to C_{60} . This interesting observation was recently applied in order to obtain an indirect proof of the covalent attachment of pyrrolidine fragments to single-walled carbon nanotubes (SWCNT). The authors applied the same conditions described by Martín *et al.*,⁷² by heating a sample of pyrrolidino-SWCNT in the presence of C_{60} to act as dipolarophile and the corresponding pyrrolidinofullerene compound was detected, thus confirming the efficient trapping of the thermally generated azomethine ylide.⁷³



97a: R = R₂ = H, R₁ = COOEt

97b: R = C(=O)Ph, R₁ = COOEt, R₂ = H

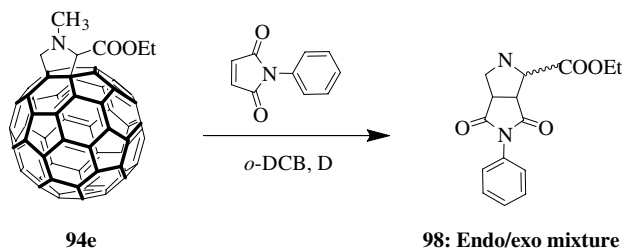
97c: R = H, R₁ = COOMe, R₂ = *p*-MeOPh (*Cis*)

97d: R = H, R₁ = COOMe, R₂ = *p*-MeOPh (*Trans*)

Figure 20. N-unsubstituted or N-benzoyl C₆₀ derivatives.

In order to unravel the mechanism of the retro-cycloaddition process, Filippone *et al.*,⁷⁴ recently reported a detailed study with new pyrrolidino-fullerene compounds, namely *N*-unsubstituted or *N*-benzoyl containing derivatives (Figure 20). Interestingly, the nature of the substituent on the pyrrolidine nitrogen atom played an important role in the retro-cyclization process. Thus, whereas *N*-methyl or *N*-H groups underwent the retro-cycloaddition reaction quantitatively, the presence of a benzoyl group prevented or complicated this process.⁷⁴

In order to prove the formation of the azomethine ylide as an intermediate resulting from the retro-cycloaddition process, the authors carried out trapping experiments using *N*-phenylmaleimide as the dipolarophile. Compound **94e** was refluxed in *o*-DCB in the presence of *N*-phenylmaleimide, and the reaction afforded cycloadduct **98**, resulting from the cycloaddition of the *in situ* generated azomethine ylide the *N*-phenylmaleimide, in 19% yield as an endo:exo mixture 66:33 (Scheme 18). This interesting finding clearly confirmed that the reaction mechanism of the retro-cycloaddition process occurred by thermal removal of the azomethine ylide as a 1,3-dipole, which was generated *in situ* under the experimental conditions.⁷⁴



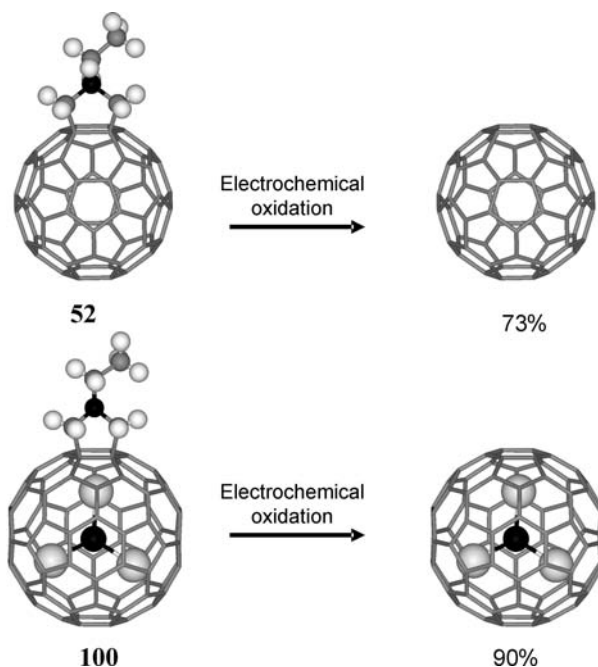
Scheme 18. Trapping experiments using *N*-phenylmaleimide as dipolarophile.

In agreement with the experimental findings, theoretical calculations carried out at the DFT level and using the two-layered ONIOM approach, predicted that the presence of the dienophile was not required for the cleavage of the azomethine ylide from the fullerene surface which, after *in situ* generation under thermal conditions, was trapped by the dipolarophile. However, for the *N*-unsubstituted fulleropyrrolidine, the participation of the dipolarophile in assisting the cleavage of the 1,3 dipole was also possible and, therefore, this alternative mechanism cannot be totally ruled out.⁷⁴

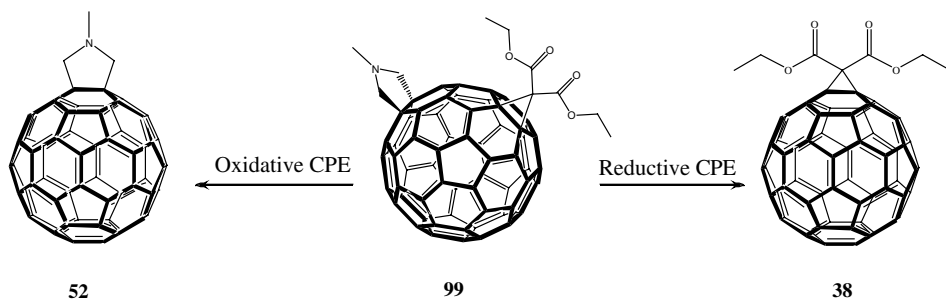
Guryanov *et al.*,⁷⁵ described an alternative protocol to achieve the retro-cycloaddition of pyrrolidinofullerenes. The authors reported that the quantitative retro-cycloaddition of pyrrolidinofullerenes under microwave irradiation and in an ionic liquid (1-methyl-3-*n*-octyl-imidazolium tetrafluoroborate) does not require any other additives. The combination of microwave irradiation in an ionic liquid offers the unique opportunity for very efficient flash-thermal activation in conjunction with a strong stabilization of ionic intermediates or reactants. In this case, the ionic liquid served as an ideal medium to solvate the incipient 1,3-dipole whose release in solution was likely assisted by electrostatic interactions with the complementary ions of the solvent.⁷⁵ In agreement with the mechanism proposed by Filippone *et al.*,⁷⁴ cycloreversion occurred through the formation of a reactive 1,3-dipolar intermediate which was expected to be stabilized by the ionic liquid environment.

4.1.1. Electrochemical retro-cycloaddition of pyrrolo [3,4:1,2] [60]fullerenes

Lukoyanova *et al.*,⁷⁶ had reported an alternative way to induce the retro-cycloaddition of pyrrolidinofullerenes using electrochemical techniques. The authors induce the retro-process by CPE at an applied potential determined from CV experiments. Compound **99** displays an irreversible oxidation process which was assigned to a pyrrolidine-based oxidation and therefore, CPE was conducted at a potential 100 mV more positive than this oxidation wave. After CPE, the reaction mixture was purified to yield the parent C₆₀ (73%) for compound **52** and Sc₃N@C₈₀ (90%) for compound **100** (Scheme 19). Another important contribution from this work was the selective removal by electrochemical methods of targeted addends (pyrrolidine or cyclopropane rings) from the fullerene derivative **99** (Scheme 20). The pyrrolidine group is easily and selectively removed by electrochemical oxidative electrolysis to obtain **38** and the cyclopropane ring is selective removed by electrochemical reductive electrolysis to obtain **52**, both processes in reasonable yields.⁷⁶



Scheme 19. Electrochemical retro-cycloaddition of N-Ethyl pyrrolidino[3,4:1,2][60] fullerene (99) and N-ethyl pyrrolidinofullerene $\text{Sc}_3\text{N}@\text{C}_{80}$ (100). Reproduced from Reference 76 with permission. Copyright Wiley-VCH Verlag GmbH & Co. KGaA.



Scheme 20. Electrochemical retro-cycloaddition and retro-cyclopropanation of the *e*-bis-adduct 99.

4.1.2. Endohedral derivatives and their stability

Pinzón *et al.*,⁷⁷ recently described the synthesis, electrochemistry and photo-physical studies of two novel [5,6]pyrrolidine- I_h - $\text{Sc}_3\text{N}@\text{C}_{80}$ (101 and 102) (Figure 21). Thermal stability studies of mixture of the two compounds were carried out in open air, following the retro-cycloaddition process by HPLC.

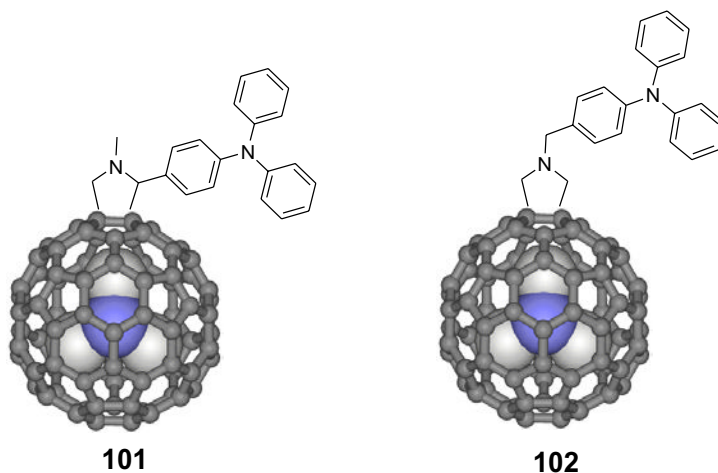


Figure 21. Triphenylaminofulleropyrrolidine Electron Donor-Acceptor Conjugates (**101** and **102**). Reprinted from Reference 77 with permission. Copyright 2010 American Chemical Society.

It was observed that the intensity of the peak corresponding to compound **101** decreased faster than for **102**. These observations could be explained by the relative thermodynamic stability of the corresponding azomethyne ylides, which were intermediates during the decomposition process. This is probably due to the triphenylamine substituent in the C-2 position which stabilizes the corresponding azomethine ylide, therefore favoring its removal from the fullerene.⁷⁷ This trend had also been observed in other pyrrolidine functionalized endohedral fullerenes. Pinzón *et al.*,⁷⁸ reported the retro-cycloaddition observed at room temperature for a phthalocyanine-substituted pyrrolidine containing $Y_3N@C_{80}$. As already discussed in this chapter, fulleropyrrolidine adducts undergo retro-1,3-dipolar cycloadditions under thermal⁷³ or electrochemically oxidative conditions.⁷⁶ This process seems to happen even faster in the case of $Y_3N@C_{80}$ derivatives containing electron donor units, probably due to their marked difference in electronic properties.

4.2. Retro-cycloaddition reaction of isoxazolo[3,4:1,2][60]fullerenes

The most studied and versatile derivatives obtained by 1,3-dipolar cycloaddition have been, so far, pyrrolidino[3,4:1,2][60]fullerenes. However other fullerene-fused with pentagonal heterocyclic rings, such as isoxazolino[4,5:1,2][60]fullerenes, are also known to show appealing chemical, electrochemical and

photophysical properties.⁷⁹ Isoxazolinofullerenes have been obtained by addition of nitrile oxides to [60]fullerene in moderate yields. In contrast to other pentagonal heterocycles, isoxazolines undergo a number of reactions that result in ring cleavage. Opening isoxazolines involves N-O and C=N bond reduction, and different reagents, such as TiCl_3 , LiNaH_4 or H_2 and Raney Nickel, have been used to reduce aliphatic and aromatic isoxazolines.⁸⁰

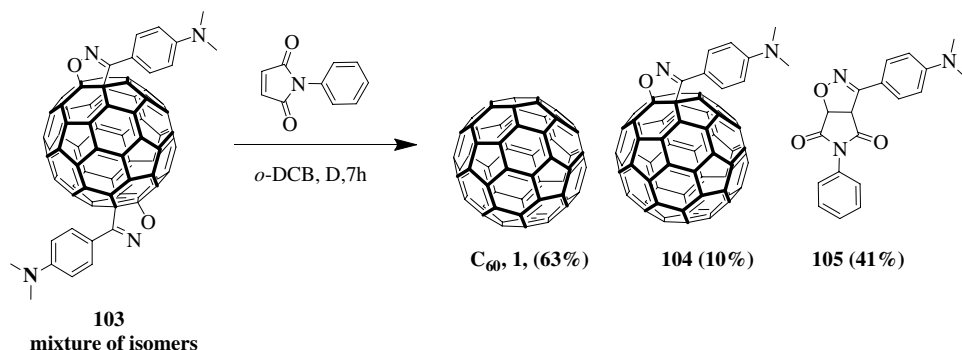
4.2.1. Chemical retro-cycloaddition

Da Ros *et al.*,⁸¹ described the first efficient method for the quantitative retro-cycloaddition of isoxazolinofullerenes. The authors reported that the treatment of isoxazolinofullerenes with Mo(CO)_6 in refluxing chlorobenzene leads quantitatively to pristine fullerene and the respective nitrile, resulting from the further reduction of the nitrile oxide formed in the retro-cycloaddition process. Similar results were obtained with excess of DIBAL-H in toluene at room temperature.⁸¹

Martín *et al.*,⁸² applied the same conditions reported for the retro-cycloaddition of fulleropyrrolidines in order to investigate the scope of this methodology for the case of isoxazolinofullerenes. In this case the highest efficiency for the retro-cycloaddition was observed by refluxing the isoxazolinofullerene derivative in *o*-DCB using an excess of maleic anhydride and copper triflate as a catalyst. The authors confirmed the loss of the nitrile oxide by carrying out a trapping experiment in the presence of *N*-phenylmaleidimide. Thus, reaction of a regioisomeric mixture of bis-adducts of **103** with *N*-phenylmaleidimide in refluxing anhydrous chlorobenzene afforded a mixture of C_{60} monoadduct **104** and cycloadduct **105** resulting from the 1,3-dipolar cycloaddition of nitrile oxide to *N*-phenylmaleidimide (Scheme 21).⁸²

4.2.2. Electrochemical retro-cycloaddition

Since pyrrolidine adducts can be easily removed from fullerenes by CPE, similar attempts to induce the retro-cycloaddition of isoxazolinofullerenes were performed.⁸² Isoxazolinofullerenes display very positive oxidation potentials, near the oxidative potential of C_{60} , and close to the limit of the solvent potential window, suggesting that oxidative removal of the isoxazoline rings would be more difficult than for the corresponding pyrrolidines. Indeed, after performing CPE of isoxazolinefullerene, only the presence of the starting isoxazolinofullerene was detected by different techniques. Therefore, and contrary to that observed for pyrrolidinofullerenes, isoxazolinofullerenes exhibit remarkable stability under oxidative conditions.⁸²



Scheme 21. Trapping experiments using N-phenylmaleidimide as dipolarophile, in order to capture the nitrile oxide resulting from the thermally induced retrocycloaddition of isoxazolinofullerene **103**.

4.3. Retro-cycloaddition reaction of pyrazolino[3,4:1,2][60]fullerenes

Although pyrrolidino[3,4:1,2][60]fullerenes have been the most studied fullerene derivatives; other fullerene-based compounds like pyrazolino-fullerenes display interesting properties.⁸³ Pyrazolino[60]fullerenes have been obtained by addition of nitrile imines to [60]fullerene in good yields. Nitrile imines are efficiently prepared by dehydrohalogenation of halohydrazones, obtained in turn by chlorination or bromination of the corresponding hydrazone.

4.3.1. Chemical retro-cycloaddition

In order to determine if the experimental conditions previously used for the retro-cycloaddition of fulleropyrrolidines and fulleroisoxazolines are suitable for 2-pyrazolinofullerenes, Delgado *et al*,⁸⁴ followed the same general protocol: excess of dipolarophile, as well as copper triflate to facilitate the retro-cycloaddition process. According to the experimental findings, C-aryl-N-aryl-2-pyrazolino[60]fullerenes **106a–d** do not undergo an efficient retro-cycloaddition process under a variety of experimental conditions, which reveals that these compounds are thermally stable fullerene derivatives (Figure 22). In contrast, the presence of an alkyl chain in the carbon atom of the pyrazole ring results in an easier cleavage of the 1,3 dipole, leading to pristine C₆₀ in good yields (72%). These results show the importance of the thermal stability in order to

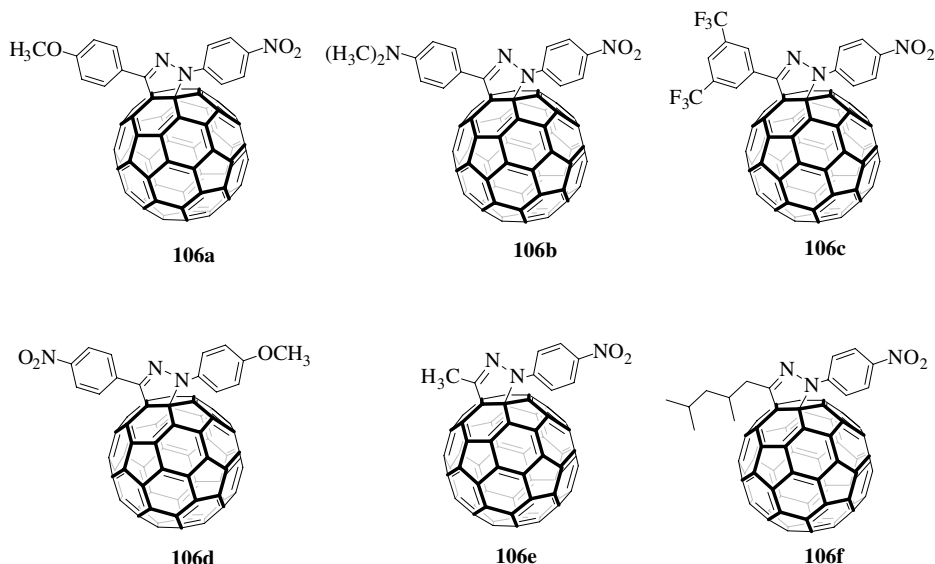


Figure 22. 2-pyrazolinofullerenes investigated for the thermal retrocycloaddition.

prepare new C_{60} -based materials, as well as the nature of the substituents (alkyl or aryl) which has a strong influence on the thermal stability of the cycloadducts. In particular, this is a key issue in photovoltaic cells, where long exposures to sunlight results in drastic temperature increases of the photo- and electro-active materials.⁸⁴

4.3.2. Competitive retro-cycloaddition of fullerene dimers

Delgado *et al.*,⁸⁵ have recently reported the preparation and photovoltaic applications of a new family of fullerene based compounds, namely, soluble [60] and [70]fullerene homodimers **107a** and **107c** and the [60]/[70] heterodimer **107b**, linked through 2-pyrazolino-pyrrolidino bridges (Figure 23). These dimers represent the first example of covalently bonded pyrrolidino-pyrazolino-fullerenes and offer a unique opportunity to study the competitive retro-cycloaddition of both pyrrolidine and pyrazoline fragments fused on the fullerene cage. Delgado *et al.*,⁸⁶ have also studied the competitive retro-cycloaddition reaction that takes place in these dimers (**107a–c**) by means of thermally induced treatment in the presence of an excess of dipolarophile (maleic anhydride) as well as copper triflate ($CuOTf_2$). The competitive retrocycloaddition process that takes place on these dimers was also studied by mass spectrometry and theoretical calculations at the density

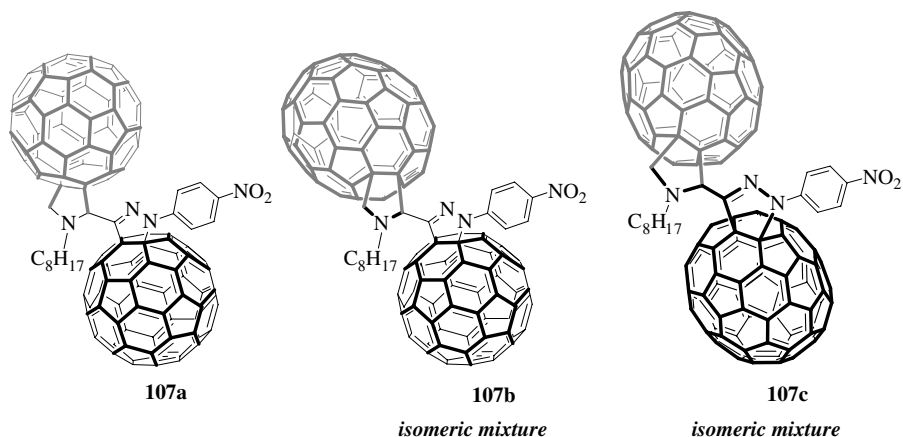


Figure 23. [60] and [70]fullerene homodimers (**107a** and **107c**) and the [60]/[70]heterodimer (**107b**), linked through 2-pyrazolino-pyrrolidino bridges.

functional theory (DFT) level, using the two-layered ONIOM approach. According to the experimental findings, dimers **107a–c** undergo an efficient retro-cycloaddition of the pyrrolidine ring in this study. In contrast, the retro-cycloaddition reaction of 2-pyrazolinofullerenes is less favored. Evidence of the occurrence of this process was obtained both by HPLC and MS-MALDI, to support these, in good agreement with that predicted by theoretical calculations.⁸⁶

5. Conclusions and Outlook

Retro-cycloaddition reactions of fullerenes offer a wide array of possibilities to prepare derivatives with a wide range of potential applications. Diels–Alder and retro-Diels–Alder reactions have been applied as a fullerene separation method (*i.e.* separation of endohedral metallofullerenes from classical fullerenes and empty cages), and also as a methodology to protect-deprotect fullerenes to obtain highly symmetrical multi-adducts that otherwise are difficult to prepare. These reactions have also been used to open fullerene cages in order to encapsulate atoms and molecules and then close them to produce endohedral fullerenes, a procedure known as “molecular surgery”. The cyclopropanation and retro-cyclopropanation reactions have been used for the preparation of pure constitutional isomers of higher fullerenes (C_{2v} - C_{78} and C_{84}) as well as enantiomerically pure intrinsically chiral higher fullerenes (fC - C_{76} , fA - C_{76} , fC - C_{84} and fA - C_{84}). These reactions have also been used to

synthesize fulleropyrrolidine derivatives in higher yields than their direct synthesis provides and multiple cyclo-propane-adducts from higher adducts by “walk-on-the-sphere” phenomenon.

Acknowledgments

Financial support from the National Science Foundation (Grant DMR-0809129 to S.C. and LE) is greatly appreciated. This material is based on work supported by the National Science Foundation while LE was working there. Any opinion, findings and conclusions or recommendations expressed in this material are those of the authors and do not necessarily reflect the views of the NSF.

This work was supported by the MEC of Spain (projects CTQ2008–00795 and CTQ2008–03077 and Consolider-Ingenio 201°C-07–25200), the CAM (project P-PPQ-000225–0505), the DIUE of the Generalitat de Catalunya (project 2009SGR637), and the ESF (project 05-SONS-FP-021). J.L.D. thanks the MICINN for a Ramón y Cajal Fellowship, cofinanced by the EUSocial Funds.

References

1. Chaur, M. N.; Melin, F.; Ortiz, A. L.; Echegoyen, L. *Angew. Chem.* **2009**, *121*, 7650–7675. *Angew. Chem. Int. Ed.* **2009**, *48*, 7514–7538.
2. Manolopoulos, D. E.; May J. C.; Down, S. E. *Chem. Phys. Lett.* **1991**, *181*, 105–111.
3. Fowler, P. W.; Batten, R. C.; Manolopoulos, D. E. *J. Chem. Soc. Faraday Trans.* **1991**, *87*, 3103–3104.
4. Schmalz, T. G.; Seitz, W. A.; Klein, D. J.; Hite, G. E. *Chem. Phys. Lett.* **1986**, *130*, 203–207.
5. Kroto, H. W. *Nature* **1987**, *329*, 529–531.
6. Kadish, K. M.; Ruoff, R. S. (Eds.) *Fullerenes: Chemistry, Physics and Technology*; John Wiley & Sons, Inc., USA, **2000**, p. 91.
7. Hirsch, A.; Brettreich, M. (Eds.) *Fullerenes: Chemistry and Reactions*; Wiley-VCH Verlag GmbH & Co. KGaA, Weinheim, **2005**.
8. Langa, F.; Nierengarten, J.-F. (Eds.) *Fullerenes: Principles and Applications*; RSC Publishing, Cambridge, **2007**, p. 15.
9. Manoharan, M.; de Proft, F.; Geerlings, P. *J. Org. Chem.* **2000**, *65*, 6132–6137.
10. Rubin, Y.; Khan, S.; Freedberg, D. I.; Yeretzian, C. *J. Am. Chem. Soc.* **1993**, *115*, 344–345.
11. Kräutler B.; Maynollo, J. *Angew. Chem.* **1995**, *107*, 69–71. *Angew. Chem. Int. Ed. Engl.* **1995**, *34*, 87–88.
12. Giovane, L. M.; Barco, J. W.; Yadav, T.; Lafleur, A. L.; Marr, J. A.; Howard, J. B.; Rotello, V. M. *J. Phys. Chem.* **1993**, *97*, 8560–8561.

13. Schlueter, J. A.; Seaman, J. M.; Taha, S.; Cohen, H.; Lykke, K. R.; Wang, H. H.; Williams, J. M. *J. Chem. Soc. Chem. Commun.* **1993**, 11, 972–974.
14. Sarova, G. H.; Berberan-Santos, M. N. *Chem. Phys. Lett.* **2004**, 397, 402–407.
15. Lamparth, I.; Maichle-Mössmer, C.; Hirsch, A. *Angew. Chem.* **1995**, 107, 1755–1757. Lamparth, I.; Maichle-Mössmer, C.; Hirsch, A. *Angew. Chem. Int. Ed. Engl.* **1995**, 34, 1607–1609.
16. Wang, G.-W.; Saunders, M.; Cross, R. J. *J. Am. Chem. Soc.* **2001**, 123, 256–259.
17. Pang, L. S. K.; Wilson, M. A. *J. Phys. Chem.* **2003**, 97, 6761–6763.
18. Wang, G.-W.; Chen, Z.-X.; Murata, Y.; Komatsu, K. *Tetrahedron* **2005**, 61, 4851–4856.
19. Herranz, M. A.; Echegoyen, L. *New J. Chem.* **2004**, 28, 513–518.
20. Isaacs, L.; Haldimann, R. F.; Diederich, F. *Angew. Chem.* **1994**, 107, 2434–2437. Isaacs, L.; Haldimann, R. F.; Diederich, F. *Angew. Chem. Int. Ed.* **1994**, 33, 2339–2342.
21. Isaacs, L.; Seiler, P.; Diederich, F. *Angew. Chem.* **1995**, 107, 1636–1639. Isaacs, L.; Seiler, P.; Diederich, F. *Angew. Chem. Int. Ed.* **1995**, 34, 1466–1469.
22. Boudon, C.; Gisselbrecht, J.-P.; Gross, M.; Isaacs, L.; Anderson, H. L.; Faust, R.; Diederich, F. *Helv. Chim. Acta* **1995**, 78, 1334–1344.
23. Cardullo, F.; Isaacs, L.; Diederich, F.; Gisselbrecht, J.-P.; Boudon, C.; Gross, M. *Chem. Commun.* **1996**, 6, 797–799.
24. Isaacs, L.; Diederich, F.; Haldimann, R. F. *Helv. Chim. Acta* **1997**, 80, 317–342.
25. Cardullo, F.; Seiler, P.; Isaacs, L.; Nierengarten, J.-F.; Haldimann, R. E.; Diederich, F.; Mordasini-Denti, T.; Thiel, W.; Boudon, C.; Gisselbrecht, J.-P.; Gross, M. *Helv. Chim. Acta* **1997**, 80, 343–371.
26. An, Y.-Z.; Ellis, G. A.; Viado, A. L.; Rubin, Y. *J. Org. Chem.* **1995**, 60, 6353–6361.
27. Lamparth, I.; Maichle-Mössmer, C.; Hirsch, A. *Angew. Chem.* **1995**, 108, 1294–1296. Lamparth, I.; Maichle-Mössmer, C.; Hirsch, A. *Angew. Chem. Int. Ed. Engl.* **1995**, 34, 1607–1609.
28. Kräutler, B.; Müller, T.; Maynollo, J.; Gruber, K.; Kratky, C.; Ochsenbein, Ph.; Schwarzenbach D.; Bürgi, H.-B. *Angew. Chem.* **1996**, 108, 1294–1296. Kräutler, B.; Müller, T.; Maynollo, J.; Gruber, K.; Kratky, C.; Ochsenbein, Ph.; Schwarzenbach D.; Bürgi, H.-B. *Angew. Chem. Int. Ed. Engl.* **1996**, 35, 1204–1208.
29. Schwenninger, R.; Müller, T.; Kräutler, B. *J. Am. Chem. Soc.* **1997**, 119, 9317–9318.
30. (a) Zhang, S.; Lukoyanova, O.; Echegoyen, L. *Chem.-Eur. J.* **2006**, 12, 2846–2853. (b) Ortiz, A. L.; Rivera, D. M.; Athans, A. J.; Echegoyen, L. *Eur. J. Org. Chem.* **2009**, 2009, 3396–3403. (c) Rodríguez-Morgade, M. S.; Plonska-Brzezinska, M. E.; Athans, A. J.; Carbonell, E.; de Miguel, G.; Guldi, D. M.; Echegoyen, L.; Torres, T. *J. Am. Chem. Soc.* **2009**, 131, 10484–10496.
31. Prato, M.; Suzuki, T.; Foroudian, H.; Li, Q.; Khemani, K.; Wudl, F.; Leonetti, J.; Little, R. D.; White, T.; Rickborn, B.; Yamago, S.; Nakamura, E. *J. Am. Chem. Soc.* **1993**, 115, 1594–1595.
32. Chuang, S.-C.; Clemente, F. R.; Khan, S. I.; Houk, K. N.; Rubin, Y. *Org. Lett.* **2006**, 8, 4525–4528.
33. (a) Chuang, S.-C.; Sander, M.; Jarrosson, T.; James, S.; Rozumov, E.; Khan, S. I.; Rubin, Y. *J. Org. Chem.* **2007**, 72, 2716–2723. (b) Sander, M.; Jarrosson, T.; Chuang, S.-C.; Khan, S. I.; Rubin, Y. *J. Org. Chem.* **2007**, 72, 2724–2731.
34. Lee, J. K.; Wang, Y.-M.; Choa, S.; Wudl, F.; Heeger, A. J. *Org. Electron.* **2009**, 10, 1223–1227.

35. (a) Guhr, K. I.; Greaves, M. D.; Rotello, V. M. *J. Am. Chem. Soc.* **1994**, *116*, 5997–5998. (b) Nie, B.; Hasan, K.; Greaves, M. D.; Rotello, V. M. *Tetrahedron Lett.* **1995**, *36*, 3617–3618. (c) Maeda, Y.; Miyashita, J.; Hasegawa, T.; Wakahara, T.; Tsuchiya, T.; Nakahodo, T.; Akasaka, T.; Mizorogi, N.; Kobayashi, K.; Nagase, S.; Kato, T.; Ban, N.; Nakajima, H.; Watanabe, Y. *J. Am. Chem. Soc.* **2005**, *127*, 12190–12191. (d) Ge, Z.; Duchamp, J. C.; Cai, T.; Gibson, H. W.; Dorn, H. C. *J. Am. Chem. Soc.* **2005**, *127*, 16292–16298. (e) Cai, T.; Xu, L.; Anderson, M. R.; Ge, Z.; Zuo, T.; Wang, X.; Olmstead, M. M.; Balch, A. L.; Gibson, H. W.; Dorn, H. C. *J. Am. Chem. Soc.* **2006**, *128*, 8581–8589.
36. Bingel, C. *Chem. Ber.* **1993**, *126*, 1957–1959.
37. González, S.; Martín, N.; Guldi, D. M. *J. Org. Chem.* **2003**, *68*, 779–791.
38. (a) Diederich, F.; Dietrich-Buchecker, C.; Niergartent, J.-F.; Sauvage, J.-P. *Chem. Commun.* **1995**, *7*, 781–782.; (b) Brettreich, M. Hirsch, A. *Tetrahedron Lett.* **1998**, *39*, 2731–2734.
39. Nakamura, Y.; Minami, S.; Iizuka, K.; Nishimura, J. *Angew. Chem.* **2003**, *115*, 3266–3270. Nakamura, Y.; Minami, S.; Iizuka, K.; Nishimura, J. *Angew. Chem. Int. Ed. Engl.* **2003**, *42*, 3158–3162.
40. (a) Arias, F.; Yang, Y.; Echegoyen, L.; Lu, Q.; Wilson, S. R.; *Proc. Electrochem. Soc.* **1995**, *10*, 200–212 (b) Keshavarz-K., M.; Knight, B.; Haddon, R. C.; Wudl, F. *Tetrahedron* **1994**, *52*, 5149–5159.
41. Kessinger, R.; Crassous, J.; Herrmann, A.; Rüttimann, M.; Echegoyen, L.; Diederich, F. *Angew. Chem.* **1998**, *110*, 2022–2025. *Angew. Chem. Int. Ed.* **1998**, *37*, 1919–1922.
42. Kessinger, R.; Fender, N. S.; Echegoyen, L. E.; Thilgen, C.; Echegoyen, L.; Diederich, F. *Chem.-Eur. J.* **2000**, *6*, 2184–2192.
43. Kordatos, K.; Bosi, S.; Da Ros, T.; Zambon, A.; Lucchini, V.; Prato, M. *J. Org. Chem.* **2001**, *66*, 2802–2808.
44. Beulen, M. W. J.; Echegoyen, L.; Rivera, J. A.; Herranz, M. A.; Martín-Domenech, A.; Martín, N. *Chem. Commun.* **2000**, *11*, 917–918.
45. (a) Nuretdinov, I. A.; Yanilkin, V. V.; Gubskaya, V. P.; Maksimiyuk, N. I.; Berezhnaya, L. Sh. *Russ. Chem. Bull.* **2000**, *49*, 427–429. (b) Yanilkin, V. V.; Nastapova, N. V.; Gubskaya, V. P.; Morozov, V. I.; Berezhnaya, L. Sh.; Nuretdinov, I. A. *Russ. Chem. Bull.* **2002**, *51*, 72–77. (c) Nuretdinov, I. A.; Morozov, V. I.; Gubskaya, V. P.; Yanilkin, V. V.; Berezhnaya, L. Sh.; Il'yasov, A. V. *Russ. Chem. Bull.* **2002**, *51*, 813–816. (d) Yanilkin, V. V.; Morozov, V. I.; Toropchina, A. V.; Nastapova, N. V.; Gubskaya, V. P.; Berezhnaya, L. Sh.; Nuretdinov, I. A. *Fullerenes, Nanotubes and Carbon Nanostructures*, **2004**, *12*, 221–227.
46. Nicholson, R. S.; Shain, J. *Anal. Chem.* **1995**, *37*, 190–195.
47. Herranz, M. A.; Beulen, M. W. J.; Rivera, J. A.; Echegoyen, L.; Díaz, M. C.; Illescas, B. M.; Martín, N. *J. Mater. Chem.* **2002**, *12*, 2048–2053.
48. (a) Brezova, V.; Stasko, A.; Rapta, P.; Domschke, G.; Barti, A.; Dunsch, L. *J. Phys. Chem.* **1995**, *99*, 16234–16241. (b) Diekers, M.; Hirsch, A.; Pyo, S.; Rivera, J. A.; Echegoyen, L. *Eur. J. Org. Chem.* **1998**, *1998*, 1111–1121 (c) Shu, L.; Pyo, S.; Rivera, J. A.; Echegoyen, L. *Inorg. Chim. Acta* **1999**, *292*, 34–40. (d) Brezova, V.; Stasko, A.; Dvoranova, D.; Asmus, K.-D.; Guldi, D. M. *Chem. Phys. Lett.* **1999**, *300*, 667–675. (e) Da Ros, T.; Prato, M.; Guldi, D. M.; Ruzzi, M.; Pasimeni, L. *Chem.-Eur. J.* **2001**, *7*, 816–827.

49. (a) Stevenson, G. R.; Recter, R. C.; Ross, D. G.; Frye, D. G. *J. Phys. Chem.* **1984**, *88*, 5763–5764. (b) G. R. Stevenson, *J. Phys. Chem.* **1998**, *92*, 493–496. (c) Stevenson, G. R.; Echegoyen, L. *J. Phys. Chem.* **1972**, *76*, 1439–1442. (d) Wang, S. K.; Wan, J. K. S. *Can. J. Chem.* **1973**, *51*, 753–759.
50. (a) Maki, A. H.; Geske, D. H. *J. Am. Chem. Soc.* **1961**, *83*, 1852–1860. (b) Stevenson, G. R.; Echegoyen, L. *J. Phys. Chem.* **1973**, *77*, 2339–2342.; (c) Stevenson, G. R.; Echegoyen, L.; Hidalgo, H. *J. Phys. Chem.* **1975**, *79*, 152.
51. Herranz, M. A.; Cox, C. T.; Echegoyen, L. *J. Org. Chem.* **2003**, *68*, 5009–5012.
52. Herranz, M. A.; Diederich, F.; Echegoyen, L. *Eur. J. Org. Chem.* **2004**, 2299–2316.
53. Carano, M.; Echegoyen, L. *Chem.–Eur. J.* **2003**, *9*, 1974–1981.
54. Tulythan, B.; Geiger, W. E. *J. Am. Chem. Soc.* **1985**, *107*, 5960–5967.
55. Oçafrain, M.; Herranz, M. A.; Marx, L.; Thilgen, C.; Diederich, F.; Echegoyen, L. *Chem.–Eur. J.* **2003**, *9*, 4811–4819.
56. Konarev, D. V.; Khasanov, S. S.; Vorontsov, I. I.; Saito, G.; Antipin, M. Y.; Otsuka, A.; Lyubovskaya, R. N., *Chem. Commun.* **2002**, *21*, 2548–2549.
57. Cheng, F.; Murata, Y.; Komatsu, K. *Org. Lett.* **2002**, *4*, 2541–2544.
58. Kessinger, R.; Gómez-López, M.; Boudon, C.; Gisselbrecht, J.-P.; Gross, M.; Echegoyen, L.; Diederich, F. *J. Am. Chem. Soc.* **1998**, *120*, 8545–8546.
59. (a) Hirsch, A. *The Chemistry of the Fullerenes*; Thieme; Stuttgart, **1994**. (b) Hirsch, A.; Lamparth, I.; Karfunkel, H. R. *Angew. Chem.* **1994**, *106*, 453–455. Hirsch, A.; Lamparth, I.; Karfunkel, H. R. *Angew. Chem. Int. Ed. Engl.* **1994**, *33*, 437–438.
60. Djojo, F.; Herzog, A.; Lamparth, I.; Hampel, F.; Hirsch, A. *Chem.–Eur. J.* **1996**, *2*, 1537–1547.
61. Echegoyen, L. E.; Djojo, F. D.; Hirsch, A.; Echegoyen, L. *J. Org. Chem.* **2000**, *65*, 4994–5000.
62. (a) Fender, N. S.; Nuber, B.; Schuster, D. I.; Wilson, S. R.; Echegoyen, L. *J. Chem. Soc. Perkin Trans.* **2000**, *2*, 1924–1928.
63. Hawkins, J. M.; Meyer, A. *Science* **1993**, *260*, 1918–1920.
64. Boudon, C.; Gisselbrecht, J.-P.; Gross, M.; Herrmann, A.; Rüttimann, M.; Crassous, J.; Cardullo, F.; Echegoyen, L.; Diederich, F. *J. Am. Chem. Soc.* **1998**, *120*, 7860–7868.
65. (a) Crassous, J.; Rivera, J.; Fender, N. S.; Shu, L. H.; Echegoyen, L.; Thilgen, C.; Hermann, A.; Diederich, F. *Angew. Chem.* **1999**, *111*, 1716–1721. (b) Crassous, J.; Rivera, J.; Fender, N. S.; Shu, L. H.; Echegoyen, L.; Thilgen, C.; Hermann, A.; Diederich, F. *Angew. Chem. Int. Ed.* **1999**, *38*, 1613–1617.
66. Moonen, N. N. P.; Thilgen, C.; Echegoyen, L.; Diederich, F. *Chem. Commun.* **2000**, *5*, 335–336.
67. (a) Herranz, M. A.; Rivera, J. A.; Alvarado, R. J.; Martín, N.; Thilgen, C.; Diederich, F.; Echegoyen, L. *J. Supramol. Chem.* **2001**, *1*, 299–303. (b) Herranz, M. A.; Echegoyen, L.; Beulen, M. W. J.; Rivera, J. A.; Martín, N.; Illescas, B.; Díaz, M. C. *Proc. Electrochem. Soc.* **2002**, *12*, 307–317.
68. (a) Burley, G. A.; Keller, P. A.; Pyne, S. G.; Ball, G. E. *Chem. Commun.* **1998**, *22*, 2539–2540. (b) Burley, G. A.; Keller, P. A.; Pyne, S. G.; Ball, G. E. *Chem. Commun.* **2000**, *18*, 1717–1718. (c) Burley, G. A.; Keller, P. A.; Pyne, S. G.; Ball, G. E. *Chem. Commun.* **2001**, *6*, 563–564. (d) Burley, G. A.; Keller, P. A.; Pyne, S. G.; Ball, G. E. *J. Org. Chem.* **2002**, *67*, 8316–8330.
69. (a) Da Ros, T.; Prato, M. *Chem. Commun.* **1999**, 663–669. (b) Bosi, S.; Da Ros, T.; Spalluto, G.; Prato, M. *Eur. J. Med. Chem.* **2003**, *38*, 913–923.

70. (a) Prato, M. *Top. Curr. Chem.* **1999**, 734, 173–187. (b) Prato, M.; Martín, N. *J. Mater. Chem.* **2002**, 12, 7–ix. (c) Giacalone, F.; Martín, N. *Chem. Rev.* **2006**, 106, 5136–5190. (d) Giacalone, F.; Martín, N. (Eds.). *Fullerene Polymers*; Wiley-VCH, Weinheim, Germany, **2009**.
71. (a) Maggini, M.; Scorrano, G.; Prato, M. *J. Am. Chem. Soc.* **1993**, 115, 9798–9799. (b) Prato, M.; Maggini, M. *Acc. Chem. Res.* **1998**, 31, 519–526. (c) Tagmatarchis, N.; Prato, M. *Synlett* **2003**, 6, 768–779.
72. Martín, N.; Altabe, M.; Filippone, S.; Martín-Domenech, A.; Echegoyen, L.; Cardona, C. M. *Angew. Chem. Int. Ed.* **2006**, 45, 110–114.
73. Brunetti, F. G.; Herrero, M. A.; Muñoz, J. M.; Giordani, S.; Díaz-Ortiz, A.; Filippone, S.; Ruaro, G.; Meneghetti, M.; Prato, M.; Vázquez, E. *J. Am. Chem. Soc.* **2007**, 129, 14580–14581.
74. Filippone, S.; Izquierdo Barroso, M.; Martín-Domenech, A.; Osuna, S.; Solà, M.; Martín, N.; *Chem. -Eur. J.* **2008**, 14, 5198–5206.
75. Guryanov, I.; Montellano Lopez, A.; Carraro, M.; Da Ros, T.; Scorrano, G.; Maggini, M.; Prato, M.; Bonchio, M. *Chem. Commun.* **2009**, 3940–3942.
76. Lukoyanova, O.; Cardona, C. M.; Altabe, M.; Filippone, S.; Martín Domenech, A.; Martín, N.; Echegoyen, L. *Angew. Chem. Int. Ed.* **2006**, 45, 7430–7433.
77. Pinzón, J. R.; Gasca, D. C.; Sankaranarayanan, S. G.; Bottari, G.; Torres, T.; Guldi, D. M.; Echegoyen, L. *J. Am. Chem. Soc.* **2009**, 131, 7727–7734.
78. Pinzón, J. R.; Cardona, C. M.; Herranz, M. A.; Plonska-Brzezinska, M. E.; Palkar, A.; Athans, A. J.; Martín, N.; Rodríguez-Forte A.; Poblet, J. M.; Bottari, G.; Torres, T.; Gayathri, S. S.; Guldi, D. M.; Echegoyen, L. *Chem.-Eur. J.* **2009**, 15, 864–877.
79. (a) Meier, M. S.; Poplawska, M. *J. Org. Chem.* **1993**, 58, 4524–4525. (b) Martín, N.; Illescas, B. *J. Org. Chem.* **2000**, 65, 5986–5995. (c) Langa, F.; de la Cruz, P.; Espíldora, E.; Gonzalez-Cortés, A.; de la Hoz, A.; López-Arza, V.; *J. Org. Chem.* **2000**, 65, 8675–8684.
80. Meier, M. S.; Poplawska, M. *Tetrahedron* **1996**, 52, 5043–5052.
81. Da Ros, T.; Prato, M.; Novello, F.; Maggini, M.; De Amici, M.; De Micheli, C. *Chem. Commun.* **1997**, 59–60.
82. Martín, N.; Altabe, M.; Filippone, S.; Martín-Domenech, A.; Martínez-Alvarez, R.; Suarez, M.; Plonska-Brzezinska, M. E.; Lukoyanova, O.; Echegoyen L. *J. Org. Chem.* **2007**, 72, 3840–3846.
83. Langa, F.; Oswald, F. C. R. *Chim.* **2006**, 9, 1058–1074.
84. Delgado, J. L.; Oswald, F.; Cardinali, F.; Langa, F.; Martín, N. *J. Org. Chem.* **2008**, 73, 3184–3188.
85. Delgado, J. L.; Espíldora, E.; Liedtke, M.; Sperlich, A.; Rauh, D.; Baumann, A.; Deibel, C.; Dyakonov, V.; Martín, N.; *Chem.-Eur. J.* **2009**, 15, 13474–13482.
86. Delgado, J. L.; Osuna, S.; Bouit, P.-A.; Martínez-Alvarez, R.; Espíldora, E.; Solà, M.; Martín, N. *J. Org. Chem.* **2009**, 74, 8174–8180.

This page intentionally left blank

Chapter 11

Porphyrin-Fullerene Supramolecular Chemistry

Peter D.W. Boyd,^{,†} Ali Hosseini,[†] John D. van Paauwe[†]
and Christopher A. Reed[‡]*

*[†]Department of Chemistry, The University of Auckland,
Private Bag 92019, Auckland 1142, New Zealand*

*[‡]Department of Chemistry, University of California,
Riverside Riverside, California 92521, USA*

1. Introduction	375
2. Molecular Porphyrin Hosts for Fullerenes	376
3. The Porphyrin-Fullerene Interaction	378
4. Cobalt(II) Porphyrins and Fullerenes	380
4.1. Synthesis of bis-porphyrins	381
4.2. Binding Constants and Charge Transfer Bands	381
4.3. X-ray Structures of T _{3,4,5} -OMe ⁻ PP Cocrystallates	383
5. Conclusions	387
Acknowledgments	387
References	387

1. Introduction

The conversion of light into chemical energy in photosynthetic bacteria is achieved by efficient light harvesting and excitation energy transfer to a bacteriochlorophyll “special pair”. A spatially and electronically separated radical ion

*Corresponding author. Email: pdw.boyd@auckland.ac.nz

pair is then formed *via* a sequence of rapid short-range electron transfer (ET) reactions along a redox gradient to give a long-lived (1 s) charge separated state: $(\text{Bchl})_2^+ \text{-quinoneB}^-$.¹ A major effort is underway to mimic this process and develop artificial photosynthetic systems for solar energy capture by linking of synthetic models of the natural components into a functional assembly.²⁻⁴

Combinations of fullerene⁵ (*e.g.* C_{60} and C_{70}) and porphyrin chromophores are highly suited to this purpose.^{2,6} Uniquely, the small 3-D reorganization energies of fullerenes following electron transfer from porphyrins leads to ultrafast charge separation and very slow charge recombination, as in the photosynthetic reaction centre (PRC).^{7,8} Elaborate covalently-linked combinations of fullerenes and porphyrins with auxiliary donors and acceptors in the form of triads, tetrads and pentads mimic the key features of this process. They form radical ion pair states in high quantum yield, with long lifetimes comparable to the PRC,⁹⁻¹² features crucial to efficient solar energy conversion.^{4,13} In contrast, the PRC uses a supramolecular arrangement of donors and acceptors in a protein matrix.¹

Many approaches to such arrangements have used electrostatic assembly,¹⁴ hydrogen bonding¹⁵ and coordination chemistry assembly.¹⁶ We have developed a supramolecular approach in which donors and acceptors self assemble using dispersive (van der Waals) attractions between the components. A key element of this approach is based on the discovery that fullerenes and porphyrins are naturally attracted to each other.¹⁷⁻²⁰ In solid state co-crystallates, there is an unusually close approach (*ca.* 2.7 Å) of the curved surface of the fullerene to the centre of a planar porphyrin, and this interaction persists in solution. This supramolecular recognition motif has allowed fullerenes to be rationally incorporated into discrete molecular assemblies,²¹⁻²³ porphyrin nanotubes²⁴ and infinite arrays of porphyrins.²⁵

There is evidence of preorganisation of fullerenes and porphyrins in composite clusters formed in mixed acetonitrile/toluene solution from mixtures of C_{60} and monomeric porphyrin molecules. When electrophoretically deposited on nanostructured SnO_2 films these clusters can be used to form a supramolecular photoelectrochemical device. It has been found that the efficiency of such constructs depends on the molecular arrangements of porphyrin and fullerene moieties and that this correlates with porphyrin substituent.²⁶

In this Chapter we present some recent results on the effect of porphyrin metallation with cobalt(II) in porphyrin-fullerene supramolecular chemistry for both molecular host-guest complexes and solid state assemblies.

2. Molecular Porphyrin Hosts for Fullerenes

The fullerene-porphyrin recognition element has now been incorporated into a variety of molecular hosts containing two suitably oriented porphyrins capable

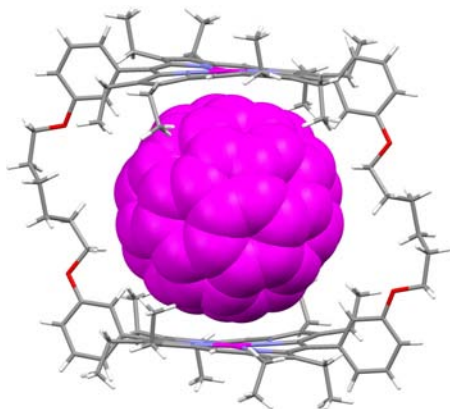


Figure 1. X-ray structure of a cyclic bisporphyrin- C_{60} complex.²³

of incorporating a fullerene between them. The main requirement for a good fit between a fullerene (C_{60} or C_{70}) guest and the porphyrin host has been found to be a separation of about 12 Å between the porphyrins connected by an appropriate linker. A range of cyclic and acyclic polyporphyrin hosts now exists with a wide variation of fullerene binding constants from 10^3 to 10^6 M^{-1} .

Cyclic bisporphyrins connected by two hexyl linkers, Figure 1, were first used by Aida, Tashiro and coworkers.^{23, 27} These formed complexes with both C_{60} and C_{70} and are still the strongest reported free base porphyrin hosts for fullerenes (7.94×10^5 and 1.58×10^7 M^{-1} for C_{60} and C_{70} respectively in toluene solution).

Molecular acyclic porphyrin hosts were first reported using Pd linked 4-pyridylporphyrins, Figure 2, with smaller binding constants (5200 M^{-1} for C_{60} in toluene solution).^{21, 22} A variety of acyclic *bis*-porphyrin hosts are now known.^{28–31} By selection of an appropriate linker, such as a hydrogen bonded isophthaloyl group ($1.0 \times 10^5 M^{-1}$ for C_{60} in toluene)²⁸ or a lower rim functionalized calix[4]arene ($2.5 \times 10^4 M^{-1}$ for C_{60} in toluene),^{29, 30} comparable binding to cyclic hosts can be achieved for fullerenes.

A recent extensive study of fullerene binding by calixarene-linked *bis*-porphyrin hosts has shown that the binding constants depend on porphyrin substituent, metal ion and solvent.³⁰ The binding strength calix[4]arene-linked bisporphyrin supramolecular hosts, (**A**), for C_{60} and C_{70} may be controlled over many orders of magnitude (*e.g.* 3×10^3 to $4.1 \times 10^6 M^{-1}$; C_{60}) by variation porphyrin of substituent **P** and solvent.³⁰

Porphyrin to fullerene charge transfer bands are observed in the host-guest complexes of (**1**), Figure 3, whose position is independent of solvent

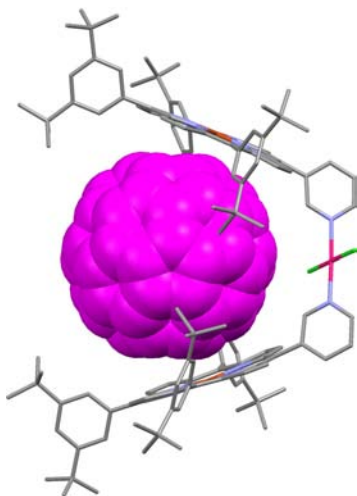
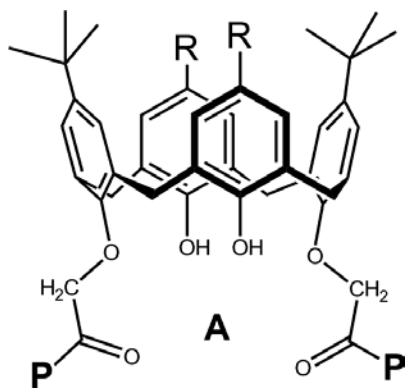


Figure 2. X-ray structure of a palladium linked bis-porphyrin- C_{60} complex.²²



but dependent on porphyrin functionalization, metallation and the fullerene guest, Figure 4.³⁰

3. The Porphyrin-Fullerene Interaction

The magnitude of binding of pristine fullerenes with porphyrin hosts has been found to be remarkably similar for both free base, zinc porphyrin and many transition metal porphyrins but increases for some second and third row metallocporphyrins such as Rh(III) and Ir(III).³² This increased binding strength has been attributed to more significant M-C metal-ligand binding.

It is now apparent that the major contribution to the attraction energy between unmetallated porphyrins and fullerenes is due to dispersive interactions

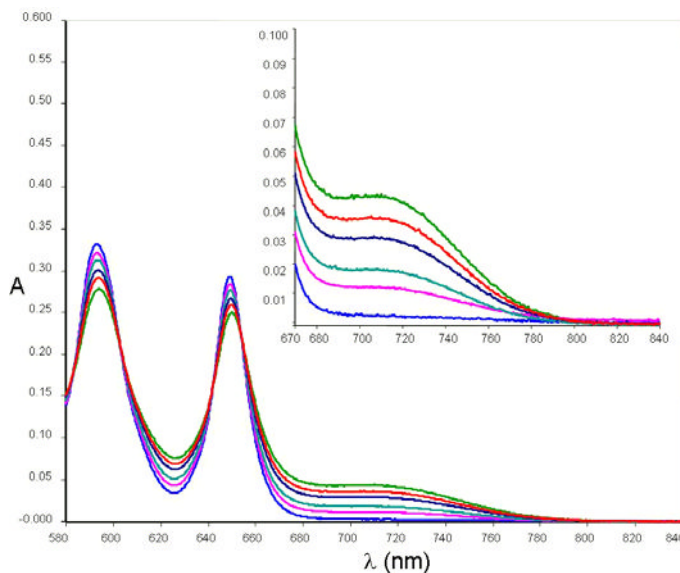


Figure 3. UV-vis titration of **1** with C_{60} in toluene solution showing charge transfer band in the NIR region.

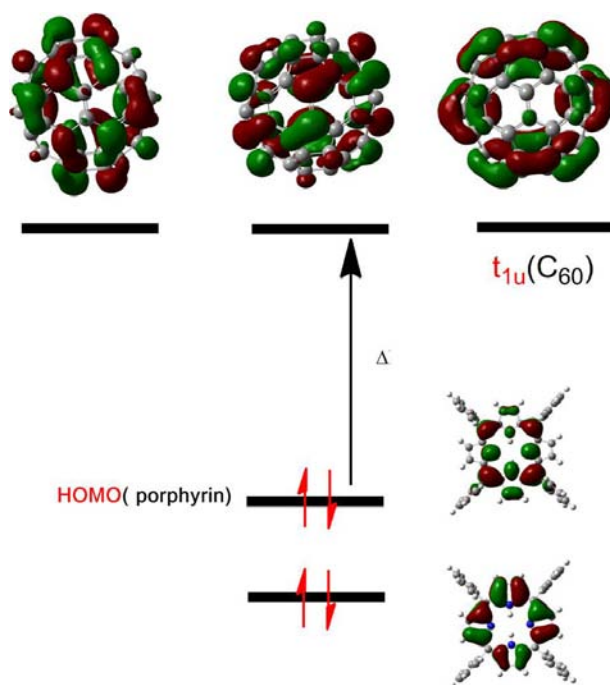


Figure 4. Tetraphenylporphyrin HOMO — C_{60} LUMO orbitals associated with the porphyrin to fullerene charge transfer band (740 nm H_2TPP).

Table 1. Calculated binding energies of porphine and Znporphine for Fullerenes, kcal/mol (TZP basis set ADF). Values in parentheses are corrected for basis set superposition errors.

		C ₆₀	C ₇₀
H ₂ porphine	KT1/TZP	-11.29(-9.59)	-11.32(-9.53)
	BLYP-D/TZP	-16.89	-17.80
	PBE-D/TZP	-10.98	—
Zn porphine	KT1/TZP	-12.91(-10.87)	-12.51(-10.44)
	BLYP-D/TZP	-18.49	-19.80
	PBE-D/TZP	-12.75	—

(van der Waals) between the two π systems. There have been a range of theoretical methods applied to this problem. Initially it was found that simple molecular mechanics models (which include van der Waals terms) reproduced the structural features of both cocrystallate and host-guest complexes.^{18,33} Density functional methods appeared to give attractive interactions, however the nature of the physical approximations in early density functionals did not allow for medium to long range interactions. The erratic performance of these calculations could be related to a combination of basis set superposition errors and the inability of functional to account for long range interactions.^{34–35} Using wavefunction based methods Jung and Head-Gordon calculated the interaction energy of C₆₀ and tetraphenylporphyrin to be -31.5 kcal mol⁻¹ using a scaled opposite spin MP2 method (in comparison to a molecular mechanics estimate of -31.6 kcal mol⁻¹).³⁶ Recent dispersion corrected density functional models such as those of Grimme have been developed.³⁷ These DFT-D models have been applied to the interaction between free base and metal porphyrin derivatives and C₆₀ by Liao, Watts and Huang.³⁵ Table 1 shows some typical interaction energies calculated for porphine with C₆₀ and C₇₀.³⁸

4. Cobalt(II) Porphyrins and Fullerenes

The effect of a metal in the porphyrins in *bis*-porphyrin hosts for fullerenes is less known. There are a number of reports that compare free-base porphyrins to zinc porphyrins but this metallation has only a minor effect on fullerene binding constants and on the subsequent photochemistry.

There are two reports on the effect of cobalt(II) metallation of a porphyrin on fullerene binding constants, both in elaborate *bis*-porphyrins.^{23,30} In neither case was the difference in binding constant between free-base and Co(II) porphyrin more than a factor of three. On the other hand in the present work the Co(II) derivative of a calixarene-linked *bis*-porphyrin showed a ten-fold

enhancement of the C_{60} binding and a lesser three to five fold enhancement with C_{70} . Normally, binding constants for C_{70} exceed those of C_{60} by more than an order of magnitude.¹⁷ In order to understand these effects on binding constants, and attempt to correlate them with structural and spectroscopic data, we have undertaken a more complete study of calixarene metalloporphyrin hosts and fullerene guests. Cobalt porphyrins offer a potentially better opportunity to improve fullerene binding and enhance photochemical performance. They meet the needs of air stability and ready synthesis.

4.1. Synthesis of bis-porphyrins

The calixarene-linked porphyrins **1**–**2** used in this study are shown in Figure 5. Compound **1** has been reported previously³⁰ and **2** was prepared by similar methods from the parent unsubstituted calixarene. Compound **2** was designed to investigate if upper rim *t*-butyl groups have a significant influence on fullerene binding constants. Since calixarenes adopt a “pinched cone” conformation upon complexation of a guest, steric hindrance between conflicting *t*-butyl groups on the upper rim might contribute to lower fullerene affinities relative to calixarenes with substituent-free rims.

Cobalt(II) was inserted into the porphyrins using cobalt acetate and full metallation in Co-1 and Co-3 was verified by UV-vis spectroscopy.

4.2. Binding Constants and Charge Transfer Bands

Fullerene binding constants were measured in toluene solution by standard UV-vis titration methods.³⁰ Table 2 lists the data. The removal of *t*-butyl

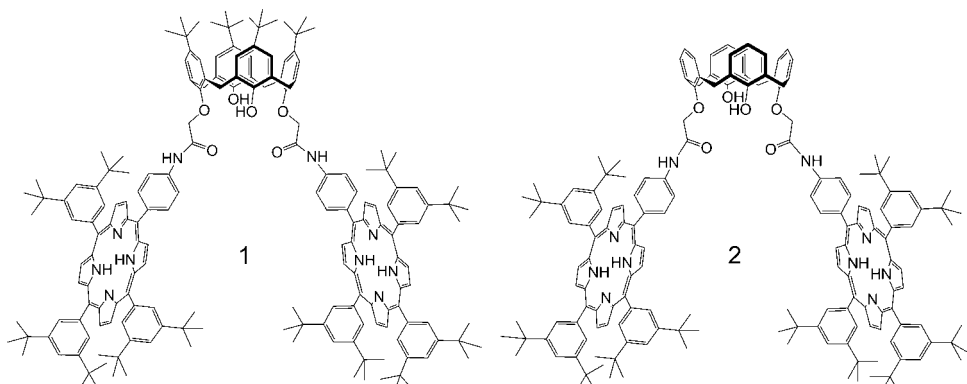
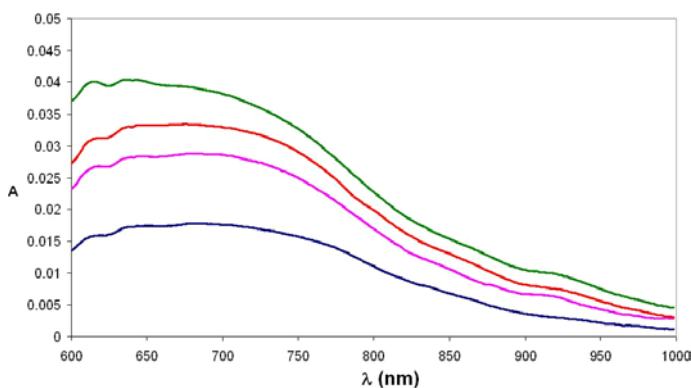


Figure 5. Calixarene *bis*-porphyrins.

Table 2. Binding Constants ($\times 10^3$) for Fullerenes of **1**, **2** and **3** in Toluene(298K).

		$K, C_{60} (M^{-1})$	$K, C_{70} (M^{-1})$
1	H2	26(4)	234(20)
	Co(II)	250(14)	1,200(100)
2	H2	35(0.5)	550(15)
	Co(II)	345(28)	1,800(300)

**Figure 6.** UV-vis titration of the cobalt(II) derivative of **1** in the NIR region.

groups on the calixarene upper rim of **2** is seen to lead to a moderate enhancement of fullerene affinity for both C_{60} and C_{70} relative to **1**. This is consistent with the notion of the sterically bulky *t*-butyl groups hindering adoption of the optimum pinched cone conformation in the adduct.

Both Co(II) *bis*-porphyrins in toluene show an increase by a factor of *ca.* 10 in their binding constants for C_{60} relative to the corresponding free-base or Zn(II) porphyrins. This corresponds to an increase in the free energy of binding of *ca.* 5.8 kJ.mole⁻¹. A similar increase is observed in the analogous *bis*-porphyrin host with 2,4,5 trimethoxyphenyl porphyrin substituents (11,000 M⁻¹ for C_{60} , 150,000 M⁻¹ for C_{70} in toluene). In contrast analogous data for C_{70} show no more than a difference of factor of 3 to 5 times.

The trend in C_{60} affinities, Co > Zn ~ free-base, is reflected in the porphyrin-to-fullerene charge transfer band. As shown in Figure 6, a broad absorption associated with charge transfer in Co-**1**· C_{60} is centered *ca.* 690 nm. The corresponding band in Zn-**1**· C_{60} is at 740 nm while that in **1**· C_{60} is 720 nm. From an analysis of the width and intensity of the bands, the electronic coupling constants V are 1158, 758 and 699 cm⁻¹ for the Co, Zn and

free-base complexes respectively. This indication of strongest electronic interaction for Co is consistent with its highest affinity.

4.3. X-ray Structures of $T_{3,4,5\text{-OMe}}$ PP Cocrystallates

The above affinity and charge transfer spectral data suggest that C_{60} can more closely approach cobalt porphyrins than their free-base or zinc analogues. In order to investigate whether these differences can be revealed by X-ray structure data, we turned from *bis*-porphyrins to a study of cocrystallates of fullerenes with tetra(3,4,5-trimethoxyphenyl)-porphyrins.

Free-base $H_2T_{3,4,5\text{-OMe}}$ PP cocrystallizes with C_{60} from toluene solution in a 1:2 ratio to give $H_2T_{3,4,5\text{-OMe}}$ PP·2 C_{60} ·2toluene.³⁹ As shown in Figure 7, each porphyrin is complexed by a pair of fullerenes, one each side of the porphyrin. The fullerenes are centered over the porphyrins and have a zigzag extended structure with closest fullerene-fullerene contact 3.17 Å. The closest fullerene C atom to porphyrin 24-atom mean plane is 2.70 Å.

The corresponding zinc structure crystallizes with an inverted stoichiometry having a 2:1 porphyrin to fullerene ratio as well as six toluene solvate molecules, 2($ZnT_{3,4,5\text{-OMe}}$ PP)· C_{60} ·6toluene.⁴⁰ While an isostructural motif might have been expected based on binding constant similarity, the X-ray structure indicates the reason why they are different. As shown in Figure 8, each zinc porphyrin is connected to its neighbour *via* axial coordination by a

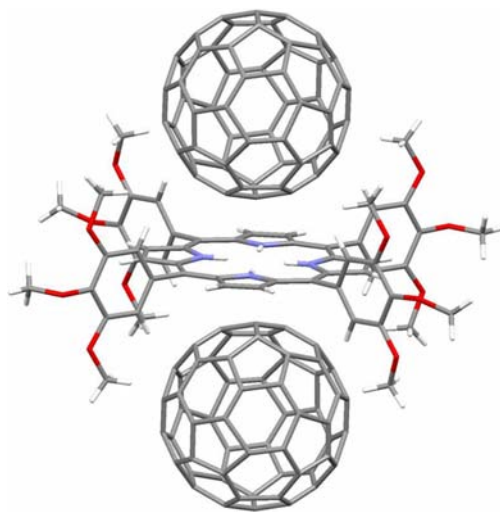


Figure 7. X-ray Structure $H_2T_{3,4,5\text{-OMe}}$ PP·2 C_{60} ·2toluene.

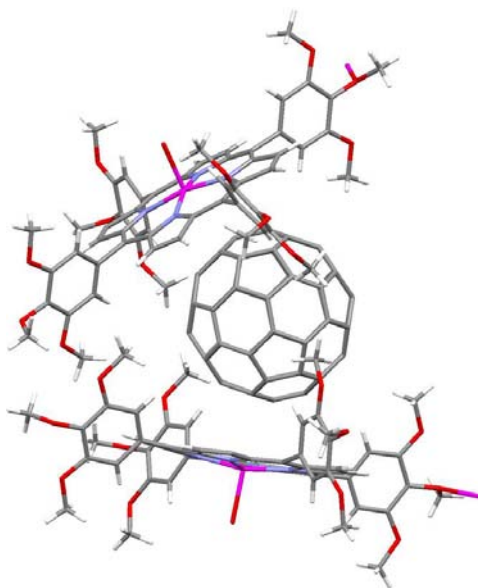


Figure 8. X-ray structure of $2(\text{ZnT}_{3,4,5\text{-OMe}}\text{PP})\cdot\text{C}_{60}\cdot 6\text{toluene}$ showing a *bis*-porphyrin-like packing of C_{60} by five coordinate zinc porphyrins.

4-methoxyphenyl group leading to a *bis*-porphyrin-like packing. Each fullerene is complexed to a pair of zinc porphyrins. Despite these differences between the free-base and Zn systems, the closest fullerene C atom to porphyrin 24-atom mean plane in the Zn complex is 2.68 Å, almost identical to that in the free-base analogue. Thus, the near equivalence of binding constants for zinc and free-base porphyrins is reflected in the near equivalence of their fullerene to porphyrin distances.

The corresponding cobalt structure crystallizes with the more common 1:1 porphyrin to C_{60} ratio with formula $\text{Co}(\text{T}_{3,4,5\text{-OMe}}\text{PP})\cdot\text{C}_{60}\cdot 1.5\text{toluene}$. As shown in Figure 9, a linear alternating column replaces the zigzag extended motif and the closest fullerene C to 24-atom mean porphyrin plane distances are 2.58 and 2.60 Å. On average, the separations in the cobalt complex are nearly 0.1 Å closer than in the zinc or free-base analogues.⁴¹ Again this correlates with binding constants.

The closest $\text{Co}\cdots\text{C}$ distances are 2.67 and 2.72 Å to a 6:6 ring juncture, alkene-like bond of C_{60} . A columnar structure formed from $\text{Co}(\text{T}_{3,5\text{-tert-Bu}}\text{PP})$ and C_{60} show $\text{Co}\cdots\text{C}$ approaches of 2.58–2.61 Å⁴² whilst those in cobalt octaethylporphyrin cocrystallates are 2.67 Å.¹⁹ These distances are shorter than the van der Waals separation (*ca.* 3.0 Å) but longer than the distance expected for Co-C coordinate bond to an alkene (< 2.3 Å), Figure 10.

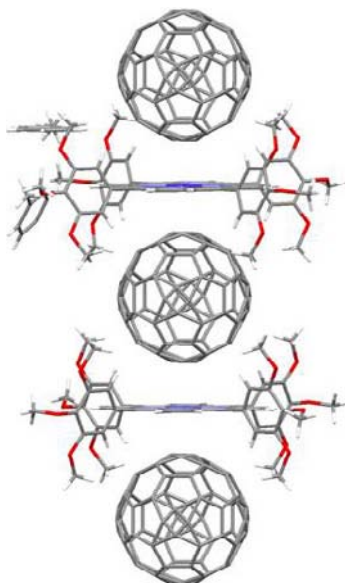


Figure 9. X-ray structure of $\text{Co}(\text{T}_{3,4,5\text{-OMe}}\text{PP})\cdot\text{C}_{60}\cdot 1.5\text{toluene}$ showing linear alternating column of cobalt porphyrins and C_{60} .

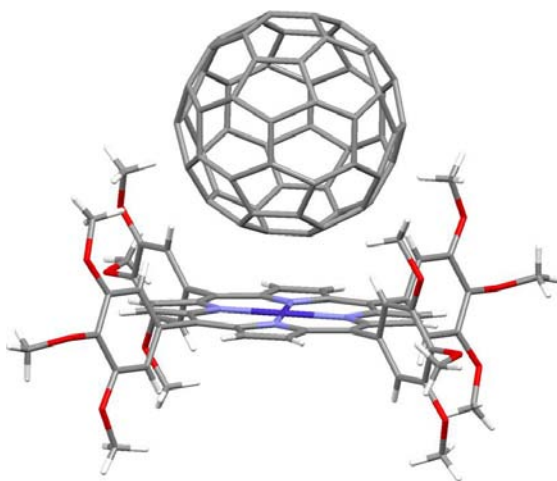


Figure 10. X-ray structure of $\text{Co}(\text{T}_{3,4,5\text{-OMe}}\text{PP})\cdot\text{C}_{60}\cdot 1.5\text{toluene}$ showing approach of C_{60} to the cobalt porphyrin plane.

Nevertheless, they are entirely consistent with a weak coordinate bond and this provides a rationale for the increased binding constant of the Co derivative relative to the Zn and free-base analogues. Dispersion-corrected DFT calculations qualitatively support the idea of an additional weak coordinate

bond for cobalt relative to zinc even though they do not quantitatively reproduce the Co-C bond distances.³⁵

C₆₀ versus C₇₀. The remaining question concerns the lack of a comparable increase in binding constant when C₇₀ binds to cobalt porphyrins. With its egg shape, the equatorial belt of C₇₀ presents a flatter and therefore larger surface to the porphyrin than C₆₀ and this larger van der Waals interaction readily rationalizes the generally larger binding constants of C₇₀ to porphyrins relative to C₆₀.¹⁷ Why would the opportunity for an additional interaction from weak coordinate Co-C bonding not be manifest in a comparable stronger binding of C₇₀? There are two possibilities: either the porphyrin presents steric hindrance to binding the larger fullerene, or the more aromatic equatorial belt of C₇₀ is less unable to engage in alkene-like coordinate bonding.

A choice between these two alternatives can be made on the basis of the crystal structure of the 1:1 cocrystallate Co(T_{3,4,5}-OMe PP)·C₇₀·CHCl₃·1.5toluene where C₇₀ is sandwiched between porphyrins in familiar zigzag chains (Figure 11).⁴³ As expected, the flatter equatorial region of C₇₀ is centered over the porphyrin. There is no steric hindrance to fitting C₇₀ into the cavity formed by the porphyrin aryl substituents. Indeed, the methyl substituents of the 3- and 5-methoxy groups embrace the fullerene with presumably attractive C-H... π interactions. The closest fullerene C to mean 24-atom porphyrin plane distances range from 2.72 to 2.77 Å and the C...Co distances are 2.73 and 2.79 Å.

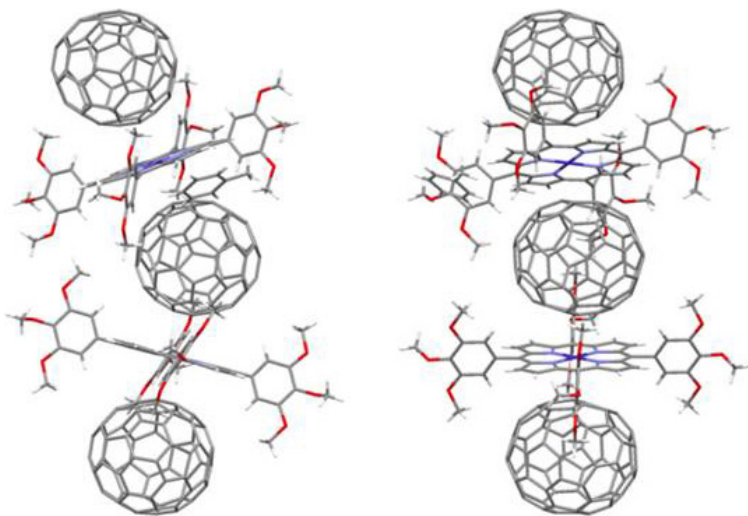


Figure 11. X-ray structure of cocrystallate Co(T_{3,4,5}-OMe PP)·C₇₀·CHCl₃·1.5toluene showing two views of the alternating zigzag array of C₇₀ with the cobalt porphyrin

These distances are all long compared to the corresponding distances in the C_{60} adduct and are comparable to the distances found in free-base porphyrin C_{70} cocrystallates.¹⁷ Thus, we conclude that the less alkene-like nature of the C-C bonding in the equatorial belt of C_{70} compared to C_{60} , diminishes the ability of C_{70} to engage in coordinate bonding to metalloporphyrins, thereby leaving the binding constants similar to that of the free base. This subtle difference in the bonding possibilities of C_{60} and C_{70} has not been recognized previously.

5. Conclusions

This work provides an explanation for understanding the trends in binding constants of fullerenes to cobalt porphyrins relative to zinc and free-base porphyrins. It also explains why C_{70} binding constants may not follow those of C_{60} . All other things being equal, the metallation of a porphyrin with cobalt can be expected to produce an order of magnitude increase in binding constant of C_{60} due to coordinate bond formation. On the other hand, the relative increase for C_{70} is marginal because C_{70} is intrinsically less suitable for alkene-like coordination to a metalloporphyrin. EPR experiments support this suggestion.⁴⁴ A study of a covalent cobaltporphyrin fullerene dyad($\text{Co}\cdots\text{C}$ 2.71–2.73 Å) suggest both a local alkene C to Co σ donation and a porphyrin π to fullerene π donation interaction are present.⁴⁴ The factor of 10 increase in both applications by increasing the lattice energy of cocrystallates and by altering the lifetime of the charge separated state from the nano- to microsecond timescale.⁴⁵ Indeed, the increase in lattice energy should make these materials easier to synthesize than their free-base or zinc counterparts.

Acknowledgments

This work was supported by the Marsden Fund and The University of Auckland Faculty Research Development Fund.

References

1. Deisenhofer, J.; Norris, J. Academic Press, San Diego, **1993**.
2. Kamat, P. J. *Phys. Chem. C* **2007**, *111*, 2834–2860.
3. Alstrum-Acededo, J. H.; Brennaman, M. K.; Meyer, T. J. *Inorg. Chem.* **2004**, *44*, 6802–6827.
4. (a) Gust, D.; Moore, T. A.; Moore, A. L. *Acc. Chem. Res.* **2001**, *34*, 40–48. (b) Gust, D.; Moore, T. A.; Moore, A. L. *Acc. Chem. Res.* **2009**, *42*, 1890–1898.

5. Langa, F.; Nierengarten, J.-F. (Eds.). *Fullerenes: Principles and Applications*; RSC Nanoscience and Nanotechnology Series, **2007**.
6. Guldi, D. M. *Phys. Chem. Chem. Phys.* **2007**, *9*, 1400–1420.
7. Fukuzumi, S.; Ohkubo, K.; Imahori, H.; Guldi, D. M. *Chem.–Eur. J.* **2003**, *9*, 1585–1593.
8. Kobori, Y.; Yamauchi, S.; Akiyama, K.; Tero-Kubota, S.; Imahori, H.; Fukuzumi, S.; No, J. R. *Proc. Nat. Acad. Sci.* **2005**, *102*, 10017–10022.
9. Imahori, H.; Tamaki, K.; Guldi, D. M.; Luo, C.; Fujitsuka, M.; Ito, O.; Sakata, Y.; Fukuzumi, S. *J. Am. Chem. Soc.* **2001**, *123*, 2607–2617.
10. Guldi, D. M.; Imahori, H.; Tamaki, K.; Kasiwagi, Y.; Yamada, H.; Sakata, Y.; Fukuzumi, S. *J. Phys. Chem. A* **2004**, *108*, 541–548.
11. Imahori, H.; Sekiguchi, Y.; Kashiwagi, Y.; Sato, T.; Araki, Y.; Ito, O.; Yamada, H.; Fukuzumi, S. *Chem.–Eur. J.* **2004**, *10*, 3184–3196.
12. Saha, S.; Johansson, E.; Flood, A. H.; Tseng, H.-R.; Zink, J. I.; Stoddardt, J. F. *Chem.–Eur. J.* **2005**, *11*, 6846–6858.
13. Guldi, D. M. *Chem. Soc. Rev.* **2002**, *31*, 22–36.
14. (a) Balbinot, D.; Atalick, S.; Guldi, D. M.; Hatzimarinaki, M.; Hirsch, A.; Jux, N. *J. Phys. Chem. B* **2003**, *107*, 13273–13279. (b) Guldi, D. M.; Prato, M. *Chem. Comm.* **2004**, 2517–2525.
15. Wessendorf, F.; Gnichwitz, J.-F.; Sarova, G. H.; Hager, K.; Hartnagel, U.; Guldi, D. M.; Hirsch, A. *J. Am. Chem. Soc.* **2007**, *129*, 16057–16071.
16. (a) Wilson, S. R.; MacMahon, S.; Tat, F.; Jarowski, P. D.; Schuster, D. I. *Chem. Comm.* **2003**, 226–227. (b) D'Souza, F.; Gadde, S.; Zandler, M. E.; Arkady, K.; El-Khouly, M. E.; Fujitsuka, M.; Ito, O. *J. Phys. Chem. A* **2002**, *106*, 12393–12404. (c) El-Khouly, M. E.; Ito, O.; Smith, P. M. D'Souza, F. *J. Photochem. Photobiol. C* **2004**, *5*, 79–104. (d) D'Souza, F.; Ito, O. *Coord. Chem. Rev.* **2005**, *249*, 1410–1422. (e) D'Souza, F.; Chitta, R.; Gadde, S.; Islam, D.-M.; Shafiqul, S.; Schumacher, A. L.; Zandler, M. E.; Araki, Y.; Ito, O. *J. Phys. Chem. B* **2006**, *110*, 25240–25250. (f) Schmittel, M.; Kishore, R. S. K.; Bats, J. W. *Org. Biomol. Chem.* **2007**, *5*, 78–86.
17. Boyd, P. D. W.; Reed, C. A. *Acc. Chem. Res.* **2005**, *38*, 235–242.
18. Boyd, P. D. W.; Hodgson, M. C.; Chaker, L.; Rickard, C. E. F.; Oliver, A. G.; Brothers, P. J.; Bolskar, R.; Tham, F. S.; Reed, C. A. *J. Am. Chem. Soc.* **1999**, *121*, 10487–10495.
19. Olmstead, M. M.; Costa, D. A.; Maitra, K.; Noll, B. C.; Phillips, S. L.; Van Calcar, P. M.; Balch, A. L. *J. Am. Chem. Soc.* **1999**, *121*, 7090–7097.
20. Konarev, D. V.; Neretin, I. S.; Slovokhotov, Y. L.; Yudanov, E. I.; Drichko, N. V.; Shul'ga, Y. M.; Tarasov, B. P.; Gumanov, K. L.; Batsanov, A. S.; Howard, J. A. K.; Lyubovskaya, R. N. *Chem.–Eur. J.* **2001**, *7*, 2605–2616.
21. Sun, D.; Tham, F. S.; Reed, C. A.; Chaker, L.; Burgess, M.; Boyd, P. D. W. *J. Am. Chem. Soc.* **2000**, *122*, 10705–10705.
22. Sun, D.; Tham, F. S.; Reed, C. A.; Chaker, L.; Boyd, P. D. W. *J. Am. Chem. Soc.* **2002**, *124*, 6604–6612.
23. (a) Tashiro, K.; Aida, T. *Chem. Soc. Rev.* **2007**, *36*, 189–197. (b) Zheng, J.-Y.; Tashiro, K.; Hirabayashi, Y.; Kinbara, K.; Saigo, K.; Aida, T.; Sakamoto, S.; Yamaguchi, K.; *Angew. Chem. Int. Ed.* **2001**, *40*, 1857.
24. Nobukuni, H.; Shimazaki, Y.; Tani, F.; Naruta, Y. *Angew. Chem. Int. Ed.* **2007**, *46*, 8975–8978.

25. Sun, D.; Tham, F. S.; Reed, C. A.; Boyd, P. D. W. *Proc. Nat. Acad. Sci.* **2002**, *99*, 5088–5092.
26. (a) Imahori, H. *J. Mat. Chem.* **2007**, *17*, 31–41. (b) Imahori, H.; Ueda, M.; Kang, S.; Hayashi, H.; Hayashi, S.; Kaji, H.; Seki, S.; Saeki, A.; Tagawa, S.; Umeyama, T.; Matano, Y.; Yoshida, K.; Isoda, S.; Shiro, M.; Tkachenko, N. V.; Lemmetyinen, H. *Chem.–Eur. J.* **2007**, *13*, 10182–10193. (c) Hasobe, H. T.; Saito, K.; Kamat, P. V.; Troiani, V.; Qiu, H.; Solladie, N.; Kim, K. S.; Park, J. K.; Kim, D.; D’Souza, F.; Fukuzumi, S. *J. Mat. Chem.* **2007**, *17*, 4160–4170.
27. (a) Shoji, Y.; Tashiro, K.; Aida, T. *J. Am. Chem. Soc.* **2010**, *132*, 5928. (b) Shoji, Y.; Tashiro, K.; Aida, T. *J. Am. Chem. Soc.* **2004**, *126*, 6570.
28. Wu, Z.-Q.; Shao, X.-B.; Li, C.; Hou, J.-L.; Wang, K.; Jiang, X.-K.; Li, Z.-T. *J. Am. Chem. Soc.* **2005**, *127*, 17460.
29. Dudic, M.; Lhotak, P.; Stibor, I.; Petrickova, H.; Lang, K. *New J. Chem.* **2004**, *28*, 85–89.
30. Hosseini, A.; Taylor, S.; Accorsi, G.; Armaroli, N.; Reed, C. A.; Boyd, P. D. W. *J. Am. Chem. Soc.* **2006**, *128*, 15903–15913.
31. (a) Schmittl, M.; He, B.; Bice, Prasenjit, M. *Org. Lett.* **2008**, *10*, 2513. (b) Tong, L. H.; Wietor, J.-L.; Clegg, W.; Raithby, P. R.; Pascu, S. I.; Sanders, J. K. M. *Chem.–Eur. J.* **2008**, *14*, 3035. (c) Marois, J.-S.; Cantin, K.; Desmarais, A.; Morin, J. F. *Org. Lett.* **2008**, *10*, 33.
32. (a) Tashiro, K.; Hirabayashi, Y.; Aida, T.; Saigo, K.; Fujiwara, K.; Komatsu, K.; Sakamoto, S.; Yamaguchi, K. *J. Am. Chem. Soc.* **2002**, *124*, 12086. (b) Yanagisawa, M.; Tashiro, K.; Yamasaki, M.; Aida, T. *J. Am. Chem. Soc.* **2007**, *129*, 11912. (c) Ouchi, A.; Tashiro, K.; Yamaguchi, K.; Tsuchiya, T.; Akasaka, T.; Aida, T. *Angew. Chem. Int. Ed.* **2006**, *45*, 3542.
33. Schuster, D. I.; Jarowski, P. D.; Kirschner, A. N.; Wilson, S. R. *J. Mater. Chem.* **2002**, *12*, 2041.
34. (a) Wang, J. B.; Lin, Z. Y. *J. Am. Chem. Soc.* **2003**, *125*, 6072. (b) Shepard, M. J.; Paddon-Row, M. N. *J. Por. Phthal.* **2002**, *6*, 783.
35. (a) Liao, M.-S.; Watts, J. D.; Huang, M.-J. *J. Phys. Chem. B* **2007**, *111*, 4374. (b) Liao, M. S.; Watts, J. D.; Huang, M. J. *Phys. Chem. Phys. Chem.* **2009**, *11*, 4365. (c) Liao, M.-S.; Watts, J. D.; Huang, M. J. *Phys. Chem. Phys. Chem.* **2009**, *11*, 6072.
36. Jung, Y.; Head-Gordon, M. *Phys. Chem. Phys. Chem.* **2006**, *8*, 2831–2840.
37. Grimme, S. *J. Comp. Chem.* **2004**, *25*, 1463.
38. (a) te Velde, G.; Bickelhaupt, F. M.; van Gisbergen, S. J. A.; Fonseca-Guerra, C.; Baerends, E. J.; Snijders, J. G.; Ziegler, T. *J. Comput. Chem.* **2001**, *22*, 931. (b) ADF 2009.01, SCM, Vrije Universiteit Amsterdam, The Netherlands. <http://www.scm.com>.
39. Crystal data for $\text{H}_2\text{T(OMe)}_3\text{PP.2C}_{60}\text{.2toluene}$, purple block, empirical formula, $\text{C}_{95}\text{H}_{27}\text{N}_2\text{O}_6$, fw 1292.19, T 87 K, monoclinic, $P2_1/n$, $a = 13.9603(2) \text{ \AA}$, $b = 17.4971(2) \text{ \AA}$, $c = 23.2376(2) \text{ \AA}$, $\alpha = 90^\circ$, $\beta = 93.3380(10)^\circ$, $\gamma = 90^\circ$, $V = 5666.50(11) \text{ \AA}^3$, $Z = 4$, $D_c = 1.515 \text{ Mg/m}^3$, $\mu = 0.095 \text{ mm}^{-1}$, $F(000) = 2636$, crystal size $0.34 \times 0.30 \times 0.24 \text{ mm}^3$, $\Theta_{\text{max}} = 25.8^\circ$, index ranges $-17 \leq h \leq 15$, $-21 \leq k \leq 21$, $-28 \leq l \leq 28$, reflections collected = 49767, independent reflections = 10812, data/restraints/parameters 10812/2688/1148. There is a disordered C_{60} molecule (disordered site occupancy ratio 60.5%/39.5%) and a disordered toluene molecule (disordered site occupancy ratio 50%/50%). Full matrix least-squares refinement on F^2 was carried out to give R indices $[I > 2\sigma(I)]$, $R1 = 0.0898$, $wR2 = 0.1962$ and $\text{GOF} = 1.108$.

40. Crystal data for **ZnT(OMe)₃PP.0.5C₆₀.3toluene**, purple needle, empirical formula, C₁₀₇H₆₈O₁ N₄Zn, fw 1667.02, T 87 K, orthorhombic Pcan, a = 18.8546(3) Å, b = 28.1962(3) Å, c = 30.1102(3) Å, α = 90°, β = 90°, γ = 90°, V = 16007.4(3) Å³, Z = 8, D_c = 1.383 Mg/m³, μ = 0.342 mm⁻¹, F(000) = 6912, crystal size 0.34 × 0.32 × 0.18 mm³, Θ_{max} = 25.1°, index ranges -22 ≤ h ≤ 19, -26 ≤ k ≤ 33, -35 ≤ l ≤ 29 reflections collected = 79391, independent reflections = 14200, Data/restraints/parameters 14200/3283/1414. All non hydrogen atoms were identified after isotropic refinement of the initial solution. The disordered fullerene moieties were initially refined using rigid group refinement. The H-atoms were included in the refinement in calculated positions riding on the atoms to which they were attached. There is a disordered C₆₀ molecule (disordered site occupancy ratio 50.0%/50.0%) and a disordered toluene molecule (disordered site occupancy ratio 50%/50%). SIMU and DELU restraints were applied to the atomic displacement parameter of all atoms. Full matrix least-squares refinement on F² was carried out to give R indices [I > 2σ(I)], R1 = 0.1136, wR2 = 0.2174 and GOF = 1.079.
41. Crystal data for **CoT(OMe)₃PP.C₆₀.1.5toluene**, purple block, empirical formula, C_{68.5}H_{37.50}Co_{0.50}N₂O₆, fw 1013.67, T 87 K, monoclinic, C2/c, a = 16.4166(3) Å, b = 25.2913(5) Å, c = 23.7733(2) Å, α = 90°, β = 108.404(1)°, γ = 90°, V = 9365.76(33) Å³, Z = 8, D_c = 1.438 Mg/m³, μ = 0.261 mm⁻¹, F(000) = 4191.4, Crystal 0.30 × 0.18 × 0.18 mm³, Θ_{max} = 26.3°, Index ranges -20 ≤ h ≤ 16, -27 ≤ k ≤ 31, -29 ≤ l ≤ 29, Reflections collected = 26178, Independent reflections = 9408, Data/restraints/parameters 9408/153/763. All non hydrogen atoms were identified after isotropic refinement of the initial solution. The H-atoms were included in the refinement in calculated positions riding on the atoms to which they were attached. There was a disordered C₆₀ molecule (disordered site occupancy ratio 50.0%/50.0%). Full matrix least-squares refinement on F² was carried out to give R indices [I > 2σ(I)], R1 = 0.1126, wR2 = 0.2392 and GOF = 1.042.
42. Ishii, T.; Kanehama, R.; Aizawa, N.; Yamashita, M.; Matsuzaka, H.; Sugiura, K.; Miyasaka, H.; Kodama, T.; Kikuchi, K.; Ikemoto, I.; Tanaka, H.; Marumoto, K.; Kurodo, S.-I. *J. Chem. Soc. Dalton Trans.* **2001**, 2975–2980.
43. Crystal data for **CoT(OMe)₃PP.C₇₀.CHCl₃.1.5toluene**, purple block, empirical formula, C_{137.50}H₆₀Cl₃CoN₄O₁₂, fw 2125.18, T 87 K, Triclinic, P -1, a = 15.4250(2) Å, b = 16.4151(2) Å, c = 18.9281(1) Å, α = 105.151(1)°, β = 98.321(1)°, γ = 94.312 (1)°, Volume = 4545.20(8) Å³, Z = 2, D_c = 1.553 Mg/m³, μ = 0.358 mm⁻¹, F(000) = 2174, Crystal 0.34 × 0.24 × 0.22 mm³, Θ_{max} = 25.69°, index ranges -18 ≤ h ≤ 18, -19 ≤ k ≤ 20, -22 ≤ l ≤ 23, reflections collected = 41194, independent reflections = 17088, data/restraints/parameters 17088/2754/2095. C₇₀ molecules (disordered site occupancy ratio 53.7%/46.3%), a disordered chloroform molecule (disordered site occupancy ratio 72.9%/27.1%), and a disordered toluene molecule (disordered site occupancy ratio 50%/50%). Full least-squares refinement on F² was carried out to give R indices [I > 2σ(I)], R1 = 0.0480, wR2 = 0.1269 and GOF = 1.035.
44. (a) Ozarowski, A.; Lee, H. M.; Balch, A. L. *J. Am. Chem. Soc.* **2003**, 125, 12606–12614.
(b) Dannhauser, J.; Donaubaue, W.; Hampel, F.; Reiher, M.; Le Guennic, B.; Corzilius, B.; Dinse, K.-P.; Hirsch, A. *Angew. Chem. Int. Ed.* **2006**, 45, 3368–3372.
45. Sutton, L. R.; Scheloske, M.; Pirner, K. S.; Hirsch, A.; Guldi, D. M.; Gisselbrecht, J.-P. *J. Am. Chem. Soc.* **2004**, 126, 10370–10381.

Chapter 12

Supramolecular Hosts for Pristine Fullerenes

*Paris E. Georghiou**

*Department of Chemistry, Memorial University of Newfoundland,
St. John's, Newfoundland and Labrador, Canada*

1. Introduction	391
2. Complexation in Organic Solutions	392
2.1. General considerations	392
2.2. Calixarene-type hosts	393
2.3. Porphyrin-containing hosts	395
2.4. Tetrathiafulvalene-containing hosts	397
2.5. Some other hosts	399
3. Conclusions	402
References	402

1. Introduction

Since the report of the discovery of “C₆₀: Buckminsterfullerene” in 1985 by Kroto, Heath, O’Brien, Curl and Smalley in their famous *Nature* paper,¹ which resulted from their attempt to account for “*the mechanism by which long-chain molecules are formed in interstellar space.*”,¹ its wonderfully symmetrical structure has continued to capture the imagination and interest of many scientists. This is not surprising for many scientific reasons, but also because over the millennia humans have been particularly fascinated with spheres, and more recently, with its rather larger analogue, the football or “soccerball”. This of course can be judged by the global (no pun intended!)

*Corresponding author. Email: parisg@mun.ca

interest in the game in which just such a spherical object is employed and watched by millions of humans. The soccerball also piqued E. Osawa's imagination and led him to discover that carbon in such a structure would be aromatic and hence likely to be stable.² In fact, to underscore this analogy further, C_{60} was referred to as "footballene", in some other early publications.³

A recent *SciFinder* search using the search term "Fullerene C_{60} " revealed a dramatic increase from that solitary 1985 *Nature* paper to, starting in 1992, approximately 1,000 papers per year, reaching a peak of around 1,600 in 1996, and since then to between 1,150 to 1,500 papers a year. Many of these papers describe a plethora of novel and highly functional derivatives of C_{60} . The number of papers specifically dealing with supramolecular complexation⁴ of "pristine" or un-derivatized C_{60} however is much smaller, and is the subject of this review. There have been excellent recent reviews on this topic published elsewhere. Complexation of C_{60} with calixarenes, which were among the earliest of the host molecules shown to be capable of extracting C_{60} into an aqueous phase by Williams and Verhoeven in 1992,⁵ and also as first shown by Atwood⁶ and coincidentally Shinkai⁷ to be capable of purifying C_{60} from a mixture of C_{60} and C_{70} in fullerite, was reviewed in excellent detail in 2001.⁸ A special *Tetrahedron* issue devoted to supramolecular chemistry of fullerenes in general appeared in 2006.⁹ A very recent particularly insightful contribution by Perez and Martin published in 2008 addressed the aspect of concave-convex complementarity between C_{60} and various host receptors.¹⁰ In that review the authors detailed many considerations which need to be considered for constructing efficient receptors for C_{60} .

The present review will attempt to review contributions on supramolecular complexation in particular with non-derivatized or "pristine" C_{60} which have been reported by various groups and which have not been covered by the previous reviews cited above. The review may not be exhaustive and may perhaps inadvertently reflect this author's bias. While many of these studies also examined the binding selectivity for C_{60} over C_{70} in many cases only the specific data for the binding constants with C_{60} will be presented herein. As well, there have been many solid-state complexes whose single-crystal X-ray structures have been published and while these are exciting and important they are outside the scope of this review, except for a few isolated examples which are presented.

2. Complexation in Organic Solutions

2.1. General considerations

There have been numerous studies involving solution complexation studies of pristine C_{60} with various host molecules and these most commonly have been

conducted by absorption spectroscopic (UV-vis), emission (fluorescence quenching) and/or NMR methods. While such solution complexation studies can yield valuable information in the form of association constants (K_{Assoc}) about the strength of the supramolecular host–guest interactions, there are particular concerns which should be noted when relying on UV-vis data alone. Our own work in this area addressed various aspects of this issue¹¹ and the reader should be reminded that C_{60} itself is capable of supramolecular self-assembly in solution: C_{60} is known to aggregate in CS_2 and as was pointed out earlier by Atwood¹² aggregation may compete with host–guest complexation and the magnitude of the apparent binding constant will be governed by the equilibrium constant of aggregation as well as by the K_{Assoc} values being determined for the putative host–guest complexation. Also, as pointed out by Pérez and Martín, and others, Stern–Volmer constants used in fluorescence-based determinations are not direct measures of binding constants since they depend on the mechanism of quenching.^{10,13} Finally, it should be noted, solution complexation behavior is also strongly solvent-dependent and also solvent solubility-limiting.

2.2. Calixarene-type hosts

The cavities of calixarenes and their many analogues and derivatives⁸ and also those of the related molecules such as cyclotrimeratrylene (CTV), resorcarenes and cyclodextrins have had obvious potential for forming “ball and socket” and/or “capsule-like”⁸ shape complementarity for forming supramolecular complexes with C_{60} and C_{70} .

Bhattacharya's group has reported binding studies of “classical” calixarenes and most recently, of *p-tert*-butylcalix[5]- and [6]arenes, **1**¹⁴ and **2**,¹⁵ respectively, with C_{60} in toluene. (Figure 1) On the basis of their analyses of their presumed charge-transfer (CT) absorption peaks noted in the UV-vis spectra derived from titration experiments and Benesi–Hildebrand analyses, they concluded that 1:1 complexes were formed with both fullerenes examined. They reported K_{Assoc} values in toluene solution of 23,600 for C_{60} (no error limits stated) with **1**; and $32,400 \pm 432 \text{ M}^{-1}$ for C_{60} with **2**, respectively. These values are considerably higher than what has been reported by others for similar calixarene: C_{60} binding studies.¹⁶ These authors also reported that in general, based upon their analysis, stronger binding constants were observed for C_{70} *i.e.* $94,460 \text{ M}^{-1}$ for C_{70} with **1**; and $110,000 \pm 5700 \text{ M}^{-1}$ for C_{70} with **2**, respectively. In the case of **2**, ¹H-NMR was also used, but only in a qualitative experiment, with no titrations being reported that would be comparable with their UV-vis studies (see discussion in Ref. 11 on the relevance for such comparisons).

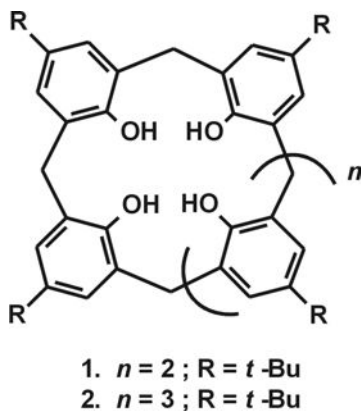


Figure 1. General structure of calix[5]arene (**1**) and calix[6]arene (**2**).

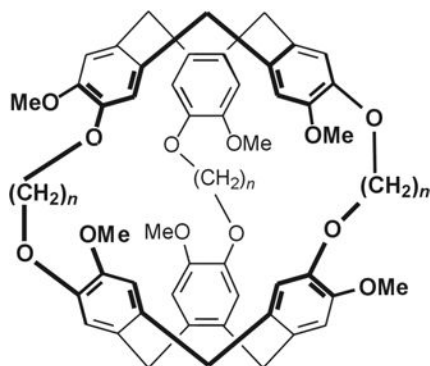


Figure 2. General structure of cryptophanes A (**3**; $n = 2$) and E (**4**; $n = 3$).

By way of contrast also with Bhattacharya’s findings and interpretations, Dong and Choi’s group reported a study on the CT and contact charge transfer (CCT) behavior¹⁷ between C₆₀ and the CTV-based cryptophanes **3** and **4** (Figure 2). These authors used a combination of absorption, fluorescence and ¹H NMR spectroscopy in order to ascertain whether supramolecular inclusion complexes are formed. They concluded that since no new absorption bands in the absorption spectra were formed, nor could any temperature-dependent equilibria be observed, that the CCT observed, was due to collisions between the electron-donor cryptophanes and the electron-acceptor C₆₀ in agreement with Berberan–Santos’ conclusions,^{18,11} and not as a result of any host–guest encapsulation.

de Mendoza's group has developed a CTV-2-ureido-4-[1*H*]-pyrimidone host **5** (Figure 3) which was shown to be capable of selectively encapsulating

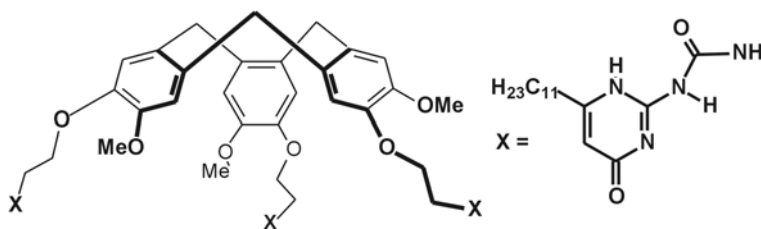


Figure 3. Structure of CTV-2-ureido-4-[1H]-pyrimidone (**5**).

C_{70} in preference to C_{60} , in THF solution, by an order of magnitude (based upon a 1:1 binding model). This preference is due to the formation of a dimeric capsule which can be used to purify C_{70} from fullerite and fullerene mixtures by a subsequent reversible decomplexation.¹⁹ This host was shown, as predicted, to be able to also selectively bind C_{84} by another order of magnitude over C_{70} .²⁰

Among recent novel calixarene-like hosts for C_{60} which have been synthesized, Wang and coworkers²¹ reported the synthesis of a series of *N,O*-bridged calix[1]arene[4]pyridines **6–9** which show much higher binding constant values with C_{60} than the “classical” calixarenes or homooxacalixarenes. These new compounds are the first species which contain an odd-number of rings with two different heteroatom bridges and two different aromatic components. The compounds all formed 1:1 complexes with C_{60} with K_{Assoc} values as determined by fluorescence titrations which ranged from $35,113 \pm 106$ for **6** to as high as $49,494 \pm 1,581 \text{ M}^{-1}$ for **9**. Previously,²² using similar fluorescence quenching titrations the same group showed that azacalix[5]-, azacalix[8]- and azacalix[10]pyridines **10–12** also formed 1:1 complexes with C_{60} with K_{Assoc} values $2.6 \times 10^5 \pm 0.01 \times 10^5$, $4.6 \times 10^5 \pm 0.02 \times 10^5$ and $3.0 \times 10^5 \pm 0.008 \times 10^5$ (Figure 4).

2.3. Porphyrin-containing hosts

Despite the fact that they do not have obvious shape complementarity of being concave hosts to the convex C_{60} or C_{70} or other fullerenes, porphyrins and metalloporphyrins are well-known to be very effective fullerene hosts.^{10,23} There is intense interest in such hosts since they are electron-rich and they can be used as biomimetic photosensitizing electron-donors, being capable of absorbing light in the visible-to-near IR region, and have favorable redox potentials.²⁴ The supramolecular binding of porphyrin hybrids to the electron-acceptor fullerenes is of on-going interest and is addressed more fully elsewhere in this volume. The binding ability of these types of hosts to C_{60} ,

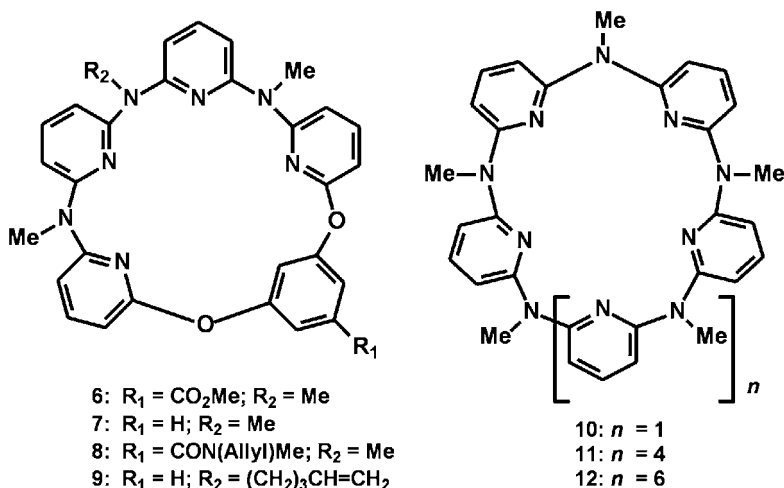


Figure 4. Structures of Wang and coworkers' compounds 6–12.

for example, can be orders of magnitude higher (*e.g.* $K_{\text{Assoc}} = 1.8 \times 10^8 \text{ M}^{-1}$ in dichlorobenzene has been reported by Aida's group for a *bis*-porphyrin²⁵), than what have been determined with most of the other macrocyclic cavity-containing hosts examined thus far, with the exception of some recent TTF-hybrid hosts which will be described in the following section.

Some new recent porphyrin-calixarene conjugates were recently reported by Lhoták and coworkers who produced molecular tweezers based upon combining four porphyrin molecules onto wide-rim Schiff base-containing scaffolds of tetra-*O*-propoxy-calix[4]- and thiacalix[4]arenes **13** and **14** which are in *1,3-alternate* conformations²⁶ (Figure 5).

They determined binding constants of between $2.0 - 6.0 \times 10^3 \text{ M}^{-1}$ in benzene and/or toluene solutions for 1:1 C_{60} complexation with these new hosts, including their corresponding reduced Schiff base-imine derivatives **13a**, **14a** using UV-vis and ^1H NMR spectroscopy. In general, slightly higher binding was observed for the calix[4]arene-based rather than the thiacalixarene-based compounds. Relatively higher $\text{C}_{70}:\text{C}_{60}$ binding selectivities were also observed for the unreduced imine-containing hosts. An analogous molecular tweezer **15** consisting of *tert*-butyl group-bearing zinc-porphyrins in the *1,3-alternate* positions of a oxacalix[2]arene[2]pyrimidine²⁷ scaffold, was found to be highly selective for C_{70} ($K_{\text{Assoc}} = 3.0 \times 10^4 \text{ M}^{-1}$ in benzene- d_6) with little, or no, supramolecular complexation with C_{60} being detected. The NMR data for these conjugates clearly show that as would be expected, the binding of the fullerenes are to the porphyrin moieties (Figure 6).

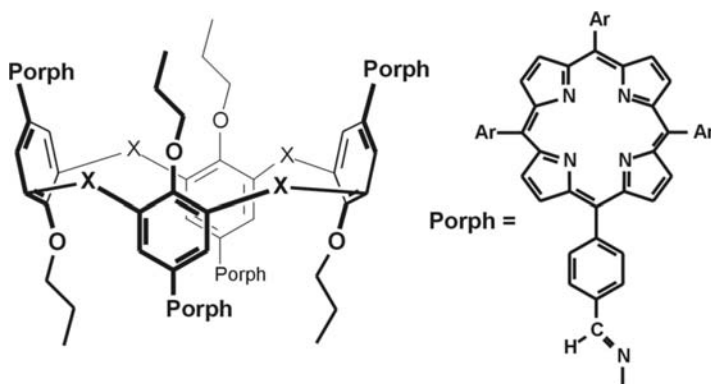


Figure 5. Porphyrin-calixarene conjugates **13** ($\text{X}=\text{CH}_2$) and **14** ($\text{X}=\text{S}$).

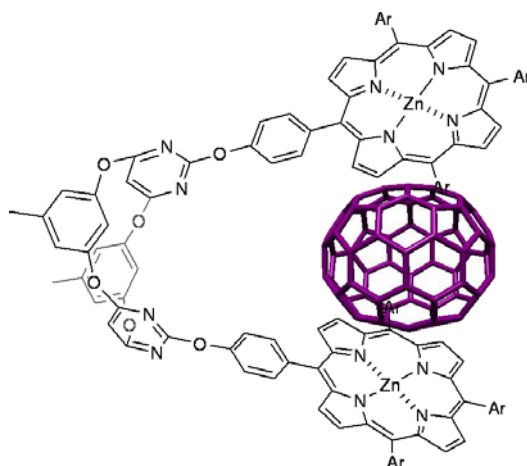


Figure 6. C_{70} -selective bis(Zn-porphyrin) tweezer **15**, Ar = *t*-Bu (not an X-ray structure). Reproduced from Reference 27 with permission of Elsevier, 2010.

A creative [3]rotaxane-porphyrin conjugate, built onto the rotaxane scaffold was reported by the Morin group.²⁸ This molecular tweezer variant showed K_{Assoc} values of 4.6×10^3 in toluene for 1:1 binding with C_{60} and 1.0×10^4 with C_{70} as determined by UV-vis spectroscopy. Although these values are similar to those seen with simpler calixarene-porphyrin conjugates, this work nevertheless presents a novel paradigm.

2.4. Tetrathiafulvalene-containing hosts

The strong electron-donor capability of the π -extended tetrathiafulvalene (TTF) analogue 2-[9-(1,3-dithiol-2-ylidene)anthracen-10(9H)-ylidene]-1,3-dithiole

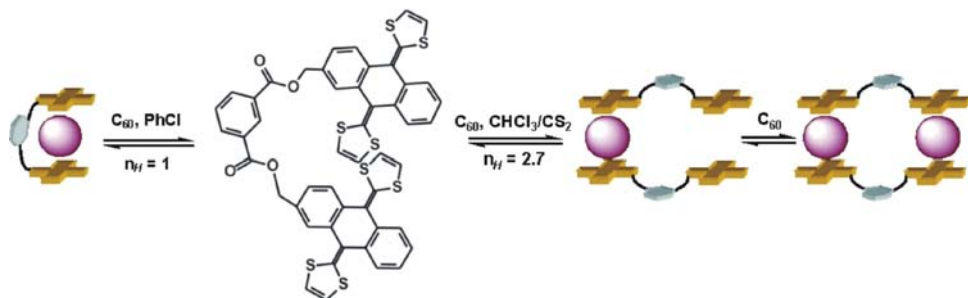


Figure 7. Proposed mechanism of C_{60} complexation with **16** by Martín and coworkers. Reproduced from Reference 29 with permission of American Chemical Society, 2006.

(“exTTF”), was employed for the first time by Martín and coworkers in a molecular tweezer. This tweezer is analogous to those employing porphyrins but with a difference being that exTTF has a distorted curved shape.^{10,29} In that seminal 2006 report, two exTTF arms of the molecular tweezer are joined to a central isophthaloyl fulcrum/spacer to form **16**. Different modes of binding to C_{60} were observed in different solvents: in chlorobenzene, C_{60} binds to **16** in a 1:1 fashion with a $K_{\text{Assoc}} = 2.98 \pm 0.12 \times 10^3 \text{ M}^{-1}$. In $\text{CHCl}_3/\text{CS}_2$ however, a sigmoidal curve from the titration experiment is observed, indicative of a positive “homotropic cooperative effect” with an apparent binding constant of $3.56 \pm 0.16 \times 10^3 \text{ M}^{-1}$. Titrations in both cases showed clear unambiguous isosbestic points; in chlorobenzene it is at $\lambda = 483 \text{ nm}$ and in $\text{CHCl}_3/\text{CS}_2$ it is at $\lambda = 451 \text{ nm}$, both the isosbestic points and the respective Jobs plots analyses implying apparent 1:1 binding. The sigmoidal curve in the $\text{CHCl}_3/\text{CS}_2$ however, was further analyzed and interpreted to be consistent with the formation of a tetrameric structure in which two C_{60} molecules are sandwiched between two molecules of **16** and which is facilitated by the formation of the initial 1:1 complex. A follow-up study employed ^1H NMR titrations to compare the binding constants of **16** with C_{60} with some analogous non-exTTF based receptors affirmed the importance of the receptor- C_{60} concave-convex complementarity.³⁰

Based upon these findings Martín’s group has produced two new highly effective exTTF-containing hosts. One of these, **17**, is a macrocycle, which is formed by tethering two exTTF molecules at two positions on each exTTF.³¹ The final macrocyclic ring-closing step was achieved *via* a RCM using a Grubb’s catalyst to afford a product that was an inseparable mixture of *E* and *Z* (Figure 8) and which was used as such. A strong CT band is formed upon titration with the C_{60} in chlorobenzene and as was seen with **16**, an isosbestic point is formed, at $\lambda = 451 \text{ nm}$. A 1:1 binding stoichiometry was confirmed in the usual manner and a $\log K_{\text{Assoc}}$ value of 6.5 ± 0.5 to 6.1 ± 0.2

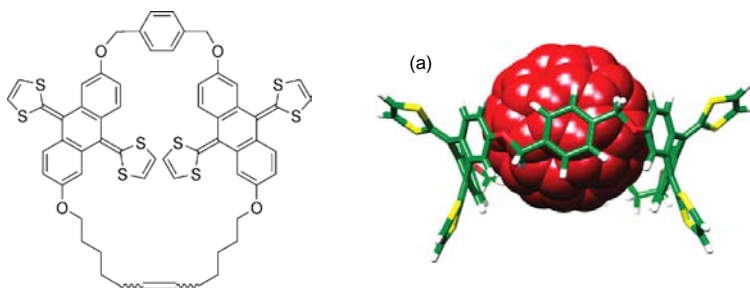


Figure 8. Macrocycle **17** containing two tethered exTTFs moieties and (a) computer-generated image of putative **17**:C₆₀ complex. Reproduced from Reference 31 with permission of American Chemical Society, 2010.

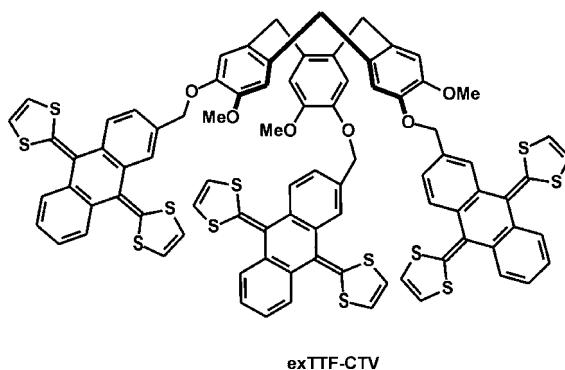


Figure 9. Structure of the tripodal CTV-exTTF host **18**. Reproduced from Reference 32 with permission of American Chemical Society, 2010.

was determined, representing a three-orders of magnitude increase over that measured with **16**. With this host, $\log K_{\text{Assoc}}$ was estimated to be 8.4 ± 0.2 .

The tripodal CTV-exTTF host **18** had $\log K_{\text{Assoc}}$ values of 5.3 ± 0.2 with C₆₀ and 6.3 ± 0.6 for C₇₀ chlorobenzene, values which are similar to those seen for **17**.³² These values are higher than most binding constants that have been observed with other hosts and C₆₀ with the exception of Aida's Rh(III)³³- and Ir(III)-metalloprophyrin²⁵ based hosts. However as noted by the authors, the inherent chirality of the CTV scaffold holds promise for enantioselective discrimination of the *D*₂ isomers of C₇₆ and C₈₄.³²

2.5. Some other hosts

In their 2008 review, Perez and Martin¹⁰ described some other concave receptors such as those that are corannulene ring-based,³⁴ and others that are cyclic [*n*]para-phenylacetylenes.³⁵ Since these show only relatively modest

($\sim 1 - 3 \times 10^3 \text{ M}^{-1}$) binding constants with C_{60} or C_{70} and no new developments have been reported since the Perez and Martin review was published, they will not be discussed any further here.

Among the few new “socket”-type of receptors are those based upon a C_{3v} -symmetrical tribenzotriquinacene (“TBTQ”) *e.g.* **19** scaffold. Vokmer³⁶ described two elaborately constructed and highly rigid TBTQ-derived hosts which were capable of binding C_{60} . Their complexation experiments were conducted using UV-vis and ^1H NMR spectroscopy using a 1:1 mixture of CS_2 and chloroform- d_1 and considered 1:1 and 1:2 binding between guest and host. Reasonable agreement between the data using the two methods was obtained. UV-vis titrations gave $K_1 = 2908 \pm 360$ and $K_2 = 2076 \pm 300$ for C_{60} with one of the hosts, and $K_1 = 5608 \pm 220$ and $K_2 = 673 \pm 160$ with the other. The ^1H NMR titrations gave, using the same hosts $K_1 = 2351 \pm 750$ and $K_2 = 1819 \pm 860$ values and $K_1 = 5328 \pm 580$ and $K_2 = 1376 \pm 260$ values, respectively. An X-ray structure for a $\text{C}_{60}:\text{host}:(\text{toluene})_3$ complex was also reported.

The C_{3v} -symmetrical *tris*(thianthreno)-TBTQ **20**, (Figure 10) by analogy with the C_{5v} -symmetrical corannulene “fly trap”^{34a} was also capable of weak 1:1 binding with C_{60} in benzene- d_6 ($K_{\text{Assoc}} = 977 \pm 56$) and in toluene- d_8 ($K_{\text{Assoc}} = 497 \pm 37$) but also failed to reveal any complexation in CS_2 .³⁷ For C_{70} in benzene- d_6 $K_{\text{Assoc}} = 463 \pm 49$ and in toluene- d_8 $K_{\text{Assoc}} = 233 \pm 42$ values were determined, a reversal, albeit relatively small, in the $\text{C}_{60}/\text{C}_{70}$ selectivity usually seen with most of the other hosts reviewed. Single-crystal X-ray structures of $(\text{C}_{60})_2:\mathbf{20}:(\text{PhCl})_{2.5}$ complex and also of $\text{C}_{60}:\mathbf{19a}:(\text{toluene})$ were obtained. Hexabromo-“methyl hat” **19a** is a precursor to **20**.³⁷ Notably, no solution complexation between either C_{60} or C_{70} and **19a** could be

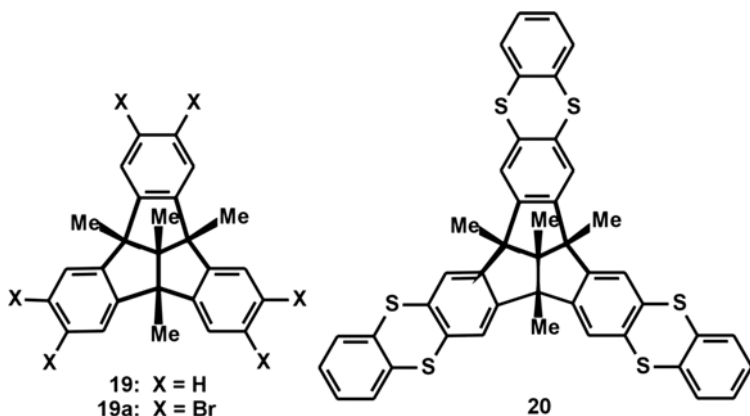


Figure 10. Structures of tribenzoquinocenes **19**–**20**.

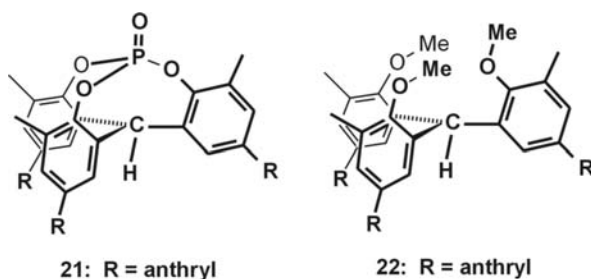


Figure 11. Structures of Kobayashi's triarylphosphate **21** and precursor **22**.

detected. Similar phenomena have been reported by others who have characterized solid inclusion complexes formed with C_{60} and other hosts, for which no solution complexation was observed.

Kobayashi and coworkers recently reported the synthesis of **21** a *p*-substituted triarylphosphate (Figure 11) which was shown to be a new C_3 -symmetric host for C_{60} .³⁸ The binding constant, $K_{\text{Assoc}} = 3.5 \pm 0.2 \times 10^4 \text{ M}^{-1}$ was determined in toluene solution using fluorescence quenching. An earlier report by the same authors using fluorescence quenching showed a lower apparent $K_{\text{Assoc}} = 4.6 \pm 0.2 \times 10^4 \text{ M}^{-1}$ for the trimethoxy precursor **22**.³⁹ The X-ray structure of **22**: C_{60} however showed that the C_{60} was not included within the cavity of this host molecule but instead was included in a side-on mode with C_{60} , due to inter- and intramolecular $C-H \cdots \pi$ interactions, and formed an interesting “..two-dimensional supramolecular sheet with a hexagonal columnar space..”.³⁹ Triarylphosphate **21** was less flexible than **22** and although better preorganized for C_{60} inclusion the authors concluded that **21** was the better host since it was an “induced-fit host” for C_{60} inclusion.

An interesting octa-permethylated β -cyclodextrin (PM β -CD)-porphyrin conjugate has been synthesized by Jayawickramarajah and coworkers, which self-assembles with C_{60} into nm-length one-dimensional water-soluble nanorods.⁴⁰ Evidence for self-assembly consisting of four C_{60} molecules per unit of the (PM β -CD)-porphyrin was deduced by several techniques including FTIR, UV-vis spectroscopy, STM and thermogravimetric analysis. No binding constant determinations however, were reported.

Finally, a recent report from Fujita and coworkers describes a supramolecular inclusion of C_{60} corresponding to a local concentration of 128mM within a self-assembled spherical complex. This complex has a composition of $\text{Pd}_{12}\text{L}_{24}$ and is formed by the addition of the coronene-based ligand “L” with $\text{Pd}(\text{NO}_3)_2$. In effect, C_{60} is “dissolved” within the complex at a much higher concentration than its solubility in *e.g.* 1-chloronaphthalene (71 mM) or toluene (3.9 mM).⁴¹

3. Conclusions

In the few most recent years which are covered in this review many different and creative molecular architectures and approaches have been designed with the aim of forming stable and potentially utilizable supramolecular hosts for pristine C₆₀ in particular and C₇₀. The significant electronic properties of C₆₀ has of course, been a significant driving force. All of these efforts, of course, have built upon the extensive bodies of work and knowledge built up in the preceding years and which have been reviewed elsewhere. These aims have resulted in creative synthetic efforts and have employed challenging analytical methodologies. However despite the fact that the porphyrin-based hosts have had an important role and will continue to do so the advent of the exTTF-based hosts which Martín and coworkers have developed promises to add a new and valuable tool for further developments. It is exciting to contemplate what developments the next 25 years will bring.

References

1. Kroto, H. W.; Heath, J. R.; O'Brien, S. C.; Curl, R. F.; Smalley, R. E. *Nature* **1985**, 318, 162.
2. Osawa, E. *Kagaku* **1970**, 25, 854. In: Smalley, R. E. *Discovering the Fullerenes. Nobel Lecture*, **1996**.
3. Haymet, A. D. J. *J. Am. Chem. Soc.* **1986**, 108, 319.
4. For a very recent detailed overview of binding mechanisms in supramolecular complexes, see: Schneider, H. J. *Angew. Chem. Int. Ed.* **2009**, 48, 3924.
5. Williams, R.; Verhoeven, J. *Rec. Trav. Chim. Pays-Bas.* **1992**, 111, 531.
6. Atwood, J. L.; Koutsantonis, G. A.; Raston C. L. *Nature* **1994**, 368, 229.
7. Suzuki, T.; Nakashima, K.; Shinkai, S. *Chem. Lett.* **1994**, 699.
8. Zhong, Z.-L.; Ikeda, A.; Shinkai, S. In: *Calixarenes 2001*; Kluwer Academic Publishers, Dordrecht, the Netherlands, **2001**, pp. 476–495.
9. *Special issue on Supramolecular Chemistry of Fullerene*; Martín, N.; Nierengarten, J.-F. (Eds.). *Tetrahedron*, **2006**.
10. Pérez, E. M.; Martín, N. *Chem. Soc. Rev.* **2008**, 37, 1512.
11. Georgiou, P. E.; Tran, A. H.; Stroud, S. S.; Thompson, D. W. *Tetrahedron* **2006**, 62, 2036.
12. Atwood, J. L.; Barnes, M. J.; Gardiner, M. G.; Raston, C. L. *Chem. Commun.* **1996**, 1449.
13. For other considerations on using fluorescence spectroscopy for association constant determinations see: Stella, L.; Capodilupo, A. L.; Bietti, M. *Chem. Commun.* **2008**, 39, 4744.
14. Halder, A.; Goswami, D.; Nayak, S. K.; Chattopadhyay, S.; Bhattacharya, S. *J. Mol. Struct.* **2009**, 936, 112.
15. Halder, A.; Nayak, S. K.; Chattopadhyay, S.; Bhattacharya, S. *J. Mol. Liq.* **2010**, 151, 125.
16. For higher binding constants reported with “double-calix[5]arenes” see Haino, T.; Yanase, M.; Fukunaga, M.; Fukazawa, Y. *Tetrahedron*, **2006**, 62, 2025.

17. Zhang, C. H.; Shen, W. L.; Fan, R. Y.; Zhang, G. M.; Shangguan, L. Z.; Chao, J. B.; Shuang, S. M.; Dong, C. A.; Choi, M. M. F.; *Anal. Chim. Acta.* **2009**, *650*, 118.
18. Sarova, G.; Berberan-Santos, M. N. *J. Phys. Chem. B.* **2004**, *108*, 17261–17268.
19. Huerta, E.; Metselaar, G. A.; Fragosó, A.; Santos, E.; Bo, C.; de Mendoza, J. *Angew. Chem. Int. Ed.* **2007**, *46*, 202.
20. Huerta, E.; Cequier, E.; de Mendoza, J. *Chem. Commun.* **2007**, 5016.
21. Wu, J.-C.; Wang, D.-X.; Huang, Z.-T.; Wang, M.-X. *Tetrahedron Lett.* **2009**, *50*, 7209.
22. Liu, S.-Q.; Wang, D.-X.; Zheng, Q.-Y.; Wang, M.-X. *Chem. Commun.* **2007**, 3856.
23. For recent reviews, see: (a) Boyd, P. D. W.; Reed, C. A. *Acc. Chem. Res.* **2005**, *38*, 235. (b) Beletskaya, I.; Tyurin, V. S.; Tsivadze, A. Y.; Guillard, R.; Stern, C. *Chem. Rev.* **2009**, *109*, 1659. (c) Perez, E. M.; Martín, N. *Pure Appl. Chem.* **2010**, *82*, 523.
24. D'Souza, F.; Ito, O. *Chem. Commun.* **2009**, *33*, 4913.
25. Yanagisawa, M.; Tashiro, K.; Yamasaki, M.; Aida, T. *J. Am. Chem. Soc.* **2007**, *129*, 11912.
26. Kundrat, O.; Kas, M.; Tkadlecova, M.; Lang, K.; Cvacka, J.; Stibor, I.; Lhoták, P. *Tetrahedron Lett.* **2007**, *48*, 6620.
27. Van Rossom, W.; Kundrát, O.; Ngo, T. H.; Lhoták, P.; Dehaen, W.; Maes, W. *Tetrahedron Lett.* **2010**, *51*, 2423.
28. Marois, J.-S.; Cantin, K.; Desmarais, A.; Morin, J.-F. *Org. Lett.* **2008**, *10*, 33.
29. Perez, E.; Sanchez, L.; Fernandez, G.; Martín, N. *J. Am. Chem. Soc.* **2006**, *128*, 7172.
30. Perez, E. M.; Capodilupo, A. L.; Fernandez, G.; Sánchez, L.; Viruela, P. M.; Viruela, R.; Ortí, E.; Bietti, M.; Martín, N. *Chem. Commun.* **2008**, 4567.
31. Isla, H.; Gallego, M.; Perez, E. M.; Viruela, R.; Orti, E.; Martín, N. *J. Am. Chem. Soc.* **2010**, *132*, 1772.
32. Huerta, E.; Isla, H.; Perez, E. M.; Bo, C.; Martín, N.; de Mendoza, J. *J. Am. Chem. Soc.* **2010**, *132*, 5351.
33. Zheng, J.-Y.; Tashiro, K.; Hirabayashi, Y.; Kinbara, K.; Saigo, K.; Aida, T.; Sakamoto, S.; Yamaguchi, K. *Angew. Chem. Int. Ed.* **2001**, *40*, 1857.
34. (a) Georghiou, P. E.; Tran, A. H.; Mizyed, S.; Bancu, M.; Scott, L. T. *J. Org. Chem.* **2005**, *70*, 6158. (b) Sygula, A.; Fronczek, F. R.; Sygula, R.; Rabideau, P.; Olmstead, M. *J. Am. Chem. Soc.* **2007**, *129*, 3842.
35. Kawase, T.; Kurata, H. *Chem. Rev.* **2006**, *106*, 5250.
36. Bredenkotter, B.; Henne, S.; Volkmer, D. *Chem.-Eur. J.* **2007**, *13*, 9931.
37. Georghiou, P. E.; Dawe, L. N.; Tran, H. A.; Strube, J.; Neumann B.; Stammer, H. G.; Kuck, D. *J. Org. Chem.* **2008**, *73*, 9040.
38. Kobayashi, J.; Domoto, Y.; Kawashima, T. *Chem. Lett.* **2010**, *39*, 134.
39. Kobayashi, J.; Domoto, Y.; Kawashima, T. *Chem. Commun.* **2009**, *41*, 6186.
40. Fathalla, M.; Li, S.; Diebold, U.; Alb, A.; Jayawickramarajah, J. *Chem. Commun.* **2009**, 4209.
41. Suzuki, K.; Takao, K.; Sato, S.; Fujita, M. *J. Am. Chem. Soc.* **2010**, *132*, 2544.

This page intentionally left blank

Index

- @, symbol signifying endohedral structures, 147
- A₂B-building block
 - fifth generation dendron formation, 11–13
 - second generation dendron formation, 11
- Absorption coefficient, metallic SWNTs, 793
- Absorption due to the chromophore, photorefractive materials, photosensitizer, 648
- Acetylenes, porphyrin-bridge-fullerene molecules, 451–452
- Acid-purified MWNTs, enhancement of thermal conductivity, 769
- Acoustic phonon mismatch, as cause for low thermal conductivity of polymeric/CNT composites, 776
- Acting potential, DNA/SWNT hybrids, 810–813
- Activation energy, retro-Diels-Alder reaction, 328
- Activation for esterification, C₆₀ fullerene carboxylic acids, 3, 9, 11, 13–15
- Activation free energies
 - charge separation process, symmetrical rotaxanes, 486
 - ferrocene-tethered fullerene rotaxanes, 495
- Activation of carboxylic acid function, reaction with polypropyleneimines, fullerene building blocks, 9–10
- Addition chemistry, fullerenes, 669–670
- Addition reactions. *see also*
 - Cycloaddition
 - covalent sidewall (and tip) functionalization of carbon nanotubes, addition of carbenes and nitrenes, 297–298
 - nucleophilic, intramolecular, 35–38
- Adsorbed photon-to-current efficiency (APCE), fullerenes, 596–601, 603–604, 608, 622, 627
- AgO₂CCF₃, synthesis of PFAFs, 107

- AlCl₃, precipitation of
 - metallofullerenes. *see* Lewis acids
- Alcohol groups protection, key step for convergent fullerodendrimer preparation, 14
- Alignment, CNTs, 738
 - chemical and biochemical sensors, 734
 - co-deposition with conducting polymers, 719–720
 - electric conductivity of CNT-polymer composites, 723–725
 - electrochemical polymerization, 711–714
 - mechanical properties of CNT-polymer composites, 729
 - and thermal conductivity, 764–765, 769
- Alkenes, fullerenes, synthesis, 34, 39–40, 45
- Alkyne-azide click reactions, fullerene building blocks, 18–21
- Allotropic forms of carbon, of nanoscale dimensions, 668
- Amidation reactions, organic functionalization of oxidized carbon nanotubes, 293–295
- Amine-tethered fullerene rotaxanes
 - temperature effect, 500–501
 - unsymmetrical, 498–504
- Amines, aromatic, C₆₀-bridges, 466–467
- Angers and Amsterdam's C₆₀-PDI assemblies
 - concept of antenna, 25
 - concept of super-absorbing fullerenes, 27–35
 - incorporation of C₆₀-PDI dyads in bulk-heterojunction, 35–38
 - photophysics, 27–35
 - synthesis of bay-substituted C₆₀-PDI dyads and corresponding electrochemical behavior, 25–27
- Aniline-functionalized nanocarbons, as precursors for porphyrin nanohybrids, 531–532
- Anion, catalysis, 52–53
- Anisotropic pseudocontact interactions, cerium-encapsulated metallofullerenes, 148–149
- Antenna effect
 - Angers and Amsterdam's C₆₀-PDI assemblies, 25
 - photoactive electron donor-C₆₀ and electron acceptor C₆₀ dyads, 18
- APCE. *see* Adsorbed photon-to-current efficiency
- Arc generator, *in situ* formation of PFAFs, 103–105
- Armchair SWNTs
 - analytical theory of the symmetry breaking, 798–805
 - chiral vector classification, 759
 - thermal conductivity, 760
- Aromatic amine donors, symmetrical fullerene rotaxanes, 483
- Aromatic amines, C₆₀-bridges, 466–467
- Aromatic molecules, individual solubilization of CNTs, 251–253
- Aromatic solvents, and PFAFs, 132–133
- Aromatic systems, phthalocyanines, 59
- Artificial photosynthetic systems. *see also* Supramolecular artificial photosynthesis
 - electron transfer reactions
 - binding strength, 210
 - donor and electron acceptor subunits, 209
 - reorganization energy, 209
 - porphyrin-fullerenes, 376
- Asymmetric catalysis. *see* Catalysis
- Asymmetric energy coupling, photorefractive materials, 638

- Asymmetric energy exchange, two-beam coupling, 642
- Asymmetric induction, fullerenes, 51–53
- Atomic force microscopy, carbon nanotubes, 286–287
- Attenuation factor β , charge transfer in molecular wires, 676
- Au DENs. *see* Gold dendrimer-encapsulated nanoparticles
- Axle charge effects, ferrocene-tethered fullerene rotaxanes, 495–498
- Axle length, bis-porphyrins, 487–489
- Axle length effects, ferrocene-tethered fullerene rotaxanes, 495–498
- Azidirine, 1,3-dipolar cycloaddition, onto carbon nanotube surface, 300
- Azomethine ylides, 1,3-dipolar cycloaddition with azomethine ylide endohedral metallofullerenes, 165–167
- onto carbon nanotube surface, 298–300
- Back-electron transfer, intramolecular, CNC-(H₂P)_n nanohybrids, 535
- Band gap opening
- metallic armchair SWNTs, 802
- metallic SWNTs, 790–794
- Band gap parameters, metallic SWNTs, 803
- Bandstructure
- of carbon SWNTs, effect of surface functionalization, 788
- pristine metallic SWNT near the Fermi point, 792
- Bandstructure calculations, DNA/SWNT hybrids, 805–810
- Bandstructure modulation, due to symmetry breaking, 797
- Beam amplification by photorefractive materials, 638
- Bending, of CNTs inside the polymer matrix, as cause for low thermal conductivity, 776
- 1-Benzyl-1,4-dihydronicotinamide dimer (BNA)₂, destacking of CSCNTs, 526–527
- BF₃-ethanol catalysis, C₆₀
- fullerene-porphyrin synthesis, 2–6
- BHJ. *see* Bulk-heterojunction solar cells
- BIE. *see* Boundary integral equation
- Binding constants
- cobalt(II), porphyrins and fullerenes, 381–383
- fullerenes, 382
- Binding energies, porphines and fullerenes, 380
- BING-C₆₀-adduct. *see* C₆₀-BING-adduct
- Bingel C₆₀ adduct associated with Pcs
- Langmuir-Blodgett films, 63
- Si(IV)Pc, 63–64
- Bingel-Hirsch adducts, PFAFs, 137–138
- Bingel-Hirsch reaction
- endohedral metallofullerenes, 168–170
- phthalocyanine fullerene assemblies, 61, 63
- retro-cyclopropanation reaction, 339
- Bingel reaction, C₆₀-donor dyads and triads formation, 10–11
- Biochemical sensors, polymer composites of carbon nanotubes, 733–735
- Biocompatible structures, phthalocyanine-SWNT systems, 91
- Biosurfactants, for CNT solubilization, 248
- Bis*-acetylenes, porphyrin-bridge-fullerene molecules, 443–449
- Bis*-biphenylamines, photoinduced electron transfer processes, 483–486

- Bis*-porphyrins
 - acyclic, 377
 - calixarene, 377, 380–381
 - cyclic, 377
 - molecular dynamic calculations, 488–489
 - photoinduced electron transfer processes, 486–491
 - synthesis, 381
 - X-ray structure, 377–378
- Bis*-silylation, endohedral metallofullerenes, 156–160
 - chemical reactivity, 157–158
- Bistable rotaxanes, definition, 670
- BNA₂. *see* 1-Benzyl-1,4-dihydronicotinamide dimer
- Boundary integral equation (BIE)
 - method, thermal conductivity in CNTs, 766
- Bovine serum albumin, phthalocyanine-SWNT systems, 91
- Bridges. *see also* C₆₀-bridge-donor systems
 - charge-separation (*see* Charge-separation)
 - porphyrin-bridge-fullerene molecules (*see* Porphyrin excitation)
- Brillouin zone (BZ), two-dimensional, of graphene, 795
- Buckminsterfullerenes, historical considerations, 391–392
- Bulk CNTs
 - SWNT-graphite composites, thermal conductivity, 764–765
 - for thermal conductive materials, 761–765
 - MWNT bundles, 761–763
 - MWNT films, 761–762
 - SWNT films, 763–764
- Bulk-heterojunction solar cells
 - concept of antenna effect, 25
 - incorporation of C₆₀-PDI, 35–38
 - indium tin oxide electrodes, 35–36
 - organic, molecular fullerene based donor-acceptor layer, 426
 - [6,6]-phenyl C₆₁-butyric acid methyl ester, theoretical principle, 36
 - P3HT, 339
 - solution-processed, deposition, 608, 620–622
- Bulk-heterojunction (BHJ) solar cells, Diels-Alder adducts of substituted isobenzofurans, 339
- BZ. *see* Brillouin zone
- ¹³C-NMR spectroscopy
 - Ce@C_{2v}-C₈₂, 148
 - Ce₂@D_{2h}(5)-C₇₈, 151
 - Ce₂@D_{5h}-C₈₀, 152
 - dimetallofullerenes, 149–152
 - La@C_{2v}-C₈₂, 147
 - La₂@D₂(10611)-C₇₂, 149
 - La₂@D_{3h}(5)-C₇₈, 150
 - monometallofullerenes, 147–148
 - Sc₂C₂@C_{3v}-C₈₂, 153–154
 - Sc₃C₂@I_v-C₈₂ anions, 154
 - Sc₃N@I_h-C₈₀, 153
- C₁-C₇₀(CF₃)₁₀. *see also* C₇₀ PFAFs
 - one-step synthesis, 115
 - Schlegel diagram, 116
- C₆₀-based dyads, photosensitizer in photoreactive materials, 658–664
- C₆₀-BING-adduct, photophysical and electrochemical data, 34
- C₆₀-bridge-donor systems
 - long linkages
 - C₆₀-phenylenevinylene-extTTF, 468–470
 - C₆₀-thiophenevinylene-ferrocene, 468–469
 - short linkages
 - C₆₀-bridge-aromatic amines, 466–467

- C₆₀-bridge-ferrocenes, 467–468
- C₆₀-exTTF ensembles, as molecular wires, 677–682
- C₆₀ fullerene-adducts
 - NIR absorption spectra, 33
 - photophysical and electrochemical data, 34
- C₆₀ fullerene alkyne-azide click reactions, copper catalyzed, 16–22
- C₆₀ fullerene alkynes, click reactions, copper mediated Huisgen 1,3-dipolar cycloaddition, 16–18, 24–28
- C₆₀ fullerene azides, click reactions, copper mediated Huisgen 1,3-dipolar cycloaddition, 19–20, 22–24
- C₆₀ fullerene benzaldehydes
 - construction of functionalized porphyrins, 2–6
 - synthesis, 2–4
- C₆₀ fullerene bis-adducts
 - click chemistry, with fullerene building blocks, 16–22
 - porphyrins, copper mediated Huisgen 1,3-dipolar cycloaddition, 21–22
- C₆₀ fullerene-bis-cyclopropane-adducts, by macrocyclization reaction, 3
- C₆₀ fullerene carboxylic acids, activation for esterification, 3, 9, 11, 13–15
- C₆₀ fullerene-containing dendrimers, structures, 7
- C₆₀ fullerene functionalized with donor units
 - electroactive electron donor-C₆₀ and electron acceptor-C₆₀ dyads, 11–17
 - synthetic strategies, 10–11
- C₆₀ fullerene hexa-adducts, with fullerene building blocks
 - click chemistry, 22–28
 - copper mediated Huisgen 1,3-dipolar cycloaddition, 24–28
- C₆₀ fullerene mono-adducts, click chemistry, with fullerene building blocks, 16–22
- C₆₀ fullerene porphyrins
 - bis(meta-substituted-phenyl) porphyrin, synthesis, 4
 - metalation of porphyrin with Zn(OAc)₂, 6
 - photophysical properties, 5
 - synthesis
 - BF₃-ethanol cocatalysis, 2–6
 - copper mediated Huisgen 1,3-dipolar cycloaddition, 21–24
 - tetrasubstituted-phenyl porphyrin, synthesis, 6–7
- C₆₀ fullerenes
 - electrochemical properties, 2–4
 - as electron acceptor in multifunctional hybrid cells, 683–689
 - functionalization, click chemistry, 16–22, 24–28
 - intramolecular nucleophilic reaction
 - alcohols and thiols, 37
 - phenols, 36
 - macrocyclic bis-adducts, 3
 - mono- and bis-adducts, 16–22
 - multi-step synthesis, with fullerene building blocks, 2
 - Pauson-Khand reaction, 39–45
 - photophysical and electrochemical data, 34
 - porphyrins (*see* Porphyrins)
 - redox potentials, 155
 - solubility, 6
 - supramolecular hosts for, 391–401
 - calixarene-type hosts, 392–395
 - corannulene ring-based hosts, 399–400

- porphyrin-containing hosts, 395–397
 - TBTQ-based hosts, 400
 - triarylphosphate-based hosts, 401
 - TTF-containing hosts, 397–399
- C₆₀ hexakis-adducts, 24–28
 - with 12 building blocks, click reactions, 22–28
 - porphyrins, copper mediated Huisgen 1,3-dipolar cycloaddition, 23–24
- C₆₀-perylene-3,4:9,10-bis(dicarboximide) dyads
 - concept of super-absorbing fullerenes, 27–34
 - electrochemical properties, 27
 - energy transfer rates, 29, 31
 - femto- and nanosecond transient absorption spectra, 30
 - photoelectrochemistry, 21–24
 - photophysics, 27–35
 - properties and applications, 18–24
 - synthesis and corresponding electrochemical behavior, 25–27
 - synthetic strategy, 26
- C₆₀-perylene-3,4-mono(dicarboximide) dyads
 - electrochemical properties, 39
 - synthesis, 38
 - voltammograms, 39
- C₆₀ PFAFs, Schlegel diagrams, 117–119
- C₆₀-[6,6]-phenyl C₆₁-butyric acid methyl ester dyads, synthesis, 10–11
- C₆₀- π -extended TTF dyads and cascade, electron transfer process, 15
- C₆₀-porphyrin rotaxane
 - HOMO, 504
 - LUMO, 504
- C₆₀ radical anion
 - femtosecond transient absorption spectra, 35
 - NIR absorption spectra, 33
- C₆₀-tetrathiofulvalene dyads, absorption spectra, 14
- C₆₀-dimethylaniline, photophysics, 11–12
- C₇₀ PFAFs, Schlegel diagrams, 120–122
- C₇₀-selective bis(Zn-porphyrin) tweezer, 397
- C-C coupling chemistry catalyzed by palladium, covalent sidewall (and tip) functionalization of carbon nanotubes, 308
- Cage frameworks, endohedral metallofullerenes, 147–154
- Cages, fullerenes. *see* Fullerene cages
- Calixarene-type hosts, for C₆₀ fullerenes, 392–395
- Calixarenes, linkage for porphyrin-fullerenes, binding strength, 377, 380–382
- Cancer phototherapy, phthalocyanine-carbon nanotubes, 91
- Capacitors, electrochemical, polymer composites of carbon nanotubes, 735–737
- CAPTEAR. *see* Chemically adjusting plasma temperature, energy, and reactivity
- Carbon allotropes, nanoscale, 668
- Carbon nanodiamond (ND)-porphyrin assemblies, for light-energy conversion, 537–540
- Carbon nanohorn (NH), compared to other nanomaterials, 520
- Carbon nanosheets. *see* Graphene nanosheets
- Carbon nanotube (CNT)/DNA hybrids, solubilized CNTs, 249–251

- Carbon nanotube (CNT)-fullerene
 composite systems, electrochemical
 deposition, 618–620
- Carbon nanotube (CNT) assemblies,
 84–89
 covalent
 electron donor, 85
 smalley procedure, 84–85
 non-covalent
 donor-acceptor nanohybrids,
 90
 magnetization, 90
 π - π interactions, 89
 single-walled-carbon
 nanohorns, 91
 phthalocyanine macrocycle, 85
 phthalocyanine-MWNT systems,
 86
 phthalocyanine-SWNT systems,
 cycloaddition, 86–88
 Zn(II)Pc, 85
- Carbon nanotube field-effect transistor
 (CNT-FED), 700, 743
 scheme, 740–741
- Carbon nanotube (CNT)
 solubilization. *see also* Solubilized
 carbon nanotubes
 basic solubilization/dispersion
 techniques, 246
 charge-transfer interactions from
 porphyrins to CNTs, 252
 π - π interaction
 between polycyclic aromatic
 compounds and CNT
 sidewalls, 251
 between polyimides and
 SWNT surfaces, 254
 surfactants for, 247–248
- Carbon nanotubes (CNTs)
 alternatives, functionalized
 graphenes, 742
 applications, supramolecular
 chemistry, 312–315
- characterization, 276–291
 atomic force microscopy,
 286–287
 electron microscopy, 289–291
 recent advances, 271–316
 scanning probe microscopy,
 285–288
 spectroscopic characterization,
 278–285
 thermogravimetric analysis,
 276–278
- composites with polymers (*see*
 Polymer composites of carbon
 nanotubes)
- composites with silicone elastomer,
 enhancement of thermal
 conductivity, 771–772
- conformational defects, and
 thermal conductivity, 760–762
- covalent functionalization, recent
 advances, 271–316
- covalent sidewall (and tip)
 functionalization, 295–310
 1,3-dipolar cycloaddition,
 298–301
 addition of carbenes and
 nitrenes, 297–298
 C-C coupling chemistry
 catalyzed by palladium,
 308
 diazonium coupling, 306–308
 Diels-Alder cycloadditions,
 301–303
 direct arylations, 306–308
 free-radical additions,
 304–305
 grafting of polymers, 309–310
 halogenation, 296–297
 mechanochemical
 functionalizations, 310
 nucleophilic and electrophilic
 additions, 303–304
 ozonolysis, 308–309

- reduction and reductive alkylations, 305–306
- covalent surface chemistry, 291–310
 - amidation and esterification, 292–295
 - covalent sidewall (and tip) functionalization, 295–310
 - oxidation, 292
- cup-stacked, 522–524
- donor-acceptor molecules, 84
- double functionalization reactions, 312
- ferrocene hybrid materials, 300–301
- functionalization (*see also* Functionalization)
 - basics, 246
 - effect on thermal conductivity, 776–778
- organic functionalization, 291–312
 - endohedral filling inner empty cavity, 311–312
 - non-covalent adsorption or wrapping of functional molecules, 310–311
- spectroscopic characterization
 - electron energy loss spectroscopy (EELS), 278
 - emission spectroscopy, 283–284
 - infrared spectroscopy, 282–283
 - nuclear magnetic resonance spectrometry, 284–285
 - resonance Raman spectroscopy, 278–280
 - UV-vis-NIR absorption spectroscopy, 280–282
 - X-ray photoelectron spectroscopy, 285
- structural connection with graphite and graphene, 520
- synthesis, 274–276
- for thermal conductive materials, 756–778
- thermal conductivity
 - BIE method, 766
 - enhancement ratio, 767
 - molecular dynamics (MD) simulations, 766
- type, structure and properties, 273–274
- Catalysis
 - asymmetric, 51
 - complexes, cobalt and dicobalt, 41–44
 - cycloadditions
 - chiral ligands, 52
 - enantioselective, 49–55
 - pyrolysis, 713
 - reduction of oxygen or hemoglobin, 702
- Catenanes
 - molecular machines, composition, 670
 - NMR spectra, 226
 - supramolecular artificial photosynthesis, 210–216
- [3]catenates
 - synthesis, 228–229
 - building blocks, 229
 - chromatographic purification, 235
 - introduction of porphyrin moiety, 232
 - MALDI-TOF analysis, 230, 233, 237
 - NMR spectra, 230
 - nonsymmetrical, 228
 - synthesis of triazole-linked, 234
- Ce@C_{2v}-C₈₂
 - electrophilic carbene addition, molecular structures and characterization of adducts, 162–163

- redox potentials, 155
- Ce@C_{2v}-C₈₂ anions
 - positions, and movements of
 - encaged cer atoms, 148–149
 - ¹³C-NMR spectra, 148
 - structure, 149
- Ce₂@D₂(10611)-C₇₂, ¹³C-NMR spectra, 150
- Ce₂@D_{2h}(5)-C₇₈, ¹³C-NMR spectra, 151
- Ce₂@D_{3h}(5)-C₇₈, bis-silylation, structures and electronic properties, 159–160
- Ce₂@D_{5h}-C₈₀
 - ¹³C-NMR spectra, 152
 - cage framework and positions of the metal atoms, 150, 152
- Ce₂@I_h-C₈₀
 - bis-silylation, structures and electronic properties, 158–159
 - electrophilic carbene addition, molecular structures and characterization of adducts, 164
- CeSc₂N@I_h-C₈₀, ⁴⁵Sc-NMR spectra, 153
- C₂F₅I, C₃F₇I, C₄F₉I, C₆F₁₃I, and C₁₂F₂₅I, synthesis of perfluoroalkylfullerenes (PFAFs), 112–114
- CF₃I, synthesis of PFAFs, 108–111
- Charge density, DNA/SWNT hybrids, 810–811
 - DNA perturbation, 812–813
- Charge distributions, DNA/SWNT hybrids, 807–808
- Charge generation
 - photosensitizers in PR materials, 656
 - quantum efficiency, photorefractive measurements, 641
- Charge recombination (CR), 482
 - activation free energies, photoinduced electron transfer processes, 486
 - in fullerene based donor-acceptor dyads
 - energetic properties, 407
 - in organized molecular films, 436
 - molecular bridges
 - electron transfer, 442
 - energy diagrams, 460–461
 - rate constants, 448–456, 459, 463, 467–473
 - scheme, 466
 - steps, 447, 451, 465
 - triphenylamines, photoinduced electron transfer processes, 502
- Charge-separated (CS) state, CNC-(H₂P)_n nanohybrids, 533–535
- Charge separation (CS)
 - activation free energies, photoinduced electron transfer processes, 486
 - bis-porphyrins, 490
 - DNA/SWNT hybrids, 812–814
 - in fullerene based donor-acceptor dyads, in organized molecular films, 435
 - molecular bridges
 - conjugated bridges, 473
 - isolated bridges, 470–473
 - photoinduced, 465
 - photosensitizing, 442, 456–458
 - rate constants, 445–453, 455, 459–463, 465–469
 - scheme, 444–445
 - steps, 443–445, 448, 451, 465
 - photoinduced, 594–595
 - phytochlorin-fullerene dyad, 412
 - porphyrin-fullerene dyads
 - dependence on dyad geometry, 411
 - energetic properties, 406–407
 - rotaxanes, 482

- photoinduced electron
 - transfer processes, 485–486
- triphenylamines, photoinduced
 - electron transfer processes, 502
 - via exciplex relaxation, thermodynamic parameters, 414
- Charge-transfer (CT) bands
 - cobalt(II), porphyrins and fullerenes, 381–383
 - porphyrin to fullerene, 379
- Charge-transfer (CT) complexes, photorefractive materials, photosensitizer, 647
- Charge-transfer (CT) interactions
 - donor-acceptor dyads, photodynamics, 410–411
 - from porphyrins to CNTs, 252
- Charge transport, through molecular wires, 676
- Charge transporting molecule, photorefractive materials, 640
- Charge trapping, photorefractive materials, 651
- CHARMM (Chemistry at Harvard Macromolecular Mechanics)
 - analytical theory of the symmetry breaking in DNA/SWNT hybrids, 799
 - electronic properties of DNA/SWNT hybrids, 807
- CHCl_3 , as solvent for rotaxanes, 671–674
- Chemical adsorption, deposition
 - coordination bonding systems, 627–628
 - hydrogen-bonding systems, 622–627
 - solution-processed bulk-heterojunction solar cells, 620–622
- Chemical functionalization
 - of CNTs, effect on thermal conductivity, 777
 - fullerenes, 669–670
 - of graphene nanosheets, effect on thermal conductivity, 781–783
- Chemical polymerization, preparation, polymer composites of carbon nanotubes, 708–711
- Chemical retro-cyclopropanation reaction
 - reductive ring opening-retro-Bingel reaction, 357
 - selective removal of methano addends, 357
- Chemical sensors, polymer composites of carbon nanotubes, 733–735
- Chemically adjusting plasma temperature, energy, and reactivity (CAPTEAR), metallofullerenes, synthesis, 187–191
- Chemistry
 - Bingel-Hirsch reactions, 168–170
 - carbon nanotubes
 - 1,3-dipolar cycloaddition, 298–301
 - addition of carbenes and nitrenes, 297–298
 - amidation reactions, 293–295
 - C-C coupling chemistry
 - catalyzed by palladium, 308
 - diazonium coupling, 306–308
 - Diels-Alder cycloadditions, 301–303
 - direct arylations, 306–308
 - esterification reactions, 292–293
 - fluorination, 296–297
 - free-radical additions, 304–305
 - grafting of polymers, 309–310
 - halogenation, 296–297
 - Heck coupling, 308–309
 - nucleophilic and electrophilic additions, 303–304
 - oxidation, 292

- ozonolysis, 308–309
 - reduction and reductive alkylations, 305–306
 - Suzuki coupling, 308–309
- of endohedral metallofullerenes, 156–175
 - 1,3-dipolar cycloaddition, 165–168
 - bis-silylation, 156–160
 - Diels-Alder reaction, 170–173
 - electrophilic carbene addition, 160–165
 - nucleophilic addition, 168–170
 - radical reaction, 173–175
- fullerene building blocks, 1–28
 - click chemistry, 16–28
 - for dendrimer synthesis, 6–16
 - double Bingel addition, 3
 - for porphyrin synthesis, 2–6
 - regioselective
 - macrocyclization reaction, 3
 - oxations and reductions, endohedral metallofullerenes, 155–156
- Chemistry at Harvard Macromolecular Mechanics. *see* CHARMM
- Chiral angle, of SWNTs, 788
- Chiral indexes, carbon nanotubes, high resolution transmission electron microscopy, 289
- Chiral SWNTs
 - chiral vector classification, 759
 - thermal conductivity, 760
- Chiral vectors, for classification of SWNTs, 759
- Chirality
 - fullerenes, 34, 46, 49–55
 - ligands, 51–52
- Chlorophyll, 208
- Chromophores
 - in molecular photoelectrochemistry, 683
 - porphyrins, 376, 686–689
- Circular dichroism
 - DNA/SWNT hybrids, 815–819
 - in non-chiral SWNTs, 789
- Click chemistry
 - C₆₀ fullerenes, functionalization, 16–22
 - fullerene azides and alkynes
 - copper mediated Huisgen 1,3-dipolar cycloaddition, 16–22, 24–28
 - hexakis-adducts bearing 12 building blocks, 22–28
 - mono- and bis-adducts, 16–22
 - fullerene building blocks, 16–28
 - fullerene hexa-adducts, 22–28
 - fullerene mono- and bis-adducts, 16–22
- Click reaction
 - additives, 220
 - carbon nanotubes assemblies, phthalocyanine-SWNT systems, 88
 - synthesis of ferrocene-C₆₀-rotaxane, 216–217, 219
- Cluster fullerenes
 - Bingel-Hirsch adducts, chemical reactivity, 169–170
 - cage frameworks, positions, and movements of encaged species, 153–154
 - [6,6]-closed and [5,6]-closed pyrrolidino adducts, cluster movements, 167
 - electronic structures, 153
 - [6,6]-open derivatives, 175
- CNC-(C₆₀)_n composite clusters, 527–528
 - current-voltage characteristics, 529–530
 - incident-photon-to-current conversion (IPCE) values, 529

- photocurrent generation process, 530–531
- CNC-(H₂P)_n nanohybrids
 - formation of the charge-separated state, 533–535
 - intramolecular back-electron transfer, 535
 - IPCE values, 536
 - OTE/SnO₂ and OTE/TiO₂ electrodes, 536–537
 - photoexcitation, 533
 - production, 531–532
 - thermogravimetric analysis, 532–533
 - UV-vis absorption spectra, 533
- CNCs. *see* Cup-shaped nanocarbons
- CNT-FET. *see* Carbon nanotube field-effect transistor
- CNT-filled polymeric nanocomposites. *see* Polymer composites of carbon nanotubes
- CNTs, carbon nanotubes. *see* Carbon nanotubes
- Cobalt(II)
 - complexes, fullerenes, 41–44
 - Pauson-Khand reaction, 39–45
 - porphyrin-fullerene supramolecular chemistry
 - binding constants and charge transfer bands, 381–383
 - comparison to other metals, 380–381
 - synthesis of bis-porphyrins, 381
 - X-ray structures of T_{3,4,5-ome}PP cocrystallates, 383–387
 - UV-vis titration, 382
- Complexation, C₆₀ fullerenes, in organic solutions, 392–401
- Complexes, catalysis
 - cobalt and dicobalt, 41–44
 - fuller-1,n-enynes, 44
 - geometry, 44
- Composite clusters, CNC-(C₆₀)_n, 527–528
- Composite systems. *see also* Polymer composites of carbon nanotubes
 - carbon nanotube-fullerenes, electrochemical deposition, 618–620
 - porphyrin-fullerenes, electrochemical deposition, 613–618
- Conductivity, electric, polymer composites of carbon nanotubes, 722–724
- Conformational defects, CNTs, and thermal conductivity, 760–762
- Conformational flexibility, phthalocyanine-C₆₀ pseudorotaxane-like complexes, 77
- Contact charge transfer (CCT), between C₆₀ and CTV-based cryptophanes, 394
- Controlled potential electrolysis (CPE)
 - electrochemically induced retro-cyclopropanation reactions
 - C₆₀ fullerene derivatives, 340–352
 - C₇₀ fullerene derivatives and higher fullerenes, 352–355
 - isoxazolo[3,4:1,2]-[60]fullerenes, 365
 - pyrrolo [3,4:1,2]-[60]fullerenes, 362–363
 - walk-on-the-sphere rearrangements, 355–357
 - stability of Diels-Alder adducts, 332
- Convergent synthesis, fullerodendrimers, 11–13
- Coordination bonding systems, deposition, 622–627
- Corannulene ring-based hosts, for C₆₀ fullerenes, 399–400

- Correlation spectroscopy (COSY),
¹⁹F NMR spectra of PFAFs,
 127–129
- COSY. *see* Correlation spectroscopy
- Coulomb perturbation, of DNA
 backbone, DNA/SWNT hybrids,
 808–809
- Covalent bonds, phthalocyanine
 fullerene assemblies, comparison with
 metal-ligand bonds, 82
- Covalent phthalocyanine-carbon
 nanotube systems, 84–89
- Covalent phthalocyanine-fullerene
 systems, 61–75
- Covalent sidewall (and tip)
 functionalization, carbon nanotubes,
 295–310
 1,3-dipolar cycloaddition,
 298–301
 addition of carbenes and nitrenes,
 297–298
 C-C coupling chemistry catalyzed
 by palladium, 308
 diazonium coupling, 306–308
 Diels-Alder cycloadditions,
 301–303
 direct arylations, 306–308
 free-radical additions, 304–305
 grafting of polymers, 309–310
 Halogenation, 296–297
 mechanochemical
 functionalizations, 310
 nucleophilic and electrophilic
 additions, 303–304
 oxidation, 292
 ozonolysis, 308–309
 reduction and reductive
 alkylations, 305–306
- Covalent surface chemistry
 carbon nanotubes, 291–310
 covalent sidewall (and tip)
 functionalization, 295–310
 oxidized carbon nanotubes,
 amidation and esterification,
 292–295
- Covalently linked donor-fullerene
 systems, electrochemical deposition,
 609–610
- Cp. *see* Cyclopentadiene
- CPE. *see* Controlled potential
 electrolysis
- CR. *see* Charge recombination process
- Crown ethers
 insertion in oligo-thiophene
 bridges, 461–462
 supramolecular, 80–82
- Cryptophane hosts, for C₆₀ fullerenes,
 394
- Crystallography. *see* X-ray
 crystallography
- CS. *see* Charge separation
- CSCNTs. *see* Cup-stacked carbon
 nanotubes
- CT. *see* Charge transfer
- CTV. *see* Cyclotrimeratrylene
- CuAAC. *see* Huisgen-Sharpless-Medal-
 Cu(I)-catalyzed-1,3-dipolar
 cycloaddition
- Cup-shaped nanocarbons (CNCs)
 for light-energy conversion,
 524–530
 porphyrin-functionalized, for light-
 energy conversion, 530–537
 production of individual, by the
 electron-transfer reduction,
 526–527
- Cup-stacked carbon nanotubes
 (CSCNTs)
 for light-energy conversion,
 522–524
 size distributions, 526
 solid-state EPR spectra, 524–525
 TEM images and size
 distributions, 525–526

- [Cu(phen)₂]⁺ complex, supramolecular artificial photosynthesis, 213
- CV. *see* Cyclic voltammogram
- Cyclic [n]*para*-phenylacetylenes, as hosts for fullerenes, 399–400
- Cyclic voltammogram (CV)
 - PFAFs, 135
 - Pt/MWNT/PBI nanocomposites, 259–262
- [2+2] Cyclizations, thermally induced, 45–46
 - cyclobutenes, 45
- Cycloaddition, carbon nanotubes assemblies, phthalocyanine-SWNT systems, 86–88
- Cycloaddition chemistry, used for PFAFs, 137–138
- Cycloaddition reactions. *see also* Retro-cycloaddition reactions
 - [60]fullerenes
 - isoxazolo[3,4:1,2], 365
 - pyrazolino[3,4:1,2], 366–367
 - pyrrolo[3,4:1,2], 359–363
- Cyclobutenes, [2+2] cycloadditions, 45–49
- Cyclopentadiene (Cp), Diels-Alder reaction, with La@C_{2v}-C₈₂, 170–171
- Cyclopropane-adducts, C₆₀ fullerenes, 3
- Cyclopropanation reaction. *see* Retro-cyclopropanation reaction
- Cyclotrimeratrylene (CTV)-type hosts, for C₆₀ fullerenes, 393–395
- DA. *see* Donor-acceptor
- Damping factor β . *see also* C₆₀-bridge-donor systems; Charge-separation; Porphyrin excitation
 - molecular bridges, 442–443
- DBU. *see* 1,8-Diazabicyclo[5.4.0]undec-7-ene
- Deep traps, photorefractive materials, 651
- Defects, in CNTs, conformational defects, 760–762
- Delocalization of electron densities, porphyrin-fullerene dyads, 415
- Dendrimers
 - containing fullerene, structures, 7
 - convergent synthesis, with fullerene building blocks, 10–16
 - divergent synthesis, with fullerene building blocks, 8–10
 - polypropyleneamine core, 9–10
 - synthesis, with fullerene building blocks, 6–16
- Density functional theory (DFT), PFAFs experimental and predicted Raman spectra, 126
 - structure compared to X-ray-diffraction experiments, 104, 130
- Density of states (DOS), metallic SWNTs, 791–792
- Deposition
 - co-deposition, polymer composites of carbon nanotubes, 716–722
 - electrochemical
 - carbon nanotube-fullerene composite systems, 618–620
 - covalently linked donor-fullerene systems, 609–610
 - fullerenes and derivatives, 608–609
 - noncovalently linked donor-fullerene systems, 610–613
 - porphyrin-fullerene composite systems, 613–618
 - layer-by-layer, 605–608
 - spin-coating and chemical adsorption
 - coordination bonding systems, 627–628

- hydrogen-bonding systems, 622–627
- solution-processed bulk-heterojunction solar cells, 620–622
- vacuum, 608
- Destacking, of CNCs, 526–527
- Dexter mechanism
 - C₆₀-bridges, 470–471
 - photo- and electroactive fullerene dyads, 5–6
- 1,8-Diazabicyclo[5.4.0]undec-7-ene (DBU), regioselective macrocyclization reaction, 3
- Diazonium coupling, covalent sidewall (and tip) functionalization of carbon nanotubes, 306–308
- Dicobalt, complexes, fullerenes, 41–44
- Dielectric permittivity, DNA/SWNT hybrids, 812–814
- Diels-Alder adducts
 - of substituted isobenzofurans
 - bulk-heterojunction solar cells, 339
 - fullerene cage opening, 337–338
 - molecular surgery, 337
 - tethered reactive units, 338
 - thermal *vs.* electrochemical stability, 327–333
- Diels-Alder cycloadditions, covalent sidewall (and tip) functionalization of carbon nanotubes, 301–303
- Diels-Alder reaction. *see also* Retro-Diels Alder reaction
 - endohedral metallofullerenes, 170–173
 - La@C_{2v}-C₈₂, with cyclopentadiene, 170–171
 - phthalocyanine fullerene assemblies, 62
- Diffraction efficiency, four wave mixing, 643–644
- Dimetallofullerenes
 - ¹³C-NMR spectra, 149–152
 - cage frameworks, positions, and movements of encaged species, 149–152
 - [6,6]-closed and [5,6]-closed pyrrolidino adducts, metal positions, 166–167
 - magnetic properties, 149–151
- Dimethylaniline (DMA), C₆₀ dyads. *see* C₆₀[3]dimethylaniline
- Diphenylmethanofullerene-perylenediimide dyads and triads, photoelectrochemistry, 24
- 1,3-Dipolar cycloaddition
 - covalent sidewall (and tip) functionalization of carbon nanotubes, 298–301
 - endohedral metallofullerenes, 165–168
 - with azomethine ylide, 165–166
 - fullerene building blocks, alkyne-azide click reactions, 18–21
- Dipolar cycloaddition reactions
 - chemical retro-cycloaddition of pyrrolo[3,4:1,2], 359–364
 - electrochemical retro-cycloaddition of pyrrolo [3,4:1,2] [60]fullerenes, 362–363
 - endohedral derivatives and their stability, 363–364
- Dirac Hamiltonian, for a massless particle, low energy excitations of SWNT, 798
- Direct arylations, covalent sidewall (and tip) functionalization of carbon nanotubes, 306–308
- Disilanes, porphyrin-bridge-fullerene molecules, 462–463
- Dispersed CNTs. *see* Solubilized carbon nanotubes
- Divergent synthesis

- fullerodendrimers, 8–10
- polyamidoamine dendrimers, 313–315
- DNA/SWNT hybrids
 - charge distributions, 807–808
 - DNA wrap, influence on optical properties, 790
 - electronic properties, 787–819
 - acting potential, 810–813
 - charge separation, 812–814
 - circular dichroism, 815–819
 - dielectric permittivity, 812–814
 - metallic SWNTs, 790–794
 - numerical modeling, 805–810
 - optical absorption, 814–815
 - photoluminescence maps, 814–815
 - rigorous analysis for armchair SWNTs, 798–805
 - screening factor, 812–814
 - self-consistent charge density, 810–813
 - semiconductor SWNTs, 794–798
 - symmetry breaking, 790–819
 - tight binding band structure calculations, 805–810
 - modeling of, Hamiltonian, 805–806
 - “natural” optical activity, 817
 - potential of DNA, 803, 811
 - solubilized CNTs, 249–251
 - supercells for SWNTs, 808–809
 - tight binding charge density, DNA perturbation, 812–813
 - wavefunctions for electronic states, 815–816
 - wrap characterization, by breaking of the helical symmetry, 789
 - wrap number, 802–803
- Donor, second, photoinduced electron transfer processes, 505
- Donor-acceptor (DA)
 - metallo-supramolecular complexes, Ti(IV)phthalocyanine, 82
- Donor-acceptor (DA) molecules
 - carbon nanotubes, 84
 - phthalocyanine fullerene assemblies
 - covalent, 60
 - non-covalent interactions, 76
- Donor-acceptor (DA) nanohybrids. *see also* Electron donor-acceptor nanohybrids
 - carbon nanotubes assemblies, 90
- Donor-acceptor (DA) systems, 406. *see also* Fullerene based donor-acceptor systems
- Donor-fullerene systems
 - covalently linked, electrochemical deposition, 609–610
 - noncovalently linked, electrochemical deposition, 610–613
- Donor systems
 - C₆₀-bridge-donor systems, 465–470
 - electrons (*see also* Charge separation; Lowest unoccupied molecular orbital)
- Dopamine sensing, phthalocyanine-carbon nanotubes, 92
- Doping, ECPs, 698, 709–712
 - PPY-films, 719
 - sensor applications, 733–734
- Dorn method, synthesis of metallic nitride fullerenes, 188–189
- Double-bridged dyads, phthalocyanine fullerene assemblies, 63
- Double functionalization reactions, carbon nanotubes, 312
- Double intramolecular Pauson-Khand reaction. *see* Pauson-Khand reaction
- Double photodynamic therapy (PDT), phthalocyanine-carbon nanotubes, 91

- Double-stranded DNA (dsDNA), as surfactant for CNT solubilization, 249
- Double-walled carbon nanotubes (DWCNTs/DWNTs)
 definition, 246
 polymer composites of carbon nanotubes, 699, 730, 741
 structure and properties, 273–274
- dsDNA. *see* Double-stranded DNA
- Dunsch method, synthesis of metallic nitride fullerenes, 188–189
- DWCNTs. *see* Double-walled carbon nanotubes
- DWNTs. *see* Double-walled carbon nanotubes
- Dy@C_{2v}-C₈₂, Bingel-Hirsch reactions, 170
- Dynamic light scattering (DLS)
 measurements, CSCNTs, 526
- ECP. *see* Electronically conducting polymer
- ECSA. *see* Electrochemically active surface area
- Effective density of traps,
 photorefractive measurements, 641
- Effective medium approach (EMA),
 thermal conductivity in CNTs, 766
- Elastomers, in polymeric/nanotube composites, thermal conductive materials, 770
- Electric-arc reactor, scheme, 190
- Electric-arc synthesis, oxometallic fullerenes, 189–191
- Electric conductivity
 doping (*see* Doping)
 polymer composites of carbon nanotubes, 722–724
- Electro and photoactive fullerene dyads. *see* Energy and electron transfer in photo- and electroactive fullerene dyads
- Electrocatalysts, for fuel cells using soluble CNTs, 258–262
- Electrochemical band gap,
 metallofullerenes, 201–203
- Electrochemical capacitors, polymer composites of carbon nanotubes, 735–737
- Electrochemical deposition
 carbon nanotube-fullerene composite systems, 618–620
 covalently linked donor-fullerene systems, 609–610
 fullerenes and derivatives, 608–609
 noncovalently linked donor-fullerene systems, 610–613
 porphyrin-fullerene composite systems, 613–618
 scheme, 720
- Electrochemical polymerization,
 preparation, polymer composites of carbon nanotubes, 711–716
- Electrochemical retro-cycloaddition, 363
- Electrochemical stability, Diels-Alder adducts, 327–333
- Electrochemically active surface area (ECSA), Pt/MWNT/PBI nanocomposites, 259–262
- Electrochemically controllable molecular shuttles, 673
- Electrochemically induced retro-cyclopropanation reactions. *see* Controlled potential electrolysis; Retro-cyclopropanation reaction
- Electrochemistry, polymer composites of carbon nanotubes, 724–729
- Electrodes, self-assembled monolayers
 gold, 596–601
 indium tin oxide, 601–605
- Electron acceptors
 photoelectrochemical and photovoltaic devices, 594

- photoinduced charge transfer, 406, 442
- photosensitizers in PR materials, 651
- Electron-donating materials, phthalocyanines, 60
- Electron donor-acceptor molecules
 - application to light-energy conversion, 519–540
 - cup-shaped nanocarbons, 524–530
 - cup-stacked carbon nanotubes, 522–524
 - nanodiamond-porphyrin assemblies, 537–540
 - porphyrin-functionalized CNCs, 530–537
 - photoinduced electron transfer processes, 480
- Electron donor-fullerene multi-ring interlocked systems
 - artificial photosynthetic systems, 209–210
 - catenates, 228–232
 - ferrocene- C_{60} -rotaxane, 216–221
 - structural characterization, 226–228
 - supramolecular artificial photosynthesis, 210–216
 - Zn(II)-porphyrin- C_{60} -rotaxane, 221–224
 - Zn(II)-porphyrin- CC_{60} -[2]catenates, 224–225
- Electron donors
 - amine-tethered fullerene rotaxanes, 498
 - electron transfer, molecular bridges (*see* C_{60} -bridge-donor systems; Charge separation; Porphyrin excitation)
- Electron energy loss spectroscopy (EELS), Carbon nanotubes, 278
- Electron-ion (EI) mass spectroscopy, characterization of PFAFs, 103, 114, 124
- Electron microscopy
 - carbon nanotubes, 289–291
 - scanning electron microscopy, carbon nanotubes, 289–291
 - transmission electron microscopy, carbon nanotubes, 289
- Electron transfer (ET). *see also* [2+2] Cyclizations; Cycloaddition; Energy and electron transfer in photo- and electroactive fullerene dyads; Pauson-Khand reaction; Photoinduced electron transfer
 - after light illumination, rotaxanes, 513
 - analysis of rate constants, 415–416
 - in artificial photosynthetic systems, 209–210
 - binding strength, 210
 - donor and electron acceptor subunits, 209
 - reorganization energy, 209
 - catalysis, chiral fullerenes, 49–55
 - fullerene based systems, 424–437
 - photodynamics, 408–424
 - intramolecular, 35–38
 - alcohols and thiols, 37–38
 - cycloaddition, 35–37
 - fullerenes, 34–35
 - phenols, 35–36
 - in organized molecular films
 - energy transfer and excitation annihilation, 432–435
 - interlayer charge transfer and photocurrent generation, 435–436
 - intramolecular and intermolecular charge transfer in films, 426–432

- theoretical analysis of exciplex reaction rates, 428–430
 - porphyrin-fullerene, 376–377, 380–381, 384–386
 - probing with π -conjugated oligomers, 677
 - thermodynamic and kinetic parameters, 406–407
 - van der Waals, porphyrin-fullerene, 376
- Electron transfer (ET) theory, exciplex intermediate, 429–430
 - reaction acceleration, 437
 - temperature dependence, 413–414
- Electronic states, CNTs, 254–258
- Electronic structure, of DNA/SWNT hybrids. *see* DNA/SWNT hybrids
- Electronic tuning, by chemical functionalization, 175–179
- Electronically conducting polymers (ECPs), 698, 708–709, 730, 733–737
- Electrophilic carbene addition, endohedral metallofullerenes, 160–165
- Electropolymerization, preparation, polymer composites of carbon nanotubes, 716–722
- Electrostatic interactions, layer preparation, 605–607, 620
- EMA. *see* Effective medium approach
- EMF. *see* Endohedral metallofullerene
- Emission spectroscopy, carbon nanotubes, 283–284
- Enantioselectivity, cycloadditions, fullerenes, 49–55
- Encaged species, cage frameworks, positions, and movements of, 147–154
- Endohedral atom-doping, fullerenes, 146
- Endohedral derivatives, electron donor-acceptor conjugates, 364
- Endohedral filling inner empty cavity, carbon nanotubes, 311–312
- Endohedral fullerenes
 - carbon allotropes, 34
 - synthesis, 188–189
- Endohedral metallofullerenes (EMF). *see also* Metallofullerenes
 - Bingel-Hirsch reactions, 168–170
 - cage frameworks, positions, and movements of encaged species, 147–154
 - chemical reactivity, 157–158
 - chemistry, 156–175
 - connection between encaged metal atom and cage, 148
 - electronic structures, 146
 - electronic tuning, by chemical functionalization, 175–179
 - functionalized
 - HOMO-LUMO energy gaps and levels, 176–179
 - redox potentials, 175
 - isolated pentagon rule isomers, 147
 - new vistas, 145–180
 - pristine
 - electronic properties, 154–156
 - redox potentials, 155
 - symbol and numbering systems, 147
 - synthesis, 188–189
 - trimetallic nitride, phthalocyanine fullerene assemblies, 68
- Energy and electron transfer in photo- and electroactive fullerene dyads
 - fullerene-C₆₀ functionalized with donor units
 - electroactive electron donor-C₆₀ dyads, 11–17
 - synthetic strategies, 10–11
 - light-harvesting C₆₀-based dyads

- association of perylene-3,4:9,10-bis(dicarboximide) with C₆₀, 18–24
 - photoactive electron donor-C₆₀ and electron acceptor C₆₀ dyads, 17
 - principles and applications, 4–10
- Energy gaps, molecular orbitals, phthalocyanine fullerene assemblies, 69
- Energy levels, photorefractive materials, 640
- Energy transfer
 - in bilayer films, 433
 - fullerene based donor-acceptor systems, 432–435
 - intramolecular, 46–47
- Enhancement ratio, thermal conductivity in CNTs, 767
- EnT. *see* Energy transfer
- Enzymes, as biosensors in carbon-nanotubes
 - glucose oxidase, 720, 733–734
 - lactate oxidase, 734
- Epoxy resin, composites with SWNTs, enhancement of thermal conductivity, 773–775
- EPR spectra, CSCNTs, 524–525
- Er₃N@I_h-C₈₀, Bingel-Hirsch adduct, molecular structure, 169–170
- Esterification reactions, organic functionalization of oxidized carbon nanotubes, 292–293
- ET. *see* Electron transfer; Photoinduced electron transfer
- Exciplex energetics, porphyrin and phthalocyanine-fullerene dyads, 422–424
- Exciplex intermediates
 - analysis with semi-quantum electron transfer theory, 413–414
 - donor-acceptor dyads, photodynamics, 411–420
 - formation and relaxation, thermodynamic parameters, 414
 - phthalocyanine-fullerene dyads, 417–420
 - phytochlorin-fullerene dyads, 412–413
 - porphyrin-fullerene dyads
 - energetic properties, 406–407
 - lifetime, 417
 - relaxation in donor-acceptor dyad multi-layers, 430–431
 - relaxation in molecular film, 428
 - relaxation in solution, 414–417, 428
 - quantum tunneling, 419–420
 - reaction mechanisms, 419–420
 - reaction rates, theoretical analysis, 428–430
- Excitation
 - C₆₀, 656
 - fullerenes, C₆₀-bridge-donor systems, 465–470
 - low energy, of SWNTs, 798
 - porphyrins (*see* Porphyrin excitation)
- Excitation annihilation, fullerene based donor-acceptor systems, 432–435
- Excitation density, in Langmuir-Blodgett films, of fullerene based donor-acceptor dyads, 434–435
- Excited states
 - singlet, 422
 - triplet, 482
- Exciton-exciton annihilation, in donor-acceptor dyad films, 434–435
- Exciton generation, photorefractive materials, photosensitizer, 646
- Exohedral adducts, endohedral metallofullerenes

- bis-silylation, 156–160
- electrophilic carbene addition, 160–165
- Extended tetrathiafulvalene (exTTF), 397–399
 - linking to C_{60} , 677–682
- f*-CNTs, functionalized carbon nanotubes. *see* Carbon nanotubes
- ^{19}F NMR spectra, synthesis of PFAFs, 115–116, 127–129
- FeCl_3 , precipitation of metallofullerenes. *see* Lewis acids
- FELS. *see* Electron energy loss spectroscopy
- Fermi contact, cerium-encapsulated metallofullerenes, 148–149
- Fermi levels, and van-Hove peaks, semiconductor SWNTs, 794
- Ferrocene- C_{60} -rotaxane synthesis, 216–221
 - building blocks, 218
 - click reaction, 216–217, 219–220
 - final stoppering reaction, 217
 - synthetic route, 218
- Ferrocene-nanotube hybrid materials, formation via 1,3-dipolar cycloaddition, 300–301
- Ferrocene-tethered unsymmetrical fullerene rotaxanes, 491–498
- Ferrocenes
 - C_{60} -bridges, 467–468
 - C_{60} -thiophenevinylenes, 468–469
- FET. *see* Carbon nanotube field-effect transistor
- Fiber, fullerene, 83
- Field-effect transistor. *see* Carbon nanotube field-effect transistor
- Films
 - deposition
 - electrochemical, 608–620
 - layer-by-layer, 605–608
 - spin-coating and chemical adsorption, 620–628
 - vacuum, 608
 - Langmuir-Blodgett, 595–596
 - self-assembled monolayers, 596–605
 - van der Waals interactions, 605–606, 612
- Flexible rotaxanes, temperature effect, 491–495
- Flow-tube reactor, synthesis of PFAFs, 108
- Fluorene (oFL) oligomers, linked to exTTF, molecular wires, 677–682
- Fluorescence intensity, Zn(II)Pc chromophore, phthalocyanine fullerene assemblies, 78
- Fluorination, carbon nanotubes, 296–297
- “Footballene,” 392
- Förster energy transfer, in photo- and electroactive fullerene dyads, 5
- Förster resonance mechanism, C_{60} -bridges, 470–471
- Four-wave mixing measurements, photorefractive, 643
- FP. *see* Fulleropyrrolidine
- Franck-Condon plot, photoexcitation relaxation of porphyrin-fullerene dyads, 415–416
- Free-radical additions, covalent sidewall (and tip) functionalization of carbon nanotubes, 304–305
- Fuel cells, using soluble CNTs, 258–262
- Fuller-1,6-enynes, fullerene building blocks
 - [2+2] cyclizations, 45–46
 - chemical structure, 39
 - fulleroallenes, 46–47
 - Pauson-Khand reaction, 39–45
 - theoretical study, 47–48

- Fullerene adduct UV-vis absorption
 - and emission spectra, fullerene- C_{60}
 - functionalized with donor units, 13
- Fullerene assemblies
 - covalent, 61–75
 - non-covalent, 75–83
- Fullerene based donor-acceptor dyads
 - exciplex relaxation, 430–431
 - exciton-exciton annihilation, 434–435
 - Langmuir-Blodgett films,
 - excitation density, 434–435
 - in organized molecular films
 - charge recombination, 436
 - charge separation, 435
- Fullerene based donor-acceptor systems
 - charge transfer
 - dynamics of photoinduced, 405–437
 - interlayer, 435–436
 - intramolecular and intermolecular, 426–432
 - and molecular interactions, 407–408
 - and recombination, 410–411
 - with covalent linkers, 408–410
 - electron transfer
 - organized molecular films, 424–437
 - photodynamics, 408–410
 - reaction schemes, 422–424
 - energy transfer
 - and excitation annihilation, 432–435
 - intramolecular, 420–421
 - exciplex intermediate,
 - photodynamics, 410–411
 - face-to-face configuration, 409–410
 - non-covalent linkage, 410
 - organized molecular films,
 - deposition methods, 425–426
 - reorganization energy, 406–407
 - solutions, 405–437
 - triplet state, 421–422
- Fullerene building blocks
 - alkynes, click reactions, 16–18
 - azides, click reactions, 19–20
 - chemistry, 1–28
 - click chemistry, 16–28
 - with fullerene hexa-adducts, 22–28
 - with fullerene mono- and bis-adducts, 16–22
- dendrimers
 - convergent synthesis, 10–16
 - divergent synthesis, 8–10
 - synthesis, 6–16
- porphyrin derivatives, synthesis, 2–6, 23–24
- reaction with polypropyleneimines,
 - activation of carboxylic acid function, 9–10
- Fullerene cages
 - cluster movements inside, 153–154
 - metallic oxide clusters, 186–188
 - isolation, 191–200
 - reactivity, 200–203
 - synthesis, 188–191
 - UV characterization, 203
- Fullerene/CNT composite systems,
 - electrochemical deposition, 618–620
- Fullerene derivatives
 - cyclopropane ring removal, 348
 - digital simulations of
 - electrochemical properties, 345
 - isolation of enantiomerically pure chiral C_{76} , 354
 - isolation of three constitutional isomers, 355
 - methano C_{70} fullerene derivatives, 353
 - as photosensitizers in PR materials, 655–658
 - C_{60} -based dyads, 658–664

- synthesis of regioselective tris-adducts, 351–352
- Fullerene excitation, C₆₀-bridge-donor systems
 - long linkages, 468–470
 - short linkages, 465–468
- Fullerene fiber, 83
- Fullerene-filled CNTs, solubilization
 - with pyrene-based dispersants, 251
- [60]Fullerene-[70]fullerene mixtures, photosensitizers in photorefractive materials, 651–655
- Fullerene-N-oxide combinations, for radical stabilization, 674–675
- Fullerene-rich dendrimers, convergent and divergent synthesis, 8–16
- Fullerene ring opening, 358
- Fullerene rotaxanes. *see also* Photoinduced electron transfer processes
- Fullerene solubility improvement, retro-Diels-Alder reaction, 339
- Fullerene-stopped molecular shuttles, 671–673
- Fullerenes. *see also* C₆₀ fullerenes; Endohedral metallofullerenes; Photosensitizers in photorefractive materials
 - building from fuller-1,6-enynes (*see* Fuller-1,6-enynes)
 - chemical functionalization, 669–670
 - chiral, 34, 46, 49–55
 - [2+2] cyclizations, thermally induced, 45–47
 - definition and history, 667–669
 - electrochemical deposition, 608–609 (*see also* Electrochemical deposition)
 - electron accepting properties, 406
 - electron acceptors, 442, 594
 - endohedral, 34, 188–189
 - endohedral atom-doping, 146
 - higher, 34
 - intramolecular
 - cycloadditions, 34–38 (*see also* Cycloadditions)
 - ene reaction, 46–47
 - metallofullerenes (*see* Metallic oxide clusters; Metallofullerenes)
 - Pauson-Khand reaction, 39–45
 - photochemistry, bridges (*see* C₆₀-bridge-donor systems; Charge separation; Porphyrin excitation)
 - photoelectrochemical and photovoltaic devices (*see* Photoelectrochemical devices)
 - porphyrins
 - bridges (*see* Porphyrin excitation)
 - cobalt (II), 380–387
 - interaction, 376, 378–380
 - molecular hosts, 376–378
 - solid state, 376
 - supramolecular hosts for, 391–401
- [60]Fullerenes. *see* C₆₀ fullerenes
- Fulleroallenes, synthesis, 46–47
- Fullerodendrimers
 - C₆₀ subunits at each branching units, 10–16
 - convergent synthesis
 - activation of carboxylic acid function as key to the synthesis, 9
 - (*p*-methoxybenzyl) protecting group, 13
 - reagents and conditions, 10–16
 - successive esterification and deprotection steps, 11–13
 - divergent synthesis
 - reagents and conditions, 8–10
 - solubility and spectroscopic characterization of the compounds, 10

- with polypropyleneimine core, 10
 - solubilizing groups, 14
 - stannoxane core, reagents and conditions, 16–18
 - t*-butyl ester function as branching unit, 14–15
- Fulleropyrrolidine (FP)
 - femtosecond transient absorption spectra, 35
 - stabilization by N-oxides, 675
- Functional aromatic molecules, individual solubilization of CNTs, 251–253
- Functionalization
 - of C_{60}
 - regiospecific, 335–336
 - topochemical, 335–336
 - of CNTs (*see* Carbon nanotubes)
 - covalent, recent advances, 271–316
 - of graphene (*see* Graphene nanosheets)
 - of SWNT surface (*see* Single-walled nanotubes)
- Functionalized clusterfullerenes
 - carbene adducts, electronic properties, 175
 - electronic properties and redox potentials, 179
 - redox potentials, 177
- Functionalized dimetallofullerenes
 - bis-silyl adducts, electronic properties and redox potentials, 178–179
 - pyrrolidino adducts, electronic properties and redox potentials, 179
 - redox potentials, 177
- Functionalized endohedral metallofullerenes
 - HOMO-LUMO energy gaps and levels, 176–179
 - redox potentials, 175
- Functionalized fullerene derivatives. *see* Molecular electronics
- Functionalized monometallofullerenes, electronic properties and redox potentials
 - benzyl adducts, 178–179
 - Bingel adducts, 176–177
 - bis-silyl adducts, 175
 - Diels-Alder adducts, 177–178
 - nitrated benzyl adducts, 179
- Functionalized nanotubes. *see* Carbon nanotubes
- Functionalized silica, isolation of metallic oxide clusters in fullerene cages, 192–196
- FWM. *see* Four-wave mixing
- Gain coefficient
 - C_{60} -based dyads as photosensitizers, 659
 - liquid crystal mixtures doped with C_{60} , 653
 - two-beam coupling, 643
- Gating effect, photosensitizers in photorefractive materials, [6,6]-PCBM, 657
- Glucose oxidase (GOX), doping of carbon-nanotubes, biosensors, 720, 733–734
- GNs. *see* Graphene nanosheets
- Gold dendrimer-encapsulated nanoparticles (Au DENs), attached on multi-walled carbon nanotube surface, 295–296
- Gold electrodes
 - phthalocyanine-carbon nanotubetube sensors, 92
 - self-assembled monolayers, 596–601
- GOX. *see* Glucose oxidase
- GR. *see* Graphene
- Gradient-temperature gas-solid (GTGS) reactor, synthesis of PFAFs, 110–111, 119

- Grafting of polymers, covalent sidewall (and tip) functionalization of carbon nanotubes, 309–310
- Graphene (GR)
 alternative to CNTs, 742
 carbon allotropes, 34
 structural connection with graphite and CNTs, 520
- Graphene lattice, translation vectors, DNA/SWNT hybrids, 800
- Graphene nanosheets (GNs)
 functionalization, effect on
 thermal conductivity, 781–783
 for thermal conductive materials
 definition, 778
 polymeric/GN composites, 779–783
 preparation, 779
 thermal conductivity of composites compared to GMP-composites, 780
- Graphite
 composites with SWCNTs, thermal conductivity, 764–765
 structural connection with graphene and CNTs, 520
- Graphite nanoplatelets. *see* Graphene nanosheets
- Graphitic microparticles (GMPs), thermal conductivity of composites compared to GN-composites, 780
- Halogenation, covalent sidewall (and tip) functionalization of carbon nanotubes, 296–297
- Hamiltonian
 for a massless particle, low energy excitations of SWNT, 798
 modeling of DNA/SWNT hybrids, 805–806
 perturbation of DNA wrapping, DNA/SWNT hybrids, 801–802
- Hartree theory, applied to DNA/SWNT hybrids, 805, 809
- Heck coupling, functionalization of carbon nanotube surfaces, 308–309
- Helical perturbation
 due to DNA wrapping, DNA/SWNT hybrids, 801–802
 selection rules for, 803
- High resolution transmission electron microscopy (HRTEM), carbon nanotubes, chiral indexes and number of walls, 289
- Higher fullerenes, carbon allotropes, 34
- Highest occupied molecular orbital (HOMO). *see also*
 Photoelectrochemical devices
 in C₆₀-exTTF systems, 679–682
 DNA/SWNT hybrids, 815–816
 molecular bridges (*see* C₆₀-bridge-donor systems; Charge separation; Porphyrin excitation)
 phthalocyanine fullerene assemblies, 69
 tetraphenylporphyrin, 379
- Highly aligned carbon-nanotubes, 729
 and CNT films, 711–714
 and PANI films, 723–725
 and P3OT films, 704–705, 738–740
 and PPY films, 708–713, 717–720, 734
- Highly aligned SWCNTs, thermal conductivity, 763–764
- Hole-transporting materials, photorefractive materials, photoconductor, 648
- HOMO. *see* Highest occupied molecular orbital
- HOMO-LUMO electron distribution
 amine-tethered fullerene rotaxanes, 498

- functionalized endohedral metallofullerenes, 176–179
- Hopping, thermally activated incoherent, 676
- Host-guest complexes, porphyrin-fullerene, 380–382
- H_2P^{8+} , as excited-state electron donor, in multifunctional hybrid cells, 686–689
- HPLC-based PFAF purifications, 119–123
- HPLC traces, synthesis of PFAFs, 107, 111, 115–116
- HRTEM. *see* High resolution transmission electron microscopy
- Huisgen 1,3-dipolar cycloaddition fullerene hexakis-adducts, azides and alkynes, 24–28 fullerene mono- and bis-adducts, azides and alkynes, 16–22
- Huisgen-Sharpless-medal-Cu(I)-catalyzed-1,3-dipolar cycloaddition, 216
- Hydrogen-bonding systems, deposition, 622–627
- Imide oligomers, containing phenylethynyl groups. *see* Phenylethynyl terminated imide
- Impurities, effect on thermal conductivity of CNTs, 774
- INADEQUATE. *see* Incredible natural abundance double quantum transfer experiment
- Incident photon to charge carrier generation efficiency (IPCE)
 - CNC-(C_{60})_n composite clusters, 529
 - CNC-(H_2P)_n nanohybrids, 536
 - CSCNTs, 523–524
- Incident photon-to-current efficiency (IPCE)
- Hydrogen bonding systems, 624–627
- ITO electrodes, 602–605
- Langmuir-Blodgett films, 596
- Non-covalent linked donor-fullerene systems, 610–613
- Porphyrin-fullerene composite systems, 617–620
 - SAM on gold electrodes, 600–601
- Incoherent hopping, thermally activated, 676
- Incredible natural abundance double quantum transfer experiment (INADEQUATE), $Ce@C_{2v}-C_{82}$ anions, 148
- Indium tin oxide (ITO) electrodes
 - bulk-heterojunction solar cells, 35–36
 - conduction band, 601
 - for determination of electronic states of isolated SWNTs, 255–258
 - modification, 732
 - molecular photoelectrochemistry, 683–688
 - self-assembled monolayers, 601–605
 - of porphyrin-PDI- C_{60} triad, 23
- Individual CNTs. *see also* Multi-walled carbon nanotubes; Single-walled carbon nanotubes
 - predicted thermal conductivity, 756–757
 - for thermal conductive materials, 757–761
- Individually solubilized CNTs
 - characterizations of, 247
 - using functional aromatic molecules, 251–253
 - using surfactant micelles, 247–248

- Infrared spectroscopy, carbon nanotubes, 282–283
- Interactions. *see also* Charge transfer
 anisotropic pseudocontact, cerium-encapsulated metallofullerenes, 148–149
 electrostatic, layer preparation, 605–607, 620
 interchromophore, porphyrin-fullerene dyads, 408–413
 metal-ligand, phthalocyanine fullerene assemblies, 78–80
 π – π
 carbon nanotubes assemblies, 89
 between polycyclic aromatic compounds and CNT sidewalls, 251
 between polyimides and SWNT surfaces, 254
 Van der Waals
 layer preparation, 605–606, 612
 molecular porphyrin hosts for fullerenes, 376, 380, 386
 Watson-Crick hydrogen bonding, phthalocyanine fullerene assemblies, 77
- Interchromophore interactions, porphyrin-fullerene dyads, 408–413
- Interfacial thermal resistance, tube-tube, 771
- Interlayer charge transfer and photocurrent generation, fullerene based donor-acceptor systems, 435–436
- Interlocked electron donor-acceptor molecules, photoinduced electron transfer processes, 480
- Intramolecular and intermolecular charge transfer in films, fullerene based donor-acceptor systems, 426–432
- Intramolecular back-electron transfer, CNC-(H₂P)_n nanohybrids, 535
- Intramolecular energy transfer, fullerene based donor-acceptor systems, 420–421
- Intramolecular photoinduced electron transfer, phthalocyanine fullerene assemblies, 72
- Intramolecular reactions. *see also* Pauson-Khand reaction
 cycloadditions, 34–38
 ene reaction, 46–47
 theoretical study, intramolecular reactions of fuller-1,6-enynes, 47–49
- Intrarotaxane hydrogen bonding, stabilization of fulleropyrrolidine, 675
- Iodine function, phthalocyanine fullerene assemblies, covalent, 66–67
- IPCE. *see* Incident photon to charge carrier generation efficiency; Incident photon-to-current efficiency
- IPR. *see* Isolated pentagon rule
- Irreversible Diels-Alder reaction, endohedral metallofullerenes, 172–173
- Isolated pentagon rule (IPR), reactions and retro-reactions of fullerenes, 326
- Isolated pentagon rule (IPR) isomers
 Ce₂@D_{5h}-C₈₀, 152
 La₂@D_{3h}(5)-C₇₈, 150
 M@C_{2v}-C₈₂, 147
 numbering system for endohedral metallofullerenes, 147
- Isolated (n,m) SWNTs, redox potentials, 255–258
- ITO. *see* Indium tin oxide
- Knudsen cell, as a chemical microreactor, synthesis of PFAFs, 105

- La@C₂(10612)-C₇₂C₆H₃Cl₂, radical coupling product, molecular structure, 173–174
- Lactate oxidase, doping of carbon-nanotubes, biosensors, 734
- La@C_{2v}-C₈₂
 Bingel-Hirsch reactions, 168
 bis-silylation, 157
 cage frameworks, ¹³C-NMR spectra, 147
 Diels-Alder reaction, with
 1,2,3,4,5-pentamethylcyclopentadiene, 170–172
 electrophilic carbene addition, molecular structures and characterization of adducts, 162–163
 photoirradiation, with α,α,2,4-tetrachlorotoluene, 173
 redox potentials, 155
- La@C_{2v}-C₈₂CBr(COOEt)₂, Bingel-Hirsch adduct, molecular structure, 168–169
- La@C_{2v}-C₈₂(C₆H(C₄)(C₂NO(C₂), formation by Diels-Alder reaction, 171–172
- La@C_{2v}(3)-C₈₀C₆H₃Cl₂, radical coupling product, molecular structure, 173–174
- La@C_{2v}-C₈₂CHClC₆H₃Cl₂, formation by photoirradiation, 173
- La@C_{2v}-C₈₂[CH(COOEt)₂]₂, Bingel-Hirsch adduct, molecular structure, 168–169
- La@C_{2v}-C₈₂(Cp*), molecular structure, 170–172
- La₂@D₂(10611)-C₇₂
¹³C-NMR spectra, 149
 electrophilic carbene addition, molecular structures and characterization of adducts, 162–163
- ¹³⁹La-NMR spectra, 149–150
 non-isolated pentagon rule cage, 149–150
- La₂@D₂(10611)-C₇₂ hexaanions, electronic structure and stability, 149
- La₂@D_{3h}(5)-C₇₈
¹³C-NMR spectra, 150
 cage framework and positions of the metal atoms, 150–151
 electrophilic carbene addition, 163
 redox potentials, 155
- La@D_{3h}-C₇₄C₆H₃Cl₂, radical coupling product, molecular structure, 173–174
- La₂@I_h-C₈₀
 bis-silylation, structures and electronic properties, 158–159
¹³C-NMR spectra, 151
 cage framework and positions of the metal atoms, 150–151
 1,3-dipolar cycloaddition, with azomethine ylide, 165–166
 electrophilic carbene addition, structures and electronic properties of adducts, 164–165
¹³⁹La-NMR spectra, 151
- Langmuir-Blodgett (LB) films
 deposition of fullerene based donor-acceptor layers, 425
 fullerene based donor-acceptor layers, exciplex relaxation, 430–431
 photoelectrochemical devices, fullerenes, 595–596
 phthalocyanine fullerene assemblies, 63
- Langmuir-Blodgett (LB) technique, carbon nanotube-fullerene composite systems, 711
- Langmuir-Schäfer (LS) methods, deposition of fullerene based donor-acceptor layers, 425

- Laser-desorption mass spectrometry,
matrix-assisted, characterization of
PFAFs, 124
- Layer-by-layer deposition, 605–608
- Layers. *see* Films
- LB. *see* Langmuir-Blodgett
- Lewis acid conditions, fullerene ring
opening, 358
- Lewis acids, precipitation methods
correlation of metallofullerenes
versus Lewis acid stages, 201
kinetic data, 201
metallofullerenes in general,
196–198
stage 1 metallofullerenes, 198–199
stage 2 metallofullerenes,
199–200
- Ligands, chirality, 51–52
- Light-energy conversion
by electron donor-acceptor
nanohybrids, 519–540
photoinduced electron transfer
processes, rotaxanes, 482
- Light-harvesting C_{60} -based dyads. *see*
also Perylene-3,4:9,10-
bis(dicarboximide)
Angers and Amsterdam's C_{60} -PDI
assemblies
concept of antenna, 25
incorporation of C_{60} -PDI
dyads in bulk-
heterojunction, 35–38
photophysics, 27–35
synthesis of bay-substituted
 C_{60} -PDI dyads and
corresponding
electrochemical behaviour,
25–27
association of PDI with C_{60} , 38–39
association of perylene-3,4:9,10-
bis(dicarboximide) with C_{60} ,
properties and applications,
18–24
photoactive electron donor- C_{60} and
electron acceptor- C_{60} dyads, 17
- Light intensity (LI) grating,
photorefractive materials, 638
- Light polarization, and one-electron
absorption spectrum, in
DNA/SWNT hybrids, 790
- Liquid crystal mixtures doped with C_{60} ,
gain coefficient, photosensitizers in
PR materials, 653
- Low energy excitations, of SWNTs,
Dirac Hamiltonian, 798
- Lowest unoccupied molecular orbital
(LUMO)
 C_{60} , associated with porphyrin to
fullerene charge transfer band,
379
 C_{60} -exTTF systems, 679–682,
815–816
molecular bridges (*see* C_{60} -bridge-
donor systems; Charge
separation; Porphyrin excitation)
phthalocyanine fullerene
assemblies, 69
- LOX. *see* Lactate oxidase
- LS. *see* Langmuir-Schäfer
- LUMO. *see* Lowest unoccupied
molecular orbital
- Macrocycles, in rotaxanes, 671–674
- Magnetic field alignment, of CNTs in
polymeric/CNT composites,
enhancement of thermal
conductivity, 773–774
- Magnetization, carbon nanotubes
assemblies, non-covalent, 90
- MALDI. *see* Matrix-assisted laser-
desorption
- Marcus equation, photorefractive
materials, photosensitizer, 647
- Marcus formula, electron transfer, in
molecular fullerene based donor-
acceptor layer, 429

- Marcus inverted region, charge-recombination processes, 461
- Mass spectrometry (MS). *see also*
 - Electron-ion (EI) mass spectroscopy
 - characterization of PFAFs, 123–124
 - in situ* formation of PFAFs, 105
- Matrix-assisted laser-desorption (MALDI) MS, characterization of PFAFs, 113, 124
- $M@C_{2v}-C_{82}$
 - electrophilic carbene addition, sides of attack, 161
 - positions, and movements of encaged metal atoms, 147–148
- $M@C_{2v}-C_{82}$ anions, cage frameworks, ^{13}C -NMR spectra, 147
- MD. *see* Molecular dynamics
- Mechanical movements, rotaxanes, 480
- Mechanics, polymer composites of carbon nanotubes, 729–730
- Mechanochemical functionalizations, covalent sidewall (and tip) functionalization of carbon nanotubes, 310
- Melting, preparation, polymer composites of carbon nanotubes, 706–708
- Metal carbides, inside fullerene cages, 153–154
- Metal complexes, and PFAFs, 132
- Metal-ligand bonds, phthalocyanine fullerene assemblies, comparison with covalent bonds, 82
- Metal-ligand interactions, phthalocyanine fullerene assemblies, 78–80
- Metal-semiconductor transition, metallic SWNTs, 790–794
- Metal trifluoroacetates, synthesis of PFAFs, 105–107
- Metallic nitride clusters, in azafullerene cages
 - precipitation, 198, 201
 - synthesis, 189
- Metallic nitride fullerenes (MNF). *see also* Metallic oxide clusters in fullerene cages
 - synthesis, 188–189
- Metallic oxide clusters, in fullerene cages
 - comparison to electrochemical band gap, 201–203
 - comparison with other fullerenes, 200–201
 - isolation, 191–200
 - selective precipitation method using Lewis acids, 196–200
 - stir and filter approach, 192–196
 - synthesis, 188–191
 - UV characterization, 203
- Metallic SWNTs
 - absorption coefficient, 793
 - band gap opening, and metal-semiconductor transition, 790–794, 802
 - band gap parameters, 803
 - density of states, 791–792
- Metallofullerenes (MFs). *see also* Endohedral metallofullerenes; Metallic oxide clusters
 - internal electron transfers, 154
 - $M_{3n}@C_{80}$
 - phthalocyanine fullerene assemblies, 68
 - Prato reaction, 70
 - precipitation, 197–199
 - kinetic data, 201
 - solar cells, 71
- Metalloporphyrins, hosts for fullerenes, 381, 387
- Metallosupramolecular complexes, Ti(IV)phthalocyanine, 82

- MF. *see* Metallofullerene
- Mixing, preparation, polymer
composites of carbon nanotubes,
703–706
- MNAF. *see* Metallic nitride cluster in
azafullerene cage
- MNF. *see* Metallic nitride fullerene
- Mobile charge generation, quantum
efficiency, 641
- Mobile charges, photorefractive
materials, 640
- Molecular bridges
C₆₀-bridge-donor systems (*see* C₆₀-
bridge-donor systems)
charge-separation processes (*see*
Charge separation)
porphyrin-bridge-fullerene
molecules (*see* Porphyrin
excitation)
- Molecular donor-acceptor conjugates,
in multifunctional hybrid cells, 687
- Molecular donor and acceptor building
blocks, in multifunctional hybrid
cells, 684
- Molecular dynamics (MD) calculations
bis-porphyrins, 488–489
ferrocene-tethered fullerene
rotaxanes, 496–497
n,n-di(tert-butyl-
biphenyl)benzenamine,
symmetrical rotaxanes, 483–485
thermal conductivity in CNTs, 766
triphenylamines, 507–509
- Molecular electronics
with functionalized fullerene
derivatives
chemical methods, 669–670
history, 667–669
molecular machines, 670–675
molecular
photoelectrochemistry,
682–689
molecular wires (*see* Molecular
wires)
with logic switching elements,
photoinduced electron transfer
processes, 480
- Molecular films
dynamics of photoinduced charge
transfer, 405–437
photovoltaic applications, 425
- Molecular glasses, photorefractive
materials, 646
- Molecular machines
design and preparation, 670–675
rotaxanes, 481
- Molecular orbital (MO). *see* Highest
occupied molecular orbital; Lowest
unoccupied molecular orbital
- Molecular photoelectrochemistry,
682–689
chromophores, 683
donor-acceptor conjugates, 687
donor and acceptor building
blocks, 684
indium tin oxide electrodes,
683–688
multifunctional hybrid cells,
682–688
porphyrins as chromophores,
686–689
role of polyelectrolytes, 683–684
- Molecular shuttles. *see also* Rotaxanes
NLO response, 674
reverse switching, 672
solvent and electrochemically
controllable, 673
solvent switchable, 671–672
- Molecular surgery, Diels-Alder adducts
of substituted isobenzofurans, 337
- Molecular tweezers, as hosts for
fullerenes
porphyrin-based, 396–397
TTF-based, 397–399

- Molecular wires
 attenuation factor b , 676
 C_{60} -exTTF ensembles, 677–682
 properties and preparation, 675–682
 structural tunability, 675
 thermally activated incoherent hopping, 676
 unidirectional transport of charges, (as a key feature), 676
- Monolayers. *see* Self-assembled monolayers
- Monometallofullerenes
 Bingel-Hirsch reactions, 168–169
 ^{13}C -NMR spectra, 147–148
 cage frameworks, positions, and movements of encaged species, 147–149
 electronic structures, 147–149
 photoirradiation, 173
 solubility, 173
- MS. *see* Mass spectrometry
- Multi-ring interlocked fullerene systems
 chlorophyll, 208
 electron transfer reactions in artificial photosynthetic systems, 209–210
 natural energy transfer, 208–209
 preparation strategies, 239
 structural characterization, 226–228
 NMR spectra, 226
 structural characterization, 227
 triazole rings, 226
 supramolecular artificial photosynthesis, 210–216
 synthesis of [3]catenates, 228–232
 synthesis of Zn(II) -porphyrin- C_{60} -[2]catenates, 221–224
 synthesis of Zn(II) -porphyrin- C_{60} -rotaxane, 216–221
- Multi-step synthesis, C_{60} fullerene, chemical reactivity, 2
- Multi-walled carbon nanotubes (MWCNTs/MWNTs), 34
 acid-purified, enhancement of thermal conductivity, 769
 attached gold dendrimer-encapsulated nanoparticles, 295–296
 carbon nanotubes assemblies, 83
 composites with PETI, enhancement of thermal conductivity, 773
 composites with polymers (*see also* Polymer composites of carbon nanotubes)
 composites with polystyrene, enhancement of thermal conductivity, 767
 composites with sodium dodecyl sulfate, enhancement of thermal conductivity, 772
 definition, 246
 individual, thermal conductivity, 757–758
 Pt/MWNT/PBI nanocomposites, 258–262
 structure and properties, 273–274
 thermogravimetric analysis, 277
- Multifunctional hybrid cells, molecular photoelectrochemistry, 682–688
- Multiple step electron transfer, rotaxanes, 513
- MWCNTs. *see* Multi-walled carbon nanotubes
- MWNTs. *see* Multi-walled carbon nanotubes
- N-methylpyrrolidine ring structures, phthalocyanine fullerene assemblies, 64–65

- N-oxides, combined with fullerenes, for radical stabilization, 674–675
- Nanocarbons (CNCs), cup-shaped, for light-energy conversion, 524–530
- Nanocomposites, CNT-filled polymeric. *see* Polymer composites of carbon nanotubes
- Nanodevices, potential of nanomaterials for constructing of, 519–521
- Nanodiamond (ND)-porphyrin assemblies
 IPCE values, 539
 for light-energy conversion, 537–540
 photoinduced electron transfer, 539–540
 with tetrakis(*p*-carboxyphenyl)porphyrin, 538–540
- Nanohorn (NH), compared to other nanomaterials, 520
- Nanohybrids, electron donor-acceptor, for light-energy conversion, 519–540
- Nanomachines. *see* Molecular machines
- Nanoscience/nanotechnology, and molecular electronics, 669
- Nanostructured carbon materials, principle structures, 520
- Nanotube-fullerene composite systems. *see* Carbon nanotube-fullerene composite systems
- Nanotube functionalization, in thermal conductive materials, 776–778
- Nanotube/polymer composites, solubilized CNTs, 254
- Nanowires. *see* Molecular Wires
- Natural energy transfer, 208
- “Natural” optical activity, DNA/SWNT hybrids, 817
- ND. *see* Nanodiamond
- Net gain coefficient, two-beam coupling, 643
- Nitride fullerenes. *see* Metallic nitride fullerenes
- Nitrogen gasification, for removing PMMA from SWNT-PMMA composites, 774–776
- NLO. *see* Non-linear optical
- NLOphore, photorefractive materials, 649–650
- NLOphores in PR composites, 650
- NMR spectroscopy. *see also* ^{13}C -NMR spectroscopy
 characterization of PFAFs, 127–128
- N,N-di(tert-butyl-biphenyl)benzenamine (BBA)
 molecular dynamic calculations, 485–486
 photoinduced electron transfer processes, symmetrical rotaxanes, 483
- Non-chiral SWNTs, showing circular dichroism, 789
- Non-covalent adsorption, carbon nanotubes, 310–311
- Non-covalent phthalocyanine systems
 with fullerenes, 75–83
 with nanotubes, 89–93
- Noncovalently linked donor-fullerene systems, electrochemical deposition, 610–613
- Non-isolated pentagon rule (IPR) isomers, $\text{La}_2@D_2(10611)\text{-C}_{72}$, 149
- Non-linear optical (NLO) behavior, phthalocyanine-SWNT systems, 89
- Non-linear optical (NLO) chromophore, 650
- Non-linear optical (NLO) response
 molecular shuttles, 674
 photorefractive measurements, 641
- Nuclear magnetic resonance spectrometry, carbon nanotubes, 284–285. *see also* ^{13}C -NMR spectroscopy

- Nucleophilic addition
 - covalent sidewall (and tip)
 - functionalization of CNTs, 303–304
 - endohedral metallofullerenes, 168–170
 - intramolecular
 - alcohols and thiols, 37–38
 - phenols, 35–37
- Numerical modeling, of DNA/SWNT hybrids, electronic properties, 805–810
- Octa-permethylated β -cyclodextrin (PM β -CD)-porphyrin, host for C₆₀ fullerenes, 401
- Octaethylporphyrin (OEP), and PFAFs, 132
- oFL. *see* fluorene (oFL) oligomers
- Oligo-silanes, porphyrin-bridge-fullerene molecules, 464
- Oligophenylene-vinylene (OPV)-C₆₀ dyads
 - organic solar cells, 15–17
 - photovoltaic conversion, 15
- Oligothiophene-vinylenes, porphyrin-bridge-fullerene molecules, 455–456
- Oligothiophenes, porphyrin-bridge-fullerene molecules
 - crown ethers, 461–462
 - long bridges, 456–461
- OMF. *see* Oxometallic fullerene
- “One-dimensional” conductors. *see* molecular wires
- One-electron absorption spectrum, and light polarization, in DNA/SWNT hybrids, 790
- One-electron Schrödinger equation, modeling of DNA/SWNT hybrids, 805
- Onsager model of charge
 - recombination, photorefractive materials, photosensitizer, 647
- oPPE. *see* para-phenyleneethynylene
- oPPV. *see* para-phenylenevinylene
- Optical absorption, DNA/SWNT hybrids, 814–815
- Optical activity, DNA/SWNT hybrids, 817
- Optical selection rules, lift of, in DNA/SWNT hybrids, 790
- Optical switching, bistable rotaxanes, 670
- Optical transparent electrodes (OTEs)
 - casting of CSCNTs, 522–524
 - CNC-(C₆₀)_n composite clusters, 529–531
- Optoelectronics
 - bistable rotaxanes, 670
 - C₆₀-based dyads, 658
- OPV. *see* Oligophenylenevinylene
- Organic functionalization, carbon nanotubes, 291–312
 - covalent surface chemistry, 291–310
 - endohedral filling inner empty cavity, 311–312
 - non-covalent adsorption or wrapping of functional molecules, 310–311
- Organic materials, photorefractivity, 640
- Organic molecular electronics, with functionalized fullerene derivatives. *see* Molecular electronics
- Organic reactions
 - C₆₀ fullerenes, macrocyclization, 3
 - endohedral metallofullerenes
 - 1,3-dipolar cycloaddition, 165–168
 - bis-silylation, 156–160
 - Diels-Alder reaction, 170–173
 - electrophilic carbene addition, 160–165
 - nucleophilic addition, 168–170

- radical reaction, 173–175
- Organic solar cells, 481
 - bulk heterojunction, molecular fullerene based donor-acceptor layer, 426
 - OPV- C_{60} dyads, 15–17
- Organic solutions, complexation of C_{60} fullerenes, 392–401
- Organized molecular films
 - fullerene based donor-acceptor layer
 - Langmuir-Blodgett, 425
 - Langmuir-Schäfer methods, 425
 - self-assembled monolayers, 426
 - fullerene based donor-acceptor systems
 - deposition methods, 425–426
 - dynamics of photoinduced charge transfer, 405–437
 - electron transfer, 424–437
 - for photovoltaic applications, 425
- OTE/ SnO_2 and OTE/ TiO_2 electrodes
 - casting of CSCNTs, 522–524
 - CNC-(C_{60})_n composite clusters, 529–531
 - CNC-(H_2P)_n nanohybrids, 536–537
 - ND-TCPP nanoclusters, 538–540
- Oxidations
 - carbon nanotubes, covalent functionalization, 292
 - metallofullerenes, redox potentials, 155–156, 175–179
 - poly(3-octylthiophene) (P3OT), 708–709
- Oxometallic fullerenes (OMF). *see also*
 - Metallic oxide clusters in fullerene cages
 - synthesis, 188–191
 - UV characterization, 203
- Ozonolysis, covalent sidewall (and tip) functionalization of carbon nanotubes, 308–309
- p*-xylene solvent molecules, and PFAFs, 132–133
- PAMAM. *see* Polyamidoamine
- PANI, carbon-nanotubes. *see* Polyaniline
- para*-phenyleneethynylene (oPPE), linked to exTTF, molecular wires, 677–682
- para*-phenylenevinylene (oPPV), linked to exTTF, molecular wires, 677–682
- Paramagnetic NMR shift analysis
 - clusterfullerenes, 153
 - dimetallofullerenes, 150–152
 - monometallofullerenes, 148
- Partial absorption coefficient, DNA/SWNT hybrids, 817
- Pauson-Khand (PK) reaction
 - double intramolecular, scheme, 42
 - fuller-1,6-enynes, scheme, 40
 - [60]fullerene, 39–45
- PBI. *see* Polybenzimidazole
- Pc. *see* Phthalocyanine
- PCBM. *see* [6,6]-phenyl- C_{61} -butyric acid methyl ester
- PDDA^{nt}. *see* Poly(diallyl-dimethylammonium) chloride
- PDI. *see* Perylene-3,4:9,10-bis(dicarboximide)
- PDT. *see* Double photodynamic therapy
- PEFCs. *see* Polymer electrolyte fuel cells
- pentaCp*. *see* 1,2,3,4,5-Pentamethylcyclopentadiene
- 1,2,3,4,5-Pentamethylcyclopentadiene (Cp*), Diels-Alder reaction, with La@ C_{2v} - C_{82} , 170–172
- Percolation threshold, lack of, in polymeric/nanotube composites, 768

- Perfluoroalkylfullerenes (PFAFs)
 and aromatic solvents, 132–133
 characterization
 mass spectrometry, 123–124
 NMR spectroscopy, 127–128
 vibrational and UV-vis spectroscopy, 125–126
 X-ray crystallography, 128–133
 chemical properties, 137–139
 cyclic voltammograms, 135
 derivatization, 137–139
 DFT predicted and experimental Raman spectra, 126
 DFT structure compared to X-ray-diffraction experiments, 104, 130
 electrochemical properties, 135–136
 isolation
 purification methods, 119–123
 selective syntheses of PFAFs, 115–119
 and metal complexes, 132
 physical properties, 134
 reduction potentials, 135–136
 synthesis
 general remarks, 102
 reactions with metal trifluoroacetates, 105–107
 reactions with perfluoroalkyl iodides, 107–114
 in situ, in an arc generator or mass spectrometer, 103–105
 steps, 102–103
- Perfluoroalkyl iodides, synthesis of PFAFs, 107
 reactions with C_2F_5I , C_3F_7I , C_4F_9I , $C_6F_{13}I$, and $C_{12}F_{25}I$, 112–114
 reactions with CF_3I , 108–111
- Perfluoroalkyl (R_F) radical precursors, role in synthesis of PFAFs, 102
- Perturbation dependence, of surface/interface layer of SWNTs, 788
- Perturbation, model potential, to describe the DNA perturbation, 811
- Perylene-3,4,9,10-bis(dicarboximide) (PDI)
 association with C_{60} , 18–24
 electrochemical data, 32
 photophysical data, 32
 UV-vis absorption and emission spectra, 20
- Perylene-3,4-mono(dicarboximide) (PMI)
 association with C_{60} , 38–39
 electrochemical data, 32
 photophysical data, 32
- PET. *see* Photoinduced electron transfer
- PETI. *see* Phenylethynyl terminated imide
- PFAFs. *see* Perfluoroalkylfullerenes
- Phase separation risk, polymer materials, 645
- P3HD- C_{60} solar cells, concept of antenna effect, 26
- [6,6]-Phenyl C_{61} -butyric acid methyl ester (PCMB)
 bulk-heterojunction, theoretical principle, 36
 cost of production, 115
 photophysical and electrochemical data, 34
 photosensitizer in photoreactive materials, 657–658
 phthalocyanine fullerene assemblies, starting material, 74
- Phenyleneacetylenes, porphyrin-bridge-fullerene molecules, 449–451

- Phenylenevinylenes, porphyrin-bridge-fullerene molecules, 452–455
- Phenylethynyl terminated imide (PETI), composites with MWNTs, enhancement of thermal conductivity, 773
- Phonon group velocity, and Umklapp process, zigzag SWNTs, 759
- Photo- and electroactive fullerene dyads. *see* Energy and electron transfer in photo- and electroactive fullerene dyads
- Photoconductive devices, phthalocyanine-carbon nanotubes, 92–93
- Photoconductivity, photorefractive measurements, 641
- Photoconductors, photorefractive materials, 648–649
- Photodynamics
 - charge transfer and recombination in fullerene based dyads, 410–411
 - electron transfer in fullerene based dyads, 408–410
 - reaction schemes, 422–424
 - exciplex intermediate in fullerene based dyads, 411–420
 - intramolecular energy transfer in fullerene based dyads, 420–421
 - triplet state in fullerene based dyads, 421–422
- Photoelectrochemical devices
 - fullerenes
 - electrochemical deposition, 608–620
 - Langmuir-Blodgett films, 595–596
 - layer-by-layer deposition, 605–608
 - properties and requirements, 594–595
 - self-assembled monolayers, 596–605
 - spin-coating deposition and chemical adsorption, 620–628
 - vacuum deposition, 608
 - SWNTs, potential, 521
- Photoexcitation. *see also* Excitation C_{60} , 656
 - phthalocyanine-fullerene dyads in molecular layers, 431–432
- Photogeneration, PR materials, 638
 - efficiencies, 652
- Photohyperthermia (PHT) cancer
 - phototherapy, phthalocyanine-carbon nanotubes, 91
- Photoinduced charge separation
 - fullerenes, 594–595
 - polymer- C_{60} interface, 739
 - Porphyrin-fullerene dyads, reaction mechanism and temperature dependency of reaction rate constant, 419–420
 - rotaxanes, 481
- Photoinduced charge transfers, fullerene based donor-acceptor systems, dynamics, 405–437
- Photoinduced electron transfer (PET), 739. *see also* C_{60} -bridge-donor systems; Charge separation; Electron transfer; Porphyrin excitation
 - energy and electron transfer in photo- and electroactive fullerene dyads, 6–10
 - exciplex intermediate
 - phthalocyanine-fullerene dyads, 417–420
 - porphyrin-fullerene dyads, 410–417
 - intramolecular, phthalocyanine fullerene assemblies, 72
 - nanodiamond (ND)-porphyrin assemblies, 539–540

- phthalocyanine fullerene
 - assemblies, 63
 - symmetrical fullerene rotaxanes
 - bis-biphenylamines, 483–486
 - bis-porphyrins, 486–491
 - unsymmetrical fullerene rotaxanes
 - three components, 504–512
 - two component amine-tethered, 498–501
 - two component ferrocene-tethered, 491–495
- Photoirradiation,
 - monometallofullerenes, 173
- Photoluminescence maps,
 - DNA/SWNT hybrids, 814–815
- Photoluminescence (PL) spectroscopy,
 - characterizations of CNTs, 247
 - isolated (n,m) SWNTs, 255–257
- Photorefractive characterization
 - techniques, 641
- Photorefractive (PR) materials, 644
 - energy levels, 640
 - NLOphore, 649–650
 - photoconductor, 648–649
 - photosensitizer, 646–648
 - trap, 650–651
- Photorefractivity effect, 639
- Photorefractivity fundamentals, 638
 - organic materials, 640–641
- Photorefractivity test, fullerenes as
 - photosensitizers in photorefractive materials, 641–643
- Photosensitizers, 640
 - photoelectrochemical devices,
 - fullerenes, 597, 600, 609–610, 625–627
 - in photorefractive materials, 644, 646–648
 - [6,6]-PCBM, 657–658
 - C₆₀-based dyads, 658–664
 - four-wave mixing, 643–644
 - [60]fullerene derivatives as, 655–657
 - NLOphore, 649–650
 - photoconductor, 648–649
 - photorefractivity in organic materials, 640–641
 - pristine fullerene and fullerene-fullerene mixtures, 651–655
 - trap, 650–651
 - two-beam coupling, 641–643
- Photosynthesis. *see* Artificial
 - photosynthetic systems; Supramolecular artificial photosynthesis
- Photosynthetic performance mimicry,
 - phthalocyanines, 60
- Photosynthetic reaction center (PRC),
 - fullerenes, 376
- Photovoltaic cells. *see also* Solar cells
 - fullerene-polymer
 - examples of commercially available, 3
 - using covalent donor-C₆₀-systems, 15
- Photovoltaic conversion, OPV-C₆₀
 - dyads, 15
- Photovoltaic devices. *see also*
 - Photoelectrochemical devices
 - constructed of SWNTs, potential, 521
 - polymer composites of carbon nanotubes, 732
- Photovoltaics, artificial photosynthetic
 - systems, 209
- PHT. *see* Photohyperthermia
- P3HT. *see* Poly(3-hexylthiophene)
 - dyads (*see* Poly(3-hexylthiophene) dyads)
- Phthalocyanine-C₆₀ pseudorotaxane-like complexes, 76–77
- Phthalocyanine-carbon nanotubes (Pc-CNT) assemblies
 - cancer phototherapy, 92
 - covalent, 84–89

- dopamine sensing, 92
- non-covalent, 89–93
- photoconductive devices, 92–93
- Phthalocyanine-fullerene assemblies
 - Bingel-Hirsch reaction, 61
 - comparison of bonding strengths, 82
 - Diels-Alder reactions, 62
 - donor-acceptor molecules, 60
 - non-covalent, 76
 - double-bridged dyads, 63
 - hexagonal columnar mesophases, 68
 - iodine function, 66–67
 - key starting materials, tris(tert-butyl) monoiodo Zn(II)Pc, 65
 - Langmuir-Blodgett films, 63
 - macrocycle, 80
 - metal-ligand interactions, 78
 - molecular orbitals, energy gaps, 69
 - photoinduced electron transfer, 63
 - polymer structures, 73–74
 - Prato reaction, 61, 69
 - N-methylpyrrolidine ring structures, 64–65
 - sonogashira coupling reaction, 67
 - sonogashira cross-coupling reaction, 71
 - starting material, [6,6]-phenyl- C_{61} -butyric acid methyl ester, 74
 - tosylhydrazones, 74–75
 - trimetallic nitride templated endohedral metallofullerenes ($M_3n@C_{80}$), 68
 - Watson-Crick hydrogen bonding interactions, 77
- Phthalocyanine-fullerene dyads
 - combined with perylene diimide as antenna layer, transient absorption spectra, 433
 - exciplex intermediates, 418–419
 - in photoinduced electron transfer, 417–420
 - molecular layers, photoexcitation reaction scheme, 431–432
 - ultrafast optical spectroscopy, transient absorption and emission, 417–418
- Phthalocyanines (Pc)
 - aromatic system, 59
 - electron-donating materials, 60
 - macrocycle, 80
 - electron donor, 85
 - MWNT systems, 86
 - photosynthetic performance mimicry, 60
 - sandwich complexes, 68
 - SWNT systems, 91
 - carbon nanotubes assemblies, 86
 - dendritic structures, 91
 - nonlinear optical behavior, 89
- Phytochlorin-fullerene dyads
 - face-to-face configuration, 408–410
 - photoinduced electron transfer
 - transient absorption and emission, 411–413
 - ultrafast optical spectroscopy, 412
 - photoreactions, exciplex intermediate, 412–413
- π -conjugated molecular wires, 676
- π -conjugated oligomers, platform for probing electron-transfer processes, 677
- π - π interaction
 - carbon nanotubes assemblies, supramolecular systems, 89
 - between polycyclic aromatic compounds and CNT sidewalls, 251
 - between polyimides and SWNT surfaces, 254
- PK reaction. *see* Pauson-Khand reaction

- PM β -CD. *see* octa-permethylated β -cyclodextrin
- PMI. *see* Perylene-3,4-mono(dicarboximide)
- PMPS. *see* Poly(methylphenylsilane)
- Point charge model, compared to case of partial charges, DNA/SWNT hybrids, 807–808
- Poly(3-hexylthiophene) (P3HT), bulk-heterojunction, theoretical principle, 36
- Poly(3-octylthiophene) (P3OT)
 carbon-nanotubes
 electrical conductivity, 724
 photovoltaic device, 732
 highly aligned carbon-nanotubes, 704
 coating, 705
 photosensitivity, 738–740
 oxidation, 708–709
- Polyacetylenes bearing PDI units, photoelectrochemistry, 24
- Polyamidoamine (PAMAM), divergent dendrimer synthesis, 313–315
- Polyaniline
 carbon-nanotubes, 702–704, 734–738
 deposition, 709–714
 monomers, 701
 properties, 728–731
 synthesis, 720
 electronically conducting polymers, 698, 733
 highly aligned carbon-nanotubes, properties, 723–725
 nanofiber, 742
- Polybenzimidazole (PBI), solubilization of CNTs, 254
 Pt/MWNT/PBI nanocomposites, 258–262
- Polycyclic aromatic compounds, π – π interaction with CNT sidewalls, 251
- Poly(diallyl-dimethylammonium) chloride (PDDAⁿ⁺), in molecular photoelectrochemistry, 683–685
- Polyelectrolytes, as glue for layer-by-layer deposition on ITO electrodes, 683–684
- Polyimides, solubilization of CNTs, 254
- Polymer composites of carbon nanotubes
 chemical polymerization, 708–711
 doping (*see* Doping)
 effect of impurities on thermal conductivity, 774
 effect of nitrogen gasification on thermal conductivity, 774–776
 effect of vacuum impregnation on thermal conductivity, 775
 electrochemical polymerization, 711–716
 electropolymerization, 716–722
 general, 697–700
 lack of thermal percolation, 768
 magnetic field alignment, effect on thermal conductivity, 773–774
 preparation
 chemical polymerization, 708–711
 co-deposition by electropolymerization, 716–722
 electrochemical polymerization, 711–716
 general, 700–703
 melting, 706–708
 solution processing, 703–706
 properties
 electric conductivity, 722–724
 electrochemical, 724–729
 mechanical, 729–730
 thermal stability, 730–732
 prospective applications

- chemical and biochemical sensors, 733–735
- electrochemical capacitors, 735–737
- other foreseeable applications, 737–741
- photovoltaic devices, 732
- self-assembly, 702, 711, 741
- solubilization of CNTs, 254
- as thermal conductive materials
 - calculations and theoretical predictions, 765–767
 - effects of nanotube functionalization, 776–778
 - elastomers, 770
 - thermoplastics, 767–770
 - thermosets, 772–776
- tube-tube interfacial thermal resistance, 771
- Polymer electrolyte fuel cells (PEFCs), PBI nanocomposites, 258
- Polymer PR materials, preparation, 644–646
- Polymer structures, phthalocyanine fullerene assemblies, 73–74
- Polymeric/GN composites, for thermal conductive materials, 779–783
- Polymers, conducting. *see* electronically conducting polymers
- Poly(methyl methacrylate) (PMMA), composites with SWNTs, enhancement of thermal conductivity, 769, 774–775
- Poly(methylphenylsilane) (PMPS), photogeneration efficiencies, 652
- Poly(*N*-vinylcarbazole) (PVK), photosensitizers in PR materials, 652–654
- Polypropyleneimine (PPI), fullerodendrimers formation, 9–10
- Polypyrrole (PPY)
 - carbon-nanotubes, 736–737
 - coating, 734–735
 - properties, 723–728
 - electronically conducting polymers, 698, 733
 - highly aligned carbon-nanotubes, 708–713
 - deposition, 717–720
- Poly(styrene-4-sulfonate) (PSSⁿ), in molecular photoelectrochemistry, 683–685
- Polystyrene-MWNT composites, enhancement of thermal conductivity, 767
- Polystyrene-SWNT composites, enhancement of thermal conductivity, 769–770
- Porphyrin-based CNT dispersants, 252–253
- Porphyrin-benzoquinone dyads, reorganization energy, 415
- Porphyrin-bridge-fullerenes. *see* Porphyrin excitation
- Porphyrin-containing hosts, for C₆₀ fullerenes, 395–397
- Porphyrin excitation. *see also* Excitation
 - acetylene bridges, 451–452
 - bisacetylene bridges, 443–449
 - disilane bridges, 462–463
 - oligosilane bridges, 464
 - oligothiophene bridges, 456–462
 - oligothiophene-vinylene bridges, 455–456
 - phenyleneacetylene bridges, 449–451
 - phenylenevinylene bridges, 452–455
- Porphyrin-fullerene bridges. *see* Porphyrin excitation
- Porphyrin-fullerene composite systems
 - electrochemical deposition, 613–618
 - interaction, 376, 378–380
- Porphyrin-fullerene dyads
 - charge separation, 406–407

- delocalization of electron densities, 415
- energy of exciplex intermediate, 422
- excited singlet states, 422
- face-to-face configuration, 408–410
- intramolecular exciplex, 406–407
- photochemical characterizations, 410–411
- photodynamics, differing distances of donor and acceptor, 417
- photoexcitation relaxation
 - Franck-Condon plot, 415–416
 - time resolved spectroscopy studies, 416–417
- photoinduced electron transfer, 419–420
 - exciplex intermediate, 410–417
 - transient absorption and emission, 411
 - ultrafast optical spectroscopy, 412
- reorganization energy, 406–407
- strongly and weakly coupled chromophores, reaction schemes in non-polar and polar solvents, 423–424
- Porphyrin-fullerene supramolecular chemistry
 - cobalt(II)
 - binding constants and charge transfer bands, 381–383
 - synthesis of bis-porphyrins, 381
 - X-ray structures of $T_{3,4,5\text{-ome}}$ PP cocrystallates, 383–387
 - molecular porphyrin hosts for fullerenes, 376–378
 - self assembling, 376
- Porphyrin-functionalized CNCs, for light-energy conversion, 530–537. *see also* CNC-(H_2P)_n nanohybrids
- Porphyrin-nanodiamond (ND) assemblies, for light-energy conversion, 537–540
- Porphyrin-PDI- C_{60} triad, self-assembled monolayers, photoelectrochemistry, 23
- Porphyrin rotaxanes, amine-tethered, 501–504
- Porphyrins. *see also* bis-Porphyrins
 - as chromophores, 376
 - in multifunctional hybrid cells, 683, 686–689
 - hosts for fullerenes, 376–378
 - cobalt (II), 380–387
 - in multifunctional hybrid cells, 2–6
 - palladium, 378
 - synthesis by click reactions, 21–24
 - synthesis with fullerene building blocks, 2–6
 - zinc, 380, 383–387
 - synthesis, *bis*-porphyrins, 381
- P3OT. *see* Poly(3-octylthiophene)
- PPI. *see* Polypropyleneimine
- PPY. *see* Polypyrrole
- PR. *see* Photorefractivity
- Prato reaction
 - fulleropyrrolidines formation, 10–11
 - N-methylpyrrolidine ring structures, 64–65
 - phthalocyanine fullerene assemblies, 61
- PRC. *see* Photosynthetic reaction center
- Precipitation, metallofullerenes, 197–199, 201
- Pristine endohedral metallofullerenes
 - electronic properties, 154–156
 - redox potentials, 155
- Pristine fullerenes
 - binding, porphyrin hosts, 378
 - fabrication, vacuum deposition, 608

- photosensitizers in photorefractive materials, 651–655
- supramolecular hosts for, 391–401
- Propargylfulleropyrrolidines
 - formation of allene-containing fullerenes, 48
 - mechanisms for the cyclization, 50
 - reactivity, 49
- Protic acid conditions, fullerene ring opening, 358
- Proton conductors, Pt/MWNT/PBI nanocomposites, 258
- Pseudorotaxane-like complexes, supramolecular systems, 76–77
- PSS^{na}. *see* Poly(styrene-4-sulfonate)
- Pt/MWNT/PBI nanocomposites, 258–262
- PVK. *see* Poly(*N*-vinylcarbazole)
- Pyrene-based CNT dispersants, 251
- Pyrolysis, catalytic, 713
- Pyrrolidines. *see*
 - Propargylfulleropyrrolidines
- Pyrrolidinodimetallofullerene, [6,6]-closed and [5,6]-closed adducts, 165–166
- Pyrrolo, C₆₀ fullerene porphyrins formation, 3–6
- Radical coupling reaction, endohedral metallofullerenes with $\alpha,\alpha,2,4$ -tetrachlorotoluene, 173
- Radical ion pair (RIP)
 - lifetimes
 - in C₆₀-exTTF systems, 677
 - in flexible rotaxanes, 494
 - molecular bridges, 442–444, 448, 466–467, 470, 474–475
 - photoinduced electron transfer processes, 483
- Radical reaction, endohedral metallofullerenes, 173–175
- Radical stabilization, by fullerene-N-oxide combinations, 674–675
- Radical trifluoromethylation, endohedral metallofullerenes, 174–175
- Raman spectra, characterization of PFAFs, 126
- Randles equivalent electric circuit, 728–729
- RCP. *see* Redox conducting polymer
- Reactions of fullerenes. *see also*
 - Retroreactions
 - competitive retro-cycloaddition of fullerene dimers, pyrazolino [3,4:1,2] [60]fullerenes, 367
 - electrochemical retro-cycloaddition, isoxazolo [3,4:1,2] [60]fullerenes, 365
 - isolated pentagon rule, 326
 - principal characteristics, 326
 - pyrrolo [3,4:1,2] [60]fullerenes
 - chemical retro-1,3-dipolar cycloaddition reactions, 359–364
 - electrochemical retro-1,3-dipolar cycloaddition reactions, 362–363
- Redox chemistry, solubilized CNTs. *see* Solubilized carbon nanotubes
- Redox conducting polymers (RCPs), 698
- Redox potentials
 - clusterfullerenes, 177
 - dimetallofullerenes, 177
 - endohedral metallofullerenes, 154–156, 175
 - isolated (n,m) SWNTs, 255–258
 - monometallofullerenes, 176
- Redox reaction, and determination of electronic states of CNTs, 254–258
- Reduction potentials, PFAFs, 135–136

- Reductions, metallofullerenes, 155–156, 175–179
- Reductive alkylations, covalent sidewall (and tip) functionalization of carbon nanotubes, 305–306
- Regioselective intramolecular *cis-1* cycloadditions, fullerenes, 34–38
- Regiospecific functionalization of C₆₀, retro-Diels-Alder reaction, 335–336
- Reorganization energy
 - electron transfer reactions, 208
 - fullerenes, 213
 - porphyrin-benzoquinone dyads, 415
 - porphyrin-fullerene dyads, 406–407
- Resonance Raman spectroscopy, carbon nanotubes, 278–280
- Retro-1,3-dipolar cycloaddition reactions
 - azomethine ylide as an intermediate, 360–361
 - endohedral derivatives and their stability, 363–364
 - pyrrolo [3,4:1,2] [60]fullerenes
 - chemical, 359–364
 - electrochemical, 362–363
 - selective removal by
 - electrochemical methods, 362
 - stabilization of ionic intermediates, 362
- Retro-cycloaddition reaction of isoxazolo[3,4:1,2] [60]fullerenes
 - chemical retro-cycloaddition, 365
 - electrochemical retro-cycloaddition, 365
- Retro-cycloaddition reaction of pyrazolino[3,4:1,2] [60]fullerenes
 - chemical retro-cycloaddition, 366
 - competitive retro-cycloaddition of fullerene dimers, 367
- Retro-cyclopropanation reaction
 - addends migration on fullerene surface, 350
- addition-elimination Bingel-Hirsch reaction, 339
- C₆₀ fullerene derivatives, 340–350
- C₇₀ fullerene derivatives and higher fullerenes, 352–355
- Coulometric reductions, 340, 344
- cyclic voltammetry, 340
- electrochemically induced, 340
 - isomerization, 349–352
- fullerene derivatives
 - controlled potential
 - electrolysis (CPE), 340–341
 - isolation of enantiomerically pure chiral C₇₆, 354
 - isolation of three
 - constitutional isomers, 355
 - methano C₇₀ fullerene derivatives, 353
 - synthesis of regioselective tris-adducts, 351–352
- methanofullerene decomposition, 340
- nucleophilic attacks on fullerenes, 339
- spiromethanofullerenes, Bingel-like addends, 343
- walk-on-the-sphere
 - rearrangements, 350–352
- Retro-Diels-Alder reaction. *see also* Diels-Alder reaction
 - activation energy, 331
 - adducts of substituted
 - isobenzofurans and c60, 337–339
 - aromaticity reduction, 330
 - bulk-heterojunction solar cells, 339
 - dimethylantracene (DMA) as a reversible template, 335

- fullerene solubility improvement, 339
- orthogonal transposition approach, 335–337
 - regiospecific functionalization of C_{60} , 335–336
 - synthetic transformation sequence, 336
 - topochemical functionalization of C_{60} , 335–336
- redox potentials, 332
- reversible tether-directed remote functionalization, 334
- tether-directed remote functionalization, 333–335
- thermal *vs.* electrochemical stability of adducts, 327–333
 - aromaticity reduction, 330
 - weight lost from the anthracene moiety, 329
- thermodynamic parameters, 330–331
- Reverse switching molecular shuttles, 672
- Reversible tether-directed remote functionalization, 334
- RIP. *see* Radical ion pair
- Rotaxanes. *see also* Molecular shuttles; Photoinduced electron transfer molecular machines, composition, 670
 - NMR spectra, 226
 - solvents for, 671–674
 - succinamide station, 672
 - supramolecular artificial photosynthesis, 210–216
 - symmetrical, 483–491
 - unsymmetrical, 491–512
- SAFA. *see* Stir and filter approach
- SAMs. *see* Self-assembled monolayers
- ^{45}Sc -NMR spectroscopy
 - $\text{CeSc}_2\text{N}@I_b\text{-C}_{80}$, 153
 - $\text{Sc}_3\text{N}@I_b\text{-C}_{80}$, 153
- Scanning electron microscopy (SEM), carbon nanotubes, 289–291
- Scanning probe microscopy, carbon nanotubes, 285–288
 - atomic force, 286–287
 - scanning tunneling, 287–288
- Scanning transmission electron microscopy (STEM), carbon nanotubes, 289–290
- Scanning transmission electron microscopy-high angular annular dark-field (STEM-HAADF), gold nanoparticles encapsulated in dendrimers, 290
- Scanning tunneling microscopy (STM), carbon nanotubes, 287–288
- $\text{Sc}_2\text{C}_2@C_{3v}(8)\text{-C}_{82}$, electrophilic carbene addition, molecular structures and characterization of adducts, 165
- $\text{Sc}_2\text{C}_2@C_{3v}\text{-C}_{82}$
 - ^{13}C -NMR spectra, 153–154
 - electronic structure, 154
- $\text{Sc}_3\text{C}_2@I_b\text{-C}_{80}$, electrophilic carbene addition, molecular structures and characterization of adducts, 165
- $\text{Sc}_3\text{C}_2@i_b\text{-C}_{80}$, pyrrolidino adducts, molecular structures and characterization, 168
- $\text{Sc}_3\text{C}_2@I_v\text{-C}_{82}$ anions, 154
- SCCNTs (stack-cup carbon nanotubes). *see* Cup-stacked carbon nanotubes
- Schlegel diagrams
 - $C_1\text{-C}_{70}(\text{CF}_3)_{10}$, 116
 - C_{60} PFAFs, 117–119
 - C_{70} PFAFs, 120–122
- Sc_3N clusters, inside fullerene cages, 153
- $\text{Sc}_3\text{N}@D_{3h}(5)\text{-C}_{78}$
 - Bingel-Hirsch reactions, chemical reactivity, 170

- pyrrolidino adducts, molecular structures and characterization, 168
- Sc₃N@I_h-C₈₀
 - bis-silylation, structures, electronic properties, and thermodynamic stability, 160
 - cage framework and motion of the Sc₃N cluster, 153
 - electronic structure, 153
 - NMR spectra, 153
 - redox potentials, 155
- Sc₃N@I_h-C₈₀, irreversible Diels-Alder reaction, with in situ generated *o*-quinodimethane, 172–173
- Sc₂O@C₈₂, 199–200. *see also* Metallic oxide clusters
- Sc₄O₂@C₈₀, 192–196. *see also* Metallic oxide clusters
- Sc₄O₃@C₈₀. *see also* Metallic oxide clusters
 - isolation, 192–196
 - precipitation, 198–199
- Screening factor, DNA/SWNT hybrids, 812–814
- Sealed glass ampoule reactor, synthesis of PFAFs, 109
- Second donor, photoinduced electron transfer processes, triphenylamine, 505
- Self-assembled complexes. *see* Supramolecular complexes
- Self-assembled monolayers (SAMs)
 - fullerenes, 426
 - on gold electrodes, 596–601
 - on indium tin oxide electrodes, 601–605
 - porphyrin-PDI-C₆₀ triad, photoelectrochemistry, 23
- Self-assembly, polymer composites of carbon nanotubes, 702, 711, 741
- Self-consistent charge density, DNA/SWNT hybrids, 810–813
- SEM. *see* Scanning electron microscopy
- Semiconductor SWNTs
 - circular polarization, new absorption lines in, 794–798
 - Fermi levels, and van-Hove peaks, 794
- Sensitizer. *see* Photosensitizers
- Sensors
 - chemical and biochemical, polymer composites of carbon nanotubes, 733–735
 - phthalocyanine-carbon nanotubes, 92
- Shallow traps, photorefractive materials, 651
- Si(IV)Pc, phthalocyanine fullerene assemblies, 63–64, 73
 - triad molecules, 72
- Silica. *see* Functionalized silica
- Silicone elastomer, composites with CNTs, 771–772
- Single-stranded DNA (ssDNA), as surfactant for CNT solubilization, 249–250
- Single-walled-carbon nanohorns (SWNH), nanotube assemblies, non-covalent, 91
- Single-walled carbon nanotubes (SWCNTs/SWNTs)
 - bandstructure, effect of surface functionalization, 788
 - carbon nanotubes assemblies, 83
 - classification by chiral vectors, 759
 - composites with epoxy resin, enhancement of thermal conductivity, 773–775
 - composites with graphite, thermal conductivity, 764–765
 - composites with polymers, 699–706, 710–716, 720–742
 - composites with polystyrene, enhancement of thermal conductivity, 769–770
 - cycloadditions, 34

- definition, 246
 - functionalization
 - Birch reduction and reductive alkylation, 305
 - diazonium coupling, 306
 - fluorination, 296–297
 - Heck and Suzuki coupling, 308–309
 - radical additions, 304–305
 - via amid linkage, 293–295
 - via ester linkage, 292–293
 - highly aligned, thermal conductivity, 763–764
 - individual, defect-free, metallic, thermal conductivity, 756–761
 - as key building blocks for
 - photoelectro-chemical and photovoltaic devices, 521
 - low energy excitations, Dirac Hamiltonian, 798
 - molecular model, 703
 - photoelectrochemical devices, 618–620
 - photoluminescence spectroscopy, 247
 - properties
 - and applications, 519–521
 - optical, 787–819
 - and structure, 273–274
 - redox potentials, 255–258
 - solubilization
 - using double- and single-stranded DNA molecules, 249–250
 - using functional aromatic molecules, 251–253
 - using surfactant micelles, 247–248
 - surface functionalization, 788
 - zigzag, thermal conductivity, 759–760
- Smalley procedure, carbon nanotube assemblies, 84–85
- Sodium dodecyl sulfate (SDS)
 - composites with CNTs, enhancement of thermal conductivity, 772
 - as surfactant for CNT solubilization, 247
- Sodium dodecylbenzene sulfonate (SDBS), as surfactant for CNT solubilization, 248
- Solar cells. *see also*
- Photoelectrochemical devices;
- Photovoltaic cells
 - bulk-heterojunction
 - incorporation of C₆₀-PDI, 35–38
 - PCMB, 36
 - P3HT, 36
 - metallofullerenes, 71
 - OPV-C₆₀ dyads, 15–17
 - P3HT dyads, suggested mechanism, 37
 - solution-processed bulk-heterojunction, deposition, 608, 620–622
- Solubilization/dispersion techniques, CNTs, overview, 246
- Solubilized carbon nanotubes, redox chemistry
 - characterizations of individually solubilized CNTs, 247
 - determination of electronic states, 254–258
 - DNA/carbon nanotube hybrids, 249–251
 - electrocatalysts for fuel cells, 258–262
 - individually solubilized CNTs, 247–248
 - introduction, 245–246
 - nanotube/polymer composites, 254
 - using functional aromatic molecules, 251–253

- Solution-processed bulk-heterojunction solar cells, deposition, 608, 620–622
- Solution processing, polymer composites of carbon nanotubes, 703–706
- Solvent controllable molecular shuttles, 673
- Solvent switchable molecular shuttles, 671–672
- Solvents, polar and nonpolar, C₆₀-porphyrin rotaxane, 504
- Sonogashira coupling reaction, phthalocyanine fullerene assemblies, 67, 71
- Space charge, photorefractive materials, 638
- Spacer molecules, phthalocyanine fullerene assemblies, 60, 65–67
- Spectroscopy. *see also* ¹³C-NMR spectroscopy; Electron-ion mass spectroscopy; Ultrafast optical spectroscopy
 - correlation spectroscopy, ¹⁹F NMR spectra of PFAFs, 127–129
 - electron energy loss spectroscopy, carbon nanotubes, 278
 - emission spectroscopy, carbon nanotubes, 283–284
 - infrared spectroscopy, carbon nanotubes, 282–283
 - nuclear magnetic resonance spectrometry, carbon nanotubes, 284–285
 - photoluminescence
 - characterizations of CNTs, 247
 - isolated (n,m) SWNTs, 255–257
 - resonance Raman spectroscopy, carbon nanotubes, 278–280
 - UV-vis, characterization of PFAFs, 125–126
 - UV-vis-NIR absorption spectroscopy, carbon nanotubes, 280–282
 - vibrational, characterization of PFAFs, 125–126
 - X-ray photoelectron spectroscopy, carbon nanotubes, 285
 - ⁸⁹Y-NMR, Y₃N@I_h-C₈₀, 153
- Spin-coating deposition
 - coordination bonding systems, 627–628
 - hydrogen-bonding systems, 622–627
 - solution-processed bulk-heterojunction solar cells, 620–622
 - SWNTs, 709
- Spiromethanofullerenes, Bingel-like addends, 343
- ssDNA. *see* Single-stranded DNA
- Stack-cup carbon nanotubes (SCCNTs). *see* Cup-stacked carbon nanotubes
- Stannoxane core, fullerodendrimers, reagents and conditions, 16–18
- STEM. *see* Scanning transmission electron microscopy
- STEM-HAADF. *see* Scanning transmission electron microscopy-high angular annular dark-field
- Stereochemistry. *see also* Chirality fullerenes, 55
- Stevenson method, synthesis of metallic nitride fullerenes, 188–189
- Stir and filter approach (SAFA), isolation of Metallic oxide clusters in fullerene cages, Sc₄O₂@C₈₀ and Sc₄O₃@C₈₀, 192–196
- Stone-Wales defects, CNTs, 760–761
- Stoppers, components of rotaxanes, 670
- Substrate perturbation, effect on surface/interface layer of SWNTs, 788

- Succinamide station, in rotaxanes, 672
- Super-absorbing fullerenes, C_{60} -PDI dyads, 27–34
- Supercells, for SWNTs, modeling of DNA/SWNT hybrids, 808–809
- Supramolecular artificial photosynthesis, 210–216. *see also* Artificial photosynthetic systems
- building blocks, tetrapyrrolic macrocycles, 213
 - catenanes, 210–216
 - construction of photoactive nanoscale structures, 211
 - fullerene introduction into interlocked molecules, 213–216
 - intrinsic submolecular movements, 211
 - metal coordination, $[Cu(phen)_2]^+$ complex, 213
 - porphyrinic pigments, 213
 - rotaxanes, 210–216
 - template-directed synthesis, 211
 - template synthesis of catenanes, original protocol, 212
 - zinc(II) porphyrins, 213
- Supramolecular chemistry, 480
- carbon nanotubes, 312–315
 - porphyrin-fullerene, 378–380
 - cobalt(II), 380–387
 - molecular hosts, 376–378
- Supramolecular complexes, fullerene based donor-acceptor systems, 410
- Supramolecular hosts
- calixarene-type, 392–395
 - $PM\beta$ -CD-porphyrin-based, 401
 - porphyrin-containing, 395–397
 - for pristine fullerenes, 391–401
 - TBTQ-based, 400
 - triarylphosphate-based, 401
 - TTF-containing, 397–399
- Supramolecular systems
- π - π interaction, 89
 - phthalocyanine based, 76
 - $Zn(II)Pc_2-(C_{60})_2$, 80–82
- Supramolecular triad, 68
- Surface functionalization, of SWNTs, with helically wrapped singlestranded DNA, 788
- Surface/interface layer of SWNTs, dependence on substrate perturbation, 788
- Surfactant micelles, individual solubilization of CNTs, 247–248
- Surfactants, for CNT solubilization, 247–248
- ssDNA, 249–250
- Suzuki coupling, functionalization of carbon nanotube surfaces, 308–309
- SWCNTs. *see* Single-walled carbon nanotubes
- SWNH. *see* Single-walled-carbon nanohorns
- SWNT. *see* Single-walled carbon nanotubes
- SWNT-PMMA composites, enhancement of thermal conductivity, 769
- using nitrogen gasification, 774–776
- Symmetrical fullerene rotaxanes
- bis-biphenylamines, 483–486
 - bis-porphyrins, 486–491
 - synthetic routes and structures, 488
 - temperature dependence, photoinduced electron transfer processes, 486
- Symmetry breaking
- analytical theory, armchair SWNTs, 798–805
 - DNA/SWNT hybrids
 - bandstructure modulation, 797

- effect of DNA wrap, 790
 - electronic properties of, 790–819
- TEM images, CSCNTs, 525–526
- tert*-butyl group-bearing zinc-porphyrins, 396–397
- Tether-directed remote functionalization
 - anchor-tether-reactive group, 334
 - synthesis of novel fullerene-acetylene hybrid carbon allotropes, 334–335
- Tetrakis(*p*-carboxyphenyl)porphyrin (TCPP), ND clusters, 538–540
- Tetrathiafulvalene (TTF)-containing hosts, for C₆₀ fullerenes, 397–399
- Tetrathiofulvalene dyads, solar cells, suggested mechanism, 37
- Thermal conductive materials
 - based on carbon nanotubes, 756–778 (*see also* Polymer composites of carbon nanotubes)
 - bulk CNTs, 761–765
 - effects of nanotube functionalization, 776–778
 - elastomers, 770–772
 - individual CNTs, 757–761
 - thermoplastics, 767–770
 - thermosets, 772–776
 - based on graphene nanosheets, 778–784
- Thermal conductivity, CNTs. *see* specific CNTs
- Thermal percolation, polymeric/nanotube composites, 768
- Thermal stability
 - Diels-Alder adducts, 327–333
 - polymer composites of carbon nanotubes, 730–732
- Thermally activated incoherent hopping, molecular wires, 676
- Thermally induced reactions
 - [2+2] cyclizations, fullerenes, 45–46
 - intramolecular ene reaction, fulleroallenes, 46–47
 - theoretical study, intramolecular reactions of fuller-1,6-enynes, 47–49
- Thermogravimetric analysis (TGA)
 - carbon nanotubes, 276–278
 - CNC-(H₂P)_n nanohybrids, 532–533
- Thermoplastics, in polymeric/nanotube composites, thermal conductive materials, 767–770
- Thermosets, in polymeric/nanotube composites, thermal conductive materials, 772–776
- Thiophenevinylene-ferrocenes, C₆₀-bridges, 468–469
- Tight binding bandstructure calculations, DNA/SWNT hybrids, 805–810
- Tight binding charge density, DNA/SWNT hybrids, DNA perturbation, 812–813
- Ti(IV) phthalocyanine, metallosupramolecular complexes, 82
- Titration, UV-vis
 - charge transfer band, 379
 - cobalt(II) derivative, 382
 - methods, 381
- TMFs. *see* Trifluoromethylfullerenes
- TNT. *see* Trimetallic nitride templated
- Topochemical functionalization of C₆₀, retro-Diels-Alder reaction, 335–336
- Tosylhydrazones, phthalocyanine fullerene assemblies, 74–75
- Transient absorption measurements
 - amine-tethered fullerene rotaxanes, 499–500

- C_{60} -porphyrin rotaxane, 504–505
 - exciplex relaxation, fullerene based donor-acceptor dyad multi-layers, 430–431
 - ferrocene-tethered rotaxanes, 494
 - triphenylamines, 510
- Transient absorption spectra
 - bilayer formed by phthalocyanine-fullerene dyads and perylene diimide, 433
 - phthalocyanine-fullerene dyads, 417–418
 - phytochlorin-fullerene dyad, 411–413
 - porphyrin-fullerene dyads, in molecular film, 427–428
- Translation vectors, graphene lattice, DNA/SWNT hybrids, 800
- Transmission electron microscopy (TEM), carbon nanotubes, 289
- Trapping site, photorefractive materials, 650–651
- Triarylphosphate-based hosts, for C_{60} fullerenes, 401
- Tribenzotriquinacene (TBTQ)-based hosts, for C_{60} fullerenes, 400
- Trifluoromethylation, of solid C_{60} with CF_3I gas, scheme, 103
- Trifluoromethylfullerenes (TMFs),
 - synthesis of PFAFs
 - arc generator, 103–104
 - general remarks, 102–103
- Trimetallic nitride clusters, endohedral metallofullerenes
 - cage framework, movement of the cluster and electronic structures, 153–154
 - chemical reactivity, 169–170
- Trimetallic nitride templated (TNT) endohedral metallofullerenes ($M_3N@c80$), phthalocyanine fullerene assemblies, 68
- Triphenyl amines (TPA), photoinduced electron transfer processes, 498–502
- Triplet states, fullerene based donor-acceptor systems, 421–422
- Tripodal CTV-exTTF, as hosts for fullerenes, 399
- Tris(tert-butyl) monoiodo Zn(II)Pc, phthalocyanine fullerene assemblies, 65
 - Sonogashira coupling reaction, 67
- TTF. *see* Tetrathiofulvalene
- Tube-tube interfacial thermal resistance, CNT-polymer composites, 771
- Tweezer molecules, as hosts for fullerenes
 - porphyrin-based, 396–397
 - TTF-based, 397–399
- Two-beam coupling, photorefractive measurements, 641
- Two-dimensional (2D) Brillouin zone, of graphene, 795
- Ultrafast optical spectroscopy
 - phthalocyanine-fullerene dyads, 417–418
 - phytochlorin-fullerene dyads, 411–413
 - porphyrin-fullerene dyads, 411
- Umklapp process, and phonon group velocity, zigzag SWNTs, 759
- Unidirectional transport of charges, in molecular wires, 676
- Unsymmetrical fullerene rotaxanes
 - three components
 - C_{60} -porphyrin rotaxane with ferrocene as a second donor, 504–505
 - triphenylamine as a second donor, 505–512
 - two components amine-tethered, 498–501

- fullerene-tethered porphyrin
 - rotaxanes, 501–504
 - two components ferrocene-tethered, 491
 - axle charge and length effects, 495–498
 - temperature effect of flexible rotaxane, 491–495
- UV-vis-NIR absorption spectroscopy, carbon nanotubes, 280–282
- UV-vis spectroscopy
 - metallofullerenes, 203
 - PFAFs, 125–126
- UV-vis titration, porphyrin-fullerenes
 - charge transfer band, 379
 - cobalt(II) derivative, 382
 - methods, 381
- Vacancies, as conformational defects in CNTs, 760–762
- Vacuum deposition
 - pristine fullerenes, 608
 - SWNTs, 739
- Vacuum impregnation, of CNTs in polymeric/CNT composites, enhancement of thermal conductivity, 775
- Van der Waals interactions
 - layer preparation, 605–606, 612
 - molecular porphyrin hosts for fullerenes, 376, 380, 386
- Van Hove singularities
 - at the edge of the Brillouin zone of graphene, 795
 - and Fermi levels, semiconductor SWNTs, 794
- Vibrational spectroscopy, characterization of PFAFs, 125–126
- Watson-Crick hydrogen bonding
 - interactions, phthalocyanine fullerene assemblies, 77
- Wavefunctions, for electronic states, DNA/SWNT hybrids, 815–816
- Wrap characterization, by breaking of the helical symmetry, DNA/SWNT hybrids, 789
- Wrap number, DNA/SWNT hybrids, 802–803
- Wrapping
 - of DNA in DNA/SWNT hybrids, influence on optical properties, 790
 - of functional molecules, carbon nanotubes, 310–311
- X-ray crystallography, characterization of PFAFs, 128–133
- X-ray photoelectron spectroscopy, carbon nanotubes, 285
- X-ray structures, fullerenes
 - Bis*-porphyrins, 377–378
 - T_{3,4,5-omc}PP cocrystallates, 383–387
- ⁸⁹Y-NMR spectroscopy, Y₃N@I_b-C₈₀, 153
- Y@C_{2v}-C₈₂, radical trifluoromethylation, 174
- Y₃N@I_b-C₈₀, Bingel-Hirsch adduct, 169–170
- Y₃N@I_b-C₈₀C(CO₂CH₂Ph)₂, Bingel-Hirsch adduct, 170
- Young's modulus, polymer composites of carbon nanotubes, 699–700, 729–730, 741
- zigzag SWNTs, thermal conductivity, 759–760
- Zinc phthalocynine (ZnPc). *see* Zn(II)Pc
- Zn(II) porphyrin (ZnP), 213
 - fullerenes
 - binding constants, 380
 - close approach, 383–387

- pristine, 378
- photoinduced electron transfer processes, 486–487
- Zn(II)-porphyrin- C_{60} -[2]catenates, synthesis, 224–225
 - MALDI-TOF analysis, 224
 - molecular models, 228
 - precursors, 225
 - synthetic route, 225
- Zn(II)-porphyrin- C_{60} -rotaxane, synthesis, 221–224
 - final stoppering reaction, 221
 - MALDI-TOF analysis, 224
 - molecular models, 228
 - synthetic route, 223
- Zn(II)Pc, carbon nanotubes assemblies, 85
- Zn(II)Pc₂-(C_{60})₂, crown-ether, supramolecular, 80–82
- Zn(II)Pc- C_{60} dyads, supramolecular systems, phthalocyanine fullerene assemblies, 79
- Zn(II)Pc chromophore, fluorescence intensity, phthalocyanine fullerene assemblies, 78
- ZnP. *see* Zinc(II) porphyrin
- ZnP⁸⁺, as excited-state electron donor, in multifunctional hybrid cells, 686–689
- ZnP-[3]catenate, MALDI-TOF analysis, 233
- ZnPc. *see* Zn(II)Pc